A KINETIC STUDY OF THE DISSOLUTION OF NATURAL AND SYNTHETIC SPHALERITE IN AQUEOUS SULPHURIC ACID AND IN ACIDIC FERRIC SULPHATE MEDIA

by

Bernard Verbaan
B.E. (Chem. Eng., Hons.), M.Sc. (Eng.)

This thesis is submitted in partial fulfilment of the requirements for the degree of Doctor of Philosophy in the Department of Chemical Engineering, University of Natal.

PREFACE

I hereby declare that the material incorporated in this thesis is my own original and unaided work except where specific acknowledgement is made, and has not been submitted for a degree at any other university or institution.

B. VERBAAN

Department of Chemical Engineering,
University of Natal,
Durban.

December, 1977.

To

RHODA , LOIS and JANICE

ACKNOWLEDGEMENTS

I wish to acknowledge and thank the following people and institutions :

Professor E.T. Woodburn who as supervisor of this project rendered invaluable advice and assistance;

The University of Natal for financial assistance and for providing laboratory and office facilities;

Mr D.W. Penn and the workshop staff of the Chemical Engineering Department for setting up the apparatus and making numerous modifications;

The National Institute of Metallurgy for providing a bursary and funds to finance this project;

Mr M. Dawson and Dr. R. Roman for their advice and encouragement, especially during the initial stages of this project;

Messrs W.G. Mandersloot and D. Cloete of the Council for Scientific and Industrial Research for providing the loan of a Ströhlein surface area meter;

Dr. I. Forster of the Geology Department of the University of Natal for his assistance in conducting optical microscopic examinations.

My wife, Rhoda , for typing this thesis.

A B S T R A C T

Four sphalerites (synthetic, high grade natural, moderately impure flotation concentrate and highly impure flotation concentrate) were leached in acid sulphate media without and with ferric ions present under the following conditions :-

Case (i) $[Fe^{3+}]_o : [H_2SO_4]_o = 0,0$

Case (ii) $[Fe^{3+}]_o : [H_2SO_4]_o \geq 1,8$

Case (iii) $[Fe^{3+}]_o : [H_2SO_4]_o \leq 0,1$

Extensive data for leaching under these conditions are tabulated. Kinetic mechanisms based on Langmuir-Hinschelwood adsorption theories were proposed, and leaching models were developed for different assumed rate limiting steps. The initial rate and overall forms of the models were tested using experimental data.

Leaching under case (i) conditions

Non-oxidative dissolution took place with Zn^{2+} and H_2S the predominant reaction products. The H_2S partial pressure was monitored continuously and solution samples were taken for analysis at discrete time intervals.

Vibratory (i.e. attrition) milling eliminated very large differences observed in the leaching characteristics of course size fractions of the

natural sphalerites.

The initial rate form of a model based on a dual site reaction mechanism and on either H^+ adsorption or reaction product desorption rate control was found to fit the data for the synthetic and vibratory milled forms of sphalerite. The most impure vibratory milled sphalerite adsorbed Zn^{2+} and H_2S very strongly, and this resulted in product desorption rate control. Vibratory milled forms of the high grade natural sphalerite and the moderately impure flotation concentrate, exhibited virtually identical initial rate dissolution kinetics, despite large differences in their chemical compositions.

Leaching under case (ii) conditions

Oxidative dissolution took place with Zn^{2+} and elemental sulphur the predominant reaction products. Scanning electron microscope photographs of leached and unleached particles showed the sulphur present on the particle surface. These photographs, and optical microscope photographs of etched polished sections, showed that dissolution took place in a complex way.

A model based on ferric ion adsorption as the rate limiting step was proposed and confirmed experimentally. The model demonstrated a proportional dependency of the rate on the area and ferric ion concentration, and an inverse dependency on the hydrogen ion concentration. For a -90,0 + 63,0 μm size fraction, the three natural sphalerites exhibited virtually identical dissolution rates per unit area.

The effect of ball milling or vibratory milling the sphalerites fine, was to increase the rate per unit area for the most impure natural sphalerite but decrease the rate per unit area for the high grade natural sphalerite.

It was shown that for course size fractions of sphalerite, the most impure sphalerite which leached slowest under case (i) conditions (i.e. adsorbed H^+ poorly) leached fastest under case (ii) conditions (i.e. adsorbed Fe^{3+} strongly). The reverse was true for the high grade natural sphalerite.

Except in the case of synthetic sphalerite leaching under case (i) conditions, no correlation was shown to exist between the way the B.E.T. measured area changed, and the way the calculated active area changed during leaching.

Leaching under case (iii) conditions

Oxidative and non-oxidative dissolution, as well as H_2S oxidation by Fe^{3+} occured simultaneously. The extents to which oxidative or non-oxidative dissolution occured could be explained in terms of the hydrogen ion and ferric ion adsorption characteristics of the sphalerites.

The ferric ion oxidation of H_2S was studied in the absence and presence of solids, and the presence of sphalerite or activated charcoal catalysed this reaction. No advantage was gained by leaching in the presence of activated charcoal with or without Fe^{3+} present, unless conditions were such that H_2S was formed as a product of reaction.

N O M E N C L A T U R E

Latin Symbols

A_o	initial specific surface area, as determined using a N_2 adsorption technique.
A	specific surface area of a sphalerite during leaching.
A'	area coefficient defined by equation F. 8 .
A_E	pre-exponential factor appearing in Arrhenius type equations (e.g. equation 3. 35).
A_{SPH}	surface area calculated theoretically for a solid sphere.
a	constant appearing in equation F. 7 .
B	a constant used in equation F. 3 .
C_i	molar concentration of specie i
$\overline{D}$	mean diameter of particle, representing the arithmetic mean of the upper and lower size fraction limits.
E_a	activation energy with units (m J / kg-mol)
K	equilibrium constant, generally subscripted
K_ϕ	proportionality constant defined by equation 2.1.
k	rate constant, generally subscripted.
k_f ; k_r	forward and reverse rate constants appearing in equation 1.1.
M	mass of solid in reactor.
MV_i	molar volume of specie i .
MW_i	molecular weight of specie i .
P_{H_2S}	H_2S partial pressure .
R	universal gas constant (when used in Arrhenius type equation with E_a expressed in m J / kg-mol units, R = 8 305,6).

r	rate of reaction, usually subscripted (e.g. $(r_A)_o = \frac{d[Zn^{2+}]}{dt}$).
r^* or r^Θ	rate of reaction per unit area, usually subscripted.
T	temperature.
t	time.
X	extent of reaction.

Greek Symbols

ε	voidage, as defined by equation 2.6.
$\eta(X)$	specific surface area change function, defined by equation F.4.
Θ	leaching slectivity factor, defined by equation 6.2.
$\lambda(\bar{D})$	specific initial rate constant ratio, as defined by equation 3.45.
μ or μm	micron (10^{-6} m).
ν_i	activity coefficient of specie i.
ρ_i	density of specie i.
ϕ	active site concentration, defined by equation 2.1.
$\phi(X)$	active site concentration change function.
$\psi_i(X)$	active site ratio function, defined by equations 4.1 to 4.4 for i = 1 to 4.
$\Omega(X)$	rate constant ratio defined by equation 4.10.
ω	rate constant ratio defined by equation 5.5.
ω^*	H_2S oxidation rate ratio, defined by equation 6.5.
∞	infinity.

Subscripts

a	refers to adsorbed specie, (e.g. $[Fe^{3+}]_a$).
E	as in A_E.
exp	refers to values measured directly from experimental data.
eq	refers to the equilibrium state (e.g. K_{eq}).
fit	refers to values of a variable or parameter which are obtained by a regression fitting technique.
g	refers to the gas phase.
ℓ	refers to the liquid phase.
mod	refers to the modified rate constant defined by equation 5.4.
MA	as in $K_{A_{MA}}$ (equation 2.37); refers to the mass action equilibrium constant.
o	refers to initial value of a parameter (e.g. $[H_2SO_4]_o$ or M_o etc.
ref	refers to reference lines fitted through -90,0 + 75,0 μm and -75,0 + 63,0 μm data points on Arrhenius type plots of case (ii) data (figures 3.18 - 3.20) and defined by equation 3.45.
TOT	total, as in $[Fe]_{TOT}$, the total iron dissolved.
v	refers to vacant sites.

Superscripts

o	refers to the elemental state of a specie such as elemental sulphur : S^o
✱	as in $r^{✱}$, referring to rate per unit area
⊖	as in $r^{⊖}$ referring to rate per unit area squared.
—	representing the mean value of a parameter, such as $\bar{D}$

Special Operators

[ ]	indicates that the concentration of the specie enclosed is referred to (e.g. $[H_2SO_4]$).
d	differential, as in $\frac{d[Zn^{2+}]}{dt}$.
Σ	cummulative summation operator.
•	represents an active site on the sphalerite surface.
Δ	difference, as in equation 3.29.

C O N T E N T S

CHAPTER 1

REVIEW OF PREVIOUS WORK

Introduction

Current pyrometallurgical technology for the production of zinc from sphaleritic flotation concentrate is often associated with atmospheric discharge of sulphur dioxide rich gases or sulphuric acid by-product disposal problems. Such problems may be overcome by hydrometallurgical zinc recovery processes. This thesis reports results relating to a study of one such hydrometallurgical route, namely the dissolution of sphalerite in aqueous acidic ferric sulphate. In this process the sphaleritic zinc reports as zinc ions in solution, and the sulphidic sulphur reports predominantly as elemental sulphur.

Although the results of semi-quantitative research on this process have been reported, very few complete kinetic studies for the whole system are available - in particular where natural rather than synthetic sphalerite was used. The presence of elemental oxygen and conditions of elevated temperature and pressure frequently made it virtually impossible to isolate and study the effects and role of hydrogen ions and ferric ions in the dissolution mechanism. The most popular theory postulates that the hydrogen ions react with zinc sulphide to produce zinc ions and dissolved hydrogen sulphide gas, followed by the homogeneous phase oxidation of H_2S by ferric ions.

A review of the current literature revealed that several workers have studied the kinetics of H_2S production by leaching synthetic sphalerite in aqueous sulphuric acid without elemental oxygen or ferric ions present. Other workers have studied the homogeneous oxidation of dissolved H_2S gas by ferric ions with no sphaleritic solids present in the reactor.

However, the evidence produced to date is inconclusive relating to the sequential H_2S production and oxidation model. The effects of adsorption of ionic species, sulphur blinding and other topochemical phenomena have often been neglected.

The present study and in particular the following literature review consequently includes within its scope of investigation:

(i) the kinetics of leaching natural and synthetic sphalerite in aqueous sulphuric acid as well as in aqueous acidic ferric sulphate media;

(ii) the kinetics of oxidising H_2S by ferric ions in aqueous sulphuric acid in the absence as well as in the presence of sphalerite particles;

(iii) the sphalerite surface area characteristics before and after leaching, the effects of sulphur blinding of the surface and other aspects relating to the topography of sphalerite particles.

1.1 LEACHING IN AQUEOUS SULPHURIC ACID

Romankiw (1962, 1965) produced a model for the dissolution of synthetic sphalerite in aqueous sulphuric acid by fitting the paramenters of a proposed rate expression to experimental data, with the following result.

$$\frac{d[Zn^{2+}]}{dt} = \frac{d[H_2S]}{dt} = M_o A_o \eta(X) \left(k_f[H^+] - k_r[H_2S]^{0,5}[Zn^{2+}]^{0,5}\right) \quad \ldots\ldots\ldots \quad 1.1$$

The equilibrium constant which fitted the experimental equilibrium results was established as:

$$K_{eq} = \frac{[Zn^{2+}]^{0.5}[H_2S]^{0.5}}{[H^+]} \quad \ldots\ldots\ldots \quad 1.2$$

and the overall stoichiometry of the reaction was proposed as:

$$ZnS + H_2SO_4 \rightleftharpoons ZnSO_4 + H_2S \quad \ldots\ldots\ldots \quad 1.3$$

Romankiw proposed that the dissolution mechanism for ZnS could be represented by the reactions:

$$Zn^{2+}_{(s)} \rightarrow Zn^{2+}_{(\ell)}$$

$$S^{2-}_{(s)} \rightarrow S^{2-}_{(\ell)} \quad \ldots\ldots\ldots \quad 1.4$$

No fundamentally sound attempt was made to include the possible effects of adsorption of reactants onto,

or desorption of products from the sphalerite surface, or to propose the mechanism for the conversion of the S^{2-} ions to H_2S.

Verhulst (1974) leached synthetic sphalerite and tested the fit of equation 1.1 to his data. Apart from establishing an apparant square root dependency of the leaching rate on the solid area exposed, the equation did fit. No attempt was made to propose a mechanism.

Pohl (1954) demonstrated that the initial rate of dissolution of ZnS in aqueous sulphuric acid possessed a first order dependency on the hydrogen ion concentration. However, he presented evidence which suggested that HS^- was the most likely initial product of reaction of ZnS with H^+ to form H_2S . Pohl implied that the dissolution mechanism proceeded via an intermediate activated complex, thus :

$$ZnS + H^+ + H_2O \rightleftharpoons \underset{\text{(activated complex)}}{(ZnSH,\ (x-1)\ H_2O)^+} + H_2O$$

$$\downarrow\uparrow$$

$$\underset{\text{(solvated zinc ion)}}{(Zn,\ H_2O)^{2+}} + HS^- \qquad \text{..... 1. 5}$$

However, no attempt was made to relate the kinetics to surface phenomena or area.

Locker and de Bruyn (1969) demonstrated the proportional dependence of the initial rate on the area, and the first order dependency of the initial rate on $[H^+]$ when dissolving group II - IV semi-conductor compounds (including ZnS) in various

nonoxidising acids (including aqueous sulphuric acid). Results were presented which suggested that the activation energy of the foreward reaction was independent of the impurity content or crystal structure of the ZnS, but was very dependent on the nature of the solution - which affected the properties of the solid-liquid interface. The overall dissolution rate was found to be very dependent on the impurity content or crystal structure of the material, owing to the effect these parameters had on the number of reactive surface sites available for reaction.

The following dissolution mechanism was proposed:

(i) The initial adsorption of H^+, preferentially on sulphur sites, was the rate determining step.

(ii) The surface reaction product which dissociated to HS^- reacted with H^+ to form H_2S, which was transported away from the solid.

An initial rate equation was proposed which included terms for the potential of the H^+ ion at the distance of closest approach before adsorption onto the surface; the potential gradient between the solid surface and the bulk fluid; and a dissolution activation energy which was dependent on the surface bonding characteristics and on the interaction between the charged solid surface and the ions in solution.

No attempt was made to assign numerical values to these various terms, or fit the proposed rate equation to experimental data. Neither was any attempt made to include the effects of the reverse reaction in their proposed mechanisms or rate expressions.

The author is unaware of any fundamental research in which the kinetics or mechanisms of dissolving natural sphaleritic material in aqueous sulphuric acid have been studied.

1.2 OXIDATION OF H_2S BY Fe^{3+}

Veltman (1968), Exner (1969) and Verhulst (1974) have proposed that the mechanism for the dissolution of sphalerite in acidic ferric sulphate media consists of the initial production of H_2S according to equation 1.3, followed by the irreversible homogeneous phase oxidation of the H_2S by Fe^{3+} to elemental sulphur as follows:

$$H_2S + 2\,Fe^{3+} \rightarrow S^o + 2\,H^+ + 2\,Fe^{2+} \quad \ldots\ldots\ldots \quad 1.6$$

Verhulst (1974) tentatively suggested that the presence of sphalerite solids catalysed this reaction, but produced no evidence to conclusively prove this theory. The author is unaware of any attempts to demonstrate whether sphalerite does in fact catalyse reaction 1.6 or not. Verhulst studied the homogeneous phase oxidation of H_2S by Fe^{3+} and produced the following rate expression:

$$\frac{d[H_2S]}{dt} = \frac{2d[Fe^{3+}]}{dt} = 0{,}947 \times 10^{14} \exp\left(\frac{-67{,}72}{RT}\right) \times \frac{[H_2S]^{1.44}[Fe^{3+}]^{1.68}}{[H_2SO_4]^{2.49}} \quad \ldots\ldots\ldots \quad 1.7$$

Moldenhauer (1926) established a similar rate equation but with a 2nd order dependency of the rate on the $[Fe^{3+}]$, and an approximately 2nd order inverse dependency of the rate on the $[H_2SO_4]$. However, the activation energy appeared to vary as a function of the acid concentration, and the dependence of the rate on acid concentration appeared to vary as a function of temperature. The author did not attempt to resolve this anomaly, and these results have been disregarded for the purpose of this thesis.

Verhulst proposed several mechanisms in an attempt to explain the dependence of the reaction rate on the H_2S, Fe^{3+} and H_2SO_4 concentrations as shown in equation 1.7. None were entirely satisfactory because his experiments were designed primarily to produce kinetic rate expressions of practical importance rather than to provide a basis for establishing the most probable mechanism.

1.3 LEACHING IN ACIDIC FERRIC SULPHATE

Dutrizac (1974) published an extensive review on the use of ferric ion as a leaching medium. He commented that most of the works available for review were intended merely to demonstrate that

sphalerite could be readily dissolved under certain conditions, and consequently the kinetics were not extensively studied. In particular, studies in which only ferric ions were present as the oxidant were rare. Many studies included the presence of elemental oxygen and this made it difficult to determine the kinetics or mechanisms.

Elemental oxygen present in the system could react electrochemically with the sphalerite as proposed by Exner (1969) or Habashi (1970):

$$\text{Anodic oxidation:} \quad ZnS \rightarrow Zn^{2+} + S^{o} + 2e \qquad \text{..... 1.8}$$
$$\text{Cathodic reduction:} \quad O_2 + 2H^{+} + 2e \rightarrow H_2O$$

or be consumed by re-oxidising ferrous ions to their ferric state as follows:

$$2FeSO_4 + H_2SO_4 + O_2 \rightarrow Fe_2(SO_4)_3 + H_2O \qquad \text{..... 1.9}$$

Only the results of studies in which ferric ions were the sole oxidant are referred to in this thesis.

Kuzminkh (1950) leached two different natural sphalerites in acidic ferric sulphate media under the following conditions:

20,0 g/ℓ	≤	Pulp density	≤	152,0 g/ℓ
2,5 g/ℓ	≤	$[H_2SO_4]$	≤	20,0 g/ℓ
20,0 g/ℓ	≤	$[Fe^{3+}]$	≤	80,0 g/ℓ
80,0 °C	≤	Temperature	≤	100,0 °C
0	≤	$[Zn^{2+}]_o$	≤	80,0 g/ℓ

where $[Zn^{2+}]_o$ is the initial zinc ion concentration in solution.

The following results were observed:

(i) An activation energy was observed such that diffusion rate control was suspected.

(ii) The dissolution rate was directly proportional to the initial mass of sphalerite present.

(iii) The dissolution rate was approximately proportional to the ferric ion concentration.

(iv) The dissolution rate was inversely proportional to the sulphuric acid concentration.

(v) Increasing the initial zinc ion concentration in the solution for a given set of conditions, only slightly reduced the rate of dissolution.

(vi) Elemental sulphur was produced stoichiometrically in accordance with the overall reaction:

$$ZnS + Fe_2(SO_4)_3 \rightarrow ZnSO_4 + 2FeSO_4 + S^o \quad \ldots\ldots\ldots \quad 1.10$$

(vii) The two sphalerites which were mineralogically very different, leached initially at similar rates under equivalent conditions. However, under similar conditions the maximum zinc which could be dissolved was in excess of 80,0% for one of the sphalerites and only about 33,0% for the other. It was suspected that in the latter case the fine intergrowth of different minerals was such that the ZnS was combined with FeS in solid solution as a

complex $ZnFeS_2$ compound. Other compounds similar to this one (for example, chalcopyrite - $CuFeS_2$) were claimed to be very stable in acidic ferric sulphate solutions.

(viii) The presence of H_2S was not reported.

No attempt was made to explain the mechanism of the dissolution reactions.

Verhulst (1974) leached synthetic sphalerite in aqueous sulphuric acid in the presence of small ferric ion concentrations so that H_2S was detected. However, the resultant rates of production of H_2S were significantly different to rates predicted by solving the two differential rate equations 1.1 and 1.7 simultaneously. Verhulst did not consider the possibility of Fe^{3+} attacking the sphalerite directly.

He did, however, suggest that the sphalerite present in the system may have catalysed the oxidation reaction, but his data was inadequate to prove this. No attempt was made to propose a mechanism for the reactions.

1.4 SURFACE PHENOMENA ASSOCIATED WITH SPHALERITE LEACHING

In order to develop mathematical expressions which meaningfully model and permit comparisons to be made between the dissolution kinetics of different

sphalerites, some measure of the accessible active site concentration needs to be incorporated in the models. Furthermore, the way in which the active site concentration varies during the course of dissolution should be known.

The surface area, as measured by B.E.T. N_2 or Krypton gas adsorption techniques, is often assumed to be proportional to the active site concentration of a given mineral. Clearly such measurements would include the surface area of gangue and other non-sphaleritic material associated with sphalerite, and the surface area of pores and cracks within the sphalerite particles which are not necessarily accessible to leaching.

Lovell (1975) presented evidence which demonstrated that the pretreatment of a given mineral significantly affected the B.E.T. gas adsorption surface area determination. For example, ground samples of galena which had been screened and elutriated in the same way gave surface areas ranging between 158,0 and 220,0 $m^2 kg^{-1}$. Galena samples containing surface xanthate generally gave lower areas than those with surfaces of either pure Pb S or containing oxidation products such as $PbSO_4$.

Factors such as preheating and time of exposure to air also appeared to exert some effect. Thus one could reasonably expect to experience difficulty in obtaining comparative surface area measurements for different sphalerites, especially in the case of flotation concentrates obtained from different mines which had been exposed to different, unknown milling histories and flotation reagents.

The author is unaware of any attempts to experimentally establish how the surface area of a synthetic or natural sphalerite changes during the course of leaching. The shrinking core model which assumes each particle to be represented as a solid sphere with a diameter continuously shrinking during the course of leaching, is often used as a basis for describing the manner in which the area changes during leaching.

Levenspiel (1964) and Smith (1970) use this model extensively to develop models for heterogeneous reactions in which a solid reactant is consumed. In the event of a reaction product ash layer or shell being continuously formed around an unreacted core, the diffusion of reactants to or products from the solid surface could become rate controlling and the dependence of the overall rate on the residual particle core surface area is reduced.

In the event of a stagnant fluid shell existing around a particle as a result of inadequate agitation, diffusion of species to and from the particle surface could become rate limiting, and the dependence of the leaching rate on the particle surface area becomes less.

1.5 TECHNIQUES FOR MONITORING THE REACTION KINETICS OF SPHALERITE LEACHING IN AQUEOUS SULPHURIC ACID

Romankiw (1962) and Verhulst (1974) measured the reaction kinetics of synthetic sphalerite leaching in

aqueous sulphuric acid manometrically by monitoring the increase in reactor pressure resulting from the production of H_2S. Difficulties were experienced trying to monitor the initial rates of pressure increase, and solution samples were generally taken for analysis only when equilibrium had been reached.

Consequently the effects of gas cap heating up (after introducing the solids) on the initial rate of increase in pressure and on the final pressure were difficult to establish.

Locker and de Bruyn (1969) adopted a technique in which the change in volume was monitored during the dissolution reaction. A pressure sensing device was linked to a driven piston arrangement, in order to maintain a constant pressure and measure the change in volume.

No attempt appears to have been reported to measure a solution related variable (such as zinc ion concentration). This possibly results from the fact that between the time of sampling and filtering the solids, dissolution continues. Such dissolution would tend to be accelerated in the event of H_2S desorbing from the sample to the atmosphere prior and during filtration. Since the initial rate of dissolution may be very rapid, errors resulting from continued dissolution prior to filtration would be large for samples taken shortly after commencement of the reaction. Thus it would be extremely difficult to measure initial rate kinetics in such a manner.

The author was unaware of the approach adopted by Locker and de Bruyn until only towards the completion of his project. In view of the problems associated with measuring a solution related variable as discussed above, the approach adopted in this thesis has therefore been to monitor the H_2S partial pressure.

It will be seen, in this thesis, that techniques were developed which eliminated many of the sources of error which appeared to be present in the research of Romankiw and Verhulst.

1.6 ELECTROKINETIC AND THERMODYNAMIC CONSIDERATIONS

1.6.1 Electrokinetic considerations

When a solid such as sphalerite is placed in an electrolyte such as aqueous H_2SO_4 or acidic ferric sulphate, electrokinetic phenomena generally occur as a result of the ionic diffusion, adsorption, reaction and desorption processes taking place at the active solid surface.

Potential differences are formed in the contact zone as a result of differences in mobilities of the ions. The charge transport between diffusing positive and negative ions do not cancel and an electric field is established in the absence of an external

current flowing. The potential gradient thus set up superimposes itself on any existing concentration gradient. The Nernst-Planck equation expresses the relationship between these phenomena - (Helfferick, 1962).

In addition to the electrokinetic phenomena just mentioned, an electrical double layer or potential could be set up on the solid side of the sphalerite-solution interface as a result of the establishment of equilibria for exchangeable potential determining ions such as Zn^{2+} or S^{2-} (Vermilyea, 1966).

When the concentration of charge carriers in a semi-conductor such as ZnS is large, this double layer becomes negligeable - (Woods, 1972). However, as the parameters associated with the electrokinetic and the double layer potential are difficult, if not impossible to measure, they are ignored for the purpose of this thesis. It is therefore implicitely assumed in this study that whilst these phenomena may occur, that the rate limiting steps are not dependent on them.

1.6.2 Thermodynamic considerations

The effects of concentration changes on the activities of various ionic species in solution are generally ignored in this thesis.

Thus the activity coefficients are assumed to be equal to unity so that the mass action and the equilibrium constants are equal. Under certain circumstances this assumption may not be valid, especially for solutions of higher ionic strengths. However, under initial rate conditions this assumption is probably justified.

1. 7 EFFECT OF THE MODE OF MILLING ON THE SPHALERITE DISSOLUTION RATE

Gerlach (1971 , 1973) subjected several different base metal sulphides (including sphalerite) to a vibratory (sometimes called attrition) mode of milling. He claimed that:-

a) crystal lattice straining occured which resulted in an activation of the mineral which could not be attained by ball or rod milling;

b) the extent of activation was related to measureable x - ray diffraction pattern peak broadening, which disappeared on heat - annealing the mineral in an inert environment;

c) Very large dissolution rates of the activated minerals were observed.

Beckstead, Wadsworth et al (1976) compared the leaching kinetics of attrition milled and ball milled chalcopyrite in acidic ferric sulphate media and showed inter - alia that:-

a) Attrition milling of chalcopyrite concentrate increased the specific surface area 4,73 times (after 1,0 hour milling); 5,27 times (after 2,0 hour milling); and 8,0 times (after 3,0 hour milling). However, ball milling of the same concentrate for 3,0 — 24,0 hours produced only a 2,47 — 2,93 times maximum increase in specific surface area.

b) The increase in the initial rate of dissolution of chalcopyrite was directly proportional to the initial specific surface area and independent of the mode of milling.

c) Although attrition milling did result in x-ray diffraction pattern peak broadening (which could be eliminated by heat treatment), the attrition milled chalcopyrite leached identically after the heat treatment as before.

The author is unaware of any attempt by Gerlach or anyone else to compare the leaching rate <u>per unit area</u> of vibratory milled and ball milled sphalerite, and this aspect is dealt with briefly in this thesis.

CHAPTER 2

PROPOSED SPHALERITE LEACHING MECHANISMS AND DERIVED MATHEMATICAL MODELS

2.1 Introduction

In this chapter two mechanisms are proposed for the leaching of sphalerite:

Mechanism 1 - based on single site reaction kinetics
Mechanism 2 - based on dual site reaction kinetics

Mathematical models are derived for each mechanism using Langmuir - Hinschelwood kinetic theories, in which either surface adsorption or surface desorption phenomena constitute the rate limiting step. Leaching models for the following three $[Fe^{3+}]_o : [H_2SO_4]_o$ ratios are considered:

Case (i): $[Fe^{3+}]_o : [H_2SO_4]_o = 0$
(no Fe^{3+} present)

Case (ii): $[Fe^{3+}]_o : [H_2SO_4]_o$ is large
(approximately $\geq 1,8$)

Case (iii): $[Fe^{3+}]_o : [H_2SO_4]_o$ is small
(approximately $\leq 0,1$)

Table 2.1 summarises the main features and designations of case (i), (ii) & (iii) models for mechanisms 1 and 2.

Case	$[Fe^{3+}]_o$: $[H_2SO_4]_o$	Mechanism 1* Model	Mechanism 2⊕ Model	Main feature of model
(i)	≤0,0	A	F	Leaching models based on H^+ adsorption rate control.
		B	G	Leaching models based on product desorption rate control
(ii)	≥1,8	C	H	Leaching models based on competitive adsorption of H^+ and Fe^{3+} with negligible dissolution contributed by the H^+.
(iii)	≤0,1	D	I	Models for the homogeneous phase oxidation of H_2S by Fe^{3+}.
		E	J	Leaching models based on competitive adsorption of H^+ and Fe^{3+} with significant dissolution contributed by the H^+ and Fe^{3+}, and homogeneous oxidation of H_2S by Fe^{3+} occuring simultaneously.

* Mechanism based on single site reaction kinetics
⊕ Mechanism based on dual site reaction kinetics

T A B L E 2. 1. SUMMARY OF NOMENCLATURE USED TO DEFINE THE MODELS CORRESPONDING TO CASES (i), (ii) AND (iii) OF PROPOSED MECHANISMS 1 & 2

In chapter 3 the initial rate forms of the case (i) and case (ii) leaching models are quantitatively tested using experimental initial rate results. This is done in order to discriminate between the two mechanisms, and to identify which of the models best fit the sphalerite leaching kinetics.

In chapter 4 the overall forms of the case (i) and case (ii) models selected in chapter 3 are tested by fitting to overall experimental rate data.

In chapter 5 the case (iii) models are tested qualitatively.

2. 2 GENERAL ASSUMPTIONS

In order to simplify the task of proposing mechanisms and deriving models, the following assumptions are made. Several of these assumptions relate to kinetic, electrokinetic and thermodynamic considerations discussed in section 1.6.

(i) The concepts of adsorption and kinetics rest on Langmuir - Hinschelwood theories. Smith (1970) described these theories, presented source references and gave examples in which these theories were used to formulate models for heterogeneous catalytic reaction mechanisms. A similar approach has been adopted here.

(ii) Electrokinetic phenomena which may exist at solution - solid interfaces and within

the solid are constant for a given system; do not influence leaching kinetics and can be ignored when proposing mechanisms and developing models.

(iii) Charge balance must be maintained between ionic species approaching and leaving the solid surface.

(iv) Diffusion of reactant or product species at solid - liquid and liquid - gas interfaces are not rate limiting (Romankiw (1962) and Verhulst (1974) tested for and found these phenomena to be negligible when leaching synthetic sphalerite in aqueous H_2SO_4 under conditions similar to those used in this thesis) .

(v) The total initial active site concentration ϕ_o is defined as -

$$\phi_o = K_\phi M_o A_o \qquad \ldots\ldots\ldots \quad 2.1$$

where M_o = mass of sphalerite;

A_o = specific surface area determined using a B.E.T. N_2 adsorption technique;

K_ϕ = proportionality constant relating ϕ_o to A_o.

In this study K_ϕ is implicitely incorporated into the leaching rate constants.

(vi) During leaching the total active site concentration ϕ_o consists of vacant sites ϕ_v and adsorbed sites, (i.e. sites occupied by adsorbed species). Thus -

$$\phi_o = \phi_v + \Sigma [C_i]_a \quad \ldots\ldots\ldots 2.2$$

where $[C_i]_a$ = concentration of active sites occupied by adsorbed species C_i.

Dividing equation 2.2 throughout by ϕ_v and rearranging gives -

$$\phi_v = \phi_o \Big/ \left(1{,}0 + \Sigma \frac{[C_i]_a}{\phi_v}\right) \quad \ldots\ldots 2.3$$

(vii) $[H^+]$ is equal to $[H_2SO_4]$ over the full temperature and $[H_2SO_4]$ range investigated.

(viii) Activity coefficients for various species in solution are implicitely included in the reaction rate constants, and are hence assumed to be independent of changes in ionic strength over the concentration ranges investigated.

(ix) Elemental sulphur formed in-situ in the solid reaction zone is sufficiently permeable that diffusion of ionic or other species through such a S^o layer does not become rate limiting.

(Note that the molar volumes for sphalerite and elemental sulphur are -

$$MV_{ZnS} = \frac{MW_{ZnS}}{\rho_{ZnS}} = \frac{97,37}{4,0} = 24,34 \text{ m}^3 \quad \ldots\ldots\ldots \quad 2.4$$

$$MV_{S^o} = \frac{MW_{S^o}}{\rho_{S^o}} = \frac{32,0}{2,0} = 16,0 \text{ m}^3 \quad \ldots\ldots\ldots \quad 2.5$$

where MV_i represents the molar volume of specie i;

MW_i represents the molecular weight of specie i;

ρ_i represents the density of specie i.

Assuming the S^o shell occupies the same volume as the original sphalerite from which it was formed, the voidage ε of the S^o shell should be -

$$\varepsilon = 1,0 - \frac{MV_{S^o}}{MV_{ZnS}} = 0,33 \quad \ldots\ldots\ldots \quad 2.6$$

This implies that the S^o shell is relatively porous. This fact, and the fact that S^o may be removed by attrition during the course of leaching in a well agitated reactor, is presented as justification for making this assumption.)

2.3 MECHANISM 1 BASED ON SINGLE SITE REACTION KINETICS

The following sequence of reaction steps are proposed. The equilibrium constants corresponding to each reaction step are defined here for use in section 2.4.

Adsorption

$$\cdot + H^+ \rightleftharpoons \cdot H^+ \qquad \ldots\ldots\ldots\ldots \quad 2.7$$

(where $\cdot$ represents an active ZnS site)

$$K_1 = \frac{[H^+]_a}{\phi_v [H^+]} \qquad \ldots\ldots\ldots\ldots \quad 2.8$$

(where subscript 'a' refers to the adsorbed specie)

$$\cdot + Fe^{3+} \rightleftharpoons \cdot Fe^{3+} \qquad \ldots\ldots\ldots\ldots \quad 2.9$$

$$K_2 = \frac{[Fe^{3+}]_a}{\phi_v [Fe^{3+}]} \qquad \ldots\ldots\ldots\ldots \quad 2.10$$

Dissociation of adsorbed species

$$\cdot H^+ \rightleftharpoons \cdot HS^+ \qquad \ldots\ldots\ldots\ldots \quad 2.11$$

$$K_3 = \frac{[HS^+]_a}{[H^+]_a} \qquad \ldots\ldots\ldots\ldots \quad 2.12$$

$$\cdot Fe^{3+} \rightleftharpoons \cdot FeS^{3+} \qquad \ldots\ldots\ldots\ldots \quad 2.13$$

$$K_4 = \frac{[FeS^{3+}]_a}{[Fe^{3+}]_a} \qquad \ldots\ldots\ldots\ldots \quad 2.14$$

Reaction of single dissociated specie with homogeneous phase reactants

$$\cdot HS^+ + H^+ \rightleftharpoons \cdot Zn^{2+} + H_2S \qquad \ldots\ldots\ldots\ldots \quad 2.15$$

$$K_5 = \frac{[Zn^{2+}]_a \; [H_2S]_\ell}{[HS^+]_a \; [H^+]} \qquad \ldots\ldots\ldots \quad 2.16$$

$$\cdot FeS^{3+} + Fe^{3+} \rightleftharpoons \cdot Zn^{2+} + 2Fe^{2+} + S^{o} \quad \ldots\ldots\ldots\ldots \text{ 2. 17}$$

This reaction is considered to be irreversible, and elemental sulphur is considered to have been formed in-situ. Hence :-

$$K_6 \simeq \infty \quad \ldots\ldots\ldots \text{ 2. 18}$$

Desorption of reaction products from the surface

$$\cdot Zn^{2+} \rightleftharpoons \cdot + Zn^{2+} \quad \ldots\ldots\ldots \text{ 2. 19}$$

$$K_7 = \frac{\phi_v [Zn^{2+}]}{[Zn^{2+}]_a} \quad \ldots\ldots\ldots \text{ 2. 20}$$

Diffusion of H_2S from liquid to gas phase

$$H_2S_\ell \rightleftharpoons H_2S_g \quad \ldots\ldots\ldots \text{ 2. 21}$$

$$K_8 = \frac{[H_2S]_g}{[H_2S]_\ell} \quad \ldots\ldots\ldots \text{ 2. 22}$$

If the ideal gas law is assumed to apply, then -

$$[H_2S]_g = \frac{P_{H_2S}}{RT} \quad \ldots\ldots\ldots \text{ 2. 23}$$

and for a given reactor volume, temperature and $[H_2SO_4]$ -

$$K_9 = K_8 \, RT = \frac{P_{H_2S}}{[H_2S]_\ell} \quad \ldots\ldots\ldots \text{ 2. 24}$$

K_9 represents the distribution coefficient K_D which relates the partial pressure of the H_2S in the gas cap to the liquid phase H_2S concentration. An empirical equation expressing K_D in terms of H_2SO_4 and temperature is determined and presented in Appendix E (equation E.27)

Homogeneous phase oxidation of H_2S by Fe^{3+}

A detailed study of this reaction is beyond the scope of this work, and consequently no attempt is made to propose a mechanism for this reaction. Equation 1.7 by Verhulst is accepted in section 2.4.3.1 as representing a model which describes the kinetics of this reaction.

Mechanism 1 implies that only H^+, Fe^{3+} and Zn^{2+} ions are adsorbed, hence from equations 2.8 2.10 and 2.20 -

$$\frac{[H^+]_a}{\phi_v} = K_1 [H^+] \quad \ldots\ldots\ldots \quad 2.25$$

$$\frac{[Fe^{3+}]_a}{\phi_v} = K_2 [Fe^{3+}] \quad \ldots\ldots\ldots \quad 2.26$$

and $$\frac{[Zn^{2+}]_a}{\phi_v} = \frac{[Zn^{2+}]}{K_7} \quad \ldots\ldots\ldots \quad 2.27$$

If $$K_8 = 1.0 / K_7 \quad \ldots\ldots\ldots \quad 2.28$$

then $$\frac{[Zn^{2+}]_a}{\phi_v} = K_8 [Zn^{2+}] \quad \ldots\ldots\ldots \quad 2.29$$

Hence substituting for the $\frac{C_i a}{\Phi_v}$ terms in equation 2.3 gives the vacant active site concentration in terms of known values of total active site concentration; the homogeneous phase concentrations of the adsorbed species; and unknown values of the adsorption and desorption equilibrium constants. Thus:-

$$\Phi_v = \Phi_o / (1.0 + K_1 [H^+] + K_2 [Fe^{3+}] + K_8 [Zn^{2+}]) \quad \ldots\ldots\ldots\ldots \quad 2.30$$

2.4 DERIVATION OF MODELS BASED ON MECHANISM 1

2.4.1 Case (i) $[Fe^{3+}]_o : [H_2SO_4]_o = 0,0$

2.4.1.1 Model A (based on the asumption that H^+ adsorption represented by equation 2.7 is rate limiting)

In section 1.1 it was reported that Locker and de Bruyn (1969) demonstrated that the activation energies of the initial dissolution reaction for different sphalerites were equal and independent of the impurity content or crystal structure of each sphalerite. They proposed that the initial adsorption of H^+ was the rate limiting step.

The rate equation representing equation 2.7 is

$$r_A = k_1 \Phi_v [H^+] - k_2 [H^+]_a \quad \ldots\ldots\ldots\ldots \quad 2.31$$

Subsequent steps represented by equations 2.11, 2.15,

2.19 and 2.21 may be considered to be at equilibrium. Equation 2.31 may be expressed in terms of homogeneous phase concentrations as follows:

From equation 2.12 $[H^+]_a = [HS^+]_a / K_3$;

from equation 2.16 $[HS^+]_a = \dfrac{[Zn^{2+}]_a \ [H_2S]}{K_5 \ [H^+]}$;

and from equation 2.20 $[Zn^{2+}]_a = \dfrac{\phi_v \ [Zn^{2+}]}{K_7}$.

Consecutive substitution into equation 2.31 gives -

$$r_A = k_1 \ \phi_v \ [H^+] - \frac{k_2}{K_5 \ K_7 \ K_3} \frac{\phi_v \ [Zn^{2+}] \ [H_2S]_\ell}{[H^+]} \qquad \ldots\ldots\ldots \ 2.32$$

Let $k_3 = \dfrac{k_2}{K_3 K_5 \ K_7}$ $\qquad \ldots\ldots\ldots \ 2.33$

Then substituting equation 2.33 into 2.32 and rearranging gives -

$$r_A = \phi_v \left(k_1 [H^+] - k_3 \frac{[Zn^{2+}] \ [H_2S]_\ell}{[H^+]} \right) \qquad \ldots\ldots \ 2.34$$

Substitution for ϕ_v by equation 2.30 gives :-

$$r_A = \frac{\phi_o}{(1.0 + K_1 \ [H^+] + K_8 \ [Zn^{2+}])} \left(k_1 [H^+] - k_3 \frac{[Zn^{2+}] \ [H_2S]_\ell}{[H^+]} \right) \qquad \ldots\ldots\ldots \ 2.35$$

The initial rate form of equation 2.35 is:-

$$r_{A_o} = \frac{k_1 \phi_o [H^+]_o}{(1.0 + K_1 \ [H^+]_o + K_8 \ [Zn^{2+}]_o)} \qquad \ldots\ldots \ 2.36$$

As equilibrium is approached and $r_A \longrightarrow 0$ the mass action constant $K_{A_{MA}}$ may be expressed as:-

$$K_{A_{MA}} = \frac{k_1}{k_3} = \frac{[Zn^{2+}] \ [H_2S]_\ell}{[H^+]^2} \qquad \ldots\ldots\ldots \ 2.37$$

(In section 2. 2 (assumption (viii)) it was assumed that the activity coefficients for the various species are incorporated in the reaction rate constants.) The thermodynamic equilibrium constant $K_{A_{EQ}}$ is thus -

$$K_{A_{EQ}} = K_{A_{MA}} \cdot \frac{\nu_{Zn^{2+}} \; \nu_{H_2S}}{\nu_{H^+}^2} \quad \ldots\ldots\ldots \quad 2.\ 38$$

where ν_i represents activity coefficient of specie i.

2. 4. 1. 2 Model B (based on the assumption that Zn^{2+} desorption represented by equation 2. 19 is rate limiting)

In view of Locker and de Bruyn's observation discussed in section 2. 4. 1. 1, the only other active site related step in Mechanism 1 which is likely to be independent of the impurity content or crystal structure of the sphalerite is the desorption of ions from active sites.

The rate equation for equation 2. 19 is -

$$r_B = k_4 \; [Zn^{2+}]_a - k_5 \; \phi_v \; [Zn^{2+}] \quad \ldots\ldots\ldots \quad 2.\ 39$$

Steps preceeding and subsequent to the reaction expressed by equation 2. 19 are assumed to be at equilibrium.

Equation 2. 39 may be expressed in terms of homogeneous phase concentrations as follows:

From equation 2.16 : $[Zn^{2+}]_a = \frac{K_5 [HS^+]_a [H^+]}{[H_2S]_\ell}$

From equation 2.12 : $[HS^+]_a = K_3 [H^+]_a$

From equation 2.8 : $[H^+]_a = K_1 \phi_v [H^+]$

Consecutive substitution into equation 2.39 gives -

$$r_B = k_4 K_1 K_3 K_5 \phi_v \left(\frac{[H^+]^2}{[H_2S]_\ell} - k_5 \phi_v [Zn^{2+}] \right) \quad \ldots\ldots\ldots \quad 2.40$$

Let $$k_6 = k_4 K_1 K_3 K_5 \quad \ldots\ldots\ldots \quad 2.41$$

Substitute for ϕ_v and $k_4 K_1 K_3 K_5$ in equation 2.40 by equations 2.30 and 2.41 respectively and rearrange :

$$r_B = \frac{\phi_o}{(1 + K_1 [H^+] + K_8 [Zn^{2+}])} \left(K_6 \frac{[H^+]^2}{[H_2S]_\ell} - k_5 [Zn^{2+}] \right) \quad \ldots\ldots\ldots \quad 2.42$$

The initial rate form of equation 2.42 is :

$$r_{B_o} = \frac{\phi_o k_6 [H^+]_o^2}{(1,0 + K_1 [H^+]_o + K_8 [Zn^{2+}]_o)[H_2S]_{\ell_o}} \quad \ldots\ldots\ldots \quad 2.43$$

and the mass action and equilibrium constants for equation 2.42 are :

$$K_{B_{MA}} = \frac{k_6}{k_5} = \frac{[Zn^{2+}] [H_2S]_\ell}{[H^+]^2} \quad \ldots\ldots\ldots \quad 2.44$$

$$K_{B_{EQ}} = K_{B_{MA}} \times \frac{\nu_{Zn^{2+}} \nu_{H_2S}}{\nu_{H^+}^2} \quad \ldots\ldots\ldots \quad 2.45$$

2. 4. 2 Case (ii) $[Fe^{3+}]_o : [H_2SO_4]_o \simeq 1,8$

2. 4. 2. 1 Model C

(based on the assumption that Fe^{3+} and H^+ adsorb competitively and that for large $[Fe^{3+}]_o : [H_2SO_4]_o$ the H^+ contributes negligibly to the dissolution reaction)

In section 1. 3 it was reported that Kuzminkh (1950) established that two mineralogically very different sphalerites initially leached at similar rates under equivalent conditions. Furthermore the initial dissolution rate was found to be approximately proportional to the $[Fe^{3+}]$. Equation 2. 9 is the only active site related step in Mechanism 1 which involves Fe^{3+} species which can take place independently of the mineralogical properties, and at rates proportion to the initial Fe^{3+} .

Kuzminkh also reported reaction rates to be inversely proportional to $[H_2SO_4]$. In order to explain this it is assumed here that the Fe^{3+} ions adsorb and react at much faster rates than do the H^+ ions. Consequently the proportion of active sites occupied by relatively slow adsorbing and reacting H^+ ions increases with increasing H_2SO_4 . This in turn proportionally decreases the concentration of vacant sites available for Fe^{3+} adsorption and reaction. At high $[Fe^{3+}]_o : [H_2SO_4]_o$ ratios the contribution of the H^+ reaction to the overall dissolution rate is assumed to be negligibly small in comparison to the contribution by the parallel Fe^{3+} reactions.

Thus the dissolution rate equation describing

equation 2. 9 is -

$$r_C = k_7 \Phi_v [Fe^{3+}] - k_8 [Fe^{3+}]_a \quad \ldots\ldots\ldots \quad 2.46$$

Since the reaction described by equation 2. 1 is irreversible, the reverse component of equation 2. 46 reduces to zero. Thus equation 2. 46 may be expressed as -

$$r_C = k_7 \Phi_v [Fe^{3+}] \quad \ldots\ldots\ldots \quad 2.47$$

According to Mechanism 1 the only species adsorbed on the surface are H^+ , Fe^{3+} and Zn^{2+}.

Substituting for Φ_v in equation 2. 47 by equation 2. 3 gives -

$$r_C = \frac{k_7 \Phi_o [Fe^{3+}]}{(1,0 + \Sigma \frac{[C_i]_a}{\Phi_v})} \quad \ldots\ldots\ldots \quad 2.48$$

Substituting

equation 2. 8 : $\frac{[H^+]_a}{\Phi_v} = K_1 [H^+]$

equation 2. 10 : $\frac{[Fe^{3+}]_a}{\Phi_v} = K_2 [Fe^{3+}]$

and equation 2. 29 : $\frac{[Zn^{2+}]_a}{\Phi_v} = K_8 [Zn^{2+}]$

into equation 2. 48 gives -

$$r_C = \frac{k_7 \Phi_o [Fe^{3+}]}{(1,0 + K_1 [H^+] + K_2 [Fe^{3+}] + K_8 [Zn^{2+}])} \quad \ldots\ldots\ldots \quad 2.49$$

If it is assumed that the H^+ ions are much more strongly adsorbed than the Fe^{3+} or Zn^{2+} ions (i.e. $K_{H^+} \gg K_{Fe^{3+}}$ or $K_{Zn^{2+}}$) and that $K_1 [H^+] \gg 1,0$, equation 2.49 reduces to -

$$r_C = \frac{k_7 \, \Phi_o \, [Fe^{3+}]}{K_1 \, [H^+]} \qquad \ldots\ldots\ldots \quad 2.50$$

Let $$k_8 = \frac{k_7}{K_1} \qquad \ldots\ldots\ldots \quad 2.51$$

then $$r_C = k_8 \, \Phi_o \, \frac{[Fe^{3+}]}{[H^+]} \qquad \ldots\ldots\ldots \quad 2.52$$

Equation 2.52 also represents the initial rate of dissolution of sphalerite in high $[Fe^{3+}]_o : [H_2SO_4]_o$ ratio leach media, and is basically in agreement with the observations reported by Kuzminkh (i.e. proportional dependency of rate on initial area and $[Fe^{3+}]_o$, and inverse dependency of the rate on $[H_2SO_4]_o$).

2.4.3 Case (iii) : $[Fe^{3+}]_o : [H_2SO_4]_o \leq 0,1$

2.4.3.1 Model D (Homogeneous oxidation of H_2S by Fe^{3+})

It is proposed that the empirical model developed by Verhulst (1974) and represented by equation 1.7 describes the kinetics of the homogeneous oxidation of H_2S by Fe^{3+}. Model D may be represented as -

$$r_D = \frac{d[H_2S]}{dt} = -\, 0,947 \times 10^{14} \, \exp\left(\frac{-67,72}{RT}\right) \times \frac{[H_2S]^{1,44}_{\ell} \, [Fe^{3+}]^{1,69}}{[H_2SO_4]^{2,49}} \qquad \ldots\ldots \quad 2.53$$

2.4.3.2 Model E (based on the assumption that H^+ and Fe^{3+} adsorb competitively; that for low $[Fe^{3+}]_o : [H_2SO_4]_o$ ratio both the H^+ and Fe^{3+} contribute significantly to the dissolution; and that H_2S formed by the H^+ is homogeneously oxidised by Fe^{3+})

In section 1.3 it was reported that Verhulst leached synthetic sphalerite in aqueous sulphuric acid with low Fe^{3+} initially present. The H_2S partial pressure was monitored and observed to reach a peak and then decrease. He proposed that equation 1.1 described the H_2S formation kinetics and that the H_2S was oxidised homogeneously by the Fe^{3+} ions (at a rate described by equation 1.7). Comparison of the experimental rate data with computed solutions of the two simultaneous differential rate equations 1.1 and 1.7 demonstrated that the experimental H_2S pressure reached a peak and decreased significantly faster than the computed H_2S pressure. He proposed the possibility that the H_2S oxidation by Fe^{3+} may have been catalysed by the sphalerite solids present in the reactor.

In this study it is proposed that for low $[Fe^{3+}]_o : [H_2SO_4]_o$, Fe^{3+} and H^+ adsorption are both slow steps occuring simultaneously and at comparable rates (reaction in parallel). The H_2S formed during dissolution is homogeneously oxidised by Fe^{3+} (reactions in series).

Assume that -

a) equation 2.35 has an additional term in the denominator for the adsorption of Fe^{3+} thus

$$r_A = \frac{\Phi_o}{(1,0 + K_1[H^+] + K_2[Fe^{3+}] + K_8[Zn^{2+}])}\left(k_1[H^+] - k_3\frac{[Zn^{2+}][H_2S]_\ell}{[H^+]}\right) \quad \ldots\ldots\ldots \quad 2.54$$

b) equations 2.54 and 2.49 represent rate expressions for the dissolution reactions occuring in parallel, and

c) equation 2.53 (representing the homogeneous oxidation of H_2S by Fe^{3+}) occurs in series with the dissolution reaction described by equation 2.54.

The overall dissolution will then be obtained by simultaneously solving the following two differential equations:

$$r_{E1} = \frac{d[Zn^{2+}]}{dt} = r_A + r_B \quad \ldots\ldots\ldots \quad 2.55$$

$$r_{E2} = \frac{d[H_2S]}{dt} = r_A - r_D \quad \ldots\ldots\ldots \quad 2.56$$

where r_A, r_B and r_D are described by equations 2.54, 2.49 and 2.53 respectively.

2. 5 MECHANISM 2 BASED ON DUAL SITE REACTION KINETICS

The following sequence of reaction steps are proposed. The equilibrium constants corresponding to each step are defined for use in section 2.6. Several steps which are identical to steps proposed for mechanism 1, are repeated here to simplify the presentation.

Adsorption

$$\cdot + H^+ \rightleftharpoons \cdot H^+ \qquad \ldots\ldots\ldots \quad 2.57$$

$$K_{11} = \frac{[H^+]_a}{\phi_v [H^+]} \qquad \ldots\ldots\ldots \quad 2.58$$

$$\cdot + Fe^{3+} \rightleftharpoons \cdot Fe^{3+} \qquad \ldots\ldots\ldots \quad 2.59$$

$$K_{12} = \frac{[Fe^{3+}]_a}{\phi_v [Fe^{3+}]} \qquad \ldots\ldots\ldots \quad 2.60$$

Dissociation

$$\cdot H^+ \rightleftharpoons \cdot HS^+ \qquad \ldots\ldots\ldots \quad 2.61$$

$$K_{13} = \frac{[HS^+]_a}{[H^+]_a} \qquad \ldots\ldots\ldots \quad 2.62$$

$$\cdot Fe^{3+} \rightleftharpoons \cdot FeS^{3+} \qquad \ldots\ldots\ldots \quad 2.63$$

$$K_{14} = \frac{[FeS^{3+}]_a}{[Fe^{3+}]_a} \qquad \ldots\ldots\ldots \quad 2.64$$

Dual site reaction of adjacent dissociated species

$$\cdot HS^{+} + \cdot HS^{+} \rightleftharpoons \cdot Zn^{2+} + \cdot H_2S_{\ell} \quad \ldots\ldots\ldots \quad 2.65$$

$$K_{15} = \frac{[Zn^{2+}]_a \; [H_2S]_a}{[HS^{+}]_a^{\,2}} \quad \ldots\ldots\ldots \quad 2.66$$

$$\cdot FeS^{3+} + \cdot FeS^{3+} \rightarrow \cdot Zn^{2+} + \cdot S^{o} + 2\,Fe^{2+} \quad \ldots\ldots\ldots \quad 2.67$$

The elemental sulphur is assumed to form in-situ. This reaction is irreversible, hence for this reaction,

$$K_{16} \simeq \infty$$

Desorption

$$\cdot Zn^{2+} \rightleftharpoons \cdot + Zn^{2+} \quad \ldots\ldots\ldots \quad 2.68$$

$$K_{17} = \frac{\phi_v [Zn^{2+}]}{[Zn^{2+}]_a} \quad \ldots\ldots\ldots \quad 2.69$$

$$\cdot H_2S \rightleftharpoons \cdot + H_2S \quad \ldots\ldots\ldots \quad 2.70$$

$$K_{18} = \frac{\phi_v [H_2S]}{[H_2S]_a} \quad \ldots\ldots\ldots \quad 2.71$$

Diffusion of H_2S from liquid to gas phase

$$H_2S_{\ell} \rightleftharpoons H_2S_g \quad \ldots\ldots\ldots \quad 2.72$$

$$K_{19} = \frac{[H_2S]_g}{[H_2S]_{\ell}} \quad \ldots\ldots\ldots \quad 2.73$$

Homogeneous oxidation of H_2S by Fe^{3+}

A study of the mechanism of this reaction is beyond the scope of this work, and equation 1.7 by Verhulst is accepted in section 2.6.3.1 as describing the oxidation kinetics.

Mechanism 2 implies that H^+, Fe^{3+}, Zn^{2+} and H_2S species are adsorbed, hence by adopting a similar approach as in section 2.3 it may be shown that:-

$$\Phi_v = \Phi_o / \left(1,0 + K_{11}\,[H^+] + K_{12}\,[Fe^{3+}] + \frac{[Zn^{2+}]}{K_{17}} + \frac{[H_2S]}{K_{18}}\right) \quad \ldots\ldots\ldots \quad 2.74$$

letting $K_{20} = \frac{1}{K_{17}}$ $\ldots\ldots\ldots$ 2.75

and $K_{21} = \frac{1}{K_{18}}$ $\ldots\ldots\ldots$ 2.76

and substituting these into equation 2.74 :-

$$\Phi_v = \Phi_o / \left(1,0 + K_{11}\,[H^+] + K_{12}\,[Fe^{3+}] + K_{20}\,[Zn^{2+}] + K_{21}\,[H_2S]\right) \quad \ldots\ldots\ldots \quad 2.77$$

2. 6 DERIVATION OF MODELS BASED ON MECHANISM 2

2.6.1 Case (i) $[Fe^{3+}]_o : [H_2SO_4]_o = 0$

2.6.1.1 Model F (based on the assumption that H^+ adsorption represented by equation 2.57 is rate limiting)

The justification for making this assumption is the same as that given in section 2.4.1.1.

The rate equation for the reaction represented by equation 2.57 is:-

$$r_F = k_{11} \phi_v [H^+] - k_{12} [H^+]_a \quad \ldots\ldots\ldots \quad 2.78$$

In a manner similar to that adopted in section 2.4.1.1 equation 2.78 can be expressed in terms of homogeneous phase concentrations as follows:

From equation 2.62 : $[H^+]_a = K_{13} [HS^+]_a$

equation 2.66 : $[HS^+]_a = \dfrac{[Zn^{2+}]_a^{0,5} [H_2S]_a^{0,5}}{K_{15}^{0,5}}$

equation 2.69 : $[Zn^{2+}]_a^{0,5} = \dfrac{[Zn^{2+}]^{0,5}}{K_{17}^{0,5}}$

and equation 2.71 : $[H_2S]_a^{0,5} = \dfrac{\phi_v^{0,5} [H_2S]^{0,5}}{K_{18}^{0,5}}$

Consecutive substitution into equation 2.78 gives -

$$r_F = k_1 \phi_v [H^+] - \frac{k_{12} K_{13} \phi_v}{K_{15}^{0,5} K_{17}^{0,5} K_{18}^{0,5}} [Zn^{2+}]^{0,5} [H_2S]^{0,5} \quad \ldots\ldots\ldots \quad 2.79$$

Let $$k_{13} = \frac{k_{12} \; K_{13}}{K_{15}^{0,5} \; K_{17}^{0,5} \; K_{18}^{0,5}} \qquad \ldots\ldots\ldots \quad 2.80$$

Substitute for ϕ_v and $k_{12} K_{13} / K_{15}^{0,5} K_{17}^{0,5} K_{18}^{0,5}$ in equation 2.79 by equations 2.77 and 2.80 and rearrange -

$$r_F = \frac{\phi_o \left(k_{11} [H^+] - k_{13} [Zn^{2+}]^{0,5} [H_2S]^{0,5}\right)}{(1,0 + K_{11} [H^+] + K_{20} [Zn^{2+}] + K_{21} [H_2S])} \quad \ldots\ldots \quad 2.81$$

The initial rate form of equation 2.81 is -

$$r_{F_o} = \frac{\phi_o \; k_{11} \; [H^+]_o}{(1,0 + K_{11} [H^+]_o + K_{20} [Zn^{2+}]_o + K_{21} [H_2S]_o)} \qquad \ldots\ldots\ldots \quad 2.82$$

and at equilibrium the mass action constant is -

$$K_{F_{MA}} = \frac{k_{11}}{k_{13}} = \frac{[Zn^{2+}]^{0,5} \; [H_2S]_\ell^{0,5}}{[H^+]} \qquad \ldots\ldots\ldots \quad 2.83$$

Note that in the event of H^+, Zn^{2+}, and H_2S each being only very weakly adsorbed so that K_{11}, K_{20} and K_{21} are very small, equation 2.81 reduces to -

$$r_F = \phi_o (k_{11} [H^+] - k_{13} [Zn^{2+}]^{0,5} [H_2S]^{0,5}) \qquad \ldots\ldots\ldots \quad 2.84$$

Also note that equations 2.84 and 2.83 are identical in form to equations 1.1 and 1.2 (which were obtained by Romankiw by regressing on synthetic sphalerite leaching data).

2.6.1.2 Model G (based on the assumption that reaction product desorption is rate limiting)

This assumption is justified by reasoning similar to that discussed in section 2.4.1.2 .

If the Zn^{2+} and H_2S species are both strongly adsorbed and desorption of both the Zn^{2+} and H_2S is necessary in order for the reaction to proceed, then the reaction describing this rate limiting situation is -

$$\cdot Zn^{2+} + \cdot H_2S \rightleftharpoons 2\cdot + Zn^{2+} + H_2S \quad \ldots\ldots \quad 2.85$$

The rate equation describing this reaction is -

$$r_G = k_{14}[Zn^{2+}]_a [H_2S]_a - k_{15}\phi_v^2 [Zn^{2+}][H_2S] \quad \ldots\ldots\ldots \quad 2.86$$

Equation 2.86 may be expressed in terms of homogeneous phase concentrations as follows :

From equation 2.66 : $[Zn^{2+}]_a [H_2S]_a = K_{15}[HS^+]_a^2$

equation 2.62 : $[HS^+]_a = K_{13}[H^+]_a$

and equation 2.58 : $[H^+]_a = K_{11}\phi_v [H^+]$

Substituting consecutively into equation 2.86 gives -

$$r_G = k_{14} K_{15} K_{13}^2 K_{11}^2 \phi_v^2 [H^+]^2 - k_{15}\phi_v^2 [Zn^{2+}][H_2S] \quad \ldots\ldots\ldots \quad 2.87$$

Let $$k_{16} = k_{14} K_{15} K_{13}^2 K_{11}^2 \quad \ldots\ldots\ldots \quad 2.88$$

Substituting for Φ_v and $k_{14}\ K_{15}\ K_{13}^2\ K_{11}^2$ in equation 2.87 by equations 2.77 and 2.88 and rearranging gives -

$$r_G = \frac{\Phi_o^2 \left(k_{16}[H^+]^2 - k_{15}[Zn^{2+}][H_2S]\right)}{\left(1,0 + K_{11}[H^+] + K_{20}[Zn^{2+}] + K_{21}[H_2S]\right)^2} \quad \ldots\ldots\ldots \quad 2.89$$

At equilibrium, the mass action constant in this case is -

$$K_{G_{MA}} = \frac{[Zn^{2+}]\ [H_2S]_\ell}{[H^+]^2} \quad \ldots\ldots\ldots \quad 2.90$$

The initial rate form of equation 2.89 is -

$$r_{G_o} = \frac{\Phi_o^2\ \ k_{16}\ [H^+]_o^2}{\left(1,0 + K_{11}[H^+]_o + K_{21}[Zn^{2+}]_o + K_{22}[H_2S]_o\right)^2} \quad \ldots\ldots\ldots \quad 2.91$$

2.6.2 Case (ii): $[Fe^{3+}]_o : [H_2SO_4]_o \geq 1,8$

2.6.2.1 Model H (based on the assumption that Fe^{3+} and H^+ adsorb competitively and that for large $[Fe^{3+}]_b : [H_2SO_4]_o$ the H^+ contributes negligibly to the dissolution reaction)

The justification for this assumption is similar to that discussed in section 2.4.2.1 .

Thus if the Fe^{3+} adsorption reaction described by equation 2.59 is rate limiting, then -

$$r_H = k_{16}\ \Phi_v\ [Fe^{3+}] - k_{17}\ [Fe^{3+}]_a \quad \ldots\ldots\ldots \quad 2.92$$

Since the dual site reaction expressed by equation 2.67 is irreversible, equation 2.92 reduces to -

$$r_H = k_{16}\,\phi_v\,[Fe^{3+}]_a \qquad \ldots\ldots\ldots \quad 2.93$$

It is seen that the rate equations based on both single site and dual site case (ii) mechanisms are identical.

Substitute for ϕ_v in equation 2.93 by equation 2.77 -

$$r_H = \frac{k_{16}\;\phi_o\;[Fe^{3+}]}{(1{,}0 + K_{11}[H^+] + K_{12}[Fe^{3+}] + K_{20}[Zn^{2+}] + K_{21}[H_2S])} \qquad \ldots\ldots\ldots \quad 2.94$$

Assuming that $K_{11} \gg K_{12}$, K_{20} or K_{21}, that $K_{11} \gg 1{,}0$; and that $k_{17} = k_{16}/K_{11}$ results in eqn. 2.94 reducing to

$$r_H = \frac{k_{17}\,\phi_o\,[Fe^{3+}]}{[H^+]} \qquad \ldots\ldots\ldots \quad 2.95$$

2.6.3 Case (iii): $[Fe^{3+}]_o : [H_2SO_4]_o \leq 0{,}1$

2.6.3.1 Model I (Homogeneous oxidation of H_2S by Fe^{3+})

It is proposed that the empirical model developed by Verhulst (1974) and represented by equation 1.7 describes the kinetics of this reaction. Thus -

$$r_I = \frac{d[H_2S]}{dt} = -0{,}947 \times 10^{14} \exp\left(\frac{-57{,}72}{RT}\right) \frac{[H_2S]_\ell^{1{,}44}\;[Fe^{3+}]^{1{,}69}}{[H_2SO_4]^{2{,}49}} \qquad \ldots\ldots\ldots \quad 2.96$$

2.6.3.2 Model J (based on the assumption that H^+ and Fe^{3+} adsorb competitively; that for low $[Fe^{3+}]_o : [H_2SO_4]_o$ ratio both the H^+ and Fe^{3+} contribute significantly to the dissolution; and that H_2S formed by the H^+ is homogeneously oxidised by Fe^{3+})

The justification offered in the preamble of section 2.4.3.2 applies here.

Assume that -

a) equation 2.81 has an additional term in the denominator for the adsorption of Fe^{3+}, thus -

$$r_F = \frac{\phi_o (k_{11}[H^+] - k_{13}[Zn^{2+}]^{0,5}[H_2S]_\ell^{0,5})}{(1,0 + K_{11}[H^+] + K_{12}[Fe^{3+}] + K_{20}[Zn^{2+}] + K_{21}[H_2S])} \quad \ldots\ldots\ldots \quad 2.97$$

b) equations 2.97 and 2.94 represent the H^+ and Fe^{3+} dissolution reactions occuring in parallel;

c) equations 2.97 and 2.96 represent the H_2S formation and oxidation reactions occuring in series.

The overall rate of dissolution for this case is obtained by simultaneously solving the following two differential rate equations :

$$r_{J1} = \frac{d[Zn^{2+}]}{dt} = r_F + r_H \quad \ldots\ldots\ldots \quad 2.98$$

$$r_{J2} = \frac{d[H_2S]_\ell}{dt} = r_F - r_I \quad \ldots\ldots\ldots \quad 2.99$$

where r_F, r_H and r_I are described by equations

2.97 , 2.94 and 2.96 respectively.

2. 7 SUMMARY OF MODELS DERIVED FOR MECHANISMS 1 AND 2

Table 2.2 summarises the case (i) models. The initial rate forms fo each of the equations are obtained by setting the negative terms in the numerators equal to zero.

Table 2.3 summarises the case (ii) models.

Table 2.4 summarises the case (iii) models.

Mech-anism	Model	Rate Control	Rate Equation	Mass Action Constant
1	A	H^+ adsorption	$r_A = \frac{\Phi_o}{(1,0 + K_1[H^+] + K_8[Zn^{2+}])}\left(k_1[H^+] - k_3\frac{[Zn^{2+}][H_2S]_\ell}{[H^+]}\right)$ 2.35	$K_{A\,MA} = \frac{k_1}{k_3} = \frac{[Zn^{2+}][H_2S]_\ell}{[H^+]^2}$ 2.37
1	B	Zn^{2+} desorption	$r_B = \frac{\Phi_o}{(1,0 + K_1[H^+] + K_8[Zn^{2+}])}\left(k_6\frac{[H^+]^2}{[H_2S]_\ell} - k_5[Zn^{2+}]\right)$ 2.42	$K_{B\,MA} = \frac{k_6}{k_5} = \frac{[Zn^{2+}][H_2S]_\ell}{[H^+]^2}$ 2.44
2	F	H^+ adsorption	$r_F = \frac{\Phi_o(k_{11}[H^+] - k_{13}[Zn^{2+}]^{0,5}[H_2S]_\ell^{0,5})}{(1,0 + K_{11}[H^+] + K_{20}[Zn^{2+}] + K_{21}[H_2S])}$ 2.81	$K_{F\,MA} = \frac{k_{11}}{k_{13}} = \frac{[Zn^{2+}]^{0,5}[H_2S]_\ell^{0,5}}{[H^+]}$ 2.83
2	G	Zn^{2+} ; H_2S desorption	$r_G = \frac{\Phi_o^2(k_{16}[H^+]^2 - k_{15}[Zn^{2+}][H_2S]_\ell)}{(1,0 + K_{11}[H^+] + K_{20}[Zn^{2+}] + K_{21}[H_2S]_\ell)^2}$ 2.89	$K_{G\,MA} = \frac{k_{16}}{k_{15}} = \frac{[Zn^{2+}][H_2S]_\ell}{[H^+]^2}$ 2.90

T A B L E 2. 2 SUMMARY OF CASE (i) (Fe^{3+} : $[H_2SO_4]$ = 0) MODELS FOR PROPOSED MECHANISMS 1 AND 2

Mechanism	Model	Rate Equation
1	C	$r_C = k_8 \phi_o \frac{[Fe^{3+}]}{[H^+]}$ 2.52
2	H	$r_H = k_{17} \phi_o \frac{[Fe^{3+}]}{[H^+]}$ 2.95

T A B L E 2. 3 SUMMARY OF CASE (ii) ($[Fe^{3+}]_o : [H_2SO_4]_o \geq 1,8$)

MODELS FOR PROPOSED MECHANISMS 1 AND 2

Mechanism	Model	Rate Equation
1	E	$r_{E1} = \dfrac{\phi_o\left(k_7[Fe^{3+}] + \left(k_1[H^+] - k_3\dfrac{[Zn^{2+}][H_2S]_\ell}{[H^+]}\right)\right)}{(1,0 + K_1[H^+] + K_2[Fe^{3+}] + K_8[Zn^{2+}])}$ 2.55
		$r_{E2} = \dfrac{\phi_o\left(k_1[H^+] - k_3\dfrac{[Zn^{2+}][H_2S]_\ell}{[H]^+}\right)}{(1,0 + K_1[H^+] + K_2[Fe^{3+}] + K_8[Zn^{2+}])} - 0,947 \times 10^{14} \exp\left(\dfrac{-67,72}{RT}\right) \dfrac{[H_2S]_\ell^{1,44}[Fe^{3+}]^{1,69}}{[H_2SO_4]^{2,49}}$ 2.56
2	J	$r_{J1} = \dfrac{\phi_o\left(k_{16}[Fe^{3+}] + \left(k_{11}[H^+] - k_{13}[Zn^{2+}]^{0,5}[H_2S]_\ell^{0,5}\right)\right)}{(1,0 + K_{11}[H^+] + K_{12}[Fe^{3+}] + K_{20}[Zn^{2+}] + K_{21}[H_2S]_\ell)}$ 2.98
		$r_{J2} = \dfrac{\phi_o\left(k_{11}[H^+] - k_{13}[Zn^{2+}]^{0,5}[H_2S]_\ell^{0,5}\right)}{(1,0 + K_{11}[H^+] + K_{12}[Fe^{3+}] + K_{20}[Zn^{2+}] + K_{21}[H_2S]_\ell)} - 0,947 \times 10^{14} \exp\left(\dfrac{-67,72}{RT}\right) \dfrac{[H_2S]_\ell^{1,44}[Fe^{3+}]^{1,69}}{[H_2SO_4]^{2,49}}$ 2.99

TABLE 2.4 SUMMARY OF CASE (iii) $([Fe^{3+}]_o : [H_2SO_4]_o \leq 0,1]$ MODELS FOR PROPOSED MECHANISMS 1 & 2

CHAPTER 3

EXPERIMENTAL TESTING OF THE INITIAL RATE FORM OF CASE (i) AND (ii) MODELS PROPOSED IN CHAPTER 2

Introduction

In this chapter the case (i) and case (ii) models developed for mechanisms 1 and 2 are tested quantitatively under initial rate conditions. Attempts are made to ascribe values to the rate and adsorption equilibrium constants for those models which do fit the data.

In chapter 4 the overall forms of the case (i) and (ii) models selected in this chapter are tested using overall leaching rate data.

In chapter 5 equation 1.7 for the homogeneous oxidation of H_2S by Fe^{3+} is tested and modified before qualitatively testing the case (iii) models using overall leaching data.

In chapter 6 (section 6.1) Scanning electron microscope photographs of unleached and leached sphalerite particles; and optical microscope photographs of etched and unetched sphalerite particles are presented

In section 3.1 the four sphalerites, the various forms in which they were used and their identifying abbreviations used in this thesis, are described.

In Appendix A the experimental apparatus is described.

In Appendix B experimental and sphalerite pre-treatment procedures are described.

In Appendix C the chemicals used in the leaching experiments are described.

In Appendix D methods of chemical analysis are given.

In Appendix E empirical expressions relating the liquid phase Zn^{2+} and H_2S concentrations to the gas phase H_2S partial pressure are determined by regressing on experimental results.

In Appendix F aspects relating to the topography of the different sphalerites are presented. In particular the B.E.T. surface areas for the different sphalerites (before and after leaching) are reported, and mathematical functions describing the change in area during leaching are derived.

In Appendix G data analysis procedures, (including that for determining the Zn^{2+} leaching rate from monitored H_2S partial pressure data) are discussed.

In Appendix H raw case (i) data ($[Fe^{3+}]_o = 0,0$) is presented graphically by plotting the P_{H_2S} versus time rate curves.

In Appendix I all case (i) experimental leaching results are fully reported in tabular form.

In Appendix J all case (ii) experimental leaching results ($[Fe^{3+}]_o : [H_2SO_4]_o \geq 1,8$) are tabulated.

In Appendixes K and L all case (iii) experimental results (i.e. Fe^{3+} oxidations of H_2S; and leaching with $[Fe^{3+}]_o : [H_2SO_4]_o \leq 0,1$) are tabulated.

3. 1 SPHALERITES USED IN THIS STUDY

3. 1. 1 GENERAL DESCRIPTION

One synthetic and three natural sphalerites were used in this investigation. The abbreviations used throughout this thesis to designate these sphalerites are shown below in capital letters between brackets, and are summarised in Table 3. 1 .

The chemical composition of each of the sphalerites are summarised in Table 3. 2 .

The following different sphalerites were used :

(i) Synthetic high grade sphalerite

A precipitated synthetic laboratory reagent grade sphalerite manufactured by the British Drug House Company - (Abbreviation : BDH.)

(ii) High grade natural sphalerite

A comparatively pure natural sphalerite from Oklohoma, U.S.A. and acquired in lump form from Wards Natural Science Establishment, Inc., New York, U.S.A. . Primary size reduction of the lumps was effected in two ways :

SPHALERITE ABBREVIATION	DESCRIPTION
B D H	Synthetic sphalerite marketed by the British Drug House Company.
W B M	Ward's ball milled high grade natural sphalerite.
W V M *	Ward's vibratory milled high grade natural sphalerite.
V M W B M *	Vibratory milled WBM sphalerite.
Z C R	Moderately impure flotation concentrate acquired from ZINCOR.
V M Z C R	Vibratory milled ZCR sphalerite.
P R	Very impure flotation concentrate acquired from Prieska.
V M P R	Vibratory milled PR sphalerite

* The WVM sphalerite was used in a relatively course granular form (eg. -75,0 + 63,0 size fraction) whilst the VMWVM sphalerite was used in a very fine form.

T A B L E 3. 1 SUMMARY OF ABBREVIATIONS AND DESCRIPTIONS OF SPHALERITES USED IN THIS THESIS

Sphalerite abbreviation	Zn %	Sulphide Sulphur %	Fe %	Cu	Pb	Cd	Ni ppm	Mg	Ca	Co ppm
ZCR * VMZCR *	61,5	31,5	7,25	155, Oppm	1,51%	0,12%	409,0	0,36%	0,63 %	237,0
PR * VMPR *	55,8	32,1	10,74	3,53%	850, Oppm	0,13%	498,0	0,17%	0,1 %	160,0
WBM * VMWBM *	66,5	32,2	0,45	382, Oppm	900, Oppm	0,48%	395,0	230,Oppm	350,Oppm	229,0
BDH *	65,4	31,0	0,12	129, Oppm	557, Oppm	83,Oppm	408,0	400,Oppm	266, Oppm	237,0

* These abbreviations described in the text and summarised in Table 3. 1

T A B L E 3. 2 AVERAGE CHEMICAL ANALYSES OF SPHALERITES USED IN THIS STUDY

a) Wet ball milling in a laboratory mill. The milled material was periodically wet screened through a 125,0μ screen, the plus fraction being returned for further milling. (Abbreviation: WBM)

b) Dry vibratory milling in a Siebtechnik laboratory attrition mill. The milled material was periodically dry screened through a 125,0μ screen, the plus fraction being returned for further milling. (Abbreviation: WVM)

(iii) Moderately impure sphalerite flotation concentrate

A moderately impure milled flotation concentrate acquired from Zincor of South Africa. The geographical origin of this material is unknown to the author. (Abbreviation: ZCR)

(iv) Highly impure sphalerite flotation concentrate

An impure milled flotation concentrate was acquired from the Prieska mine in the Cape Province of South Africa. (Abbreviation: PR)

In addition to leaching the natural sphalerites in their granular form, fully pretreated acid washed granular samples of each were extensively vibratory milled. (Abbreviations: VMWBM, VMZCR and VMPR) The surface area of these sphalerites were increased as a result of the vibratory milling from typically

100,0 m^2/kg to say, 3 000,0 m^2/kg.

It was further found that topographically induced differences in the leaching characteristics of the granular sphalerites, were largely eliminated by the extensive vibratory milling. The large increase in dissolution rates resulting from the large specific surface area exposed, permitted comparative experiments using each of the sphalerites to be conducted much more rapidly, with less sphaleritic material being required per run.

3.1.2 MINERALOGICAL PROPERTIES OF THE WBM, ZCR AND PR SPHALERITES

Mounted, polished sphalerite particles were inspected using a reflecting optical microscope.

The WBM particles were observed to consist of essentially pure sphalerite. No obvious distinctive crystallographic or mineralogical features were observed. Upon etching with concentrated sulphuric acid for different time periods, dissolution appeared to mostly take place evenly over the entire surface. Some evidence of leaching in preferential directions was however observed.

The ZCR sphalerite particles were observed to contain what appeared to be magnetite intergrowths, and pyrite appeared also to be present as separate particles. Etching with concentrated sulphuric acid revealed zonal structuring with fine sub-grain polycrystalline material at different orientations.

Etching appeared to occur preferentially along twinning zones and grain boundaries.

Figure 6.18 shows a photograph of an etched ZCR particle.

The PR sphalerite was mineralogically far more complex and interesting than the WBM and ZCR sphalerites. Anhaeusser and Lenthall (1970) reported a detailed petrographic and mineragraphic study of PR sphalerite obtained from the same source as that used by the author. Only the more obvious features observed by the author are reported here.

Three generations of sphalerite were observed. The copper impurity existed predominantly as exsolved chalcopyrite, whilst the iron impurity was present in the sphalerite lattice, as well as in the chalcopyrite.

Iron free sphalerite was observed to exist immediately adjacent to the chalcopyrite, the iron concentration increasing with distance away from the chalcopyrite. Upon etching, dissolution appeared to take place, preferentially in the zones adjacent to the chalcopyrite.

Figure 6.19 shows this phenomena, the bright yellow grains being the chalcopyrite. Fine sub-grain boundaries, twinning and other crystallographic zones of weakness were observed along which etching appeared to take place preferentially.

3. 2 EXPERIMENTAL TESTING OF CASE (i) MODELS

In this section experimental initial rate data is used to discriminate between models derived for mechanisms 1 and 2 under case (i) conditions - (i.e. $[Fe^{3+}]_o = 0,0$).

Tables 3.3 to 3.6 summarise the conditions of the experiments performed to determine the effects of stirrer speed, initial sphalerite area, H_2SO_4 concentration, temperature, initial zinc concentration, and initial H_2S_ℓ concentration. Also shown on tables 3.3 to 3.6 are the experimental and fitted initial rates, along with initial rates calculated using the final expressions developed in this section.

3. 2. 1 EFFECT OF AGITATION

Figures H1a to H1c plot $^{P}H_2S$ vs t rate curves for leaching VMWBM, VMPR and BDH sphalerites with stirrer speeds ranging from 400,0 r p m to 1500,0 r p m . No significant effect of agitation is observed. Since all other experiments were conducted at stirrer speeds greater than 800,0 rpm assumption (iv) made in section 2. 2 is justified. This is assumed to be true also in the case of the VMZCR sphalerite.

3. 2. 2 EFFECT OF INITIAL AREA Φ_o

An examination of the models summarised on table 2. 2 reveals that models A, B and F predict 1st order dependency, and model G a 2nd order dependency of the initial rate on area. Figures

Table No (-)	Initial Mass x 10^3 (kg)	Temp. (K)	Stirrer Speed (rpm)	$[H_2SO_4]_o$ (kg-mol/m^3)	$[Zn^{2+}]_o$ x 10^3 (kg-mol/m^3)	$[H_2S]_o$ x 10^3 (kg-mol/m^3)	$(r_o)_{exp}$ x 10^3 (kg-mol/m^3)	$(r_o)_{fit}$ x 10^3 (kg-mol/min m^3)	$(r_o)_{calc}$ * x 10^3 (kg-mol/min m^3)
I 1	5,0	318,0	1 000,0	1,0	0	0	5,57	5,73	4,154
I 2	10,0	318,0	1 000,0	1,0	0	0	7,46	8,33	8,31
I 3	20,0	318,0	800,0	1,0	0	0	13,70	18,1	16,62
I 4	20,0	298,0	800,0	1,0	0	0	4,86	6,68	6,10
I 5	20,0	338,0	800,0	1,0	0	0	25,30	55,60	40,19
I 6	20,0	318,0	1 150,0	1,0	0	0	21,70	22,60	16,62
I 7	10,0	318,0	1 500,0	1,0	0	0	11,80	9,29	8,308
I 8	10,0	318,0	1 000,0	0,5	0	0	4,94	4,61	4,941
I 9	10,0	318,0	1 000,0	2,0	0	0	12,60	14,20	12,60
I 10	10,0	318,0	1 000,0	1,0	15,0	0	5,28	5,30	6,119
I 11	10,0	318,0	1 000,0	1,0	25,1	0	5,56	5,60	4,843
I 12	10,0	318,0	1 000,0	1,0	53,9	0	3,68	3,57	3,635
I 13	10,0	318,0	1 000,0	0,5	0	5,0	3,89	6,47	4,941
I 14	10,0	318,0	1 000,0	1,0	0	11,9	9,19	8,18	8,308
I 15	10,0	318,0	1 000,0	2,0	0	20,0	15,30	14,00	12,60

* Calculated using equation 3.41 with parameter values shown on table 3.10

TABLE 3.3 SUMMARY OF INITIAL CONDITIONS AND RESULTS FOR EXPERIMENTAL LEACHING RUNS USING VMWBM SPHALERITE (ALL EXPERIMENTAL RESULTS TABULATED IN APPENDIX I)

$([Fe^3]_o : [H_2SO_4]_o = 0.0)$

Table No (-)	Initial Mass x 10^3 (kg)	Temp. (K)	Stirrer Speed (rpm)	$[H_2SO_4]_o$ (kg-mol/m^3)	$[Zn^{2+}]_o$ x 10^3 (kg-mol/m^3)	$[H_2S]_o$ x 10^3 (kg-mol/m^3)	$(r_o)_{exp}$ x 10^3 (kg-mol/min m^3)	$(r_o)_{fit}$ x 10^3 (kg-mol/min m^3)	$(r_o)_{calc}$ * x 10^3 (kg-mol/min m^3)
I 16	5,0	318,0	1 000,0	1,0	0	0	3,28	3,19	3,391
I 17	10,0	318,0	1 000,0	1,0	0	0	6,84	4,87	6,783
I 18	20,0	318,0	800,0	1,0	0	0	13,60	28,90	13,57
I 19	20,0	318,0	1 000,0	1,0	0	0	9,50	12,60	13,57
I 20	20,0	298,0	1 000,0	1,0	0	0	4,66	4,61	4,035
I 21	20,0	338,0	800,0	1,0	0	0	36,90	54,90	39,52
I 22	10,0	318,0	1 000,0	0,5	0	0	4,20	4,17	4,169
I 23	10,0	318,0	1 000,0	2,0	0	0	10,10	9,88	9,879
I 24	10,0	318,0	1 000,0	1,0	14,343	0	5,457	4,402	4,829
I 25	10,0	318,0	1 000,0	1,0	0	10,96	5,96	N.D.	6,783

* Calculated using equation 3.41 with parameter values shown on table 3.10

TABLE 3.4 SUMMARY OF INITIAL CONDITIONS AND RESULTS FOR EXPERIMENTAL LEACHING RUNS USING VMZCR SPHALERITE (ALL EXPERIMENTAL RESULTS TABULATED IN APPENDIX I)

($[Fe^{3+}]_o$: $[H_2SO_4]_o$ = 0,0)

Table No (-)	Initial Mass x 10^3 (kg)	Temp. (K)	Stirrer Speed (rpm)	$[H_2SO_4]_o$ (kg-mol/m^3)	$[Zn^{2+}]_o$ x 10^3 (kg-mol/m^3)	$[H_2S]_o$ x 10^3 (kg-mol/m^3)	$(r_o)_{exp}$ x 10^3 (kg-mol/min m^3)	$(r_o)_{fit}$ x 10^3 (kg-mol/min m^3)	$(r_o)_{calc}$ ⊕ x 10^3 (kg-mol/min m^3)
I 26	5,0	318,0	1 000,0	1,0	0	0	0,614	0,69	0,657
I 27	10,0	318,0	1 000,0	1,0	0	0	2,95	2,93	2,628
I 28	20,0	318,0	1 000,0	1,0	0	0	8,71	7,16	10,51
I 29	20,0	298,0	1 000,0	1,0	0	0	2,45	1,81	3,34
I 30	20,0	338,0	1 000,0	1,0	0	0	14,80	22,10	28,87
I 31	20,0	318,0	1 500,0	1,0	0	0	11,90	7,74	10,51
I 32	10,0	318,0	1 000,0	0,5	0	0	0,689	0,551	0,657
I 33	10,0	318,0	1 000,0	2,0	0	0	2,56*	2,85*	10,51
I 34	10,0	318,0	1 000,0	1,0	14,237	0	0,483	0,471	0,472
I 35	10,0	318,0	1 000,0	1,0	0	17,767	1,07	N.D.	0,969

* Values far too low owing to some unexplained error

⊕ Calculated using equation 3.41 with parameter values shown on table 3.10

TABLE 3.5 SUMMARY OF INITIAL CONDITIONS AND RESULTS FOR EXPERIMENTAL LEACHING RUNS USING VMPR SPHALERITE (ALL EXPERIMENTAL RESULTS TABULATED IN APPENDIX I)

($[Fe^{3+}]_o : [H_2SO_4]_o = 0,0$)

Table No (-)	Initial Mass x 10^3 (kg)	Temp. (K)	Stirrer Speed (rpm)	$[H_2SO_4]_o$ (kg-mol/m^3)	$[Zn^{2+}]_o$ x 10^3 (kg-mol/m^3)	$[H_2S]_o$ x 10^3 (kg-mol/m^3)	$(r_o)_{exp}$ x 10^3 (kg-mol/min m^3)	$(r_o)_{fit}$ x 10^3 (kg-mol/min m^3)	$(r_o)_{calc}$ * x 10^3 (kg-mol/min m^3)
I 36	4,0	318,0	1 000,0	1,0	0	0	3,97	4,06	4,723
I 37	10,0	318,0	1 000,0	1,0	0	0	12,00	11,20	11,80
I 38	10,0	298,0	1 000,0	1,0	0	0	3,42	2,99	4,257
I 39	10,0	338,0	1 000,0	1,0	0	0	21,80	21,30	29,03
I 40	5,0	318,0	1 000,0	0,5	0	0	2,52	2,24	2,36
I 41	4,0	318,0	1 000,0	2,0	0	0	10,8	10,5	9,45
I 42	4,0	318,0	1 000,0	1,0	14,24	0	3,34	4,34	4,72
I 43	4,0	318,0	1 000,0	1,0	0	10,85	4,39	5,17	4,72
I 45	4,0	298,0	1 000,0	1,04	0	0	1,78	1,33	1,71
I 46	4,0	298,0	1 000,0	1,04	0	0	1,85	1,56	1,71
I 47	4,0	298,0	400,0	1,04	0	0	1,36	1,12	1,71
I 48	4,0	298,0	700,0	1,04	0	0	1,79	1,48	1,71
I 49	4,0	298,0	1 000,0	1,04	0	0	1,74	1,42	1,71
I 50	8,0	298,0	1 000,0	1,04	0	0	3,24	2,40	3,43
I 51	8,0	298,0	1 000,0	1,04	0	0	2,78	2,35	3,43
I 52	6,0	298,0	1 000,0	1,04	0	0	2,70	2,17	2,57
I 53	2,0	298,0	1 000,0	1,04	0	0	1,04	0,824	0,86
I 54	4,0	298,0	1 000,0	0,513	0	0	0,871	0,670	0,88
I 55	4,0	298,0	1 000,0	0,25	0	0	0,566	0,412	0,429
I 56	4,0	298,0	1 000,0	1,95	0	0	3,26	2,71	3,345

* Calculated using equation 3.41 with parameter values shown on table 3.10

T A B'L E 3.6

SUMMARY OF INITIAL CONDITIONS AND RESULTS FOR EXPERIMENTAL LEACHING RUNS USING BDH SPHALERITE (ALL EXPERIMENTAL RESULTS TABULATED IN APPENDIX I)

$([Fe^{3+}]_o : [H_2SO_4]_o = 0,0)$

Results on tables I 45 to I 56 were performed by H. DIJS on the author's apparatus and permission was granted for the author to use the data.

3.1 and 3.2 plot $(r_o)_{exp}$ and $(r_o)_{fit}$ versus ϕ_o for experiments in which different initial masses of sphalerite were leached under similar conditions.

The VMWBM, VMZCR and BDH sphalerites each demonstrate 1st order dependency, and the VMPR a 2nd order dependency of r_o on ϕ_o.

The VMWBM and VMZCR sphalerite data superimpose and scatter closely about the dashed best fit line on figure 3.1 represented by the following equation:

$$r_o = 2,5 \times 10^{-4} \phi_o \quad \ldots\ldots\ldots \quad 3.1$$

The BDH sphalerite $(r_o)_{exp}$ data at 3,8,0 K and 298,0 K scatter around the best fit lines represented by the equations:

$$r_o = 1,64 \times 10^{-4} \phi_o \text{ (at 318,0 K)} \ldots\ldots \quad 3.2$$

$$r_o = 0,55 \times 10^{-4} \phi_o \text{ (at 298,0 K)} \ldots\ldots \quad 3.3$$

The VMPR sphalerite $(r_o)_{exp}$ data scatters around the best fit line represented by the equation:

$$r_o = 3,8 \times 10^{-6} \phi_o^2 \quad \ldots\ldots\ldots \quad 3.4$$

The VMWBM and the VMZCR sphalerites differ greatly in terms of impurity content, yet apparantly leach identically. The BDH sphalerite appears to leach at a much lower initial rate per given area. It is possible that the proportion of BET measured area consisting of active sites (represented by K_ϕ in equation 2.1) for the natural VMWBM and VMZCR

------ Calculated by eqn. 3.1

conditions			
	TEMP.	(K)	318,0
	$[H_2SO_4]$	(kg-mol/m³)	1,0
	STIRRER	(rpm)	1000,0

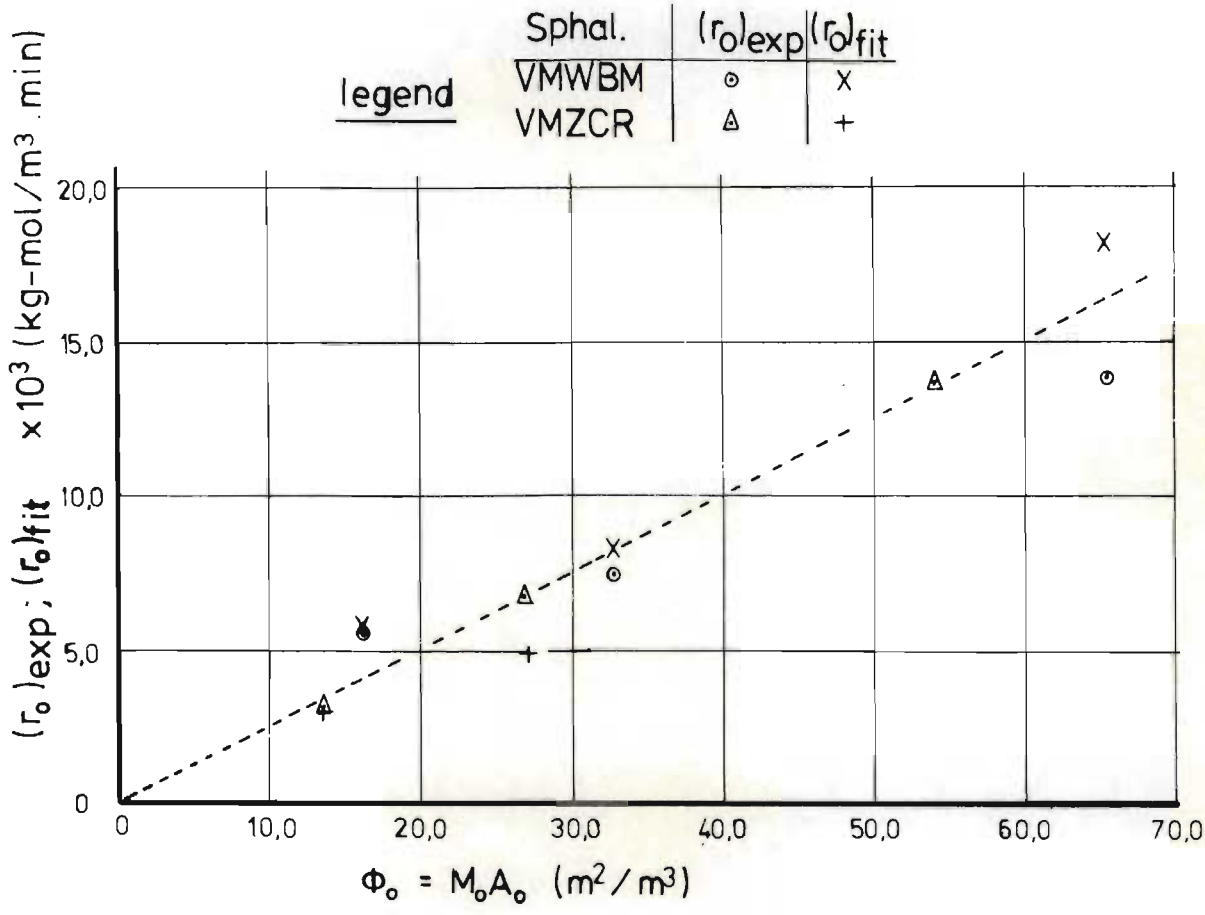

Figure 3.1 Initial rate versus total initial area for VMWBM and VMZCR sphalerites.

a Calculated by eqn. 3.2
b Calculated by eqn. 3.3
c Calculated by eqn. 3.4

conditions			
	$[H_2SO_4]$	(kg-mol/m³)	1,0
	STIRRER	(rpm)	1000,0

legend

Sphal.	$(r_o)_{exp}$	$(r_o)_{fit}$	TEMP.(K)
VMPR	⊙	X	318,0
BDH	▲	Y	318,0
BDH	▣	I	298,0

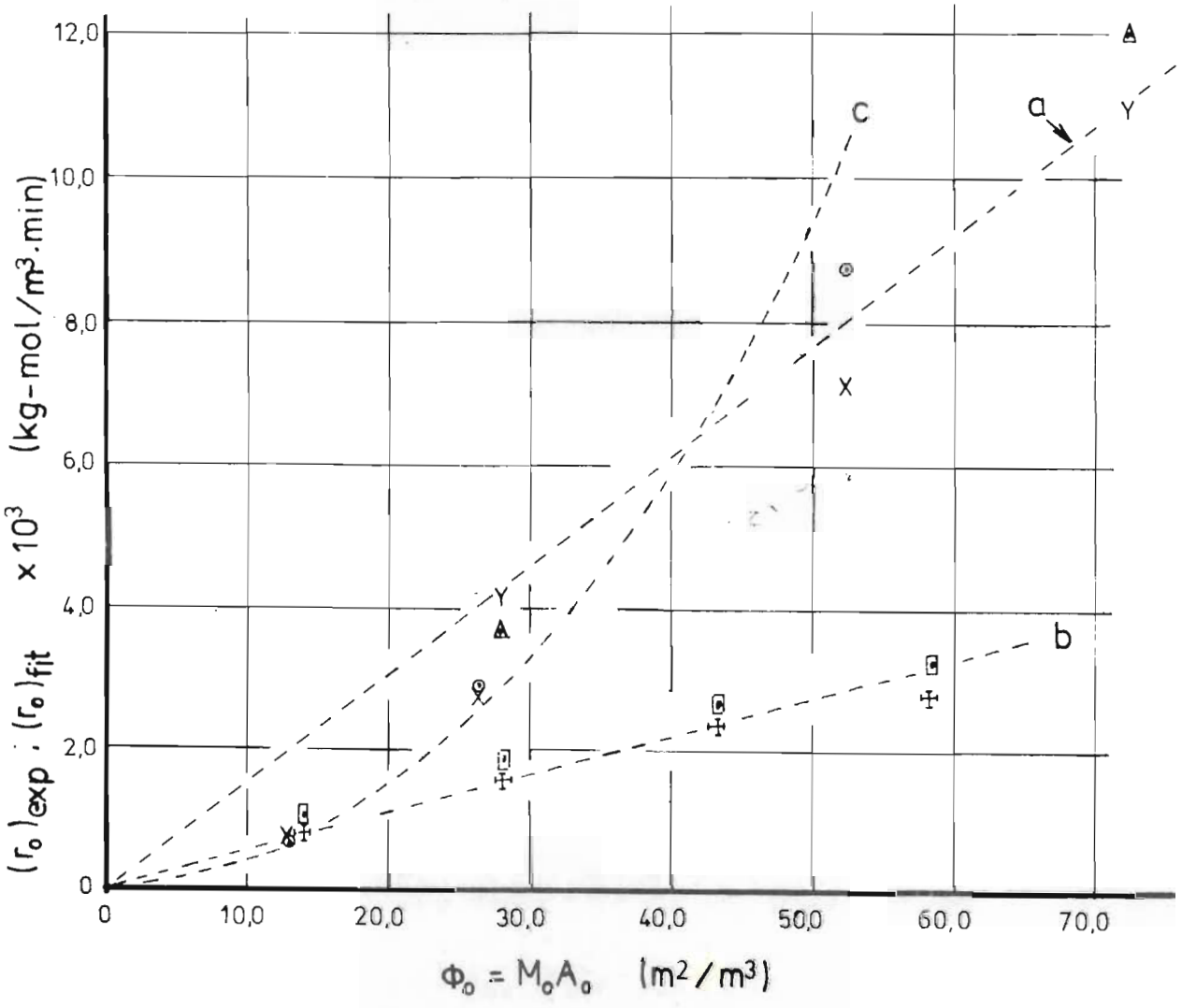

Figure 3.2 Initial rate versus total initial area for the VMPR and BDH sphalerites.

sphalerites is significantly higher than for the BDH sphalerite.

If it is assumed that $K_\phi = 1,0$ (in equation 2.1) for the VMWBM and the VMZCR sphalerites, then a value of $K_\phi = 0,61$ (i.e. $\frac{1,53 \times 10^{-4}}{2,5 \times 10^{-4}}$) will permit the initial rates of all three sphalerites (at T = 318,0 K and $[H_2SO_4]_o = 1,0$ kg-mol / m^3) to be described by the following equation :

$$r_o = 2,5 \times 10^{-4} \frac{\phi_o}{K_\phi} \qquad \ldots\ldots\ldots \quad 3.5$$

where $\phi_o = K_\phi M_o A_o$ (equation 2.1)
$K_\phi = 1,0$ for VMWBM and VMZCR sphalerites,
and $K_\phi = 0,61$ for the BDH sphalerite.

Although these results do not discriminate between models A, B and F they do justify having assumed H^+ adsorption as being the rate limiting step in developing these models. By comparing the results on figures 3.1 and 3.2 it is evident that the initial rate dependency of VMPR sphalerite is completely different to that for the two natural and the synthetic sphalerite. In fact the results for the VMPR sphalerite are in agreement with the behaviour predicted by model G for which product desorption is assumed rate limiting.

3.2.3 EFFECT OF INITIAL H_2SO_4 CONCENTRATION

An examination of the models summarised on table 2.2 reveals that models A and F predict a 1st order dependency and models B and G a 2nd order dependency of the initial leaching rates on $[H_2SO_4]_o$.

With no Zn^{2+} or H_2S initially present the models may be represented as follows:

$$\text{Model A:} \quad r_o^{*} = \frac{k_1 [H^+]_o}{(1,0 + K_1 [H^+]_o)} \quad \ldots\ldots\ldots \quad 3.6$$

$$\text{Model B:} \quad r_o^{*} = \frac{k_6 [H^+]_o^2}{(1,0 + K_1 [H^+]_o)[H_2S]_{\ell o}} \quad \ldots\ldots\ldots \quad 3.7$$

$$\text{Model F:} \quad r_o^{*} = \frac{k_{11} [H^+]_o}{(1,0 + K_{11} [H^+]_o)} \quad \ldots\ldots\ldots \quad 3.8$$

$$\text{Model G:} \quad r_o^{\Theta} = \frac{k_{16} [H^+]_o^2}{(1,0 + K_{11} [H^+]_o)^2} \quad \ldots\ldots\ldots \quad 3.9$$

$$\text{where} \quad r_o^{*} = \frac{r_o}{\Phi_o} \quad \text{for models A, B \& F} \quad \ldots\ldots\ldots \quad 3.10$$

$$\text{and} \quad r_o^{\Theta} = \frac{r_o}{\Phi_o^2} \quad \text{for model G} \quad \ldots\ldots\ldots \quad 3.11$$

Figure 3.3 plots $(r_o^{*})_{exp}$ and $(r_o^{*})_{fit}$ for the VMWBM and VMZCR sphalerites. A definite non-linearity is evident.

Equation 3.6 and 3.8 each have two unknowns, k_1 or k_{11} and K_1 or K_{11}. Two equations were set up for each set of data and solved for values of the unknown constants. Curve 'a' on figure 3.3 is described by the following equation for the VMWBM sphalerite:

$$r_o^{*} = \frac{3,726 \times 10^{-4}[H^+]}{(1,0 + 0,4674 [H^+])} \quad \ldots\ldots\ldots \quad 3.12$$

Curve b on fig 3.3 is described by the following equation for the VMZCR sphalerite:

$$r_o^{*} = \frac{3,996 \times 10^{-4} [H^+]}{(1,0 + 0,5954 [H^+])} \quad \ldots\ldots\ldots \quad 3.13$$

Note that for $H^+ = 1,0$, the solution for equation

a Calculated by eqn. 3.12

b Calculated by eqn. 3.13

conditions	TEMP.	(K)	318,0
	MASS	(kg)	0,010
	STIRRER	(rpm)	1000,0

	Sphal.	$(r_o)_{exp}$	$(r_o)_{fit}$	A_o (m^2/kg)
legend	VMWBM	⊙	x	3,272
	VMZCR	△	+	2,708

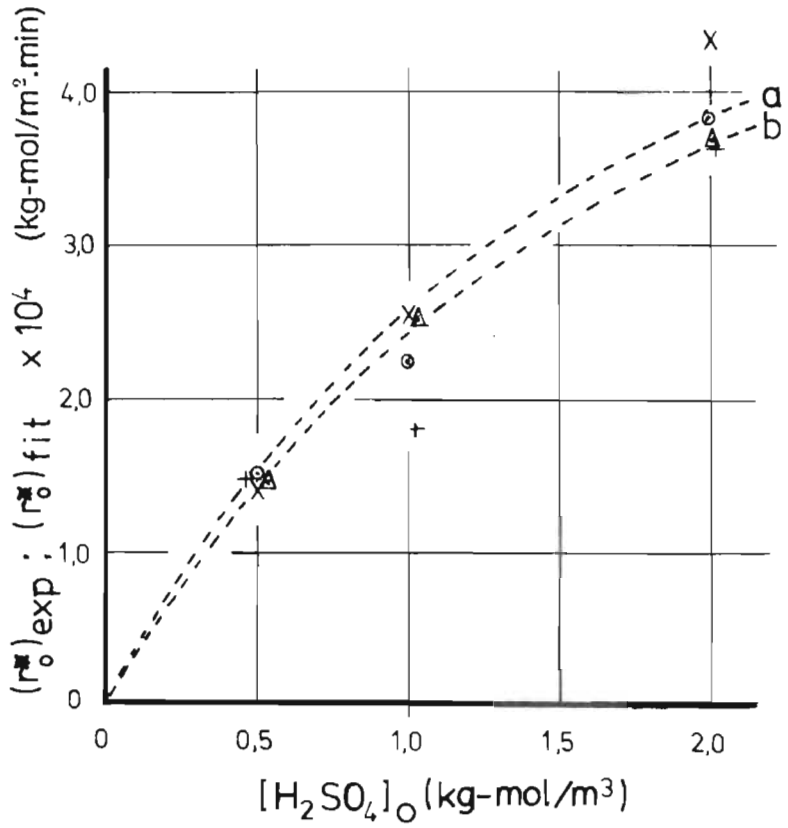

Figure 3.3 Initial specific rate versus initial H_2SO_4 concentration for the VMWBM and VMZCR sphalerites.

3. 12 is -

$$r_o^* = 2{,}539 \times 10^{-4} \quad \ldots\ldots\ldots \quad 3.\ 14$$

and for equation 3. 13 is -

$$r_o^* = 2{,}505 \times 10^{-4} \quad \ldots\ldots\ldots \quad 3.\ 15$$

These values agree very well with the value of $r_o/\phi_o = 2{,}5 \times 10^{-4}$ given by equation 3. 5 .

Figure 3. 4 plots $(r_o^*)_{exp}$ and $(r_o^*)_{fit}$ for the BDH sphalerite leaching at 318,0 K and 298,0 K. A linear dependence of r_o^* on $[H^+]_b$ is observed. According to models A or F this could suggest that the adsorption of H^+ at active synthetic sites takes place very weakly so that the adsorption constants K_1 or K_{11} (in equations 3. 6 and 3. 8) are essentially zero.

Using the values of r_o/ϕ_o from equations 3. 2 and 3. 3 for BDH sphalerites leaching at 318,0 K and 298,0 K (for $[H^+] = 1{,}0$), and letting the H^+ adsorption constants K_1 and K_{11} be zero, gives the following reduced forms of equations 3. 6 and 3. 8 :

$$r_o^* = 1{,}64 \times 10^{-4}\,[H^+] \quad (T = 318{,}0\,K) \quad \ldots\ldots\ldots \quad 3.\ 16$$

and $$r_o^* = 0{,}55 \times 10^{-4}\,[H^+] \quad (T = 298{,}0\,K) \quad \ldots\ldots\ldots \quad 3.\ 17$$

Solutions to these equations are represented on figure 3. 4 by lines 'a' and 'b' respectively.

a Calculated by eqn. 3.16

b Calculated by eqn. 3.17

conditions			
	Mass	(kg)	0,004
	Agitation	(rpm)	1 000,0

legend	Data	T (K)
⊙	$(r_o^*)_{exp}$	318,0
×	$(r_o^*)_{expfit}$	318,0
⊡	$(r_o^*)_{exp}$	298,0
+	$(r_o^*)_{expfit}$	298,0

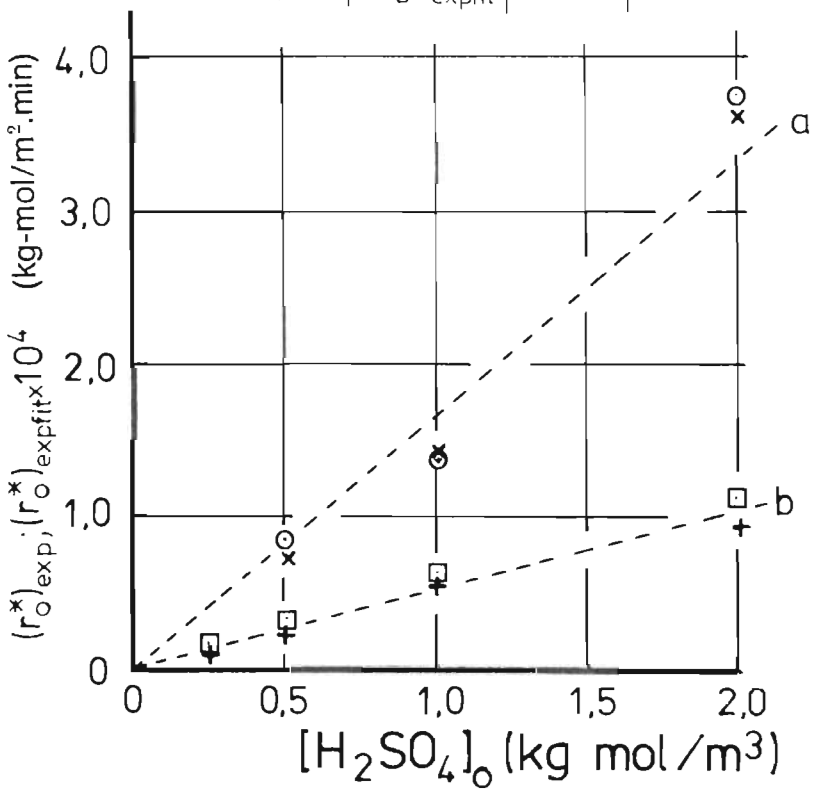

Figure 3.4 Initial specific rate versus initial H_2SO_4 concentration for the BDH sphalerite.

Figure 3.5 plots $r_o^{\oplus}$ versus $[H^+]_o$ for the VMPR sphalerite. The value at $[H^+]_o = 2,0$ is lower than the well established value at $[H^+]_o = 1,0$. This is probably due to an abnormal unidentified error, (possibly the graph paper recording the P_{H_2S} with time was advancing faster than was logged) and hence this point has been neglected . Letting $r_o/\phi_o^2 = 3,8 \times 10^{-6}$ (from equation 3.4) and assuming that in the situation of reaction products being strongly adsorbed, that the adsorption of H^+ has an insignificant effect on the kinetics (i.e. assume $K_{11} = 0,0$ in equation 3.9), permits equation 3.9 for model G to reduce to -

$$r_o^{\oplus} = 3,8 \times 10^{-6} [H^+]_o^2 \quad \ldots\ldots\ldots \quad 3.18$$

The dashed curve on figure 3.5 represents the solution to equation 3.18 and is observed to fit through the origin and two data points reasonably well.

It is apparant that none of the sphalerites exhibit 1st order and 2nd order dependencies of the initial rate on the initial area and $[H^+]_o$ respectively, as predicted by model B. Hence this model and mechanism 1 is considered invalid and will be subsequently disregarded. Additional reasons for rejecting mechanism 1 in favour of mechanism 2 are discussed in section 3.2.8 .

3.2.4 EFFECT OF INITIAL Zn^{2+} CONCENTRATION ON INITIAL RATE

According to the initial rate components of models F and G , if Zn^{2+} ions are sufficiently

-------- Calculated by eqn. 3.18

conditions			
	Temp	(K)	318.0
	Mass	(kg)	0.01
	Stirrer	(rpm)	1000.0

legend	Data
⊙	$(r_o^{\oplus})_{exp}$
x	$(r_o^{\oplus})_{fit}$

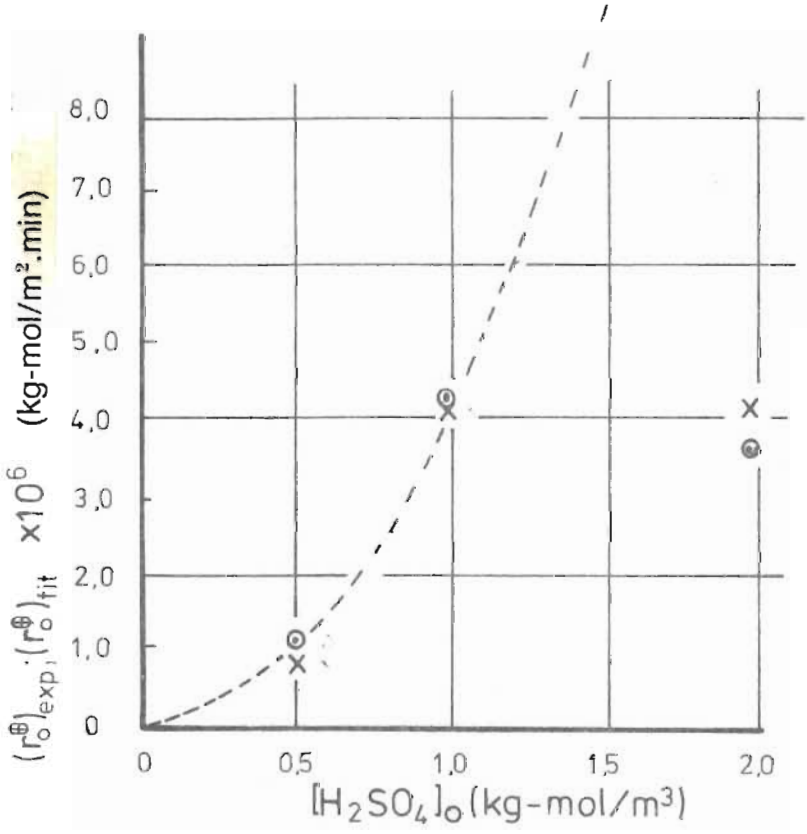

Figure 3.5 Initial specific rate versus initial H_2SO_4 concentration for VMPR sphalerite.

strongly adsorbed their presence should suppress the initial dissolution rate.

Figure 3.6 plots $[r_o^*]$ versus $[Zn^{2+}]_o$ for the VMWBM, VMZCR and BDH sphalerites. The VMWBM and VMZCR sphalerite initial rates are observed to have been significantly suppressed.

Using the values of constants given in equations 3.12 and 3.13 (for the VMWBM and VMZCR sphalerites) model F take the following forms :

For VMWBM sphalerite -

$$r_o^* = \frac{3{,}726 \times 10^{-4} [H^+]_o}{(1{,}0 + 0{,}4674 [H^+]_o + K_8 [Zn^{2+}]_o)} \quad \ldots\ldots\ldots \quad 3.19$$

and for VMZCR sphalerite -

$$r_o^* = \frac{3{,}996 \times 10^{-4} [H^+]_o}{(1{,}0 + 0{,}5954 [H^+]_o + K_8 [Zn^{2+}]_o)} \quad \ldots\ldots\ldots \quad 3.20$$

Figure 3.6 plots the solutions to equations 3.19 and 3.20 for K_8 = 30,0 35,0 45,0 50,0 and 60,0 respectively. All the points for the VMWBM and VMZCR sphalerites fall within the curves for $K_8 = 30$ and $K_8 = 60$. A value $K_8 = 35{,}0$ and $K_8 = 45{,}0$ is accepted here as representing the best average fit through the VMWBM and the VMZCR data points respectively. Consequently equations 3.19 and 3.20 take the following forms :

-------- Calculated by eqns. 3.19 and 3.20 with K_8 values as shown below.

conditions	TEMP,	(K)	318,0
	$[H_2SO_4]$	(kg-mol/m³)	1,0
	STIRRER	(rpm)	1000,0

	Sphal.	$(r_o)_{exp}$	$(r_o)_{fit}$	Mass (kg)
legend	VMWBM	⊙	x	0,010
	VMZCR	△		0,010
	BDH	✢	✡	0,004

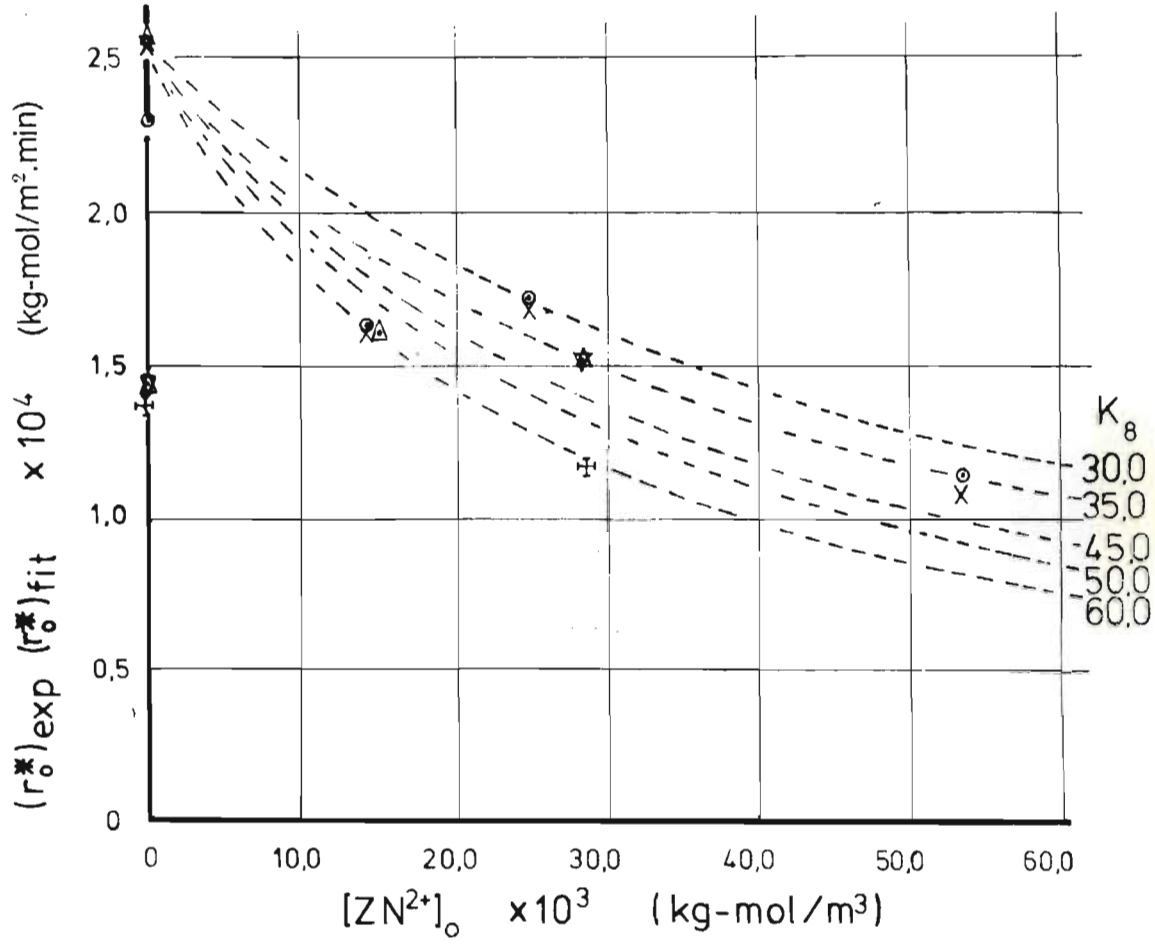

Figure 3.6 Initial specific rate versus initial zinc ion concentration for the VMWBM, VMZCR and BDH sphalerites.

For VMWBM sphalerite -

$$r_o^* = \frac{3{,}726 \times 10^{-4} \ [H^+]_o}{(1{,}0 + 0{,}4674 \ [H^+]_o + 35{,}0 \ [Zn^{2+}]_o)} \quad \ldots\ldots\ldots \ 3.\ 21$$

and for VMZCR sphalerite -

$$r_o^* = \frac{3{,}996 \times 10^{-4} \ [H^+]_o}{(1{,}0 + 0{,}5954 \ [H^+]_o + 45{,}0 \ [Zn^{2+}]_o)} \quad \ldots\ldots\ldots \ 3.\ 22$$

For the BDH sphalerite the $(r_o^*)_{fit}$ values demonstrate no suppression of the initial rate, whilst the $(r_o^*)_{exp}$ values do appear to demonstrate a suppressive effect of $[Zn^{2+}]_o$ on the initial rate. Unfortunately insufficient data is available to resolve whether Zn^{2+} ions do adsorb sufficiently strongly so as to give the Zn^{2+} adsorption equilibrium constant K_8 a finite value.

Romankiw (1962) leached synthetic sphalerite in 0,5 kg - mol / m^3 H_2SO_4 at 298,0 K with five values of Zn^{2+} over the range -

$0{,}0 \leq [Zn^{2+}]_o \leq 50{,}0 \times 10^{-3}$ kg - mol / m^3

and detected no influence of $[Zn^{2+}]_o$ on the initial leaching rate. It is accepted then that Zn^{2+} ions adsorb sufficiently weakly on BDH sphalerite that the Zn^{2+} adsorption equilibrium constant K_8 for this sphalerite is approximately zero.

Figure 3. 7 plots $(r_o^{\Theta})_{exp}$ and $(r_o^{\Theta})_{fit}$ versus $[Zn^{2+}]_o$ (where $r_o^{\Theta} = \frac{r_o}{\Phi_o^2}$) for the VMPR sphalerite, and a significant suppressive effect of the Zn^{2+} ions on the initial rate is observed. In section 3. 2. 3 the H^+ ion adsorption equilibrium constant for this sphalerite was accepted as being zero.

-------- Calculated by eqn. 3.28

conditions	Temp	(K)	318,0
	Mass	(kg)	0,01
	stirrer	(rpm)	1000,0

legend ⊙ $(r_o^{\oplus})_{exp}$ × $(r_o^{\oplus})_{fit}$

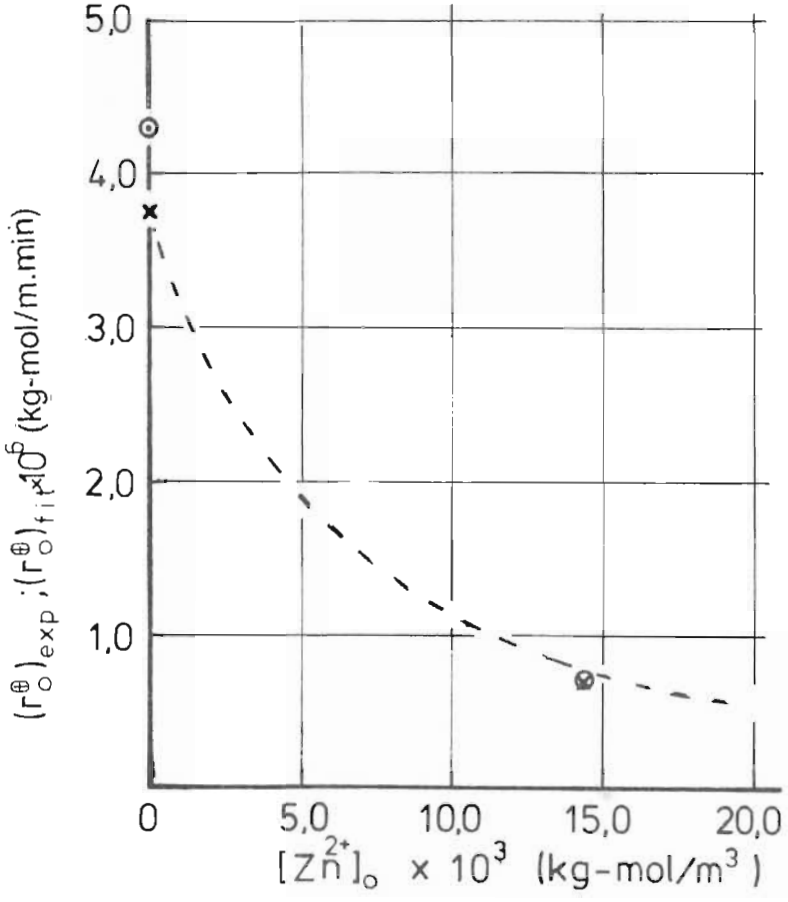

Figure 3.7 Initial specific rate versus initial zinc ion concentration for the VMPR sphalerite.

Model G therefore adopts the following form (using the rate constant value expressed in equation 3. 18) :

$$r_o^{\oplus} = \frac{3,8 \times 10^{-6} \ [H^+]_o^{\,2}}{(1,0 + K_{22}[Zn^{2+}]_b)^{\,2}} \quad \ldots\ldots\ldots \quad 3.\ 23$$

The value of K_{22} was determined as follows :

$$\text{Let} \quad 1,0 + K_{22}\,[Zn^{2+}]_b = Z \quad \ldots\ldots\ldots \quad 3.\ 24$$

Now experimentally

$r_o^{\oplus} = 0,684 \times 10^{-6}$ (at $[Zn^{2+}]_b = 14,237 \times 10^{-3}$ and $[H^+]_o = 1,0$) so that equation 3. 23 takes the form -

$$0,684 \times 10^{-6} = \frac{3,8 \times 10^{-6}}{Z^{\,2}} \quad \ldots\ldots\ldots \quad 3.\ 25$$

Hence $Z = 2,36$ 3. 26

Substituting for $[Zn^{2+}]_o$ and Z in equation 3. 24 and solving for K_{22} gives -

$$K_{22} = \frac{2,36 - 1,0}{14,237 \times 10^{-3}} = 95,53 \quad \ldots\ldots\ldots \quad 3.\ 27$$

Hence equation 3. 23 takes the form -

$$r_o^{\oplus} = \frac{3,8 \times 10^{-6} \ [H^+]_b^{\,2}}{(1,0 + 95,53\ [Zn^{2+}]_o)^{\,2}} \quad \ldots\ldots\ldots \quad 3.\ 28$$

The solution to equation 3. 28 is plotted on figure 3. 7 .

3.2.5 EFFECT OF INITIAL H_2S CONCENTRATION ON INITIAL RATE

According to mechanism 1 H_2S does not form an adsorbed specie and hence models A and B do not contain terms for the H_2S adsorption equilibrium constant in the denominator. Models F and G for mechanism 2 do contain such terms, but if the H_2S is only very weakly adsorbed such terms could have zero values. Experiments were conducted in which H_2S gas was purged into the leach reactor containing aqueous H_2SO_4 to give a significant positive H_2S partial pressure prior to injecting the sphalerite solids. The initial H_2S concentration was determined analytically.

Table 3.7 summarises $(r_o^*)_{exp}$ and $(r_o^*)_{fit}$ data for VMWBM (at three $[H^+]_o$ values); VMZCR; BDH and VMPR sphalerites leached without and with H_2S initially present. Only for the VMPR sphalerite is a significant suppression of the initial rate observed. The $(r_o^*)_{exp}$ data shows rather serious scatter (often giving larger values with H_2S present than without). Figures 3.8 to 3.11 plot the P_{H_2S} and ΔP_{H_2S} versus time rate curves for the experiments without and with H_2S initially present.

ΔP_{H_2S} is defined as :-

$$\Delta P_{H_2S} = P_{H_2S} - P_{H_2S_o} \quad \ldots\ldots\ldots \quad 3.29$$

where P_{H_2S} = measured total H_2S partial pressure;

$P_{H_2S_o}$ = measured initial H_2S partial pressure at time $t = 0$;

Table No.	Sphalerite type	$[H_2SO_4]_o$ (kg-mol/m³)	$[H_2S]_o$ x 10^3 (kg-mol/m³)	$(r_o^*)_{exp}$ (kg-mol/m².min)	$(r_o^*)_{fit}$ (kg-mol/m².min)
I 8	VMWBM	0,5	0	15,1	14,1
I 13	VMWBM	0,5	5,0	11,9	19,8
I 2	VMWBM	1,0	0	22,8	25,5
I 14	VMWBM	1,0	11,9	28,1	25,5
I 9	VMWBM	2,0	0	38,6	43,3
I 15	VM WBM	2,0	20,0	46,8	42,9
I 17	VMZCR	1,0	0	25,3	18,0
I 25	VMZCR	1,0	9,8	22,0	N.D.
I 27	VMPR	1,0	0	11,2	11,1
I 35	VMPR	1,0	17,0	4,08	N.D.
I 36	B D H	1,0	0	13,8	14,1
I 43	B D H	1,0	9,801	15,2	17,9

T A B L E 3. 7 SUMMARY OF INITIAL RATE RESULTS FOR LEACHING WITH AND WITHOUT H_2S INITIALLY PRESENT

Conditions			
	Temp.	(K)	318.0
	Mass	(kg)	0.01
	Stirrer	(rpm)	1000.0

legend	Curve (−)	$[H_2SO_4]_o$ (kg-mol/m³)	$[H_2S]_o \times 10^3$ (kg-mol/m³)	Table (−)
	a	2.0	0	I 9
	b	2.0	20.0	I15
	c	1.0	0	I 2
	d	1.0	11.9	I 14
	e	0.5	0	I 8
	f	0.5	5.0	I 13

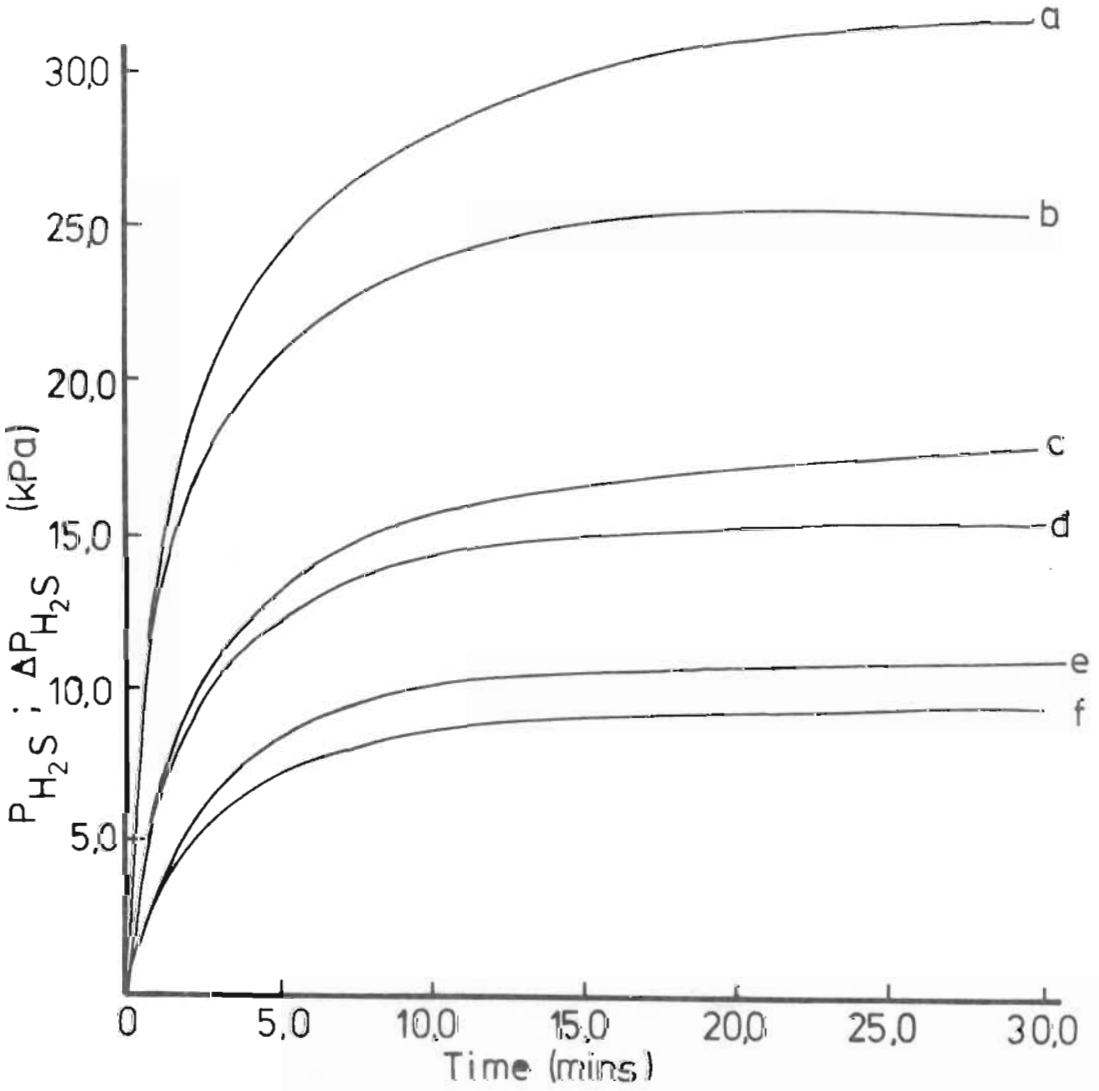

Figure 3.8 H_2S partial pressure versus time for VMWBM sphalerite without and with H_2S initially present.

Conditions			
	Mass	(kg)	0.04
	Temp.	(K)	318.0
	$[H_2SO_4]_o$	(kg-mol/m^3)	1.0
	Stirrer	(rpm)	1000.0

legend	Curve (-)	$[H_2S]_o \times 10^3$ (kg-mol/m^3)	Table (-)
	a	0	I 36
	b	9.801	I 43

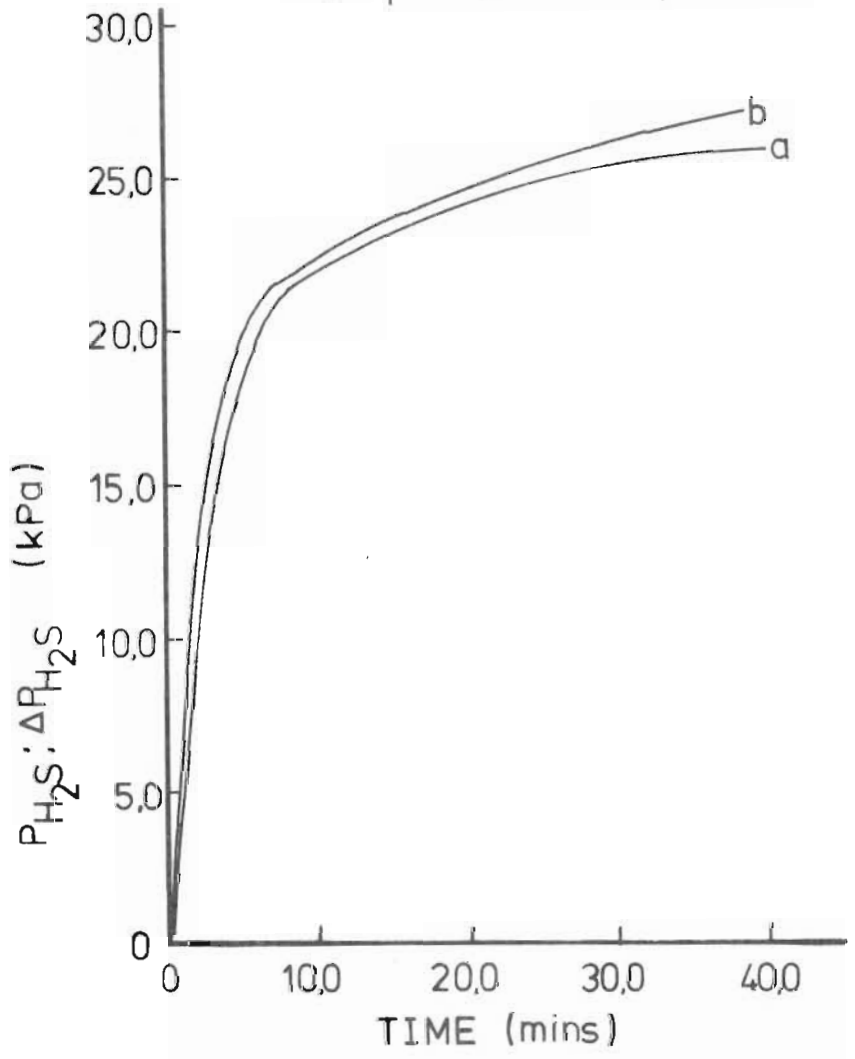

Figure 3.9 H_2S partial pressure versus time for BDH sphalerite leaching without and with H_2S initially present.

Conditions

Temp.	(K)	318,0
Mass	(kg)	0,01
$[H_2SO_4]_o$	(kg-mol/m^3)	1,0
Stirrer	(rpm)	1000,0

legend

Curve (−)	$[H_2S]_o \times 10^3$ (kg-mol/m^3)	Table (−)
a	0	I 17
b	9,8	I 25

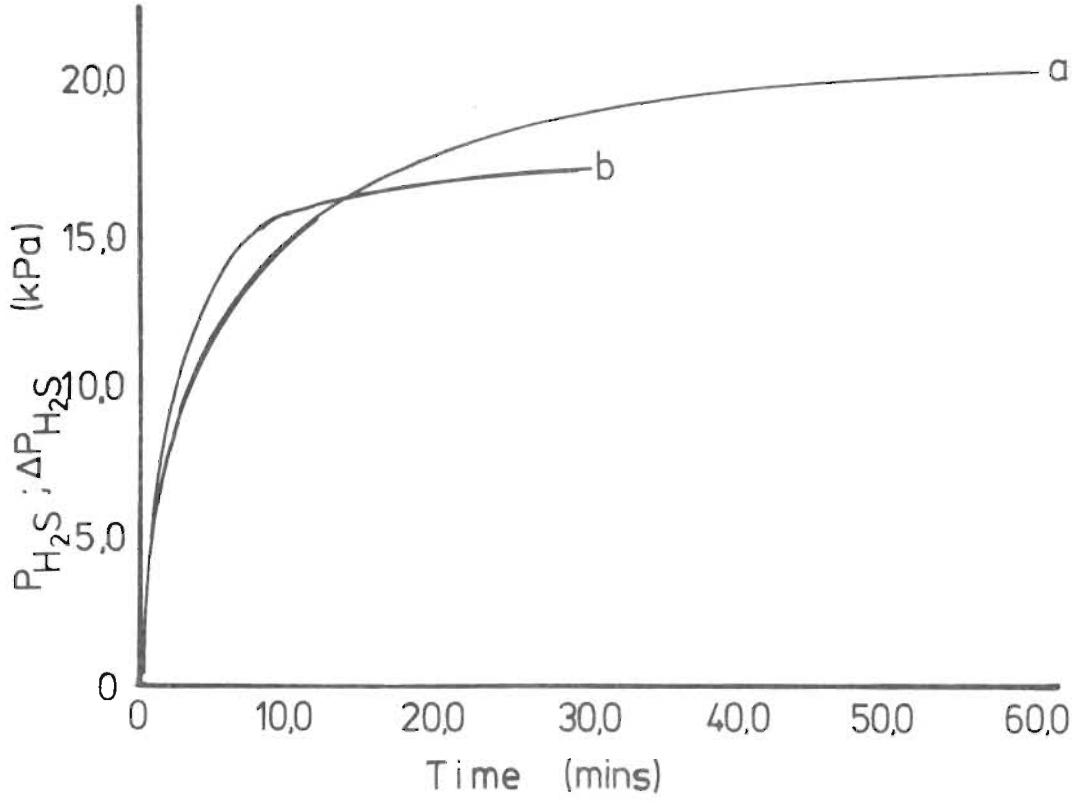

Figure 3.10 H_2S partial pressure versus time for VMZCR sphalerite leaching without and with H_2S initially present.

conditions

Temp	(K)	318,0
Mass	(kg)	0,01
$[H_2SO_4]$	(kg-mol/m³)	1,0
Stirrer	(rpm)	1 000,0

legend

	RUN (-)	Table (-)	$(P_{H_2S})_o$ (kPa)	$[H_2S]_o$ x10³ (kg-mol/m³)
a	132	I 27	0	0
b	196	I 35	11,91	18,0

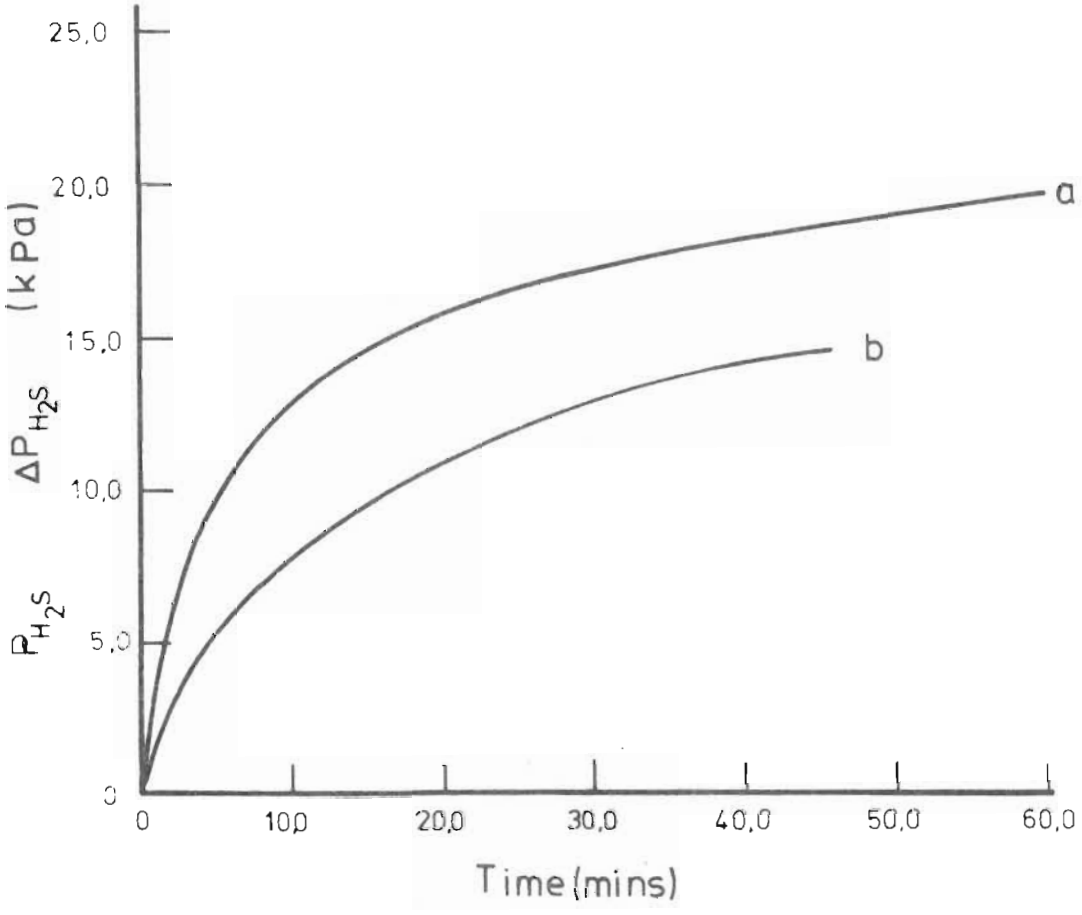

Figure 3.11 H_2S partial pressure versus time for VMPR sphalerite leaching without and with H_2S initially present.

ΔP_{H_2S} = calculated H_2S partial pressure which increases as dissolution proceeds.

The results on the figures 3.8 to 3.11 confirm that only in the case of the VMPR sphalerite does the H_2S significantly suppress the initial dissolution rate. Hence it is assumed that if H_2S adsorption does occur for the VMWBM, VMZCR and BDH sphalerites, it does so only weakly and that the H_2S adsorption equilibrium constants for these sphalerites are effectively zero.

The following form of model G can be solved to determine the H_2S adsorption equilibrium constant K_{23} for the VMPR sphalerite. Using the rate constant value contained in equation 3.18 -

$$r_o^{\oplus} = \frac{3{,}8 \times 10^{-6} [H^+]^2}{(1{,}0 + K_{23} [H_2S]_o)^2} \quad \ldots\ldots\ldots \quad 3.30$$

Let $1{,}0 + K_{23} [H_2S]_o = Z$ $\ldots\ldots\ldots$ 3.31

Now experimentally -

$r_o^{\oplus} = 1{,}55 \times 10^{-6}$ at $[H_2S]_o = 18{,}0 \times 10^{-3}$

and $[H^+]_o = 1{,}0$ so that equation 3.30 takes the form -

$$1{,}55 \times 10^{-6} = \frac{3{,}8 \times 10^{-6}}{Z^2} \quad \ldots\ldots\ldots \quad 3.32$$

Hence $Z = 1{,}66$

Substituting for H_2S_o and Z in equation 3.31 and solving for K_{23} gives -

$$K_{23} = \frac{1{,}66 - 1{,}0}{18{,}0 \times 10^{-3}} = 36{,}4 \quad \ldots\ldots\ldots \quad 3.33$$

Hence equation 3.30 takes the form -

$$r_o^{\oplus} = \frac{3,8 \times 10^{-6} [H^+]^2}{(1,0 + 36.4 [H_2S]_o)^2} \quad \ldots\ldots\ldots \quad 3.34$$

Figure 3.12 plots $(r_o^{\oplus})_{exp}$ versus $[H_2S]_o$ for the VMPR sphalerite and also plots the solution to equation 3.34.

------- Calculated by eqn. 3.34

Conditions			
	Temp.	(K)	318.0
	$[H_2SO_4]_o$	(kg-mol/m³)	1.0
	Mass	(kg)	0.01
	Stirrer	(rpm)	1000.0

legend ⊙ $(r_o^{\oplus})_{exp}$ × $(r_o^{\oplus})_{fit}$

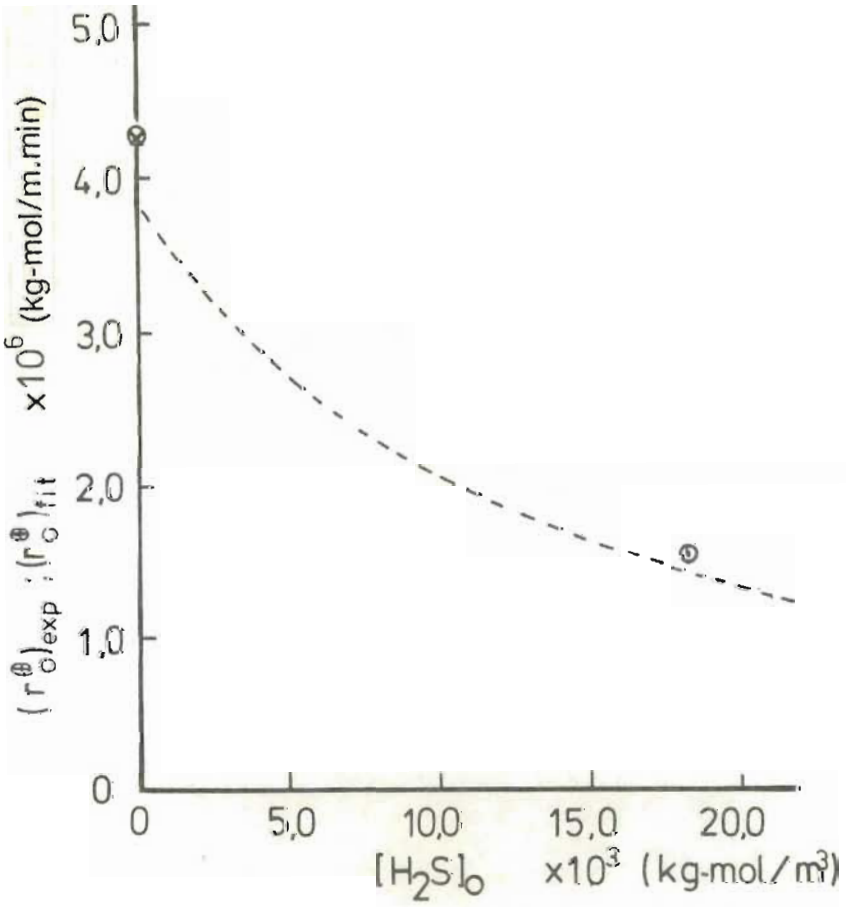

Figure 3.12 Initial specific rate versus initial H_2S concentration for VMPR sphalerite.

3.2.6 EFFECT OF TEMPERATURE ON INITIAL RATE

The leaching models F and G incorporate not only rate constants, but also adsorption equilibrium constants which are likely to be temperature dependent. For example, leaching a given sphalerite at different temperatures (but at common $[H^+]_o$; $[Zn^{2+}]_o$ or $[H_2S]_o$ values), the overall resultant measured activation energy which is ascribed to the rate constant is in fact only an apparant activation energy. In order to establish the temperature dependencies of the individual adsorption equilibrium constants it would be necessary to perform experiments at different temperatures for different values of $[H^+]_o$; $[Zn^{2+}]_o$ or $[H_2S]_o$. This has not been done in this study, nor in any other study of which the author is aware.

In order to observe the effect of temperature on the leaching of the VMWBM, VMZCR, BDH and VMPR sphalerites it is assumed that the foreward rate constants of models F and G can be described by an Arrhenius type equation, i.e. -

$$k_{11} \text{ or } k_{16} = A_E \exp\left(\frac{-E_a}{R\,T}\right) \quad \ldots\ldots \quad 3.35$$

For the VMWBM sphalerite (from equation 3.12) -

$$k_{11} = \frac{r_o\,(1{,}0 + 0{,}4674\,[H^+]_o)}{\Phi_o\,[H^+]_o} \quad \ldots\ldots\ldots \quad 3.36$$

For the VMZCR sphalerite (from equation 3.13) -

$$k_{11} = \frac{r_o\,(1{,}0 + 0{,}5954\,[H^+]_o)}{\Phi_o\,[H^+]_o} \quad \ldots\ldots\ldots \quad 3.37$$

For the BDH sphalerite (from equation 3.16) -

$$k_{11} = \frac{r_o}{\phi_o [H^+]_o} \qquad \ldots\ldots\ldots 3.38$$

For the VMPR sphalerite (from equation 3.18) -

$$k_{16} = \frac{r_o}{\phi_o^2 \, [H^+]_o^{\,2}} \qquad \ldots\ldots\ldots 3.39$$

Figure 3.13 plots log k_{11} and log k_{16} (based on $(r_o)_{exp}$ or $(r_o)_{fit}$ values) versus $\frac{1}{T}$.

All the $(k_{11})_{exp}$ and $(k_{11})_{fit}$, or $(k_{16})_{exp}$ and $(k_{16})_{fit}$ data points were linear regressed for each of the sphalerites. Table 3.8 summarises values of A_E and E_a for each sphalerite.

Sphalerite (-)	A_E (kg mol/min.m^2)	E_a x 10^{-6} (J/kg - mole)
VMWBM	1 062,0	39,43
VMZCR	35 310,0	47,75
BDH	545,1	40,17
VMPR	66,81	45,13

TABLE 3.8 SUMMARY OF PRE-EXPONENTIAL CONSTANTS A_E AND ACTIVATION ENERGIES E_a REPRESENTING THE ORIGIN AND SLOPE OF THE LINES APPEARING ON FIGURE 3.13.

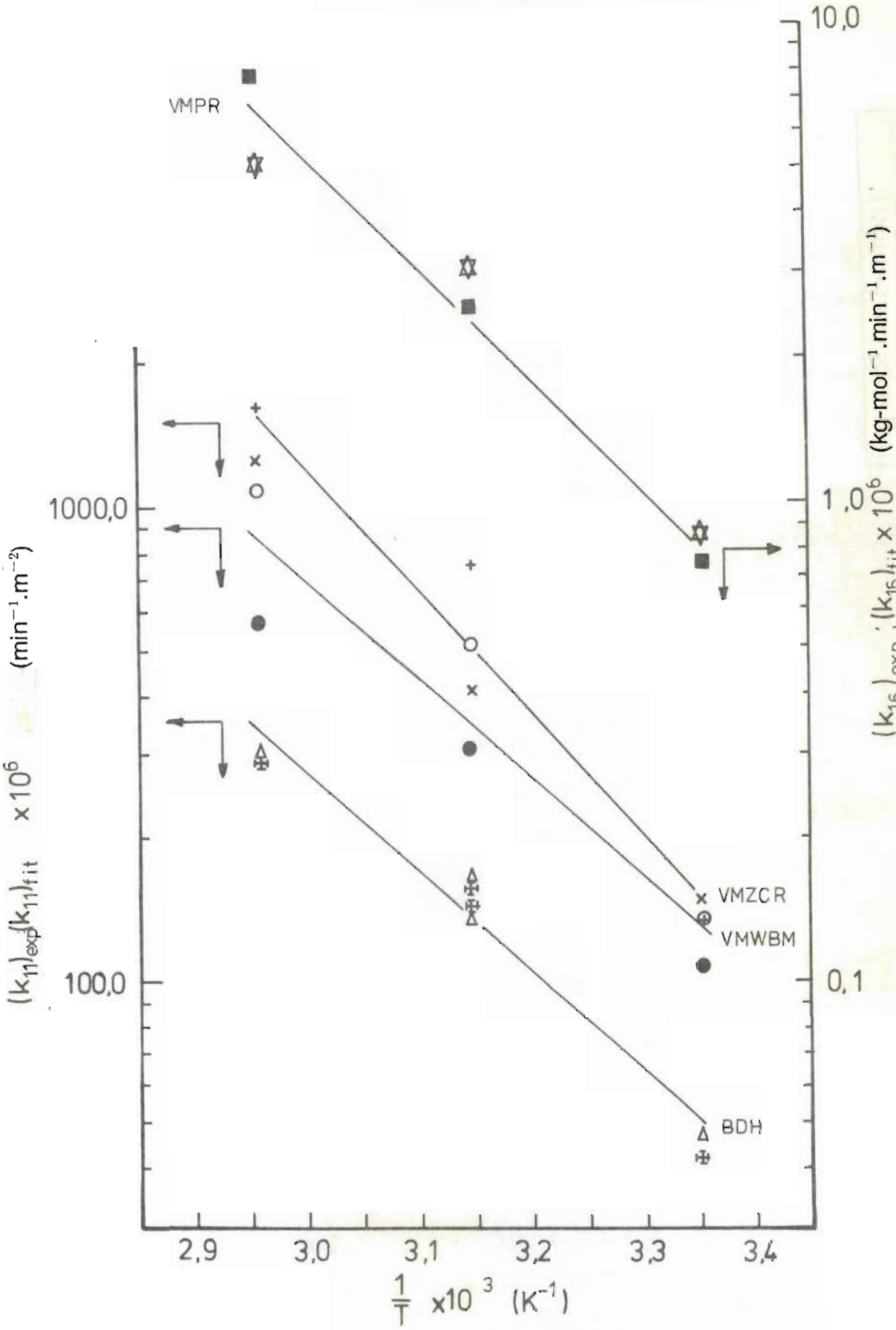

Figure 3.13 Arrhenius plot demonstrating the effect of temperature on the foreward rate constants for the VMWBM, VMZCR, VMPR and BDH sphalerites.

In order to improve the fit of final models to the data in which ϕ_o and $[H_2SO_4]_o$ were varied, pre-exponential constants may be calculated using values of the rate constants appearing previously and using the activation energy values summarised in table 3.8. Thus -

$$A_e = \frac{k_{11} \text{ or } k_{16}}{\exp\left(\frac{-E_a}{318,0}\right)} \quad \ldots\ldots\ldots \quad 3.40$$

Table 3.9 summarises the k_{11} or k_{16} values (including the equation no. containing these values) and the E_a values used to calculate A_E. It is these calculated values of A_E which are used in the final models.

Sphalerite (—)	k_{11} or k_{16} (—)	Equation number (—)	E_a x 10^{-6} (J/kg-mol)	Calculated A_E (kg-mol/m².min)
VMWBM	$3,726 \times 10^{-4}$	3.12	39,43	1 126,0
VMZCR	$3,996 \times 10^{-4}$	3.13	47,75	28 130,0
BDH	$1,64 \times 10^{-4}$	3.16	40,17	665,5
VMPR	$3,8 \times 10^{-6}$	3.18	45,13	99,24

TABLE 3.9 SUMMARY OF PRE-EXPONENTIAL CONSTANTS A_E CALCULATED USING EQUATION 3.40

3. 2. 7 FINAL FORM OF THE INITIAL RATE EQUATIONS

A general initial rate equation may be represented as follows :

$$r_o = \frac{\Phi_o^m \; A_E \exp\left(\frac{-E_a}{RT}\right) [H^+]_o^m}{\left(1,0 + K_{H^+}[H^+]_o + K_{Zn^{2+}}[Zn^{2+}]_o + K_{H_2S}[H_2S]_o\right)^m} \quad \ldots\ldots\ldots \; 3.41$$

Table 3. 10 summarises the values of all the constants in equation 3. 41 for the VMWBM, VMZCR, BDH and the VMPR sphalerites.

The calculated initial rates obtained on inserting the constants on table 3. 10 into equation 3. 41 for each sphalerite are reported in tables 3. 3 to 3. 6 . Figures 3. 14 to 3. 17 plot the $(r_o)_{exp}$ and $(r_o)_{fit}$ values versus the calculated initial rate $(r_o)_{calc}$ values reported in tables 3. 3 to 3. 6 . Generally a very good fit is observed for each sphalerite.

3. 2. 8 REASONS FOR REJECTING MECHANISM 1 IN FAVOUR OF MECHANISM 2

The following reasons are offered as justification for selecting mechanism 2 rather than mechanism 1 to describe the kinetics of sphalerite leaching under case (i) conditions ($[Fe^{3+}]_o = 0,0$) .

a) The initial rate forms of models F and G based on the dual site kinetics proposed in mechanism 2 have been shown to fit the

Sphalerite Type	m	A_E	E_a x 10^6	K_{H^+}	$K_{Zn^{2+}}$	K_{H_2S}
V M W B M	1,0	1 126,0	39,43	0,4674	35,0	0,0
V M Z C R	1,0	28 130,0	47,75	0,5954	45,0	0,0
B D H	1,0	655,5	40,17	0,0	0,0	0,0
V M P R	2,0	99,2	45,13	0.0	95,53	36,4

T A B L E 3. 1 0 SUMMARY OF CONSTANTS APPEARING IN THE GENERAL INITIAL RATE LEACHING EQUATION 3. 41

——— Line representing 1:1 correspondence between $(r_o)_{exp}$ or $(r_o)_{fit}$ and $(r_o)_{calc}$.

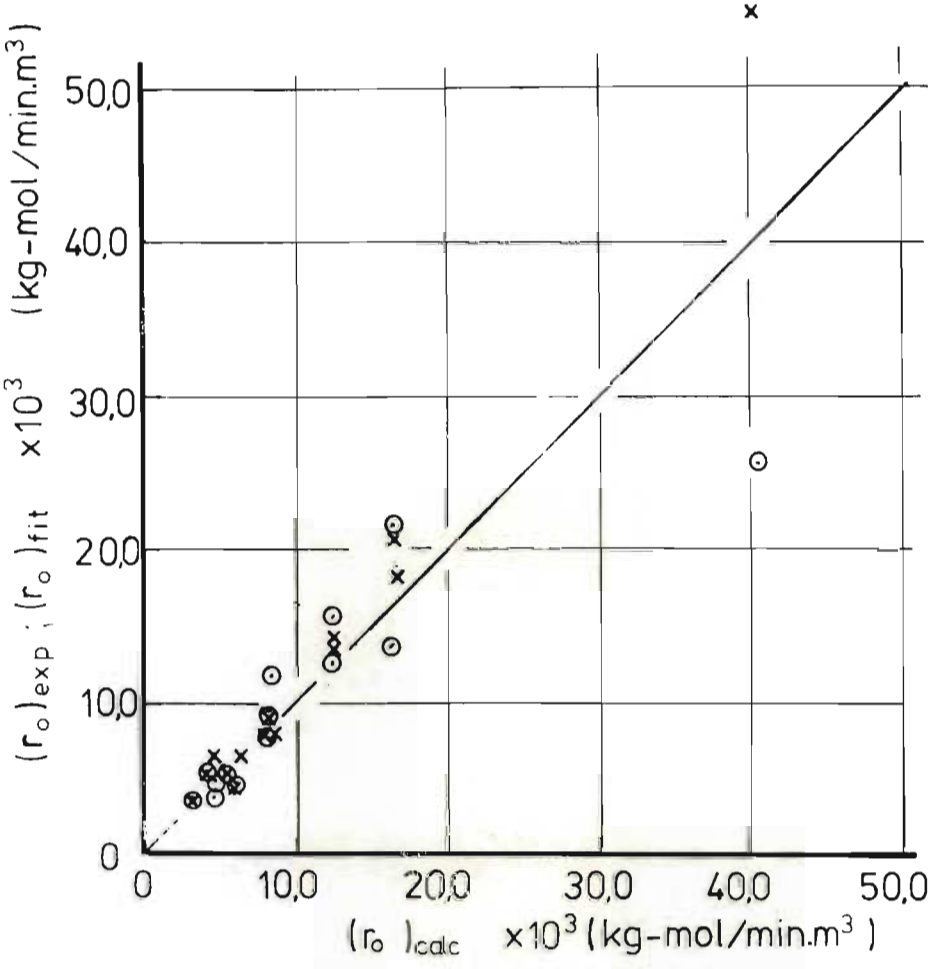

Figure 3.14 Comparison between initial rate values calculated using eqn. 3.41 with experimental and fitted initial rate values for the VM/NBM spalerite. All values are presented in table 3.3

——— Line representing 1:1 correspondence between $(r_o)_{exp}$ or $(r_o)_{fit}$ and $(r_o)_{calc}$.

legend ⊙ $(r_o)_{exp}$

× $(r_o)_{fit}$

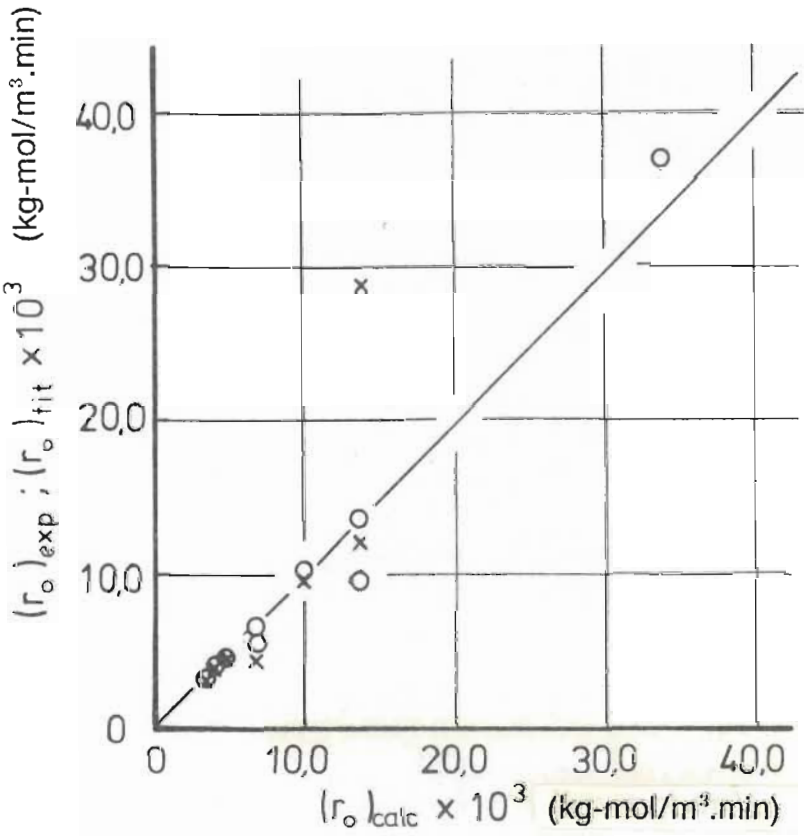

Figure 3.15 Comparison between initial rate values calculated using eqn. 3.41 with experimental and fitted initial rate values for the VMZCR sphalerite. All values are presented in table 3.4

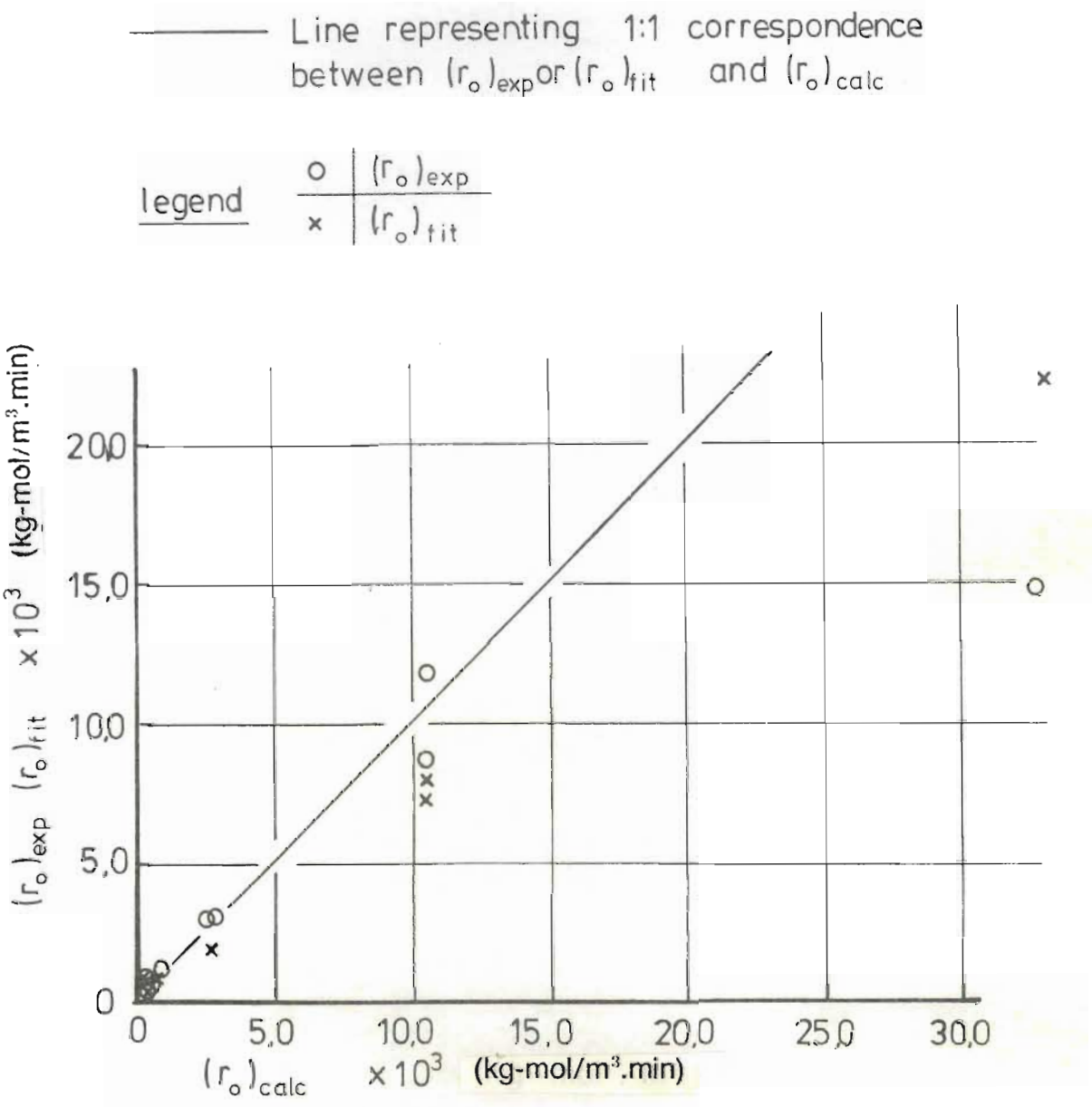

Figure 3.16 Comparison between initial rate values calculated using eqn. 3.41 with experimental and fitted initial rate values for the VMPR sphalerite. All values are presented in table 3.5.

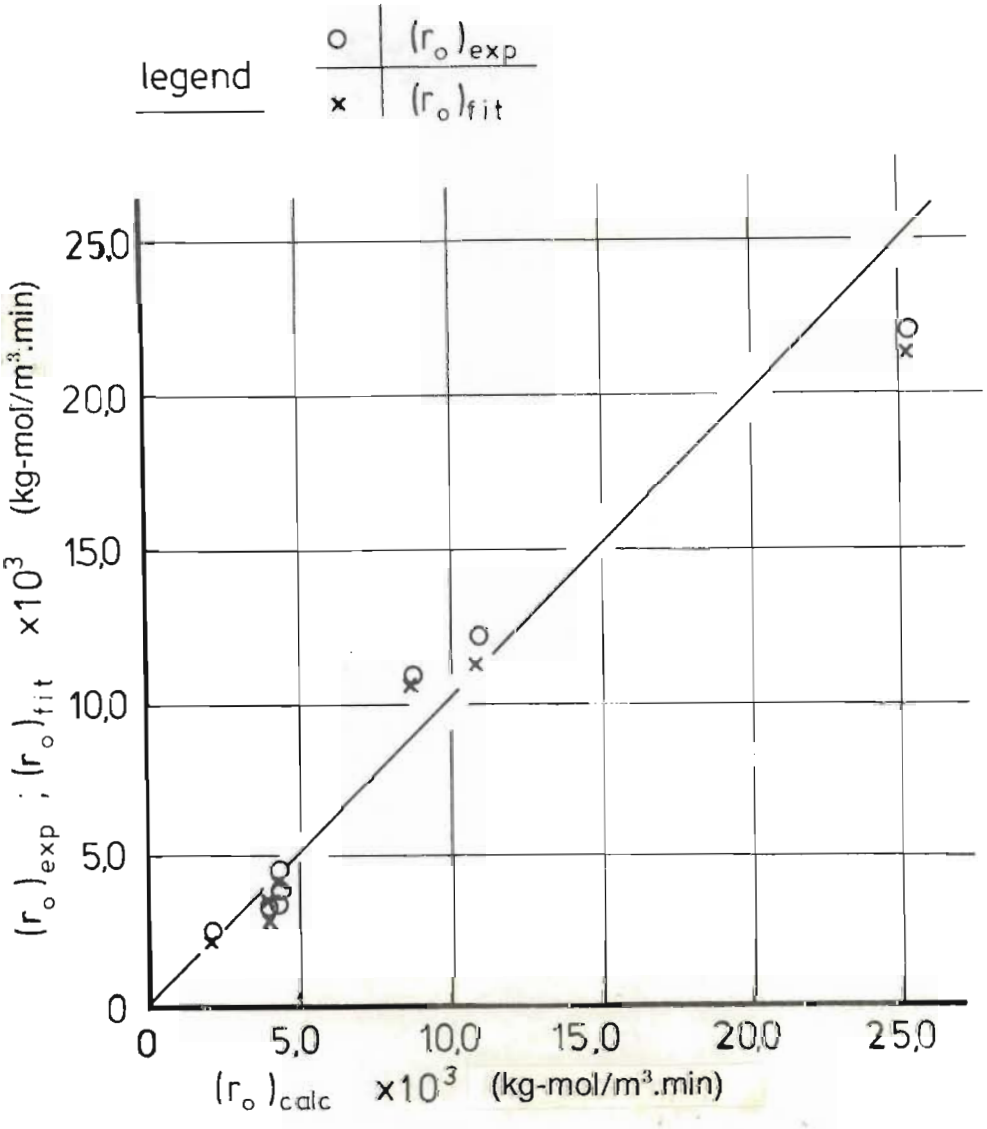

Figure 3.17 Comparison between initial rate values calculated using eqn. 3.41 with experimental and fitted initial rate values for the BDH sphalerite. All values are presented in table 3.6

initial leaching rate behaviour of the VMWBM, VMZCR and BDH sphalerites (model F) and of the VMPR sphalerite (model G). On the other hand none of the sphalerites exhibited 1st and 2nd order dependencies on the initial area and $[H^+]_o$ respectively as predicted by model B based on the single site kinetics proposed in mechanism 1.

b) When the H^+, Zn^{2+} and H_2S species adsorb only weakly so that their adsorption equilibrium constants may be considered to be zero, the overall form of model F (equation 2.81) reduced to exactly the same form of equation as that derived empirically by Romankiw (1962). This is not the case for model A, which demonstrates 1st order dependencies of the reverse reaction on $[Zn^{2+}]$ and $[H_2S]$ and an inverse dependency of the reverse reaction on $[H^+]$.

3.3 EXPERIMENTAL TESTING OF CASE (ii) MODELS ($[Fe^{3+}]_o : [H_2SO_4]_o \cong 1,8$)

Introduction

In this section model H (equation 2.95) is tested by fitting it to the experimental initial rate results of leaching granular WBM, ZCR and PR; finely milled VMWBM, VMZCR and VMPR, and synthetic

BDH sphalerite in acidic ferric sulphate media with $[Fe^{3+}]_o : [H_2SO_4]_o \geq 1,8$. Model C (equation 2.52) is identical in form to model H and is thus not referred to further.

The original objective of the experiments reported in this section was to leach the different sphalerites to various extents of zinc recovery, and then measure the surface areas of the leached particles (after washing S^o off, using CCl_4). Thus the leaching conditions were not selected primarily to study the effects of different variables (e.g. solids mass; $[Fe^{3+}]$; $[H_2SO_4]$; temperature; agitation; $[Zn]_o$ etc.) on the leaching rate, but were basically chosen for the following reasons:

a) Sufficient solids were required to give significantly measurable B.E.T. areas using the Strohlein apparatus, both before and after leaching.

b) Stoichiometrically sufficient $[Fe^{3+}]_o$ was required to permit a given mass of sphalerite solids to be leached to the desired extent.

c) For a given solids mass and $[Fe^{3+}]_o$ the temperature was selected so that the leaching rate would proceed sufficiently slowly so as to permit initial rate samples to be taken and filtered without excessive error; but not so slow as to require excessive time to achieve the desired final

extent of zinc dissolution.

d) Preliminary experiments in which free acid was initially added proceeded slowly and subsequently no H_2SO_4 was added. It was found that on dissolving the ferric sulphate crystals in sufficient double de-ionised distilled water to produce 1,0 ℓ solution, that measureable H_2SO_4 was formed in such a way that $[Fe^{3+}]_o : [H_2SO_4]_o \geq 1,8$. The H_2SO_4 formed in this way remained essentially measureably constant even after most of the Fe^{3+} had been reduced to Fe^{2+}.

Unfortunately the same reagent grade Japanese manufactured ferric sulphate crystals used to perform the bulk of the research was unobtainable towards the end of the project. Consequently a less pure technical grade of ferric sulphate powder (marketed by the British Drug House Company) was used for a few of the final experiments.

Something was present in the alternative ferric solution which seriously interfered with the H_2SO_4 determination technique, and reproducible H_2SO_4 analyses could not be performed and are consequently not presented.

All the experimental data supporting the results used in this section are comprehensively reported in tabular form in Appendix J. Besides reporting initial leaching conditions and measured $[Zn^{2+}]$, $[Fe^{3+}]$ and $[H_2SO_4]$ versus

time rate data, the tables report additional results such as final specific surface area; total filtered dry residue mass; recovered S^o mass etc. for those experiments in which these values were determined.

3. 3. 1 EXPERIMENTAL INITIAL RATE RESULTS

Tables 3.11 to 3.14 (facing figures 3. 18 to 3.21) summarise the experimental conditions and initial rate results for the different sphalerites used.

The initial rate $r_o = \left(\frac{d\,[Zn^{2+}]}{d\,t}\right)_o$ was obtained by measuring the initial slope of the $[Zn^{2+}]_o$ versus time rate curve. The rate curve was obtained by plotting the $[Zn^{2+}]$ versus time data and visually fitting a smooth curve through the data points.

In the case of the ZCR sphalerite, the rate curves frequently never passed through the origin. This probably resulted from oxidised Zn O coating on the sphalerite surface dissolving very rapidly relative to the slow rate of dissolution of the Zn S . Although attempts were made to minimise this effect, by washing the sphalerite in dilute acid during pre-treatment, not all of the oxidised material may have been removed.

The rate curve was consequently smoothed through the data to intercept the vertical axis at some $[Zn^{2+}]$ value (referred to as $[Zn^{2+}]_o$ for the case (ii) data),

and the initial rate was measured by visually fitting a straight line to the curve where it intercepts the Y - axis at the $Zn^{2+}{}_o$ value.

According to model H (equation 2.95) the initial rate :-

$$r_{H_o} = k_{18}\ \Phi_o\ \frac{[Fe^{3+}]_o}{[H^+]_o} \quad \ldots\ldots\ldots \quad 3.42$$

Let $r_{H_o}^{*}$ be the specific initial rate, i.e. -

$$r_{H_o}^{*} = r_{H_o} / \Phi_o \quad \ldots\ldots\ldots \quad 3.43$$

The reaction rate constant k_{18} is then :-

$$k_{18} = r_{H_o}^{*}\ \frac{[H^+]_o}{[Fe^{3+}]_o} \quad \ldots\ldots\ldots \quad 3.44$$

Figure 3.18 presents Arrhenius type plots of log k_{18} versus $\frac{1}{T}$ for the WBM, VMWBM and BDH sphalerites.

Figures 3.19 and 3.20 present similar plots for the ZCR and VMZCR sphalerites, and PR and VMPR sphalerites. Since most of the experiments using the granular WBM, ZCR and PR sphalerites were done using -90,0 + 75,0μm or -75,0 + 63,0μm size fractions, best fit straight lines have been visually fitted through the data points corresponding to these two size fractions. These lines provide reference values with which to make qualitative observations regarding the effects of particle size, the effect of vibratory milling of each type of sphalerite and permit comparison between the leaching

Table (-)	Size Fraction x 10^6 (m)	Temp. (K)	M_o (kg)	A_o (m^2/kg)	$[Fe^{3+}]_o$ (kg-mol/m^3)	$[H_2SO_4]_o$ (kg-mol/m^3)	$r_{H_o} \times 10^3$ (kg-mol/m^3 min)	$r_{H_o}^{*} \times 10^6$ (kg-mol/min.m^2)	$k_{18} \times 10^6$ (kg-mol/min.m^2)
J 1	-125,0 + 106,0	358,0	0,1	65,0	0,9848	N.D.	1,92	295,4	N.D.
J 2	- 90,0 + 75,0	318,0	0,15	80,0	1,039	0,822	0,667	55,58	43,97
J 3	- 75,0 + 63,0	343,0	0,1	80,0	0,824	0,337	3,3	412,5	168,7
J 4	- 75,0 + 63,0	355,5	0,1	80,0	0,795	0,298	4,29	535,7	201,0
J 5	- 75,0 + 63,0	368,0	0,1	80,0	1,504	0,561	12,5	1 563,0	582,8
J 6	- 32,0 + 24,0	318,0	0,05	140,0	0,2256	0,1224	0,555	79,29	29,31
J 7	- 24,0 + 17,0	318,0	0,05	320,0	0,217	0,123	1,0	62,50	35,43
J 8	- 17,0 + 12,0	323,0	0,03	420,0	0,1468	0,0612	0,58	46,69	19,46
J 9	VMWBM	318,0	0,02	3 272,0	0,1504	0,051	2,1	32,1	10,88
J 10	VMWBM	338,0	0,02	3 272,0	0,3044	0,0735	6,9	105,0	25,46

TABLE 3. 11 SUMMARY OF CONDITIONS AND INITIAL RATE RESULTS FOR WBM AND VMWBM SPHALERITES LEACHING UNDER CASE (ii) CONDITIONS

Table (-)	Temp. (K)	M_o (kg)	A_o (m^2/kg)	$[Fe^{3+}]_o$ (kg-mol/m^3)	$[H_2SO_4]_o$	$r_{H_o} \times 10^3$ (kg-mol/m^3 min)	$r_{H_o}^{*} \times 10^6$ (kg-mol/min.m^2)	$k_{18} \times 10^6$ (kg-mol/min.m^2)
J 44	323,0	0,05	7 200,0	0,290	0,111	9,0	25,0	9,569
J 45	343,0	0,02	7 200,0	0,1432	0,063	6,0	41,67	18,32
J 46	343,0	0,02	7 200,0	0,292	0,107	11,6	80,56	29,52
J 47	353,0	0,05	7 200,0	0,580	0,223	38,0	105,6	40,58

TABLE 3. 12 SUMMARY OF CONDITIONS AND INITIAL RATE RESULTS FOR BDH SPHALERITE LEACHING UNDER CASE (ii) CONDITIONS

a best fit line through -90.0 + 75.0 μm and -75.0 + 63.0 μm data points.

b best fit line through BDH sphal. data points.

legend

	Size fraction (μm)	
×	-90.0 + 75.0	WBM sphalerite
●	-75.0 + 63.0	
✡	-32.0 + 24.0	
+	-24.0 + 17.0	
Δ	-17.0 + 12.0	
✣	VMWBM sphalerite	
□	BDH sphalerite	

Note: exptl. conditions for each data point are summarised on tables 3.11 and 3.12.

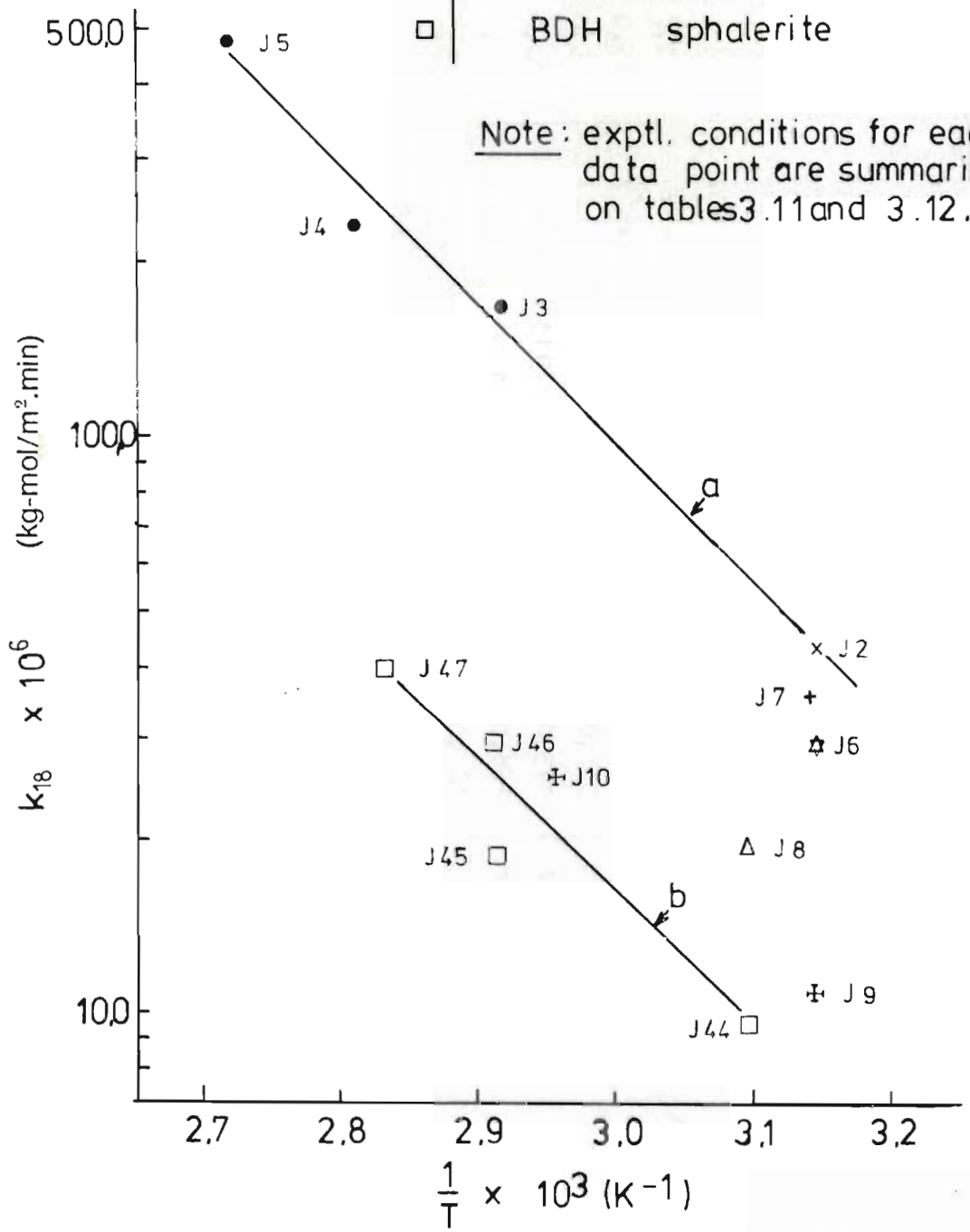

Figure 3.18 Arrhenius plot demonstrating the effect of temperature on k_{18} (as defined by eqn 3.44) for the WBM; VMWBM and BDH sphalerites.

Table (-)	Size Fraction x 10^6 (m)	Temp. (K)	M_o (kg)	A_o (m^2/kg)	$[Fe^{3+}]_o$ (kg-mol/m^3)	$[H_2SO_4]_o$ (kg-mol/m^3)	$[Zn^{2+}]_o$ x 10^3 (kg-mol/m^3)	r_{H_o} x 10^3 (kg-mol/m^3.min)	$r^*_{H_o}$ x 10^6 (kg-mol/min.m^2)	k_{18} x 10^6 (kg-mol/min.m^2)
J 11	-212,0	303,0	0,02	450,5	0,376	0,184	6,8	0,101	11,20	5,486
J 12	-212,0	323,0	0,02	450,5	0,376	0,184	6,4	0,372	41,28	20,17
J 13	-212,0	358,0	0,02	450,5	0,376	0,194	27,91	1,176	130,52	67,34
J 14	-212,0	373,0	0,02	450,5	0,376	0,184	22,9	2,357	261,59	131,20
J 15	-106,0 + 90,0	343,0	0,02	140,0	0,383	0,188	9,2	0,421	150,4	73,80
J 16	-106,0 + 90,0	358,0	0,05	140,0	N.D.	N.D.	15,0	1,867	266,7	N.D.
J 17	-106,0 + 90,0	368,0	0,02	140,0	0,362	0,19	3,3	2,32	828,6	434,9
J 18	-106,0+ 90,0	368,0	0,05	140,0	0,927	0,469	15,0	6,0	857,1	426,0
J 19	-90,0 + 75,0	338,0	0,05	150,0	0,304	N.D.	5,0	0,97	129,3	N.D.
J 20	-90,0 + 75,0	343,0	0,05	150,0	0,913	0,459	10,0	2,4	320,0	159,5
J 21	-90,0 + 75,0	368,0	0,1	150,0	1,49	0,804	30,0	11,75	783,3	422,7
J 22	-90,0 + 75,0	368,0	0,1	150,0	0,902	0,475	25,0	11,96	797,3	419,9
J 23	-75,0 + 63,0	323,0	0,1	150,0	0,886	0,454	18,0	1,32	88,0	45,09
J 24	-45,0 + 38,0	343,0	0,02	185,0	0,367	0,186	3,3	0,914	247,0	125,2
J 25	-45,0 + 38,0	368,0	0,02	185,0	0,367	0,188	3,0	3,44	929,7	478,8
J 26	-45,0 + 38,0	368,0	0,01	185,0	0,362	0,188	1,0	2,5	1 351,3	701,8
J 27	-17,0 + 12,0	323,0	0,02	420,0	0,145	0,059	4,0	0,33	39,29	16,0
J 28	VMZCR	318	0,02	2 708,0	0,144	0,0633	0	3,50	64,62	28,41
J 29	VMZCR	338	0,02	2 708,0	0,299	N.D.	0	7,00	129,2	N.D.

TABLE 3.13 SUMMARY OF LEACHING CONDITIONS AND INITIAL RATE RESULTS FOR ZCR AND VMZCR SPHALERITES LEACHING UNDER CASE (ii) CONDITIONS

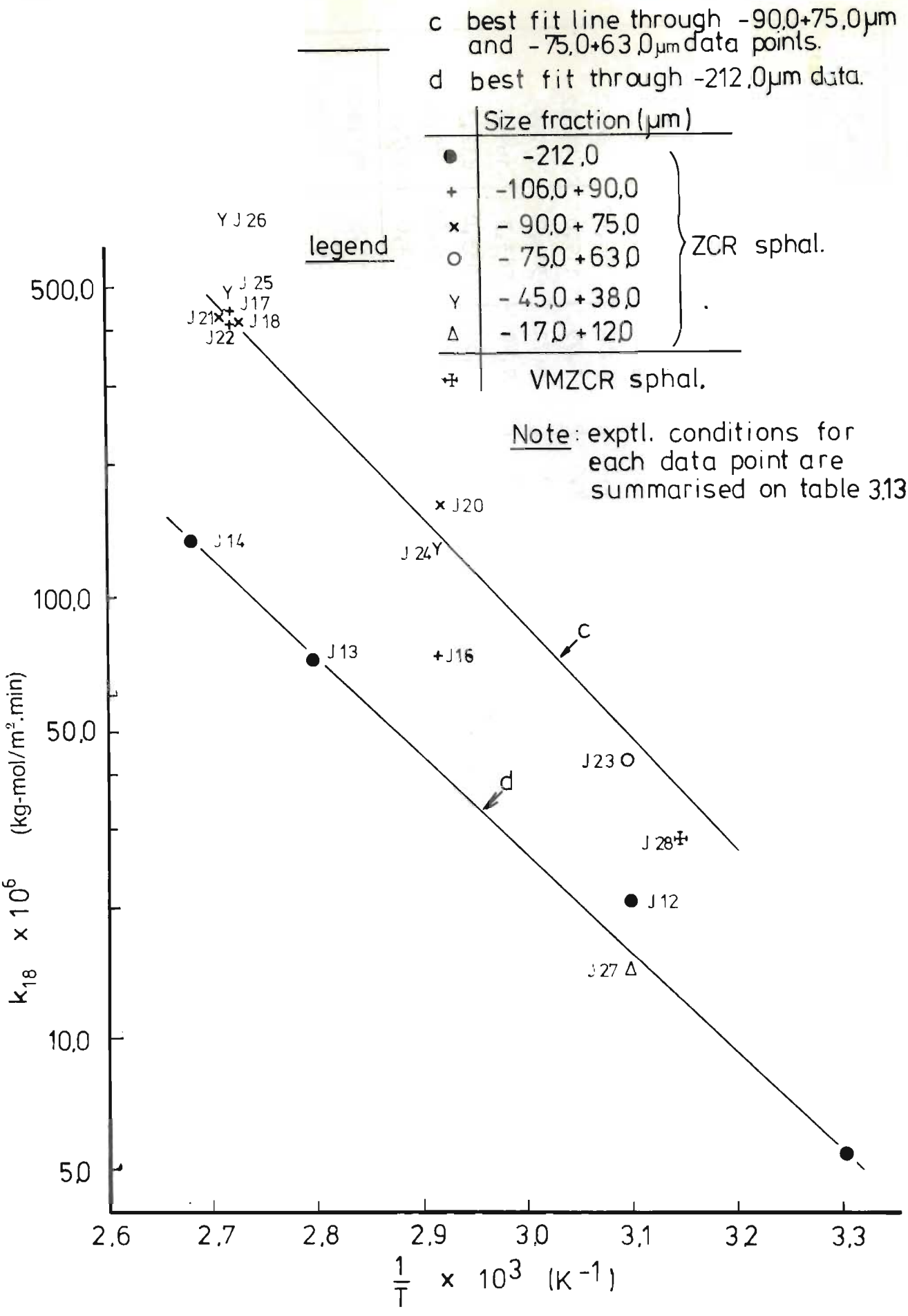

Figure 3.19 Arrhenius type plot demonstratating the effect of temperature on k_{18} (where k_{18} is defined by eqn. 3.44) for ZCR and VMZCR sphalerite.

Table (-)	Size Fraction x 10^6 (m)	Temp. (K)	M_o (kg)	A_o (m^2/kg)	$[Fe^{3+}]_o$	$[H_2SO_4]_o$	$[Zn^{2+}]_o$ x10^3	r_{H_o} x 10^3 (kg-mol/ min.m^3)	$r^*_{H_o}$ x 10^6	k_{18} x 10^6
					(kg-mol / m^3)				(kg-mol/min.m^2)	
J 30	-106,0 + 90,0	318,0	0,02	140,0	0,344	N.D.	2,0	0,40	46,40	N.D.
J 31[2]	-106,0 + 90,0	318,0	0,05	140,0	0,466	0,631	142,0[2]	0,08	11,43	15,48
J 32	-90,0 + 75,0	343,0	0,15	150,0	0,763	0,413	0	6,88	305,8	96,36
J 33[1]	-90,0 + 75,0	343,0	0,1	764,0[1]	0,412	0,222	0	5,3	69,37	37,38
J 34	-75,0 + 63,0	308,0	0,05	150,0	0,14	0,063	1,3	0,21	28,0	12,6
J 35	-75,0 + 63,0	318,0	0,05	150,0	0,279	0,111	2,0	0,50	66,67	26,52
J 36	-75,0 + 63,0	323,0	0,1	150,0	0,802	0,296	4,0	1,79	119,0	43,92
J 37	-75,0 + 63,0	343,0	0,1	150,0	0,877	0,444	0	5,71	380,7	192,7
J 38	-75,0 + 63,0	358,0	0,08	150,0	0,716	0,155	0	9,40	783,3	169,6
J 39	-75,0 + 63,0	368,0	0,1	150,0	0,806	0,322	0	30,50	2033,0	812,3
J 40	-24,0 + 17,0	318,0	0,03	320,0	0,225	0,873	3,0	0,2	20,83	80,83
J 41	-17,0 + 12,0	323,0	0,02	420,0	0,147	0,062	3,0	2,13	254,0	107,1
J 42	VMPR	318,0	0,02	2630,0	0,1432	0,0633	0	23,75	451,5	199,6
J 43	VMPR	318,0	0,02	2630,0	0,308	N.D.	0	24,0	456,3	N.D.

1) The CCl_4 washed residue from the run reported on table J 33 was used in this experiment.
2) The leach solution used in this experiment contained 0,8 ℓ of the final filtered solution of the experiment reported on table J 2.

TABLE 3.14 SUMMARY OF CONDITIONS AND INITIAL RATE RESULTS FOR PR AND VMPR SPHALERITE LEACHING UNDER CASE (ii) CONDITIONS

e best fit line through -90,0 + 75,0 μm and -75,0 + 63,0 μm data points.

legend	Size fraction (μm)	
+	-106,0 + 90,0	PR sphalerite
×	- 90,0 + 75,0	
o	- 75,0 + 63,0	
Y	- 24,0 + 17,0	
Δ	- 17,0 + 12,0	
✢	VMPR sphalerite	

Note: exptl. conditions for each data point are summarised on table 3.14

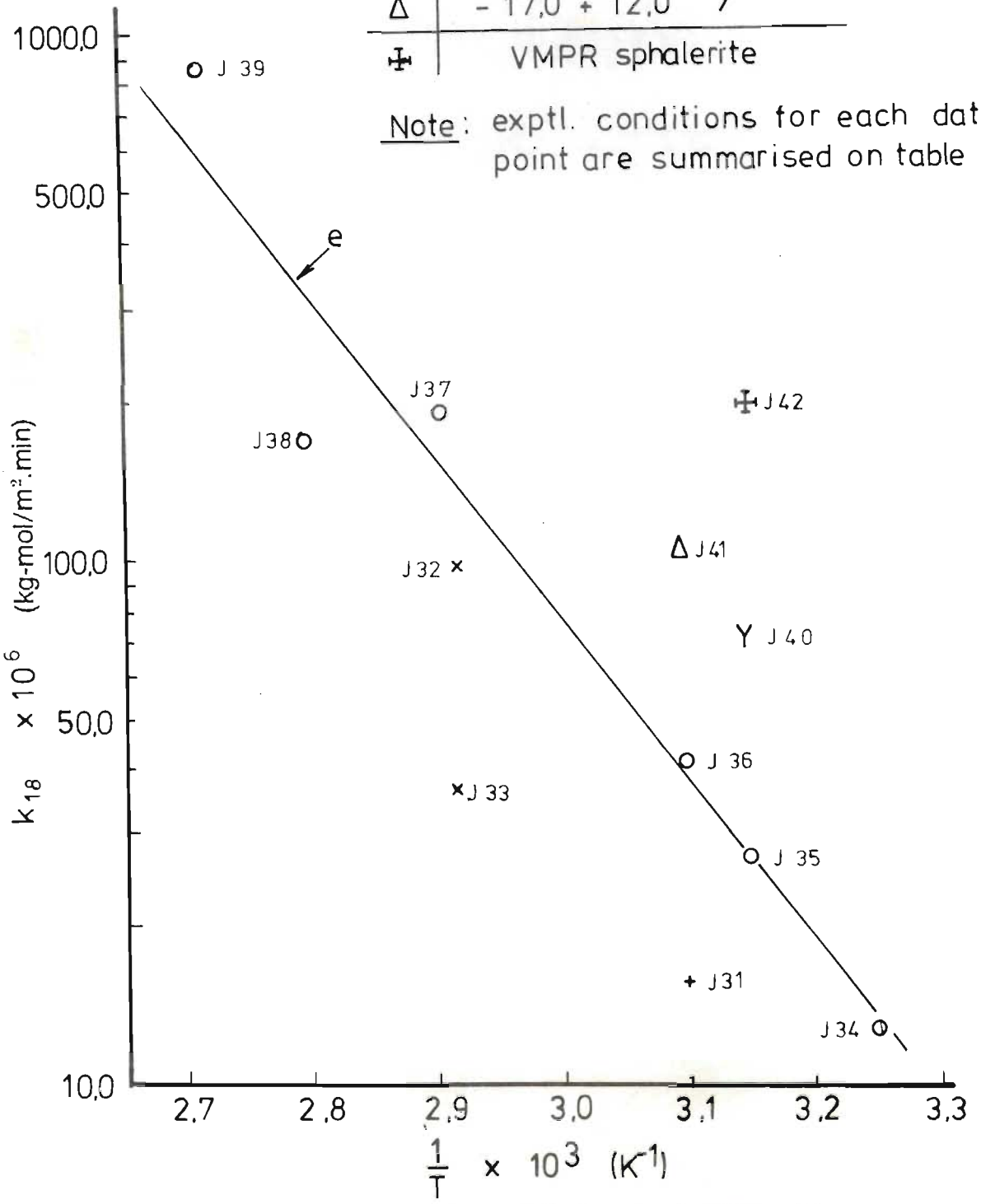

Figure 3.20 Arrhenius plot demonstrating the effect of temperature on k_{18} (where k_{18} is defined by eqn. 3.44) for the PR and VMPR sphalerites.

behaviour of different sphalerites with each other and with the BDH synthetic sphalerite.

The results for each of the sphalerites are now discussed individually.

3.3.1.1 WBM, VMWBM AND BDH SPHALERITE RESULTS

From figure 3.18 the following observations are made :

a) The line 'a' fits very well through the -90,0 + 75,0μm and -75,0 + 63,0μm WBM sphalerite size fraction data points. This suggests that over a narrow size range model H represented by equation 3.42 fits the WBM sphalerite data.

b) The activation energies represented by the slopes of the best fit lines 'a' and 'b' through the WBM and the BDH sphalerite data points are virtually identical, i.e. $E_a = -45{,}62 \times 10^6$ J / kg - mole for the WBM sphalerite and $E_a = -45{,}38 \times 10^6$ J / kg - mole for the BDH sphalerite.

c) In order to observe the effect of particle size on the leaching rate, a specific initial rate constant ratio $\lambda(\bar{D})$ is proposed as follows :

$$\lambda(\bar{D}) = \frac{k_{18}}{(k_{18})_{ref}} \qquad \ldots\ldots\ldots \quad 3.45$$

where -

k_{18} is defined by equation 3.44 ;

$(k_{18})_{ref}$ = the value of the best fit reference line 'a' on figure 3.18 at a given value of $\frac{1}{T}$;

$\overline{D}$ = arithmetic mean of the size fraction upper and lower limits (e.g. $\overline{D} = \frac{90,0 + 75,0}{2,0}$ µm for the -90,0 + 75,0 µm size fraction).

Figure 3.21 plots $\lambda(\overline{D})$ versus $\overline{D}$ for the WBM, VMWBM and BDH sphalerites. It has been assumed that the mean diameters $\overline{D}$ of the VMWBM and BDH sphalerite particles are each about 1,0µm. (Romankiw took scanning electron microscope photographs of synthetic sphalerite with a specific surface area of about 500,0 m^2/kg and estimated the mean particle diameter to be about 0,15µm).

Curve 'f' on figure 3.21 represents the best fit through the data points, and it is evident that $\lambda(\overline{D})$ decreases with decreasing $\overline{D}$. No explanation for this phenomenon is offered at this stage, and this aspect will be considered further in section 3.3.2 when the shape of the $\lambda(\overline{D})$ versus $\overline{D}$ curves of the different sphalerites are compared.

3.3.1.2 ZCR AND VMZCR SPHALERITE RESULTS

From figure 3.19 the following observations are made:

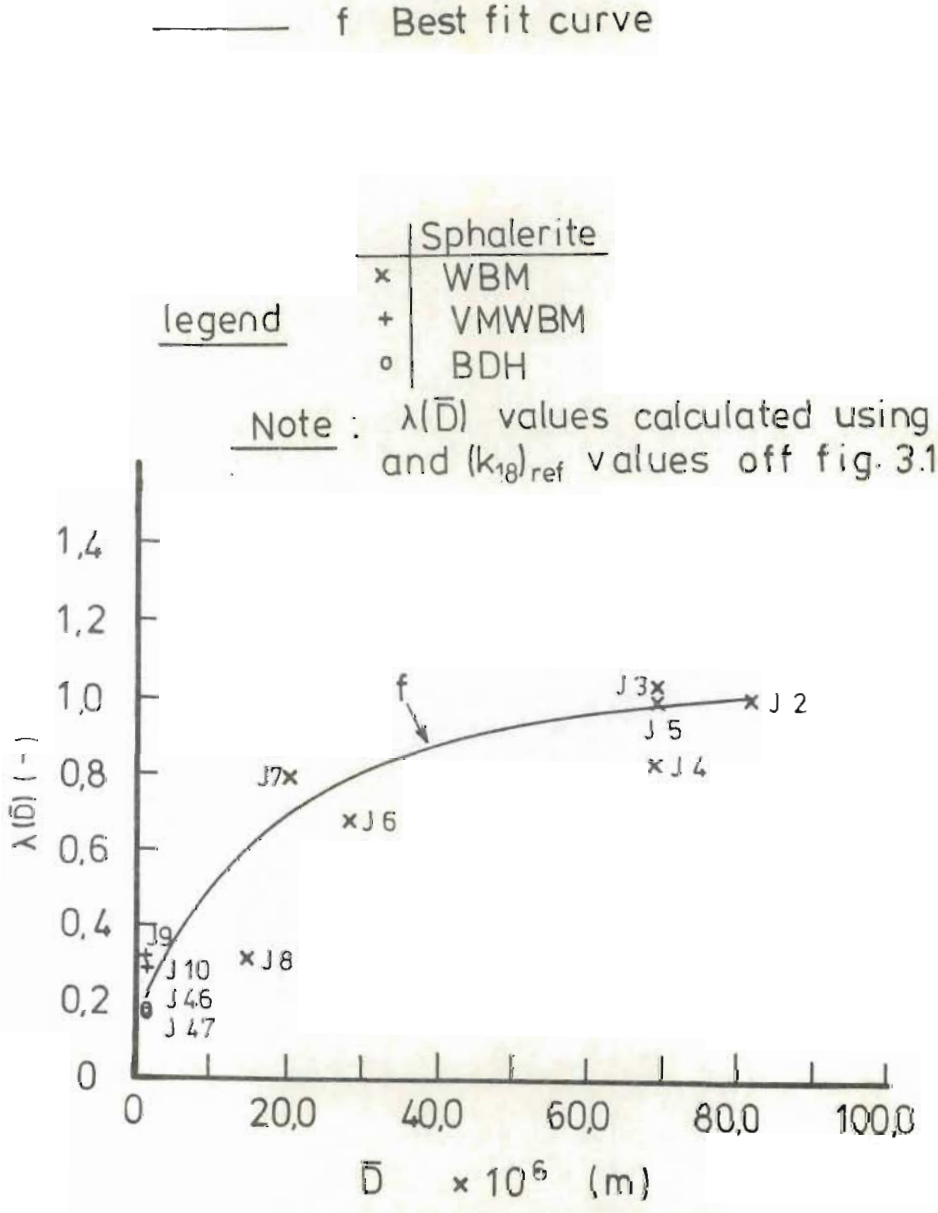

Figure 3.21 Mean diameter $\bar{D}$ versus rate constant ratio $\lambda(\bar{D})$ - (where $\lambda(\bar{D})$ is defined by equation 3.45) for the WBM, VMWBM and BDH sphalerites.

a) The line 'c' fits reasonably well through the rather limited -90,0 + 75,0 μm and 75,0 + 63,0 μm size fraction data points. This suggests that over a narrow size range model H represented by equation 3.41 fits the ZCR sphalerite data. The line 'd' fits reasonably well through the -212,0 μm fraction ZCR sphalerite, but at a consistently lower absolute value. The -212,0 μm size fraction contains all the very fine material including possibly gangue, which has been removed from the courser size fractions (e.g. -90,0 + 75,0 μm).

A significant proportion of the specific surface area for the -212,0 μm size fraction could therefore have been contributed by non-sphaleritic material, resulting in the observed lower values for the rate constant k_{18}.

b) Figure 3.22 represents a plot of $\lambda(\overline{D})$ versus $\overline{D}$ for the ZCR and VMZCR sphalerites (where $(k_{18})_{ref}$ represents values of the line 'c' on figure 3.19 at given values of $\frac{1}{T}$). The data points are rather scattered. The best fit line demonstrates that $\lambda(\overline{D})$ tends to decrease slightly as $\overline{D}$ decreases. This aspect is discussed further in section 3.3.2.

——— g Best fit curve.

legend		
	×	ZCR sphalerite
	+	VMZCR sphalerite

Note: $\lambda(\bar{D})$ values calculated using k_{18} and $(k_{18})_{ref}$ values off fig. 3.19

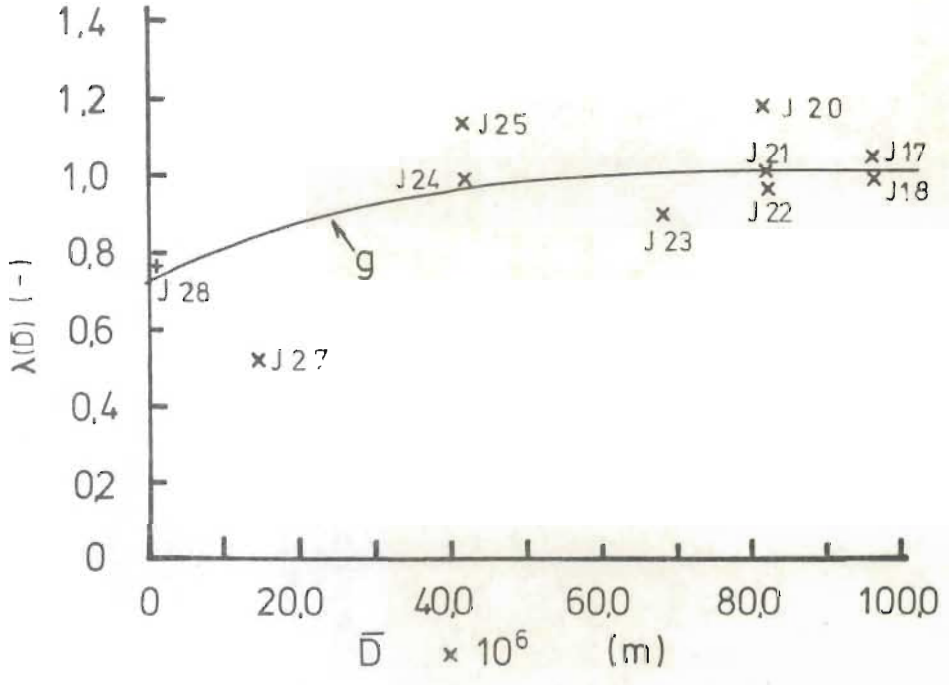

Figure 3.22 Mean diameter $\bar{D}$ versus rate constant ratio $\lambda(\bar{D})$ - (where $\lambda(\bar{D})$ is defined by equation 3.45) for the ZCR and VMZCR sphalerite.

3.3.1.3 PR AND VMPR SPHALERITE RESULTS

From figure 3.20 it is observed that:

a) The straight line 'e' fits the -90,0 + 75,0μm and -70,0 + 63,0μm size fraction data points reasonably well. This suggests that model H represented by equation 3.41 fits the PR initial rate sphalerite data.

b) Figure 3.23 plots $\lambda(\overline{D})$ versus $\overline{D}$ for the PR and VMPR sphalerites. (It has been assumed that the mean particle diameter for the VMPR sphalerite is approximately 1,0μm.) $\lambda(\overline{D})$ is observed to increase with decreasing $\overline{D}$ to a very large value for the VMPR sphalerite. This behaviour is remarkably different to that observed on figures 3.21 and 3.22 for the other sphalerites. This aspect is dealt with further, in the next section.

3.3.2 COMPARISON OF THE INITIAL RATE LEACHING BEHAVIOURS OF THE VARIOUS SPHALERITES

Figure 3.24 superimposes the best fit log k_{18} versus $\frac{1}{T}$ lines 'a' and 'b' (from figure 3.18), 'c' and 'd' (from figure 3.19) and 'e' (from figure 3.20) onto a common set of axes. Figure 3.25 superimposes the best fit $\lambda(\overline{D})$ versus $\overline{D}$ curves from figures 3.21, 3.22 and 3.23 onto a common set of axes.

——— h Best fit curve.

legend		
	×	PR sphalerite
	+	VMPR sphalerite

Note $\lambda(\bar{D})$ values calculated using k_{18} and $(k_{18})_{ref}$ values off fig. 3.20.

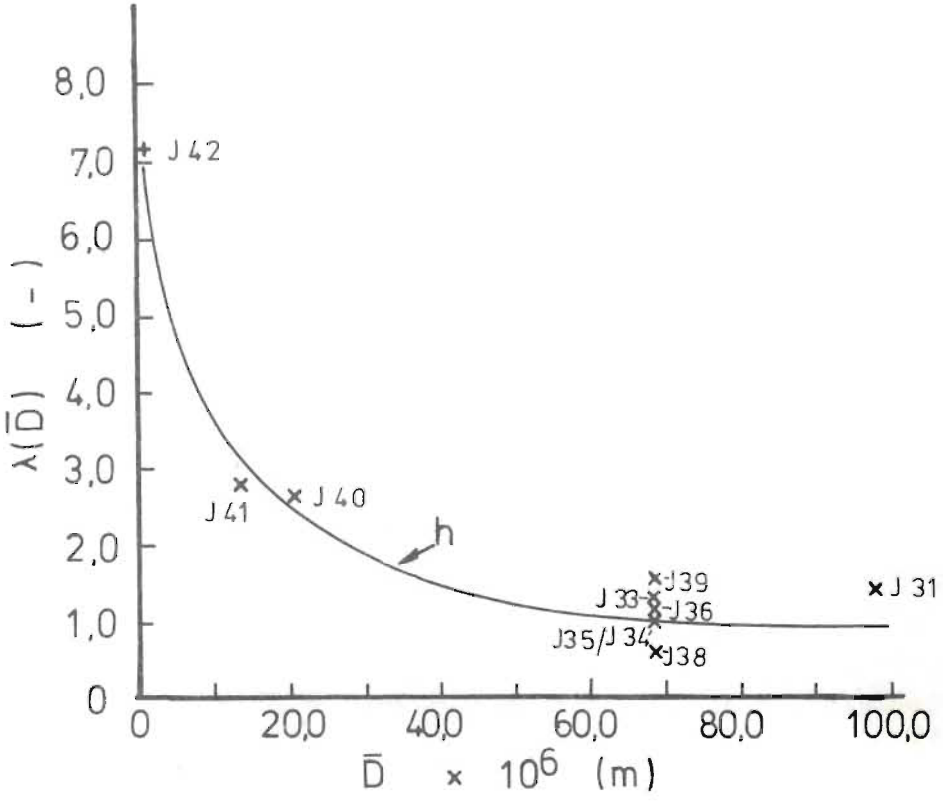

Figure 3.23 Mean diameter $\bar{D}$ versus rate constant ratio $\lambda(\bar{D})$ - (where $\lambda(\bar{D})$ is defined by equation 3.45) for the PR and VMPR sphalerites.

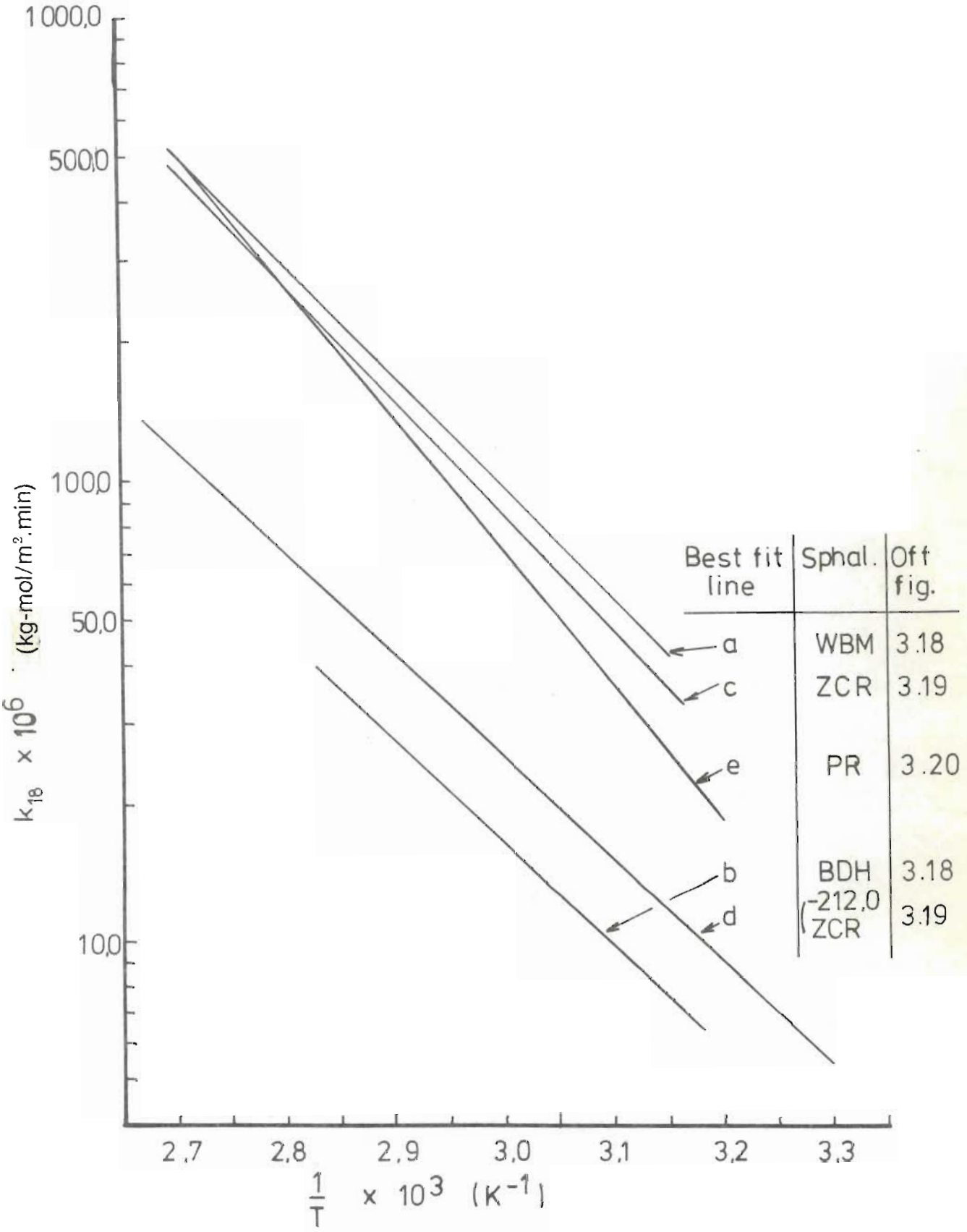

Figure 3.24 Comparison of best fit Arrhenius plots presented on figures 3.18 (WBM and BDH); 3.19 (ZCR) and 3.20 (PR).

legend	Best fit curve	Off fig.	Sphalerites
	f	3.21	WBM; VMWBM; BDH
	g	3.22	ZCR; VMZCR
	h	3.23	PR; VMPR

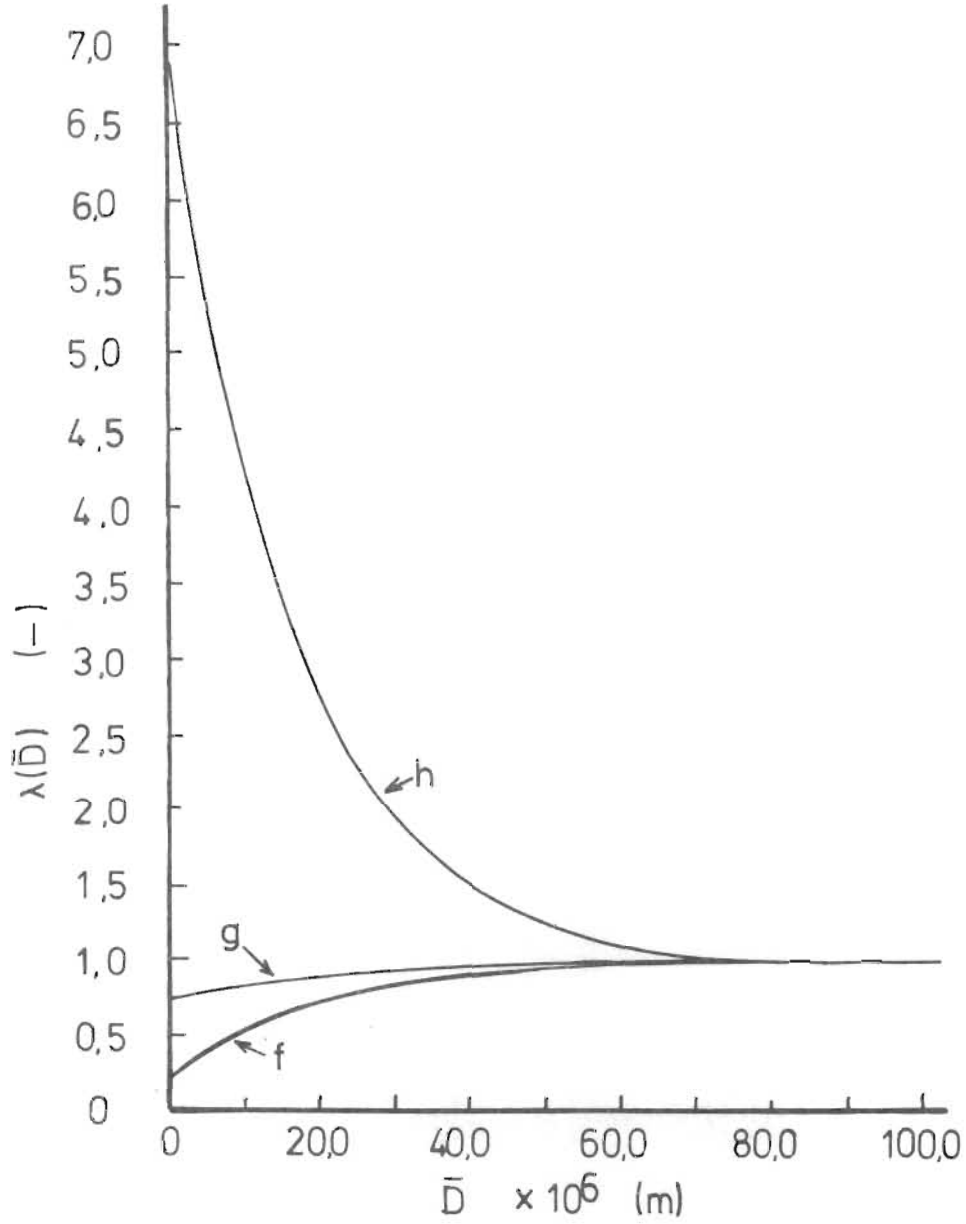

Figure 3.25 Comparison of best fit $\lambda(\bar{D})$ versus $(\bar{D})$ curves off figures 3.21; 3.22 and 3.23

Table 3. 15 summarises the pre-exponential constants and apparant activation energies represented by the best fit lines on figures 3. 18, 3. 19 and 3. 20 for the different sphalerites.

Table 3. 16 summarises the $\lambda(\bar{D})$ values for the BDH, VMWBM, VMZCR and VMPR sphalerites, along with the concentrations of the major impurities in these sphalerites (copper and iron).

From figures 3. 23 and 3. 24 and from tables 3. 16 and 3. 17 the following observations may be made :

a) The leaching rate constant k_{18} for the -90,0 + 75,0μm and -75,0 + 63,0μm size fractions of the WBM, ZCR and PR sphalerites are virtually identical (see figure 3. 23). This observation is in agreement with that made by Kuzminkh (1950) (i.e. that two mineralogically completely different sphalerites initially leached identically under comparable conditions in acidic ferric sulphate media). This observation also appears to justify the assumption made in developing model H that the initial leaching rate is Fe^{3+} adsorption rate controlling in a way which is independent of the chemical composition of the sphalerite.

b) From table 3. 15 it is apparant that except for the -212,0μm ZCR sphalerite the activation energies for the sphalerites increase

Sphalerite (-)	E_a x 10^{-6} (J/kg-mole)	A_E x 10^6	Best fit line (-)	Best fit line from fig. (-)	Copper Concentration (-)	Iron Concentration (-)
BDH	45,38	0,218	b	3.18	129,0 ppm	0,12 %
WBM	45,62	1,32	a	3.18	382,0 ppm	0,45 %
ZCR	48,33	3,11	c	3.19	155,0 ppm	7,25 %
PR	59,93	183,7	e	3.20	3,53 %	10,74 %
-212,0 ZCR	42,92	0,135	d	3.19	N. D.	N. D.

T A B L E 3.15 SUMMARY OF ACTIVATION ENERGIES E_a AND PRE-EXPONENTIAL CONSTANTS A_E FOR THE INDICATED BEST FIT LINES FOR LEACHING VARIOUS SPHALERITES UNDER CASE (ii) CONDITIONS ($[Fe^{3+}]_o : [H_2SO_4]_o \simeq 1,8$). CONCENTRATIONS OF MAJOR IMPURITIES (COPPER AND IRON) ARE ALSO SUMMARISED

Sphalerite (-)	Cu (-)	Fe (-)	$\lambda(\bar{D})$ (-)
BDH	129,0 ppm	0,12 %	0,19
VMWBM	382,0 ppm	0,45 %	0,3
VMZCR	155,0 ppm	7,25 %	0,75
VMPR	3,53 %	10,74 %	7,2

T A B L E 3. 16 SUMMARY OF CONCENTRATIONS OF MAJOR IMPURITIES (Cu and Fe) and $\lambda(\bar{D})$ FOR THE INDICATED SPHALERITES

N. B. $\lambda(\bar{D}) = \frac{k_{18}}{(k_{18})_{ref}}$ defined by equation 3. 45 .

with increasing degree of impurity of the sphalerite - i.e. BDH < WBM < ZCR < PR .

c) From figure 3. 24 it is evident that increasing the surface area of the various sphalerites by ball milling or vibratory milling, influences the leaching rate constants k_{18} for each sphalerite in unpredictable manners.

For the relatively pure WBM and VMWBM sphalerites decreasing $\bar{D}$ appears to decrease k_{18} significantly. For the moderately impure ZCR and VMZCR sphalerites, decreasing $\bar{D}$ decreases k_{18} only slightly. For the highly impure PR and VMPR sphalerites, decreasing $\bar{D}$ increases k_{18} significantly.

From table 3. 16 it is seen that $\lambda(\bar{D})$ hence leaching rate constants k_{18} for the BDH, VMWBM, VMZCR and VMPR sphalerites increase with increasing impurity content of the sphalerite, - i.e. BDH < VMWBM < VMZCR < VMPR . It appears then that vibratory milling does not cause the WBM or ZCR sphalerites to become 'activated' with respect to leaching in acidic ferric sulphate media.

The fact that the VMWBM and VMZCR sphalerites demonstrate virtually identical leaching characteristics in aqueous H_2SO_4 , is additional evidence that these sphalerites are not activated. The VMZCR sphalerite contained a much higher concentration of iron than the VMWBM sphalerite, but this did not appear to significantly influence its leaching characteristics.

Although $\lambda(\overline{D})$ (hence k_{18}) for the PR and VMPR sphalerites increases significantly with decreasing $\overline{D}$, the increase does not appear to depend on the mode of milling. It is possible that the increase in dissolution rate per unit area is related to the liberation and grinding of the chalcopyrite impurity.

Figure 6.17 presents a photomicrograph of etched PR particles. This figure and the observation of other polished sections of leached PR particles showed that dissolution occured preferentially in the vicinity of the occluded chalcopyrite zones. It is possible that -

a) the chalcopyrite dissolves -

$$Cu\,Fe\,S_2 + 4\,Fe^{3+} \longrightarrow Cu^{2+} + 5\,Fe^{2+} + 2\,S^{o}\ ; \qquad \ldots\ldots\ldots\ 3.46$$

b) the $Cu\,SO_4$ acts as a catalyst to accelerate the sphalerite dissolution :-

$$Cu\,SO_4 + Zn\,S \longrightarrow Cu\,S + Zn\,SO_4\ ; \qquad \ldots\ldots\ldots\ 3.47$$

c) the $Cu\,S$ dissolves and regenerates the Cu^{2+} ion :-

$$Cu\,S + 2\,Fe^{3+} \longrightarrow Cu^{2+} + 2\,Fe^{2+} + S^{o} \qquad \ldots\ldots\ldots\ 3.48$$

Accordingly the more finely dispersed the chalcopyrite is, the greater the catalytic effect on the dissolution of the sphalerite.

It is evident from the above that the large increase in k_{18} associated with fine milling of the PR sphalerite is not due to an activation of

the sphalerite crystal lattice. It is also evident that fine milling of the WBM and ZCR sphalerites does not result in any apparant activation, or increase in k_{18} taking place.

CHAPTER 4

TESTING OF OVERALL CASE (i) AND CASE (ii) RATE EQUATIONS

Introduction

In chapters 2 and 3 it was assumed that under initial rate conditions the initial active site concentration ϕ_o was proportional to the total specific surface area of the sphalerite solids (equation 2.1). In this chapter the way in which the active site concentration $\phi(X)$ changes during leaching under non-initial conditions is investigated.

It is assumed that the active site area change function $\phi(X)$ could possess one of the following forms:

1) $\phi(X)$ remains constant, i.e.:-

$$\psi_1(X) = \frac{\phi(X)}{\phi_o} = 1,0 \quad \ldots\ldots\ldots \quad 4.1$$

where $\psi(X)$ = Active site area ratio function.

2) $\phi(X)$ obeys shrinking core behaviour, i.e.:-

$$\psi_2(X) = \frac{\phi(X)}{\phi_o} = (1 - X)^{2/3} \quad \ldots\ldots\ldots 4.2$$

3) $\phi(X)$ varies in proportion to the B.E.T. measured specific surface area, i.e.:-

$$\psi_3(X) = \frac{\phi(X)}{\phi_o} = \eta(X) \quad \ldots\ldots 4.3$$

where $\eta(X)$ = specific area change function (as defined by eqn. F 4).

The form of $\eta(X)$ for each sphalerite was experimentally determined by measuring the specific surface area before and after leaching to various extents X. A Ströhlein area meter was used to perform single point B.E.T. N_2 adsorption measurements, and details concerning the apparatus, procedure and $\eta(X)$ determined for each sphalerite is presented in Appendix F.

4) $\phi(X)$ varies during leaching in a way which is uniquely characteristic for each sphalerite, i.e.:-

$$\psi_4(X) = \frac{\phi(X)}{\phi_o} \quad \ldots\ldots\ldots 4.4$$

where -

a) for the case (i) model F based on H^+ adsorption rate control (equation 2.81):-

$$\phi(X) = r_F \frac{(1{,}0 + K_{11}[H^+] + K_{22}[Zn^{2+}] + K_{23}[H_2S]_\ell)}{(k_{11}[H^+] - k_{13}[Zn^{2+}]^{0.5}[H_2S]^{0.5})} \quad \ldots\ldots\ldots 4.5$$

b) For the case (i) model G based on product desorption rate control (equation 2.89) :-

$$\phi(X) = r_G \left(\frac{(1,0 + K_{11}[H^+] + K_{22}[Zn^{2+}] + K_{23}[H_2S])^2}{(k_{16}[H^+]^2 - k_{15}[Zn^{2+}][H_2S]_\ell)} \right)^{0,5} \quad \ldots\ldots\ldots \quad 4.6$$

The value of the reverse rate constants k_{13} or k_{15} in equations 4.5 and 4.6 may be established using a regression technique.

c) For the case (ii) model H (equation 2.95) :-

$$\phi(X) = \frac{r_H}{k_{18}} \cdot \frac{[H^+]}{[Fe^{3+}]} \quad \ldots\ldots \quad 4.7$$

In this case the value of k_{18} was established in chapter 3 under initial rate conditions, r_H is measured directly from the rate curve and $[Fe^{3+}]$ or $[H^+]$ can be determined analytically or calculated by stoichiometry.

$\phi(X)$ can most readily be calculated for case(ii) data using equation 4.7 in which all values are known. This is done in section 4.1 using VMWBM and WBM sphalerite results as examples, and the $\psi_4(X)$ established for these sphalerite leached under case (ii) conditions are compared with $\psi_1(X)$, $\psi_2(X)$ and $\psi_3(X)$ described by equations 4.1, 4.2 and 4.3 respectively.

In section 4.2 $\phi(X)$ and the reverse reaction

rate constant k_{13} are determined using the VMWBM sphalerite case (i) leaching data as an example. The $\phi(X)$ determined for leaching this sphalerite in H_2SO_4 (with $[Fe^{3+}]_o = 0,0$) will be compared with the $\phi(X)$ determined for the sphalerites leaching under case (ii) conditions (i.e. - $[Fe^{3+}]_o : [H_2SO_4]_o \geq 1,8$).

In sections 4.3 to 4.6 $\psi_4(X)$ will be determined for the other types of sphalerite using mainly case (ii) experimental rate results.

4.1 DETERMINATION OF $\psi_4(X)$ FOR THE VMWBM AND WBM SPHALERITE LEACHING UNDER CASE (ii) CONDITIONS

Equation 4.7 was used to calculate $\phi(X)$ for VMWBM and WBM sphalerite leaching in acidic ferric sulphate media. Values of the rate constant k_{18} are summarised on table 3.11. Values for the rate of leaching ($r_H = \frac{d[Zn^{2+}]}{dt}$) at various extents of reaction X were obtained by measuring the slopes of tangents drawn on the rate curve. $[H^+]$ was analytically determined and was experimentally observed to remain constant.

$[Fe^{3+}]$ was calculated as follows:

$$[Fe^{3+}] = [Fe^{3+}]_o - 2,0 \times [Zn^{2+}] \quad \ldots\ldots\ldots \quad 4.8$$

where $[Fe^{3+}]_o$ and $[Zn^{2+}]$ were determined analytically.

Tables 4.1 and 4.2 summarise the measured and calculated results for experimental VMWBM and WBM sphalerite leaching runs.

Figure 4.1 plots $\psi_1(X)$, $\psi_2(X)$, $\psi_3(X)$ and $\psi_4(X)$ versus extent of reaction X. It is observed that $\psi_4(X)$ calculated according to equation 4.7 for model H decreases far more rapidly than any of the other $\psi(X)$ functions and is virtually identical for both the VMWBM and the WBM sphalerites. This phenomenon could be the result of one or more of the following:

a) Model H does not correctly predict the VMWBM or WBM sphalerite leaching behaviour under non-initial case (ii) conditions.

b) Elemental sulphur which forms on the sphalerite surface blinds the active sites and results in a faster decrease in the leaching rate r_H than would occur if S^o blinding did not occur.

c) The active site area does actually decrease far more rapidly than predicted by the shrinking core model $\psi_2(X)$ or the B.E.T. area change function $\psi_3(X)$.

The following purely empirical function is also plotted on figure 4.1 -

$$\psi_4(X) = 1{,}0 - \frac{1{,}065}{\left(\frac{0{,}065}{X} + 1{,}0\right)} \qquad \ldots\ldots\ldots \quad 4.9$$

$[Zn^{2+}]$ x 10^3 (kg-mol/m^3)	X (-)	$(r_H)_{exp}$ x 10^3 (kg-mol/min m^3)	$[Fe^{3+}]$ x 10^3 (kg-mol/m^3)	$\Phi(X)$ - (m^2/kg)	$\psi_4(X)$ (-)
0	0	2,1	0,1504	65,45	1,0
5,0	0,025	1,75	0,1404	58,43	0,893
10,0	0,049	1,20	0,1304	43,14	0,659
15,0	0,073	0,532	0,1204	20,71	0,316
30,0	0,147	0,338	0,0904	17,53	0,268

NOTE :- k_{18} = 10,88 x 10^{-6} (kg-mol/min m^2 m^3)

$[H^+]$ = 0,051 (kg-mol/m^3)

Temp = 318.0 (K)

T A B L E 4. 1a DETERMINATION OF ψ_4 (X) FOR VMWBM SPHALERITE LEACHING RESULTS REPORTED IN TABLE J 9

$[Zn^{2+}]$ x 10^3 (kg-mol/m^3)	X (-)	$(r_H)_{exp}$ x 10^3 (kg-mol/min m^3)	$[Fe^{3+}]$ x 10^3 (kg-mol/m^3)	$\phi(X)$ (m^2/kg)	$\psi_4(X)$ (-)
0	0	6,9	0,3044	65,62	1,00
20,0	0,098	3,24	0,2644	35,46	0,541
30,0	0,147	1,49	0,244	17,68	0,269
40,0	0,196	0,70	0,244	9,04	0,138
50,0	0,246	0,41	0,2044	5,81	0,088

NOTE :- k_{18} = 25,46 x 10^{-6} (kg-mol/m^2.min)

$[H^+]_o$ = 0,0737 (kg-mol/m^3)

Temp = 338,0 (K)

TABLE 4. 1b DETERMINATION OF ψ_4 (X) FOR VMWBM SPHALERITE LEACHING RESULTS REPORTED IN TABLE J 10

$[Zn^{2+}]$ x 10^3 (kg-mol/m^3)	X (-)	$(r_H)_{exp}$ x 10^3 (kg-mol/m^3 min)	$[Fe^{3+}]$ x 10^3 (kg-mol/m^3)	$\phi(X)$ (m^2/kg)	$\psi_4(X)$ (-)
0	0	12,5	1,504	8,0	1,0
50,0	0,049	4,94	1,404	3,39	0,423
150,0	0,147	2,92	1,204	2,33	0,292
200,0	0,197	2,44	1,104	2.13	0,166
250,0	0,246	2,10	1,004	2.01	0,252
300,0	0,3	1,50	0,904	1,60	0,20
350,0	0,344	0,96	0,804	1,15	0,144
400,0	0,393	0,63	0,704	0,86	0,108

NOTE :- k_{18} = 582,8 x 10^{-6} (kg-mol/m^2.min)

$[H^+]_o$ = 0,561 (kg-mol/m^3) Temp = 368,0 (K)

Size fraction = -75,0 + 63,0 μm

T A B L E 4. 2a DETERMINATION OF $\psi_4(X)$ FOR WBM SPHALERITE LEACHING RESULTS REPORTED IN TABLE J 5

$[Zn^{2+}]$ x10^3 (kg-mol/m^3)	X (-)	$(r_H)_{exp}$ x 10^3 (kg-mol/m^3 min)	$[Fe^{3+}]$ x 10^3 (kg-mol/m^3)	$\phi(X)$ (m^2/kg)	ψ_4 (X) (-)
0	0	4,29	0,793	8,0	1,0
30,0	0,029	2,63	0,735	5,25	0,66
60,0	0,059	1,34	0,675	2,91	0,37
85,0	0,083	1,08	0,625	2,53	0,32
110,0	0,108	0,91	0,575	2,32	0,29

NOTE :- k_{18} = 201,0 x 10^{-6} (kg-mol/m^2.min)

$[H^+]_o$ = 0,295 (kg-mol/m^3) Temp = 355,5 (K)

Size fraction = -75,0 + 63,0 µm

T A B L E 4. 2 b DETERMINATION OF ψ_4 (X) FOR WBM SPHALERITE LEACHING RESULTS REPORTED IN TABLE J 4

	Calc. using eqn.
$\psi_1(X)$	4.1
$\psi_2(X)$	4.2
$\psi_3(X)$	4.3 and F.7 with a=0,25
$\psi_4(X)$	4.9

	Sphal.	Table reporting calc. $\psi_4(X)$ values	Leaching data on table
o	WBM	4.1a	J 4
×	WBM	4.1b	J 5
□	VMWBM	4.2a	J 9
✣	VMWBM	4.2b	J 10

legend

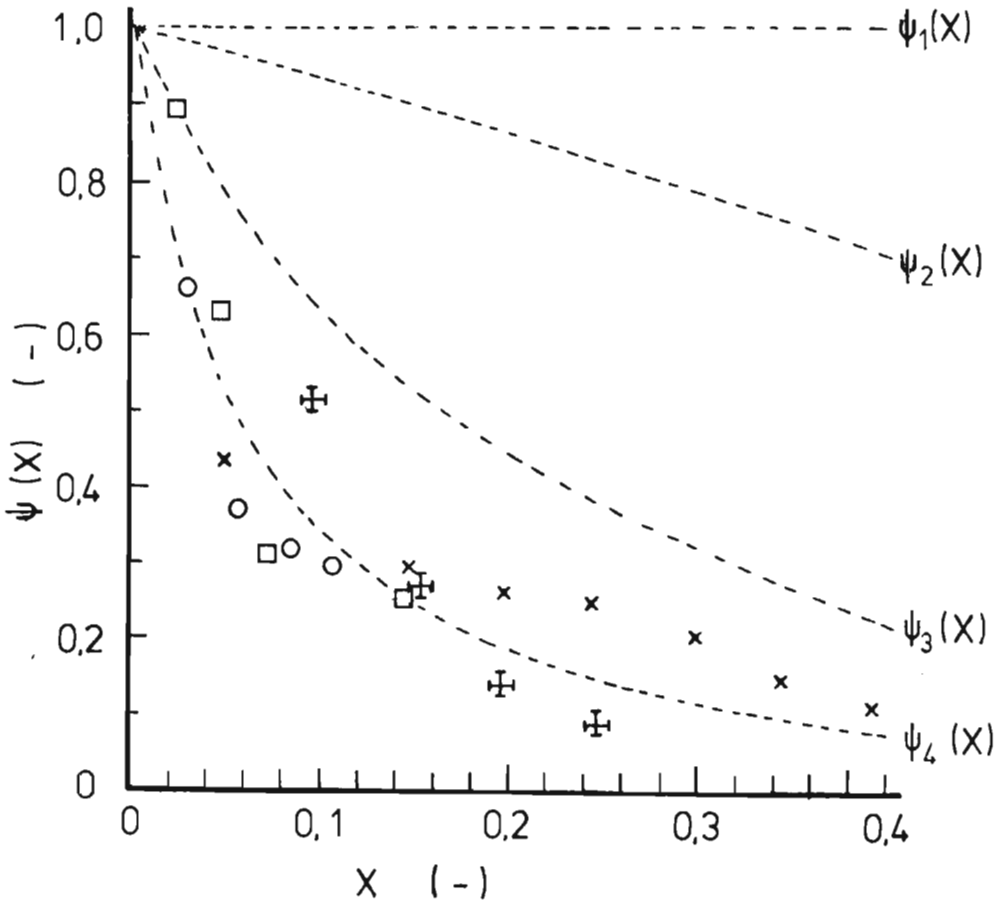

Figure 4.1 Comparison of active site area ratio functions $\psi_1(X)$; $\psi_2(X)$; $\psi_3(X)$ and $\psi_4(X)$ with $\psi_4(X)$ values calculated for WBM and VMWBM sphalerites leaching under case (ii) conditions. Values were calculated using eqns. 4.4 and 4.7.

It is observed that equation 4.9 fits the shape of the $\psi_4(X)$ versus X data points reasonably well.

4.2 DETERMINATION OF $\psi_4(X)$ FOR VMWBM SPHALERITE LEACHING UNDER CASE (i) CONDITIONS

Equation 4.5 is used (along with values for the constants K_{11}, K_{22}, K_{23} and k_{11} which are summarised in table 3.10) to calculate $\phi(X)$ for the VMWBM sphalerite leaching under case (i) conditions. However, k_{13} is also an unknown, and thus $\phi(X)$ and k_{13} are simultaneously determined as follows :-

a) For a given experiment and at different extents of reaction X, the leaching rates r_F are measured directly off the rate curve and the corresponding $[Zn^{2+}]$, $[H_2S]_\ell$ and $[H^+]$ values are calculated.

b) At each value of X, $\phi(X)$ and $\psi_4(X) = \frac{\phi(X)}{\phi_0}$ are calculated using several values of k_{13} in equation 4.5 .

c) Procedures a) and b) are repeated for other experiments conducted under different initial temperature, sphalerite mass or $[H^+]_0$ conditions.

d) The calculated $\psi_4(X)$ values at the given X values for at lease two runs are plotted against the k_{13} values. The intercept of

the best fit curves through the $\psi(X)$ and k_{13} points at each value of X for each run represents a valid solution to equation 4.5 .

The above procedure is now demonstrated using an example.

Table 4.3 presents values of $\Phi(X)$ and $\psi_4(X)$ calculated at various X values for the experimental runs reported in tables I 2 ($[H^+]_o$ = 1,0 (kg-mol/m^3)) and I 8 ($[H^+]_o$ = 0,5 (kg-mol/m^3)). All other conditions for these two runs are identical. Figure 4.2 plots the $\psi_4(X)$ versus k_{13} values presented on table 4.3.

Figure 4.3 plots $\psi_4(X)$ versus k_{13} for two runs conducted at two different temperatures (i.e. - T = 318,0 K, (table I 2) and T = 338,0 K, (table I 5)) with all other conditions constant.

Figure 4.4 plots $\psi_4(X)$ versus k_{13} for two runs conducted at two different initial masses of sphalerite (i.e. M_o = 0,005 kg (table I 1) and M_o = 0,01 kg (table I 2)), with all other conditions constant.

It is observed on each of the figures 4.2, 4.3 and 4.4 that the intercepts of the $\psi(X)$ versus k_{13} curves at the different values of X do not fall on a constant value of k_{13}. This suggests that k_{13} itself may be a function of X.

Figure 4.5 summarises the $\psi_4(X)$ versus X and figure 4.6 summarises the k_{13} versus X values at

$[H_2SO_4]_o$ (kg-mol/m^3)		0,5		1,0	
TABLE	(-)	I 2		I 8	
X (-)	k_{13}	$\phi(X)$ (m^2/kg)	$\psi_4(X)$ (-)	$\phi(X)$ (m^2/kg)	$\psi_4(X)$ (-)
0,01	0,01	25,55	0,781	28,57	0,873
	0,015	26,24	0,8	28,94	0,884
	0,02	26,96	0,824	29,31	0,896
	0,025	27,73	0,847	29,70	0,908
	0,03	28,55	0,873	30,09	0,92
	0,035	29,41	0,9	30,50	0,932
	0,04	30,32	0,927	30,92	0,945
	0,045	31,30	0,957	31,35	0,958
0,02	0,01	21,16	0,647	24,61	0,752
	0,015	22,40	0,684	25,27	0,772
	0,02	23,81	0,728	25,97	0,794
	0,025	25,4	0,776	26,70	0,816
	0,03	27,21	0,832	27,48	0,84
	0,035	29,31	0,896	28,30	0,865
0,04	0,01	12,19	0,37	16,64	0,509
	0,015	13,96	0,427	17,61	0,538
	0,02	16,32	0,50	18,70	0,571
	0,025	19,64	0,6	19,94	0,609
	0,03	24,65	0,753	21,35	0,652
	0,035	33,12	1,012	22,97	0,702
0,06	0,01	3,982	0,122	8,437	0,258
	0,015	5,088	0,155	9,252	0,283
	0,02	7,046	0,215	10,13	0,31
	0,025	11,45	0,35	11,35	0,347
	0,03	30,58	0,935	12,89	0,40
	0,035	45,66	1,40	15,07	0,461

T A B L E 4. 3 SAMPLE CALCULATIONS FOR DETERMINING $\phi(X)$ AND k_{13} OF EQUATION 4.5 AT DIFFERENT VALUES OF X. $\psi_4(X) = \frac{\phi(X)}{\phi_o}$ VALUES IN THIS TABLE ARE PLOTTED VERSUS k_{13} ON FIGURE 42

---------- Lines indicating $\psi_4(X)$ and k_{13} solutions at given values of X.

——— Best fit curves through points

Conditions			
	Temp.	(K)	318,0
	Mass	(kg)	0,01
	Stirrer	(rpm)	800,0

legend		$[H_2SO_4]_o$	Leaching data reported on table
	o	1,0	I 2
	×	0,5	I 8

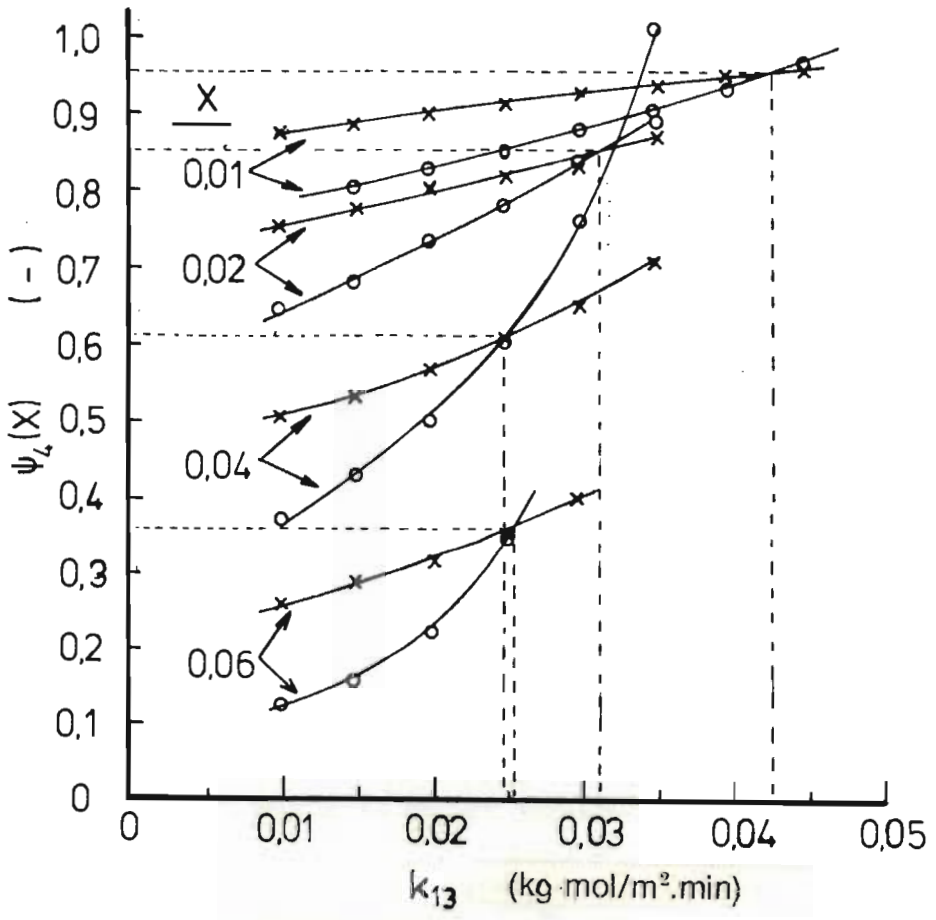

Figure 4.2 Example of graphically determing $\psi_4(X)$ and k_{13} solutions to equation 4.5 for VMWBM sphalerite leaching under case (i) conditions at two different $[H^+]_o$ values. All values plotted are presented on table 4.3

---------- Lines indicating $\psi_4(X)$ and k_{13} solutions at given values of X.

———— Best fit curves through points.

Conditions			
	$[H_2SO_4]_o$	(kg-mol/m^3)	1,0
	Mass	(kg)	0,01
	Stirrer	(rpm)	1000,0

legend		Temp. (K)	Leaching data reported in tables
	o	338,0	I 5
	×	318,0	I 2

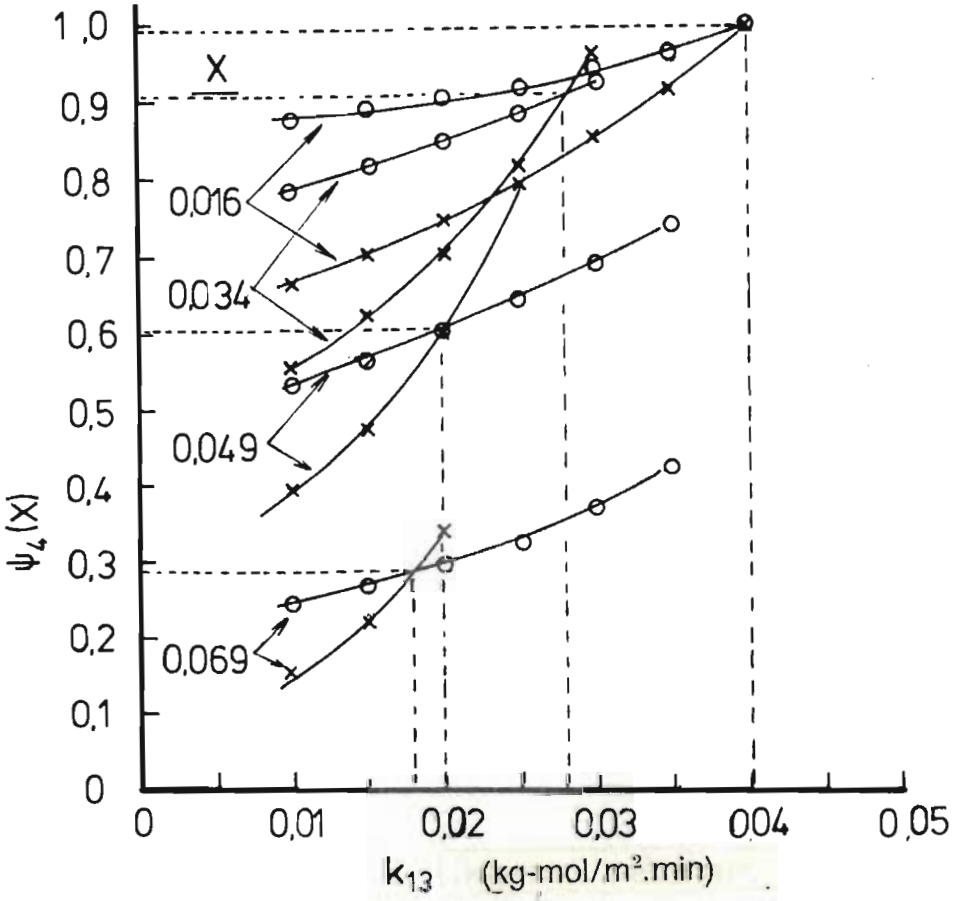

Figure 4.3 Example of graphically determining $\psi_4(X)$ and k_{13} solutions to equation 4.5 for VMWBM sphalerite leaching under case(i) conditions at two different temperatures.

- - - - - - - - Lines indicating $\psi_4(X)$ and k_{13} solutions at given values of X.

———— Best fit through points.

Conditions

Temp.	(K)	318,0
$[H_2SO_4]_o$	(kg-mol/m^3)	1,0
Stirrer	(rpm)	1000,0

legend

	$(M)_o$ (kg)	Leaching data reported on table
o	0,005	I 1
×	0,01	I 2

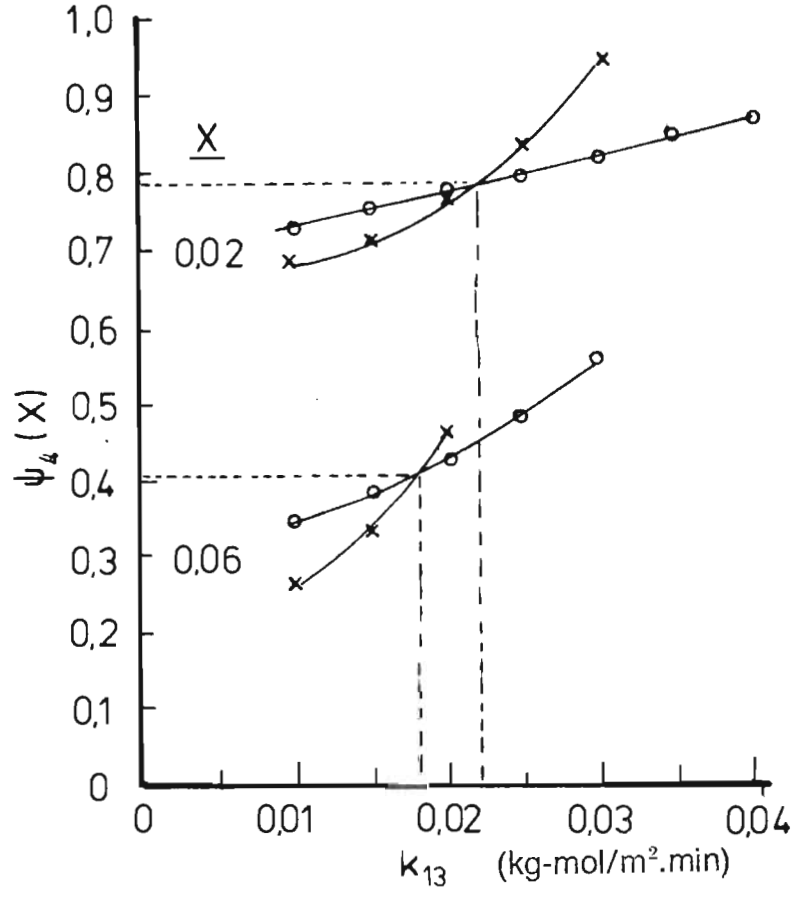

Figure 4.4 Example of graphically determining $\psi_4(X)$ and k_{13} solutions to eqn. 4.5 for VMWBM leaching under case (i) conditions with two different masses of sphalerite initially present.

	Calc. using eqn.
$\psi_1(X)$	4.1
$\psi_2(X)$	4.2
$\psi_3(X)$	4.3 and F.7 with a= 0,25
$\psi_4(X)$	4.9

legend

	From figure	Variable
o	4.2	$[H_2SO_4]_o$
×	4.3	Temp.
□	4.4	M_o

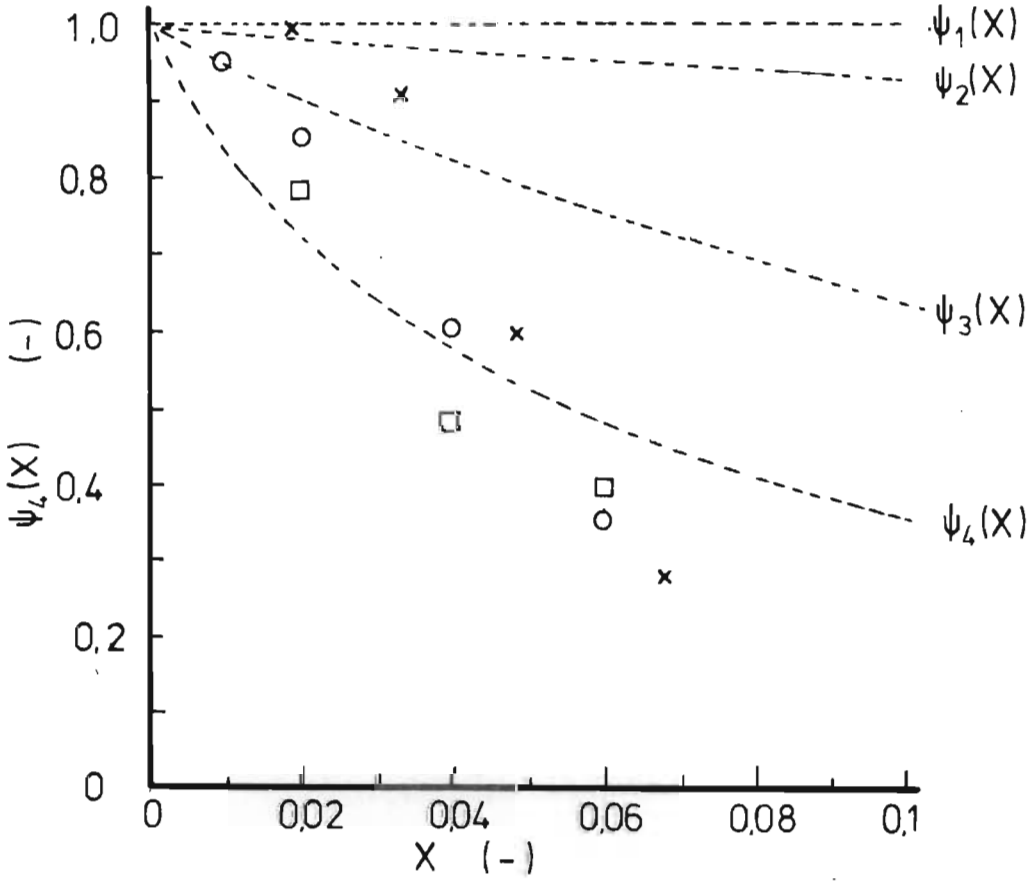

Figure 4.5 Summary of $\psi_4(X)$ versus X solution values shown on figures 4.2;4.3and 4.4.

--------- Calculated using eqn. 4.10 with $\Omega(X)$ defined by eqn. 4.11.

legend	From fig.	Variable
o	4.2	$[H_2SO_4]_o$
×	4.3	Temp.
□	4.4	M_o

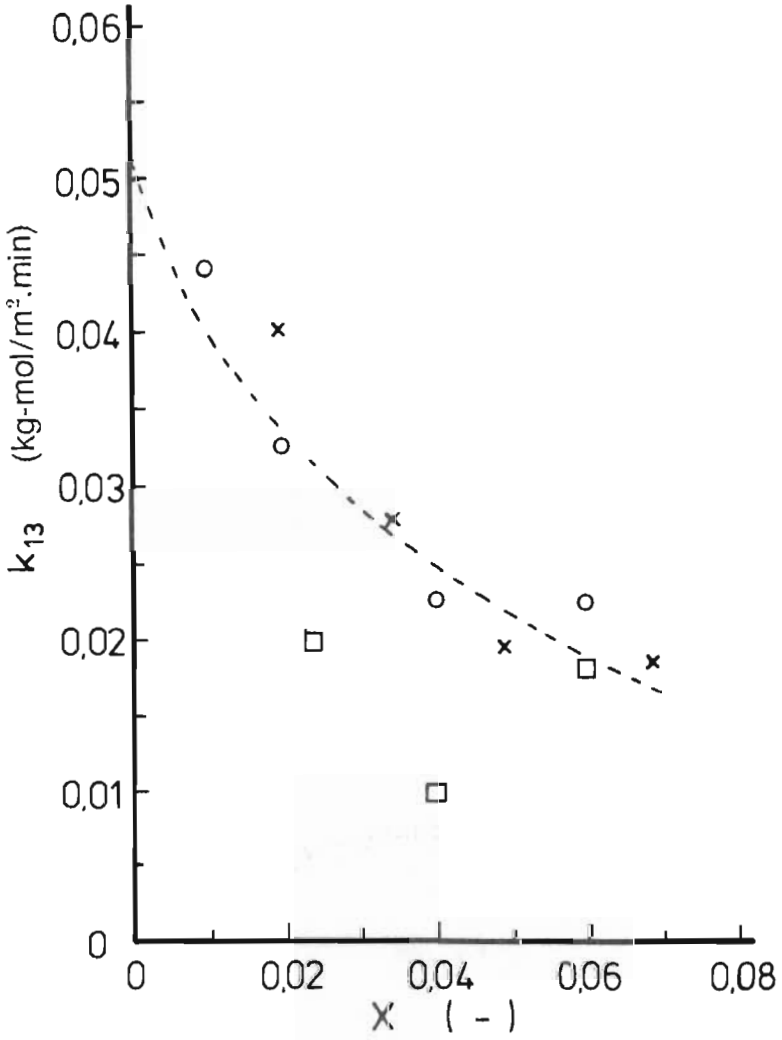

Figure 4.6 Summary of k_{13} versus X solution values shown on figures 4.2; 4.3 and 4.4

the points of interception of the curves on figures 4.2, 4.3 and 4.4.

It is observed on figure 4.5 that the $\psi_4(X)$ versus X points lie close to the curve described by equation 4.9. Figure 4.7 superimposes all the case (i) and case (ii) $\psi_4(X)$ data points presented on figures 4.5 and 4.1 respectively. Figure 4.7 also plots the function $\psi_4(X)$ described equation 4.9 as well as $\psi_1(X)$, $\psi_2(X)$ and $\psi_3(X)$.

It is observed that generally both the case (i) and case (ii) data points lie scattered about the best fit $\psi_4(X)$ curve. This is accepted as evidence that the rapid decrease in active site area is a real phenomenon, and not due to elemental sulphur blinding. This evidence is also accepted as proof that models F and H describe the kinetics of VMWBM sphalerite leaching under case (i) and case (ii) conditions over the range of variables investigated.

The results on figure 4.6 are accepted as evidence that for the VMWBM sphalerite the reverse rate constant k_{13} appearing in model F (equation 2.81) is a function of X. This suggests that as leaching progresses the residual area becomes less active. This idea is similar in concept to the variable activation energy model proposed by Brittan (1971) who proposed that in the copper segregation process the most active sites reacted first, so that the residual sites were progressively

	Calc. using eqn.
$\psi_1(X)$	4.1
$\psi_2(X)$	4.2
$\psi_3(X)$	4.3 and F.7 with a = 0,25
$\psi_4(X)$	4.9

legend

- o Case (i) data ($[Fe^{3+}]$ = 0,0) from fig 4.5
- × Case (ii) data ($[Fe^{3+}]_o : [H_2SO_4]_o \simeq 1,8$) from fig 4.1.

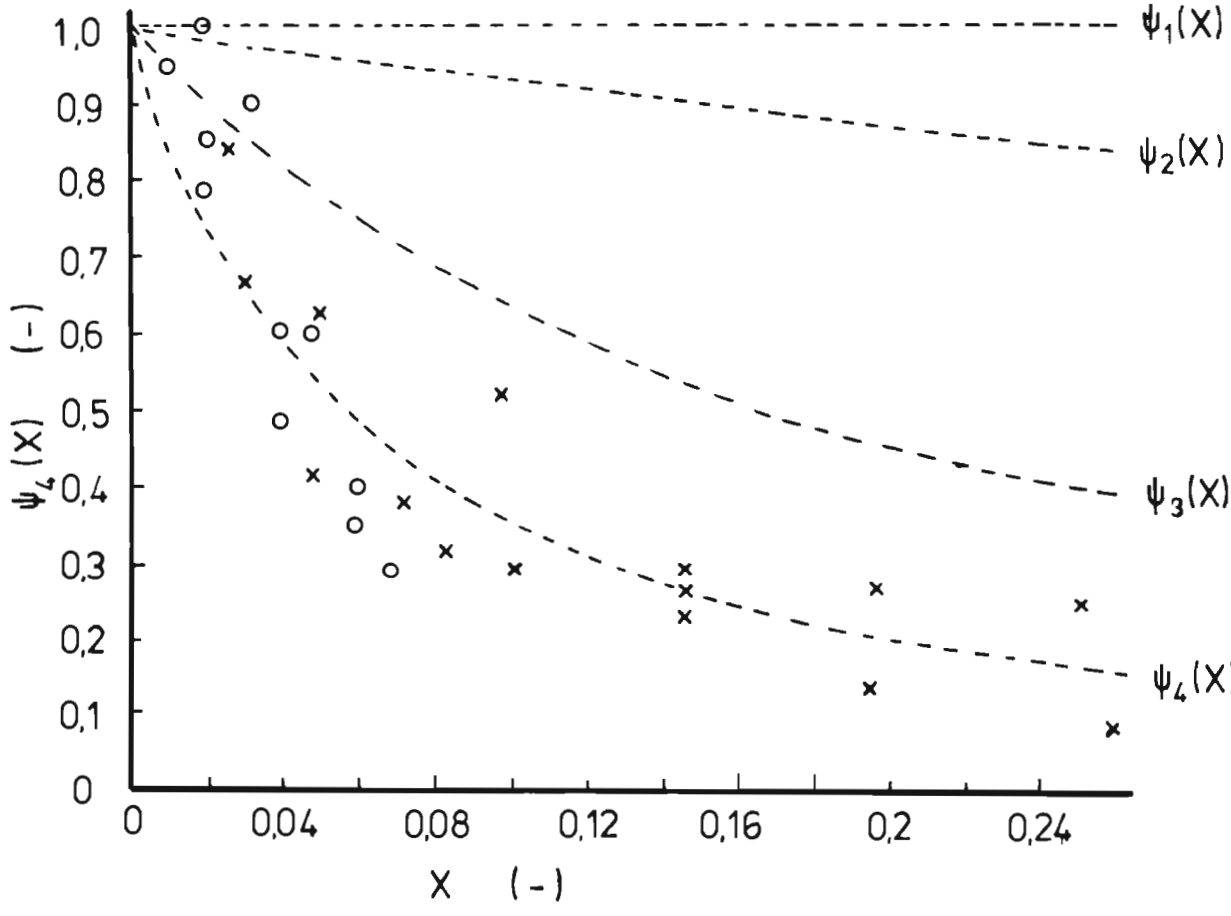

Figure 4.7 Comparison of all case (i) $\psi_4(X)$ versus X data (from fig 4.5) with all case (ii) $\psi_4(X)$ versus X data (from fig 4.1).

less active. However, for the leaching of VMWBM sphalerite, it is proposed that the activation energy of the reverse reaction is independent of X so that only the pre-exponential constant of the reverse reaction rate constant k_{13} varies with X. The effect of X on k_{13} is modelled as follows:

Let $$\Omega(X) = \frac{k_{13}}{(k_{13})_{X=0}} \quad \ldots\ldots\ldots \quad 4.10$$

where k_{13} = value of k_{13} at a given value of X;

$(k_{13})_{X=0}$ = value of k_{13} at X = 0.

Now from figure 4.6 $(k_{13})_{X=0} = 0{,}051$.

Figure 4.8 plots $\Omega(X)$ versus X for all the k_{13} points established previously and the following empirical function is seen to fit the data reasonably well.

$$\Omega(X) = 1{,}0 - \frac{1{,}04}{\frac{0{,}04}{X} + 1{,}0} \quad \ldots\ldots \quad 4.11$$

Now assume that k_{13} can be described by an Arrhenius type relationship -

$$k_{13} = A_E \exp\left(\frac{-E_a}{RT}\right) \quad \ldots\ldots\ldots \quad 4.12$$

The activation energy E_a may be established if values of k_{13} at two temperatures are known.

From equation 2.81 -

$$k_{13} = \frac{k_{11}[H^+] - r_F \dfrac{(1{,}0 + K_{11}[H^+] + K_{22}[Zn^{2+}] + K_{23}[H_2S])}{\Phi(X)}}{[H_2S]^{0,5} \quad [Zn^{2+}]^{0,5}} \quad \ldots\ldots\ldots \quad 4.13$$

-------- Calculated using eqn. 4.11.

legend o $\Omega(X) = k_{13} / (k_{13})_{X=0}$; where k_{13} values are plotted on fig 4.6 and $(k_{13})_{X=0} = 0.051$

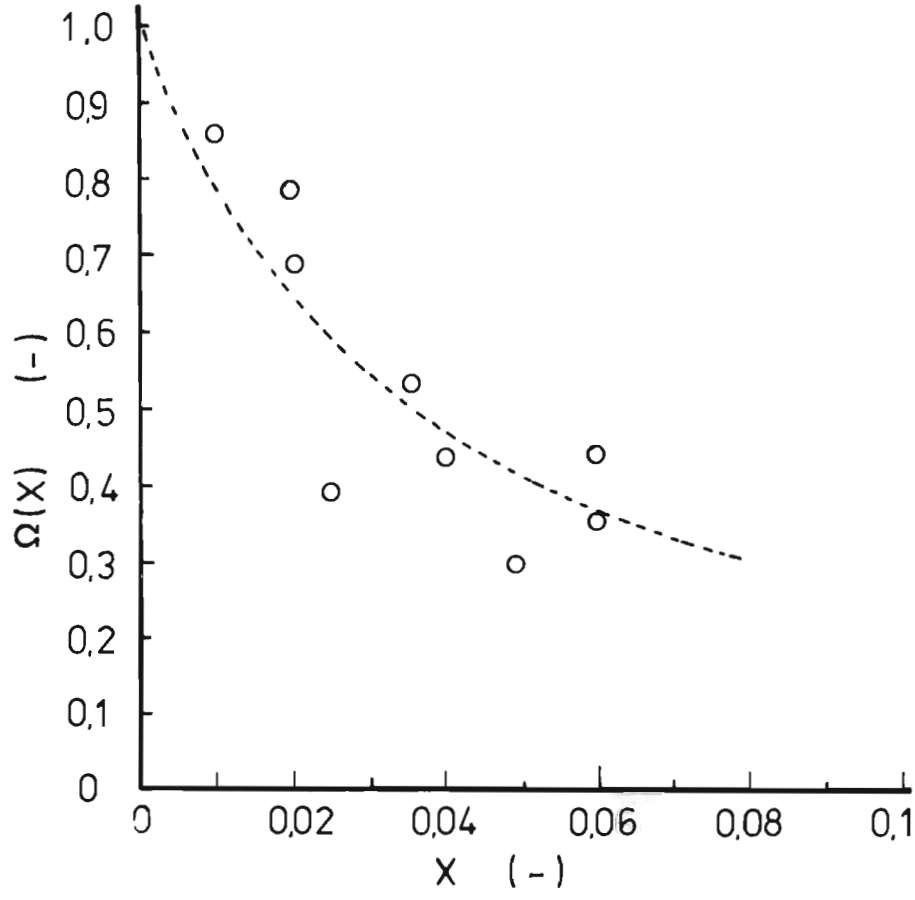

Figure 4.8 Reverse rate constant ratio $\Omega(X)$ versus X for VMWBM sphalerite leached under case (i) conditions. $\Omega(X)$ is defined by eqn. 4.10.

and since $\phi(X)$ is well described by equation 4.9, all values are known, and k_{13} may be calculated at given values of X.

Figure 4.9 plots calculated values of log k_{13} versus $\frac{1}{T}$, and from the slope the activation energy is :-

$$E_a = 26,236 \times 10^6 \text{ J / kg-mole} \quad \ldots\ldots \quad 4.14$$

From figure 4.6 it is observed that at $X = 0,0$, $k_{13} = 0,051$, therefore at 318,0 K

$$A_E = 0,051 \Big/ \exp\left(\frac{-26,236 \times 10^6}{8,31 \times 10^3 \times 318,0}\right)$$

$$= 2,49 \times 10^{-6} \quad \ldots\ldots\ldots \quad 4.15$$

Hence the final overall form of the differential rate equation for VMWBM sphalerite leaching under case (i) conditions appears as follows :

$$r_F = \frac{\psi_4(X)\,\phi_o\,(k_{11}[H^+] - \Omega(X)\,(k_{13})_o\,[H_2S]_\ell^{0,5}[Zn^{2+}]^{0,5})}{(1,0 + K_{11}[H^+] + K_{22}[Zn^{2+}] + K_{23}[H_2S])} \quad \ldots\ldots\ldots \quad 4.16$$

where : $\psi_4(X)$ is defined by equation 4.9 ;

ϕ_o is defined by equation 2.1 ;

$\Omega(X)$ is defined by equation 4.11;

$k_{11} = A_E \exp \frac{-E_a}{RT}$ and values of A_E and E_a are given in table 3.9 ;

$(k_{13})_o = A_E \exp \frac{-E_a}{RT}$ and values of A_E and E_a are given in equations 4.14 and 4.15 respectively.

Values for K_{11}, K_{22} and K_{23} are given in table 3.10 .

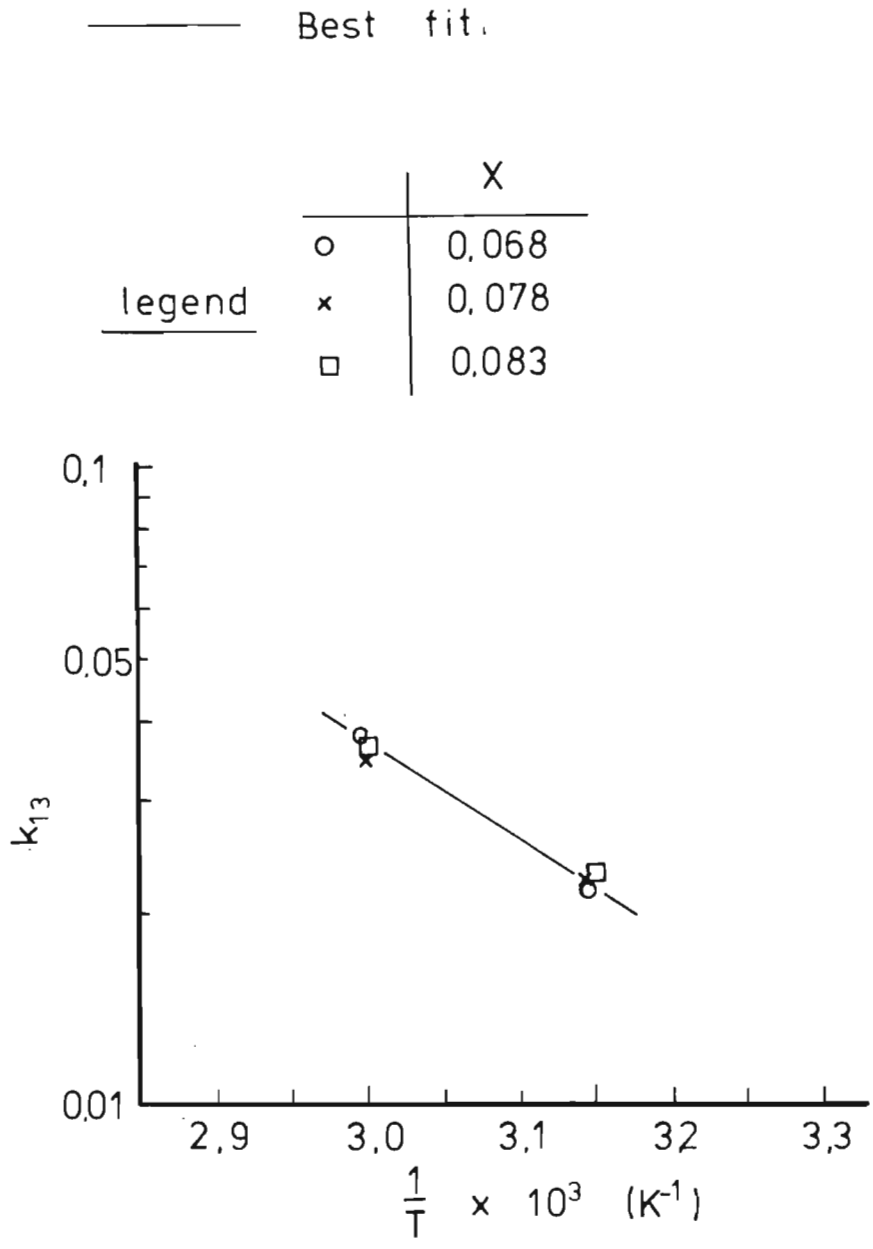

Figure 4.9 Arrhenius-type plot illustrating the effect of temperature on the reverse rate constant k_{13} for VMWBM sphalerite leaching under case(i) conditions.
The 318,0 K and 338,0K leaching results are reported in tables I 3 and I 5 respectively.

4. 3 $\psi_4(X)$ CALCULATED FOR THE VMZCR AND ZCR SPHALERITES

The same methods used in sections 4. 1 and 4. 2 to calculate $\psi_4(X)$ for the VMWBM sphalerite were applied to calculate $\psi_4(X)$ for the VMZCR sphalerite. In addition, case (ii) data was used to calculate $\psi_4(X)$ for the ZCR sphalerite. Figure 4. 10 summarises the calculated $\psi_4(X)$ versus X data for the VMZCR and ZCR sphalerites and compares the $\psi_4(X)$ values with $\psi_1(X)$, $\psi_2(X)$ and $\psi_3(X)$ curves.

It is observed that the case (i) and case (ii) $\psi_4(X)$ values for the VMZCR sphalerite are similar to each other, but are entirely different to the case (ii) $\psi_4(X)$ values for the ZCR sphalerite. The shape of the $\psi_4(X)$ versus X curves for the VMZCR and ZCR sphalerites are observed to be significantly different to the shape of the $\psi_1(X)$, $\psi_2(X)$ curves or the $\psi_3(X)$ curve for this sphalerite.

In order to test whether sulphur blinding caused $\psi_4(X)$ for the ZCR sphalerite to decrease much faster than $\psi_3(X)$ for this sphalerite the following experiment (results reported in table J 18) was performed :-

ZCR sphalerite was leached for 60,0 minutes under case (ii) conditions prior to being filtered. All the elemental sulphur associated with the filtered residue was removed by washing with carbon tetrachloride. The washed solids were returned to the filtrate from which they were removed, with all leaching conditions identical to conditions at the time of filtration.

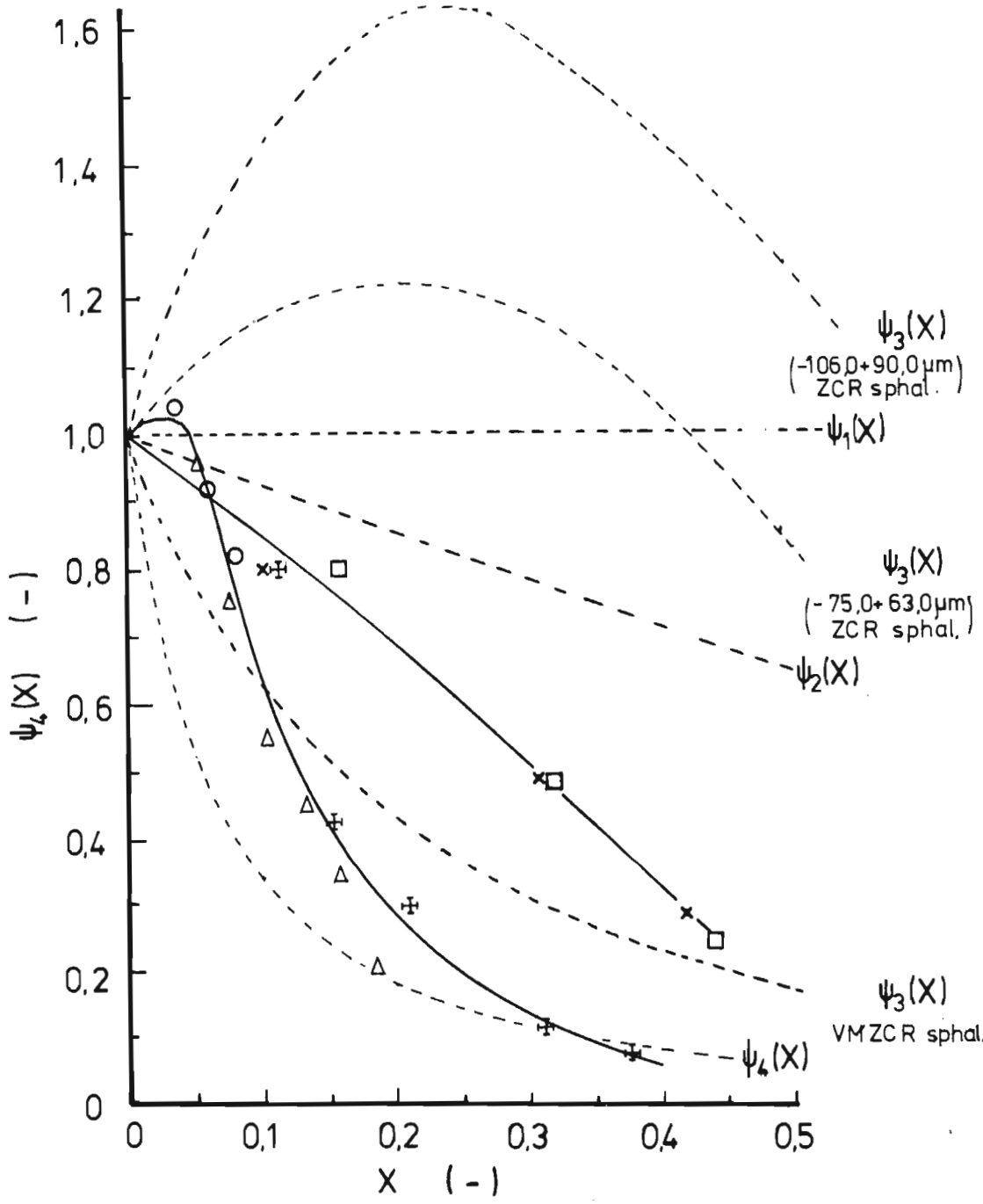

Figure 4.10 Comparison of calculated $\psi_4(X)$ versus X values for the VMZCR sphalerite (leaching under case(i)$_{\Lambda}^{\alpha\alpha(i)}$ conditions) and for the ZCR sphalerite (leaching only under case(ii) conditions) with the functions $\psi_1(X)$; $\psi_2(X)$; $\psi_3(X)$ and $\psi_4(X)$.

Figure 4. 11 plots the $[Zn^{2+}]$ versus time rate curve for the sphalerite leaching before and after sulphur removal and it is observed that sulphur removal did not result in an increase in the rate of leaching. Hence the rapid decrease in $\psi_4(X)$ is a real phenomenon, and not merely due to sulphur blinding.

It is observed on figure 4. 10 that $\psi_4(X)$ for the VMZCR and ZCR sphalerites are entirely different to $\psi_4(X)$ for the VMWBM and WBM sphalerites.

Figure 4. 12 compares three k_{13} versus X values computed for the VMZCR sphalerite with the best fit k_{13} versus X curve for the VMWBM sphalerite (from figure 4. 5). A similar order of magnitude, and dependence on X is observed.

4. 4 $\psi_4(X)$ CALCULATED FOR THE PR AND VMPR SPHALERITES

Figure 4. 13 plots $\psi_4(X)$ versus X data calculated using only case (ii) data for the VMPR and PR sphalerites. $\psi_4(X)$ is observed to decrease more rapidly for the VMPR sphalerite than for the PR sphalerite, and $\psi_4(X)$ for both sphalerites are entirely different to the shapes of the $\psi_1(X)$, $\psi_2(X)$ and $\psi_3(X)$ functions shown plotted on figure 4. 13.

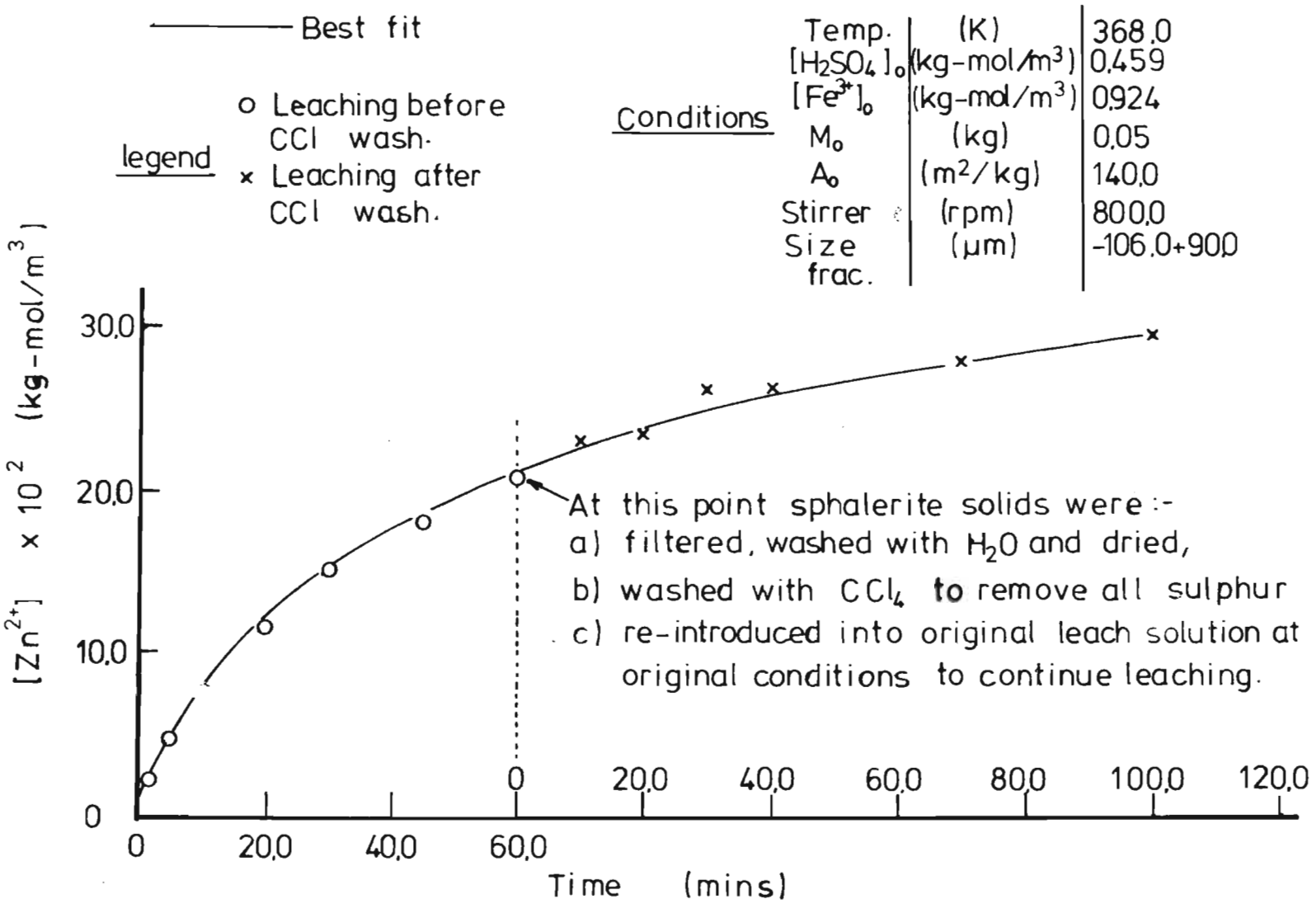

Figure 4.11 Rate curve for ZCR sphalerite (results reported in table J 18) leaching under case(ii) conditions, demonstrating the effect of removing the sulphur from the particles at X = 0.49 (t = 60.0 mins)

——— Best fit curve for VMWBM sphal. and described by eqns. 4.10 and 4.11

o Calculated k_{13} values for the VMZCR sphalerite.

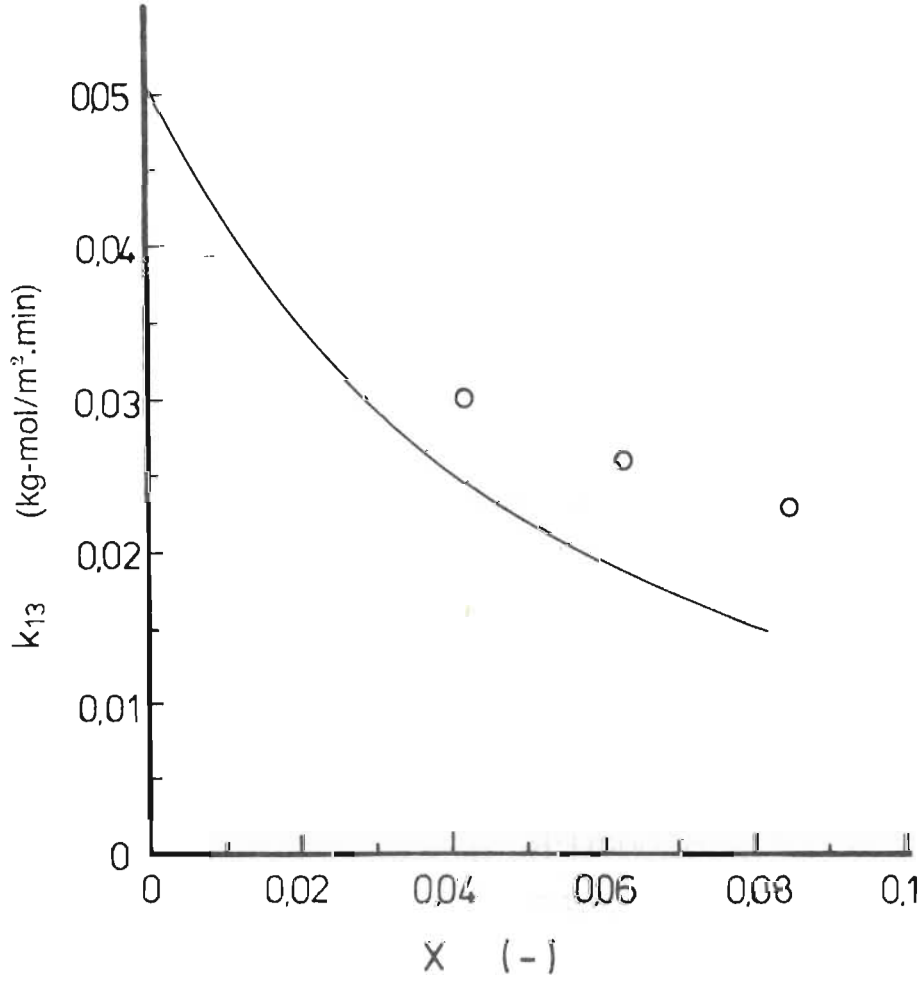

Figure 4.12 Comparison of reverse rate constant k_{13} calculated for VMZCR sphal. (using data reported in tables I 13 and I 15) with the best fit k_{13} curve (off fig 4.6) for VMWBM sphalerite.

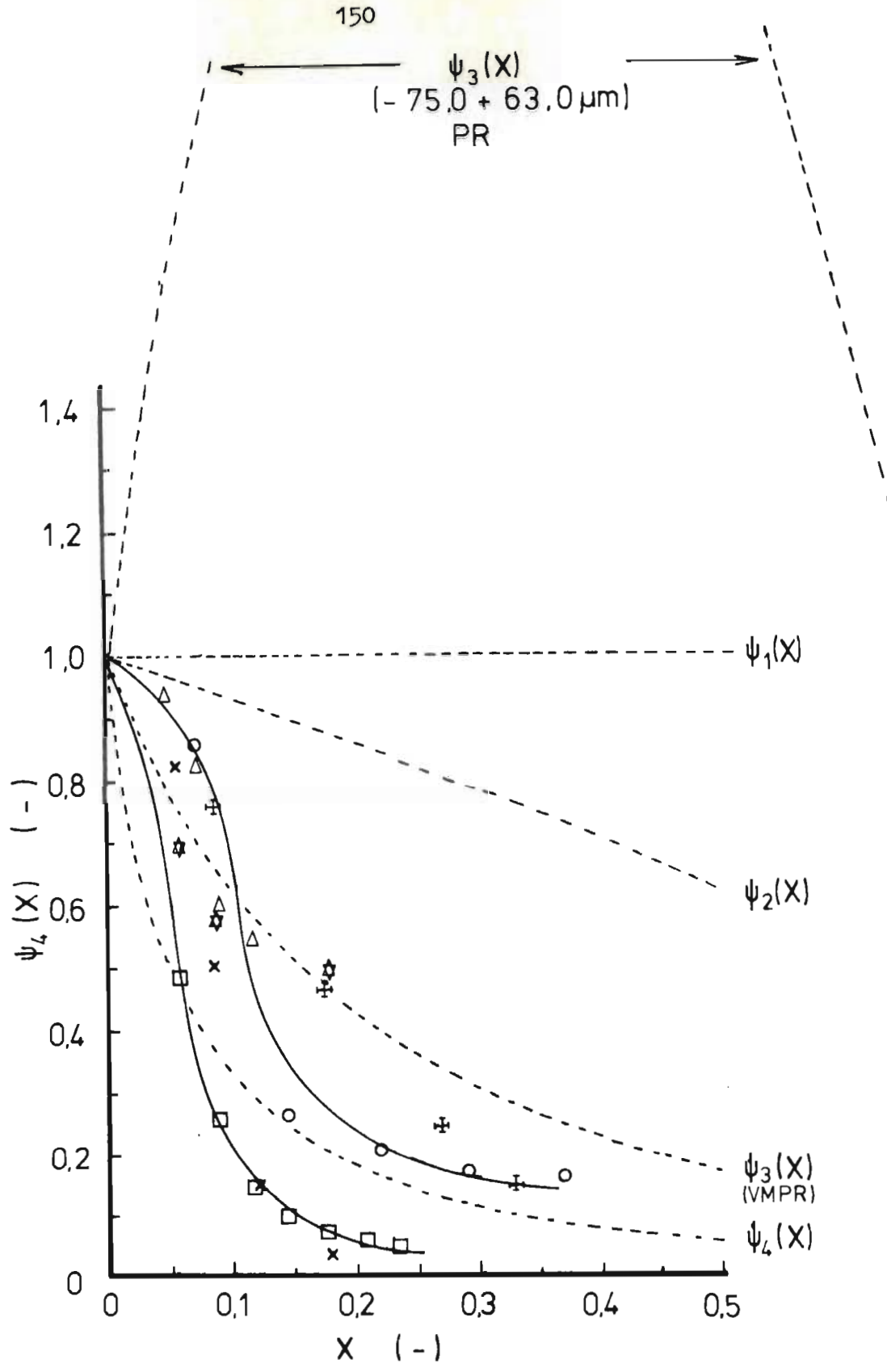

Figure 4.13 Comparison of calculated $\psi_4(X)$ versus X values for the PR and VMPR sphalerites leaching under case (ii) conditions with the functions $\psi_1(X)$; $\psi_2(X)$; $\psi_3(X)$ and $\psi_4(X)$.

4. 5 $\psi_4(X)$ CALCULATED FOR THE BDH SPHALERITE

Romankiw (1962) and Verhulst (1974) were able to demonstrate that for synthetic sphalerite leaching under case (i) conditions ($[Fe^{3+}]_o = 0,0$) the active site concentration decreases in a way described by the shrinking core model. Hence equation 4. 5 was used to calculate the reverse rate constant k_{13} under the assumption that $\phi(X)$ decreases according to shrinking core behaviour (expressed by equation 4. 2) .

Figure 4. 14 plots calculated values of k_{13} versus X , for experiments in which various masses of BDH sphalerite were leached at 25,0 ° C at various $[H_2SO_4]_o$ values. The k_{13} values are observed to be independent of X within experimental limitations, and with the limitation imposed by manually measuring the rate values r as a function of X off the rate curves. This suggests that the shrinking core model indeed predicts the change in active site area for this sphalerite.

However, figure 4. 15 plots $\psi_4(X)$ versus X for the BDH sphalerite leaching under case (ii) conditions. $\psi_4(X)$ is observed to decrease far more rapidly than $\psi_2(X)$ predicted by the shrinking core model, and very nearly as rapidly as the $\psi_4(X)$ observed for the VMWBM and WBM sphalerites.

No attempt is made to account for the differences between the calculated case (i) and case (ii) $\psi_4(X)$ values.

——— Best fit

Conditions			
	Temp.	(K)	298.0
	Stirrer	(rpm)	1000.0

legend	M_o (kg)	$[H_2SO_4]_o$ (kg-mol/m³)	Data presented in table (-)
o	0.002	1.04	I 52
Δ	0.004	1.04	I 45
□	0.004	1.95	I 55
×	0.008	1.04	I 49

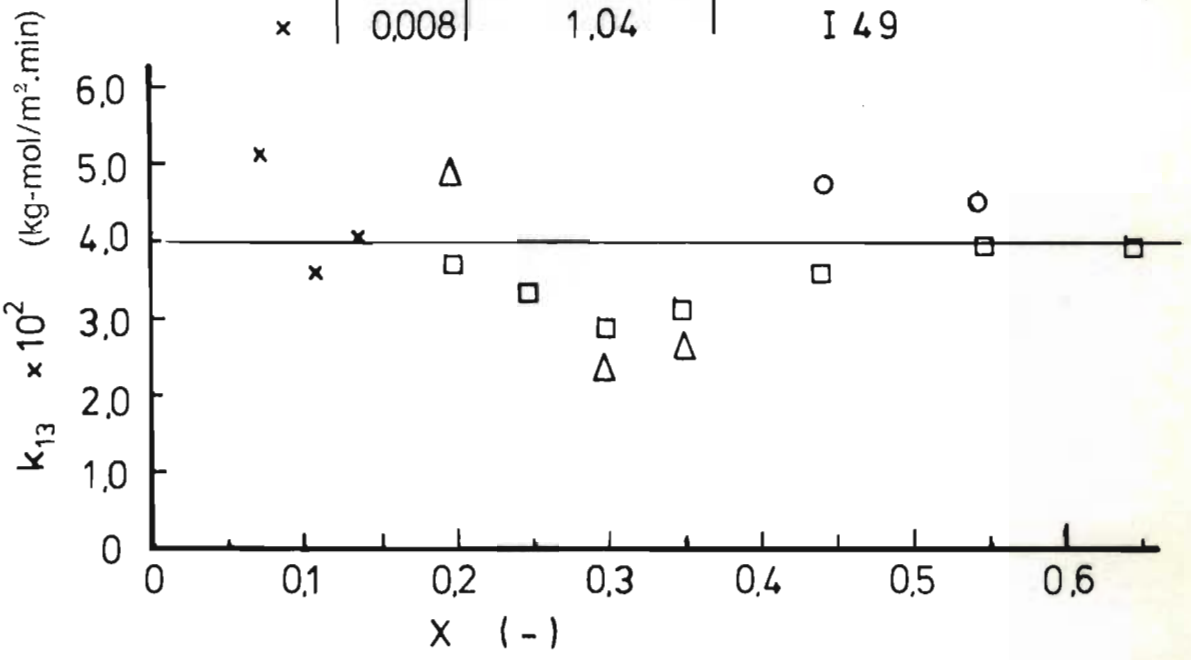

Figure 4.14 Reverse rate constant values k_{13} calculated for BDH sphalerite leaching under various case(i) conditions (using eqn. 4.5 with the assumption that $\phi(X)$ varies according to the shrinking core model eqn. 4.2)

——— Best fit through calc. $\psi_4(X)$ values

	Calculated using eqn.
$\psi_1(X)$	4.1
$\psi_2(X)$	4.2
$\psi_3(X)$	4.2
$\psi_4(X)$	4.9

legend

	M_o (kg)	$[Fe^{3+}]_o$ (kg-mol/m³)	$[H_2SO_4]_o$	Temp. (K)	Results in table
×	0,02	0,143	0,063	343,0	J 45
Δ	0,02	0,292	0,107	343,0	J 46
o	0,05	0,580	0,223	353,0	J 47

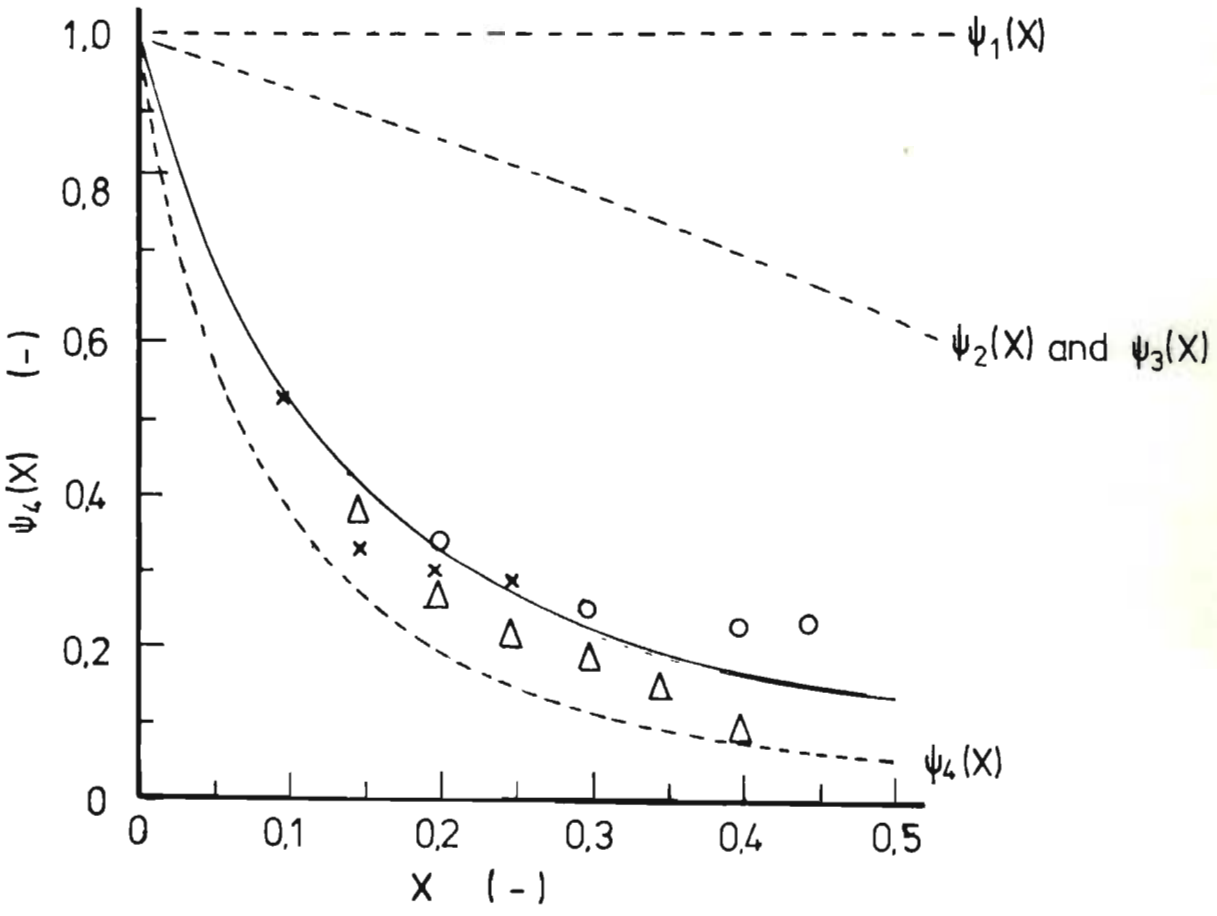

Figure 4.15 Comparison of $\psi_4(X)$ versus X values for BDH sphalerite leaching under case(ii) conditions with the functions $\psi_1(X)$; $\psi_2(X)$; $\psi_3(X)$ and $\psi_4(X)$.

4. 6 COMPARISON OF $\psi_4(X)$ FUNCTIONS CALCULATED FOR THE DIFFERENT SPHALERITES

Figure 4. 16 summarises the calculated $\psi_4(X)$ versus X best fit curves plotted previously in this chapter for the different sphalerites. It is observed that for approximately $X \leq 0,2$ $\psi_4(X)$ changes as a function of X in a unique manner for each different sphalerite. For approximately $X \geq 0,2$, the decreases in $\psi_4(X)$ with increasing X for each sphalerite are somewhat similar.

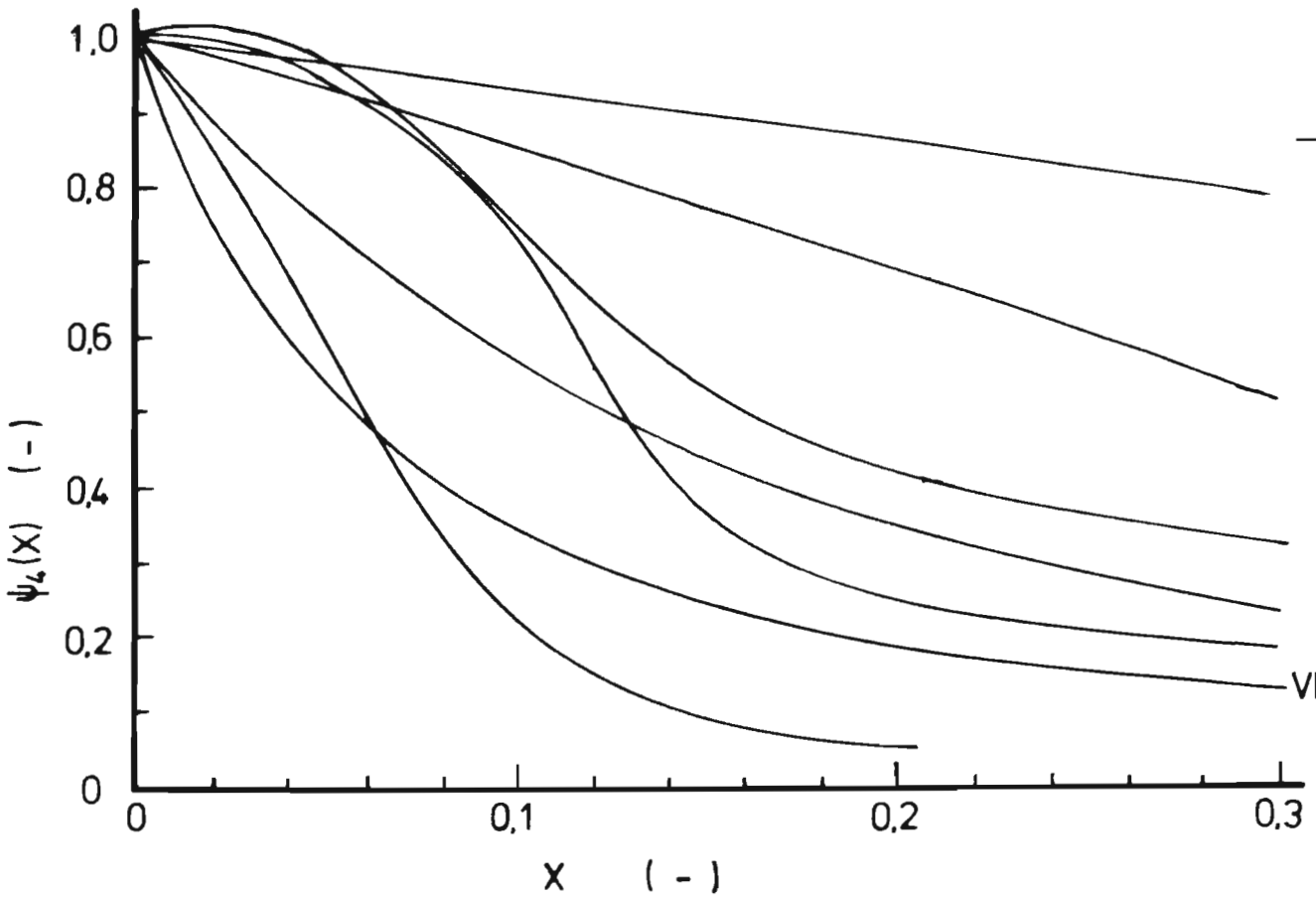

Sphalerite	Data case	Curve from
BDH	(i)	Calc. by eqn. 4.2 (shrinking core model)
ZCR	(ii)	Best fit off fig 4.10
VMZCR	(i) and (ii)	Best fit off fig 4.10
BDH	(ii)	Best fit off fig 4.15
PR	(ii)	Best fit off fig 4.13
VMWBM ; WBM	(i) and (ii)	Calc. by eqn 4.9 (see fig 4.7)
VMPR	(ii)	Best fit off fig 4.13

Figure 4.16 Comparison between the $\psi_4(X)$ versus X best fit and calculated curves for each of the sphalerites, presented previously on figures 4.7; 4.10; 4.13 and 4.15.

C H A P T E R 5

TESTING OF H_2S OXIDATION BY Fe^{3+} AND CASE (iii) LEACHING MODELS

5.1 OXIDATION OF H_2S BY Fe^{3+}

In this section model I describing the homogeneous H_2S oxidation by Fe^{3+} is tested using the results of experiments in which :-

a) H_2S was bubbled into 0,5 , 1,0 and 2,0 M H_2SO_4 before injecting Fe^{3+} into the reactor. Experiments like this were done with no solids present, and with activated charcoal initially present in the reactor. The latter results are reported in section 6.5 .

b) H_2S was generated by VMWBM, VMZCR, BDH or VMPR sphalerite solids leaching in aqueous H_2SO_4 , and Fe^{3+} was injected when the rate of increase in the H_2S partial pressure became very small. Details of the experimental procedures and analytical techniques are presented in Appendixes B and D .

Tables 5.1 to 5.5 summarise the initial experimental conditions and measured rates of oxidation of H_2S by Fe^{3+} in the total absence of solids, and in the presence of the various sphalerites.

5.1.1 TESTING MODEL I

Under initial rate conditions model I has the following form :-

$$r_{I_o} = \left(\frac{d\,[H_2S]}{dt}\right)_o = -k_I \frac{[H_2S]_o^{1,44}\,[Fe^{3+}]_o^{1,68}}{[H_2SO_4]_o^{2,49}} \quad \ldots\ldots\ldots \quad 5.1$$

where, according to Verhulst :-

$$k_I = 4{,}735 \times 10^{13} \exp\left(\frac{-67{,}72}{RT}\right) \quad \ldots\ldots\ldots \quad 5.2$$

At 318,0 K $k_I = 347{,}3$

Now define a rate constant $(k_{I_o})_{exp}$ based on equation 5.1 as follows :-

$$(k_{I_o})_{exp} = -(r_{I_o})_{exp} \times \frac{[H_2SO_4]_o^{2,49}}{[H_2S]_o^{1,44}\,[Fe^{3+}]_o^{1,68}} \quad \ldots\ldots\ldots \quad 5.3$$

where : -

$$(r_{I_o})_{exp} = \left(\frac{d\,P_{H_2S}}{dt}\right)_o \Big/ K_D$$

NOTE THAT : a) $\left(\frac{d\,P_{H_2S}}{dt}\right)_o$ is the measured initial rate of decrease in H_2S partial pressure after injecting the Fe^{3+} solution into the reactor.

TABLE	RUN NO.	$[H_2SO_4]_o$	$[Fe^{3+}]_o \times 10^3$ (kg-mol/m^3)	$[H_2S]_o \times 10^3$	$-(r_{I_o})_{exp} \times 10^3$ (kg-mol/min m^3)	① $(k_{I_o})_{exp}$	② $(k_{I_o})_{mod}$	③ ω
K 1	217	0,5	14,32	41,43	22,39	489,3	687,19	1,09
K 2	217	0,5	28,65	34,27	58,46	523,7	735, 4	1,17
K 3	216	1,0	14,32	25,54	2,309	568,9	569,0	0, 9
K 4	216	1,0	28,65	18,38	4,608	568,7	568,7	0, 9
K 5	218	2,0	14,32	25,84	0,5757	783,6	557,9	0,89
K 6	218	2,0	28,65	18,68	1,358	919,8	654,9	1,04

① Defined by eqn. 5.3
② Defined by eqn 5.4
③ Defined by eqn 5.5

Table 5.1 SUMMARY OF INITIAL EXPERIMENTAL CONDITIONS AND RATE OF HOMOGENEOUS OXIDATION OF H_2S BY Fe^{3+} (WITH NO SOLIDS PRESENT AT ALL)

TABLE	RUN NO.	$[H_2SO_4]_o$ (kg-mol/m³)	$[Fe^{3+}]_o \times 10^3$ (kg-mol/m³)	$[H_2S]_o \times 10^3$ (kg-mol/m³)	$-(r_{I_o})_{exp} \times 10^3$	$(k_{I_o})_{exp}$ ①	$(k_{I_o})_{mod}$ ②	③
K 7	172	0,48	5,5	6,5	0,453	642,7	920,8	1,46
K 8	172	0,48	13,8	4,87	1,27	582,2	834,2	1,33
K 9	176	0,97	5,5	10,32	0,222	933,1	947,1	1,51
K 10	176	0,97	13,8	9,19	0,774	819,7	832,0	1,32
K 11	175	1,95	5,5	18,11	0,112	1 192,0	859,2	1,37
K 12	175	1,95	13,8	16,6	0,631	1 623,0	1 170,0	1,86

① Defined by eqn 5.3
② " " " 5.4
③ " " " 5.5

Table 5.2 SUMMARY OF INITIAL EXPERIMENTAL CONDITIONS AND RATE OF OXIDATION OF H_2S BY Fe^{3+} IN THE PRESENCE OF VMWBM SPHALERITE SOLIDS

TABLE	RUN NO.	$[H_2SO_4]_o$	$[Fe^{3+}]_o$ x10^3	$[H_2S]_o$ x10^3	$-(r_{I_o})_{exp}$ x 10^3	$(k_I)_{exp}$ ①	$(k_I)_{mod}$ ②	ω ③
		(kg - mol / m^3)						
K 13	200	0,48	5,73	6,673	0,586	747,3	1 071,0	1,7
K 14	200	0,48	14,3	5,08	1,358	551,8	790,6	1,26
K 15	199	0,96	14,3	16,1	1,032	447,4	456,5	0,73
K 16	199	0,96	28,6	11,64	2,18	470,6	480,1	0,76
K 17	201	1,95	14,3	25,0	0,94	1 263,0	910,3	1,45
K 18	201	1,95	28,6	18,22	1,65	1 091,0	786,4	1,25
K 19	201	1,95	28,6	8,28	0,586	1 206,0	869,6	1,38

① Defined by eqn 5.3
② Defined by eqn 5.4
③ Defined by eqn 5.5

Table 5.3

SUMMARY OF INITIAL EXPERIMENTAL CONDITIONS AND RATE OF OXIDATION OF H_2S BY Fe^{3+} IN THE PRESENCE OF BDH SPHALERITE

TABLE	RUN NO.	$[H_2SO_4]_o$	$[Fe^{3+}]_o$ $\times 10^3$ (kg-mol/m³)	$[H_2S]_o$ $\times 10^3$	$-(r_{I_o})_{exp}$	① $(k_I)_{exp}$	② $(k_I)_{exp}$	③ 3
K 20	170	0,48	5,5	8,39	0,526	516,7	740,1	1,18
K 21	170	0,48	13,8	6,93	1,59	438,6	628,4	1,0
K 22	170	0,48	13,8	2,34	0,519	683,6	979,4	1,56
K 23	168	0,97	5,5	10,53	0,238	971,7	986,3	1,57
K 24	168	0,97	13,8	8,94	0,624	687,6	697,9	1,11
K 25	168	0,97	13,8	4,21	0,205	668,1	678,2	1,08
K 26	174	1,94	5,5	22,1	0,102	804,4	581,4	0,92
K 27	174	1,94	13,8	20,23	0,660	1 260,0	911,0	1,45
K 28	174	1,94	13,8	14,7	0,440	1 331,0	961,9	1,53

① Defined by eqn 5.3
② Defined by eqn 5.4
③ Defined by eqn 5.5

Table 5.4

SUMMARY OF INITIAL EXPERIMENTAL CONDITIONS AND RATE OF OXIDATION OF H_2S BY Fe^{3+} IN THE PRESENCE OF V M Z C R SPHALERITE

TABLE (-)	RUN NO. (-)	A (m^2/m^3)	$[H_2SO_4]_o$	$[Fe^{3+}]_o \times 10^3$	$[H_2S]_o \times 10^3$	$-(r_{I_o})_{exp} \times 10^3$	① $(k_{I_o})_{exp}$	② $(k_{I_o})_{mod}$	③ ω
			($kg\text{-}mol / m^3$)			($kg\text{-}mol/min\ m^3$)			
K 29	171	17,75	0,48	5,5	5,39	5,39	10 290,0	14 740,0	23,44
K 30	171	17,75	0,48	13,8	3,65	3,65	2 534,0	3 631,0	5,77
K 31	169	4,66	0,97	5,5	9,84	1,65	7 427,0	7 539,0	11,99
K 32	169	4,66	0,97	13,8	7,95	1,60	2 088,0	2 119,0	3,37
K 33	101	28,68	0,95	4,48	12,27	15,11	66 330,0	68 020,0	108,17
K 34	101	28,68	0,95	4,48	9,81	7,74	46 890,0	48 090,0	76,48
K 35	173	8,564	1,95	5,5	20,39	4,63	41 530,0	29 940,0	47,61
K 36	173	8,564	1,95	5,5	18,67	3,07	31 270,0	22 540,0	35,85
K 37	173	8,564	1,95	13,8	16,64	4,21	10 790,0	7 778,0	12,37
K 38	173	8,564	1,95	12,1	11,29	2,90	16 200,0	11 680,0	18,58

① Defined by eqn 5.3
② Defined by eqn 5.4
③ Defined by eqn 5.5

Table 5.5

SUMMARY OF INITIAL EXPERIMENTAL CONDITIONS AND RATE OF OXIDATION OF H_2S BY Fe^{3+} IN THE PRESENCE OF VMPR SPHALERITE

b) $K_D = \frac{(P_{H_2S})_o}{[H_2S]_b}$ if the initial partial pressure and concentration of H_2S are known;

c) K_D may alternatively be calculated using equation E.27.

Tables 5.1 to 5.5 also present calculated values of $(k_{I_o})_{exp}$ for each experiment.

Figure 5.1 plots the $(k_{I_o})_{exp}$ results reported on tables 5.1 and 5.2 against $[H_2SO_4]_o$, and $(k_{I_o})_{exp}$ is observed to increase with increasing $[H_2SO_4]_o$.

It was established that reducing the value of the exponent on the H_2SO_4 term in equation 5.1 from 2.49 to 2.0 resulted in a significantly better fit of the equation to the data.

Define a modified rate constant $(k_{I_o})_{mod}$ as follows :-

$$(k_{I_o})_{mod} = -(r_{I_o})_{exp} \cdot \frac{[H_2SO_4]^{2,0}}{[H_2S]_o^{1,44}[Fe^{3+}]_o^{1,68}} \quad \ldots\ldots\ldots \quad 5.4$$

where $(r_{I_o})_{exp}$ is defined as before.

Tables 5.1 to 5.5 present the calculated $(k_{I_o})_{mod}$ values for each experiment.

To facilitate comparison of the various results, define a rate constant ratio ω as follows :-

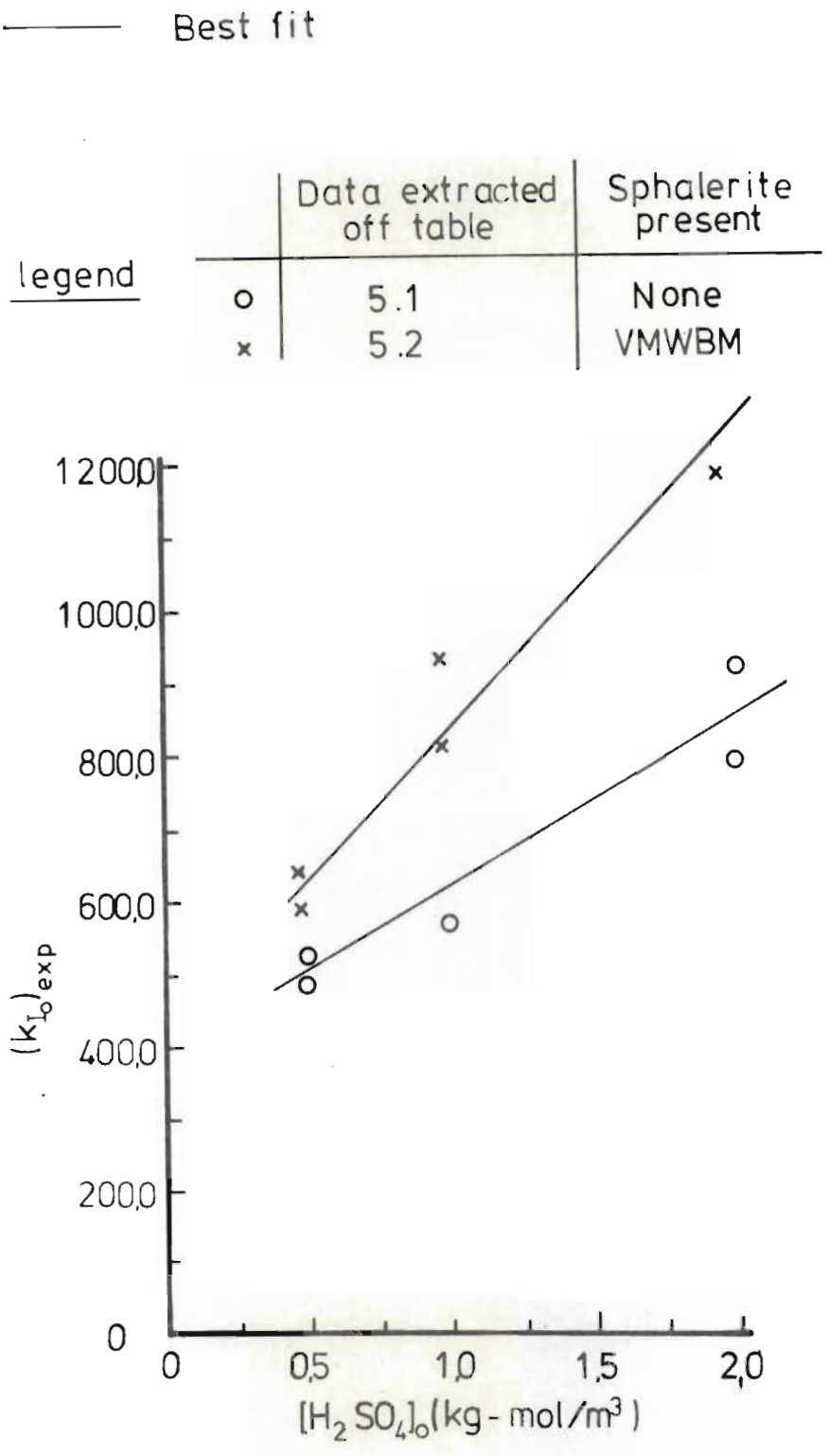

Figure 5.1 H_2S oxidation rate constant $(k_{I_o})_{exp}$ versus $[H_2SO_4]_o$. $(k_{I_o})_{exp}$ was calculated using the Verhulst model as expressed by eqn 5.3

$$\omega = \frac{(k_{I_o})_{mod}}{628,8} \qquad \ldots\ldots\ldots\ 5.5$$

where $(k_{I_o})_{mod}$ is defined by equation 5.4. The value 628,8 is the arithmetic mean of the $(k_{I_o})_{mod}$ values calculated for the purely homogeneous experiments on table 5.1.

Table 5.6 summarises the arithmetic mean and standard deviation of the $(k_{I_o})_{exp}$, $(k_{I_o})_{mod}$ and ω values for the results presented on tables 5.1 to 5.5.

The following observations are made concerning the results summarised on table 5.6 :-

a) Except when VMPR solids were present, the standard deviations for the $(k_{I_o})_{mod}$ values were significantly less than for the $(k_{I_o})_{exp}$ values. This suggests that the modified form of model I (represented by equation 5.6) fits the data significantly better than the original form of model I (represented by equation 5.1).

b) The ω values for the experiments performed in the presence of the sphalerite solids are significantly larger than in the purely homogeneous case where no solids were present. In particular ω for the case where VMPR sphalerite solids were present is very large, and the standard deviation for this case is so large as to suggest that the modified Verhulst equation does not fit.

Sphalerite present	$(\bar{k}_{I_o})_{exp}$	S	$(\bar{k}_{I_o})_{mod}$	S	$\bar{\omega}$	S
None	640,7	167,2	628,8	74,4	1,0	0,12
VMWBM	965,5	389,1	927,2	127,8	1,48	0,2
BDH	828,3	355,1	766,4	224,8	1,22	0,36
VMZCR	818,0	311,2	796,1	162,5	1,27	0,26
VMPR	23 534,9	21 890,3	21 607,7	21 508,6	34,36	34,2

T A B L E 5. 6 SUMMARY OF THE ARITHMETIC MEAN AND STANDARD DEVIATIONS OF THE $(k_{I_o})_{exp}$, $(k_{I_o})_{mod}$ AND ω VALUES PRESENTED ON TABLES 5. 1 TO 5. 5

Figure 5.2 plots ω versus A, where A is the B.E.T. area in the reactor at the time of injecting the Fe^{3+}. It is observed that ω increases with increasing A, and that ω is significantly larger after the first injection of Fe^{3+} than after subsequent introductions of Fe^{3+}.

This suggests that the presence of the various sphalerite solids catalyse the H_2S oxidation reaction, and that S^o formed on the surface blinds active sites and reduces the catalytic effect.

The ω values increase in the order :

no solids < BDH < VMWBM < VMZCR $\ll$ VMPR .

It may then be concluded that :-

i) the presence of sphalerite solids does catalyse the Fe^{3+} oxidation of H_2S, particularly in the case of the VMPR sphalerite ;

ii) the modified form of the Verhulst equation fits the oxidation kinetics better than the original form, and for the homogeneous oxidation of H_2S by Fe^{3+} the modified Verhulst equation may be expressed as follows :-

$$\frac{d[H_2S]}{dt} = -(k_I)_{mod} \times \frac{[H_2S]^{1,44}\,[Fe^{3+}]^{1,68}}{[H_2SO_4]^{2,0}} \quad \ldots\ldots\ldots \quad 5.6$$

with $(k_I)_{mod} = 8,572 \times 10^{13} \exp \frac{-67,72}{RT}$

and at 318,0 K : $(k_I)_{mod} = 628,8$.

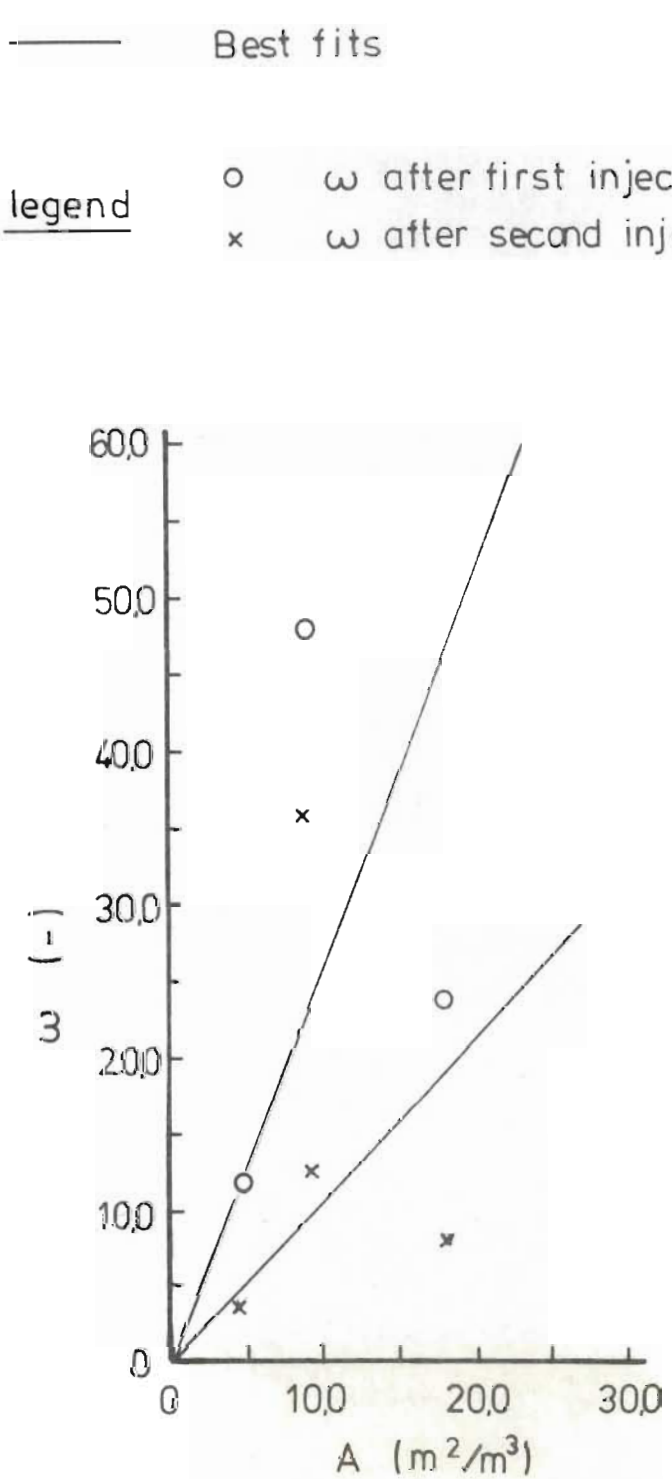

Figure 5.2 H_2S oxidation rate constant ratio ω (defined by eqn 5.5) versus the total VMPR sphalerite surface area A present. The catalytic effect of the VMPR solids on the Fe^{3+} oxidation of H_2S is evident. Data on this figure was extracted off table 5.5

5. 2 QUALITATIVE RESULTS OF LEACHING VARIOUS SPHALERITES UNDER CASE (iii) CONDITIONS ($[Fe^{3+}]_o : [H_2SO_4]_o \leq 0,1$)

Equations 2.98 and 2.99 (summarised on table 2.4) represents model J proposed for the leaching of VMWBM, VMZCR and BDH (but not VMPR) sphalerites under case (iii) conditions. According to mechanism 2 proposed in chapter 2, when leaching these sphalerites under case (iii) conditions -

a) the $S^=$ species react with adsorbed Fe^{3+} to form S^o in situ (oxidative leaching) ;

b) the $S^=$ species react with adsorbed H^+ to form H_2S (non-oxidative leaching) ;

c) the H_2S and Fe^{3+} react homogeneously.

These reactions take place simultaneously.

In section 5.1 it was demonstrated that the oxidation of H_2S by Fe^{3+} was catalysed by the sphalerite surface present. Since this catalytic effect has not been studied in detail or been allowed for in model J, the results of leaching the various sphalerites under case (iii) conditions are merely dealt with qualitatively in this section.

Table 5.7 summarises the conditions for the experiments in which VMWBM, VMZCR, BDH and VMPR sphalerites were leached under case (iii) conditions. It is observed that case (i) experiments - ($[Fe^{3+}]_o = 0,0$) have been included in table 5.7 for comparative purposes. Thus, in this section the $[Zn^{2+}]$ versus time and P_{H_2S} versus time rate curves for leaching without Fe^{3+} and with low initial

TABLE	RUN NO.	$[H_2SO_4]_o$ (kg-mol/m^3)	$[Fe^{3+}]_o \times 10^3$ (kg-mol/m^3)	
I 8	172	0,5	0	
L 1	180	0,5	13,75	
I 2	176	1,0	0	
L 2	177	1,0	13,75	VMWBM
L 3	178	1,0	27,50	SPHALERITE
L 4	179	1,0	55,01	(M_o = 0,01 kg)
L 5	210	1,0	57,03	
I 9	175	2,0	0	
L 6	181	2,0	13,75	
I 17	167	1,0	0	VMZCR
L 14	207	1,0	28,67	SPHALERITE
L 15	211	1,0	57,3	(M_o = 0,01 kg)
I 36	199	1,0	0	BDH
L 16	206	1,0	28,67	SPHALERITE
L 17	208	1,0	114,67	(M_o = 0,004 kg)
I 27	132	1,0	0	VMPR
L 18	209	1,0	14,32	SPHALERITE
L 19	205	1,0	28,67	(M_o = 0,01 kg)

NOTES :- 1) Temp. = 318,0 K

2) Stirrer = 1 000,0 rpm

TABLE 5.7 SUMMARY OF EXPERIMENTAL CONDITIONS FOR VMWBM, VMZCR, BDH AND VMPR SPHALERITES LEACHING UNDER CASE (i) AND (iii) CONDITIONS

concentrations of Fe^{3+} are compared.

In chapter 6 (section 5) the results of leaching VMWBM sphalerite with activated charcoal present under case (i) and case (iii) conditions are presented.

5.2.1 VMWBM SPHALERITE LEACHING UNDER CASE (iii) CONDITIONS

Figures 5.3a and 5.3b plot $[Zn^{2+}]$ versus time and P_{H_2S} versus time rate curves for VMWBM sphalerite leaching without and with low $[Fe^{3+}]_o$ present. Figure 5.4 plots $[Zn^{2+}]$ versus $[Fe^{3+}]_o$ at different discrete time intervals; where the $[Zn^{2+}]$ values were either experimentally determined or interpolated off the curves on figure 5.3.

It is observed that the amount of $[Zn^{2+}]$ leached after a given time interval initially decreases to a minimum as $[Fe^{3+}]_o$ increases.

From figure 5.3b it is observed that as $[Fe^{3+}]_o$ increases, the measurable amount of H_2S formed decreases. For $[Fe^{3+}]_o = 27{,}5 \times 10^{-3}$ (kg-mol/m^3), the P_{H_2S} is observed to increase to a maximum at about t = 5,0 mins., and then decrease to zero. After 30 mins the P_{H_2S} is observed to increase again. It is apparant that for $[Fe^{3+}]_o = 55{,}0 \times 10^{-3}$ (kg-mol/m^3), negligible measureable H_2S is formed.

Figures 5.5a and 5.5b plot $[Zn^{2+}]$ versus time and P_{H_2S} versus time rate curves for VMWBM sphalerite leaching without and with Fe^{3+} initially

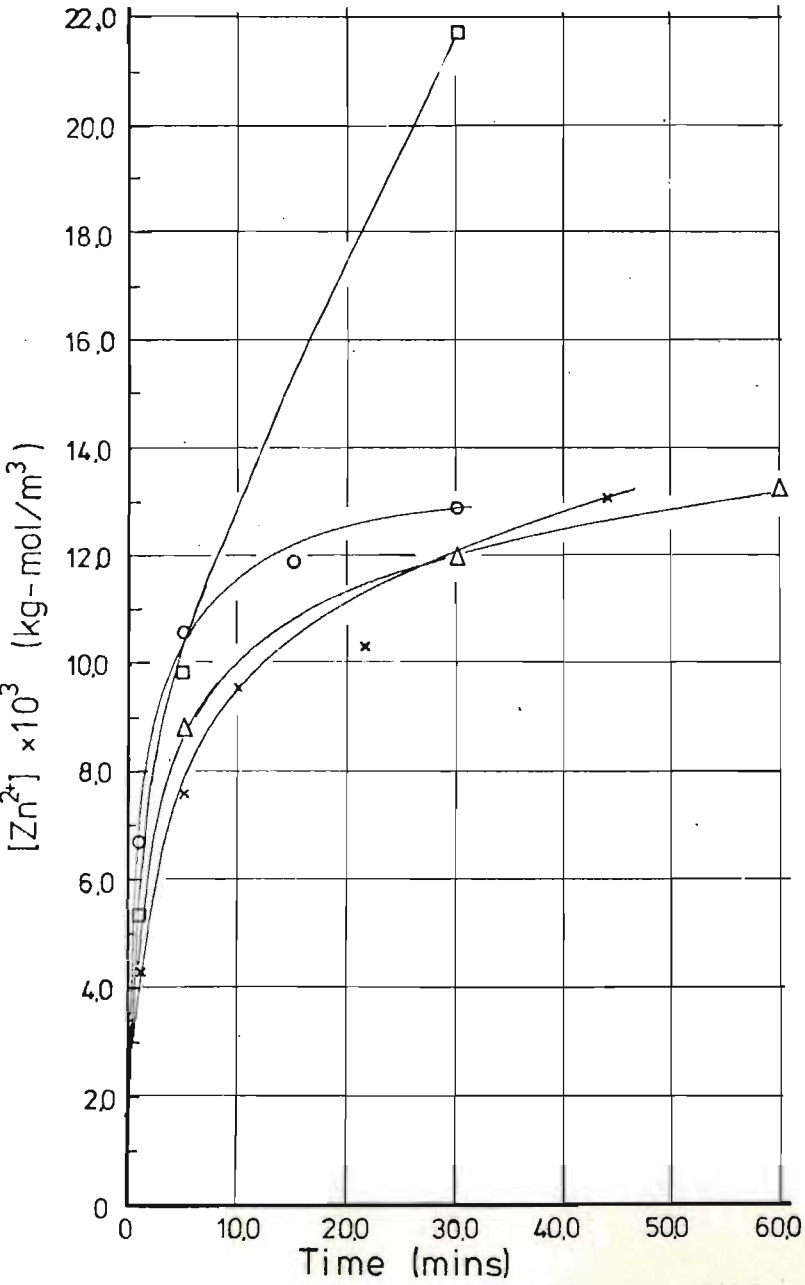

(on fig 5.3a) Best fit through exptl. $[Zn^{2+}]$ data.

legend

Points	Curves	Data on table	$[Fe^{3+}]_o \times 10^3$ (kg-mol/m^3)
o	a	I 2	0
×	b	L 2	13,75
Δ	c	L 3	27,50
□	d	L 4	55,00

conditions

$[H_2SO_4]_o$ (kg-mol/m^3)		1,0
Temp.	(K)	318,0
M_o	(kg)	0,01
Stirrer	(rpm)	1000,0

Fig. 5.3a

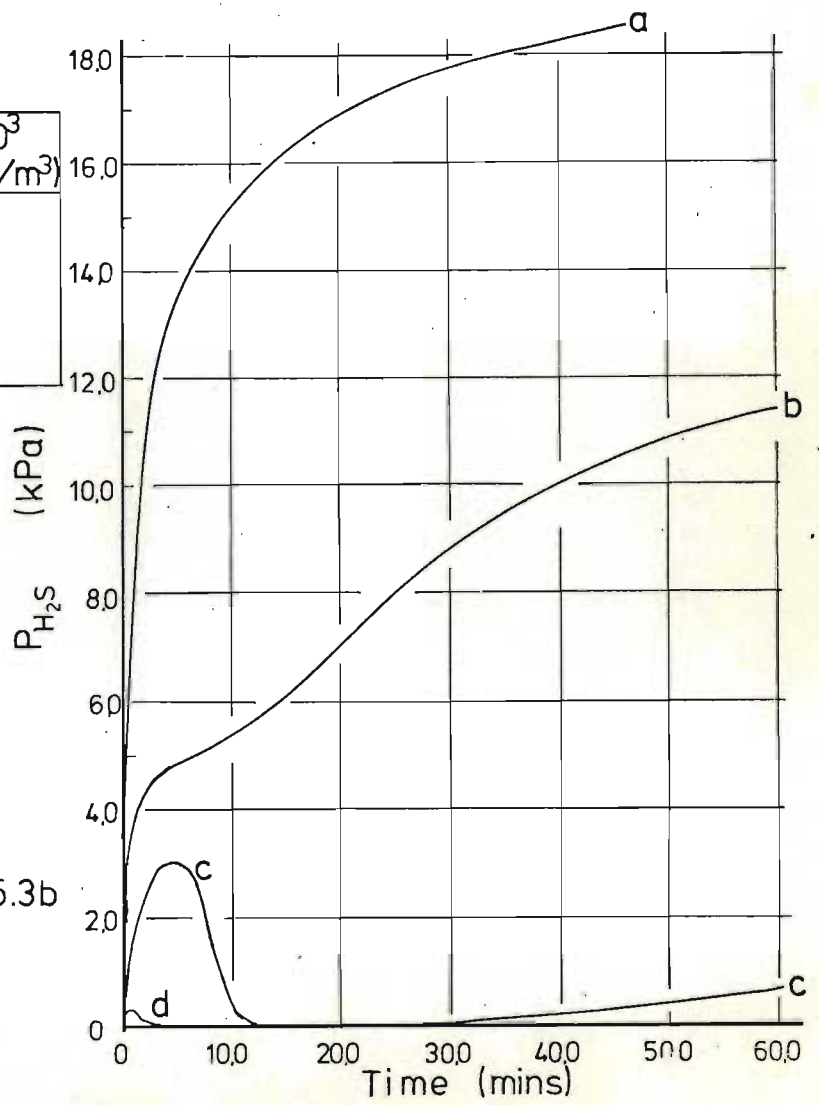

Fig 5.3b

Figures 5.3a and 5.3b Comparison between case(i) and case(iii) exptl. $[Zn^{2+}]$ and P_{H_2S} leaching results for VMWBM sphalerite.

——— Best fit

legend
o Exptl. $[Zn^{2+}]$ values
× $[Zn^{2+}]$ values interpolated off fig 5.3a

conditions

$[H_2SO_4]_o$	(kg-mol/m)	1,0
Temp.	(K)	318,0
M_o	(kg)	0,01
Stirrer	(rpm)	1000,0

Time (mins)
15,0

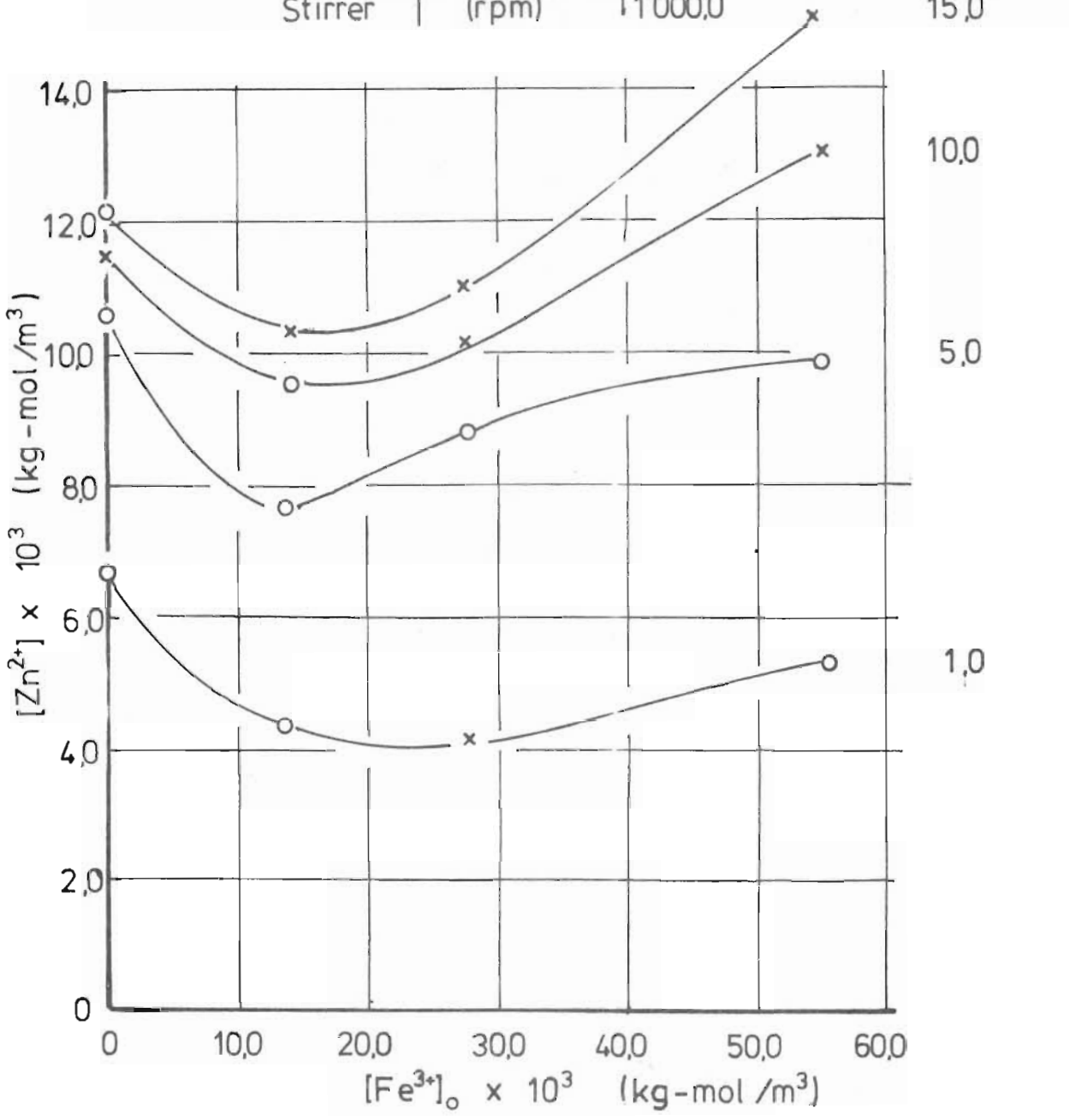

Figure 5.4 Effect of initial $[Fe^{3+}]$ on the amount of Zn^{2+} produced from VMWBM sphalerite during different time intervals.

——— Best fit through exptl. $[Zn^{2+}]$ data.
(on fig 5.5a)

Point (-)	Curve (-)	Data on table	$[Fe^{3+}]_o \times 10^3$ (kg-mol/m^3)	$[H_2SO_4]_o$
o	a	I 9	0	2,0
×	b	L 6	13,75	2,0
Δ	c	I 2	0	1,0
□	d	L 2	13,75	1,0
+	e	I 8	0	0,5
•	f	L 1	13,75	0,5

legend

Temp.	(K)	318,0
M_o	(kg)	0,01
Stirrer	(rpm)	1000,0

conditions

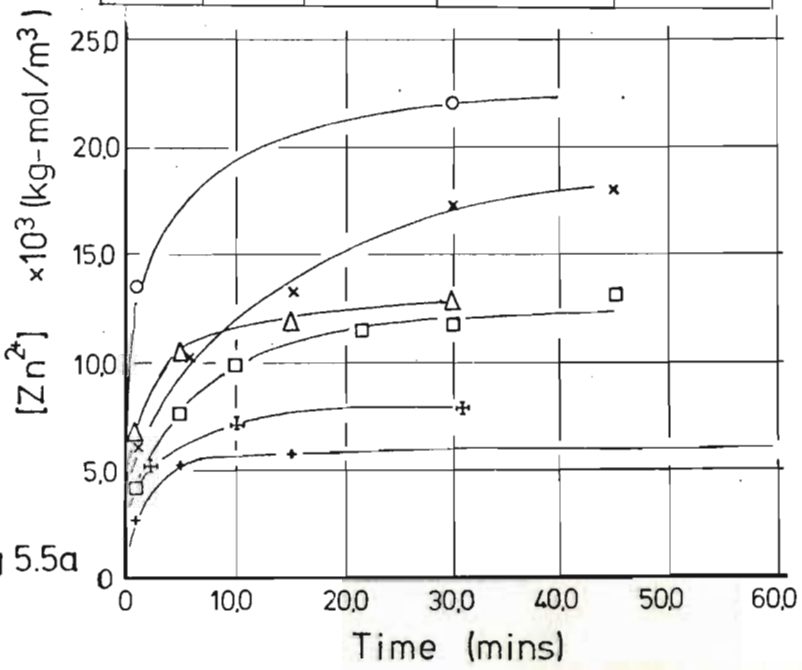

Fig 5.5a

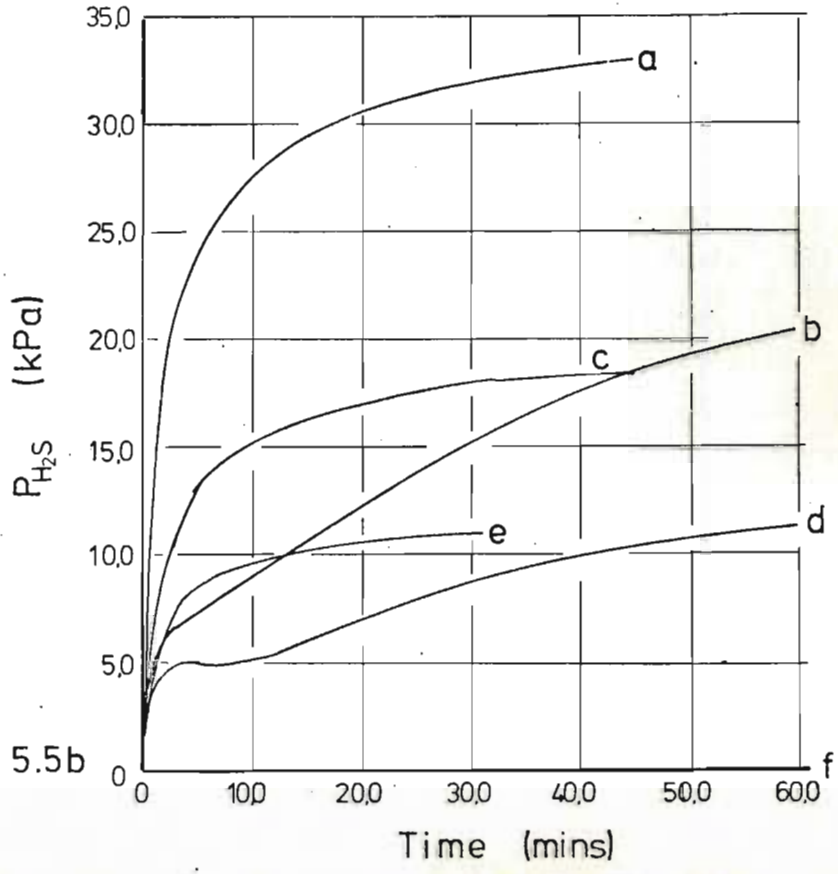

Fig 5.5b

Figures 5.5a and 5.5b Comparison between case(i) and case(iii) exptl. $[Zn^{2+}]$ and P_{H_2S} results for VMWBM sphalerite at different $[H_2SO_4]_o$ values.

present, at three different H_2SO_4 concentrations. From figure 5.5a it is observed that the apparant suppression of the initial leaching rate resulting from adding Fe^{3+}, increases with increasing $[H_2SO_4]_o$. From figure 5.5b it is observed that as the $[H_2SO_4]_o$ decreases, so the measureable amount of H_2S formed decreases (and in fact was zero at $[H_2SO_4]_o$ = 0,5).

5.2.2 VMZCR SPHALERITE LEACHING UNDER CASE (iii) CONDITIONS

Figures 5.6a and 5.6b plot the $[Zn^{2+}]$ versus time and P_{H_2S} versus time rate curves for the VMZCR sphalerite leaching without and with Fe^{3+} initially present. On figure 5.6b the P_{H_2S} is observed to increase to maximum (with Fe^{3+} initially present), before decreasing to a non-zero minimum value. It is probable that during vibratory milling of the acid pre-treated ZCR sphalerite to produce the VMZCR sphalerite, CO_2 forming gangue was liberated. The formation of an inert gas such as CO_2 would account for the non-zero minimum observed on figure 5.6b.

From figure 5.6a it is observed that addition of Fe^{3+} apparantly suppressed the dissolution rate, but to a significantly less extent for a given Fe^{3+} concentration than in the case of the VMWBM sphalerite (figure 5.3a).

(on fig 5.6a) Best fit through exptl $[Zn^{2+}]$ data.

Point (-)	Curve (-)	Data on table	$[Fe^{3+}]_o \times 10^3$ (kg-mol/m^3)
○	a	I 17	0
×	b	L14	28,67
Δ	c	L15	57,30

Legend

Conditions

$[H_2SO_4]_o$ (kg-mol/m^3)		1,0
Temp.	(K)	318,0
M_o	(kg)	0,01
Stirrer	(rpm)	1000,0

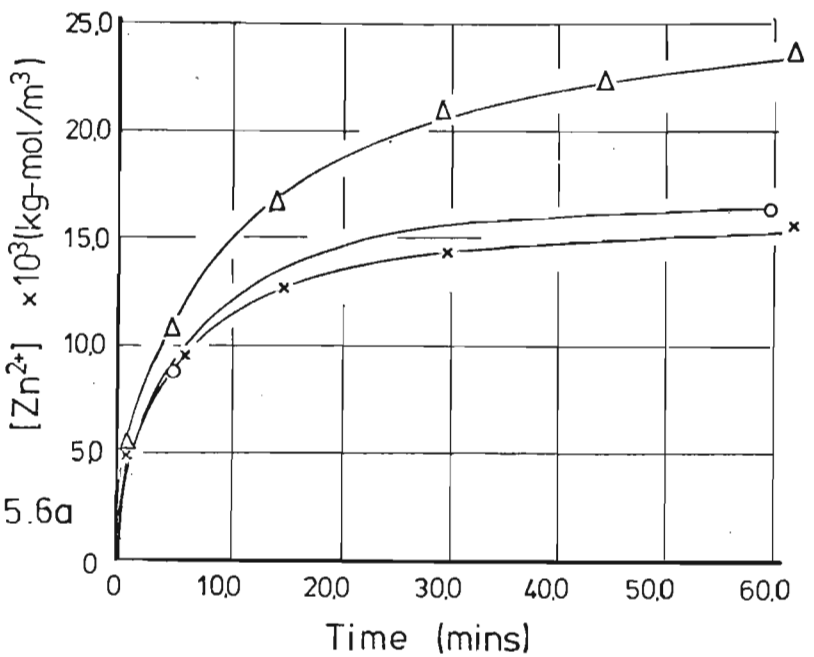

Fig 5.6a

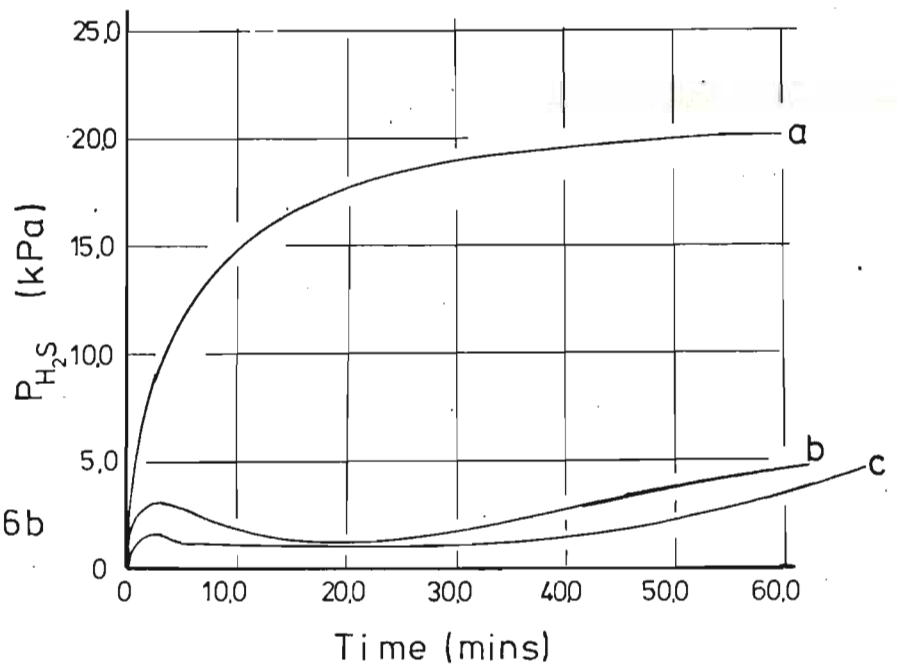

Fig 5.6b

Figures 5.6a and 5.6b Comparison between case (i) and case (iii) exptl. $[Zn^{2+}]$ and P_{H_2S} leaching data for VMZCR sphalerite.

5.2.3 BDH SPHALERITE LEACHING UNDER CASE (iii) CONDITIONS

Figures 5.7a and 5.7b plot the $[Zn^{2+}]$ versus time and P_{H_2S} versus time rate curves for the BDH sphalerite leaching without and with Fe^{3+} initially present. It is observed on figure 5.7a that the initial rate is suppressed significantly as a result of adding Fe^{3+} to the system.

On figure 5.7b it is observed that for $[Fe^{3+}]_o$ = 0,1147 kg-mol/m^3, the P_{H_2S} rapidly goes through a very small maximum and decreases to a constant non-zero value. It may be possible that an inert gas was formed, but it is more likely that during the reaction start-up experimental error resulted in a shift in the zero base line.

5.2.4 VMPR SPHALERITE LEACHING UNDER CASE (iii) CONDITIONS

Figures 5.8a and 5.8b plot $[Zn^{2+}]$ versus time and P_{H_2S} versus time rate curves for VMPR sphalerite leaching under case (iii) conditions. It is observed on figure 5.8a that adding Fe^{3+} progressively increases the initial leaching rate.

According to the overal reaction stoichiometry:

$$ZnS + 2Fe^{3+} \longrightarrow Zn^{2+} + S^{o} + 2Fe^{2+}$$

Thus for $[Fe^{3+}]_o$ = 14,32 x 10^{-3} and 28,67 x 10^{-3} kg-mol/m^3, $[Zn^{2+}]$ = 7,16 x 10^{-3} or 14,335 x 10^{-3}

(on fig 5.7a) Best fit through exptl. $[Zn^{2+}]$ data.

legend

Point	Curve	Data on table	$[Fe^{3+}]_o \times 10^3$ (kg-mol/m^3)
o	a	I 36	0
Δ	b	L16	28,67
×	c	L17	114,57

conditions

$[H_2SO_4]$	(kg-mol/m^3)	1,0
Temp.	(K)	318,0
M_o	(kg)	0,004
Stirrer	(rpm)	1000,0

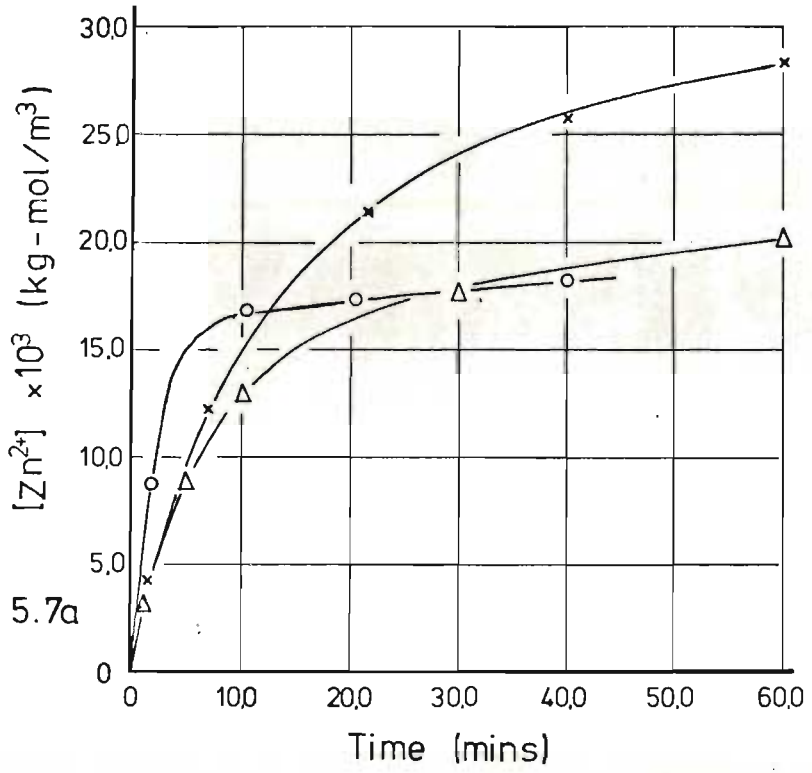

Fig 5.7a

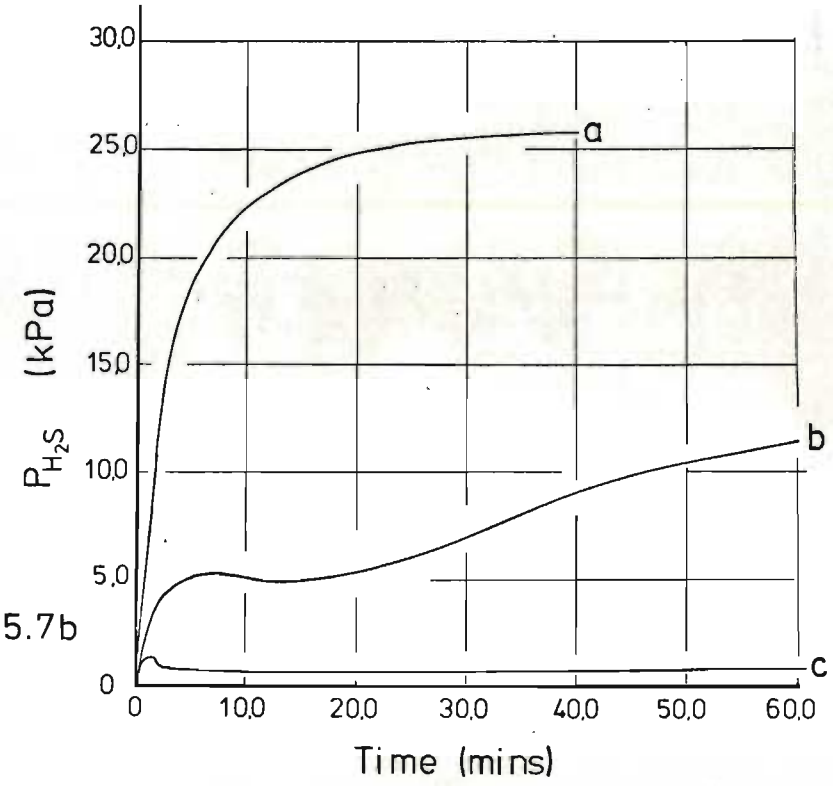

Fig 5.7b

Figures 5.7a and 5.7b Comparison between case(i) and case(ii) exptl. $[Zn^{2+}]$ and P_{H_2S} leaching data for BDH sphalerite.

(on fig 5.8a) Best fit through exptl. $[Zn^{2+}]$ data.

legend

Point (-)	Curve (-)	Data on table	$[Fe^{3+}]_o \times 10^3$ (kg-mol/m^3)
o	a	I 27	0
×	b	L 18	14,32
Δ	c	L 19	28,67

conditions

$[H_2SO_4]_o$	(kg-mol/m^3)	1,0
Temp.	(K)	318,0
M_o	(kg)	0,01
Stirrer	(rpm)	1000,0

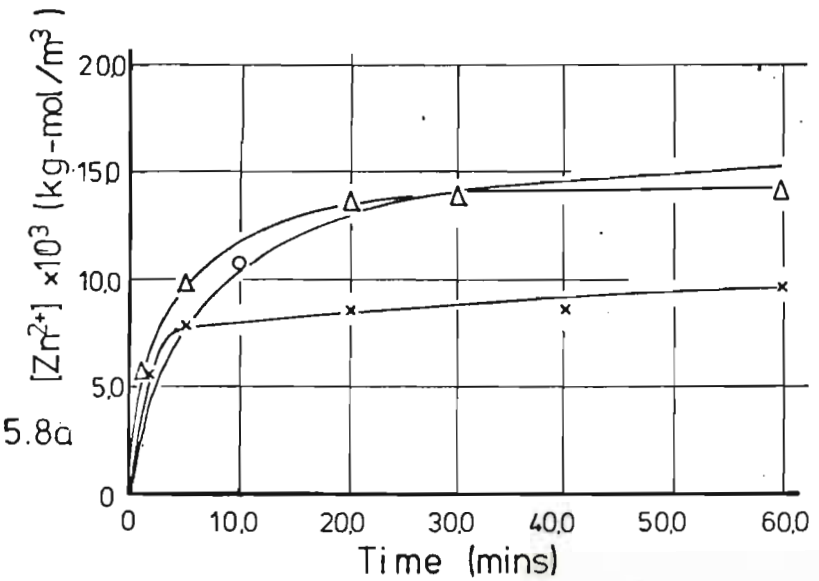

Fig 5.8a

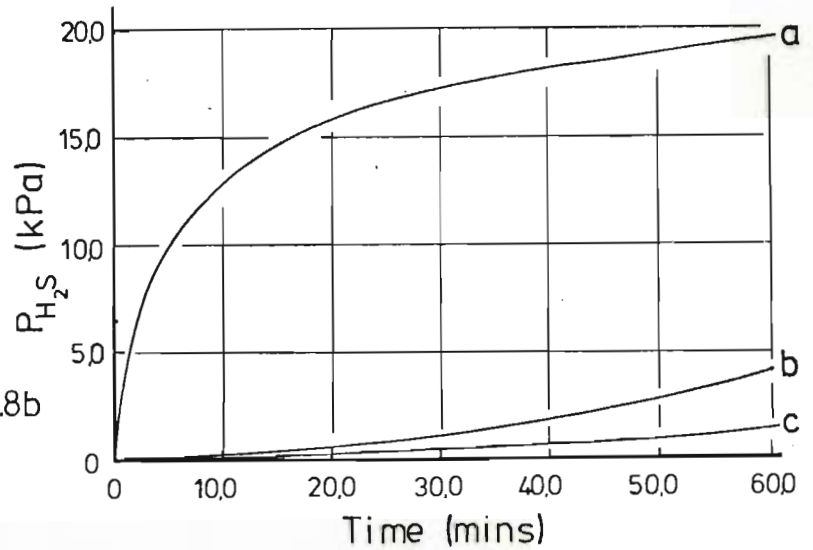

Fig 5.8b

Figures 5.8a and 5.8b Comparison between case(i) and case(iii) exptl. $[Zn^{2+}]$ and P_{H_2S} leaching data for VMPR sphalerite.

kg-mol/m^3 will be leached into solution respectively.

It is seen on figure 5.8 a that the leaching rates decrease rapidly as these $[Zn^{2+}]$ values are approached. On figure 5.8 b it is observed that negligible measureable H_2S is initially formed.

5.2.5 COMPARISON BETWEEN THE LEACHING OF VMWBM, VMZCR, BDH AND VMPR SPHALERITES UNDER CASE (iii) CONDITIONS

Figure 5.9 a plots $[Zn^{2+}]$ versus time for the four different sphalerites each leaching with $[Fe^{3+}]_o = 28,0 \times 10^{-3}$ kg-mol/m^3. Figure 5.9 b plots P_{H_2S} versus time for the four sphalerites leaching without Fe^{3+} and with $[Fe^{3+}]_o = 28,0 \times 10^{-3}$ kg-mol/m^3.

It is observed on figure 5.9 b that the added Fe^{3+} has least effect on the P_{H_2S} versus time rate curve for the BDH sphalerite. At time $t = 5,0$ mins it is observed that the P_{H_2S} for the different sphalerites increases in the order -
VMPR $<$ VMZCR $<$ VMWBM $<$ BDH .

On figure 5.9 a it can be seen that at time $t = 5,0$ mins, the $[Zn^{2+}]$ varied between 0,009 and 0,01 kg-moles/m^3 for each of the sphalerites. These results suggest that under the case (iii) condition being considered here, the BDH sphalerite leached non-oxidatively to a significant extent as well as oxidatively, whilst the VMPR sphalerite leached mainly non-oxidatively. The proportion of the dissolution occuring non-oxidatively for the four sphalerites

legend

Sphal. type	Point (-)	Curve (-)	Data on table	$[Fe^{3+}]_o \times 10^3$ (kg-mol/m³)	M_o (kg)
VMWBM		a	I 2	0	0,01
VMWBM	Δ	b	L 3	27,50	0,01
VMZCR		c	I 17	0	0,01
VMZCR	×	d	L 14	28,67	0,01
VMPR		e	I 27	0	0,01
VMPR	□	f	L 19	28,67	0,01
BDH		g	I 36	0	0,004
BDH	+	h	L 17	28,67	0,004

(on fig 5.9a) Best fit through exptl. $[Zn^{2+}]$ data.

conditions

$[H_2SO_4]_o$ (kg-mol/m³)		1,0
Temp.	(K)	318,0
Stirrer	(rpm)	1000,0

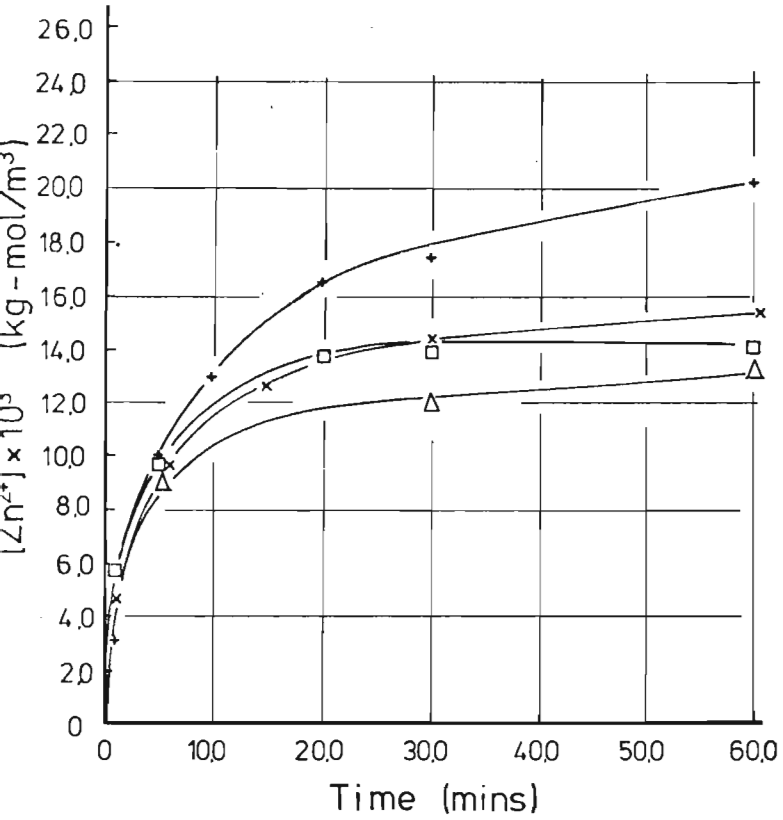

Fig 5.9a

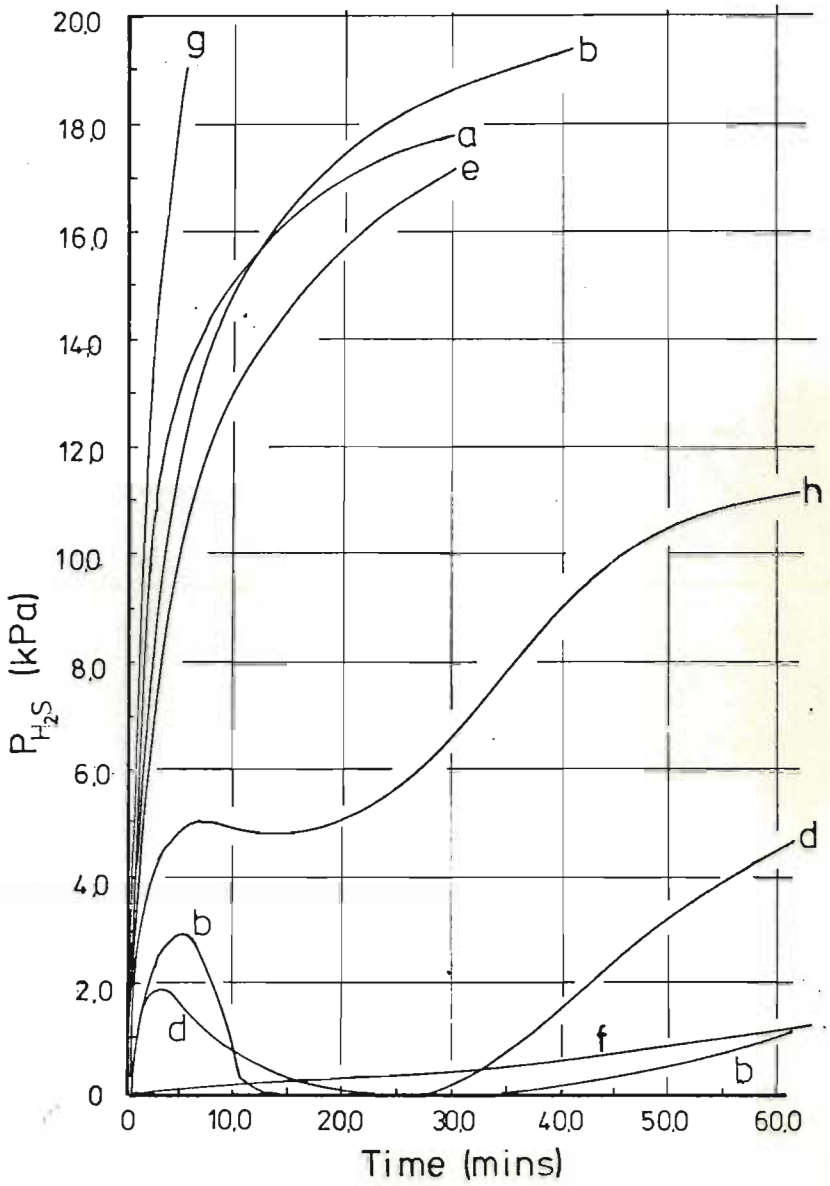

Fig 5.9b

Figures 5.9a and 5.9b Comparison of the exptl. $[Zn^{2+}]$ and P_{H_2S} rate curves for the VMWBM, VMZCR, VMPR and BDH sphalerites leaching under case(iii) conditions. (P_{H_2S} curves for leaching under case(i) conditions are also plotted.)

thus appears to increase in the order -
BDH < VMWBM < VMZCR < VMPR .

5. 3 OVERALL DISCUSSION OF RESULTS REPORTED IN SECTIONS 5. 1 AND 5. 2

It is proposed that many of the phenomena observed in sections 5. 1 and 5. 2 may be explained in terms of Langmuir-Hinschelwood adsorption theories. In particular it is proposed that the four sphalerites exhibit different capacities to adsorb ferric ions, with the Fe^{3+} adsorption capacities varying as follows :-

BDH < VMWBM < VMZCR $\ll$ VMPR .

Evidence to support this proposal is as follows :-

a) In section 3.3 it was demonstrated that the rates of leaching these sphalerites under case (ii) conditions increases in the order proposed above.

b) In section 5. 1 it was shown that (apart from the VMZCR sphalerite) the sphalerites catalysed the oxidation reaction in the above mentioned order.

c) In section 5. 2. 5 it was demonstrated that for the four different sphalerites leaching under case (iii) conditions, the proportion of the dissolution which occurs non-oxidatively increases for the sphalerites in the order shown above.

However, it is difficult to explain why the initial rates of dissolution are suppressed with small additions of Fe^{3+}, (see figure 5.4). It is possible that electrokinetic theories could explain this phenomena more satisfactorily than adsorption theories.

C H A P T E R 6

MISCELLANEOUS ADDITIONAL RELEVENT OBSERVATIONS

The purpose of this chapter is to present additional relevent qualitative results, which could not be conveniently included elsewhere in this thesis.

6. 1 SCANNING ELECTRON MICROSCOPIC (S.E.M.) AND OPTICAL MICROSCOPIC (O.M.) PHOTOGRAPHS OF VARIOUS UNLEACHED AND LEACHED SPHALERITE PARTICLES

Figures 6. 1 to 6. 13 present S.E.M. photographs of WBM, ZCR and PR sphalerite particles:-

a) before leaching (figures 6. 1, 6. 2, 6. 4 and 6. 9) ;

b) after leaching under case (ii) conditions but before washing with CCl_4 so that elemental sulphur formed in-situ is visible, (figures 6.6, 6. 7, 6. 10 and 6. 12) ;

c) after leaching under case (ii) conditions

and after washing with CCl_4 to remove all elemental sulphur, (figures 6.3, 6.5, 6.8, 6.11 and 6.13).

The captions provide full descriptions for each of the S.E.M. photographs.

Figures 6.14 to 6.16 present O.M. photographs of polished sections of WBM, ZCR and PR sphalerite particles, demonstrating in particular the internal cracks and pores present inside particles. The captions further describe these photographs.

Figures 6.17 and 6.18 present O.M. photographs of etched ZCR and PR sphalerite polished sections. Preferential zones of leaching are observed, particularly in the vicinity of the chalcopyrite inclusions in the case of the PR sphalerite. These photographs are also further described in their captions.

The following general observations may be made and conclusions drawn from inspecting all the photographs.

1) The WBM, ZCR and PR sphalerite particles all possess rough external surfaces, and contain significant numbers of internal cracks or pores. This helps explain the results presented in Appendix F which show that the measured B.E.T. areas for these sphalerites are much larger than one would expect, had they been considered solid spheres; the excess area being contributed by external roughness, and

internal cracks or pores.

2) The surfaces of the leached particles appear much rougher than those of the unleached particles (especially for the PR sphalerite). This explains why the B.E.T. areas of leached particles increased when leaching the PR and ZCR sphalerites (figures F 5 and F 6).

It is difficult, however, to explain why the WBM sphalerite B.E.T. area decreased during leaching approximately according to the shrinking core model prediction (figure F 4).

3) Figures 6. 7, 6. 10 and 6. 12 show that for PR, ZCR and WBM sphalerites leaching to similar extents in acidic ferric sulphate media -

(i) the PR sphalerite forms a very dense sulphur coating;

(ii) the ZCR sphalerite forms elemental sulphur coatings in specific zones of the particle;

(iii) the WBM sphalerite appears to form pits and cracks filled with elemental sulphur.

In each case elemental sulphur on the surface is distinctly visible.

4) From figures 6. 16 and 6. 17 it is evident that the PR sphalerite contains large amounts of chalcopyrite inclusions. From figures 6. 17 and 6. 18 it is evident that PR and ZCR sphalerites demonstrate complex etching patterns. In the case of the PR sphalerite, etching takes place preferentially in the vicinity of chalcopyrite inclusion zones.

(facing figs 6.1 to 6.5)

FIGURE 6.1 — S.E.M. photograph of unleached WBM sphalerite particles (from -75,0 + 63,0μm size fraction). Magnification: 200,0 x

FIGURE 6.2 — S.E.M. photograph of unleached ZCR sphalerite particles (from -75,0 + 63,0μm size fraction). Magnification: 200,0 x

FIGURE 6.3 — S.E.M. photograph of CCl_4 washed leached ZCR sphalerite particles (from -90,0 + 75,0μm size fraction). Particles taken from final leach residue of experiment reported on table J 21. Extent leached: X = 0,68 Magnification: 200,0 x

FIGURE 6.4 — S.E.M. photograph of unleached PR sphalerite particles (from -75,0 + 63,0μm size fraction). Magnification: 200,0 x

FIGURE 6.5 — S.E.M. photograph of CCl_4 washed leached PR sphalerite particles (from -75,0 + 63,0μm size fraction). Particles taken from final residue of experiment reported on table J 39. Extent leached: X = 0,33 Magnification: 200,0 x

Figure 6.1 100,0 µm

Figure 6.2 100,0µm

Figure 6.3 100,0µm

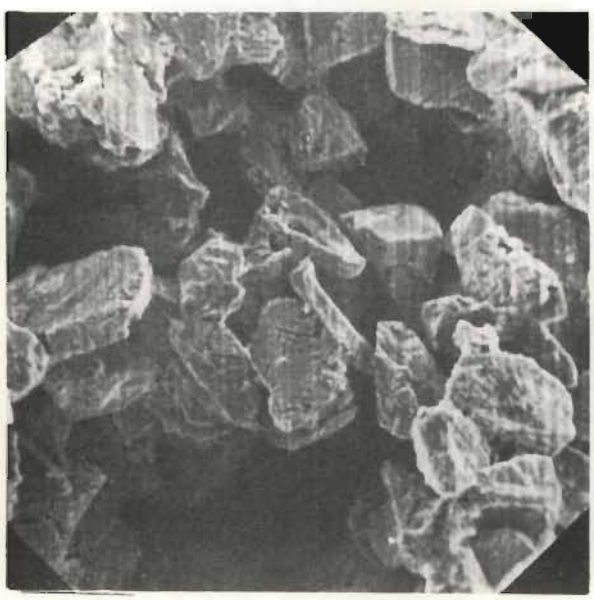

Figure 6.4 100,0µm

Figure 6.5 100,0µm

(facing figures 6.6 to 6.11)

FIGURE 6.6 S.E.M. photograph of the unwashed surface of a single leached PR particle (from -75,0 + 63,0μm size fraction), taken from leach reactor during experiment reported on table J 37. The initial layer of elemental sulphur formed in-situ is clearly visible.
Extent leached : X = 0,017
Magnification : 3000,0 x

FIGURE 6.7 S.E.M. photograph of an unwashed leached PR sphalerite particle (from -75,0 + 63,0μmsize fraction), taken from the final residue of the experiment reported in table J 39. The elemental sulphur coating the particle is clearly visible.
Extent leached : X = 0,33
Magnification : 780,0 x

FIGURE 6.8 S.E.M. photograph of a CCl_4 washed leached PR sphalerite particle (from -75,0 + 63,0μmsize fraction), taken from the final leach residue of the experiment reported in table J 39. Preferential zones of leaching are a distinguishing feature.
Extent leached : X = 0,33
Magnification : 1000,0 x

FIGURE 6.9 S.E.M. photograph of an unleached ZCR sphalerite particle (from -106,0 + 90,0μmsize fraction.
Magnification: 1000,0 x

FIGURE 6.10 S.E.M. photograph of the unwashed surface of a single ZCR particle (from -90,0 + 75,0μm size fraction), taken from the final leach residue of experiment reported in table J 22. Light areas on photograph represents unleached particle , whilst grey areas are in-situ elemental sulphur.
Extent leached : X = 0,38
Magnification : 4000,0 x

FIGURE 6.11 S.E.M. photograph of the CCl_4 washed surface of a ZCR sphalerite particle (from -90,0 + 75,0μmsize fraction) taken from the residue of the experiment reported in table J 21.
Extent leached : X = 0,68
Magnification : 1000,0 x

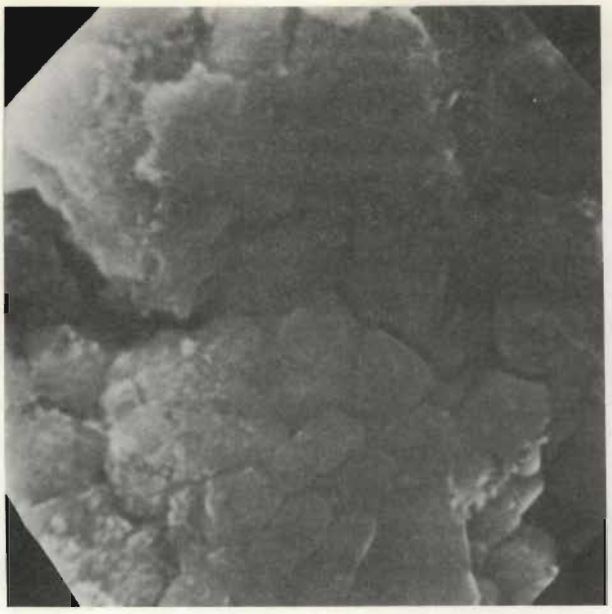

Figure 6.6 10,0µm

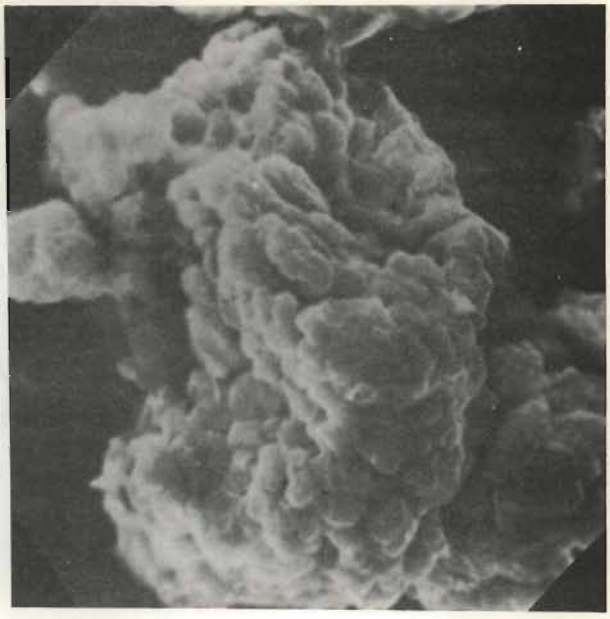

Figure 6.7 25,0µm

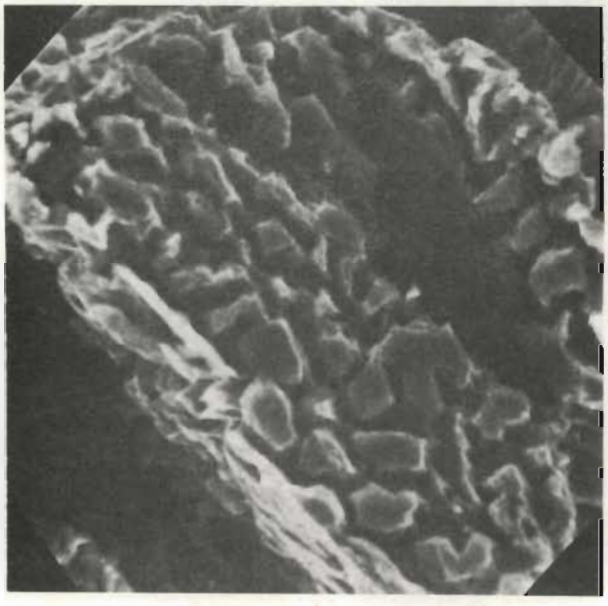

Figure 6.8 20,0µm

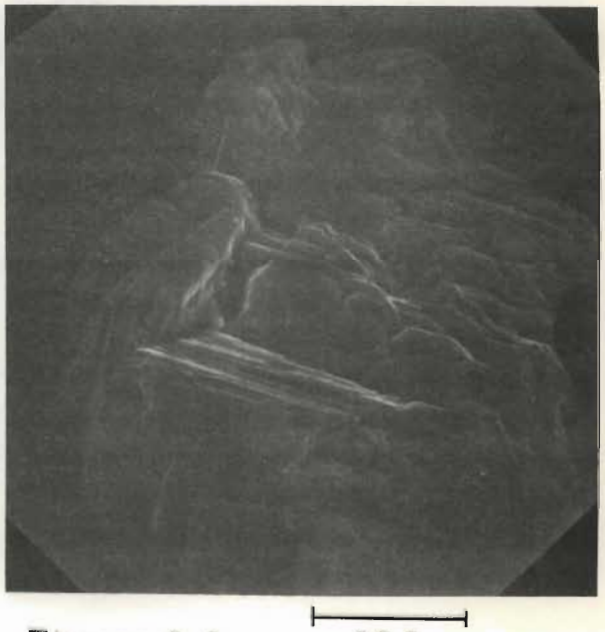

Figure 6.9 20,0µm

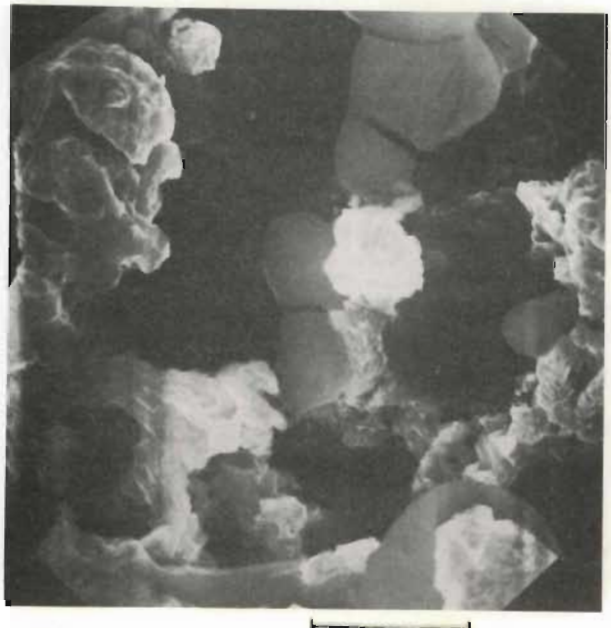

Figure 6.10 5,0µm

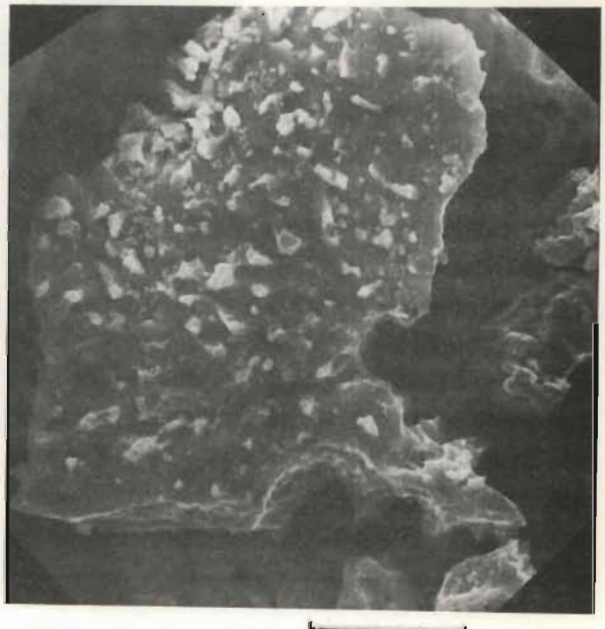

Figure 6.11 20,0µm

(facing figures 6.12 to 6.16)

FIGURE 6.12 S.E.M. photograph of an unwashed leached WBM sphalerite particle (from -75,0 +63,0μm size fraction), taken from the final leach residue of the experiment reported in table J5. Sulphur on the surface is visible.
Extent leached : X = 0,38
Magnification : 1 000,0 x

FIGURE 6.13 S.E.M. photograph of a CCl_4 washed leached WBM sphalerite particle (from -75,0 +63,0μm size fraction), taken from the final leach residue of the experiment reported in table J4.
Extent leached : X = 0,11
Magnification : 2 000,0 x

FIGURE 6.14 O.M. photograph of a polished section of WBM sphalerite particles (from -75,0 +63,0μm size fraction). Internal cracks are visible.
Magnification : Approx. 4 000,0 x

FIGURE 6.15 O.M. photograph of a polished section of ZCR sphalerite particles (from -75,0 + 63,0μm size fraction). Internal cracks are visible.
Magnification : Approx. 4 000,0 x

FIGURE 6.16 O.M. photograph of a polished section of PR sphalerite particles (from -75,0 + 63,0μm size fraction) etched for 17,0 seconds with sodium hypochlorite. Bright spots represent chalcopyrite inclusions. Internal cracks are visible.
Magnification : Approx. 4 000,0 x

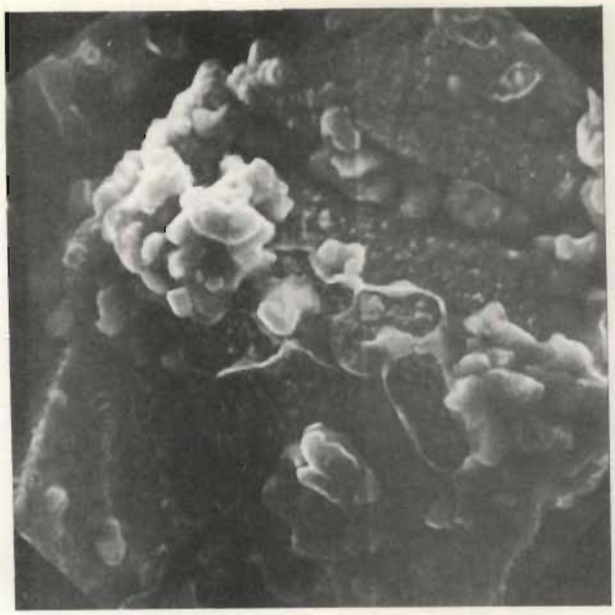

Figure 6.12 20,0µm

Figure 6.13 10,0µm

Figure 6.14

Figure 6.15

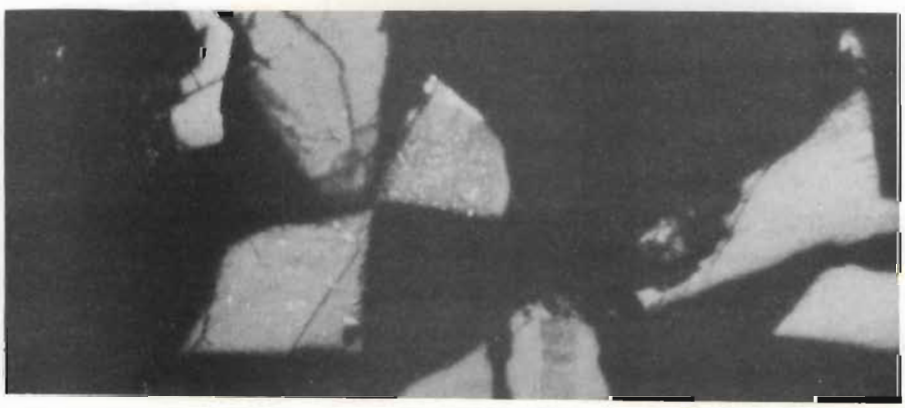

Figure 6.16

(facing figures 6.17 and 6.18)

FIGURE 6.17 O.M. photograph of a polished section of PR sphalerite particles (from -75,0 + 63,0μm size fraction), etched for 5,0 minutes with concentrated H_2SO_4. Bright spots represent chalcopyrite inclusions. Etching took place preferentially in the vicinity of the chalcopyrite zones.

Magnification : Approx. 400,0 x

FIGURE 6.18 O.M. photograph of a polished section of a single ZCR sphalerite particle (from -90,0 + 75,0μm size fraction), etched for 2,0 minutes with concentrated H_2SO_4. A complex etching pattern is observed.

Magnification : Approx. 800,0 x

Figure 6.17

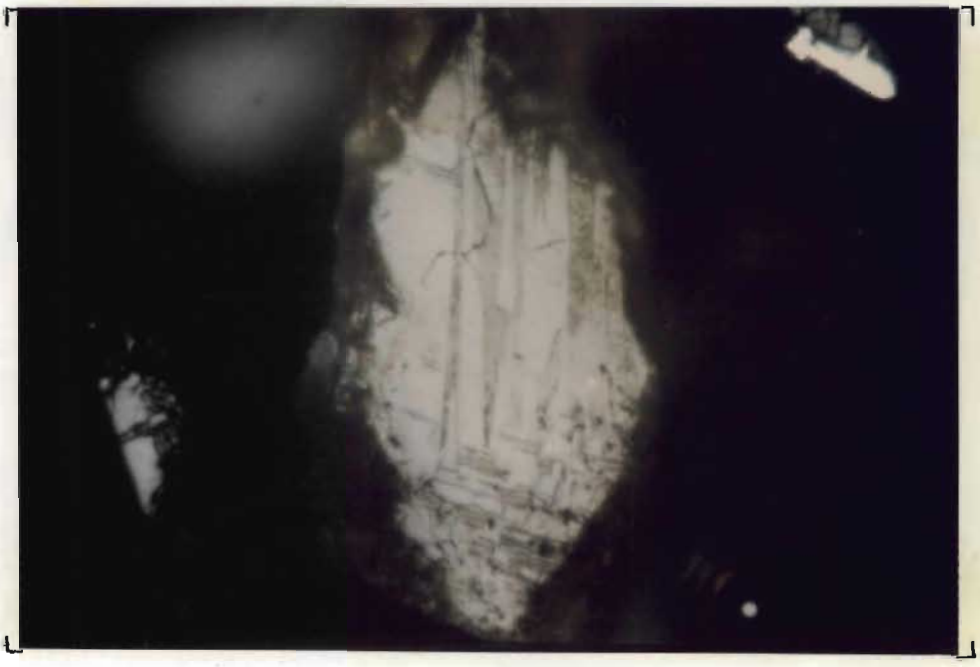

Figure 6.18

6. 2 RELATIONSHIP BETWEEN THE FORMATION OF ZINC IONS AND ELEMENTAL SULPHUR FOR SPHALERITE LEACHING UNDER CASE (ii) CONDITIONS

Figure 6. 19 plots $[Zn^{2+}]$ versus $[S^{o}]$. The zinc ion and elemental sulphur concentration were measured directly using the techniques described in Appendix D. The results of experiments using ZCR sphalerite (reported in tables J 18, J 20, J 21 and J 22) are not included on figure 6. 19 as a soxhlet apparatus was not used to extract the sulphur in these experiments. The values of all the points plotted on figure 6. 19 are presented in the tables of Appendix J.

It is observed that except for the BDH sphalerite, all the points lie closely scattered about a straight line which passes through the origin and has a slope of one.

This means that the molar concentrations of Zn^{2+} and S^{o} formed are approximately equal; and suggests that when leaching with relatively high $[Fe^{3+}]$: $[H_2SO_4]$ ratios in the absence of oxygen, negligible S^{o} or $S^{=}$ are oxidised to sulphate species.

In the case of the BDH sphalerite the ratio $[Zn^{2+}]$: $[S^{o}]$ is significantly greater than one. This was probably due to the fact that the BDH particles were much finer than those of any of the other sphalerites, and not all the S^{o} was extracted in a given time interval using CCl_4 in a soxhlet apparatus.

——— Line representing a 1:1 ratio of $[Zn^{2+}]$ to $[S^{o}]$.

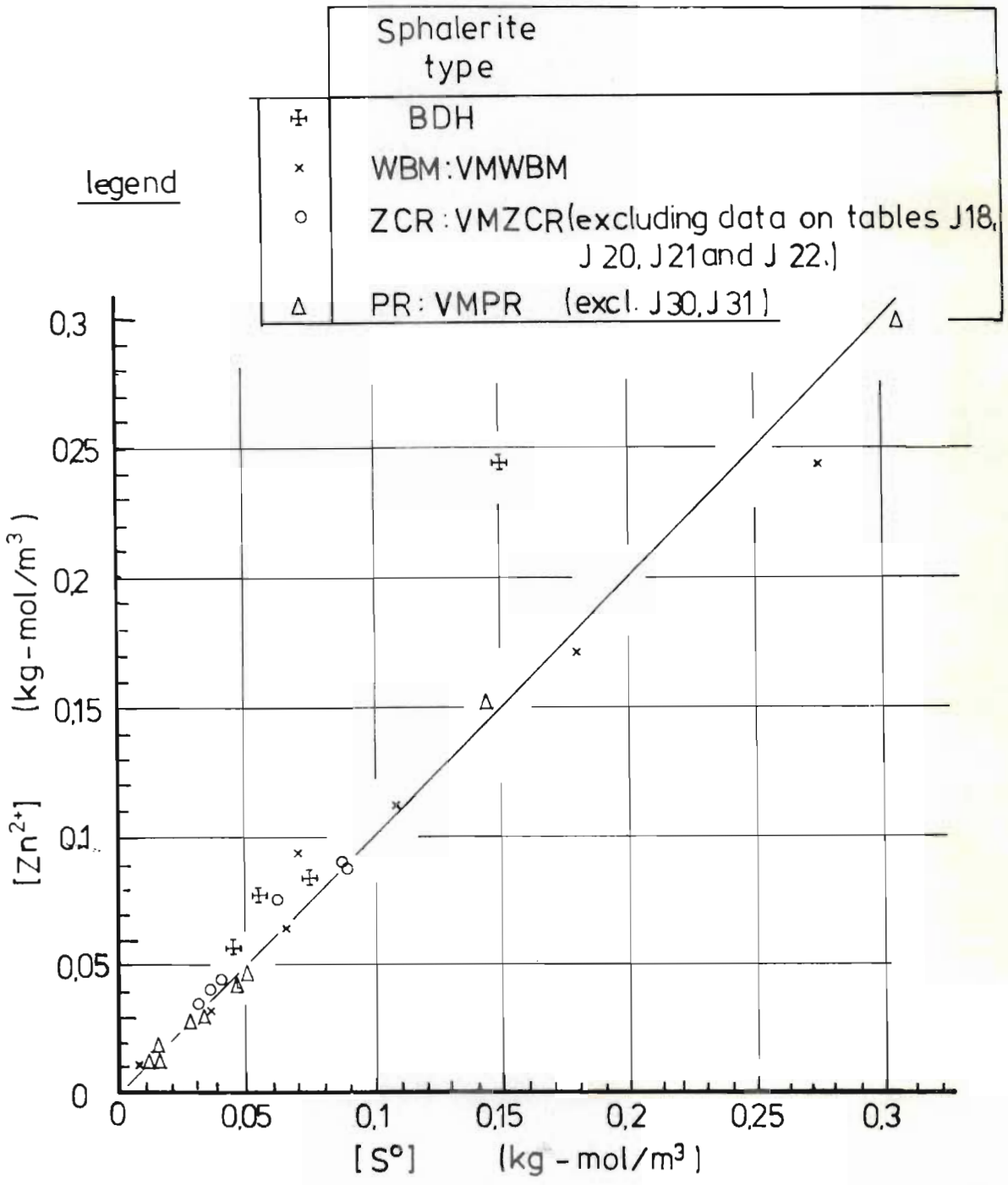

Figure 6.19 Plot of $[Zn^{2+}]$ versus elemental S recovered, demonstrating the stoichiometric production of S^{o} during the leaching of the various sphalerites under case (ii) conditions. All plotted data point values were extracted from the tables in Appendix J. See text for a more detailed description of the results presented on this figure.

From tables J 44 to J 47 it is observed that the $[Zn^{2+}] : [S^{o}]$ ratio for the experiments using 0,05 kg BDH sphalerite was significantly greater than for the experiments using only 0,02 kg BDH sphalerite.

6. 3 THE LEACHING OF VARIOUS SIZE FRACTIONS OF WBM, ZCR AND PR SPHALERITES IN H_2SO_4

In chapters 3 and 4 the leaching behaviour of the BDH and vibratory milled sphalerites under case (i) conditions were studied. In this chapter the leaching behaviour of various size fractions of the granular WBM, ZCR and PR sphalerites in H_2SO_4 are examined qualitatively. Table 6.1 summarises the conditions for such experiments.

Figures 6. 20 to 6. 22 plot $[Zn^{2+}]$ versus time rate curves for three size fractions of the WBM, ZCR and PR sphalerites respectively. Figure 6. 23 plots the $[Zn^{2+}]$ versus time rate curves of one size fraction for each of these sphalerites. The following observations may be made :-

a) The ZCR and PR sphalerites both exhibit apparant initial 'induction' periods during which the rates of dissolution progressively increase to a maximum and then decrease.

b) The WBM sphalerite does not exhibit an induction period, but commences leaching at a maximum rate which progressively decreases with time.

c) The initial leaching rates for the WBM

TABLE NO. (-)	SPHALERITE (-)	SIZE FRACTION x 10^6 (m)
I 56	WBM	-125,0 + 106,0
I 61	WBM	- 75,0 + 53,0
I 62	WBM	- 17,0 + 12,0
I 63	ZCR	-125,0 + 106,0
I 64	ZCR	- 75,0 + 53,0
I 65	ZCR	- 17,0 + 12,0
I 66	PR	-125,0 + 106,0
I 67	PR	- 75,0 + 53,0
I 68	PR	- 17,0 + 12,0

Other conditions:

Temp. = 318,0 (K)

Stirrer = 1 000,0 (rpm)

$[H_2SO_4]_o$ = 1,0 (kg-mol/m^3)

Initial Mass = 0,045 (kg)

T A B L E 6.1 SUMMARY OF EXPERIMENTS IN WHICH WBM, ZCR AND PR SPHALERITES WERE LEACHED IN H_2SO_4

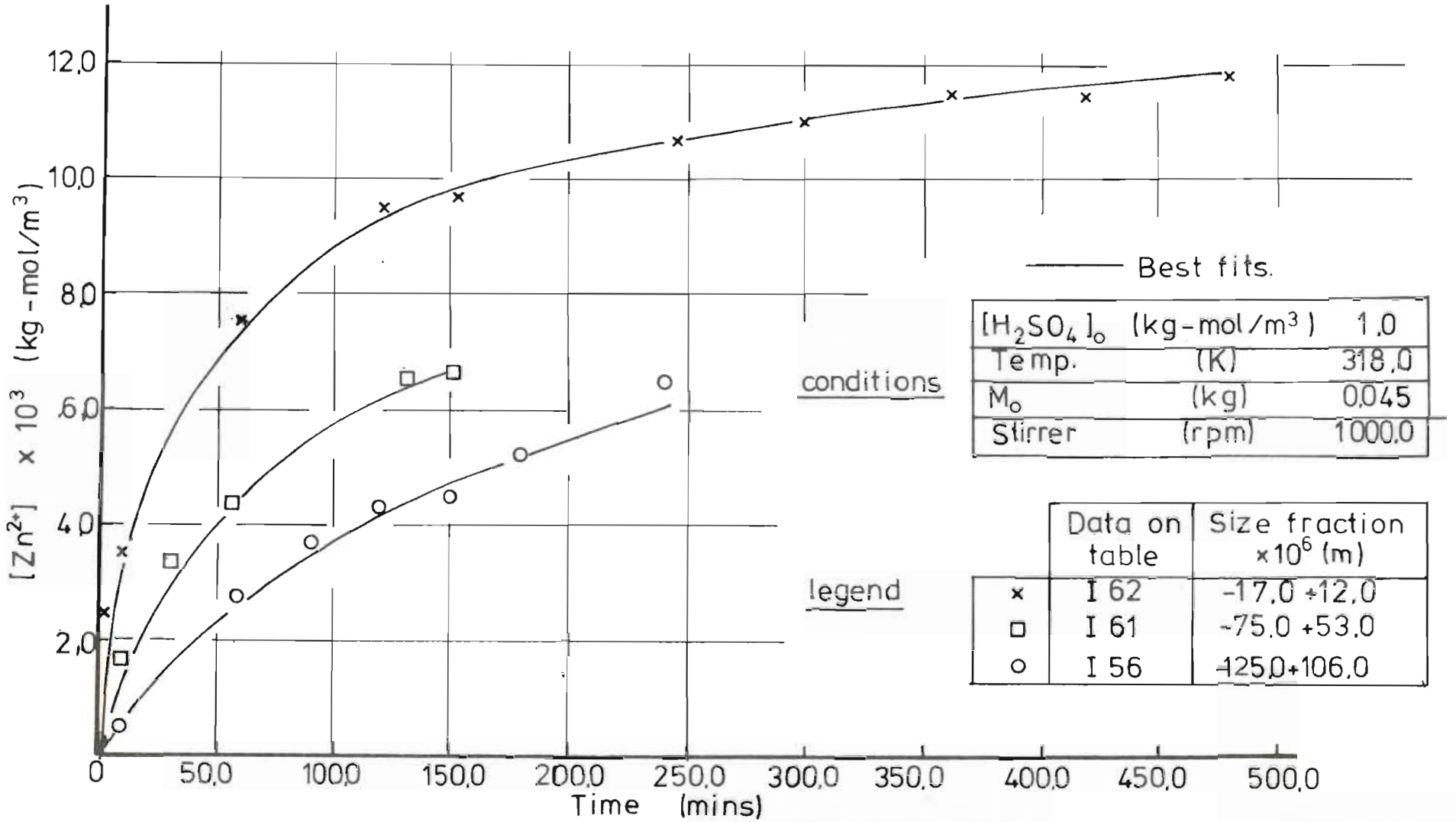

Figure 6.20 Exptl. rate curves for leaching various size fractions of WBM sphalerite under case(i) conditions ($[Fe^{3+}]_o$; $[H_2SO_4]_o$ = 0.0)

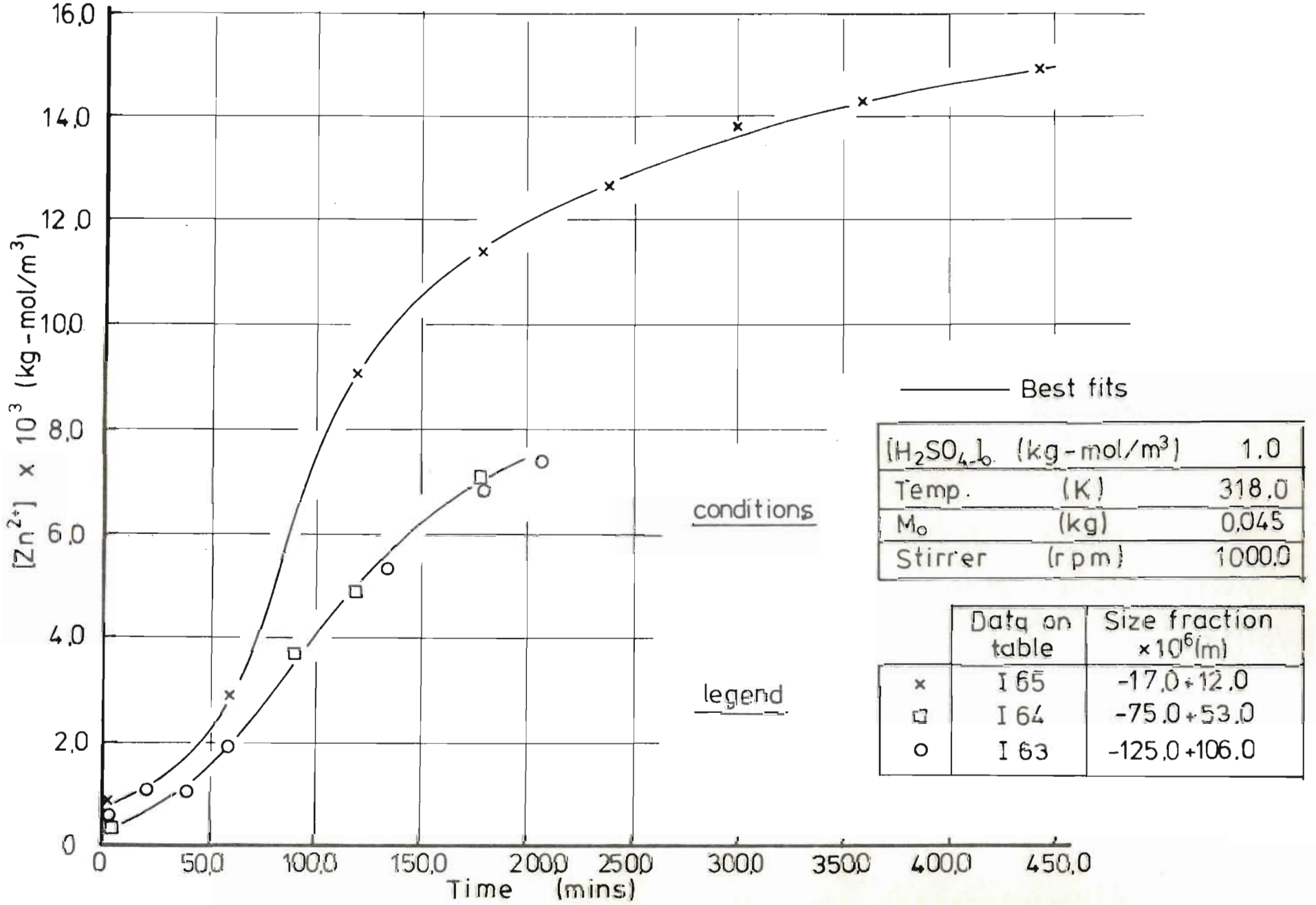

Figure 6.21 Exptl. rate curves for leaching various size fractions of ZCR sphalerite in H_2SO_4.

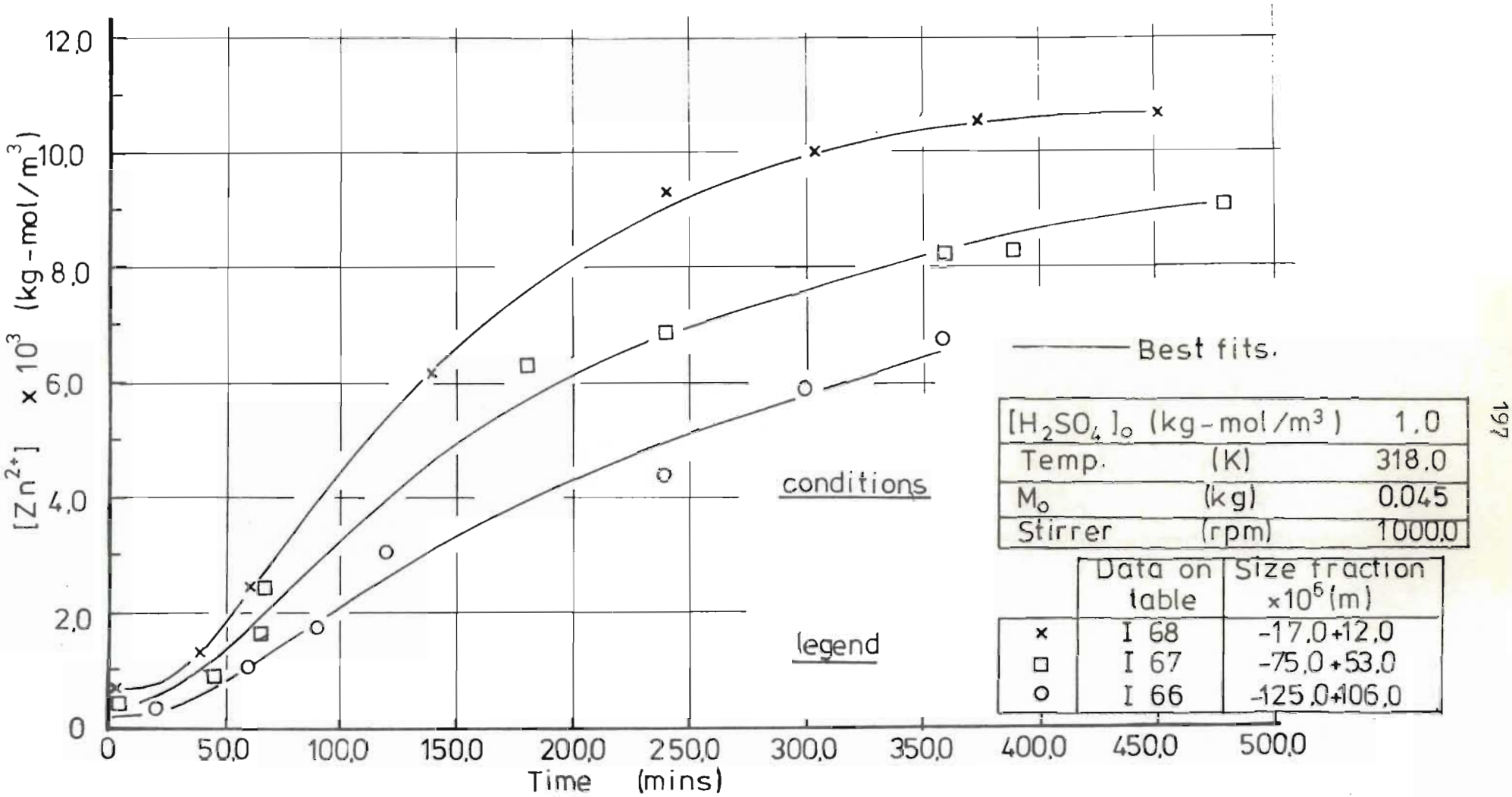

Figure 6.22 Exptl. rate curves for leaching various size fractions of PR sphalerite in H_2SO_4.

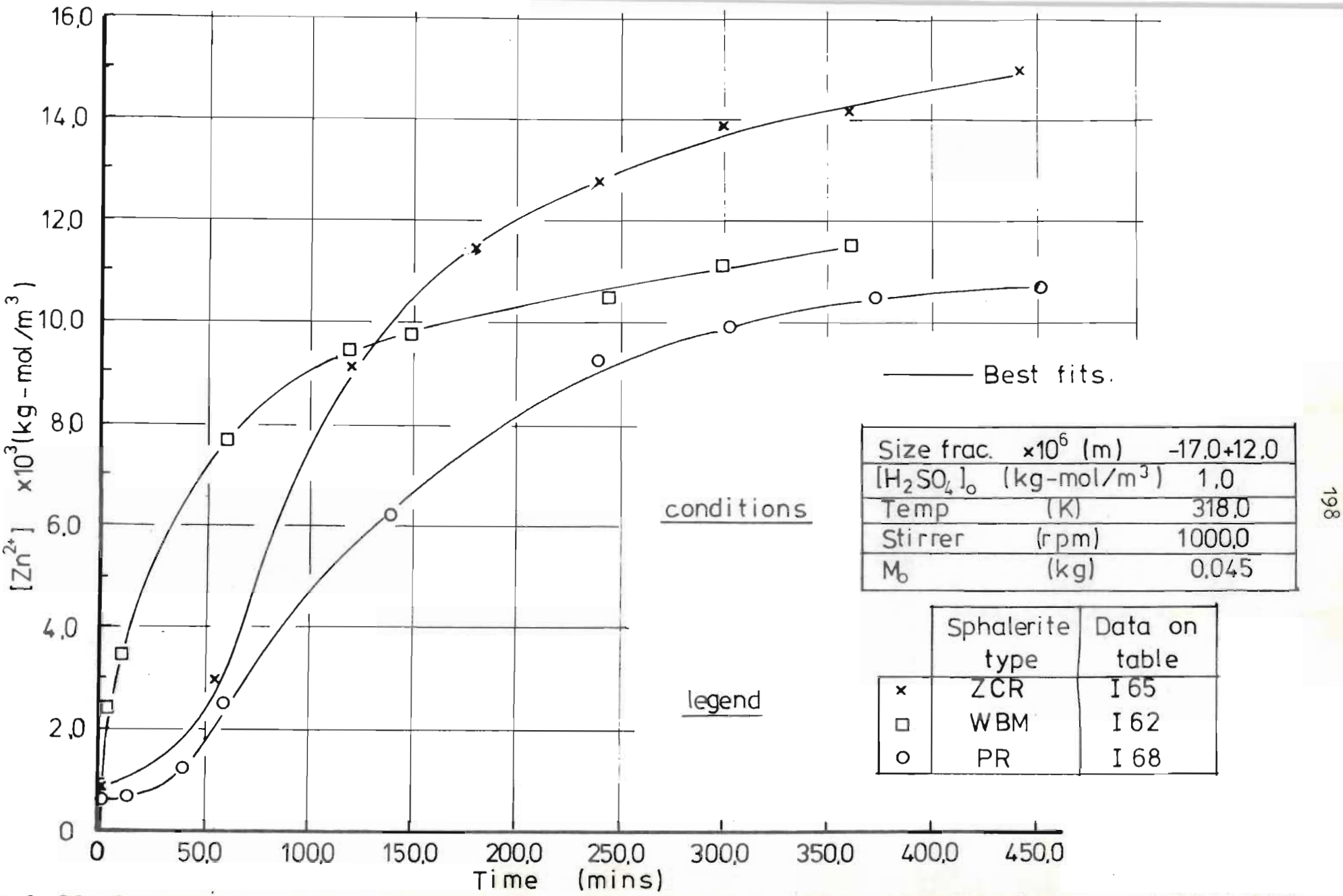

Figure 6.23 Comparison of the leaching rate curves for the -17.0+12.0 μm size fraction of WBM, ZCR and PR leaching in H_2SO_4.

sphalerite are very much greater than those for the ZCR and PR sphalerites.

These observations are important when compared to the results of leaching the vibratory milled forms of these sphalerites. In chapter 3 it was shown that the VMWBM and VMZCR sphalerites leached virtually identically in H_2SO_4. Furthermore, the VMPR sphalerite leached in H_2SO_4 without exhibiting any apparant induction period.

These results demonstrate that milling the sphalerites very fine results in the elimination of large apparant differences in the H_2SO_4 leaching behaviours of the WBM, ZCR and PR sphalerites.

Figure 6.24 compares the leaching rate curves for -17,0 + 12,0μm WBM, ZCR and PR sphalerites leaching under both case (i) and case (ii) conditions. From figures 6.24 the following observations may be made :-

a) The characteristic apparant induction behaviour exhibited when leaching under case (i) conditions is completely absent when leaching under case (ii) conditions.

b) Although $[H_2SO_4]_o$ = 1,0 (kg-mol/m^3) and M_o = 0,045 kg for the case (i) experiments, and $[H_2SO_4]_o$ = 0,06 (kg-mol/m^3) and M_o = 0,02 kg for the case (ii) experiments, the case (ii) leaching rates are very much greater than the case (i) leaching rates.

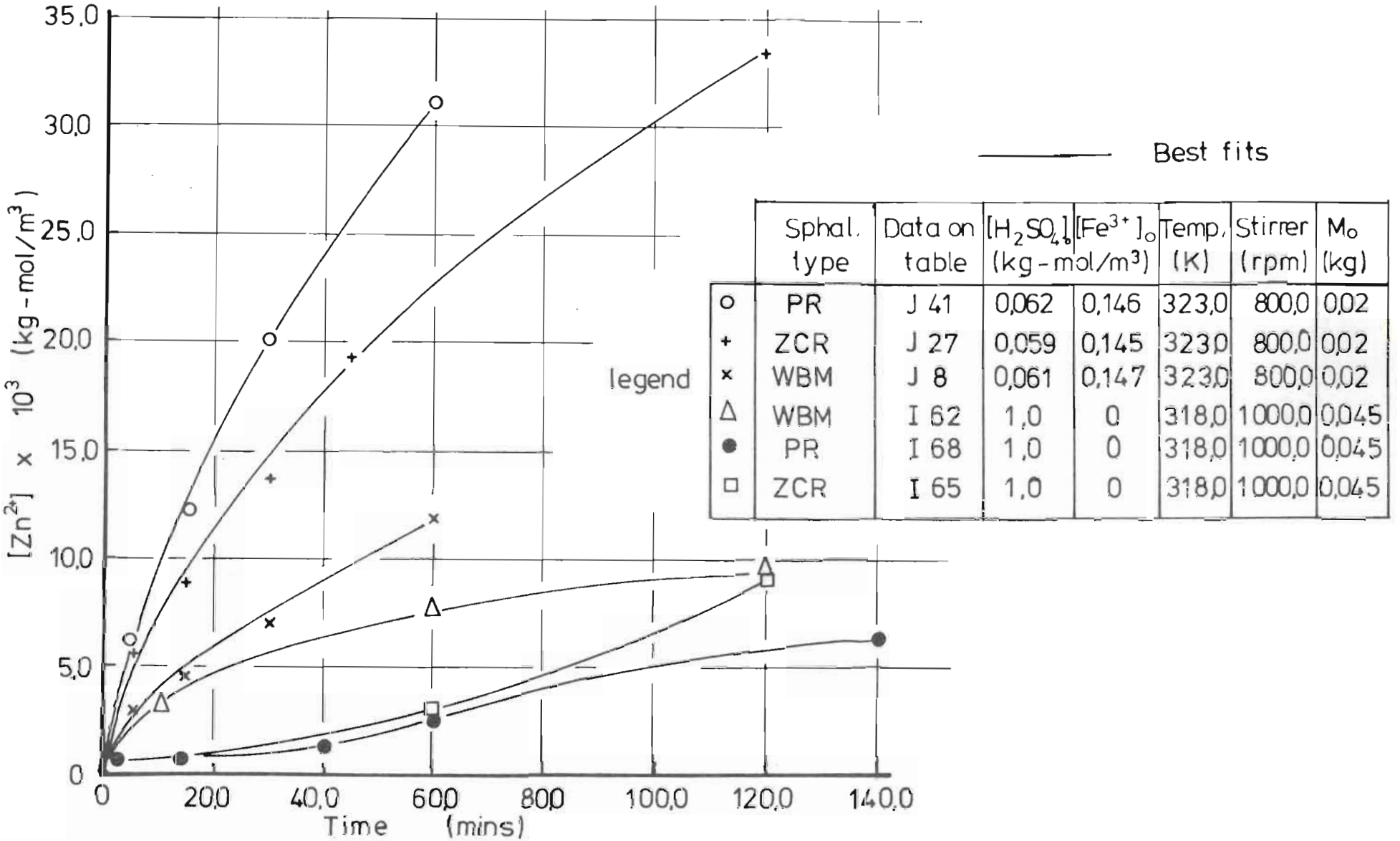

	Sphal. type	Data on table	$[H_2SO_4]_o$ (kg-mol/m^3)	$[Fe^{3+}]_o$	Temp. (K)	Stirrer (rpm)	M_o (kg)
○	PR	J 41	0,062	0,146	323,0	800,0	0,02
+	ZCR	J 27	0,059	0,145	323,0	800,0	0,02
×	WBM	J 8	0,061	0,147	323,0	800,0	0,02
△	WBM	I 62	1,0	0	318,0	1000,0	0,045
●	PR	I 68	1,0	0	318,0	1000,0	0,045
□	ZCR	I 65	1,0	0	318,0	1000,0	0,045

Figure 6.24 Comparison of rate curves for WBM, ZCR and PR sphalerite (-17,0+12,0 μm size fraction) leaching under case(i) ($[Fe^{3+}]_o = 0,0$) and under case(ii) ($[Fe^{3+}]_o : [H_2SO_4]_o \geq 1,8$) conditions.

This evidence further disproves the theory that dissolution, under case (ii) conditions, takes place non-oxidatively, followed by the homogeneous oxidation of H_2S by Fe^{3+}. Were this theory in fact correct, the case (ii) leaching rate curves on figure 6.24 would all have lay below the case (i) leaching rate curves.

c) The PR sphalerite which leached slowest under case (i) conditions, leached fastest under case (ii) conditions. The rates which increase in the order PR $<$ ZCR $<$ WBM when leaching under case (i) conditions is completely reversed (i.e. WBM $<$ ZCR $<$ PR) when leaching under case (ii) conditions.

These results suggest that in terms of the models presented in chapter 2 (based on Langmuir-Hinschelwood kinetics), the the adsorption of H^+ by the sphalerites increases in the order PR $<$ ZCR $<$ WBM, but that the adsorption of Fe^{3+} by the sphalerites increases in the order :- WBM $<$ ZCR $<$ PR.

6.4 DISSOLUTION OF IRON AND COPPER FROM SPHALERITE

In several experiments conducted under case (i) conditions, attempts were made to measure the dissolved iron and copper as well as the zinc concentrations. Attempts to do this for experiments conducted under

case (ii) conditions were unsuccessful (owing to the large Fe^{3+} initially present in relation to the very small amounts of iron dissolved).

No dissolved copper was detected for sphalerite leaching under case (i) conditions. However, in certain case (ii) experiments, technical grade ferric sulphate was dissolved, and dissolved copper was detected in the leach solution prior to adding the sphalerite. Upon adding the sphalerite, the copper concentration rapidly reduced to zero. It is proposed that the following reaction is responsible for preventing copper ions remaining in solution:-

$$CuSO_4 + ZnS \rightarrow ZnSO_4 + CuS\downarrow \quad \text{..... 6. 1}$$

Figure 6. 25 plots the total concentration of dissolved iron (Fe^{2+} plus Fe^{3+} species), i.e. $[Fe]_{TOT}$ versus time for the -17,0 + 12,0μm size fraction of the WBM, ZCR and PR sphalerites leaching in 1,0 molar H_2SO_4.

It is observed that iron enters solution significantly faster for the PR sphalerite than for the ZCR or WBM sphalerites. Hence only the dissolution of iron from PR sphalerite is considered further in this section.

Figures 6. 26 and 6. 27 superimpose the Zn^{2+} versus time and $[Fe]_{TOT}$ versus time rate curves for two size fractions of PR sphalerite, and for VMPR sphalerite, leaching under case (i) conditions.

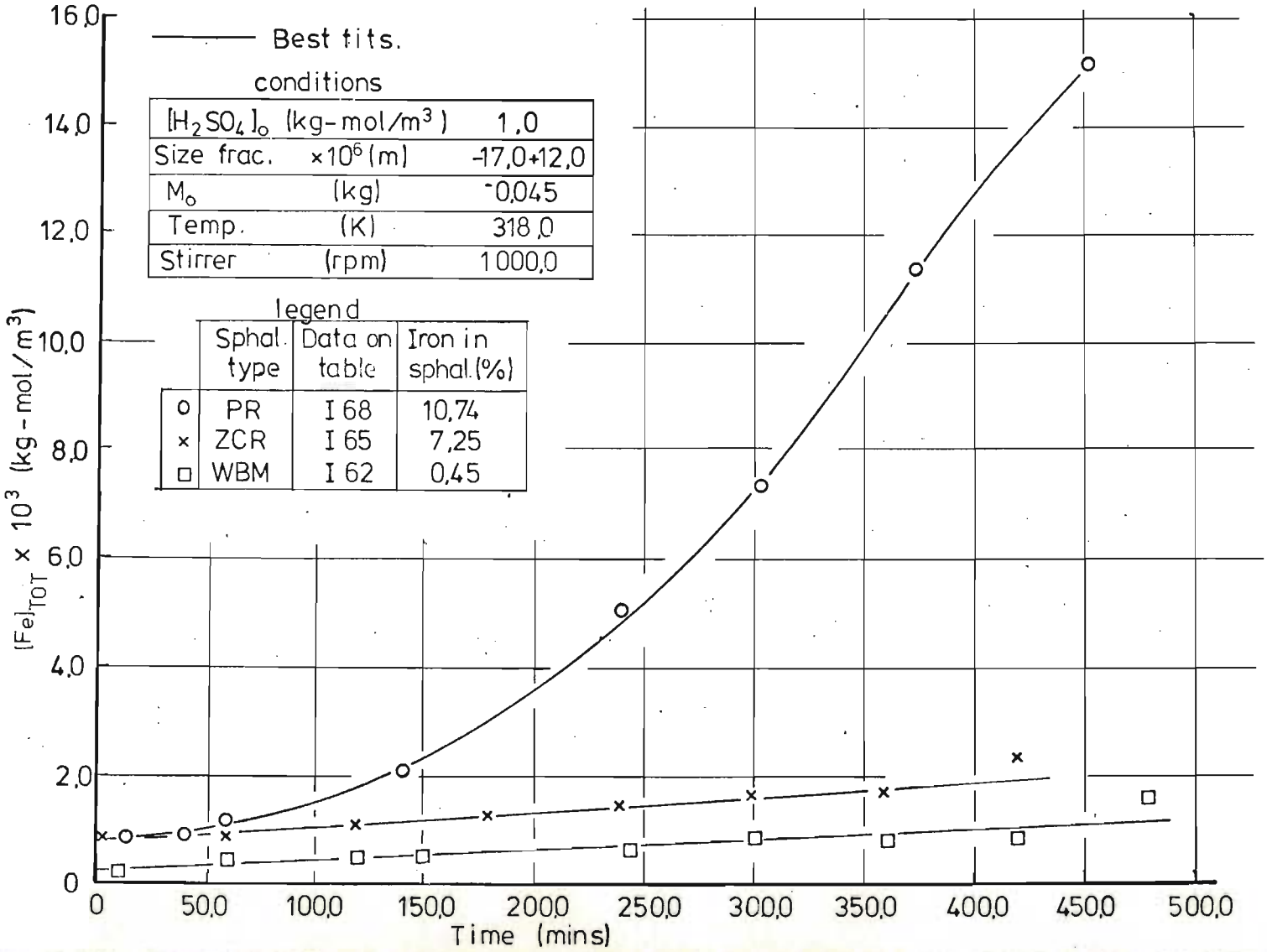

Figure 6.25 Experimental rate curves comparing the dissolution of iron during the leaching of PR, ZCR and WBM sphalerites (-17,0+12,0 μm size fraction) in H_2SO_4.

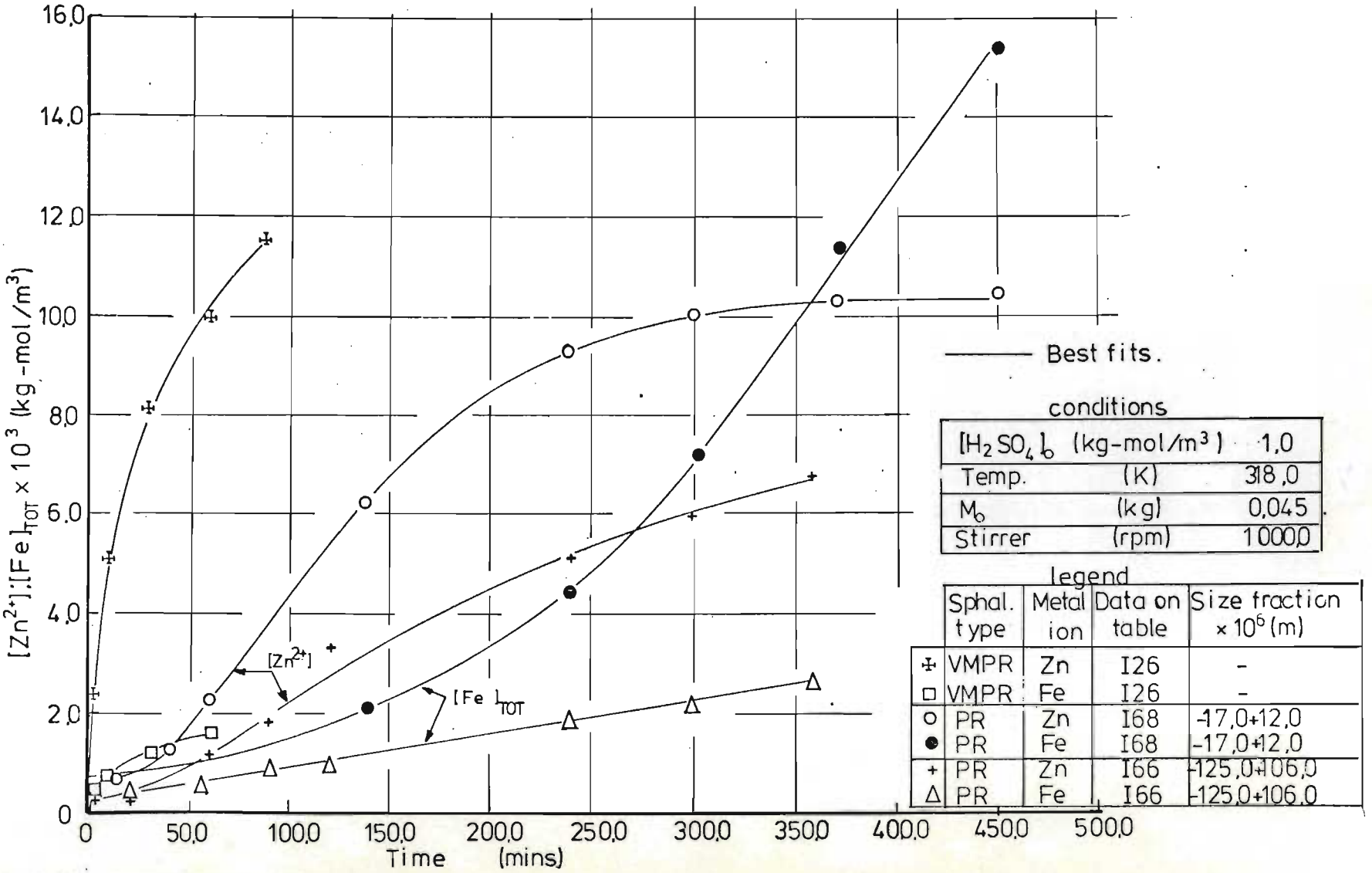

Figure 6.26 Comparison of zinc and iron dissolution rate curves for PR and VMPR sphalerites leaching in H_2SO_4 (with $[Fe^{3+}]_o$=0,0)

——— Best fits.

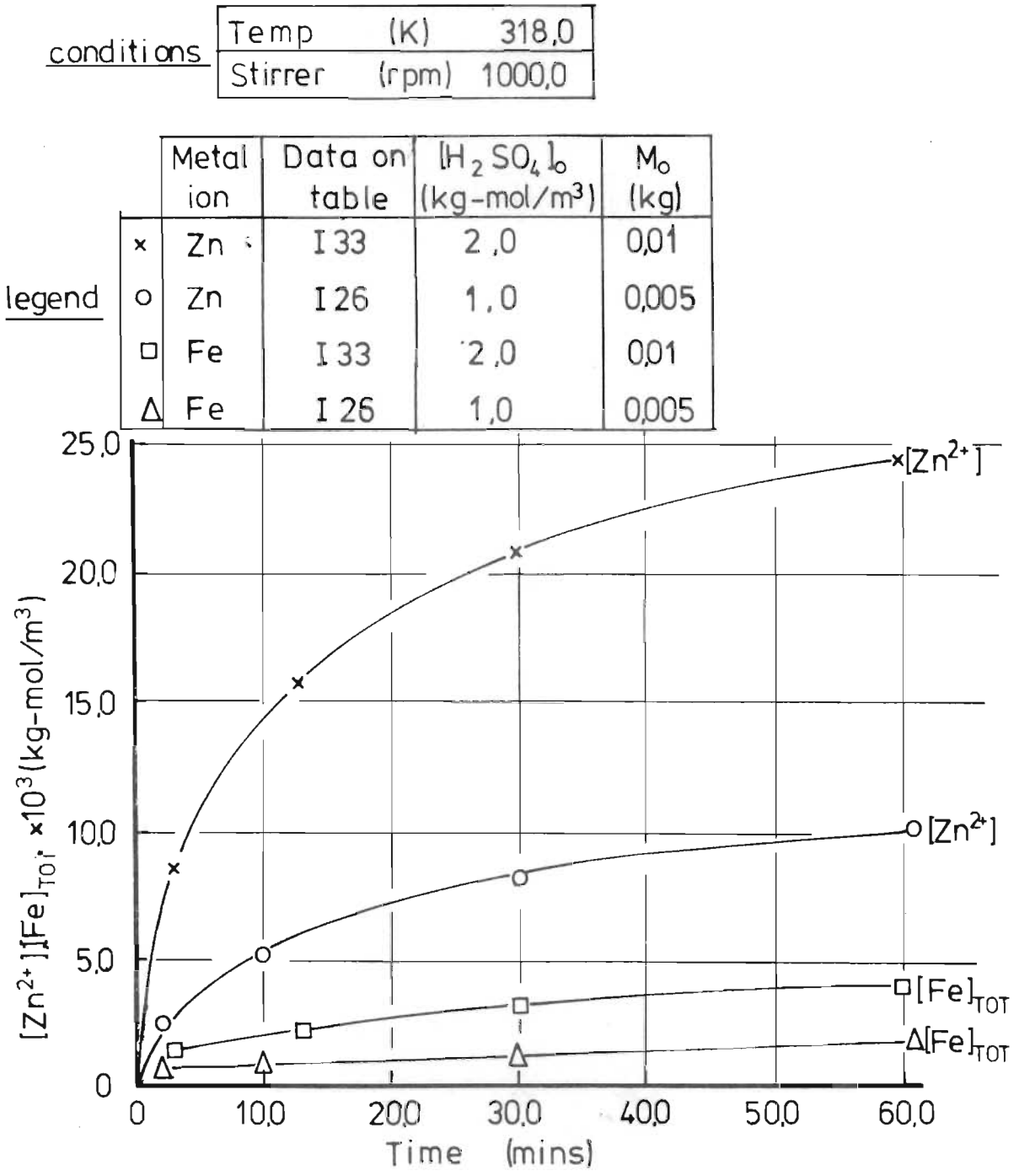

Figure 6.27 Comparison between zinc and iron dissolution rate curves for VMPR sphalerite leaching in H_2SO_4.

In order to compare the rates of dissolution of the zinc and iron from the sphalerite , a selectivity factor is defined as follows :-

$$\Theta = \frac{X_{[Zn^{2+}]}}{X_{[Fe]_{TOT}}} \quad \ldots\ldots\ldots \quad 6.2$$

where

$$X_{[Zn^{2+}]} = [Zn^{2+}] / [Zn]_o \quad \ldots\ldots\ldots \quad 6.3$$

$$X_{[Fe]_{TOT}} = [Fe^{2+}] / [Fe]_{TOT,O} \quad \ldots\ldots\ldots \quad 6.4$$

$X_{[Zn^{2+}]}$ and $X_{[Fe]_{TOT}}$ are the extents of zinc and iron dissolved; whilst $[Zn^{2+}]_o$ and $[Fe]_{TOT,O}$ are the initial molar concentrations of undissolved zinc and iron in the sphalerite.

Figure 6. 28 plots the selectivity factor Θ versus time for three size fractions of PR sphalerite leaching in 1 M H_2SO_4 ; and for VMPR leaching in 1,0 M H_2SO_4 and in 2,0 M H_2SO_4. From figure 6. 28 it is observed that the result of vibratory milling the PR sphalerite was to vastly increase Θ

6. 5 OXIDATION OF H_2S BY Fe^{3+} IN THE PRESENCE OF ACTIVATED CHARCOAL

The author conducted preliminary tests which demonstrated that the presence of activiated charcoal catalysed the oxidation of H_2S by Fe^{3+}. H. Dijs subsequently conducted a series of controlled experiments using the author's apparatus with the understanding that the results be made available to the author for publication in this thesis. The

conditions

Temp.	(K)	318,0
Stirrer	(rpm)	1000,0

legend

	Sphal. type	Data on table	Size fraction $\times 10^6$ (m)	M_o (kg)	$[H_2SO_4]_o$ (kg-mol/m^3)
⊹	VMPR	I 33	-	0,01	2,0
□	VMPR	I 26	-	0,005	1,0
○	PR	I 68	-17,0+12,0	0,045	1,0
Δ	PR	I 67	-75,0+53,0	0,045	1,0
×	PR	I 66	-125,0+106,0	0,045	1,0

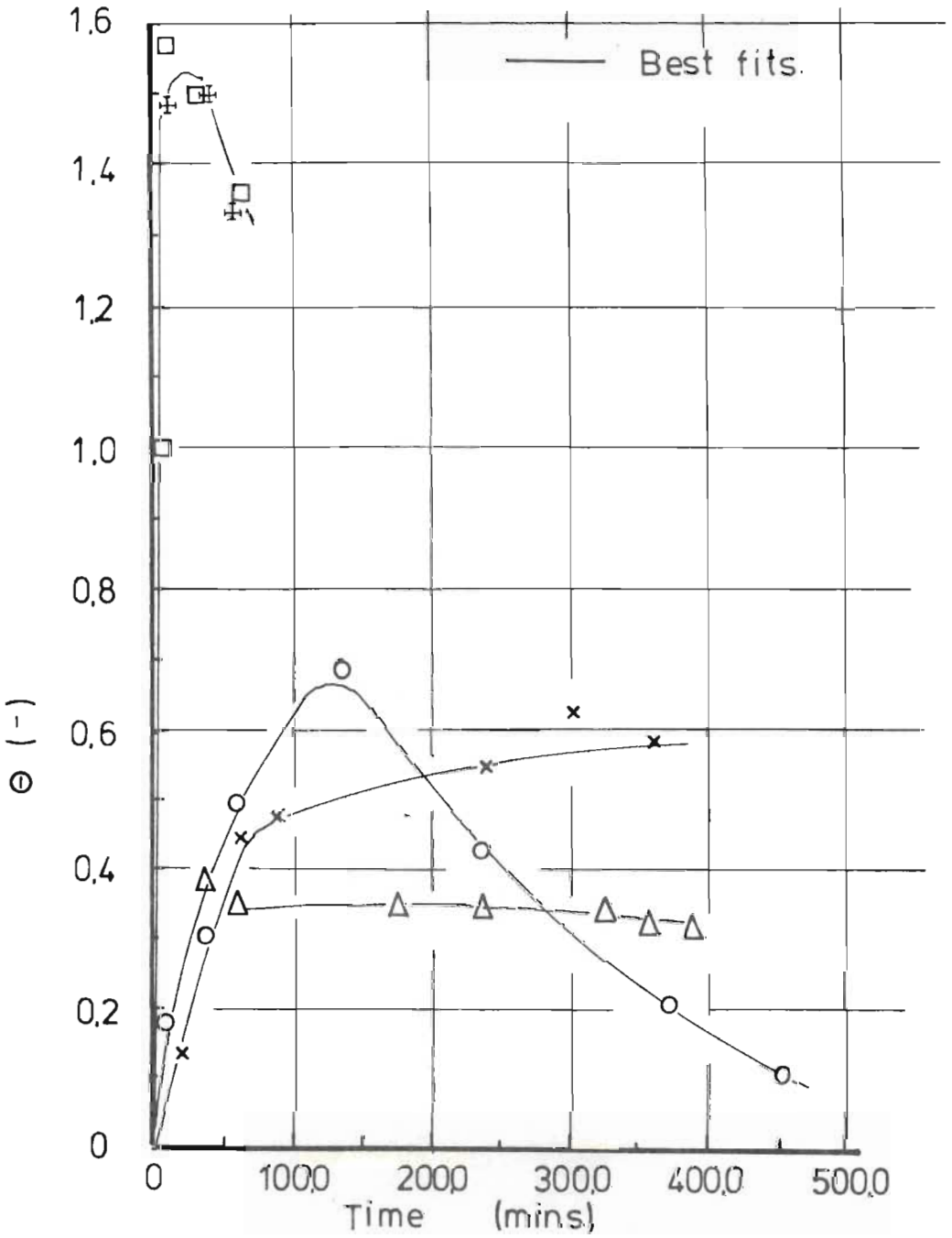

Figure 6.28 Comparison of the selectivities Θ associated with the dissolution of zinc and iron from three sizes of PR sphalerite, and from VMPR sphalerite leaching in H_2SO_4.

full results of these experiments are presented in tables K 39 to K 42 .

The experiments consisted of :-

(i) purging H_2S gas into 1,0 M H_2SO_4 without and with various masses of activated charcoal initially present. The reagent grade activated charcoal used was marketed by the British Drug House Company and had a specific surface area (determined by the author using the B E T N_2 adsorption method) of 0,75 x 10^6 m^2/kg. The H_2S partial pressure was monitored during purging and during the subsequent reaction with Fe^{3+}.

(ii) With the H_2S partial pressure at steady state, solution samples were drawn and the H_2S concentration was determined analytically.

(iii) A volume of concentrated Fe^{3+} solution was injected into the reactor, and the pressure decay curve was monitored and recorded.

Table 6. 2 summarises the experimental conditions for the four runs, and presents the measured values of $(P_{H_2S})_o$ and $\left(\frac{dP_{H_2S}}{dt}\right)_o$. The initial rates were expressed in terms of $\frac{d[H_2S]}{dt}$ by dividing $\left(\frac{dP_{H_2S}}{dt}\right)_o$ by the measured distribution coefficient, K_D for H_2S.

Table No.	M_o (Act.Char) (kg)	$[Fe^{3+}]_o$ x 10^3 (kg-mol / m^3)	$[H_2S]_o$ x 10^3 (kg-mol / m^3)	$\left(\frac{dP_{H_2S}}{dt}\right)_o$ (kPa/min)	$(P_{H_2S})_{o,eq.}$ (kPa)	$-\left(\frac{d[H_2S]}{dt}\right)_{o,exp}$ (kg - mol / m^3.min)	$-\left(\frac{d[H_2S]}{dt}\right)_{o,mod}$ (kg - mol / m^3.min)	ω^* (-)
K 39	0	36,5	21,7	3,43	26,21	2,861	1,74	1,64
K 40	0,003	50,5	22,1	9,21	26,77	7,605	3,08	2,47
K 41	0,01	51,5	21,8	22,33	26,35	18,44	3,12	5,91
K 42	0,02	53,4	22,2	53,0	26,85	43,77	3,32	13,19

NOTE 1) $[H_2SO_4]_o$ = 1,0 for each experiment

2) Temperature = 298,0 ° K for each experiment

3) Stirrer speed = 1 000,0 r p m for each experiment

4) $\left(\frac{d[H_2S]}{dt}\right)_{mod}$ defined by equation 5. 7

T A B L E 6. SUMMARY OF CONDITIONS AND RESULTS OF OXIDISING H_2S BY Fe^{3+} IN AQUEOUS H_2SO_4 IN THE PRESENCE OF VARIOUS MASSES OF ACTIVATED CHARCOAL. RESULTS ARE TABULATED IN APPENDIX H 3

The initial homogeneous rate of H_2S oxidation by Fe^{3+} was calculated using the modified Verhulst equation 5.7. Figure 6.29 plots ω^* versus the initial mass of activated charcoal added, where:-

$$\omega^* = \frac{\text{Experimental initial rate}}{\text{Initial rate calculated using equation 5.6}} \quad \ldots\ldots\ldots\ldots \quad 6.5$$

A linear relationship exists which clearly demonstrates and proves that activated charcoal catalyses the oxidation of H_2S by Fe^{3+}. No attempt has been made here to propose a mechanism for the catalysis phenomena.

6.6 EFFECT OF ACTIVATED CHARCOAL ON THE LEACHING OF VMWBM SPHALERITE IN H_2SO_4 WITH AND WITHOUT Fe^{3+} PRESENT

Table 6.3 summarises the conditions of experiments in which VMWBM sphalerite was leached in aqueous sulphuric acid with and without Fe^{3+} and/or activated charcoal present.

Figures 6.30a and 6.30b plot $[Zn^{2+}]$ versus time and P_{H_2S} versus time for experiments conducted under such conditions that a H_2S partial pressure could be monitored. The following observations are made from these figures :-

a) The presence of activated charcoal (but no Fe^{3+}) results in an increase in the $[Zn^{2+}]$ versus time rate curve, but a decrease in the P_{H_2S} versus time rate curve. This suggests that the activated charcoal adsorbs H_2S more readily than Zn^{2+}. This has the

——— Best fit with origin $\Theta = 1,0$ at $M_o = 0,0$

o Data reported on table 6.2

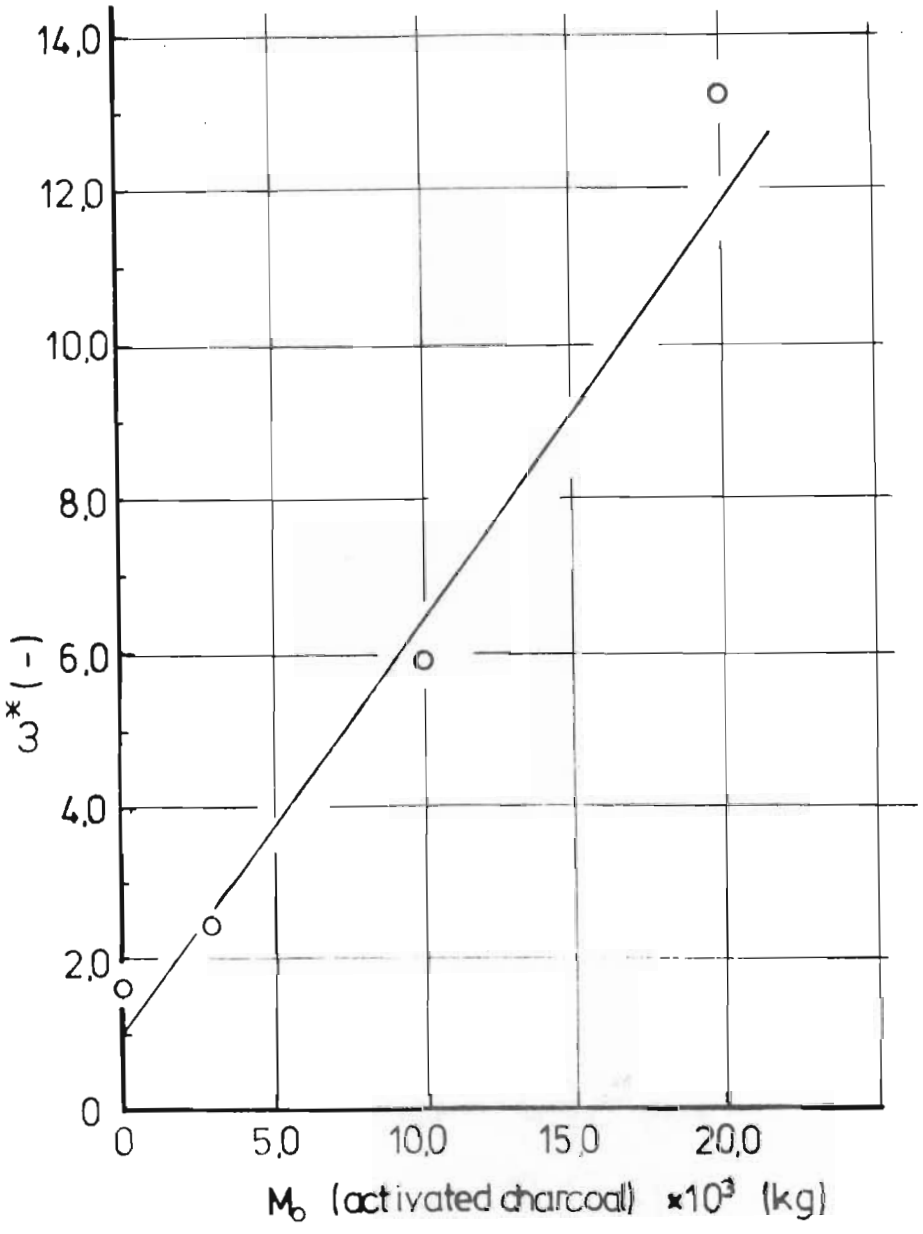

Figure 6.29 Demonstration of the catalytic effect of activated charcoal on the oxidation of H_2S by Fe^{3+}. The initial oxidation rate ratio ω^* is defined by eqn. 6.5.

TABLE NO. (-)	$[Fe^{3+}]_o \times 10^3$ (kg-mol / m^3)	MASS OF ACT. CHARCOAL (kg)
I 2	0	0
L 2	13,75	0
L 7	0	0,005
L 8	0	0,01
L 9	13,75	0,005
L 4	55,0	0
L 10	57,3	0,01
L 11	57,3	0,02

Temp. = 318,0 (K)
M_o(sphal) = 0,01 (kg)
Stirrer = 1 000,0 (rpm)
$[H_2SO_4]_o$ = 1,0 (kg-mol / m^3)

T A B L E 6. 3 SUMMARY OF CONDITIONS FOR EXPERIMENTS IN WHICH VMWBM SPHALERITE WAS LEACHED WITH AND WITHOUT Fe^{3+} OR ACTIVATED CHARCOAL PRESENT

conditions			
	$[H_2SO_4]_o$	(kg-mol/m^3)	1,0
	Temp.	(K)	318,0
	M_o(sphal)	(kg)	0,01
	Stirrer	(rpm)	1000,0

Point (-)	Curve (-)	Data on table	$[Fe^{3+}]_o \times 10^3$ (kg-mol/m)	M_o(activated charcoal)-(kg)
Δ	a	I2	0	0
○	b	L2	13,75	0
●	c	L7	0	0,005
□	d	L8	0	0,01
×	e	L9	13,75	0,005

——— Best fit through $[Zn^{2+}]$ data.

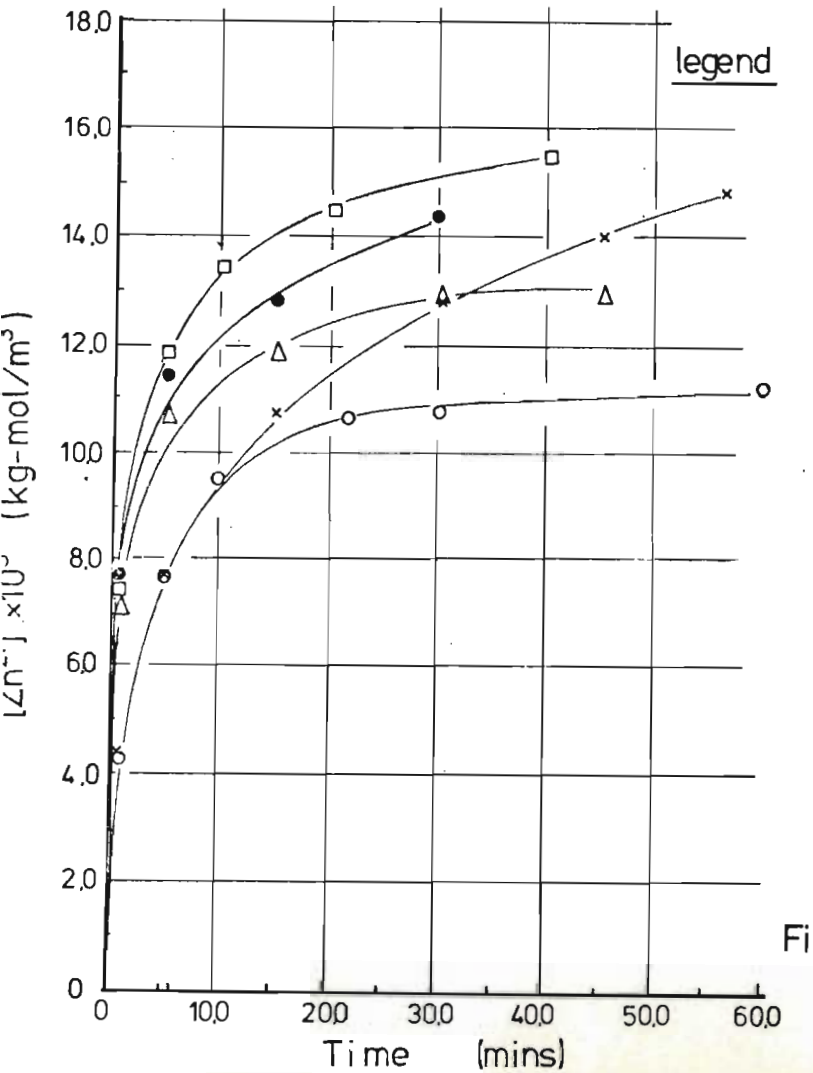

Fig 6.30a

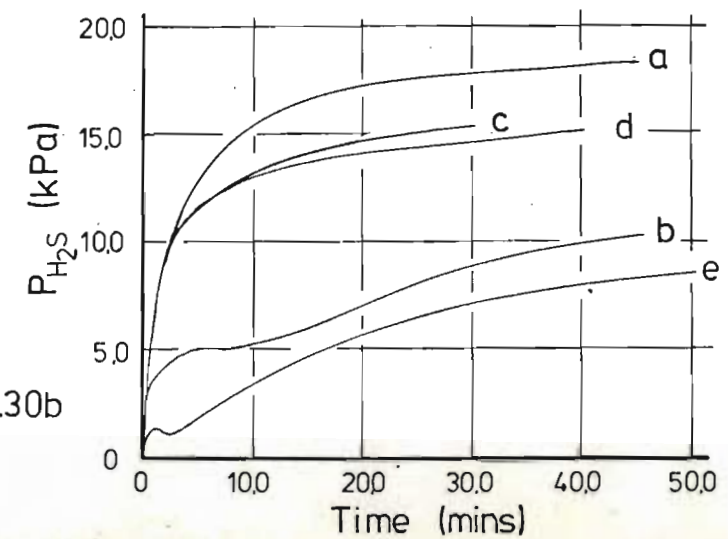

Fig 6.30b

Figures 6.30a and 6.30b Comparison of exptl. $[Zn^{2+}]$ and P_{H_2S} rate curves for VMWBM sphalerite leaching in H_2SO_4 without and with Fe^{3+} and/or activated charcoal initially present.

effect of permitting more Zn^{2+} to go into solution in order to achieve equilibrium according to the overall reaction stoichiometry :-

$$Zn\,S + H_2SO_4 \rightleftharpoons Zn\,SO_4 + H_2S \quad \ldots\ldots\ldots \quad 6.6$$

b) The presence of Fe^{3+} alone (but no activated charcoal) suppressed the $[Zn^{2+}]$ versus time and P_{H_2S} versus time rate curves, as was observed and discussed in chapter 5 (section 5.2.1).

c) The presence of Fe^{3+} and activated charcoal had no effect on the initial rate of Zn^{2+} formation (compared to the case referred to in b).
However, the $[Zn^{2+}]$ versus time curve for $t \geq 10{,}0$ mins. was increased and the overall P_{H_2S} versus time was greatly decreased (compared to the case referred to in b).

Figure 6.31 plots $[Zn^{2+}]$ versus time for VMWBM sphalerite leaching in H_2SO_4 with and without activated charcoal with sufficient initial Fe^{3+}. present, so that no significant H_2S partial pressure was detected. The initial rate of leaching appeared to be unaffected by the presence of the activated charcoal. However, the subsequent rates of leaching with activated charcoal present increased more rapidly, and then decreased more rapidly than the rate of leaching without activated charcoal present.

——— Best fits.

conditions

$[H_2SO_4]_o$	(kg-mol/m^3)	1,0
Temp.	(K)	318,0
M_o(sphal)	(kg)	0,01
Stirrer	(rpm)	1000,0

legend

	Data on table	$[Fe^{3+}]_o \times 10^3$ (kg-mol/m^3)	M_o (activated charcoal)-(kg)
o	L 4	55,0	0
×	L 10	57,3	0,01
Δ	L 11	57,3	0,02

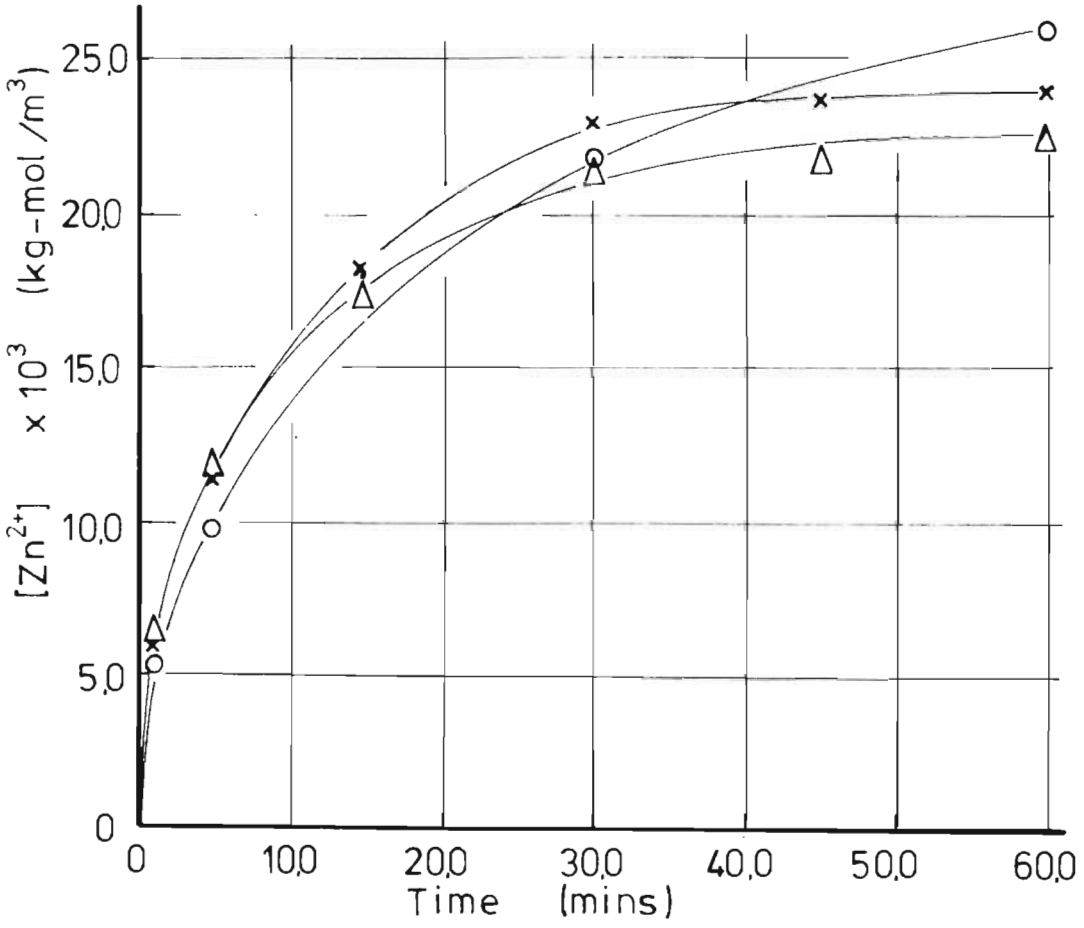

Figure 6.31 Exptl. $[Zn^{2+}]$ rate curves for VMWBM sphalerite leaching in H_2SO_4 with sufficient Fe^{3+} initially present so that no P_{H_2S} is detectable, and with activated charcoal present.

Furthermore, the final $[Zn^{2+}]$ value for the experiment conducted with 0,02 kg activated charcoal present, was less than that for the experiment conducted with only 0,01 kg activated charcoal present.

It was not possible to establish what concentration of zinc or ferric ions was adsorbed onto the activated charcoal surface. The adsorption of Zn^{2+} onto the activated charcoal could possibly explain why the $[Zn^{2+}]$ at $t = 60,0$ mins. was apparantly lower with 0,02 kg activated charcoal than with 0,01 kg activated charcoal present.

From the above it appears that -

1) the presence of activated charcoal renders the greatest advantage when leaching VMWBM sphalerite in H_2SO_4 with no initial ferric ions present;

2) the presence of activated charcoal renders no apparant advantage when leaching VMWBM sphalerite in H_2SO_4 with sufficiently high $[Fe^{3+}]_o$ such that no detectable P_{H_2S} is evident.

6.7 DISSOLUTION OF WVM SPHALERITE UNDER CASE (i) CONDITIONS

In section 3.1.1 the technique for producing WVM sphalerite was described. In short, the Wards sphalerite acquired originally in lump form was dry milled in a vibratory (i.e. attrition) mill, and screened into discrete size fractions. The WBM was wet ball milled before drying and screening.

Figure 6.32 compares the $[Zn^{2+}]$ and P_{H_2S} rate curves for -90,0 + 75,0 μm and -75,0 + 63,0 μm size fractions of WVM with the same size fractions of WBM sphalerite. It is observed that for the -90,0 + 75,0 μm particles, the WBM sphalerite apparantly leaches faster, but that for the -75,0 + 63,0 μm particles the WBM and WVM leach at virtually identical rates. It is apparant that the act of vibratory milling does not activate the WVM and results in faster leaching for this sphalerite.

Figure 6.33 compares the specific surface area versus $\bar{D}$ (where $\bar{D}$ is the arithmetic mean of the size fraction upper and lower limits) for the WVM and WBM sphalerites. A B.E.T. N_2 adsorption technique was used to measure the specific surface area.

It is observed that for a given $\bar{D}$, the WVM sphalerite generally has a lower A_o value than the WBM sphalerite. No attempt is made to explain this phenomenon.

onditions

M_o	(kg)	0,05
$[H_2SO_4]_o$	(kg-mol/m^3)	1,0

(on fig. 6.32a) Best fit through exptl. $[Zn^{2+}]$ data.

egend

Point (-)	Curve (-)	Sphal. type	Stirrer (rpm)	Size fraction $\times 10^6$(m)	Data on table
o	a	WBM	800,0	-90,0+75,0	I 57
×	b	WVM	800,0	-90,0+75,0	I 58
□	c	WBM	1000,0	-75,0+63,0	I 59
Δ	d	WVM	1000,0	-75,0+63,0	I 60

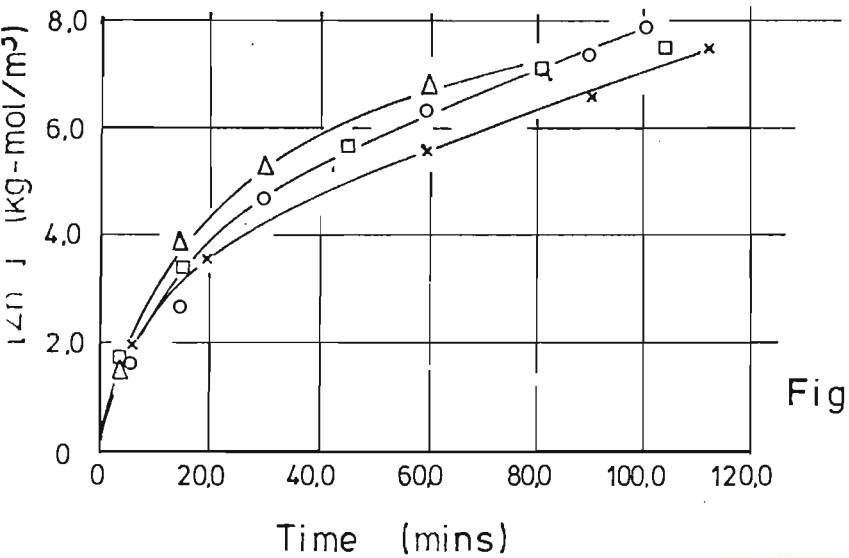

Fig 6.32a

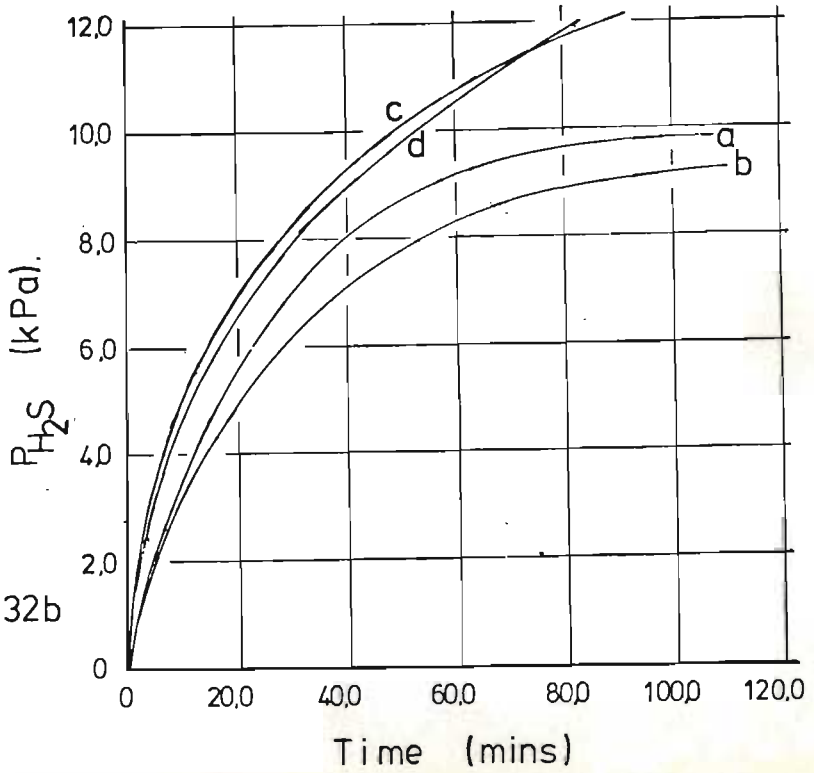

Fig 6.32b

igures 6.32a-b Comparison between the $[Zn^{2+}]$ and P_{H_2S} rate curves for ball milled (WBM) and vibratory milled (WVM) sphalerite leaching under case(i) conditions.

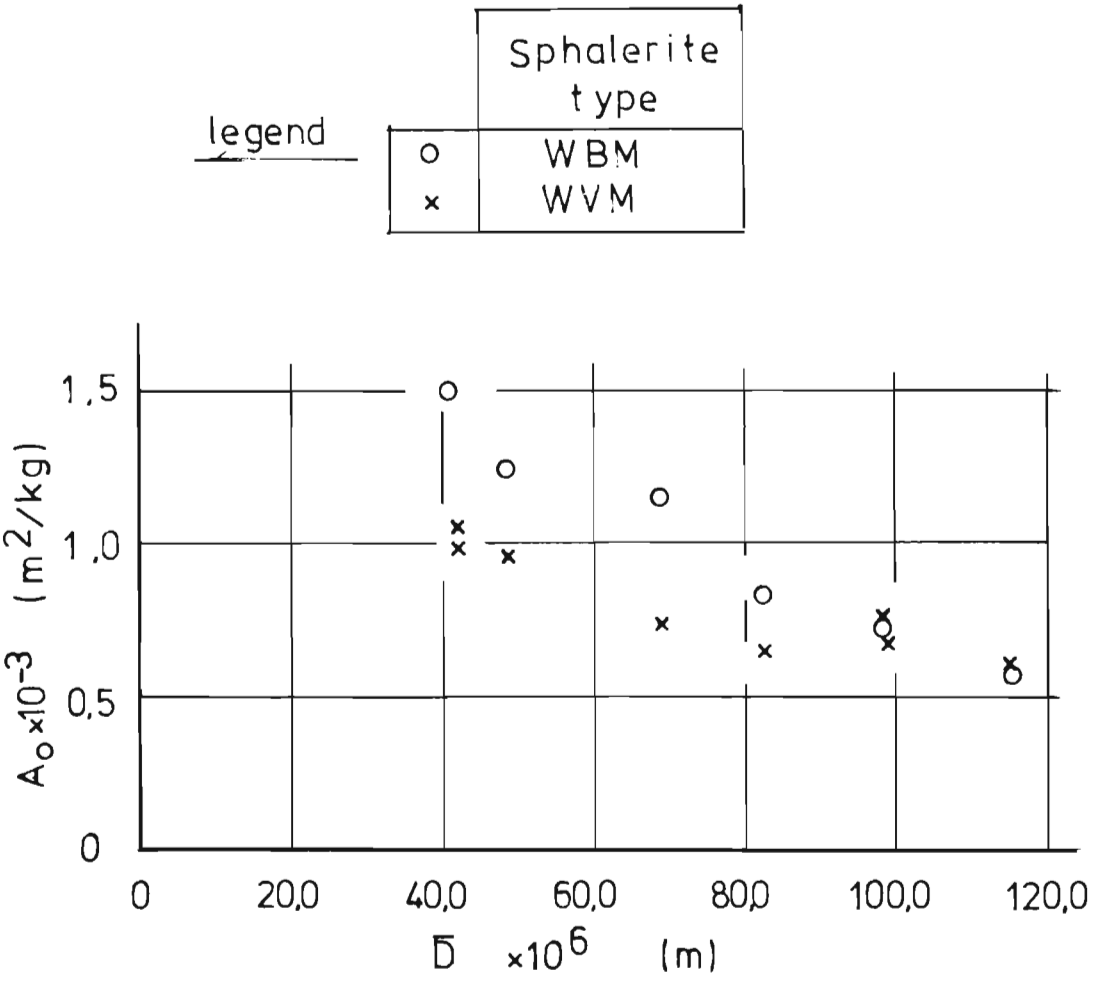

Figure 6.33 Comparison between the specific surface areas of WBM and WVM sphalerites.

6.8 THE POSSIBILITY OF S^o ASH DIFFUSION BECOMING RATE LIMITING DURING SPHALERITE DISSOLUTION UNDER CASE (ii) CONDITIONS

Wen (1968) presented a test to differentiate between chemical and diffusion rate control. Without repeating his derivation, he demonstrated that for the heterogeneous reaction of solids in which an ash layer formed, plotting lot (time) versus log $(1,0 - (1,0 - X)^{0,333})$ produced a line with a slope of 1,0 or 2,0 depending on whether chemical reaction, or ash diffusion respectively was rate controlling.

Figure 6.34 represents such plots for the BDH, VMWBM and VMPR sphalerites.

Figure 6.35 represents such plots for the WBM, ZCR and PR sphalerites. Very little accurate data was generally collected within the first 5,0 or 10,0 minutes. It is observed in the case of the WBM and PR sphalerites that chemical reaction appeared to be rate limiting up to about log (time) = 1,5 (i.e. t = 30,0 mins) and thereafter S^o ash diffusion appeared to be rate limiting. The slopes for each of the other types of sphalerite approximated 2,0 over the range of data plotted, suggesting that S^o ash diffusion was rate limiting.

This evidence conflicts with the results in chapter 4 (sections 4.1 and 4.7) which showed that for VMWBM sphalerite the calculated change in active site concentration (X) with X was the same for dissolution under case (i) conditions as it was for dissolution under case (ii) conditions. No elemental sulphur was formed under case (i) conditions.

Furthermore, in section 4.3 results were reported in which ZCR sphalerite was partially leached before removal from the acidic ferric sulphate media, washed in CCl_4 to remove S^o and then resubmitted for leaching in the original solution. No increase in rate was evident suggesting that diffusion through a S^o layer was not rate limiting.

Tiwari (1976) investigated the leaching of zinc sulphide in aqueous sulphuric acid using dissolved SO_2 gas as the oxidant. It was established that chemical reaction was initially rate controlling and that subsequently the rate limiting step became diffusion through a sulphur ash layer. The kinetics of the chemical reaction and ash diffusion control regimes was modelled.

NOTE: Wen's test for diffusion control is valid only for the initial stages of reaction (equation 16 presented by Wen (1968) is a valid approximation to equation 11 only under such circumstances); and for smooth spherical particles (which were not used for this thesis).

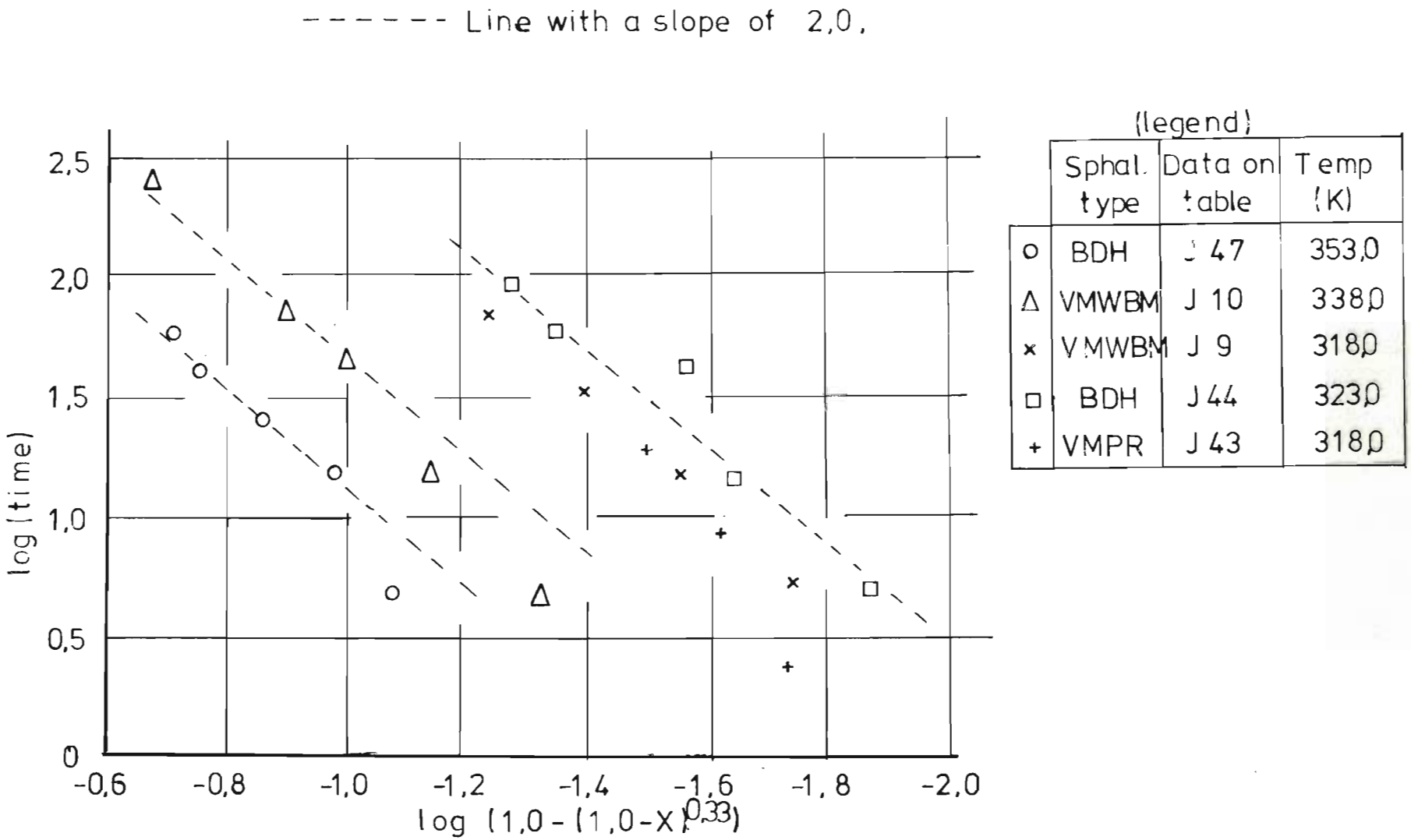

Figure 6.34 Plots of case(ii) leaching data for BDH, VMWBM and VMPR sphalerites. According to WEN(1968) a slope of 2,0 suggests that S° ash diffusion is rate limiting.

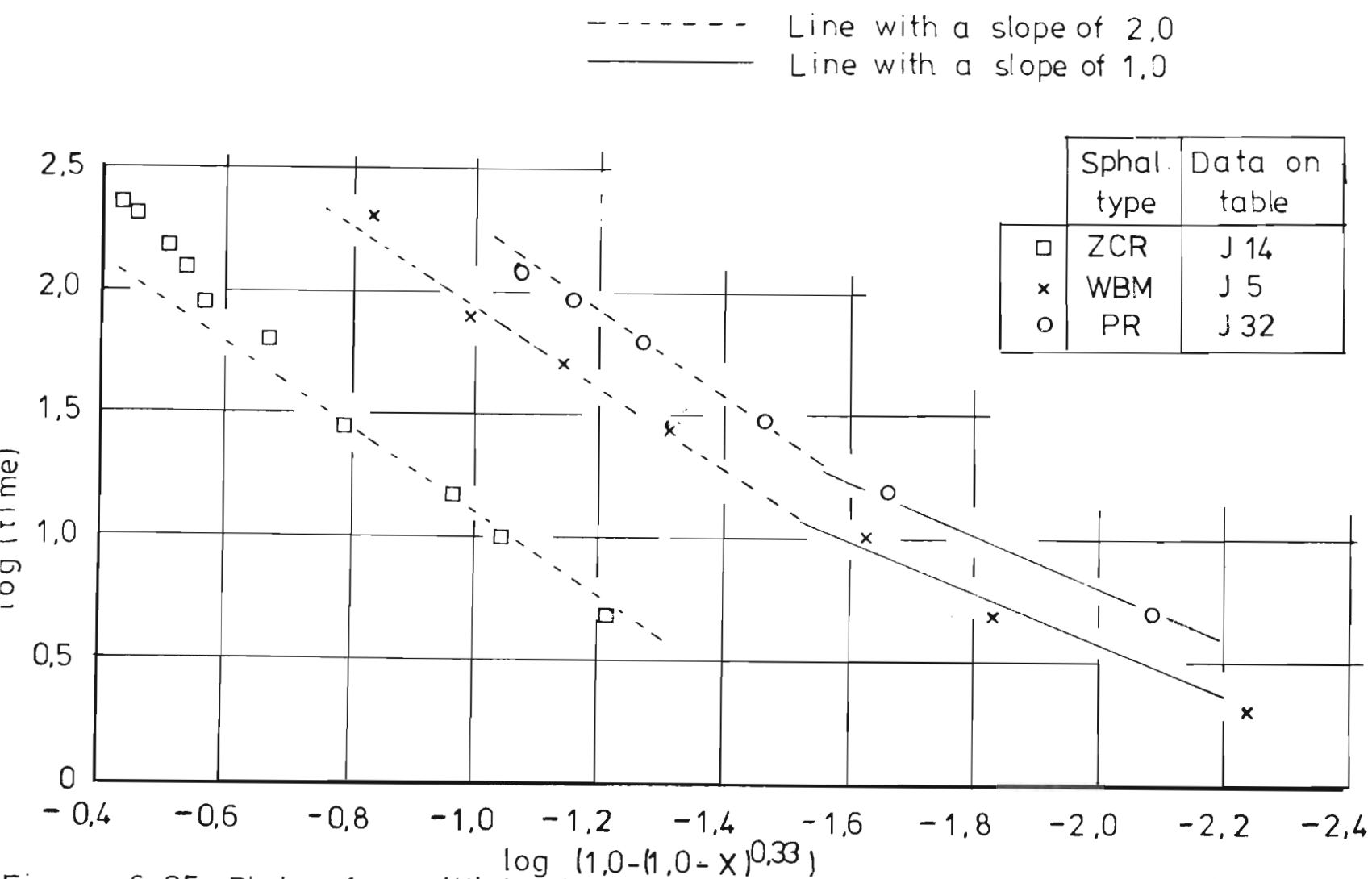

Figure 6.35 Plots of case(ii) leaching data for the WBM, ZCR and PR sphalerites. According to WEN (1968), a slope of 2,0 suggests that S° ash diffusion is rate limiting and a slope of 1,0 suggests that chemical reaction is rate limiting.

CHAPTER 7

SUMMARY AND CONCLUSIONS

The aim of this thesis was to fundamentally study the dissolution kinetics of a synthetic and three different natural sphalerites in acidic sulphate media under the following conditions :-

Case (i)	$[Fe^{3+}]_o$	:	$[H_2SO_4]_o = 0,0$
Case (ii)	$[Fe^{3+}]_o$	:	$[H_2SO_4]_o \geq 1,8$
Case (iii)	$[Fe^{3+}]_o$	:	$[H_2SO_4]_o \leq 0,1$

The manner in which this work was carried out and the results obtained are now summarised.

7.1 LITERATURE REVIEW

A review of the literature showed that very few fundamental sudies of the dissolution of natural sphalerite under case (i), (ii) or (iii) conditions had been reported. The role and effect of changes in the spalerite surface area had generally been neglected. Some controversy seemed to exist regarding the effect of vibratory (i.e. attrition) milling on the sphalerite dissolution kinetics.

Many studies were complicated by the presence of elemental oxygen and pressure conditions in the system. Consequently the roles of the hydrogen and

ferric ions were poorly understood.

It appeared to be generally accepted that the dissolution of sphalerite in acidic ferric sulphate media takes place non-oxidatively with H_2S first being produced, and that the H_2S is then oxidised homogeneously by the ferric ion. Some evidence was presented which suggested that the oxidation of the H_2S by the Fe^{3+} could be catalysed by the sphalerite present.

7.2 THEORETICAL ASPECTS

Dissolution mechanisms based on Langmuir-Hinschelwood adsorption theories were proposed and tested, and the following mechanism involving dual site reaction of adsorbed species in a well agitated system was favoured.

Adsorption:

$$\bullet + H^+ \rightleftharpoons \circ H^+ \quad \ldots\ldots\ldots \quad 2.57$$

$$\bullet + Fe^{3+} \rightleftharpoons \bullet Fe^{3+} \quad \ldots\ldots\ldots \quad 2.59$$

Dissociation:

$$\bullet H^+ \rightleftharpoons \circ HS^+ \quad \ldots\ldots\ldots \quad 2.61$$

$$\bullet Fe^{3+} \rightleftharpoons \circ FeS^{3+} \quad \ldots\ldots\ldots \quad 2.63$$

Dual site reaction of adjacent dissociated species:

$$\bullet HS^+ + \bullet HS^+ \rightleftharpoons \circ Zn^{2+} + \circ H_2S_\ell \ldots \quad 2.65$$

$$\bullet FeS^{3+} + \bullet FeS^{3+} \rightleftharpoons \bullet Zn^{2+} + \bullet S^o + 2\,Fe^{2+} \quad \ldots\ldots\ldots \quad 2.65$$

Desorption:

$$\bullet Zn^{2+} \rightleftharpoons \bullet + Zn^{2+} \quad \ldots\ldots\ldots \quad 2.68$$

$$\circ H_2S \rightleftharpoons \circ + H_2S_\ell \quad \ldots\ldots\ldots \quad 2.70$$

Diffusion of H_2S from liquid to gas phase:

$$H_2S_\ell \rightleftharpoons H_2S_g \quad \ldots\ldots\ldots \quad 2.72$$

No mechanism was proposed for the homogeneous

oxidation of H_2S by Fe^{3+}, and an empirical model (equation 1.7) developed by Verhulst (1974) was accepted as describing the kinetics for this reaction.

The following model was developed for dissolution under case (i) conditions in which adsorption or desorption steps were assumed to be rate limiting :-

$$\frac{d\,[Zn^{2+}]}{d\,t} = \frac{\phi_o^m \left(k_f\,[H^+]^m - k_r\,[Zn^{2+}]^{m/2,0}\,[H_2S]_\ell^{m/2,0} \right)}{\left(1,0 + K_{H^+}[H^+] + K_{Zn^{2+}}[Zn^{2+}] + K_{H_2S}[H_2S]_\ell\right)^m} \quad \ldots\ldots\ldots \quad 2.81 : 2.89$$

where m = 1,0 when adsorption is rate limiting;
m = 2,0 when desorption is rate limiting.

The model developed for dissolution under case (ii) conditions was :-

$$\frac{d\,[Zn^{2+}]}{d\,t} = k\,\phi_o\,\frac{[Fe^{3+}]}{[H^+]} \quad \ldots\ldots\ldots \quad 2.95$$

The models developed for dissolution under case (iii) conditions were very complex and are summarised in table 2.4.

7.3 EXPERIMENTAL ASPECTS

The following types and forms of sphalerite were leached under case (i), (ii) and (iii) conditions. (The abbreviations used in the text to identify each sphalerite are shown enclosed by brackets.)

A synthetic sphalerite (BDH);
A hand picked high grade natural sphalerite; which was ball milled (WBM); course vibratory milled (WVM) and vibratory milled fine (VMWBM);

A moderately impure industrial flotation concentrate used in a granular form (ZCR) or after vibratory milling fine (VMZCR);

A highly impure industrial flotation concentrate used in a granular form (PR) or after vibratory milling fine (VMPR).

The chemical compositions and mineralogies of these sphalerites are reported in this thesis.

7.3.1 LEACHING UNDER CASE (i) CONDITIONS

1) The sphalerites were leached in a 1 ℓ glass bowl reactor. Solution samples were taken at discrete time intervals during leaching, filtered and analysed for Zn^{2+}. The H_2S partial pressure was monitored continuously. The effects of the following variables were investigated:
$[H_2SO_4]_o$; M_o ; A_o ; Temperature ; agitation ; $[Zn^{2+}]_o$; $[H_2S]_o$.

2) Most of the experimentation was done using the VMWBM , VMZCR , BDH and VMPR sphalerites . The models expressed by equations 2.81 and 2.89 fitted the initial rate dissolution kinetics for these four sphalerites.

3) The active site concentration Φ varied during leaching in a way which was unique for each sphalerite. The way in which Φ changed was not related to the change in specific surface area (as measured using a B.E.T. N_2 adsorption technique), or to the shrinking core or any other simple model.

4) The shapes of the WBM and ZCR sphalerite dissolution rate curves were very different, the latter demonstrating an apparant induction period (as did the PR sphalerite). However, the VMWBM and VMZCR sphalerites leached virtually identically, without any evidence of an induction period.

5) The Zn^{2+} adsorption equilibrium constants for each sphalerite were observed to increase in the order :-
BDH < VMWBM < VMZCR < VMPR
(The dissolution rate per unit area of these sphalerites leaching under case (ii) conditions also increase in this order. This suggests that the adsorption of positive metal ions increase for the sphalerites in this order).

7.3.2 LEACHING UNDER CASE (ii) CONDITIONS

1) Under case (ii) conditions no H_2S partial pressure was detected, and it was shown that equal amounts of zinc ions and elemental sulphur were formed.

2) The -90,0 + 63,0 µm size fractions of WBM, ZCR and PR sphalerites leached virtually identically. For the PR sphalerite the leaching rate per unit area increased with decreasing particle size to a maximum for the vibratory milled VMPR sphalerite. This apparant activation appeared to be due to the liberation of chalcopyrite impurity rather than due to the mode of milling.

For the WBM sphalerite the leaching rate per unit area decreased with decreasing particle size to a minimum for the vibratory milled VMWBM sphalerite, to a value which was close to that observed for the synthetic BDH sphalerite. Consequently no apparant activation effect was observed.

A slight decrease in leaching rate per unit area with decrease in particle size was observed for the ZCR sphalerite.

3) Photographs of unleached and leached sphalerite particles were taken using a Scanning Electron Microscope. Elemental sulphur was observed to coat the WBM, ZCR and PR sphalerite particles which had been leached under case (ii) conditions.

Optical microscope photographs of etched and unetched polished sections of WBM, ZCR and PR sphalerites were taken which revealed that dissolution generally occured preferentially at specific zones and in a complex manner.

The experimental and theoretical evidence regarding the effect of the sulphur coating on case (ii) dissolution kinetics, tends to be conflicting.

7.3.3 LEACHING UNDER CASE (iii) CONDITIONS

1) It was shown that for leaching under case (iii) conditions, oxidative dissolution (which produced S^{o}) and non-oxidative dissolution (which produced H_2S) occur ed simultaneously.

2) The presence of small Fe^{3+} concentrations tended to suppress the initial rate of dissolution of the BDH, VMWBM and VMZCR sphalerites in a manner which could not be satisfactorily explained in terms of adsorption theories.

3) Experiments were conducted in which H_2S (produced either by purging H_2SO_4 with H_2S, or by leaching various sphalerites) was oxidised by Fe^{3+} injected into the reactor. The resultant decrease in P_{H_2S} with time was monitored. It was shown that the sphalerite solids catalysed the oxidation reaction, and that the catalytic effect was very large for the VMPR sphalerite. It was also shown that activated charcoal strongly catalysed the Fe^{3+} oxidation of H_2S.

4) The presence of activated charcoal enhanced the dissolution of sphalerite in acidic ferric sulphate media, only when conditions were such that H_2S was a product of the dissolution reaction.

7.4 CONCLUSIONS

1) Extensive experimental data are reported for the dissolution of a synthetic and three natural sphalerites under case (i), (ii) or (iii) conditions, and for the oxidation of H_2S by Fe^{3+} in the absence or presence of these sphalerites or activated charcoal.

2) It was possible to use the Langmuir-Hinschelwood adsorption theories to propose mechanisms and develop models which fitted the initial rate kinetic data for leaching sphalerite in acid sulphate media without or with Fe^{3+} present.

3) Dissolution took place non-oxidatively (under case (i) conditions); oxidatively (under case (ii) conditions), or both non-oxidatively and oxidatively at the same time (under case (iii) conditions). The extents and rate at which oxidative or non-oxidative dissolution took place, and the catalytic effect of the sphalerites on the Fe^{3+} oxidation of H_2S, could be interpreted in terms of the adsorption characteristics of the sphalerites.

4) Scanning electron microscope photographs of particles leached under oxidative conditions showed the presence of elemental sulphur on the surface. However, the evidence is conflicting as to whether the sulphur results in diffusion rate control.

5) The way in which the specific area (as measured using a N_2 adsorption technique) changed during leaching generally bore no relationship to the calculated change in active area.

6) The effects of milling the natural sphalerites fine depended on the chemical composition of the sphalerites, and not on the mode of milling. Thus vibratory milling and ball milling which apparantly resulted in an activation effect in the case of the PR sphalerite, caused no such effect for the WBM and ZCR sphalerites.

7) Decreasing the exponent on the H_2SO_4 term from 2,49 to 2,0 in the Verhulst model for the Fe^{3+} oxidation of H_2S (equation 1.7), resulted in a significantly better fit of the model to experimental data. The presence of sphalerite or activated charcoal exerted significant catalytic effects on the oxidation of H_2S by Fe^{3+}.

8) The presence of activated charcoal did not result in enhanced sphalerite dissolution rates, unless conditions were such that H_2S was a product of reaction.

CHAPTER 8

REFERENCES

ANHAEUSSER C.R. and LENTHALL D.H.

"A petrographic and mineragraphic study of selected borehole intersections of the Prieska copper-zinc lode, Northwestern Cape Province."
Economic Geology Research Unit, University of the Witwatersrand, Johannesburg.
(August, 1970)

BECKSTEAD L.W., WADSWORTH M.E. et al

"Acid ferric sulphate leaching of attritor ground chalcopyrite concentrates".
International Symposium on Copper Extraction and Refining, Los Angeles. (February, 1976)

BRITTAN M.I.

"A kinetic model of copper segregation and its application to Torco plant design."
Inst. Min. and Metall. C 262 - C 272
(December, 1971)

C. R. C. PRESS, INC.

Handbook of Chemistry and physics. 55th Edition (April, 1974)

DUTRIZAC J.E. and MAC DONALD R.J.C.

"Ferric ion as a leaching medium".
Minerals Science Engineering: 6, (2), 59 - 100 , (April, 1974)

EXNER F., GERLACH J., PAWLEK F.

"Pressure leaching of ZnS"
Erzmetall 22, (5), 219 - 227 (1969)
(NIM Translation No. 174)

GEAR C.W.
"The Automatic Integration of Ordinary Differential Equations".
Communication of the A.C.M. 3, (14), 176 - 178, (1971)

GEAR C.W.
"Difsub for Solution of Ordinary Differential Equations".
Communication of the A.C.M. 3, (14), 185 - 189, (1971)

GERLACH J.
"Method for the processing of sulphide, arsenide or antimonide ores."
Patent Application. Federal Republic of Germany. Central Patents office. File no: P 2136 143.1 (30th July, 1971)
(NIM Translation No: 430.
Address: National Institute for Metallurgy,
Private Bag X 3015,
Randburg, 2125,
South Africa.)

GERLACH J.
"Activation and leaching of chalcopyrite concentrates with dilute sulphuric acid."
A.I.M.E. International Symposium on Hydrometallurgy. Chicago (1973).

HABASHI F.
"Principle of Extractive Metallurgy :
Vol. 1, General Principles
Vol. 2, Hydrometallurgy
Gordon and Breach, New York, (1970)

HELFFERICK, F.
"Ion exchange".
Mc Graw Hill, New York, (1962)

JAN J.
"A kinetic study on the pressure leaching of sphalerite".
Ph D thesis, University of Denver, (1974)

JOHNE R., SEVERIN D.
"Die oberflächenmessung mit dem Areameter"
Zeitschrift für technische Chemie, Verfahrenstechnik und Apparatewesen, 37, (1), 57-61 (1965)

KUZMINKH I.N. and YAKOUTOVA E.L.
"Action of solutions of ferric sulphate on zinc sulphide".
Jnl. of Applied Chem. of the U.S.S.R., vol 23, 1197 - 1202, (1950)

LEVENSPIEL O.

"Chemical Reaction Engineering".
John Wiley and Sons, Inc. New York
(1964)

LOCKER L.D. and de BRUYN P.L.

"The kinetics of dissolution of II - VI semiconductor compounds in nonoxidising acids".
Jnl. Electrochem. Soc. : Electrochemical Science 116, (12), 1659 - 1665, (December, 1969)

LOVELL V.M.

"The effect of certain pretreatments on the surface area of various minerals, determined by the B.E.T. method".
Powder Technology 12, 71 - 76 (1975)

MOLDENHAUER W.

"Über die Reduktion von ferrisalzen mit schwefelwasserstof."
Zeitzchrift für Electrochemie und Angewandte Physikalische Chemie
Vol. 32 (1926)
(NIM Translation No. 590 entitled :-
'On the reduction of ferric salts by H_2S '.)

NELDER J.A., MEAD R.

"A simplex method for function minimisation".
Computer Science 7, 308 - 313, (1965).

PERRY J.H.

"Chemical Engineers Handbook" 4th Edition, (1963). Mc Graw - Hill Chemical Engineering Series.

POHL H.A.

"The formation and dissolution of metal sulphides".
American Chem. Soc. Jnl., vol 76, 2182 - 2184 (1954)

ROMANKIW L.T.

"Kinetics of dissolution of zinc sulfide in aqueous sulfuric acid".
Ph D thesis submitted to Massachusetts Inst. of Technology (August, 1962).

ROMANKIW L.T., de BRUYN P.L.

"Kinetics of dissolution of zinc Sulphide in aqueous sulphuric acid".
Unit Processes in Hydrometallurgy,
Met. Soc. Conferences 74, Dallas,(1963)

SMITH J.M.

"Chemical Engineering Kinetics."
2nd Edition . Mc Graw - Hill , (1970)

TIWARI B.

"The kinetics of oxidation of zinc sulfide and hydrogen sulfide by sulfur dioxide in aqueous sulfuric acid".
Columbia University, Eng. Sc. D. (1976)

VELTMAN H., O ' KANE P.T.

"Accelerated Pressure leaching of Zn S Concentrates".
97th Annual Meeting of A.I.M.E., New York, (1968)

VERHULST D.

"Kinetics of Oxidation of Hydrogen Sulphide and Zinc Sulphide by Ferric Iron in Sulphuric Acid solution".
Ph D thesis, University of Columbia, New York, (1974)

Available: Xerox University Microfilms, Ann Arbor, Michegan, U.S.A.
Order no. 75 - 12,369

VERMILYEA D.A.

"The dissolution of ionic compounds in aqueous media".
Jnl. of the Electrochemical Soc., 113 , (10), 1067 - 1070 , (October, 1966)

VOGEL A. I.

"A text book of quantitative inorganic analysis, including elementary instrumental analysis".
3rd Edition. (1961). Longmans, Green & Co. Ltd., London.

WEN C.Y.

"Noncatalytic hetergeneous solid fluid reaction models".
Ind. Eng. Chem. 60,(9), 34-54,(1968).

APPENDIX

A P P E N D I X A

DESCRIPTION OF LEACHING APPARATUS

Introduction

Figure A. 1 schematically illustrates the apparatus used to leach sphalerite in aqueous sulphuric acid, and to oxidise H_2S by Fe^{3+} in the presence or absence of sphalerite or other solids. Basically the same apparatus was used to leach sphalerite in acidic ferric sulphate, the main difference being that in many runs the H_2S partial pressure was known to be negligible and no attempt was made to monitor the reactor pressure.

Figure A. 2 presents a photograph of an overall view of the leaching circuit and figure A. 3 a close-up photograph of the reactor bowl and head.

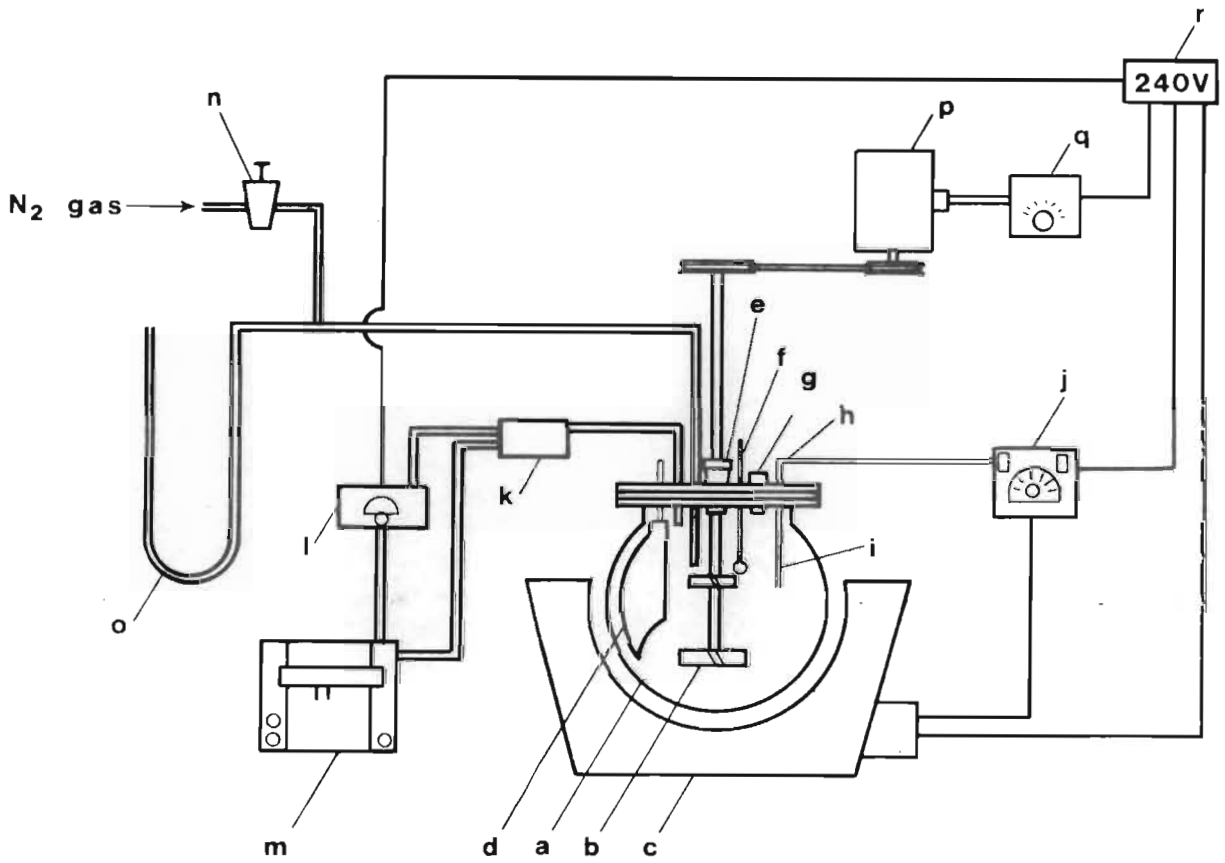

Description

a 1 l Glass Quickfit reactor
b Ti impellers and stirrer shaft
c Isopad heating mantle
d Perspex baffle
e PTFE graphite packed stuffing box
f Thermometer
g Sampler containing septum
h Fe–Co Thermocouple
i Oil filled glass thermowell
j Plastocomp temperature controller
k Kyoga O-100 kPa pressure transducer
l Regulated 5 mV power source
m Goerz chart recorder
n Pressure regulator
o Hg manometer
p Reliance 0,75 kJ/s d.c. motor
q Thyristor d.c. voltage regulator
r 240 V mains power supply

N.B. (1) Cooling effected by heat radiation, and narrow bore rubber coil looped around outside of reactor through which tap water is passed.

(2) N_2 gas and Hg manometer only used to purge reactor solution and calibrate the pressure transducer, but removed during leaching

FIGURE A.1. Schematic diagram of leaching apparatus

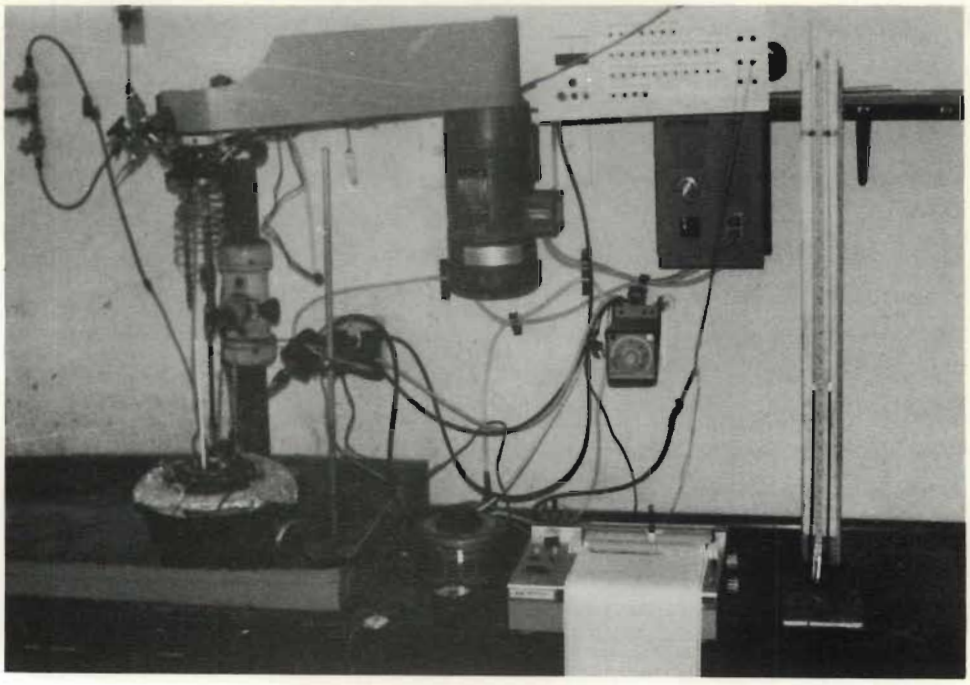

Figure A.2 Overall view of leaching apparatus. Refer to text and fig. A.1 for description and details.

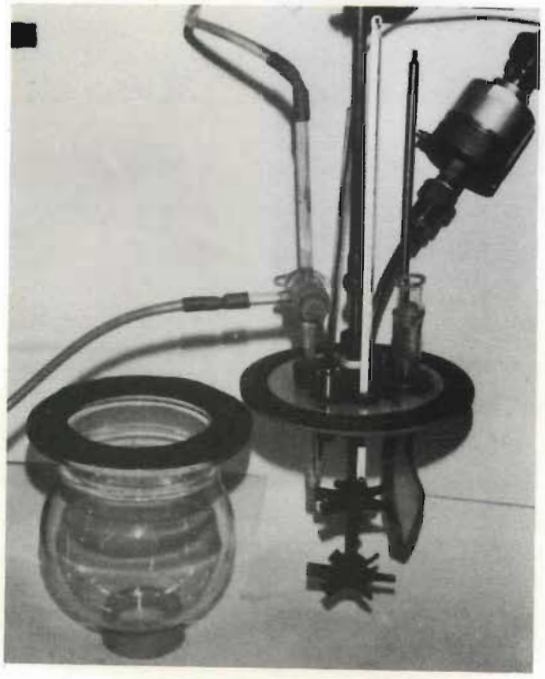

Figure A.3 Close-up view of reactor bowl and head. Refer to text and fig A.1 for description and details.

A. 1 REACTOR

Figure A. 3 shows a close-up view of the reactor which consisted of a spherical 1 ℓ Quickfit glass bowl. A flat P.V.C. top was machined with multiple ports to permit access into the reactor. A flat expanded rubber gasket was fitted between the ground glass reactor flange and the P.V.C. top. A mild steel ring counter sunk into the P.V.C. top enabled the top and the reactor flange to be tightly clamped together with a spring clip, (visible on Figure A. 2). Pressures of up to 40,0 kPa could be tolerated before leakage occured.

A titanium shaft passed through a stuffing box into the reactor, and two downward pumping titanium impellars were fitted, 0,05 m apart at the bottom of the shaft. The teflon (or P.T.F.E.) dry stuffing box was packed with Chesterton self forming graphite tape.

A shaped perspex baffle was installed in the reactor to help induce turbulence. The total internal volume of the reactor with top, impellar, baffle etc. fitted, was approximately $1,35 \times 10^{-3}$ m^3 .

A. 2 TEMPERATURE CONTROL

An oil-filled thermowell containing a "Thermocoax" Fe-Co thermocouple was installed in the reactor. A Philips Plastocomp temperature controller related the

thermocouple millivolt signal to a set point, and operated a relay switch. The relay switch passed 240 V mains current through a variable voltage transformer to an "Isopad" heating unit. A thermometer calibrated in 0,1 K was used to accurately monitor the temperature of the reactor contents.

Cooling was effected manually when necessary by passing mains water through narrow bore rubber tubing looped around the outside of the reactor. (It was found that passing cooling water through the reactor gas cap to a cooling coil inside the reactor, caused intolerable fluctuations of the monitored pressure owing to cooling of the gas in the gas cap.)

Many of the experiments were conducted at 318,0 K as at this temperature the control system functioned best. Temperature could generally be controlled to approximately ±0,25 K .

A. 3 STIRRER SPEED CONTROL

A "Saftronic" single phase thyristor controller was used to drive a "Reliance" 0,75 K J/s D.C. motor. The titanium reactor stirrer was connected via a rubber coupling to the drive shaft of apparatus used previously by the author to conduct pressure leaching experiments. The stirrer speed was measured using a 0 to 10 000 r.p.m. tachometer.

A. 4 GAS CAP PRESSURE MONITORING

The reactor pressure was transduced to a milli-volt output signal using either a Kyowa model PG - 1 KU (0 - 100,0 k Pa range) or a model PG - 2 KU (0 - 200,0 k Pa range) transducer. The pressure transducer was activated by a 5,0 m V D.C. regulated current, and the transducer output was recorded using a "Goerz" potentiometric flatbed recorder. A source of N_2 gas (used to purge the reactor contents), was connected to a mercury manometer so that when the reactor was closed and pressurised the recorder output of the transducer signal could be calibrated against the measured H g manometer head difference.

A. 5 SAMPLE INTRODUCTION

It was important to be able to measure the initial rate of increase of the reactor pressure due to H_2S evolution, when the reaction commenced. Pressure increases due to the gas cap heating up after switching on the reactor, and increases associated with the introduction of the solids thus had to be minimised.

A 10,0 ml or 20,0 ml plastic hypodermic syringe, with the front cut off, was therefore filled with sphalerite sample and the syringe front was sealed with a rubber stopper. The syringe with sample was fitted into the reactor top, (shown in Figure A. 3),

and the sphalerite sample was 'injected' into the reactor after initial steady state had been attained.

The introduction of large samples (for example > 20,0 g), necessitated pouring the solids into the reactor through a funnel and sealing the reactor as rapidly as possible. This procedure unfortunately permitted the ingress of air (hence elemental oxygen), and permitted the gas cap to cool.

A. 6 SOLUTION SAMPLING AND FILTERING

A stainless steel cylinder was obtained into which a gas chromatograph self-sealing rubber septum could be fitted. This device was installed in the reactor top, and solution samples could be injected into, or withdrawn from, the reactor through a 7,0 - 10,0 cm long 20 or 22 guage hypodermic exploratory needle. The self-sealing septum ensured that the reactor pressure was not accidently released on withdrawing the needle.

Even solutions containing -90,0 + 75,0 micron size fraction suspended solids could be sampled in this manner. The use of needles larger than 18 - 20 guage, resulted in rapid destruction of the septa.

The procedure adopted to filter the solution samples depended on the nature of the suspended solids.

It was found that for samples containing relatively course sphalerite particles (say larger than 10,0 micron mean diameter), upon holding a 2,0 or 5,0 ml hyperdermic sampling syringe horizontally, the solids rapidly settled out of solution. With the needle off, and the syringe kept in a horizontal position, the clear solid-free leach solution could be carefully expelled from the syringe. Generally less than 30,0 seconds elapsed between the time of sampling, and solids separation.

Solution samples containing synthetic or fine vibratory milled sphalerite were quickly injected from the sampling syringe into a gouch cruscible containing a layer of analytical grade asbestos wool deposited on the glass frit.

Filteration under vacuum ensured that the time elapsed between sampling and solids separation, was generally less than approximately 20,0 seconds.

APPENDIX B

DESCRIPTION OF EXPERIMENTAL PROCEDURE AND PRETREATMENT OF NATURAL SPHALERITES

B.1 DESCRIPTION OF EXPERIMENTAL PROCEDURE

Introduction

The procedure adopted for leaching sphalerite in acidic ferric sulphate was basically the same as for leaching in aqueous sulphuric acid - with the important exception that frequently no attempt was made to monitor the reactor pressure in the former case. Only the procedure for leaching in aqueous sulphuric acid and injecting Fe^{3+} into the system when the rate of increase of the H_2S partial pressure became very small, will therefore be described below.

B.1.1. INITIAL PREPARATIONS

(i) While heating the reactor (containing 1 ℓ aqueous H_2SO_4 but no sphalerite) to the desired temperature, N_2 gas was purged

into the solution for up to 30,0 minutes. Sufficient agitation was maintained using the stirrer, to finely disperse the N_2 gas bubbles.

(ii) With the N_2 gas switched off and the reactor sealed, the agitation rate was set at 800,0 - 1 000,0 r.p.m. and the system left to reach thermal equilibrium at the exact desired temperature. Themometers installed in both the gas cap and the solution demonstrated that these zones achieved thermal equilibrium at the same temperature within 1,0 - 2,0 minutes.

(iii) The desired chart recorder graph paper drive speed and transducer millivolt scale expansion were set. All information relating to the experimental conditions were recorded on the recorder graph paper, and the recorder chart drive was switched on.

B. 1. 2. COMMENCEMENT OF REACTION

The following sequence of actions was performed as rapidly as possible:

(i) The stirrer was switched off.

(ii) The solids were injected into the reactor.

(iii) The reactor was momentarily vented to atmospheric pressure and then tightly sealed.

(iv) The stirrer and stop watch (calibrated in 0,2 second intervals) were simultaneously switched on.

B. 1. 3. SAMPLING DURING THE COURSE OF REACTION

(i) Samples were taken at desired time intervals by injecting, for example 5 ml leach solution similar to that initially in the reactor , and then withdrawing 5 ml leach solution. In this way the total pressure within the reactor was affected minimally. The dilution and cooling effects introduced by injecting 5 ml into 1,0 ℓ solution was found to be negligibly small.

(ii) The solution sample was filtered (as described in section A. 6.).

(iii) An A-grade pipette was used to pipette 1,0 ml of the filtered leach sample into a 100,0 ml volumetric flask containing slightly acidified double de-ionised distilled water. The solution in the flask was made up to 100,0 ml , and transferred to an appropriately labled bottle which was tightly sealed. The diluted samples were analysed for dissolved zinc or other metal ion using atomic adsorption techniques - (Appendix D. 1.) .

(iv) Sampling was continued at regular time

intervals until the rate of increase in the reactor pressure became very small.

B. 1. 4. INJECTION OF Fe^{3+} INTO THE REACTOR

In several experiments, H_2S gas was purged into the H_2SO_4 solution, without any sphalerite being present. However, the only difference the presence of sphalerite made as regards procedure, was that it was then not possible to analytically determine the H_2S concentration in solution. Therefore, whether the H_2S partial pressure was generated by leaching sphalerite or injecting H_2S gas, the following procedure was adopted, once the P_{H_2S} was relatively constant.

(i) By experience it was found that the presence of, for example VMPR or activated charcoal in the reactor, resulted in catalysis of the H_2S oxidation by the Fe^{3+}. Thus the chart recorder drive speed was increased prior to injecting the ferric.

(ii) An exact volume (2,0 or 5,0 ml for example), of the reactor solution was removed. (Switching off the stirrer during this operation eliminated gas being withdrawn with the liquid phase.)

(iii) An identical volume (to that removed) of highly concentrated Fe^{3+} solution was rapidly injected into the reactor.

(iv) The initial rate of decrease of the P_{H_2S} was measured and taken as being proportional to the initial rate of H_2S oxidation by the Fe^{3+}.

(v) Frequently there was sufficient residual H_2S after all the Fe^{3+} had been reduced to Fe^{2+}, to repeat steps (ii) - (iv) using different volumes of injected Fe^{3+}. Thus initial rates of H_2S oxidation could be measured using different initial H_2S and Fe^{3+} concentrations.

(vi) The samples drawn in step (ii) were sometimes filtered and diluted in order to analyse the Zn^{2+} or total Fe concentrations.

B. 1. 5. FILTERATION AND WASHING OF FINAL LEACHED SOLIDS

Frequently the entire final leach solution was filtered and washed in order to collect all the residual solid leached material and determine the total final surface area. This was especially so in those experiments in which sphalerite solids had been leached to relatively large extents of zinc recovery in acidic ferric sulphate media. The procedure adopted was as follows:

(i) The leach solution was filtered under vacuum in a buchner funnel using Whatman (number 1) qualitative grade filter paper.

(It was necessary to use finer paper when filtering BDH or vibratory milled sphalerite solids.)

(ii) The filter cake was washed with several cake displacements of distilled water.

(iii) The filter cake was oven dried at between 100,0 - 105,0 °C, and weighed.

(iv) In the case of granular solids leached in acidic ferric sulphate media, a small mass of solids was sometimes removed and kept for subsequent S.E.M. observation.

(v) The dried solids were washed with CCl_4 in a Soxhlet apparatus to remove all elemental sulphur.

(vi) The CCl_4 washed solids were oven dried and weighed. The elemental sulphur was recovered by distilling off the CCl_4 solvent (which was recycled) and drying the precipitated S^o.

(vii) The mass of S^o was weighed.

(viii) For many runs, samples of the filtrate were bottled and stored.

B. 2. PRETREATMENT OF NATURAL SPHALERITES

The PR and ZCR industrial flotation sphalerite concentrates were initially dispersed and washed in water containing Teepol detergent to break down agglomerates, and remove organic flotation reagents possibly present on the particle surfaces. The WBM sphalerite obtained in lump form was either wet ground in a laboratory ball mill or dry ground using a Siebtechnik laboratory vibratory mill.

The dispersed PR, ZCR and the milled WBM sphalerites were wet screened through a 38,0μm screen to remove the fines fraction. The +38,0μm fractions were oven dried and dry screened into several discrete size fractions ranging between 38,0 μm and 125,0μm. The -38,0μm fines were separated into discrete size fractions ranging from 38,0μm down to approximately 9,0μm using a Warman cyclosizer, and then dried.

Further pretreatment of the WBM, PR and ZCR sphalerites by washing in dilute acid resulted in the removal of oxide coatings possibly present and of gangue (most likely $MgCO_3$). Removal of the latter was found to significantly affect the specific surface areas of the PR and ZCR sphalerites.

In addition to using the WBM, PR and ZCR sphalerites in their granular form, part of the acid-washed +38,0μm size fractions were finely milled to powder consistency by extensive (5 minutes) vibratory milling in a Siebtechnik laboratory scale vibratory mill.

These vibratory milled sphalerites (designated as VMWBM, VMPR, and VMZCR) were also used in this form in leaching experiments in addition to the BDH, WBM, PR and ZCR sphalerites. The synthetic BDH sphalerite was not pretreated in any way prior to leaching.

A P P E N D I X C

CHEMICALS USED IN LEACHING EXPERIMENTS

The source and composition of the various sphalerites used have been described in Chapter 3. The leach solutions used were prepared as follows:

C. 1. AQUEOUS SULPHURIC ACID

Bulk supplies (approximately 25,0 ℓ at a time) of 1,0 M or 2,0 M H_2SO_4 were prepared by adding analar grade concentrated H_2SO_4 to double deionised distilled (d.d.d.) water. The acid concentrations were analysed and adjusted until ± 0,5% of the desired molarity had been achieved. For experiments which required 0,5 M H_2SO_4, the 1,0 M H_2SO_4 was diluted 50 : 50 with d.d.d. water.

C. 2. ACIDIC FERRIC SULPHATE SOLUTION

Solutions with desired ferric ion concentrations were generally prepared by dissolving the required mass of Kanto Chemical Co. guaranteed reagent or extra pure reagent grade ferric sulphate crystals in sufficient d.d.d. water to give 1 ℓ of solution.

Measureable free acid was formed by hydrolysis of the ferric ions (with a resultant ratio - $[Fe^{3+}] : [H_2SO_4] \simeq 2,0$) and except in isolated experiments, no additional H_2SO_4 was added. Selection of the ferric ion concentration required for each run was based on the extent of leaching and the initial mass of the sphalerite chosen for the experiment in which the solution was to be used. The ferric ion and H_2SO_4 concentrations were measured in duplicate before commencing each leach experiment.

In several experiments volumes of up to 40,0 ml concentrated (150,0 - 160,0 g/l Fe^{3+}) acidic ferric sulphate solution were added to 1 l 0,5 M, 1,0 M or 2,0 M H_2SO_4 to give solutions with low $[Fe^{3+}] : [H_2SO_4]$ ratios. No attempt was made to measure the ferric ion or changes in H_2SO_4 concentration resulting from adding such small amounts of the acidic ferric sulphate solution; and it was assumed that the acid concentration remained unaffected.

A P P E N D I X D

METHODS OF CHEMICAL ANALYSIS

D. 1. DETERMINATION OF DISSOLVED ZINC, IRON OR COPPER IN SOLUTION

A Perkin-Elmer model 303 atomic adsorption (A.A.) spectrophotometer with an air-acetylene flame, and a Tarkan flatbed chart recorder was used.

Prepared Solution

Calibration samples were prepared by diluting "Searle" 1,0 g/l zinc, iron or copper spectrophotometry standardised solutions (accurate to within $\pm$ 0,5 %) with H_2SO_4 acidified double deionised distilled water to concentrations within the A.A. manufacturer's recommended sensitivity ranges. These diluted samples were used to calibrate the A.A. adsorption as a function of metal ion concentration for analysis of leach solution samples.

Method

1) 5,0 or 10,0 ml samples of leach solution were taken and filtered as soon as possible at discrete time intervals during the course of an experiment - (see section B. 1. 3. for details of sampling procedure).

2) Small (usually 1,0 ml) aliquots of the filtered leach samples were diluted using H_2SO_4 acidified double deionised distilled water to within the metal ion concentraion ranges recommended by the A.A. manufacturer.

3) The percentage adsorption of the diluted calibration and leach samples were measured using the A.A. .

4) Percentage adsorption versus concentration calibration curves were drawn from which the metal concentrations of the leach solutions were interpolated.

5) Appropriate dilution factors were used to calculate the metal concentrations in the original leach solutions.

D. 2. FERRIC ION (Fe^{3+}) DETERMINATION

Prepared solutions

A standard 0,179 N sodium thiosulphate solution was prepared by dissolving 44,424 g $Na_2S_2O_3$ 5 H_2O in recently boiled distilled water and making up to 1,0 l. Approximately 3 drops chloroform and 0,1 g/l Na_2CO_3 was added.

Then 1,0 ml 0,179 N $Na_2S_2O_3$ = 0,01 g Fe^{3+}

Method

1) Add an excess of K I crystals to an aliquote of the leach sample.

2) Titrate with the standard sodium thiosulphate solution until the range brown colour disappears.

3) Near the end point the solution becomes pale yellow, and at this point a crystal of K I may be added to determine whether sufficient K I is present.

4) At the end point the solution is colourless.

5) Calculate the concentration of Fe^{3+} in the original leach solution.

Reactions

$$Fe_2(SO_4)_3 + KI \rightarrow 2\,FeSO_4 + I^o$$

$$I^o + Na_2S_2O_3 \rightarrow Na_2S_4O_6 + \underset{\text{(colourless)}}{NaI}$$

D. 3. H_2SO_4 DETERMINATION

Prepared solutions

a) Phenol - phthalein indicator

b) Standardised 0,2 N NaOH solution.

Method

1) A few drops of phenol-pthalein indicator is added to an aliquot of the H_2SO_4 solution.

2) The standardised NaOH is titrated until permanent red colour first appears.

3) Calculate the H_2SO_4 concentration in the original leach solution.

Reaction

$$2\,NaOH + H_2SO_4 \rightarrow Na_2SO_4 + 2\,H_2O$$

D. 4. H_2SO_4 DETERMINATION IN SOLUTIONS CONTAINING Fe^{2+} / Fe^{3+} IONS

Prepared Solutions

a) Mixed indicator - 0,2 g dimethyl yellow + 0,2 g methyl blue dissolved in 200,0 ml methanol.

b) 0,204 N Sodium carbonate prepared by dissolving 10,8110 g oven dried (at 533,0 K - 543,0 K) Na_2CO_3 with distilled water up to 1 L.

Then 1 ml 0,203 N Na_2CO_3 = 0,01g H_2SO_4

Method

1) Any ferric ion present in an aliquot of the leach solution must first be reduced to ferrous ion (i.e. add K I crystals and titrate with $Na_2S_2O_3$ as in section D. 2.).

2) Add 3 drops mixed indicator to the aliquot and titrate with the standard Na_2CO_3 solution until a green colour indicates that end point is reached.

Reaction

$$Na_2CO_3 + H_2SO_4 \rightarrow Na_2SO_4 + CO_2 + H_2O$$

D. 5. DETERMINATION OF ELEMENTAL SULPHUR IN LEACH RESIDUE

Carbon tetrachloride solvent was used in a Soxhlet apparatus to dissolve elemental sulphur from leach residue contained in a tared permeable paper thimble.

Method

1) The final leach solution is filtered through number 1 Whatman filter paper.

2) The filter cake is oven dried at 378,0 K, and allowed to cool in a dessicator.

3) The dried residue is weighed and placed in a tared permeable paper thimble.

4) The elemental sulphur is extracted from the residue in the thimble in the Soxhlet apparatus using carbon tetrachloride for six hours.

5) The residual solids and thimble are oven dried, cooled and weighed and the solids mass is calculated.

6) The amount of sulphur is determined by difference.

7) The loaded solvent is transferred to a tared

conical flask, and the CCl_4 is distilled off and condensed.

8) The conical flask containing the dried precipitated sulphur is dried, and the mass of S^o recovered is calculated.

D. 6. DETERMINATION OF DISSOLVED H_2S

Prepared solutions

a) A starch solution was prepared as described by Vogel (1961 , page 347) .

b) A 0,1 N iodine solution was prepared and standardised as described by Vogel (1961, p 354, 355) .

c) A 0,1 M Sodium arsenite solution was prepared as described by Vogel (1961)

Then 1 ml 1,0 N As_2O_3 ≡ 0,02556 g H_2S

Method

1) Place 20,0 ml standard 0,1 M sodium arsenite into a 100 ml volumetric flask.

2) Add sufficient H_2SO_4 to render solution distinctly acid.

3) Add 10,0 ml of sample and mix well.

4) Yellow precipitate of arseneous sulphide forms, but the liquid itself is colourless.

5) Make up to 100,0 ml mark with distilled water and shake thoroughly.

6) Filter mixture through dry filter paper into dry vessel.

7) Remove 50,0 ml of filtrate and neutralise with 1 M sodium bicarbonate solution.

8) Titrate with standard 0,1 M I_2 solution with a few drops starch solution to the first blue colour. Titration must be carried out between 4,0 pH 9,0 , best value being 6,5. pH must be adjusted using sodium bicarbonate.

Reactions

In water : $Na_2AsO_2 \rightarrow Na^+ + AsO_2^-$

In acid : $2AsO_2^- + 2H^+ \rightarrow As_2O_3 + H_2O$

With H_2S : $As_2O_3 + 3H_2S \rightarrow As_2S_3 + H_2O$

With I_2 : $As_2O_3 + 2I_2 + 2H_2O \rightarrow As_2O_5 + 4H^+ + 4I^-$

A P P E N D I X E

ASPECTS RELATING TO THE USE OF H_2S PARTIAL PRESSURES TO DETERMINE ZINC ION AND H_2S CONCENTRATIONS IN H_2SO_4 SOLUTION

E. 1. P_{H_2S} MONITORING OF SPHALERITE DISSOLUTION AND H_2S OXIDATION KINETICS

The overall reaction stoichiometry of sphalerite leaching in aqueous sulphuric acid is :-

$$ZnS + H_2SO_4 \rightleftharpoons ZnSO_4 + H_2S \quad \ldots\ldots\ldots\ldots \text{E. 1}$$

In the presence of a gas cap, diffusion of H_2S from the liquid to gaseous phase occurs and if diffusion is not rate limiting -

$$(H_2S)_l \rightleftharpoons (H_2S)_g \quad \ldots\ldots\ldots\ldots \text{E. 2}$$

The mole fraction of H_2S in the gas phase is related to the mole fraction of H_2S in the liquid phase by Henry's law:-

$$H_c = P_{H_2S} / x_{H_2S} \quad \ldots\ldots\ldots\ldots \text{E. 3}$$

where H_c = Henry's law constant;

P_{H_2S} = H_2S partial pressure or mole fraction of H_2S in the gas phase;

x_{H_2S} = mole fraction of H_2S in the liquid phase.

According to Perry (4th Edition) Henry's law holds well for a large number of gases under conditions such that the partial pressure of a given gas does not exceed about 100,0 kPa. The C.R.C. handbook (55th Edition) indicates that Henry's law only strictly applies to gases which do not unite chemically with the solvent.

Now for H_2S dissolved in water :—

$$x_{H_2S} = \frac{[H_2S]_l}{[H_2S]_l + [H_2O]} \qquad \text{..... E. 4}$$

where $[H_2O] = 55,56 \text{ kg - mole} / m^3$,

assuming $[H_2S]_l \ll [H_2O]$ gives -

$$x_{H_2S} = \frac{[H_2S]_l}{55,56} \qquad \text{..... E. 5}$$

Substituting equation E. 5 for x_{H_2S} in equation E. 3 gives -

$$\frac{P_{H_2S}}{[H_2S]_l} = \left(\frac{H_c}{55,56}\right) \qquad \text{..... E. 6}$$

Define a calculated distribution coefficient K_D as follows :

$$[K_D]\ \text{calc} = \frac{H_c}{55,56} \qquad \text{..... E. 7}$$

and hence also -

$$\frac{P_{H_2S}}{[H_2S]_l} = (K_D)_{calc} \quad \text{..... E. 8}$$

Equation E. 7 may be used to calculate values of K_D. Figure E.1 plots $(K_D)_{calc.}$ values (calculated using values of H_c presented by Perry) as a function of temperature for H_2S dissolved in non-acidic water. Equation E. 8 may then be used to calculate either the H_2S partial pressure (if $[H_2S]_l$ is known) or $[H_2S]_l$ (if P_{H_2S} is known) using $(K_D)_{calc}$.

Romankiw (1962) demonstrated that the solubility of H_2S was affected by the presence of H_2SO_4 in solution, and that the ratio $P_{H_2S} / [H_2S]_l$ for a given $[H_2S]_l$ value decreases with increasing H_2SO_4 concentration. The distribution coefficient may be determined experimentally by measuring the P_{H_2S} and $[H_2S]_l$, thus -

$$(K_D)_{exp} = \left(\frac{P_{H_2S}}{[H_2S]_l}\right)_{exp} \quad \text{..... E. 9}$$

In a sphalerite leaching system, in which H_2S is produced stoichiometrically along with Zn^{2+} in a reactor containing a gas cap the distribution coefficient $(K_D)_{exp}$ may be determined as follows:

According to mass balance in a system containing liquid and gaseous phases :-

$$[H_2S]_{total} = [H_2S]_l + [H_2S]_g \quad \text{..... E. 10}$$

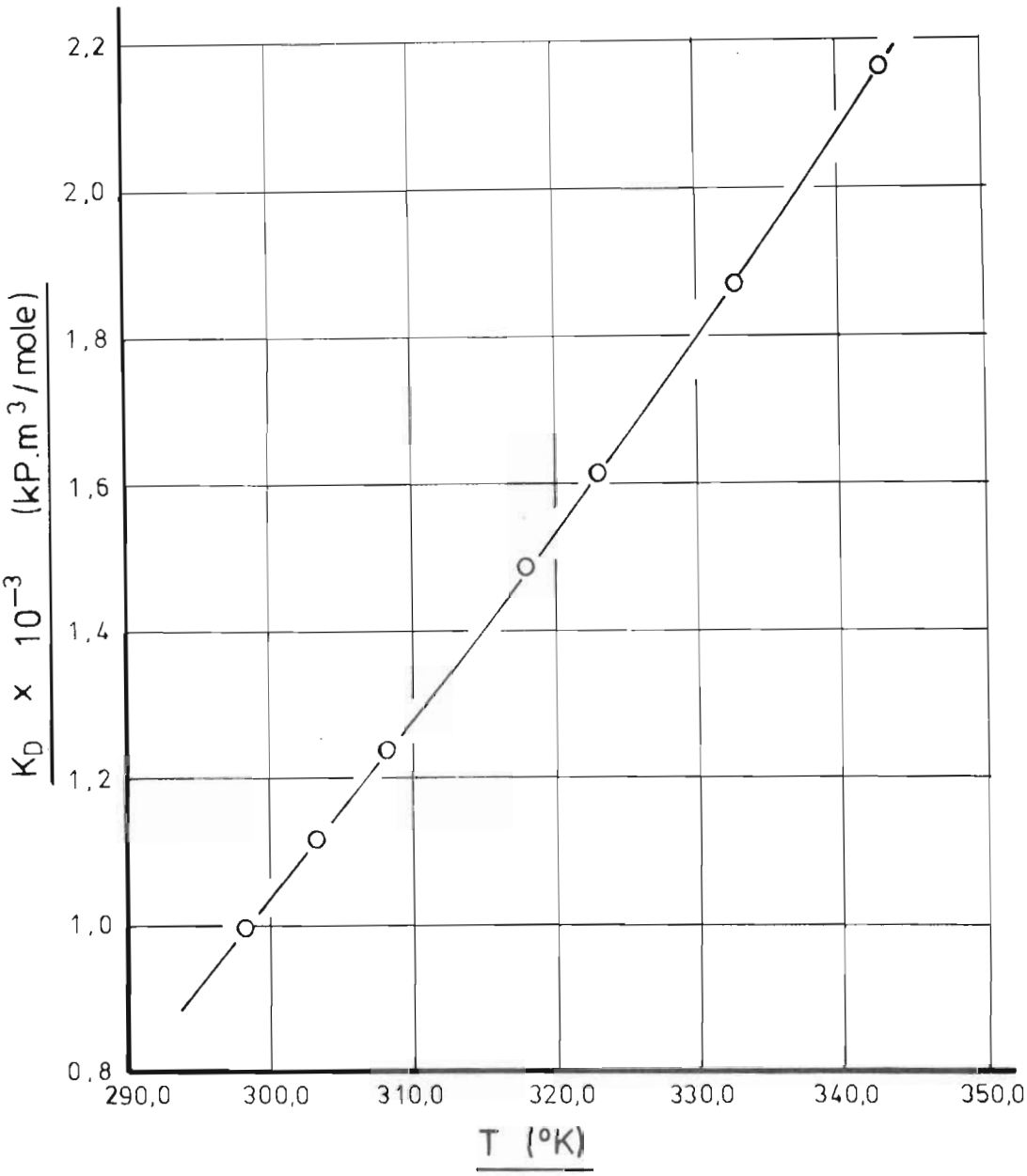

Fig.E.1 Effect of temperature T on the distribution coefficient K_D for H_2S dissolved in water.
K_D values calculated using Henry's law and tabulated Henry's constant data presented by Perry (4th edition)

Now, from the ideal gas law -

$$[H_2S]_g = \frac{P_{H_2S} \cdot V_g}{RT} \quad \text{..... E. 11}$$

and from equation E. 9 -

$$[H_2S]_l = \frac{P_{H_2S} \cdot V_l}{(K_D)_{exp}} \quad \text{..... E. 12}$$

Substituting equations E. 11 and E. 12 into E. 10 -

$$[H_2S]_{total} = \frac{P_{H_2S} \cdot V_l}{(K_D)_{exp}} + \frac{P_{H_2S} \cdot V_g}{RT} \quad \text{..... E. 13}$$

or expressed in terms of moles of H_2S per volume liquid : -

$$[H_2S]_{total} = \frac{P_{H_2S}}{(K_D)_{exp}} + \frac{P_{H_2S} \cdot V_g}{RT \cdot V_l} \quad \text{..... E. 14}$$

Rearranging equation E. 14 gives -

$$\frac{[H_2S]_{total}}{P_{H_2S}} = \frac{1}{(K_D)_{exp}} + \frac{V_g}{RT \; V_l} \quad \text{..... E. 15}$$

In a sphalerite leaching system

$$[Zn^{2+}] = [H_2S]_{total} \quad \text{..... E. 16}$$

hence

$$\frac{[Zn^{2+}]}{P_{H_2S}} = \frac{1}{(K_D)_{exp}} + \frac{V_g}{RT \; V_l} \quad \text{..... E. 17}$$

Define a distribution ratio C_D based on experimentally measured $[Zn^{2+}]$ and P_{H_2S} values,

$$(C_D)_{exp} = \frac{[Zn^{2+}]}{P_{H_2S}} \quad \ldots\ldots\ldots \text{E. 18}$$

Thus

$$(C_D)_{exp} = \frac{1}{(K_D)_{exp}} + \frac{V_g}{R\,T\,V_l} \quad \ldots\ldots \text{E. 19}$$

and rearranging equation E. 19 to express K_D in terms of C_D gives -

$$(K_D)_{exp} = 1.0 \Big/ \left((C_D)_{exp} - \frac{V_g}{R\,T\,V_l}\right) \ldots\ldots \text{E. 20}$$

The experimental distribution ratio $(C_D)_{exp}$ may therefore be determined during a leaching experiment, and the distribution coefficient $(K_D)_{exp}$ be calculated using equation E. 20. In section E. 2. an expression is developed based on experimental results which relates $(K_D)_{exp}$ to $(K_D)_{calc}$, temperature and $[H_2SO_4]$.

The expressions derived in this section are useful because during the leaching of sphalerite in aqueous H_2SO_4 solution, the H_2S partial pressure can be monitored continuously but the $[Zn^{2+}]$ need only be determined at discrete time intervals. Then having determined $(C_D)_{exp}$ from equation E. 19 and $(K_D)_{exp}$ from equation E. 20, the initial rates of Zn^{2+} or H_2S_l produced and subsequent $[Zn^{2+}]$ and $[H_2S]$ values may be calculated using measured H_2S partial pressure values in equations E. 18 and E. 9 respectively.

E. 2. RELATIONSHIPS BETWEEN EXPERIMENTAL AND THEORETICAL H_2S DISTRIBUTION COEFFICIENTS

In this section a model is developed which relates the distribution coefficient K_D of H_2S gas dissolved in aqueous H_2SO_4, to the H_2SO_4 concentration and temperature of the solution. Such a relationship is useful in that during sphalerite leaching, it is necessary only to monitor the P_{H_2S} continuously without analysing the solution for Zn^{2+} in order to follow the kinetics of the reaction. This is also true in the event of studying the homogeneous oxidation of H_2S by Fe^{3+} reaction, in systems in which the H_2S gas was bubbled into solution and the P_{H_2S} was monitored.

The distribution coefficient may be determined experimentally in a sphalerite leaching system using measured values of $(C_D)_{exp}$ (defined by equation E. 18) in equation E. 19. In Appendix I experimental H_2SO_4 leaching results are tabulated, and values of $(C_D)_{exp}$ and $(K_D)_{exp}$ are also presented in the tables.

Examination of the $(C_D)_{exp}$ values determined at discrete time intervals during the course of a leaching experiment revealed that frequently $(C_D)_{exp}$ decreased with time and tended to approach a constant value. For example figure E.2. plots $(C_D)_{exp}$ versus time for several experiments.

Any such deviations of $(C_D)_{exp}$ from constancy over the full time scale could have been caused by

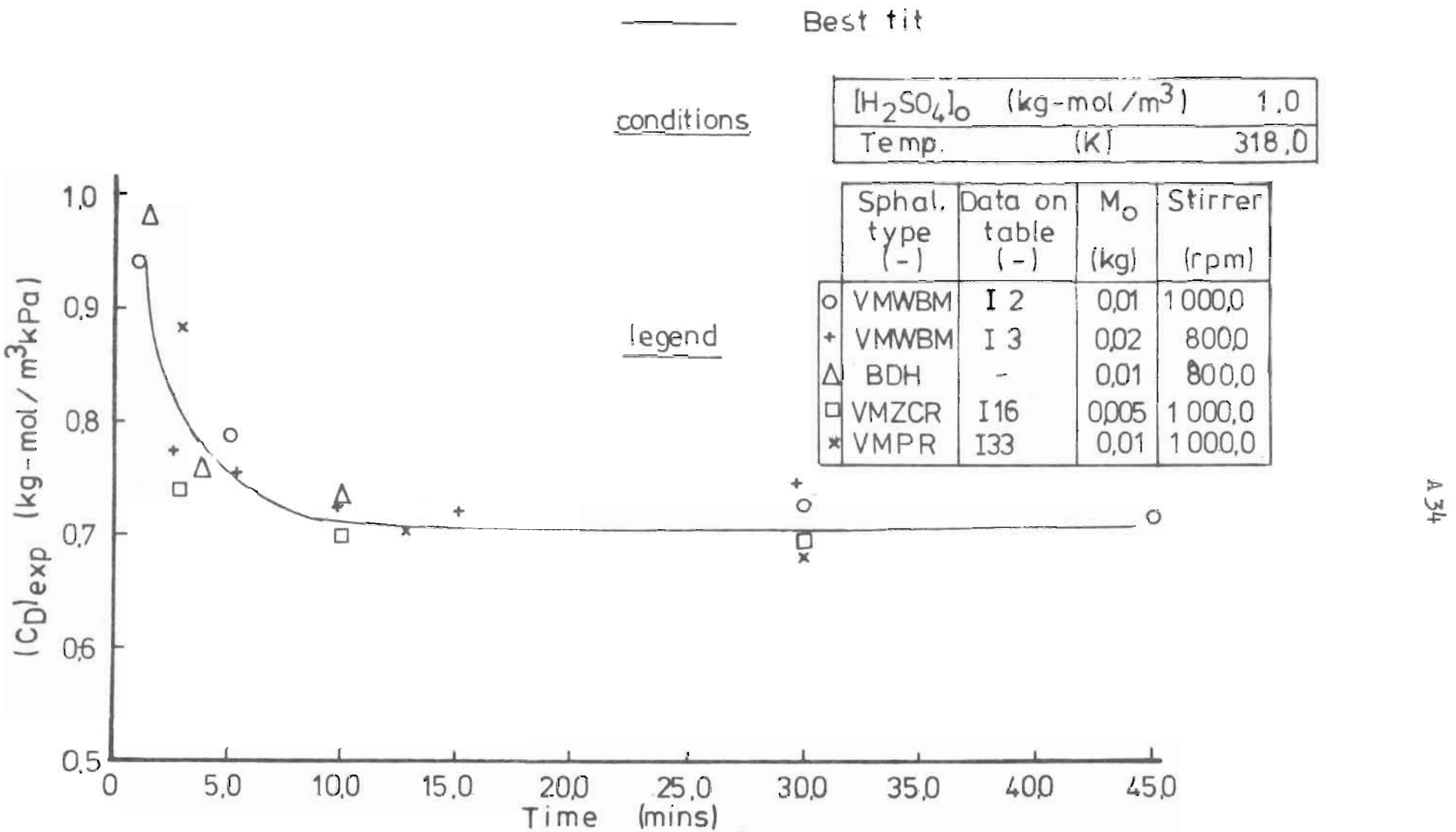

Figure E.2 Plot of $(C_D)_{exp}$ (where $(C_D)_{exp} = P_{H_2S} / [Zn^{2+}]$) versus time for various sphalerites leaching under case (i) conditions. Note that a constant value of $(C_D)_{exp}$ is approached after about time $t > 10$ mins

one or more of the following factors :

(i) For samples taken shortly after time $t = 0$; leaching continued at a significant rate during the time lag of say 20 - 30 seconds elapsing between sampling and filtering. Thus for samples taken at say $t = 1$ minute, the Zn^{2+} concentration determined analytically could be up to 50,0% greater than the true value at time of sampling. As leaching apparantly approaches equilibrium in the reactor and the leaching rate decreases one would expect this source of error to become progressively less significant.

(ii) It was often difficult to establish the true initial pressure in the reactor after introducing the sample, and then switching on the reactor, which in turn resulted in the gas cap reheating to reaction temperature simultaneously as the reaction proceeded. Thus small initial errors in P_{H_2S} would tend to affect $(C_D)_{exp}$ to greater extents shortly after $t = 0$ when the total measured P_{H_2S} was relatively large.

(iii) The stoichiometric amount of Zn^{2+} and H_2S produced may initially not have been equal.

(iv) The initial effects of Zn^{2+} or H_2S adsorption on the sphalerite particles

may have been significant.

As the reaction rate decreases and $[Zn^{2+}]$ and P_{H_2S} approach their maximum values, the effects of the above sources of deviation are minimised. Thus the final value of $(C_D)_{exp}$ determined closest to largest P_{H_2S} values for each run will be subsequently used in this thesis to calculate $(K_D)_{exp}$.

The value of V_g used in equations E 19 or E 20 was determined experimentally from the results of injecting known volumes of solution into the reactor, and measuring the corresponding change in pressure. Details of the calculations and results are presented in Appendix E. 3. . The values of V_g , V_l and R used in equation E. 19 were -

$V_g = 0{,}35 \times 10^{-3} \quad (m^3)$

$V_l = 1{,}0 \times 10^{-3} \quad (m^3)$

$R = 8{,}29 \times 10^{-3} \; (kPa \cdot m^3 / kg\text{-}mol \cdot K)$

The effects of different variables on K_D are now discussed.

E. 2. 1 EFFECT OF H_2SO_4 CONCENTRATION ON $(K_D)_{exp}$

Figure E. 3. plots $(K_D)_{exp}$ versus $[H_2SO_4]_o$ at 318,0 ° K for the different sphalerites, and demonstrates that the H_2SO_4 present in solution does significantly

——— Linear regressed fit. Line described by eqn E.2.1

conditions

Temp. (K)	318,0
Stirrer (rpm)	1000,0

legend

	Sphal. type (-)	M_o (kg)
o	VMPR	0,01
×	BDH	0,004
□	VMWBM	0,01
Δ	VMZCR	0,01

NOTE: All data point values have been extracted from the tables in Appendix I

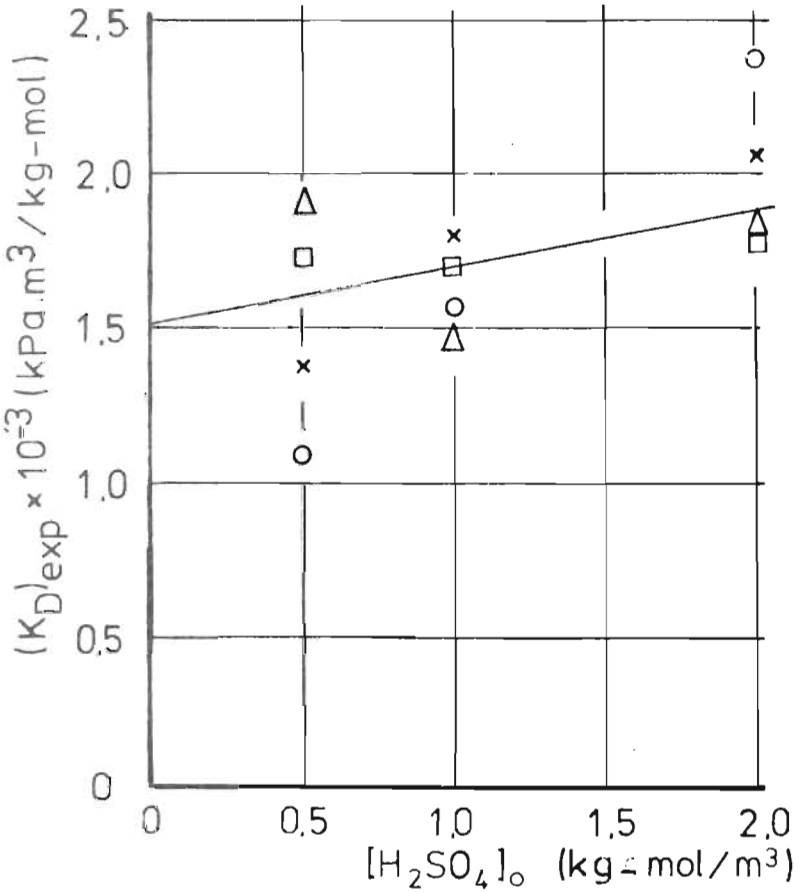

Figure E.3 Plot of experimental H_2S distribution coefficient $(K_D)_{exp}$ versus $[H_2SO_4]_o$. ($(K_D)_{exp}$ is defined by eqn. E.1.20)

influence the distribution of H_2S between the liquid and gas phases. The data points are rather widely scattered on figures E. 3. and a least squares linear regression on the data was performed with the following results:

$$(K_D)_{fit} = 1,52 \times 10^3 + 170,0 \times [H_2SO_4] \quad \ldots\ldots\ldots \text{E. 21}$$

Now $K_D = 1,484_{\times 10^3}$ (as calculated from data at 318,0 ° K), and equation E.2.1. may be expressed as

$$(K_D)_{exp} = K_D + 170,0 \times [H_2SO_4] \quad \ldots\ldots\ldots \text{E. 22}$$

This equation is consistent in that as $[H_2SO_4]$ tends to zero, $[K_D]$ tends to the theoretical value of K_D. The wide scatter in the $[K_D]_{exp}$ data is possibly the result of the various factors enumerated in the last section.

E. 2. 2 EFFECT OF TEMPERATURE ON $(K_D)_{exp}$

Figure E. 4. shows an Arrhenius type plot of $(K_D)_{exp}$ versus $\frac{1}{T}$. The data points were linear regressed with the following result:

$$\ln (K_D)_{fit} = 12,47 - 1,62 \times 10^3 \left(\frac{1}{T}\right) \quad \ldots\ldots\ldots \text{E. 23}$$

The familiar exponential form of this equation corresponds to:-

$$(K_D)_{fit} = 2,604 \times 10^5 \quad \exp\left(\frac{-13,41}{RT}\right) \quad \ldots\ldots \text{E. 24}$$

a Linear regression through exptl. points. Line a is described by eqn. E.2.3.

b Linear regession line demonstrating the effect of temp. on $(K_D)_{calc.}$. $(K_D)_{calc.}$ is the distribution coefficient for H_2S in water, calculated using Henry's law with data presented in Perry (1963).

conditions

$[H_2SO_4]_o$	(kg-mol/m^3)	1,0
Stirrer	(rpm)	800,0

legend

	Sphal type (-)	M_o (kg)
o	VMPR	0,02
×	BDH	0,01
□	VMWBM	0,02
Δ	VMZCR	0,02

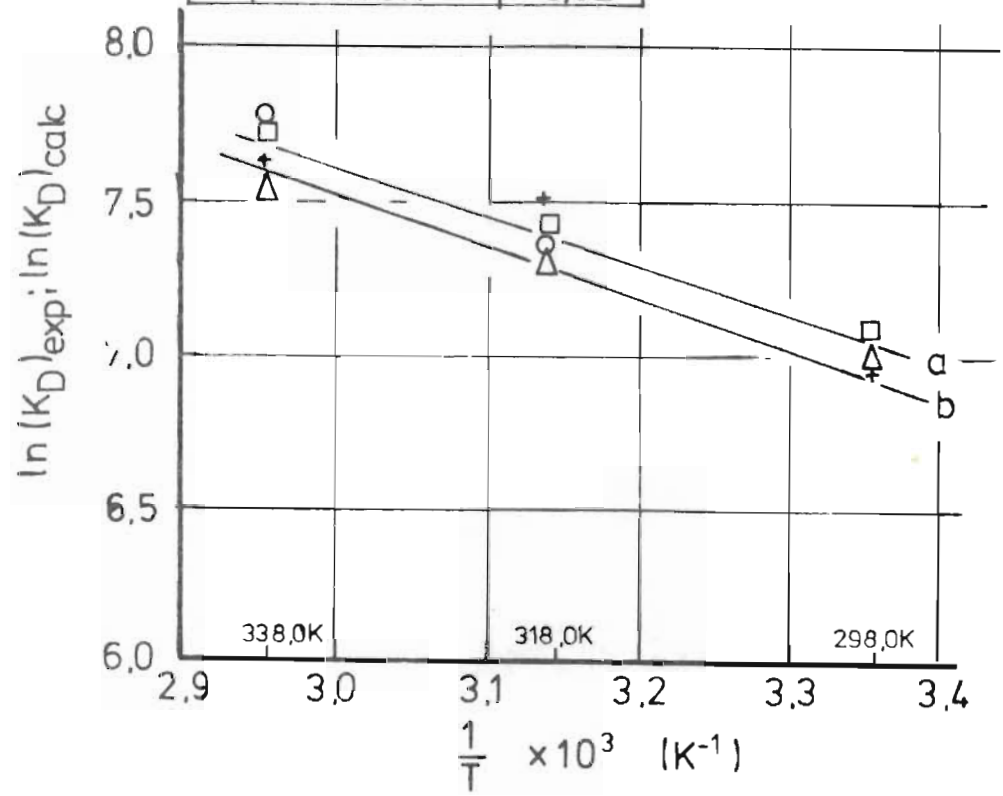

Figure E.4 Arrhenius-type plot demonstrating the effect of temperature on the H_2S distribution coefficient K_D.

The fitted values of $(K_D)_{exp}$ as a function of temperature are plotted on figure E. 4. along with the values of K_D calculated using Henry's constant. The experimental $(K_D)_{exp}$ corresponds to values obtained in 1 M H_2SO_4 solution, and consequently according to equation E. 22 one would expect the $(K_D)_{exp}$ values to be greater than the theoretical K_D values by a factor of about 0,17. This is in fact so.

E. 2. 4. OVERALL MODEL EXPRESSING $(K_D)_{exp}$ IN TERMS OF $[H_2SO_4]$ AND TEMPERATURE

As observed in equation E. 24 , the activation energy term relating the change in K_D with temperature is 13,41 mJ/kg-mol (i.e. 3,208 k cal / mole). The theoretical value for K_D at 318,0 ° K in neutral water is -

$$K_D = 1{,}484 \times 10^3$$

Therefore, at 318,0 ° K the pre-exponential constant $(K_D)_o$ will be -

$$(K_D)_o = 1{,}484 \times 10^3 / \exp\left(\frac{-13{,}41}{RT}\right) \quad \text{..... E. 25}$$

$$(K_D)_o = 2{,}379 \times 10^5$$

Hence $$K_D = 2{,}379 \times 10^5 \exp\left(-\frac{13{,}41}{RT}\right) \quad \text{..... E. 26}$$

Substituting for K_D at 318,0 ° K in equation E. 22 gives an expression which includes the effect of

H_2SO_4. Thus the final equation which may be used to calculate $(K_D)_{calc}$ as a function of temperature and $[H_2SO_4]$:-

$$(K_D)_{calc} = 2{,}379 \times 10^5 \times \exp\left(\frac{-13.41}{RT}\right) + 170{,}0 \times [H_2SO_4] \quad \ldots\ldots\ldots \text{E. 27}$$

E. 3. DETERMINATION OF REACTOR GAS CAP VOLUME

The gas cap volume with the pressure transducer and sensing tube was established by injecting a given volume of liquid into the reactor, and measuring the increase in pressure. A sample calculation is now given:

From ideal gas law -

$$P_1 V_{g1} = P_2 V_{g2} \quad \ldots\ldots\ldots \text{E. 28}$$

where P_1 = initial pressure in reactor (generally atmospheric),

V_{g1} = initial total gas volume in reactor,

P_2 = reactor pressure after injecting liquid,

V_{g2} = gas phase volume after injecting liquid.

But $V_{g2} = V_{g1} - \Delta V_\ell \quad \ldots\ldots\ldots$ E. 29

and $P_2 = P_1 + \Delta P \quad \ldots\ldots\ldots$ E. 30

where ΔV_ℓ = volume of aliquot liquid injected into reactor,

ΔP = measured increase in reactor pressure.

Hence substituting equation E. 29 into equation E. 28 -

$$P_1 V_{g1} = P_2 (V_{g1} - \Delta V_\ell) \quad \ldots\ldots\ldots \text{E. 31}$$

Rearranging equation E. 31 gives -

$$V_{g1} = \Delta V_\ell \times \left(\frac{P_2}{P_2 - P_1}\right) \quad \ldots\ldots\ldots \text{E. 32}$$

Table E. 1. summarised the results of injecting 5,0 or 10,0 ml water into the reactor containing $1{,}0 \times 10^{-3}$ m^3 solution.

It is observed that the average reactor gas cap volume was established to be $0{,}348 \times 10^{-3}$ m^3. Hence in this thesis a volume of $0{,}35 \times 10^{-3}$ m^3 has been used throughout. No attempt was made to correct the gas cap volume for the effect of density changes on the liquid volume at different temperatures.

Exptl Run (-)	P_1 (k Pa)	V_ℓ x 10^3 (m^3)	ΔP (kPa)	P_2 (k Pa)	V_{g1} x 10^3 (m^3)	Data Table (-)
197	99,67*	0,1	2,785	102,5	0,368	I 25
197	99,67*	0,1	2,689	102,4	0,381	I 25
183	100,0*	0,05	1,536	101,53	0,33	L 9
169	100,0⊖	0,05	1,421	101,421	0,357	I 26
178	100,0⊖	0,05	1,566	101,566	0,324	L 3
178	100,0⊖	0,05	1,489	101,489	0,341	L 3
180	100,0⊖	0,05	1,460	101,460	0,347	L 1
211	100,0⊖	0,05	1,489	101,489	0,341	L 15
211	100,0⊖	0,05	1,489	101,489	0,341	L 15

Average : $0,348 \times 10^{-3}$ m^3

* Measured barometric pressure

⊖ Assumed pressure

T A B L E E. 1. SUMMARY OF RESULTS FOR THE DETERMINATION OF REACTOR GAS CAP VOLUME V_{g1}

A P P E N D I X F

SURFACE AREAS OF UNLEACHED PARTICLES AND AREA CHANGES DURING LEACHING

F. 1. SPECIFIC SURFACE AREAS OF UNLEACHED SPHALERITE PARTICLES

NOTE: All A_o versus $\overline{D}$ and area change versus X data used in this section are contained within the tables presented in Appendix J. Johne (1965) describes the Ströhlein Areameter used to measure the specific surface areas reported in this thesis and the theory associated with single point B.E.T. area determinations. In actual practice, sphalerite samples weighing upto 100,0g could be used in the instrument to ensure that the total area measured fell within the recommended range ($7,0 m^2$ to $50,0 m^2$), and specific surface areas greater than $0,1 m^2/g$ could readily be determined with a significant degree of reproducibility.

Figures F. 1. and F. 2. compare the specific surface areas A_o of acid washed and acid unwashed WBM, PR and ZCR sphalerites, and the A_o values for solid spheres calculated as a function of diameter by the expression:-

$$A_o = \frac{6,0}{\overline{D}\,\rho} \; m^2/kg \qquad \ldots\ldots\ldots \text{F. 1.}$$

The density of each of the sphalerites was measured and each was found to be very close to:-

$$\rho = 4,0 \times 10^6 \; kg/m^3$$

Hence $$A_o = \frac{1,5 \times 10^{-6}}{\overline{D}} \; m^2/kg \qquad \ldots\ldots \text{F. 2.}$$

It was established that the very large decrease in A_o observed as a result of acid washing the ZCR sphalerite, was due to the removal of a gaugue, probably $MgCO_3$.

legend

	Sphal. type	Acid Washed
□	PR	No
×	PR	Yes
+	ZCR	No
o	ZCR	Yes

a A_o versus $\bar{D}$ calculated for solid spheres using equation F.2

b Best fit curves through data points.

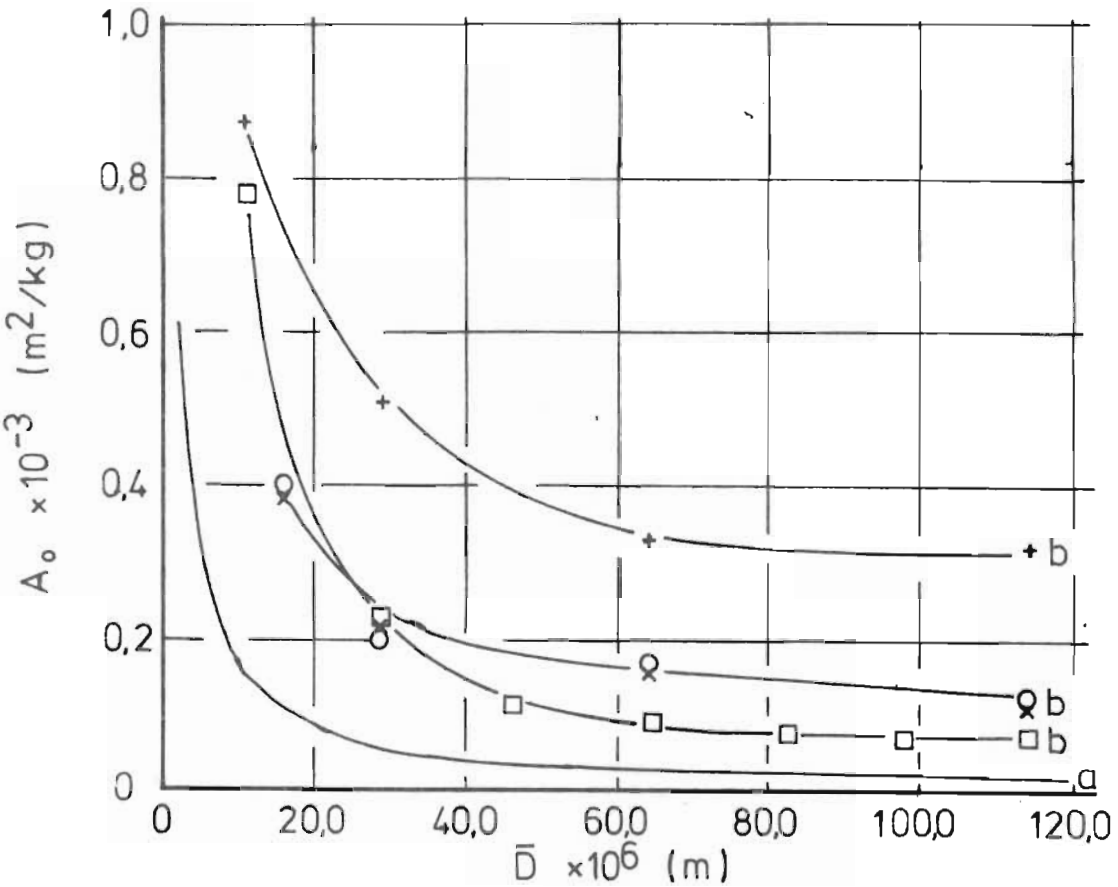

Figure F.1 Comparison of specific surface areas of PR and ZCR sphalerites before and after acid pre-treatment, with A_o values calculated for solid spheres.

legend	Sphal. type	Acid washed
×	WBM	No
o	WBM	Yes

——— a A_o versus $\bar{D}$ for solid spheres calc. using eqn. F.2

b Best fit curves through data points.

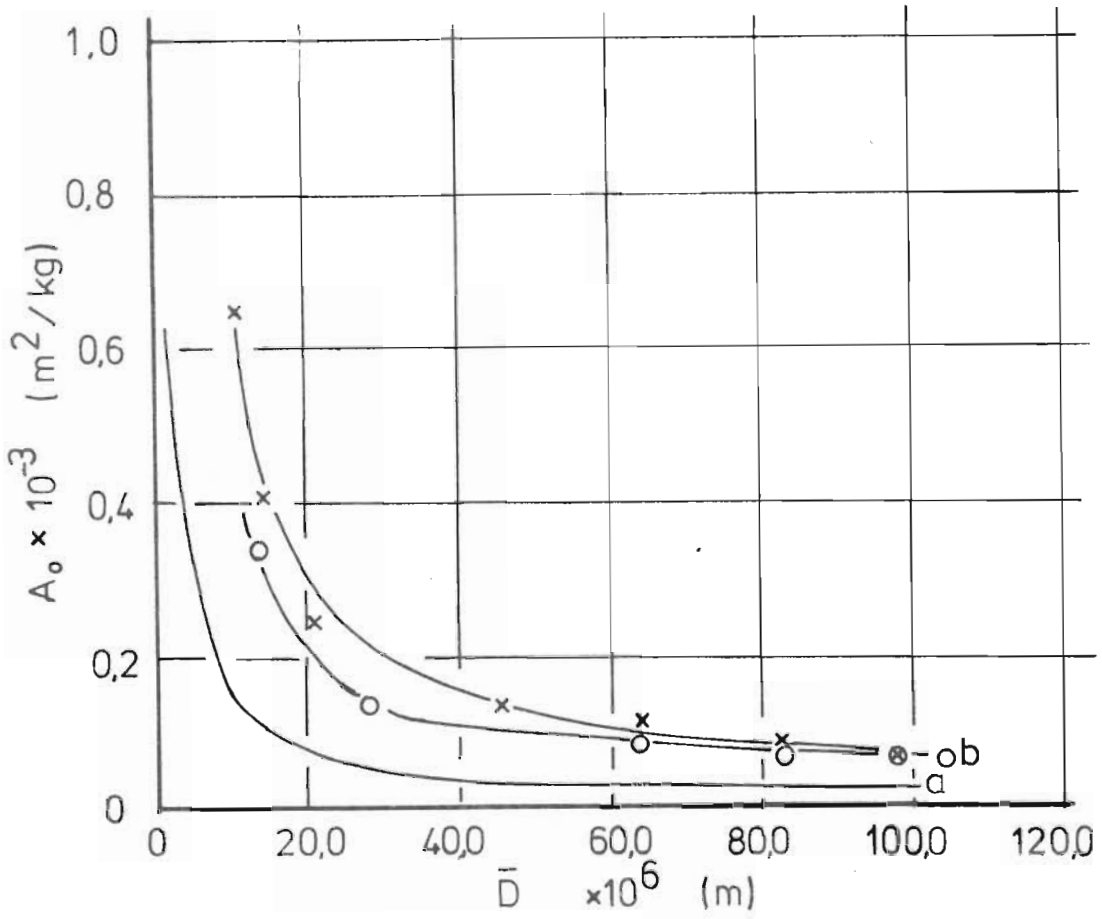

Figure F.2 Comparison of the specific surface area of WBM sphalerite before and after acid pretreatment, with A_o calculated for solid spheres using eqn. F.2.

(Relatively high concentrations of Mg^{2+} were identified in the wash solution, and unwashed ZCR particles placed in the concentrated HCl produced odourless gas bubbles which were assumed to be CO_2 gas.)

It is not obvious why acid washing changed the A_o for the PR and WBM in the way it did.

Figure F. 3 plots the ratio of the measured specific surface area $A_o : A_{sph.}$ calculated for spheres, as a function of the mean particle diameter. Linear plots are observed which are fitted by the following empirical expression which may be used to calculate the A_o for any $\overline{D}$ over the range $125{,}0 \leq \overline{D} \leq 9{,}0$ μm.

$$A_o = A_{sph.} \times (2{,}6 + B \times \overline{D}) \ m^2/g \quad \ldots\ldots\ \text{F. 3.}$$

where $B = 6{,}73 \times 10^4$ for the PR and ZCR sphalerites,

and $B = 2{,}0 \times 10^4$ for the WBM sphalerite.

Table F. 1. summarises the specific surface areas of the BDH and the vibratory milled sphalerites.

It is proposed that the surface areas of the sphalerites are significantly higher than that for smooth spheres of the same diameter because of the greater surface roughness, and the existance of internal or pore area.

The value of the intercept on the vertical axis of Figure F. 3., can be taken as an indication of the internal area (m^2/kg) which is independent of $\overline{D}$.

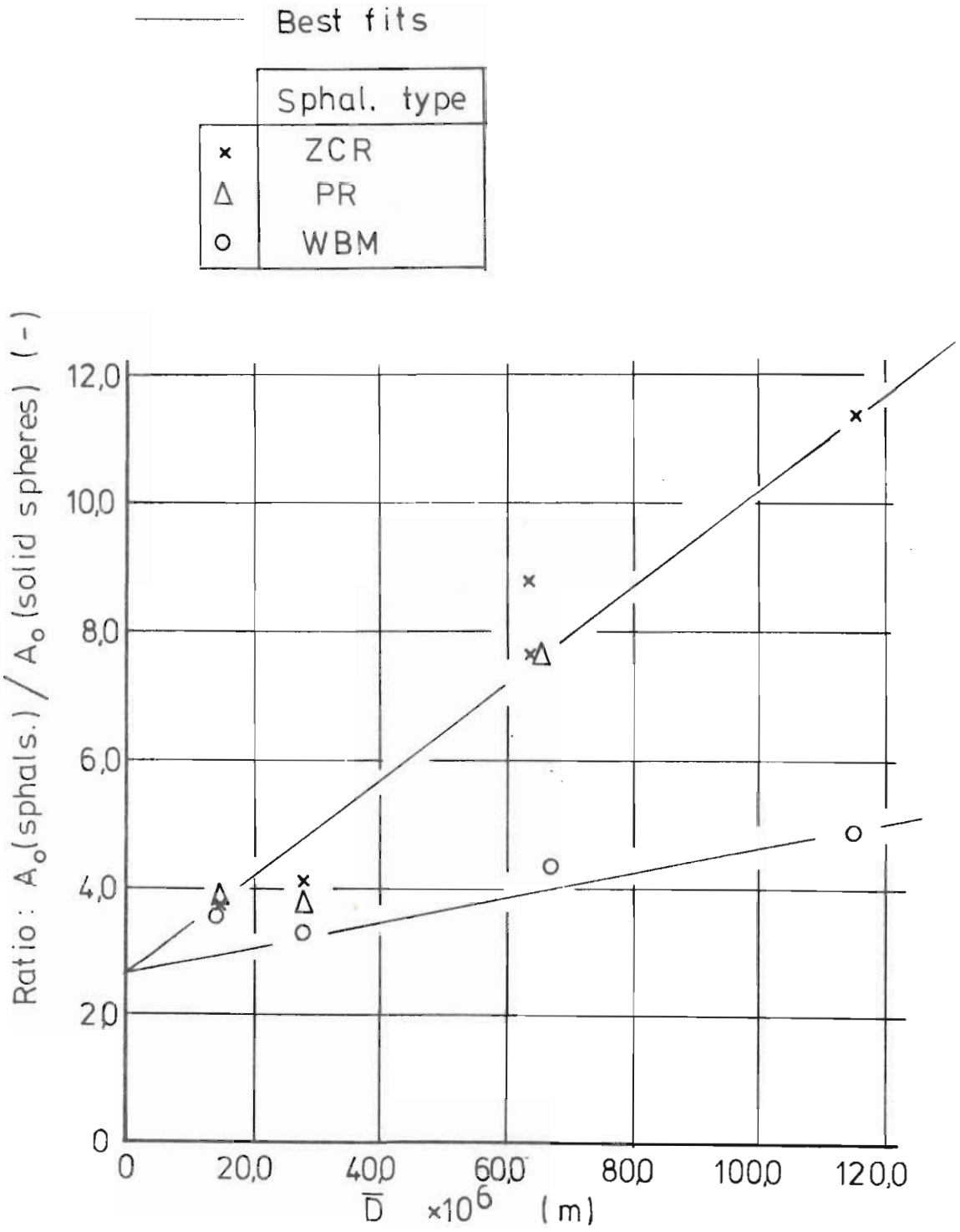

Figure F.3 Comparison of the ratios A_o (for a sphal.) to A_o (calc. for solid spheres) for the ZCR, PR and WBM sphals.

The slopes of the lines on Figure F. 3. represent the area due to roughness for a given sphalerite. (Zero slope would mean the particles were perfectly smooth.)

Therefore, if the intercept and the slope were both zero, a given substance should have a measurable surface area identical to that of smooth, solid spheres.

Figures 6. 14 to 6. 18 represent various photomicrographs taken of polished sections of WBM, ZCR and PR sphalerite particles and reveal the presence of cavities and cracks within the particles which account for the internal area.

Figures 6.1, 6.2, 6.4 & 6. 9 represent S.E.M. photographs of unleached WBM, PR and ZCR particles, and reveal the existance of surface roughness which would account for additional surface area.

F. 2. AREA CHANGES DURING LEACHING

The area remainder function $\eta(X)$ was experimentally determined for each of the different sphalerites by leaching in acidic ferric sulphate to various extents of reaction, and measuring the specific surface area A of the CCl_4 cleaned sphalerite particles using a B.E.T. N_2 adsorption technique.

The experimental value of the area of the solids

remaining in a reactor may be defined as -

$$\eta(X) = \frac{M A}{M_o A_o} \qquad \ldots\ldots\ldots \text{F. 4.}$$

or

$$\eta(X) = (1 - X)\ \frac{A}{A_o} \qquad \ldots\ldots\ldots \text{F. 5.}$$

Knowing the final $[Zn^{2+}]$ concentration, it was possible to calculate M by mass balance, and several checks showed that the calculated values agreed closely with the weighed values.

Figure F. 4. plots the experimental values of η versus X for the BDH, WBM and the VMWBM, VMPR and VMZCR sphalerites.

Curve 'a' on Figure F. 4. is the result of predicting η from an area remainder function describing the area change of shrinking solid spheres (i.e. corresponding to the shrinking core model).

$$\eta(X) = (1 - X)^{0,666} \qquad \ldots\ldots\ldots \text{F. 6.}$$

It is observed that the BDH and WBM sphalerites closely obey shrinking core behaviour. The vibratory milled sphalerites each exhibited an initial rapid decrease in area probably due to the initial rapid dissolution of the finest particles (which contributed disproportionately heavily to the total area).

The following empirical area remainder function

a Curve calculated according to the shrinking core model, (equation F. 6)

b Curve calculated using equation F.7 (with the value of 'a' = 0,25)

legend

	Sphalerite type
×	BDH
o	WBM (-75,0+63,0 µm size fraction)
□	VMWBM
Δ	VMPR
+	VMZCR

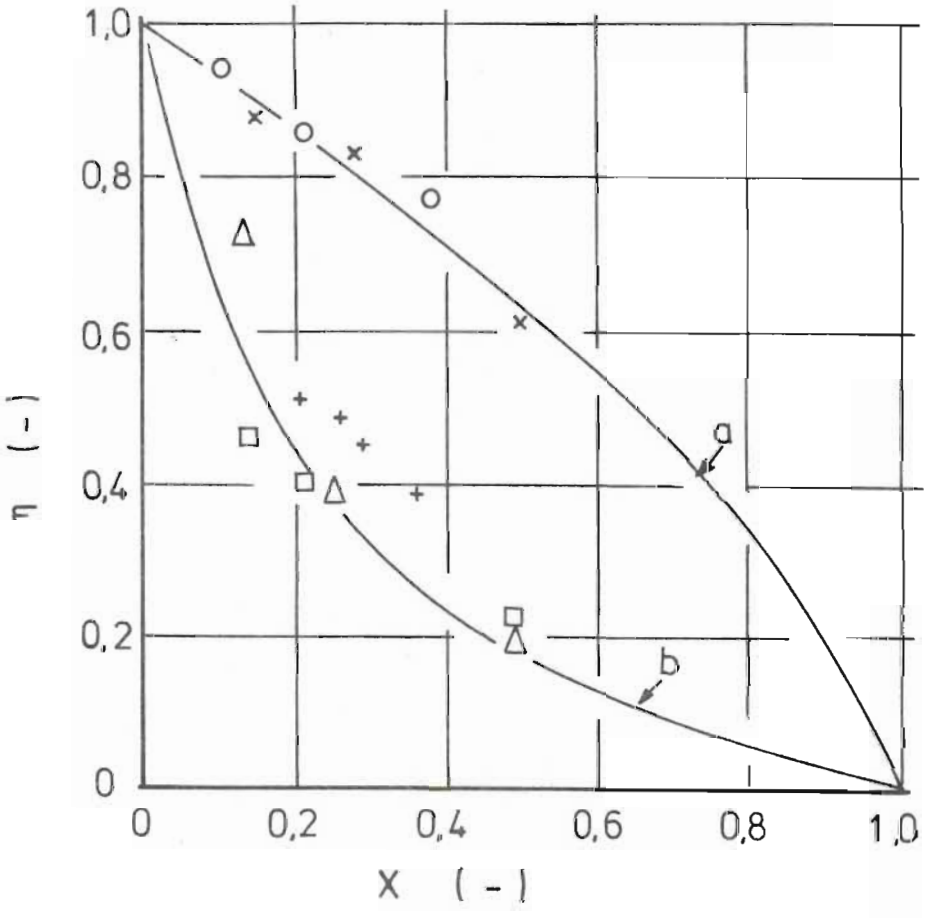

Figure F.4 Comparison between exptl. and calculated fractional area remainder η versus extent leached X results.

was found to fit this data well -

$$\eta(X) = \left(1 - \frac{a + 1}{\left(\frac{a}{X} + 1\right)}\right) \qquad \ldots\ldots\ldots \text{ F. 7.}$$

Equation F. 7. is shown plotted on Figure F. 4, and with $a = 0{,}25$ a reasonable fit is observed.

Figures F. 5. and F. 6. plot $\eta(X)$ versus X for the PR and ZCR sphalerites respectively. In both cases $\eta(X)$ rises to a maximum, the value of which is a function of $\overline{D}$, and then decreases.

This behaviour was the result of A in equation F. 4. increasing faster than M was decreasing, to a point beyond which the opposite occured.

Figures 6.3, 6.5, 6.8, 6.11 & 6.13 present S.E.M. photographs of leached PR, ZCR and WBM particles and show clearly that leaching took place faster along specific zones, resulting in pitting and consequent increases in surface area. It is not clear why the WBM then exhibits shrinking core behaviour.

Figures 6.17 and 6.18 show photomicrographs of the results of etching polished PR and ZCR particles. Visual observation through an optical microscope showed that etching took place preferentially along grain boundaries and other stressed zones.

A model which fitted the PR and ZCR area change curves on Figures F. 5. and F. 6. was developed as follows :-

a Curve calculated according to the shrinking core model (eqn. F.6)

b,c,d and e Curves calculated using eqn F.11 with $\frac{dA'}{dX}$ values shown in the legend.

legend

Points (—)	Curves (—)	Size fraction $\times 10^6$ (m)	$\frac{dA'}{dX} \times 10^{-3}$ used in eqn F.11
×	b	-17,5 +12,5	2,6
o	c	-75,0 +63,0	3,0
□	d	-90,0 +75,0	3,60
Δ	e	-106,0 +90,0	3,44

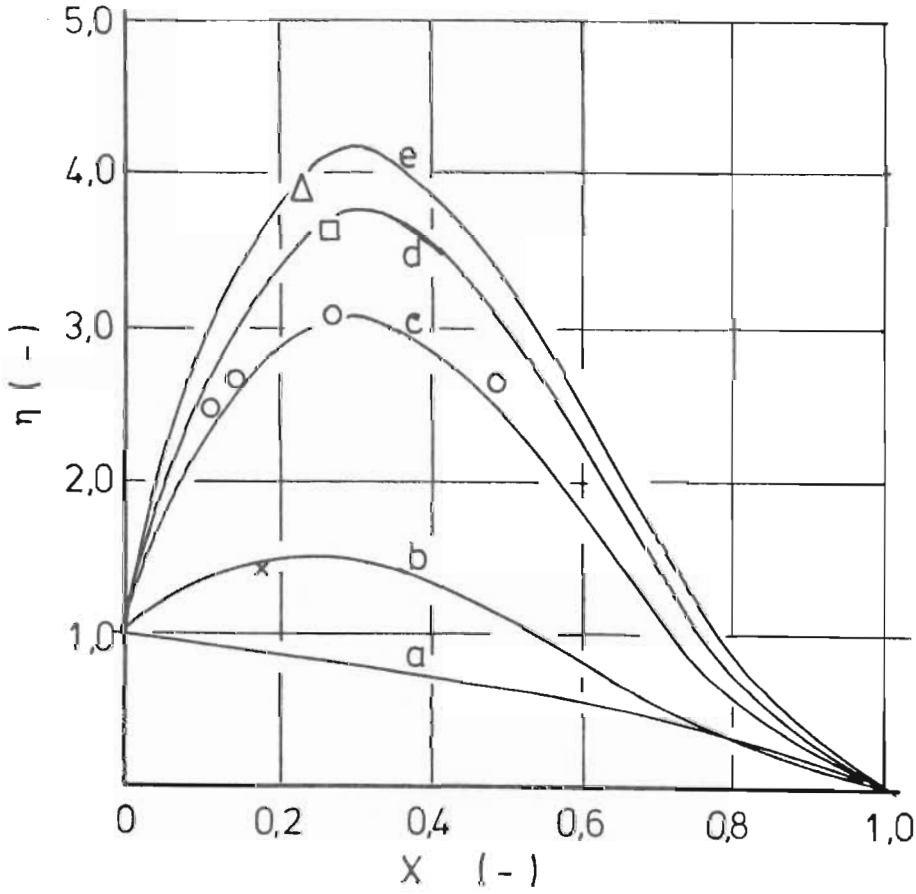

Figure F.5 Fractional area remainder η versus the extent of reaction X for Pr sphalerite. $\frac{dA'}{dX}$ and A_o values used in equation F.11 to calculate curves b,c,d and e were obtained off figs F.1; F.7 and F.8.

a Curve calculated according to the shrinking core model (eqn F.6)

b,c,d and e Curves calculated using eqn F.11 with $\frac{dA'}{dX}$ values shown in the legend.

legend

Points (–)	Curves (–)	Size fraction $\times 10^6$ (m)	$\frac{dA'}{dX} \times 10^{-3}$ used in eqn F.11
+	b	-17,5 +12,5	1,497
□	c	-75,0 +63,0	0,748
o	d	-90,0 +75,0	0,918
×	e	-106,0 +90,0	1,06

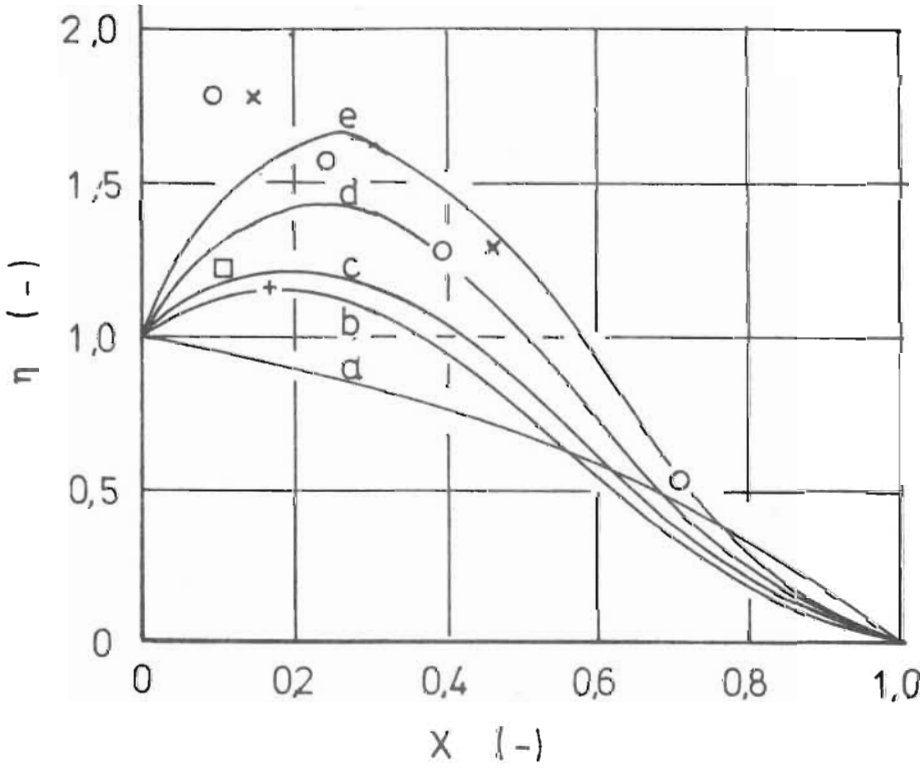

Figure F.6 Fractional area remainder η versus extent leached X for ZCR sphalerite. $\frac{dA'}{dX}$ and A_o values used in eqn F.11 to calculate curves b,c,d and e were obtained off figs F.1; F.7 and F.8.

An area coefficient A' was defined -

$$A' = \frac{A}{(1 - X)} \qquad \ldots\ldots\ldots \text{F. 8.}$$

Figure F. 7 shows examples of plotting A' versus X for the PR and ZCR sphalerites and straight lines are observed. The slopes $\frac{dA'}{dX}$ for each $\overline{D}$ were measured and plotted against $\overline{D}$ on Figure F. 8 .

In the case of the A' versus X line for ZCR sphalerite on Figure F. 7 , sphalerite had been used which had not been acid washed, and some gaugue may have still been present in the residues leached to low X, thus contributing excessive area.

From Figure F. 7 it is apparant that the straight lines may be fitted by a linear model -

$$A' = A_o + \left(\frac{dA'}{dX}\right) X \qquad \ldots\ldots\ldots \text{F. 9.}$$

Equating A' in equation F. 9 with A' in equation F. 8, produces -

$$A = \left(A_o + \left(\frac{dA'}{dX}\right) X \right) (1 - X) \qquad \ldots\ldots \text{F. 10.}$$

and equating A in equation F. 10. with A in equation F. 5 produced the area remainder function -

$$\eta(X) = \left(1{,}0 + \frac{dA'}{dX} \frac{X}{A_o}\right) (1 - X)^2 \qquad \ldots\ldots\ldots \text{F. 11.}$$

Equation F. 11. is shown plotted on Figures F. 5. and F. 6. using the experimental values of $\frac{dA'}{dX}$ shown on Figure F. 8 . The shape of the experimental $\eta(X)$ vs X data is observed to be fitted well by this function.

——— Best fit lines.

legend

	Sphal type (-)	Size fraction $\times 10^6$ (m)
×	PR	-75,0 +63,0
o	ZCR	-90,0 +75,0

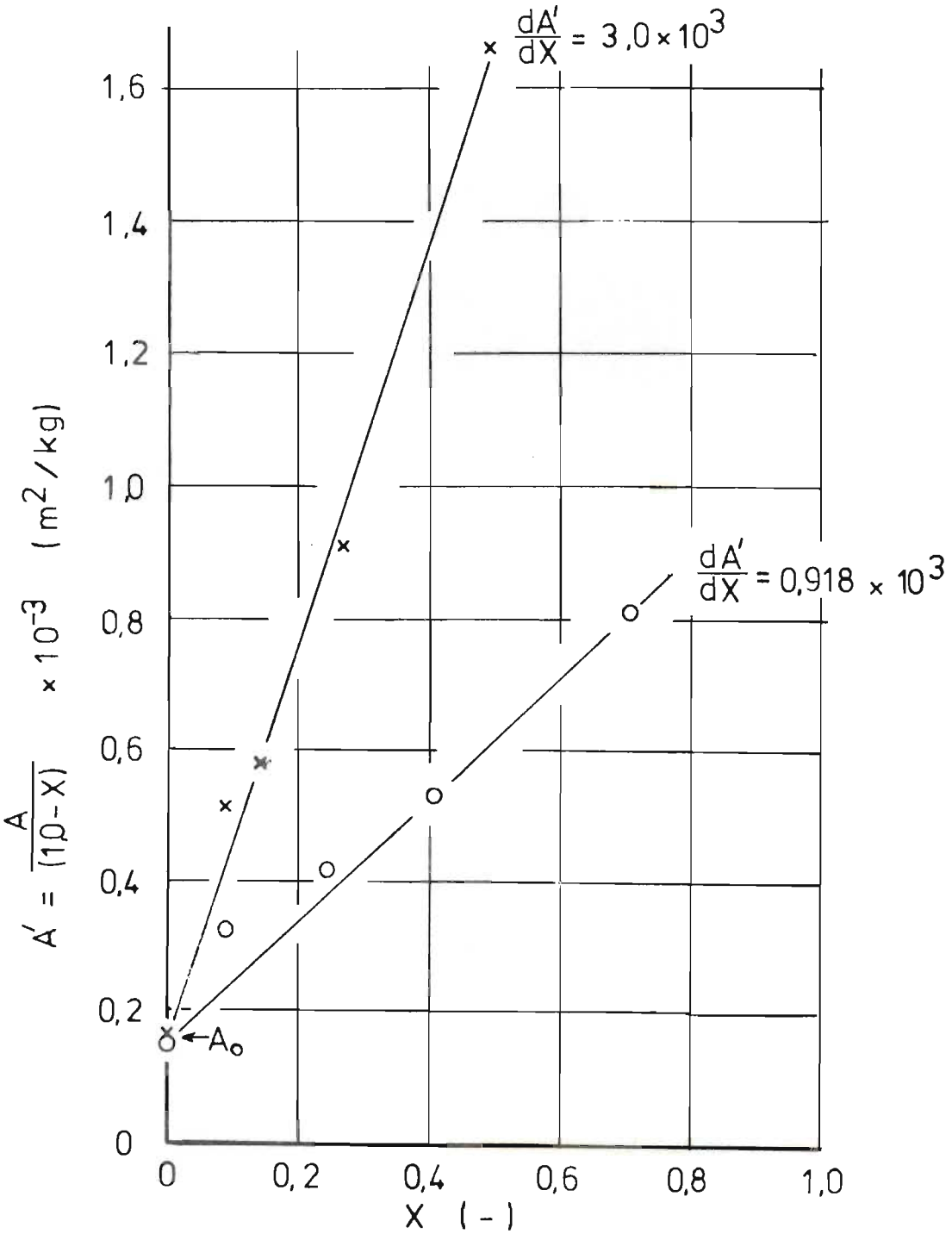

Figure F.7 Examples of plotting A' versus X for PR and ZCR sphalerites, and of measuring $\frac{dA'}{dX}$ from the slopes of the best fit lines

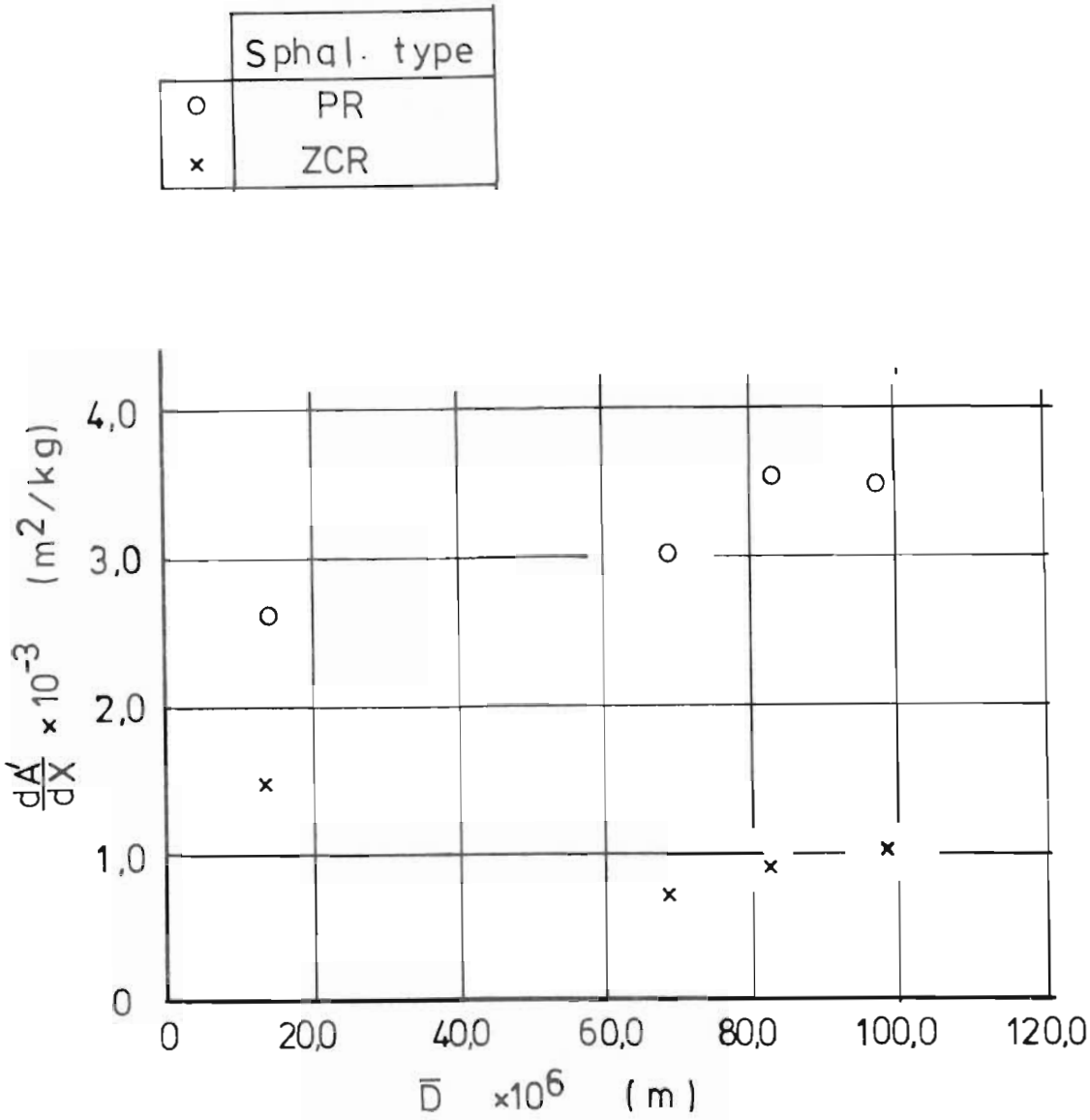

Figure F.8 $\frac{dA'}{dX}$ versus $\bar{D}$ for PR and ZCR sphalerites. The $\frac{dA'}{dX}$ values plotted here were measured off A' versus X plots as shown in the examples on figure F.7.

APPENDIX G

DATA PROCESSING PROCEDURES

G. 1 PROCESSING OF CASE (i) DATA

When sphalerite was leached in aqueous H_2SO_4 (with $[Fe^{3+}]_o = 0$), the change in H_2S partial pressure (P_{H_2S}) with time was monitored. The initial rate $\left(\frac{d P_{H_2S}}{d t}\right)_o$ was often difficult to measure directly from the P_{H_2S} versus time trace.

The following empirical equation was found to fit the shape of the P_{H_2S} versus time rate curves :-

$$P_{H_2S} = \frac{a t}{b + t} \qquad \ldots\ldots\ldots \text{ G. 1}$$

where $$\left(\frac{d P_{H_2S}}{d t}\right)_o = \frac{a}{b} \qquad \ldots\ldots\ldots \text{ G. 2}$$

and as $t \rightarrow \infty$ and equilibrium is approached

$$(P_{H_2S})_{eq} = a \qquad \ldots\ldots\ldots \text{ G. 3}$$

Values were fitted to the constants a and b of equation G. 1 by the following regression technique.

Initial guesses were assigned to the two constants a and b and equation G. 1 was integrated numerically using the computer programme DIFSUB by Gear (1971). The P_{H_2S} values at discrete time intervals were established by

unequal interval interpolation, and the sum of squares of the differences between these interpolated P_{H_2S} and the experimental P_{H_2S} values was established. A "hill-climber" optimisation routine NELM by Nelder and Mead (1965) was linked to the DIFSUB routine, and the values of the constants were changed until a convergence criterion for the sum of squares had been satisfied. As an example table G. 1 summarises experimental and calculated P_{H_2S} values at discrete time intervals for three experiments using VMWBM sphalerite leaching at three different temperatures. Very good fits are observed.

Initial rates in terms of the zinc ion concentration were determined in two ways as follows :-

$$(r_o)_{exp} = \left(\frac{d\,P_{H_2S}}{d\,t}\right)_{o,exp} \cdot (C_D)_{exp} \quad \ldots\ldots\ldots \text{G. 4}$$

and $$(r_o)_{fit} = \left(\frac{d\,P_{H_2S}}{d\,t}\right)_{o,fit} \cdot (C_D)_{calc} \quad \ldots\ldots\ldots \text{G. 5}$$

where $\left(\frac{d\,P_{H_2S}}{d\,t}\right)_{o,exp}$ = measured experimental initial rate of P_{H_2S} increase;

$\left(\frac{d\,P_{H_2S}}{d\,t}\right)_{o,fit} = \frac{a}{b}$ (as defined by equation G. 2) $\ldots\ldots\ldots$ G. 6

$(C_D)_{exp}$ = $P_{H_2S}/[Zn^{2+}]$ (with the P_{H_2S} and $[Zn^{2+}]$ being experimental values measured when the rate of increase in P_{H_2S} is low).

$(C_D)_{calc} = \left(\frac{1}{K_D}\right)_{calc} + \frac{V_g}{RT}$ ..... G. 7

(with $(K_D)_{calc}$ defined by equation E. 27).

Data on table	I 3		I 4		I 5	
Temperature (K)	318,0		298,0		338,0	
Fitted value of a	26,4		16,7		38,6	
Fitted value of b	1,07		2,39		0,41	
$(\frac{d\,P_{H_2S}}{d\,t})_{o,calc} = \frac{a}{b}$ (kPa)	24,6		6,98		95,1	
Time (mins)	$(P_{H_2S})_{exp}$ (kPa)	$(P_{H_2S})_{calc}$ (kPa)	Time (mins)	$(P_{H_2S})_{exp}$ (kPa)	$(P_{H_2S})_{calc}$ (kPa)	Time (mins)	$(P_{H_2S})_{exp}$ (kPa)	$(P_{H_2S})_{calc}$ (kPa)
0,62	9,44	9,67	1,0	4,72	4,92	0,8	24,99	25,61
0,98	12,59	12,60	1,42	6,29	6,22	1,5	31,23	30,38
1,49	15,73	15,35	2,1	7,87	7,81	2,4	34,36	33,02
2,0	17,31	17,18	3,0	9,44	9,29	5,0	36,54	35,70
2,75	19,12	18,99	4,6	11,01	10,99	10,0	37,17	37,00
			5,0	11,41	11,30			

TABLE G.1 COMPARISON OF EXPERIMENTAL P_{H_2S} RATE DATA WITH P_{H_2S} RATA DATA CALCULATED BY NUMERICALLY INTEGRATING EQUATION G.1 (i.e. $P_{H_2S} = \frac{a\,t}{b+t}$) WHICH WAS FITTED TO THE EXPERIMENTAL DATA

In the case of the BDH sphalerite, equation G. 1 did not fit the shape of the leaching rate curves very well, and on alternative initial rate was defined as follows :-

$$r_{o\ exp\ fit} = \left(\frac{d\,P_{H_2S}}{d\,t}\right)_{o,exp} \cdot (C_D)_{fit} \quad \ldots\ldots\ldots \quad G.\ 8$$

The measured and fitted values of $\left(\frac{d\,P_{H_2S}}{d\,t}\right)_o$, $(C_D)_{exp}$ and $(K_D)_{calc}$ are tabulated along with the case (i) experimental results in Appendix I.

G. 2 PROCESSING OF CASE (ii) EXPERIMENTAL DATA

When sphalerite was leached under case (ii) conditions ($[Fe^{3+}]_o : [H_2SO_4]_o \geq 1,8$), solution samples were taken, filtered and analysed for zinc by A. A. adsorption.

The initial rate of dissolution was determined by simply measuring the initial slope of the best fit curve drawn through the $[Zn^{2+}]$ versus time data points plotted on linear graph paper. Since most of the case (ii) experiments were conducted using relatively course size fractions of WBM, ZCR or PR sphalerite, the rates of dissolution were sufficiently slow to justify this direct method of initial rate measurement.

Particularly in the case of the ZCR sphalerite, zinc initially dissolved very rapidly from what was probably Zn O present in the sphalerite. The Zn S itself dissolved far slower. The result was that the initial rate of dissolution of the sphalerite frequently did not pass through the origin at $[Zn^{2+}] = 0,0$. The concentration of the initial Zn^{2+} thus formed was

designated $[Zn^{2+}]_o$. All the measured initial rate and $[Zn^{2+}]_o$ results are tabulated for the case (ii) data in Appendix J.

G. 3 PROCESSING OF H_2S OXIDATION DATA

When H_2S was purged into the reactor, the P_{H_2S} and H_2S concentration were measured to give the distribution coefficient K_D directly, i.e. -

$$(K_D)_{exp} = P_{H_2S} \Big/ [H_2S]_\ell$$

Upon injecting Fe^{3+}, oxidation of the H_2S took place and the P_{H_2S} decreased with time. The initial rate of oxidation was determined by measuring the initial slope of the P_{H_2S} versus time trace on the chart recorder output. The initial rate of reaction in terms of the H_2S concentration was then calculated as follows :-

$$(r_o)_{exp} = \left(\frac{d P_{H_2S}}{d t}\right)_{o,exp} \Big/ (K_D)_{exp}$$

In many experiments the H_2S was generated in-situ by the dissolving sphalerite and the Fe^{3+} was injected only when the rate of increase in P_{H_2S} due to dissolution was very low compared to the rate of decrease in P_{H_2S} due to oxidation of the H_2S by the Fe^{3+}.

In this case, the initial rate of decrease in P_{H_2S} was measured as described above, but the initial rate in terms of the H_2S concentration was calculated as follows :-

$$(r_o)_{calc} = \left(\frac{d P_{H_2S}}{d t}\right)_{o,exp} \Big/ (K_D)_{calc}$$

where $(K_D)_{calc}$ was calculated using equation E. 27.

The $\left(\frac{d P_{H_2S}}{d t}\right)_{o,exp}$, $(P_{H_2S})_o$, $(K_D)_{calc}$ and (where measured) the $[H_2S]_o$ values used are presented with the oxidation rate data results in the tables in Appendix K.

G. 4 PROCESSING OF CASE (iii) EXPERIMENTAL DATA

When sphalerite was leached under case (iii) conditions ($[Fe^{3+}]_o : [H_2SO_4]_o \leq 0,1$), the zinc ion concentration and the H_2S partial pressure was measured with time. This data has been dealt with qualitatively in this thesis. Hence in chapter 5 the experimental $[Zn^{2+}]$ versus time and P_{H_2S} versus time rate curves are plotted and discussed qualitatively.

A P P E N D I X H

PRESENTATION OF SELECTED CASE (i) ($[Fe^{3+}]_o$ = 0,0) RAW DATA IN GRAPHICAL FORM

All the case (i) leaching data presented in tabular form in Appendix I was interpreted in chapter 3 in terms of models derived from proposed mechanisms.

In this section, selected case (i) data is presented graphically in order to demonstrate specific aspects of the work.

H. 1 EFFECT OF AGITATION RATE ON THE RATE OF SPHALERITE DISSOLUTION

Figures H. 1a to H. 1c plot the measured H_2S partial pressure versus time rate curves at different stirrer speeds for the VMWBM, VMPR and BDH sphalerites. Although experimentally a continuous P_{H_2S} versus time curve was obtained using a chart recorder, the P_{H_2S} values at discrete time intervals were noted in order to present the results in tabular form in Appendix I. These discrete P_{H_2S} versus time data are plotted on figures H. 1 a to H. 1 c, as the continuous curves tend to superimpose on one another (making plotting and comparison difficult).

(facing Figure H.1)

legend		Data on table	Stirrer (rpm)	M_o (kg)	$[H_2SO_4]_o$ (kg-mol/m3)	Temp. (K)
Fig H.1a	×	I 3	800,0	0,02	1,0	318,0
	o	I 6	1150,0	0,02	1,0	318,0
	Δ	I 2	1 000,0	0,01	1,0	318,0
	+	I 7	1 500,0	0,01	1,0	318,0
Fig H.1b	o	I 28	1 000,0	0,02	1,0	318,0
	×	I 31	1 500,0	0,02	1,0	318,0
Fig H.1c	o	I 45	400,0	0,004	1,04	298,0
	×	I 47	700,0	0,004	1,04	298,0
	+	I 48	1 000,0	0,004	1,04	298,0

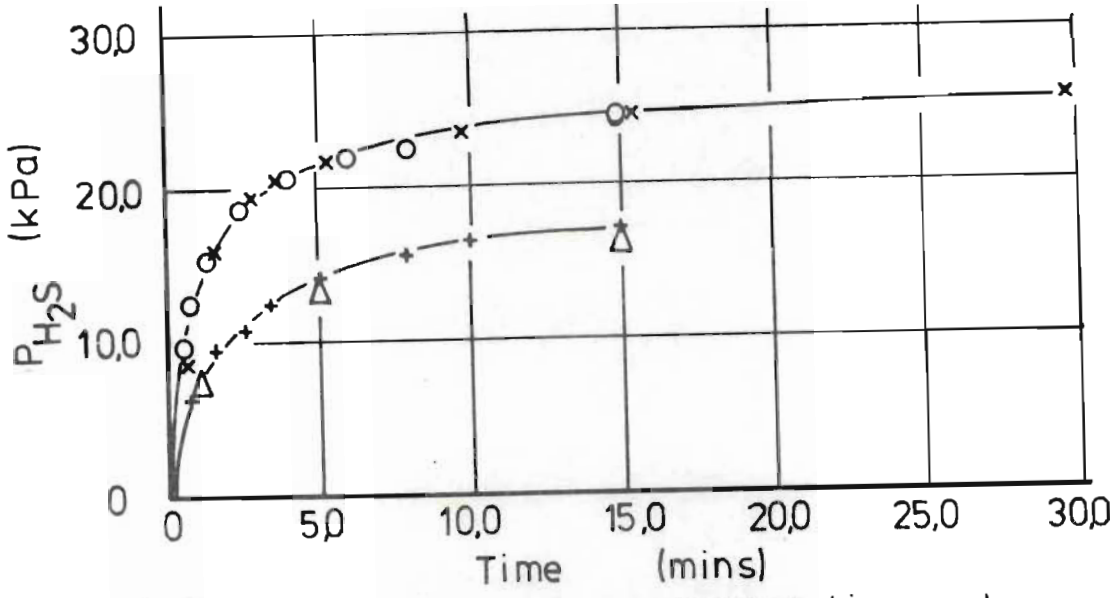

Figure H.1a Comparison of P_{H_2S} versus time rate curves at different stirrer speeds for VMWBM sphalerite.

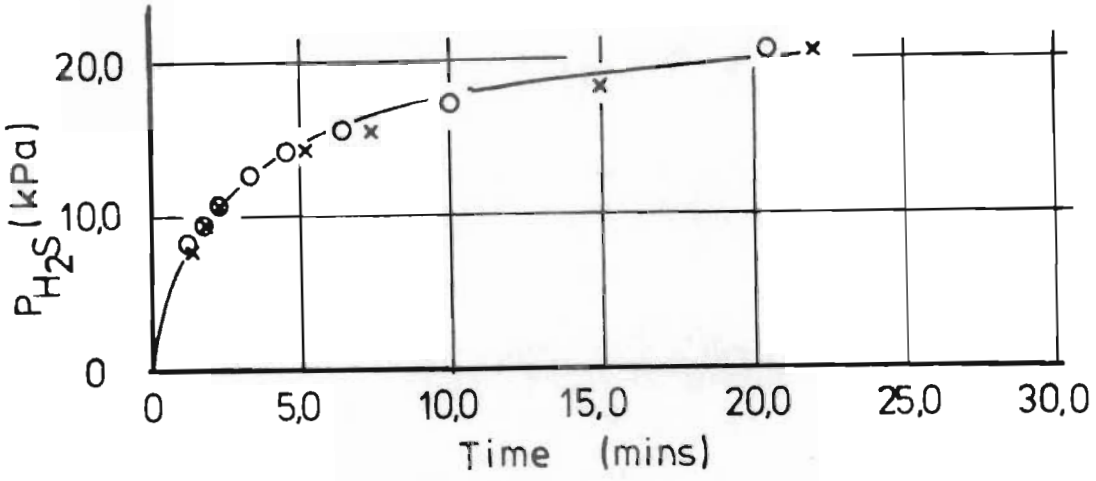

Figure H.1b Comparison of P_{H_2S} versus time rate curves at different stirrer speeds for VMPR sphalerite.

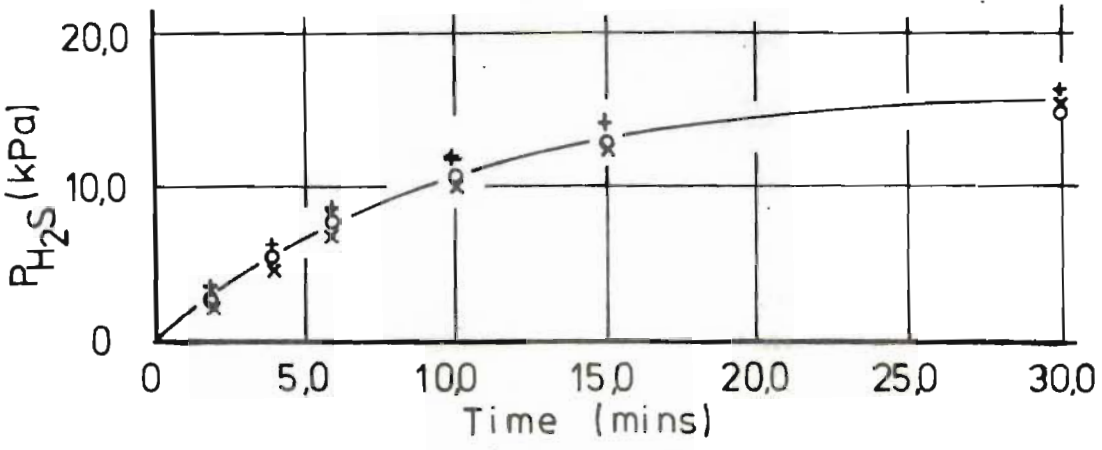

Figure H.1c Comparison of P_{H_2S} versus time rate curves at different stirrer speeds for BDH sphalerite.

No significant effect of agitation on the dissolution rate is observed, which suggests that film diffusional phenomena do not constitute the rate limiting step. This observation confirms the results discussed in section 3.2.6 (in which dissolution rate curves for experiments conducted at different temperatures were processed), which showed that the apparant activation energy of the rate limiting step for the various sphalerites were far greater than one would expect had a diffusion phenomena been rate limiting.

H. 2 EFFECT OF INITIAL SPHALERITE MASS M_o ON THE DISSOLUTION RATE

Figures H.2a and H.2b plot the P_{H_2S} versus time rate curves for different initial masses of VMWBM and BDH sphalerites. Similar plots for the VMZCR and VMPR sphalerites may be constructed from the data in Appendix I.

From figure H.2a it would appear as though the P_{H_2S} approaches significantly differently equilibrium values. However, in chapter 4 it was demonstrated that the concentration of the active sphalerite sites $\phi(X)$ decreases very rapidly as described by equation 4.9 (where $\psi_4(X) = \frac{\phi(X)}{\phi_o}$).

Thus when 0,02 kg sphalerite is present (curve a on figure H.2a), more active sphalerite is available to permit the P_{H_2S} value to approach the thermodynamic equilibrium faster, than if only 0,01 or 0,005 kg sphalerite is present. It is proposed that if leaching were permitted to proceed

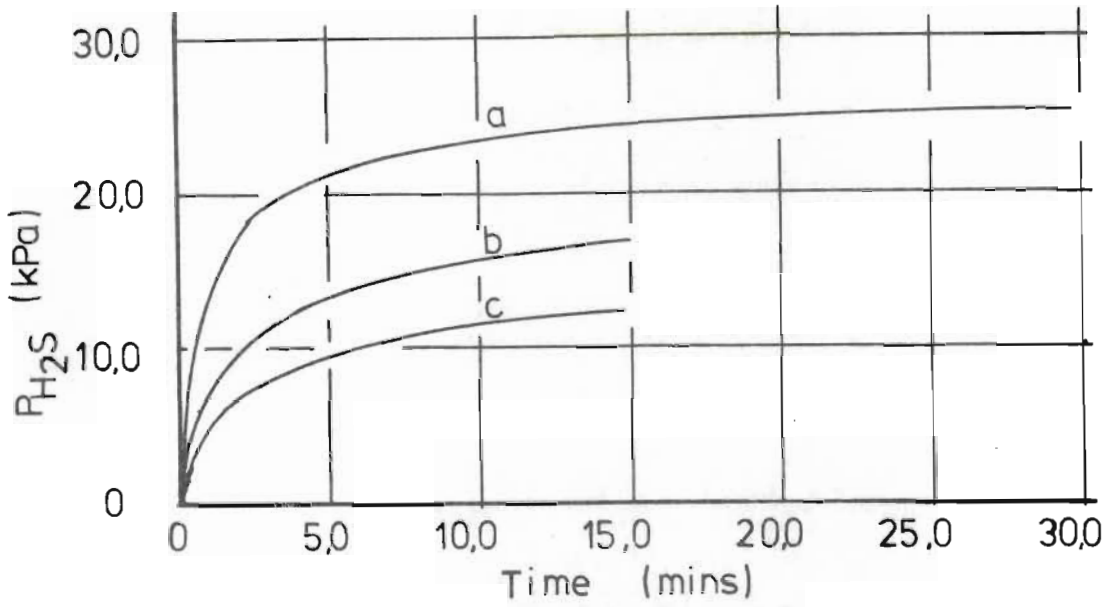

Figure H.2a Plot demonstrating the effect of M_o on the P_{H_2S} versus time rate curves for VMWBM sphalerite.

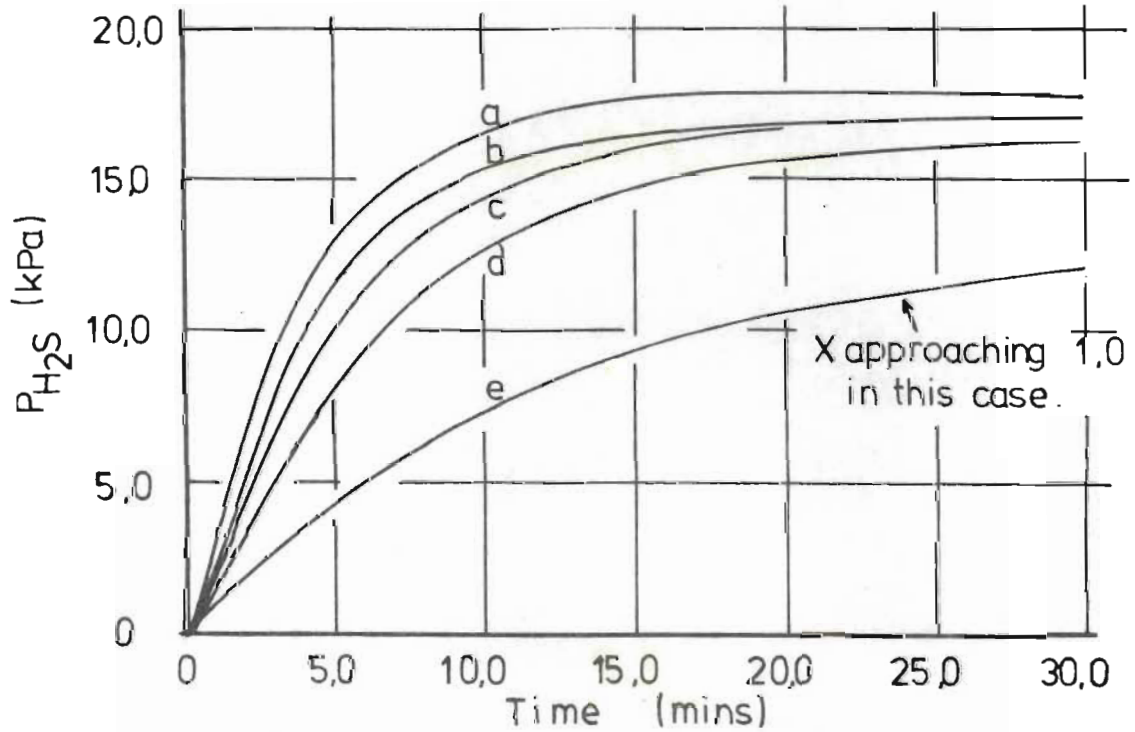

Figure H.2b Plot demonstrating the effect of M_o on the P_{H_2S} versus time rate curves for BDH sphalerite.

long enough, the three P_{H_2S} versus time curves would coincide.

In the case of the BDH sphalerite (figure H. 2 b) it was shown in chapter 4 that the active site concentration $\phi(X)$ decreases according to the shrinking core model (equation 4. 2). Equation 4. 2 describes a much slower decrease in $\phi(X)$ with X than does equation 4. 9 (for the VMWBM sphalerite). Thus the effect of M_o on the rate of approach of the P_{H_2S} to thermodynamic equilibria values for the BDH sphalerite is less than is the case for the VMWBM sphalerite.

A P P E N D I X I

TABULATED EXPERIMENTAL RESULTS

FOR LEACHING UNDER CASE (i) CONDITIONS

($[Fe^{3+}]_o$: $[H_2SO_4]_o$ = 0,0)

The procedure adopted for processing case (**i**) experimental leaching results is described in section G. **1**.

TABLE I 1

EXPERIMENTAL RUN NO. = 114
SPHALERITE LEACHING IN AQUEOUS H2SO4

SPHAL. TYPE LEACHED		= VMWBM
TEMPERATURE	(K)	= 318.00
INITIAL MASS	(KG)	= 0.0050
STIRRER SPEED	(RPM)	= 1000.0
INITIAL H2SO4	(KG-MOL/M3)	= 1.0000
SPEC.SURFACE AREA	(M2/KG)	= 3272.0
CDEXP	(KG-MOL/M3 KPA)	= .7248E-03
KDEXP	(KPA M3/KG-MOL)	= .1689E 04
KDCALC	(KPA M3/KG-MOL)	= .1654E 04

TIME (MINS)	PH2S (KPA)	ZN2+ (KG-MOL/M3)	ZN2+/PH2S (KG-MOL/M3 KPA)
0.50	3.12	N.D.	N.D.
1.00	4.69	N.D.	N.D.
1.62	6.25	N.D.	N.D.
2.49	7.81	N.D.	N.D.
4.10	9.37	N.D.	N.D.
7.20	10.93	N.D.	N.D.
14.80	12.03	.872E-02	.725E-03

MEASURED (DP/DT)0	(KPA/MIN)	=	7.68
FITTED (DP/DT)0	(KPA/MIN)	=	7.77
MEASURED (P)EQ	(KPA)	=	12.03
FITTED (P)EQ	(KPA)	=	13.40

TABLE I 2

EXPERIMENTAL RUN NO. = 176
SPHALERITE LEACHING IN AQUEOUS H2SO4

SPHAL. TYPE LEACHED		= VMWBM
TEMPERATURE	(K)	= 318.00
INITIAL MASS	(KG)	= 0.0100
STIRRER SPEED	(RPM)	= 1000.0
INITIAL H2SO4	(KG-MOL/M3)	= 1.0000
SPEC.SURFACE AREA	(M2/KG)	= 3272.0
CDEXP	(KG-MOL/M3 KPA)	= .7196E-03
KDEXP	(KPA M3/KG-MOL)	= .1704E 04
KDCALC	(KPA M3/KG-MOL)	= .1654E 04

TIME (MINS)	PH2S (KPA)	ZN2+ (KG-MOL/M3)	ZN2+/PH2S (KG-MOL/M3 KPA)
1.00	7.11	.670E-02	.943E-03
5.00	13.44	.106E-01	.790E-03
15.00	16.33	.119E-01	.728E-03
30.00	17.86	.129E-01	.720E-03
45.00	18.48	N.D.	N.D.

MEASURED (DP/DT)0	(KPA/MIN)	=	10.37
FITTED (DP/DT)0	(KPA/MIN)	=	11.30
MEASURED (P)EQ	(KPA)	=	18.48
FITTED (P)EQ	(KPA)	=	18.50

TABLE I 3

EXPERIMENTAL RUN NO. = 100
SPHALERITE LEACHING IN AQUEOUS H2SO4

SPHAL. TYPE LEACHED		= VMWBM
TEMPERATURE	(K)	= 318.00
INITIAL MASS	(KG)	= 0.0200
STIRRER SPEED	(RPM)	= 800.0
INITIAL H2SO4	(KG-MOL/M3)	= 1.0000
SPEC.SURFACE AREA	(M2/KG)	= 3272.0
CDEXP	(KG-MOL/M3 KPA)	= .7200E-03
KDEXP	(KPA M3/KG-MOL)	= .1703E 04
KDCALC	(KPA M3/KG-MOL)	= .1654E 04

TIME (MINS)	PH2S (KPA)	ZN2+ (KG-MOL/M3)	ZN2+/PH2S (KG-MOL/M3 KPA)
0.62	9.44	N.D.	N.D.
0.98	12.59	N.D.	N.D.
1.49	15.73	N.D.	N.D.
2.00	17.31	N.D.	N.D.
2.75	19.12	.148E-01	.776E-03
3.80	20.45	N.D.	N.D.
5.40	21.87	.165E-01	.755E-03
9.75	23.78	.173E-01	.727E-03
15.20	24.86	.180E-01	.723E-03
29.80	25.35	.190E-01	.748E-03

MEASURED (DP/DT)0	(KPA/MIN)	=	19.01
FITTED (DP/DT)0	(KPA/MIN)	=	24.60
MEASURED (P)EQ	(KPA)	=	25.35
FITTED (P)EQ	(KPA)	=	26.40

TABLE I 4

EXPERIMENTAL RUN NO. = 109
SPHALERITE LEACHING IN AQUEOUS H2SO4

SPHAL. TYPE LEACHED		= VMWBM
TEMPERATURE	(K)	= 298.00
INITIAL MASS	(KG)	= 0.0200
STIRRER SPEED	(RPM)	= 800.0
INITIAL H2SO4	(KG-MOL/M3)	= 1.0000
SPEC.SURFACE AREA	(M2/KG)	= 3272.0
CDEXP	(KG-MOL/M3 KPA)	= .9651E-03
KDEXP	(KPA M3/KG-MOL)	= .1214E 04
KDCALC	(KPA M3/KG-MOL)	= .1225E 04

TIME (MINS)	PH2S (KPA)	ZN2+ (KG-MOL/M3)	ZN2+/PH2S (KG-MOL/M3 KPA)
1.00	4.72	.768E-02	.163E-02
1.42	6.29	N.D.	N.D.
2.10	7.87	N.D.	N.D.
3.00	9.44	N.D.	N.D.
4.60	11.01	N.D.	N.D.
5.00	11.41	.110E-01	.965E-03
7.80	12.57	N.D.	N.D.
10.00	13.53	N.D.	N.D.
20.00	14.88	N.D.	N.D.
38.00	15.86	N.D.	N.D.

MEASURED (DP/DT)0	(KPA/MIN)	=	5.03
FITTED (DP/DT)0	(KPA/MIN)	=	6.98
MEASURED (P)EQ	(KPA)	=	16.36
FITTED (P)EQ	(KPA)	=	16.70

TABLE I 5

EXPERIMENTAL RUN NO. = 108
SPHALERITE LEACHING IN AQUEOUS H2SO4

SPHAL. TYPE LEACHED		= VMWBM
TEMPERATURE	(K)	= 338.00
INITIAL MASS	(KG)	= 0.0200
STIRRER SPEED	(RPM)	= 800.0
INITIAL H2SO4	(KG-MOL/M3)	= 1.0000
SPEC.SURFACE AREA	(M2/KG)	= 3272.0
CDEXP	(KG-MOL/M3 KPA)	= .5700E-03
KDEXP	(KPA M3/KG-MOL)	= .2247E 04
KDCALC	(KPA M3/KG-MOL)	= .2174E 04

TIME (MINS)	PH2S (KPA)	ZN2+ (KG-MOL/M3)	ZN2+/PH2S (KG-MOL/M3 KPA)
0.80	24.99	N.D.	N.D.
1.50	31.23	N.D.	N.D.
2.40	34.36	N.D.	N.D.
5.00	36.54	.194E-01	.532E-03
10.00	37.17	N.D.	N.D.
15.00	37.42	N.D.	N.D.
22.00	37.48	.214E-01	.571E-03

MEASURED (DP/DT)0	(KPA/MIN)	=	44.35
FITTED (DP/DT)0	(KPA/MIN)	=	95.10
MEASURED (P)EQ	(KPA)	=	37.48
FITTED (P)EQ	(KPA)	=	38.60

TABLE I 6

EXPERIMENTAL RUN NO. = 110
SPHALERITE LEACHING IN AQUEOUS H2SO4

SPHAL. TYPE LEACHED		= VMWBM
TEMPERATURE	(K)	= 318.00
INITIAL MASS	(KG)	= 0.0200
STIRRER SPEED	(RPM)	= 1150.0
INITIAL H2SO4	(KG-MOL/M3)	= 1.0000
SPEC.SURFACE AREA	(M2/KG)	= 3272.0
CDEXP	(KG-MOL/M3 KPA)	= .7200E-03
KDEXP	(KPA M3/KG-MOL)	= .1703E 04
KDCALC	(KPA M3/KG-MOL)	= .1654E 04

TIME (MINS)	PH2S (KPA)	ZN2+ (KG-MOL/M3)	ZN2+/PH2S (KG-MOL/M3 KPA)
0.50	9.44	N.D.	N.D.
0.80	12.59	N.D.	N.D.
1.30	15.73	N.D.	N.D.
2.44	18.88	N.D.	N.D.
3.00	20.00	.148E-01	.738E-03
4.00	20.46	N.D.	N.D.
6.00	22.03	N.D.	N.D.
8.00	22.81	N.D.	N.D.
15.00	24.71	.177E-01	.718E-03

MEASURED (DP/DT)0	(KPA/MIN)	=	30.21
FITTED (DP/DT)0	(KPA/MIN)	=	30.60
MEASURED (P)EQ	(KPA)	=	24.86
FITTED (P)EQ	(KPA)	=	25.70

TABLE I 7

EXPERIMENTAL RUN NO. = 115
SPHALERITE LEACHING IN AQUEOUS H2SO4

SPHAL. TYPE LEACHED	=	VMWBM
TEMPERATURE (K)	=	318.00
INITIAL MASS (KG)	=	0.0100
STIRRER SPEED (RPM)	=	1400.0
INITIAL H2SO4 (KG-MOL/M3)	=	1.0000
SPEC.SURFACE AREA (M2/KG)	=	3272.0
CDEXP (KG-MOL/M3 KPA)	=	.6701E-03
KDEXP (KPA M3/KG-MOL)	=	.1861E 04
KDCALC (KPA M3/KG-MOL)	=	.1654E 04

TIME (MINS)	PH2S (KPA)	ZN2+ (KG-MOL/M3)	ZN2+/PH2S (KG-MOL/M3 KPA)
0.70	6.25	N.D.	N.D.
1.60	9.37	N.D.	N.D.
2.35	10.93	N.D.	N.D.
3.40	12.49	N.D.	N.D.
5.00	14.06	N.D.	N.D.
7.90	15.62	N.D.	N.D.
10.00	16.30	N.D.	N.D.
15.00	17.05	N.D.	N.D.
22.00	17.59	.119E-01	.674E-03

MEASURED (DP/DT)0	(KPA/MIN)	=	17.65
FITTED (DP/DT)0	(KPA/MIN)	=	12.60
MEASURED (P)EQ	(KPA)	=	17.59
FITTED (P)EQ	(KPA)	=	18.50

TABLE I 8

EXPERIMENTAL RUN NO. = 172
SPHALERITE LEACHING IN AQUEOUS H2SO4

SPHAL. TYPE LEACHED	=	VMWBM
TEMPERATURE (K)	=	318.00
INITIAL MASS (KG)	=	0.0100
STIRRER SPEED (RPM)	=	1000.0
INITIAL H2SO4 (KG-MOL/M3)	=	0.5000
SPEC.SURFACE AREA (M2/KG)	=	3272.0
CDEXP (KG-MOL/M3 KPA)	=	.7151E-03
KDEXP (KPA M3/KG-MOL)	=	.1717E 04
KDCALC (KPA M3/KG-MOL)	=	.1569E 04

TIME (MINS)	PH2S (KPA)	ZN2+ (KG-MOL/M3)	ZN2+/PH2S (KG-MOL/M3 KPA)
1.00	3.75	N.D.	N.D.
2.00	6.43	.528E-02	.820E-03
5.00	8.55	N.D.	N.D.
10.00	9.70	.721E-02	.743E-03
20.00	10.51	N.D.	N.D.
32.00	11.05	.791E-02	.715E-03

MEASURED (DP/DT)0	(KPA/MIN)	=	6.91
FITTED (DP/DT)0	(KPA/MIN)	=	5.99
MEASURED (P)EQ	(KPA)	=	11.05
FITTED (P)EQ	(KPA)	=	11.80

TABLE I 9

EXPERIMENTAL RUN NO. = 175
SPHALERITE LEACHING IN AQUEOUS H2SO4

SPHAL. TYPE LEACHED	=	VMWBM
TEMPERATURE (K)	=	318.00
INITIAL MASS (KG)	=	0.0100
STIRRER SPEED (RPM)	=	1000.0
INITIAL H2SO4 (KG-MOL/M3)	=	2.0000
SPEC.SURFACE AREA (M2/KG)	=	3272.0
CDEXP (KG-MOL/M3 KPA)	=	.6926E-03
KDEXP (KPA M3/KG-MOL)	=	.1786E 04
KDCALC (KPA M3/KG-MOL)	=	.1824E 04

TIME (MINS)	PH2S (KPA)	ZN2+ (KG-MOL/M3)	ZN2+/PH2S (KG-MOL/M3 KPA)
1.00	13.13	.135E-01	.103E-02
2.00	18.44	N.D.	N.D.
5.00	24.12	N.D.	N.D.
10.00	27.69	N.D.	N.D.
20.00	30.34	N.D.	N.D.
30.00	31.69	.220E-01	.693E-03
45.00	33.04	N.D.	N.D.

MEASURED (DP/DT)0	(KPA/MIN)	=	18.19
FITTED (DP/DT)0	(KPA/MIN)	=	20.80
MEASURED (P)EQ	(KPA)	=	33.04
FITTED (P)EQ	(KPA)	=	32.90

TABLE I 10

EXPERIMENTAL RUN NO. = 185
SPHALERITE LEACHING IN AQUEOUS H2SO4

SPHAL. TYPE LEACHED	=	VMWBM+ZNSO4 at t=0
TEMPERATURE (K)	=	318.00
INITIAL MASS (KG)	=	0.0100
STIRRER SPEED (RPM)	=	1000.0
INITIAL H2SO4 (KG-MOL/M3)	=	1.0000
INITIAL ZN2+ (KG-MOL/M3)	=	0.0150
SPEC.SURFACE AREA (M2/KG)	=	3272.0
CDEXP (KG-MOL/M3 KPA)	=	.7334E-03
KDEXP (KPA M3/KG-MOL)	=	.1665E 04
KDCALC (KPA M3/KG-MOL)	=	.1654E 04

TIME (MINS)	PH2S (KPA)	ZN2+ (KG-MOL/M3)
1.00	4.90	N.D.
2.00	7.01	.153E-01
7.00	10.37	.223E-01
15.00	12.14	.233E-01
30.00	13.64	N.D.
40.00	13.96	.252E-01

MEASURED (DP/DT)0	(KPA/MIN)	=	7.20
FITTED (DP/DT)0	(KPA/MIN)	=	7.19
MEASURED (P)EQ	(KPA)	=	13.96
FITTED (P)EQ	(KPA)	=	14.10

TABLE I 11

EXPERIMENTAL RUN NO. = 186
SPHALERITE LEACHING IN AQUEOUS H2SO4

SPHAL. TYPE LEACHED	=	VMWBM+ZNSO4 at t=0
TEMPERATURE (K)	=	318.00
INITIAL MASS (KG)	=	0.0100
STIRRER SPEED (RPM)	=	1000.0
INITIAL H2SO4 (KG-MOL/M3)	=	1.0000
INITIAL ZN2+ (KG-MOL/M3)	=	0.0251
SPEC.SURFACE AREA (M2/KG)	=	3272.0
CDEXP (KG-MOL/M3 KPA)	=	.7613E-03
KDEXP (KPA M3/KG-MOL)	=	.1591E 04
KDCALC (KPA M3/KG-MOL)	=	.1654E 04

TIME (MINS)	PH2S (KPA)	ZN2+ (KG-MOL/M3)
1.00	4.80	.299E-01
5.00	8.99	N.D.
10.00	10.47	.336E-01
20.00	11.72	N.D.
30.00	12.39	.345E-01

MEASURED (DP/DT)0	(KPA/MIN)	=	7.30
FITTED (DP/DT)0	(KPA/MIN)	=	7.60
MEASURED (P)EQ	(KPA)	=	12.39
FITTED (P)EQ	(KPA)	=	12.50

TABLE I 12

EXPERIMENTAL RUN NO. = 187
SPHALERITE LEACHING IN AQUEOUS H2SO4

SPHAL. TYPE LEACHED	=	VMWBM+ZNSO4 at t=0
TEMPERATURE (K)	=	318.00
INITIAL MASS (KG)	=	0.0100
STIRRER SPEED (RPM)	=	1000.0
INITIAL H2SO4 (KG-MOL/M3)	=	1.0000
INITIAL ZN2+ (KG-MOL/M3)	=	0.0251
SPEC.SURFACE AREA (M2/KG)	=	3272.0
CDEXP (KG-MOL/M3 KPA)	=	.0
KDEXP (KPA M3/KG-MOL)	=	-.7528E 04
KDCALC (KPA M3/KG-MOL)	=	.1654E 04

TIME (MINS)	PH2S (KPA)	ZN2+ (KG-MOL/M3)
1.00	3.36	N.D.
2.30	4.80	.545E-01
3.00	5.09	N.D.
5.00	5.88	N.D.
10.50	6.97	.590E-01
20.00	7.80	N.D.
30.00	8.45	N.D.
40.00	8.87	.603E-01

MEASURED (DP/DT)0	(KPA/MIN)	=	4.99
FITTED (DP/DT)0	(KPA/MIN)	=	4.84
MEASURED (P)EQ	(KPA)	=	8.87
FITTED (P)EQ	(KPA)	=	8.63

TABLE I 13

EXPERIMENTAL RUN NO. = 195
SPHALERITE LEACHING IN AQUEOUS H2SO4

SPHAL. TYPE LEACHED		=	VMWBM(+H2S at t=0)
TEMPERATURE	(K)	=	318.00
INITIAL MASS	(KG)	=	0.0100
STIRRER SPEED	(RPM)	=	1000.0
INITIAL H2SO4	(KG-MOL/M3)	=	0.5000
INITIAL PH2S	(KPA)	=	81.17
SPEC.SURFACE AREA	(M2/KG)	=	3272.0
CDEXP	(KG-MOL/M3 KPA)	=	.7429E-03
KDEXP	(KPA M3/KG-MOL)	=	.1639E 04
KDCALC	(KPA M3/KG-MOL)	=	.1569E 04

TIME (MINS)	PH2S (KPA)	ZN2+ (KG-MOL/M3)
0.00	7.87	N.D.
0.50	10.37	N.D.
1.00	11.93	.369E-02
2.00	13.19	N.D.
5.00	14.88	.558E-02
10.00	16.13	N.D.
22.00	17.09	.685E-02
30.00	17.09	N.D.

MEASURED (DP/DT)0	(KPA/MIN)	=	5.24
FITTED (DP/DT)0	(KPA/MIN)	=	8.40
MEASURED (P)EQ	(KPA)	=	9.22
FITTED (P)EQ	(KPA)	=	16.80

Note: Measured $[H_2S]$ = 5.0×10^{3} kg-mol/m³

TABLE I 15

EXPERIMENTAL RUN NO. = 194
SPHALERITE LEACHING IN AQUEOUS H2SO4

SPHAL. TYPE LEACHED		=	VMWBM(+H2S at t=0)
TEMPERATURE	(K)	=	318.00
INITIAL MASS	(KG)	=	0.0100
STIRRER SPEED	(RPM)	=	1000.0
INITIAL H2SO4	(KG-MOL/M3)	=	2.0000
INITIAL PH2S	(KPA)	=	226.84
SPEC.SURFACE AREA	(M2/KG)	=	3272.0
CDEXP	(KG-MOL/M3 KPA)	=	.7022E-03
KDEXP	(KPA M3/KG-MOL)	=	.1756E 04
KDCALC	(KPA M3/KG-MOL)	=	.1824E 04

TIME (MINS)	PH2S (KPA)	ZN2+ (KG-MOL/M3)
0.00	22.01	N.D.
0.50	29.53	N.D.
1.00	34.55	.108E-01
2.00	38.34	N.D.
5.00	42.85	N.D.
9.00	44.94	.158E-01
20.00	46.71	.174E-01

MEASURED (DP/DT)0	(KPA/MIN)	=	21.81
FITTED (DP/DT)0	(KPA/MIN)	=	20.60
MEASURED (P)EQ	(KPA)	=	21.81
FITTED (P)EQ	(KPA)	=	48.51

Note: Measured $[H_2S]_0$ = 20.0×10^{-3} kg-mol/m³

TABLE I 17

EXPERIMENTAL RUN NO. = 167
SPHALERITE LEACHING IN AQUEOUS H2SO4

SPHAL. TYPE LEACHED		=	VMZCR
TEMPERATURE	(K)	=	318.00
INITIAL MASS	(KG)	=	0.0100
STIRRER SPEED	(RPM)	=	1000.0
INITIAL H2SO4	(KG-MOL/M3)	=	1.0000
SPEC.SURFACE AREA	(M2/KG)	=	2708.0
CDEXP	(KG-MOL/M3 KPA)	=	.8166E-03
KDEXP	(KPA M3/KG-MOL)	=	.1462E 04
KDCALC	(KPA M3/KG-MOL)	=	.1654E 04

TIME (MINS)	PH2S (KPA)	ZN2+ (KG-MOL/M3)	ZN2+/PH2S (KG-MOL/M3 KPA)
1.00	5.38	N.D.	N.D.
2.00	7.80	N.D.	N.D.
5.00	11.91	N.D.	N.D.
10.00	14.88	N.D.	N.D.
20.00	17.71	N.D.	N.D.
30.00	18.82	N.D.	N.D.
45.00	19.67	N.D.	N.D.
60.00	20.24	.165E-01	.817E-03

MEASURED (DP/DT)0	(KPA/MIN)	=	8.37
FITTED (DP/DT)0	(KPA/MIN)	=	6.60
MEASURED (P)EQ	(KPA)	=	20.24
FITTED (P)EQ	(KPA)	=	20.40

TABLE I 14

EXPERIMENTAL RUN NO. = 193
SPHALERITE LEACHING IN AQUEOUS H2SO4

SPHAL. TYPE LEACHED		=	VMWBM(+H2S at t=0)
TEMPERATURE	(K)	=	318.00
INITIAL MASS	(KG)	=	0.0100
STIRRER SPEED	(RPM)	=	1000.0
INITIAL H2SO4	(KG-MOL/M3)	=	1.0000
INITIAL PH2S	(KPA)	=	174.23
SPEC.SURFACE AREA	(M2/KG)	=	3272.0
CDEXP	(KG-MOL/M3 KPA)	=	.7630E-03
KDEXP	(KPA M3/KG-MOL)	=	.1586E 04
KDCALC	(KPA M3/KG-MOL)	=	.1654E 04

TIME (MINS)	PH2S (KPA)	ZN2+ (KG-MOL/M3)
0.00	16.90	N.D.
0.50	21.13	N.D.
1.00	24.78	.790E-02
5.00	29.10	N.D.
11.00	30.92	.109E-01
20.00	31.73	N.D.
30.00	32.07	.116E-01

MEASURED (DP/DT)0	(KPA/MIN)	=	12.04
FITTED (DP/DT)0	(KPA/MIN)	=	11.10
MEASURED (P)EQ	(KPA)	=	15.17
FITTED (P)EQ	(KPA)	=	33.40

Note Measured $[H_2S]_0$ = 11.9×10^{3} kg-mol/m³

TABLE I 16

EXPERIMENTAL RUN NO. = 168
SPHALERITE LEACHING IN AQUEOUS H2SO4

SPHAL. TYPE LEACHED		=	VMZCR
TEMPERATURE	(K)	=	318.00
INITIAL MASS	(KG)	=	0.0050
STIRRER SPEED	(RPM)	=	1000.0
INITIAL H2SO4	(KG-MOL/M3)	=	1.0000
SPEC.SURFACE AREA	(M2/KG)	=	2708.0
CDEXP	(KG-MOL/M3 KPA)	=	.7114E-03
KDEXP	(KPA M3/KG-MOL)	=	.1728E 04
KDCALC	(KPA M3/KG-MOL)	=	.1654E 04

TIME (MINS)	PH2S (KPA)	ZN2+ (KG-MOL/M3)	ZN2+/PH2S (KG-MOL/M3 KPA)
1.00	3.63	N.D.	N.D.
3.00	7.01	.520E-02	.742E-03
10.00	11.18	.780E-02	.698E-03
30.00	14.88	.103E-01	.695E-03
45.00	16.19	N.D.	N.D.
60.00	17.04	.121E-01	.711E-03

MEASURED (DP/DT)0	(KPA/MIN)	=	4.61
FITTED (DP/DT)0	(KPA/MIN)	=	4.32
MEASURED (P)EQ	(KPA)	=	17.03
FITTED (P)EQ	(KPA)	=	17.00

TABLE I 18

EXPERIMENTAL RUN NO. = 102
SPHALERITE LEACHING IN AQUEOUS H2SO4

SPHAL. TYPE LEACHED		=	VMZCR
TEMPERATURE	(K)	=	318.00
INITIAL MASS	(KG)	=	0.0200
STIRRER SPEED	(RPM)	=	800.0
INITIAL H2SO4	(KG-MOL/M3)	=	1.0000
SPEC.SURFACE AREA	(M2/KG)	=	2708.0
CDEXP	(KG-MOL/M3 KPA)	=	.7753E-03
KDEXP	(KPA M3/KG-MOL)	=	.1556E 04
KDCALC	(KPA M3/KG-MOL)	=	.1654E 04

TIME (MINS)	PH2S (KPA)	ZN2+ (KG-MOL/M3)	ZN2+/PH2S (KG-MOL/M3 KPA)
1.10	12.59	N.D.	N.D.
1.34	14.16	N.D.	N.D.
1.75	16.47	.129E-01	.785E-03
2.88	18.88	N.D.	N.D.
4.10	20.46	N.D.	N.D.
5.00	21.00	.161E-01	.769E-03
10.00	21.71	.168E-01	.775E-03
15.00	21.09	N.D.	N.D.
25.00	19.48	N.D.	N.D.
35.00	18.41	.212E-01	.115E-02
45.00	17.79	N.D.	N.D.

MEASURED (DP/DT)0	(KPA/MIN)	=	17.53
FITTED (DP/DT)0	(KPA/MIN)	=	39.20
MEASURED (P)EQ	(KPA)	=	21.71
FITTED (P)EQ	(KPA)	=	20.70

TABLE I 19

EXPERIMENTAL RUN NO. = 137
SPHALERITE LEACHING IN AQUEOUS H2SO4

SPHAL. TYPE LEACHED		= VMZCR
TEMPERATURE	(K)	= 318.00
INITIAL MASS	(KG)	= 0.0200
STIRRER SPEED	(RPM)	= 1000.0
INITIAL H2SO4	(KG-MOL/M3)	= 1.0000
SPEC.SURFACE AREA	(M2/KG)	= 2708.0
CDEXP	(KG-MOL/M3 KPA)	= .7700E-03
KDEXP	(KPA M3/KG-MOL)	= .1569E 04
KDCALC	(KPA M3/KG-MOL)	= .1654E 04

TIME (MINS)	PH2S (KPA)	ZN2+ (KG-MOL/M3)	ZN2+/PH2S (KG-MOL/M3 KPA)
1.20	12.49	N.D.	N.D.
1.85	15.62	N.D.	N.D.
2.90	18.74	N.D.	N.D.
3.20	20.15	.155E-01	.771E-03

MEASURED (DP/DT)0	(KPA/MIN)	=	12.34
FITTED (DP/DT)0	(KPA/MIN)	=	17.10
MEASURED (P)EQ	(KPA)	=	25.77
FITTED (P)EQ	(KPA)	=	31.90

TABLE I 20

EXPERIMENTAL RUN NO. = 139
SPHALERITE LEACHING IN AQUEOUS H2SO4

SPHAL. TYPE LEACHED		= VMZCR
TEMPERATURE	(K)	= 298.00
INITIAL MASS	(KG)	= 0.0200
STIRRER SPEED	(RPM)	= 1000.0
INITIAL H2SO4	(KG-MOL/M3)	= 1.0000
SPEC.SURFACE AREA	(M2/KG)	= 2708.0
CDEXP	(KG-MOL/M3 KPA)	= .1057E-02
KDEXP	(KPA M3/KG-MOL)	= .1092E 04
KDCALC	(KPA M3/KG-MOL)	= .1225E 04

TIME (MINS)	PH2S (KPA)	ZN2+ (KG-MOL/M3)	ZN2+/PH2S (KG-MOL/M3 KPA)
1.30	4.72	N.D.	N.D.
2.10	6.29	N.D.	N.D.
2.40	6.87	.750E-02	.109E-02
3.20	7.87	N.D.	N.D.
4.70	9.44	N.D.	N.D.
7.30	11.01	N.D.	N.D.
11.45	12.59	N.D.	N.D.
19.50	14.16	N.D.	N.D.
30.00	15.30	N.D.	N.D.
39.60	15.81	.167E-01	.106E-02

MEASURED (DP/DT)0	(KPA/MIN)	=	4.41
FITTED (DP/DT)0	(KPA/MIN)	=	4.81
MEASURED (P)EQ	(KPA)	=	15.42
FITTED (P)EQ	(KPA)	=	16.80

TABLE I 21

EXPERIMENTAL RUN NO. = 106
SPHALERITE LEACHING IN AQUEOUS H2SO4

SPHAL. TYPE LEACHED		= VMZCR
TEMPERATURE	(K)	= 338.00
INITIAL MASS	(KG)	= 0.0200
STIRRER SPEED	(RPM)	= 800.0
INITIAL H2SO4	(KG-MOL/M3)	= 1.0000
SPEC.SURFACE AREA	(M2/KG)	= 2708.0
CDEXP	(KG-MOL/M3 KPA)	= .6747E-03
KDEXP	(KPA M3/KG-MOL)	= .1818E 04
KDCALC	(KPA M3/KG-MOL)	= .2174E 04

TIME (MINS)	PH2S (KPA)	ZN2+ (KG-MOL/M3)	ZN2+/PH2S (KG-MOL/M3 KPA)
0.50	20.80	N.D.	N.D.
1.00	29.18	N.D.	N.D.
2.00	35.26	.203E-01	.575E-03
3.00	36.69	N.D.	N.D.
5.00	38.43	N.D.	N.D.
8.00	39.46	.240E-01	.609E-03
10.00	39.14	N.D.	N.D.
20.00	38.33	N.D.	N.D.
25.00	38.21	.258E-01	.675E-03

MEASURED (DP/DT)0	(KPA/MIN)	=	54.63
FITTED (DP/DT)0	(KPA/MIN)	=	93.90
MEASURED (P)EQ	(KPA)	=	39.46
FITTED (P)EQ	(KPA)	=	40.80

TABLE I 22

EXPERIMENTAL RUN NO. = 170
SPHALERITE LEACHING IN AQUEOUS H2SO4

SPHAL. TYPE LEACHED		= VMZCR
TEMPERATURE	(K)	= 318.00
INITIAL MASS	(KG)	= 0.0100
STIRRER SPEED	(RPM)	= 1000.0
INITIAL H2SO4	(KG-MOL/M3)	= 0.5000
SPEC.SURFACE AREA	(M2/KG)	= 2708.0
CDEXP	(KG-MOL/M3 KPA)	= .6626E-03
KDEXP	(KPA M3/KG-MOL)	= .1887E 04
KDCALC	(KPA M3/KG-MOL)	= .1569E 04

TIME (MINS)	PH2S (KPA)	ZN2+ (KG-MOL/M3)	ZN2+/PH2S (KG-MOL/M3 KPA)
1.00	3.84	N.D.	N.D.
2.00	6.34	.483E-02	.763E-03
5.00	9.03	N.D.	N.D.
15.00	11.43	.780E-02	.683E-03
35.00	12.93	.857E-02	.663E-03
39.00	13.15	N.D.	N.D.

MEASURED (DP/DT)0	(KPA/MIN)	=	6.34
FITTED (DP/DT)0	(KPA/MIN)	=	5.41
MEASURED (P)EQ	(KPA)	=	13.15
FITTED (P)EQ	(KPA)	=	13.80

TABLE I 23

EXPERIMENTAL RUN NO. = 174
SPHALERITE LEACHING IN AQUEOUS H2SO4

SPHAL. TYPE LEACHED		= VMZCR
TEMPERATURE	(K)	= 318.00
INITIAL MASS	(KG)	= 0.0100
STIRRER SPEED	(RPM)	= 1000.0
INITIAL H2SO4	(KG-MOL/M3)	= 2.0000
SPEC.SURFACE AREA	(M2/KG)	= 2708.0
CDEXP	(KG-MOL/M3 KPA)	= .6796E-03
KDEXP	(KPA M3/KG-MOL)	= .1828E 04
KDCALC	(KPA M3/KG-MOL)	= .1824E 04

TIME (MINS)	PH2S (KPA)	ZN2+ (KG-MOL/M3)	ZN2+/PH2S (KG-MOL/M3 KPA)
1.00	11.14	N.D.	N.D.
2.60	19.21	.128E-01	.666E-03
5.00	24.40	N.D.	N.D.
11.70	31.77	.208E-01	.653E-03
20.00	35.34	N.D.	N.D.
30.00	38.10	.256E-01	.671E-03
45.00	40.53	.275E-01	.680E-03

MEASURED (DP/DT)0	(KPA/MIN)	=	14.79
FITTED (DP/DT)0	(KPA/MIN)	=	14.50
MEASURED (P)EQ	(KPA)	=	40.53
FITTED (P)EQ	(KPA)	=	40.70

TABLE I 24

EXPERIMENTAL RUN NO. = 204
SPHALERITE LEACHING IN AQUEOUS H2SO4

SPHAL. TYPE LEACHED		= VMZCR+ZNSO4 att.=0)
TEMPERATURE	(K)	= 318.00
INITIAL MASS	(KG)	= 0.0100
STIRRER SPEED	(RPM)	= 1000.0
INITIAL H2SO4	(KG-MOL/M3)	= 1.0000
INITIAL ZN2+	(KG-MOL/M3)	= 0.0143
SPEC.SURFACE AREA	(M2/KG)	= 2708.0
CDEXP	(KG-MOL/M3 KPA)	= .5715E-03
KDEXP	(KPA M3/KG-MOL)	= .2279E 04
KDCALC	(KPA M3/KG-MOL)	= .1654E 04

TIME (MINS)	PH2S (KPA)	ZN2+ (KG-MOL/M3)
1.00	4.80	N.D.
2.80	8.45	.199E-01
5.00	10.66	N.D.
10.00	13.44	.214E-01
20.00	15.94	N.D.
30.00	17.48	.243E-01
32.00	17.67	N.D.

MEASURED (DP/DT)0	(KPA/MIN)	=	2.98
FITTED (DP/DT)0	(KPA/MIN)	=	5.97
MEASURED (P)EQ	(KPA)	=	17.67
FITTED (P)EQ	(KPA)	=	18.50

TABLE I 25

EXPERIMENTAL RUN NO. = 197
SPHALERITE LEACHING IN AQUEOUS H2SO4

SPHAL. TYPE LEACHED		=	VMZCR(+H2S at t=0)
TEMPERATURE	(K)	=	318.00
INITIAL MASS	(KG)	=	0.0100
STIRRER SPEED	(RPM)	=	1000.0
INITIAL H2SO4	(KG-MOL/M3)	=	1.0000
INITIAL PH2S	(KPA)	=	132.65
SPEC.SURFACE AREA	(M2/KG)	=	2708.0
COEXP	(KG-MOL/M3 KPA)	=	.7429E-03
KOEXP	(KPA M3/KG-MOL)	=	.1639E 04
KOCALC	(KPA M3/KG-MOL)	=	.1654E 04

Note: Measured $[H_2S]_o = 10.96 \times 10^{-3}$ kg-mol/m³

TIME (MINS)	PH2S (KPA)	ZN2+ (KG-MOL/M3)
0.00	12.87	N.D.
0.50	17.13	N.D.
1.00	19.59	N.D.
2.00	22.47	.746E-02
5.00	26.12	N.D.
10.00	28.52	.116E-01
20.00	29.42	N.D.
30.00	30.00	N.D.

MEASURED (DP/DT)O	(KPA/MIN)	=	8.02
FITTED (DP/DT)O	(KPA/MIN)	=	N.D.
MEASURED (P)EQ	(KPA)	=	17.13
FITTED (P)EQ	(KPA)	=	N.D.

TABLE I 26

EXPERIMENTAL RUN NO. = 169
SPHALERITE LEACHING IN AQUEOUS H2SO4

SPHAL. TYPE LEACHED		=	VMPR
TEMPERATURE	(K)	=	318.00
INITIAL MASS	(KG)	=	0.0050
STIRRER SPEED	(RPM)	=	1000.0
INITIAL H2SO4	(KG-MOL/M3)	=	1.0000
SPEC.SURFACE AREA	(M2/KG)	=	2630.0
COEXP	(KG-MOL/M3 KPA)	=	.7100E-03
KOEXP	(KPA M3/KG-MOL)	=	.1732E 04
KOCALC	(KPA M3/KG-MOL)	=	.1654E 04

TIME (MINS)	PH2S (KPA)	$[Zn^{2+}]$ $\times 10^3$ (kg-mol/m³)	$[Fe]_{TOT}$ (kg-mol/m³)	ZN2+/PH2S (KG-MOL/M3 KPA)
2.00	1.73	2.42	0.535	.140E-02
5.00	3.84	N.D.	N.D.	N.D.
10.00	6.24	5.09	0.726	.815E-03
20.00	9.27	N.D.	N.D.	N.D.
30.00	11.23	8.11	1.224	.722E-03
61.00	14.40	9.99	1.644	.694E-03
90.00	16.08	11.50	N.D.	.712E-03

MEASURED (DP/DT)O	(KPA/MIN)	=	0.86
FITTED (DP/DT)O	(KPA/MIN)	=	0.94
MEASURED (P)EQ	(KPA)	=	16.08
FITTED (P)EQ	(KPA)	=	19.10

TABLE I 27

EXPERIMENTAL RUN NO. = 132
SPHALERITE LEACHING IN AQUEOUS H2SO4

SPHAL. TYPE LEACHED		=	VMPR
TEMPERATURE	(K)	=	318.00
INITIAL MASS	(KG)	=	0.0100
STIRRER SPEED	(RPM)	=	1000.0
INITIAL H2SO4	(KG-MOL/M3)	=	1.0000
SPEC.SURFACE AREA	(M2/KG)	=	2630.0
COEXP	(KG-MOL/M3 KPA)	=	.7860E-03
KOEXP	(KPA M3/KG-MOL)	=	.1531E 04
KOCALC	(KPA M3/KG-MOL)	=	.1654E 04

TIME (MINS)	PH2S (KPA)	ZN2+ (KG-MOL/M3)	ZN2+/PH2S (KG-MOL/M3 KPA)
2.00	6.25	N.D.	N.D.
2.50	7.34	.106E-01	.144E-02
4.20	9.37	N.D.	N.D.
5.80	10.93	N.D.	N.D.
8.40	12.49	N.D.	N.D.
10.70	13.43	.106E-01	.786E-03
12.50	14.06	N.D.	N.D.
18.80	15.62	N.D.	N.D.
30.00	17.33	N.D.	N.D.
60.00	19.62	N.D.	N.D.
90.00	20.61	N.D.	N.D.
120.00	22.02	N.D.	N.D.
180.00	25.24	N.D.	N.D.

MEASURED (DP/DT)O	(KPA/MIN)	=	3.75
FITTED (DP/DT)O	(KPA/MIN)	=	39.70
MEASURED (P)EQ	(KPA)	=	17.18
FITTED (P)EQ	(KPA)	=	21.90

TABLE I 28

EXPERIMENTAL RUN NO. = 133
SPHALERITE LEACHING IN AQUEOUS H2SO4

SPHAL. TYPE LEACHED		=	VMPR
TEMPERATURE	(K)	=	318.00
INITIAL MASS	(KG)	=	0.0200
STIRRER SPEED	(RPM)	=	1000.0
INITIAL H2SO4	(KG-MOL/M3)	=	1.0000
SPEC.SURFACE AREA	(M2/KG)	=	2630.0
COEXP	(KG-MOL/M3 KPA)	=	.9000E-03
KOEXP	(KPA M3/KG-MOL)	=	.1303E 04
KOCALC	(KPA M3/KG-MOL)	=	.1654E 04

TIME (MINS)	PH2S (KPA)	ZN2+ (KG-MOL/M3)	ZN2+/PH2S (KG-MOL/M3 KPA)
1.25	8.12	.800E-02	.985E-03
1.80	9.37	N.D.	N.D.
2.23	10.93	N.D.	N.D.
3.30	12.49	N.D.	N.D.
4.50	14.06	N.D.	N.D.
6.45	15.62	N.D.	N.D.
10.00	17.18	N.D.	N.D.
21.00	20.30	.183E-01	.900E-03

MEASURED (DP/DT)O	(KPA/MIN)	=	9.68
FITTED (DP/DT)O	(KPA/MIN)	=	9.71
MEASURED (P)EQ	(KPA)	=	18.58
FITTED (P)EQ	(KPA)	=	21.30

TABLE I 29

EXPERIMENTAL RUN NO. = 136
SPHALERITE LEACHING IN AQUEOUS H2SO4

SPHAL. TYPE LEACHED		=	VMPR
TEMPERATURE	(K)	=	298.00
INITIAL MASS	(KG)	=	0.0200
STIRRER SPEED	(RPM)	=	1000.0
INITIAL H2SO4	(KG-MOL/M3)	=	1.0000
SPEC.SURFACE AREA	(M2/KG)	=	2630.0
COEXP	(KG-MOL/M3 KPA)	=	.1470E-02
KOEXP	(KPA M3/KG-MOL)	=	.7520E 03
KOCALC	(KPA M3/KG-MOL)	=	.1225E 04

TIME (MINS)	PH2S (KPA)	ZN2+ (KG-MOL/M3)	ZN2+/PH2S (KG-MOL/M3 KPA)
1.00	1.56	N.D.	N.D.
1.70	2.50	N.D.	N.D.
5.00	4.43	N.D.	N.D.
10.00	5.78	N.D.	N.D.
20.00	7.03	N.D.	N.D.
30.00	7.87	N.D.	N.D.
40.50	8.90	.132E-01	.148E-02

MEASURED (DP/DT)O	(KPA/MIN)	=	1.66
FITTED (DP/DT)O	(KPA/MIN)	=	1.89
MEASURED (P)EQ	(KPA)	=	8.59
FITTED (P)EQ	(KPA)	=	9.06

TABLE I30

EXPERIMENTAL RUN NO. = 135
SPHALERITE LEACHING IN AQUEOUS H2SO4

SPHAL. TYPE LEACHED		=	VMPR
TEMPERATURE	(K)	=	338.00
INITIAL MASS	(KG)	=	0.0200
STIRRER SPEED	(RPM)	=	1000.0
INITIAL H2SO4	(KG-MOL/M3)	=	1.0000
SPEC.SURFACE AREA	(M2/KG)	=	2630.0
COEXP	(KG-MOL/M3 KPA)	=	.5670E-03
KOEXP	(KPA M3/KG-MOL)	=	.2262E 04
KOCALC	(KPA M3/KG-MOL)	=	.2174E 04

TIME (MINS)	PH2S (KPA)	ZN2+ (KG-MOL/M3)	ZN2+/PH2S (KG-MOL/M3 KPA)
0.50	12.49	N.D.	N.D.
0.72	15.62	N.D.	N.D.
1.20	18.74	N.D.	N.D.
1.80	21.86	N.D.	N.D.
2.70	24.99	N.D.	N.D.
4.50	28.11	N.D.	N.D.
9.60	31.23	N.D.	N.D.
15.00	31.86	N.D.	N.D.

MEASURED (DP/DT)O	(KPA/MIN)	=	25.30
FITTED (DP/DT)O	(KPA/MIN)	=	37.80
MEASURED (P)EQ	(KPA)	=	32.17
FITTED (P)EQ	(KPA)	=	33.70

TABLE I 31

EXPERIMENTAL RUN NO. = 134
SPHALERITE LEACHING IN AQUEOUS H2SO4

SPHAL. TYPE LEACHED		=	VMPR
TEMPERATURE	(K)	=	318.00
INITIAL MASS	(KG)	=	0.0200
STIRRER SPEED	(RPM)	=	1500.0
INITIAL H2SO4	(KG-MOL/M3)	=	1.0000
SPEC.SURFACE AREA	(M2/KG)	=	2630.0
CDEXP	(KG-MOL/M3 KPA)	=	.9034E-03
KDEXP	(KPA M3/KG-MOL)	=	.1297E 04
KDCALC	(KPA M3/KG-MOL)	=	.1654E 04

TIME (MINS)	PH2S (KPA)	ZN2+ (KG-MOL/M3)	ZN2+/PH2S (KG-MOL/M3 KPA)
0.80	6.25	N.D.	N.D.
1.20	7.81	.800E-02	.102E-02
1.70	9.37	N.D.	N.D.
2.40	10.93	N.D.	N.D.
3.55	12.49	N.D.	N.D.
5.20	14.06	N.D.	N.D.
7.45	15.62	N.D.	N.D.
15.00	18.58	N.D.	N.D.
22.00	20.15	.182E-01	.903E-03

MEASURED (DP/DT)0	(KPA/MIN)	=	13.18
FITTED (DP/DT)0	(KPA/MIN)	=	10.50
MEASURED (P)EQ	(KPA)	=	20.61
FITTED (P)EQ	(KPA)	=	20.20

TABLE I 33

EXPERIMENTAL RUN NO. = 173
SPHALERITE LEACHING IN AQUEOUS H2SO4

SPHAL. TYPE LEACHED		=	VMPR
TEMPERATURE	(K)	=	318.00
INITIAL MASS	(KG)	=	0.0100
STIRRER SPEED	(RPM)	=	1000.0
INITIAL H2SO4	(KG-MOL/M3)	=	2.0000
SPEC.SURFACE AREA	(M2/KG)	=	2630.0
CDEXP	(KG-MOL/M3 KPA)	=	.6842E-03
KDEXP	(KPA M3/KG-MOL)	=	.1813E 04
KDCALC	(KPA M3/KG-MOL)	=	.1824E 04

TIME (MINS)	PH2S (KPA)	$[Zn^{2+}]$ $\times 10^3$ (kg-mol/m3)	$[Fe]_{TOT}$ (kg-mol/m3)	ZN2+/PH2S (KG-MOL/M3 KPA)
1.00	3.75	N.D.	N.D.	N.D.
3.00	9.76	8.64	1.40	.886E-03
5.00	13.68	N.D.	N.D.	N.D.
13.00	22.18	15.57	2.33	.702E-03
30.00	30.34	20.76	3.06	.684E-03
45.00	34.22	N.D.	N.D.	N.D.

MEASURED (DP/DT)0	(KPA/MIN)	=	3.75
FITTED (DP/DT)0	(KPA/MIN)	=	41.90
MEASURED (P)EQ	(KPA)	=	36.59
FITTED (P)EQ	(KPA)	=	4.04

TABLE I 35

EXPERIMENTAL RUN NO. = 196
SPHALERITE LEACHING IN AQUEOUS H2SO4

SPHAL. TYPE LEACHED		=	VMPR(+H2S at t = 0)
TEMPERATURE	(K)	=	318.00
INITIAL MASS	(KG)	=	0.0100
STIRRER SPEED	(RPM)	=	1000.0
INITIAL H2SO4	(KG-MOL/M3)	=	1.0000
INITIAL PH2S	(KPA)	=	122.75
SPEC.SURFACE AREA	(M2/KG)	=	2630.0
CDEXP	(KG-MOL/M3 KPA)	=	.7930E-03
KDEXP	(KPA M3/KG-MOL)	=	.1514E 04
KDCALC	(KPA M3/KG-MOL)	=	.1654E 04

Note. Measured $[H_2S]_L = 17.77 \times 10^3$ kg-mol/m3

TIME (MINS)	PH2S (KPA)	ZN2+ (KG-MOL/M3)
0.00	11.91	N.D.
0.50	12.96	N.D.
1.00	13.68	N.D.
2.00	14.98	.361E-02
5.00	17.48	N.D.
10.60	20.17	.737E-02
20.00	22.85	N.D.
30.00	24.78	N.D.
40.00	25.93	N.D.
46.00	26.31	.114E-01

MEASURED (DP/DT)0	(KPA/MIN)	=	1.35
FITTED (DP/DT)0	(KPA/MIN)	=	N.D.
MEASURED (P)EQ	(KPA)	=	14.40
FITTED (P)EQ	(KPA)	=	N.D.

TABLE I 32

EXPERIMENTAL RUN NO. = 171
SPHALERITE LEACHING IN AQUEOUS H2SO4

SPHAL. TYPE LEACHED		=	VMPR
TEMPERATURE	(K)	=	318.00
INITIAL MASS	(KG)	=	0.0100
STIRRER SPEED	(RPM)	=	1000.0
INITIAL H2SO4	(KG-MOL/M3)	=	0.5000
SPEC.SURFACE AREA	(M2/KG)	=	2630.0
CDEXP	(KG-MOL/M3 KPA)	=	.8966E-03
KDEXP	(KPA M3/KG-MOL)	=	.1309E 04
KDCALC	(KPA M3/KG-MOL)	=	.1569E 04

TIME (MINS)	PH2S (KPA)	ZN2+ (KG-MOL/M3)	ZN2+/PH2S (KG-MOL/M3 KPA)
2.00	1.34	.288E-02	.214E-02
5.00	2.69	N.D.	N.D.
15.00	4.80	.543E-02	.113E-02
30.00	8.41	.754E-02	.897E-03

MEASURED (DP/DT)0	(KPA/MIN)	=	0.77
FITTED (DP/DT)0	(KPA/MIN)	=	0.72
MEASURED (P)EQ	(KPA)	=	8.41
FITTED (P)EQ	(KPA)	=	11.80

TABLE I 34

EXPERIMENTAL RUN NO. = 203
SPHALERITE LEACHING IN AQUEOUS H2SO4

SPHAL. TYPE LEACHED		=	VMPR(+ZNSO4 at t = 0)
TEMPERATURE	(K)	=	318.00
INITIAL MASS	(KG)	=	0.0100
STIRRER SPEED	(RPM)	=	1000.0
INITIAL H2SO4	(KG-MOL/M3)	=	1.0000
INITIAL ZN2+	(KG-MOL/M3)	=	0.0142
SPEC.SURFACE AREA	(M2/KG)	=	2630.0
CDEXP	(KG-MOL/M3 KPA)	=	.0
KDEXP	(KPA M3/KG-MOL)	=	-.7528E 04
KDCALC	(KPA M3/KG-MOL)	=	.1654E 04

TIME (MINS)	PH2S (KPA)	ZN2+ (KG-MOL/M3)
1.00	0.65	N.D.
2.00	1.23	N.D.
3.00	1.83	N.D.
4.80	2.48	.176E-01
10.00	4.30	N.D.
15.50	5.84	.191E-01
20.00	6.72	N.D.
30.00	8.72	.209E-01
40.00	10.10	N.D.
50.00	11.52	N.D.
60.00	12.18	.222E-01
64.00	12.52	N.D.

MEASURED (DP/DT)0	(KPA/MIN)	=	0.65
FITTED (DP/DT)0	(KPA/MIN)	=	0.64
MEASURED (P)EQ	(KPA)	=	6.32
FITTED (P)EQ	(KPA)	=	16.80

TABLE I 36

EXPERIMENTAL RUN NO. = 199
SPHALERITE LEACHING IN AQUEOUS H2SO4

SPHAL. TYPE LEACHED		=	BDH
TEMPERATURE	(K)	=	318.00
INITIAL MASS	(KG)	=	0.0040
STIRRER SPEED	(RPM)	=	1000.0
INITIAL H2SO4	(KG-MOL/M3)	=	1.0000
SPEC.SURFACE AREA	(M2/KG)	=	7200.0
CDEXP	(KG-MOL/M3 KPA)	=	.7216E-03
KDEXP	(KPA M3/KG-MOL)	=	.1698E 04
KDCALC	(KPA M3/KG-MOL)	=	.1654E 04

TIME (MINS)	PH2S (KPA)	ZN2+ (KG-MOL/M3)	ZN2+/PH2S (KG-MOL/M3 KPA)
1.00	5.40	N.D.	N.D.
2.00	11.00	.875E-02	.795E-03
5.00	18.72	N.D.	N.D.
10.20	22.58	.164E-01	.725E-03
20.40	24.21	.172E-01	.709E-03
30.00	25.48	N.D.	N.D.
40.00	25.90	.179E-01	.690E-03

MEASURED (DP/DT)0	(KPA/MIN)	=	5.50
FITTED (DP/DT)0	(KPA/MIN)	=	N.D.
MEASURED (P)EQ	(KPA)	=	25.90
FITTED (P)EQ	(KPA)	=	N.D.

TABLE I 37

EXPERIMENTAL RUN NO. = 141
SPHALERITE LEACHING IN AQUEOUS H2SO4

SPHAL. TYPE LEACHED		= BDH
TEMPERATURE	(K)	= 318.00
INITIAL MASS	(KG)	= 0.0100
STIRRER SPEED	(RPM)	= 1000.0
INITIAL H2SO4	(KG-MOL/M3)	= 1.0000
SPEC.SURFACE AREA	(M2/KG)	= 7200.0
CDEXP	(KG-MOL/M3 KPA)	= .7732E-03
KDEXP	(KPA M3/KG-MOL)	= .1561E 04
KDCALC	(KPA M3/KG-MOL)	= .1654E 04

TIME (MINS)	PH2S (KPA)	ZN2+ (KG-MOL/M3)	ZN2+/PH2S (KG-MOL/M3 KPA)
1.00	15.05	N.D.	N.D.
2.00	23.74	N.D.	N.D.
3.15	27.01	.217E-01	.804E-03
4.00	27.95	N.D.	N.D.
5.00	28.36	N.D.	N.D.
10.00	28.49	N.D.	N.D.
16.20	28.77	.228E-01	.792E-03
20.00	28.77	N.D.	N.D.

MEASURED (DP/DT)0	(KPA/MIN)	=	15.15
FITTED (DP/DT)0	(KPA/MIN)	=	N.D.
MEASURED (P)EQ	(KPA)	=	28.89
FITTED (P)EQ	(KPA)	=	N.D.

TABLE I 38

EXPERIMENTAL RUN NO. = 140
SPHALERITE LEACHING IN AQUEOUS H2SO4

SPHAL. TYPE LEACHED		= BDH
TEMPERATURE	(K)	= 298.00
INITIAL MASS	(KG)	= 0.0100
STIRRER SPEED	(RPM)	= 1000.0
INITIAL H2SO4	(KG-MOL/M3)	= 1.0000
SPEC.SURFACE AREA	(M2/KG)	= 7200.0
CDEXP	(KG-MOL/M3 KPA)	= .1031E-02
KDEXP	(KPA M3/KG-MOL)	= .1124E 04
KDCALC	(KPA M3/KG-MOL)	= .1225E 04

TIME (MINS)	PH2S (KPA)	ZN2+ (KG-MOL/M3)	ZN2+/PH2S (KG-MOL/M3 KPA)
1.00	3.10	N.D.	N.D.
1.80	5.93	.737E-02	.124E-02
5.00	13.27	N.D.	N.D.
10.00	16.87	N.D.	N.D.
20.00	17.55	N.D.	N.D.
30.00	17.56	N.D.	N.D.
38.70	17.56	.192E-01	.110E-02

MEASURED (DP/DT)0	(KPA/MIN)	=	3.12
FITTED (DP/DT)0	(KPA/MIN)	=	N.D.
MEASURED (P)EQ	(KPA)	=	17.49
FITTED (P)EQ	(KPA)	=	N.D.

TABLE I 39

EXPERIMENTAL RUN NO. = 142
SPHALERITE LEACHING IN AQUEOUS H2SO4

SPHAL. TYPE LEACHED		= BDH
TEMPERATURE	(K)	= 338.00
INITIAL MASS	(KG)	= 0.0050
STIRRER SPEED	(RPM)	= 1000.0
INITIAL H2SO4	(KG-MOL/M3)	= 1.0000
SPEC.SURFACE AREA	(M2/KG)	= 7200.0
CDEXP	(KG-MOL/M3 KPA)	= .5670E-03
KDEXP	(KPA M3/KG-MOL)	= .2262E 04
KDCALC	(KPA M3/KG-MOL)	= .2174E 04

TIME (MINS)	PH2S (KPA)	ZN2+ (KG-MOL/M3)	ZN2+/PH2S (KG-MOL/M3 KPA)
0.85	28.11	N.D.	N.D.
1.10	31.23	N.D.	N.D.
1.44	34.36	N.D.	N.D.
2.00	37.65	.205E-01	.545E-03
2.65	39.04	N.D.	N.D.
4.00	40.23	N.D.	N.D.
5.60	40.91	.245E-01	.598E-03
10.00	41.22	N.D.	N.D.

MEASURED (DP/DT)0	(KPA/MIN)	=	36.44
FITTED (DP/DT)0	(KPA/MIN)	=	N.D.
MEASURED (P)EQ	(KPA)	=	40.60
FITTED (P)EQ	(KPA)	=	N.D.

TABLE I40

EXPERIMENTAL RUN NO. = 200
SPHALERITE LEACHING IN AQUEOUS H2SO4

SPHAL. TYPE LEACHED		= BDH
TEMPERATURE	(K)	= 318.00
INITIAL MASS	(KG)	= 0.0040
STIRRER SPEED	(RPM)	= 1000.0
INITIAL H2SO4	(KG-MOL/M3)	= 0.5000
SPEC.SURFACE AREA	(M2/KG)	= 7200.0
CDEXP	(KG-MOL/M3 KPA)	= .8649E-03
KDEXP	(KPA M3/KG-MOL)	= .1365E 04
KDCALC	(KPA M3/KG-MOL)	= .1569E 04

TIME (MINS)	PH2S (KPA)	ZN2+ (KG-MOL/M3)	ZN2+/PH2S (KG-MOL/M3 KPA)
1.00	2.69	N.D.	N.D.
2.00	5.57	.456E-02	.819E-03
5.00	8.35	N.D.	N.D.
10.00	9.89	.839E-02	.848E-03
15.00	10.12	N.D.	N.D.
20.00	10.27	.888E-02	.865E-03

MEASURED (DP/DT)0	(KPA/MIN)	=	2.91
FITTED (DP/DT)0	(KPA/MIN)	=	N.D.
MEASURED (P)EQ	(KPA)	=	10.27
FITTED (P)EQ	(KPA)	=	N.D.

TABLE I 41

EXPERIMENTAL RUN NO. = 201
SPHALERITE LEACHING IN AQUEOUS H2SO4

SPHAL. TYPE LEACHED		= BDH
TEMPERATURE	(K)	= 318.00
INITIAL MASS	(KG)	= 0.0040
STIRRER SPEED	(RPM)	= 1000.0
INITIAL H2SO4	(KG-MOL/M3)	= 2.0204
SPEC.SURFACE AREA	(M2/KG)	= 7200.0
CDEXP	(KG-MOL/M3 KPA)	= .6392E 00
KDEXP	(KPA M3/KG-MOL)	= .1000E 01
KDCALC	(KPA M3/KG-MOL)	= .1827E 04

TIME (MINS)	PH2S (KPA)	ZN2+ (KG-MOL/M3)	ZN2+/PH2S (KG-MOL/M3 KPA)
1.00	15.44	N.D.	N.D.
2.10	28.57	.189E-01	.663E-03
3.00	34.55	N.D.	N.D.
5.00	40.92	N.D.	N.D.
9.20	45.09	.267E-01	.592E-03
15.00	45.75	.285E-01	.622E-03
20.00	45.75	N.D.	N.D.

MEASURED (DP/DT)0	(KPA/MIN)	=	15.44
FITTED (DP/DT)0	(KPA/MIN)	=	N.D.
MEASURED (P)EQ	(KPA)	=	45.75
FITTED (P)EQ	(KPA)	=	N.D.

TABLE I 42

EXPERIMENTAL RUN NO. = 202
SPHALERITE LEACHING IN AQUEOUS H2SO4

SPHAL. TYPE LEACHED		= BDH+Zn_2SO_4 at t=0
TEMPERATURE	(K)	= 318.00
INITIAL MASS	(KG)	= 0.0040
STIRRER SPEED	(RPM)	= 1000.0
INITIAL H2SO4	(KG-MOL/M3)	= 1.0000
SPEC.SURFACE AREA	(M2/KG)	= 7200.0
KDCALC	(KPA M3/KG-MOL)	= .1654E 04
Initial Zn^{2+}	(kg-mol/m^3)	= .1427E-01

TIME (MINS)	PH2S (KPA)	ZN2+ (KG-MOL/M3)	ZN2+/PH2S (KG-MOL/M3 KPA)
1.00	2.98	N.D.	N.D.
2.00	5.86	.191E-01	.326E-02
3.00	8.35	N.D.	N.D.
5.00	11.52	N.D.	N.D.
10.00	15.17	.229E-01	.151E-02
20.00	16.98	N.D.	N.D.
30.00	17.86	.243E-01	.136E-02
38.00	18.25	N.D.	N.D.
40.00	1.73	N.D.	N.D.
45.00	2.11	N.D.	N.D.
53.00	2.21	.243E 02	.110E 02

MEASURED (DP/DT)0	(KPA/MIN)	=	5.89
FITTED (DP/DT)0	(KPA/MIN)	=	N.D.
MEASURED (P)EQ	(KPA)	=	18.25
FITTED (P)EQ	(KPA)	=	N.D.

TABLE I 43

EXPERIMENTAL RUN NO. = 198
SPHALERITE LEACHING IN AQUEOUS H2SO4

SPHAL. TYPE LEACHED		=	BDH+H2S att=01
TEMPERATURE	(K)	=	318.00
INITIAL MASS	(KG)	=	0.0040
STIRRER SPEED	(RPM)	=	1000.0
INITIAL H2SO4	(KG-MOL/M3)	=	1.0000
INITIAL PH2S	(KPA)	=	118.80
SPEC.SURFACE AREA	(M2/KG)	=	7200.0
KDCALC	(KPA M3/KG-MOL)	=	.1654E 04

Note Measured H_2S_b = 10.85×10^{-3} kg-mol/m^3

TIME (MINS)	PH2S (KPA)	ZN2+ (KG-MOL/M3)	ZN2+/PH2S (KG-MOL/M3 KPA)
0.00	11.52	N.D.	N.D.
0.50	14.40	N.D.	N.D.
1.40	20.93	.857E-02	.409E-03
3.00	28.04	N.D.	N.D.
5.00	31.59	N.D.	N.D.
9.00	33.80	.160E-01	.474E-03
20.00	36.30	N.D.	N.D.
30.00	37.36	N.D.	N.D.
41.50	38.70	.170E-01	.439E-03

MEASURED	(DP/DT)0	(KPA/MIN)	=	7.01
FITTED	(DP/DT)0	(KPA/MIN)	=	N.D.
MEASURED	(P)EQ	(KPA)	=	7.78
FITTED	(P)EQ	(KPA)	=	N.D.

TABLE I 44

EXPERIMENTAL RUN NO. = 153
SPHALERITE LEACHING IN AQUEOUS H2SO4

SPHAL. TYPE LEACHED		=	BDH
TEMPERATURE	(K)	=	298.00
INITIAL MASS	(KG)	=	0.0040
STIRRER SPEED	(RPM)	=	1000.0
INITIAL H2SO4	(KG-MOL/M3)	=	1.0400
SPEC.SURFACE AREA	(M2/KG)	=	7200.0
CDEXP	(KG-MOL/M3 KPA)	=	.1165E-02
KDEXP	(KPA M3/KG-MOL)	=	.9770E 03
KDCALC	(KPA M3/KG-MOL)	=	.1232E 04

TIME (MINS)	PH2S (KPA)	ZN2+ (KG-MOL/M3)	ZN2+/PH2S (KG-MOL/M3 KPA)
2.00	2.81	N.D.	N.D.
4.00	5.42	N.D.	N.D.
6.00	7.62	N.D.	N.D.
8.00	9.33	N.D.	N.D.
10.00	10.75	N.D.	N.D.
15.00	12.84	N.D.	N.D.
30.00	14.83	N.D.	N.D.
40.00	15.05	N.D.	N.D.
60.00	15.02	.194E-01	.129E-02

MEASURED	(DP/DT)0	(KPA/MIN)	=	1.39
FITTED	(DP/DT)0	(KPA/MIN)	=	N.D.
MEASURED	(P)EQ	(KPA)	=	15.08
FITTED	(P)EQ	(KPA)	=	N.D.

TABLE I 45

EXPERIMENTAL RUN NO. = 154
SPHALERITE LEACHING IN AQUEOUS H2SO4

SPHAL. TYPE LEACHED		=	BDH
TEMPERATURE	(K)	=	298.00
INITIAL MASS	(KG)	=	0.0040
STIRRER SPEED	(RPM)	=	1000.0
INITIAL H2SO4	(KG-MOL/M3)	=	1.0400
SPEC.SURFACE AREA	(M2/KG)	=	7200.0
CDEXP	(KG-MOL/M3 KPA)	=	.1165E-02
KDEXP	(KPA M3/KG-MOL)	=	.9770E 03
KDCALC	(KPA M3/KG-MOL)	=	.1232E 04

TIME (MINS)	PH2S (KPA)	ZN2+ (KG-MOL/M3)	ZN2+/PH2S (KG-MOL/M3 KPA)
2.00	3.30	N.D.	N.D.
4.00	6.40	N.D.	N.D.
6.00	9.09	N.D.	N.D.
8.00	11.13	N.D.	N.D.
10.00	12.53	N.D.	N.D.
15.00	14.70	N.D.	N.D.
30.00	16.30	N.D.	N.D.
40.00	16.40	N.D.	N.D.
60.00	16.84	.189E-01	.112E-02

MEASURED	(DP/DT)0	(KPA/MIN)	=	1.64
FITTED	(DP/DT)0	(KPA/MIN)	=	N.D.
MEASURED	(P)EQ	(KPA)	=	16.78
FITTED	(P)EQ	(KPA)	=	N.D.

TABLE I 46

EXPERIMENTAL RUN NO. = 155
SPHALERITE LEACHING IN AQUEOUS H2SO4

SPHAL. TYPE LEACHED		=	BDH
TEMPERATURE	(K)	=	298.00
INITIAL MASS	(KG)	=	0.0040
STIRRER SPEED	(RPM)	=	400.0
INITIAL H2SO4	(KG-MOL/M3)	=	1.0400
SPEC.SURFACE AREA	(M2/KG)	=	7200.0
CDEXP	(KG-MOL/M3 KPA)	=	.1165E-02
KDEXP	(KPA M3/KG-MOL)	=	.9770E 03
KDCALC	(KPA M3/KG-MOL)	=	.1232E 04

TIME (MINS)	PH2S (KPA)	ZN2+ (KG-MOL/M3)	ZN2+/PH2S (KG-MOL/M3 KPA)
2.00	2.29	N.D.	N.D.
4.00	4.66	N.D.	N.D.
6.00	6.80	N.D.	N.D.
8.00	8.57	N.D.	N.D.
10.00	10.09	N.D.	N.D.
15.00	12.57	N.D.	N.D.
30.00	15.26	N.D.	N.D.
40.00	15.73	N.D.	N.D.
60.00	16.01	.188E-01	.117E-02

MEASURED	(DP/DT)0	(KPA/MIN)	=	1.18
FITTED	(DP/DT)0	(KPA/MIN)	=	N.D.
MEASURED	(P)EQ	(KPA)	=	16.18
FITTED	(P)EQ	(KPA)	=	N.D.

TABLE I 47

EXPERIMENTAL RUN NO. = 156
SPHALERITE LEACHING IN AQUEOUS H2SO4

SPHAL. TYPE LEACHED		=	BDH
TEMPERATURE	(K)	=	298.00
INITIAL MASS	(KG)	=	0.0040
STIRRER SPEED	(RPM)	=	700.0
INITIAL H2SO4	(KG-MOL/M3)	=	1.0400
SPEC.SURFACE AREA	(M2/KG)	=	7200.0
CDEXP	(KG-MOL/M3 KPA)	=	.1165E-02
KDEXP	(KPA M3/KG-MOL)	=	.9770E 03
KDCALC	(KPA M3/KG-MOL)	=	.1232E 04

TIME (MINS)	PH2S (KPA)	ZN2+ (KG-MOL/M3)	ZN2+/PH2S (KG-MOL/M3 KPA)
2.00	3.05	N.D.	N.D.
4.00	6.04	N.D.	N.D.
6.00	8.62	N.D.	N.D.
8.00	10.61	N.D.	N.D.
10.00	12.03	N.D.	N.D.
15.00	14.23	N.D.	N.D.
30.00	15.81	N.D.	N.D.
40.00	16.13	N.D.	N.D.
55.00	16.29	.188E-01	.115E-02

MEASURED (DP/DT)0	(KPA/MIN)	=	1.55
FITTED (DP/DT)0	(KPA/MIN)	=	N.D.
MEASURED (P)EQ	(KPA)	=	16.48
FITTED (P)EQ	(KPA)	=	N.D.

TABLE I 48

EXPERIMENTAL RUN NO. = 157
SPHALERITE LEACHING IN AQUEOUS H2SO4

SPHAL. TYPE LEACHED		=	BDH
TEMPERATURE	(K)	=	298.00
INITIAL MASS	(KG)	=	0.0040
STIRRER SPEED	(RPM)	=	700.0
INITIAL H2SO4	(KG-MOL/M3)	=	1.0400
SPEC.SURFACE AREA	(M2/KG)	=	7200.0
CDEXP	(KG-MOL/M3 KPA)	=	.1165E-02
KDEXP	(KPA M3/KG-MOL)	=	.9770E 03
KDCALC	(KPA M3/KG-MOL)	=	.1232E 04

TIME (MINS)	PH2S (KPA)	ZN2+ (KG-MOL/M3)	ZN2+/PH2S (KG-MOL/M3 KPA)
2.00	3.00	N.D.	N.D.
4.00	6.01	N.D.	N.D.
6.00	8.44	N.D.	N.D.
8.00	10.51	N.D.	N.D.
10.00	11.82	N.D.	N.D.
15.00	13.93	N.D.	N.D.
30.00	15.66	N.D.	N.D.
40.00	16.04	N.D.	N.D.
60.00	16.29	.190E-01	.116E-02

MEASURED (DP/DT)0	(KPA/MIN)	=	1.49
FITTED (DP/DT)0	(KPA/MIN)	=	N.D.
MEASURED (P)EQ	(KPA)	=	16.27
FITTED (P)EQ	(KPA)	=	N.D.

TABLE I 49

EXPERIMENTAL RUN NO. = 158
SPHALERITE LEACHING IN AQUEOUS H2SO4

SPHAL. TYPE LEACHED		=	BDH
TEMPERATURE	(K)	=	298.00
INITIAL MASS	(KG)	=	0.0080
STIRRER SPEED	(RPM)	=	1000.0
INITIAL H2SO4	(KG-MOL/M3)	=	1.0400
SPEC.SURFACE AREA	(M2/KG)	=	7200.0
CDEXP	(KG-MOL/M3 KPA)	=	.1165E-02
KDEXP	(KPA M3/KG-MOL)	=	.9770E 03
KDCALC	(KPA M3/KG-MOL)	=	.1232E 04

TIME (MINS)	PH2S (KPA)	ZN2+ (KG-MOL/M3)	ZN2+/PH2S (KG-MOL/M3 KPA)
2.00	5.02	N.D.	N.D.
4.00	9.42	N.D.	N.D.
6.00	12.22	N.D.	N.D.
8.00	13.76	N.D.	N.D.
10.00	14.47	N.D.	N.D.
15.00	14.78	N.D.	N.D.
30.00	14.78	.190E-01	.129E-02

MEASURED (DP/DT)0	(KPA/MIN)	=	2.52
FITTED (DP/DT)0	(KPA/MIN)	=	N.D.
MEASURED (P)EQ	(KPA)	=	14.78
FITTED (P)EQ	(KPA)	=	N.D.

TABLE I 50

EXPERIMENTAL RUN NO. = 159
SPHALERITE LEACHING IN AQUEOUS H2SO4

SPHAL. TYPE LEACHED		=	BDH
TEMPERATURE	(K)	=	298.00
INITIAL MASS	(KG)	=	0.0080
STIRRER SPEED	(RPM)	=	1000.0
INITIAL H2SO4	(KG-MOL/M3)	=	1.0400
SPEC.SURFACE AREA	(M2/KG)	=	7200.0
CDEXP	(KG-MOL/M3 KPA)	=	.1165E-02
KDEXP	(KPA M3/KG-MOL)	=	.9770E 03
KDCALC	(KPA M3/KG-MOL)	=	.1232E 04

TIME (MINS)	PH2S (KPA)	ZN2+ (KG-MOL/M3)	ZN2+/PH2S (KG-MOL/M3 KPA)
2.00	5.44	N.D.	N.D.
4.00	9.92	N.D.	N.D.
6.00	12.88	N.D.	N.D.
8.00	14.49	N.D.	N.D.
10.00	15.39	N.D.	N.D.
15.00	16.23	N.D.	N.D.
20.00	16.62	N.D.	N.D.
30.00	16.83	.191E-01	.113E-02

MEASURED (DP/DT)0	(KPA/MIN)	=	2.46
FITTED (DP/DT)0	(KPA/MIN)	=	N.D.
MEASURED (P)EQ	(KPA)	=	16.88
FITTED (P)EQ	(KPA)	=	N.D.

TABLE I 51

EXPERIMENTAL RUN NO. = 160
SPHALERITE LEACHING IN AQUEOUS H2SO4

SPHAL. TYPE LEACHED		=	BDH
TEMPERATURE	(K)	=	298.00
INITIAL MASS	(KG)	=	0.0060
STIRRER SPEED	(RPM)	=	1000.0
INITIAL H2SO4	(KG-MOL/M3)	=	1.0400
SPEC.SURFACE AREA	(M2/KG)	=	7200.0
CDEXP	(KG-MOL/M3 KPA)	=	.1165E-02
KDEXP	(KPA M3/KG-MOL)	=	.9770E 03
KDCALC	(KPA M3/KG-MOL)	=	.1232E 04

TIME (MINS)	PH2S (KPA)	ZN2+ (KG-MOL/M3)	ZN2+/PH2S (KG-MOL/M3 KPA)
2.00	4.51	N.D.	N.D.
4.00	8.53	N.D.	N.D.
6.00	11.44	N.D.	N.D.
8.00	13.30	N.D.	N.D.
10.00	14.33	N.D.	N.D.
15.00	15.64	N.D.	N.D.
20.00	16.10	N.D.	N.D.
30.00	16.18	.193E-01	.119E-02

MEASURED (DP/DT)0	(KPA/MIN)	=	2.28
FITTED (DP/DT)0	(KPA/MIN)	=	N.D.
MEASURED (P)EQ	(KPA)	=	16.28
FITTED (P)EQ	(KPA)	=	N.D.

TABLE I 52

EXPERIMENTAL RUN NO. = 161
SPHALERITE LEACHING IN AQUEOUS H2SO4

SPHAL. TYPE LEACHED		=	BDH
TEMPERATURE	(K)	=	298.00
INITIAL MASS	(KG)	=	0.0020
STIRRER SPEED	(RPM)	=	1000.0
INITIAL H2SO4	(KG-MOL/M3)	=	1.0400
SPEC.SURFACE AREA	(M2/KG)	=	7200.0
CDEXP	(KG-MOL/M3 KPA)	=	.1165E-02
KDEXP	(KPA M3/KG-MOL)	=	.9770E 03
KDCALC	(KPA M3/KG-MOL)	=	.1232E 04

TIME (MINS)	PH2S (KPA)	ZN2+ (KG-MOL/M3)	ZN2+/PH2S (KG-MOL/M3 KPA)
2.00	1.74	N.D.	N.D.
4.00	3.51	N.D.	N.D.
10.00	7.52	N.D.	N.D.
15.00	9.42	N.D.	N.D.
30.00	12.27	N.D.	N.D.
45.00	13.05	N.D.	N.D.
60.00	13.56	N.D.	N.D.
90.00	13.85	.167E-01	.120E-02

MEASURED (DP/DT)0	(KPA/MIN)	=	0.86
FITTED (DP/DT)0	(KPA/MIN)	=	N.D.
MEASURED (P)EQ	(KPA)	=	13.88
FITTED (P)EQ	(KPA)	=	N.D.

TABLE I 53

EXPERIMENTAL RUN NO. = 162
SPHALERITE LEACHING IN AQUEOUS H2SO4

SPHAL. TYPE LEACHED		=	BDH
TEMPERATURE	(K)	=	298.00
INITIAL MASS	(KG)	=	0.0040
STIRRER SPEED	(RPM)	=	1000.0
INITIAL H2SO4	(KG-MOL/M3)	=	0.5130
SPEC.SURFACE AREA	(M2/KG)	=	7200.0
CDEXP	(KG-MOL/M3 KPA)	=	.1165E-02
KDEXP	(KPA M3/KG-MOL)	=	.9770E 03
KDCALC	(KPA M3/KG-MOL)	=	.1142E 04

TIME (MINS)	PH2S (KPA)	ZN2+ (KG-MOL/M3)	ZN2+/PH2S (KG-MOL/M3 KPA)
2.00	1.30	N.D.	N.D.
6.00	3.69	N.D.	N.D.
10.00	5.33	N.D.	N.D.
15.00	6.28	N.D.	N.D.
30.00	6.96	N.D.	N.D.
45.00	6.96	.926E-02	.133E-02

MEASURED	(DP/DT)0	(KPA/MIN)	=	0.66
FITTED	(DP/DT)0	(KPA/MIN)	=	N.D.
MEASURED	(P)EQ	(KPA)	=	6.99
FITTED	(P)EQ	(KPA)	=	N.D.

TABLE I 54

EXPERIMENTAL RUN NO. = 163
SPHALERITE LEACHING IN AQUEOUS H2SO4

SPHAL. TYPE LEACHED		=	BDH
TEMPERATURE	(K)	=	298.00
INITIAL MASS	(KG)	=	0.0040
STIRRER SPEED	(RPM)	=	1000.0
INITIAL H2SO4	(KG-MOL/M3)	=	0.2500
SPEC.SURFACE AREA	(M2/KG)	=	7200.0
CDEXP	(KG-MOL/M3 KPA)	=	.1165E-02
KDEXP	(KPA M3/KG-MOL)	=	.9770E 03
KDCALC	(KPA M3/KG-MOL)	=	.1098E 04

TIME (MINS)	PH2S (KPA)	ZN2+ (KG-MOL/M3)	ZN2+/PH2S (KG-MOL/M3 KPA)
2.00	1.53	N.D.	N.D.
6.00	3.99	N.D.	N.D.
10.00	5.44	N.D.	N.D.
15.00	6.31	N.D.	N.D.
30.00	6.76	N.D.	N.D.
45.00	6.73	.494E-02	.734E-03

MEASURED	(DP/DT)0	(KPA/MIN)	=	0.39
FITTED	(DP/DT)0	(KPA/MIN)	=	N.D.
MEASURED	(P)EQ	(KPA)	=	3.41
FITTED	(P)EQ	(KPA)	=	N.D.

TABLE I 55

EXPERIMENTAL RUN NO. = 164
SPHALERITE LEACHING IN AQUEOUS H2SO4

SPHAL. TYPE LEACHED		=	BDH
TEMPERATURE	(K)	=	298.00
INITIAL MASS	(KG)	=	0.0040
STIRRER SPEED	(RPM)	=	1000.0
INITIAL H2SO4	(KG-MOL/M3)	=	1.9500
SPEC.SURFACE AREA	(M2/KG)	=	7200.0
CDEXP	(KG-MOL/M3 KPA)	=	.1165E-02
KDEXP	(KPA M3/KG-MOL)	=	.9770E 03
KDCALC	(KPA M3/KG-MOL)	=	.1387E 04

TIME (MINS)	PH2S (KPA)	ZN2+ (KG-MOL/M3)	ZN2+/PH2S (KG-MOL/M3 KPA)
2.00	6.28	N.D.	N.D.
6.00	16.36	N.D.	N.D.
10.00	21.98	N.D.	N.D.
15.00	25.77	N.D.	N.D.
30.00	30.16	N.D.	N.D.
45.00	31.48	N.D.	N.D.
60.00	31.91	N.D.	N.D.
90.00	31.98	.333E-01	.104E-02

MEASURED	(DP/DT)0	(KPA/MIN)	=	3.14
FITTED	(DP/DT)0	(KPA/MIN)	=	N.D.
MEASURED	(P)EQ	(KPA)	=	32.06
FITTED	(P)EQ	(KPA)	=	N.D.

TABLE I 56

EXPERIMENTAL RUN NO. = 149
SPHALERITE LEACHING IN AQUEOUS H2SO4

SPHAL. TYPE LEACHED		=	-125+106 WBM
TEMPERATURE	(K)	=	318.00
INITIAL MASS	(KG)	=	0.0450
STIRRER SPEED	(RPM)	=	1000.0
INITIAL H2SO4	(KG-MOL/M3)	=	1.0000
SPEC.SURFACE AREA	(M2/KG)	=	60.0

KDCALC (KPA M3/KG-MOL) = .1654E 04

TIME (MINS)	PH2S (KPA)	$[Zn^{2+}]$ $\times 10^3$ (kg-mol/m^3)	$(Fe)_{TOT}$	ZN2+/PH2S (KG-MOL/M3 KPA)
4.00	0.50	0.489	0.43	.973E-03
10.00	1.02	0.489	0.30	.489E-03
60.00	2.74	2.754	N.D.	.100E-02
90.00	4.28	3.626	N.D.	.848E-03
120.00	4.75	4.33	0.358	.912E-03
150.00	5.79	4.56	0.681	.788E-03
180.00	5.95	5.247	0.717	.883E-03

MEASURED	(DP/DT)0	(KPA/MIN)	=	0.14
FITTED	(DP/DT)0	(KPA/MIN)	=	N.D.
MEASURED	(P)EQ	(KPA)	=	5.95
FITTED	(P)EQ	(KPA)	=	N.D.

TABLE I 57

EXPERIMENTAL RUN NO. = 55
SPHALERITE LEACHING IN AQUEOUS H2SO4

SPHAL. TYPE LEACHED		=	-90+75 WBM
TEMPERATURE	(K)	=	318.00
INITIAL MASS	(KG)	=	0.0500
STIRRER SPEED	(RPM)	=	800.0
INITIAL H2SO4	(KG-MOL/M3)	=	1.0000
SPEC.SURFACE AREA	(M2/KG)	=	80.0

KDCALC (KPA M3/KG-MOL) = .1654E 04

TIME (MINS)	PH2S (KPA)	ZN2+ (KG-MOL/M3)	ZN2+/PH2S (KG-MOL/M3 KPA)
6.00	3.65	.198E-02	.544E-03
15.00	5.61	.267E-02	.476E-03
30.00	8.30	.466E-02	.562E-03
60.00	10.49	.632E-02	.603E-03
90.00	10.85	.738E-02	.680E-03
100.00	11.18	.792E-02	.708E-03

MEASURED	(DP/DT)0	(KPA/MIN)	=	0.86
FITTED	(DP/DT)0	(KPA/MIN)	=	N.D.
MEASURED	(P)EQ	(KPA)	=	11.18
FITTED	(P)EQ	(KPA)	=	N.D.

TABLE I 58

EXPERIMENTAL RUN NO. = 56
SPHALERITE LEACHING IN AQUEOUS H2SO4

SPHAL. TYPE LEACHED		=	-90+75 WVM
TEMPERATURE	(K)	=	318.00
INITIAL MASS	(KG)	=	0.0500
STIRRER SPEED	(RPM)	=	800.0
INITIAL H2SO4	(KG-MOL/M3)	=	1.0000
SPEC.SURFACE AREA	(M2/KG)	=	80.0

KDCALC (KPA M3/KG-MOL) = .1654E 04

TIME (MINS)	PH2S (KPA)	ZN2+ (KG-MOL/M3)	ZN2+/PH2S (KG-MOL/M3 KPA)
6.00	2.80	.198E-02	.709E-03
20.00	4.56	.357E-02	.782E-03
60.00	8.32	.559E-02	.672E-03
90.00	9.19	.651E-02	.708E-03
112.00	9.36	.746E-02	.796E-03

MEASURED	(DP/DT)0	(KPA/MIN)	=	0.75
FITTED	(DP/DT)0	(KPA/MIN)	=	N.D.
MEASURED	(P)EQ	(KPA)	=	9.19
FITTED	(P)EQ	(KPA)	=	N.D.

TABLE I 59

EXPERIMENTAL RUN NO. = 189
SPHALERITE LEACHING IN AQUEOUS H2SO4

SPHAL. TYPE LEACHED	=	WBM-75+63
TEMPERATURE (K)	=	318.00
INITIAL MASS (KG)	=	0.0500
STIRRER SPEED (RPM)	=	1000.0
INITIAL H2SO4 (KG-MOL/M3)	=	1.0000
SPEC.SURFACE AREA (M2/KG)	=	0.0
KDCALC (KPA M3/KG-MOL)	=	.1654E 04

TIME (MINS)	PH2S (KPA)	ZN2+ (KG-MOL/M3)	ZN2+/PH2S (KG-MOL/M3 KPA)
3.00	1.69	.168E-02	.996E-03
6.00	2.59	N.D.	N.D.
15.00	4.51	.329E-02	.729E-03
30.00	6.88	N.D.	N.D.
45.00	8.55	.569E-02	.666E-03
60.00	9.89	N.D.	N.D.
80.00	10.85	.711E-02	.655E-03

MEASURED (DP/DT)0	(KPA/MIN)	=	0.59
FITTED (DP/DT)0	(KPA/MIN)	=	N.D.
MEASURED (P)EQ	(KPA)	=	10.85
FITTED (P)EQ	(KPA)	=	N.D.

TABLE I 60

EXPERIMENTAL RUN NO. = 192
SPHALERITE LEACHING IN AQUEOUS H2SO4

SPHAL. TYPE LEACHED	=	W -75+63
TEMPERATURE (K)	=	318.00
INITIAL MASS (KG)	=	0.0500
STIRRER SPEED (RPM)	=	100.0
INITIAL H2SO4 (KG-MOL/M3)	=	1.0000
SPEC.SURFACE AREA (M2/KG)	=	0.0
KDCALC (KPA M3/KG-MOL)	=	.1654E 04

TIME (MINS)	PH2S (KPA)	ZN2+ (KG-MOL/M3)	ZN2+/PH2S (KG-MOL/M3 KPA)
3.00	2.40	.153E-02	.637E-03
6.00	3.65	N.D.	N.D.
10.00	4.90	N.D.	N.D.
15.00	5.99	.395E-02	.659E-03
30.00	8.16	.528E-02	.647E-03
45.00	9.53	N.D.	N.D.
60.00	10.76	.681E-02	.633E-03
85.00	11.91	N.D.	N.D.

MEASURED (DP/DT)0	(KPA/MIN)	=	0.62
FITTED (DP/DT)0	(KPA/MIN)	=	N.D.
MEASURED (P)EQ	(KPA)	=	11.91
FITTED (P)EQ	(KPA)	=	N.D.

TABLE I 61

EXPERIMENTAL RUN NO. = 152
SPHALERITE LEACHING IN AQUEOUS H2SO4

SPHAL. TYPE LEACHED	=	-75+53 WBM
TEMPERATURE (K)	=	318.00
INITIAL MASS (KG)	=	0.0450
STIRRER SPEED (RPM)	=	1000.0
INITIAL H2SO4 (KG-MOL/M3)	=	1.0000
SPEC.SURFACE-AREA (M2/KG)	=	80.0

KDCALC (KPA M3/KG-MOL) = .1654E 04

TIME (MINS)	PH2S (KPA)	$[Zn^{2+}]$ $\times 10^3$	$[Fe]_{TOT}$ (kg-mol/m3)	ZN2+/PH2S (KG-MOL/M3 KPA)
2.00	0.47	0.918	0.40	.195E-02
10.00	2.36	1.606	0.40	.682E-03
30.00	4.56	3.381	0.40	.741E-03
55.00	6.69	4.406	0.40	.659E-03
130.00	7.87	6.578	0.41	.836E-03
150.00	8.81	8.108	0.54	.755E-03

MEASURED (DP/DT)0	(KPA/MIN)	=	0.23
FITTED (DP/DT)0	(KPA/MIN)	=	N.D.
MEASURED (P)EQ	(KPA)	=	0.00
FITTED (P)EQ	(KPA)	=	N.D.

TABLE I 62

EXPERIMENTAL RUN NO. = 148
SPHALERITE LEACHING IN AQUEOUS H2SO4

SPHAL. TYPE LEACHED	=	-17+12 WBM
TEMPERATURE (K)	=	318.00
INITIAL MASS (KG)	=	0.0450
STIRRER SPEED (RPM)	=	1000.0
INITIAL H2SO4 (KG-MOL/M3)	=	1.0000
SPEC.SURFACE AREA (M2/KG)	=	320.0

KDCALC (KPA M3/KG-MOL) = .1654E 04

TIME (MINS)	PH2S (KPA)	$[Zn^{2+}]$ $\times 10^3$	$[Fe]_{TOT}$ (kg-mol/m3)	ZN2+/PH2S (KG-MOL/M3 KPA)
2.00	1.56	2.402	0.27	.154E-02
10.00	4.65	3.488	0.287	.750E-03
60.00	8.34	7.649	0.484	.917E-03
120.00	8.62	9.484	0.484	.110E-02
150.00	9.68	9.683	0.537	.100E-02
245.00	17.02	10.71	0.627	.629E-03
300.00	21.71	11.09	0.86	.510E-03
363.00	26.39	11.52	0.806	.436E-03
420.00	29.45	11.52	0.86	.391E-03
480.00	30.83	11.93	1.631	.387E-03

MEASURED (DP/DT)0	(KPA/MIN)	=	0.68
FITTED (DP/DT)0	(KPA/MIN)	=	N.D.
MEASURED (P)EQ	(KPA)	=	30.83
FITTED (P)EQ	(KPA)	=	N.D.

TABLE I 63

EXPERIMENTAL RUN NO. = 151
SPHALERITE LEACHING IN AQUEOUS H2SO4

SPHAL. TYPE LEACHED	=	-125+106 ZCR
TEMPERATURE (K)	=	318.00
INITIAL MASS (KG)	=	0.0450
STIRRER SPEED (RPM)	=	1000.0
INITIAL H2SO4 (KG-MOL/M3)	=	1.0000
SPEC.SURFACE AREA (M2/KG)	=	130.0

KDCALC (KPA M3/KG-MOL) = .1654E 04

TIME (MINS)	PH2S (KPA)	$[Zn^{2+}]$ $\times 10^3$ (kg-mol/m3)	$[Fe]_{TOT}$	ZN2+/PH2S (KG-MOL/M3 KPA)
2.00	0.01	0.512	0.55	.786E-01
20.00	-0.39	1.071	0.88	N.D.
40.00	0.48	1.085	0.41	.225E-02
60.00	1.19	1.973	0.58	.166E-02
135.00	4.81	5.278	0.84	.110E-02
180.00	6.79	6.884	1.47	.101E-02

TABLE I 64

EXPERIMENTAL RUN NO. = 150
SPHALERITE LEACHING IN AQUEOUS H2SO4

SPHAL. TYPE LEACHED	=	-75+53 ZCR
TEMPERATURE (K)	=	318.00
INITIAL MASS (KG)	=	0.0450
STIRRER SPEED (RPM)	=	1000.0
INITIAL H2SO4 (KG-MOL/M3)	=	1.0000
SPEC.SURFACE AREA (M2/KG)	=	160.0

KDCALC (KPA M3/KG-MOL) = .1654E 04

TIME (MINS)	PH2S (KPA)	$[Zn^{2+}]$ $\times 10^3$ (kg-mol/m3)	$[Fe]_{TOT}$	ZN2+/PH2S (KG-MOL/M3 KPA)
3.00	0.08	0.304	0.41	.382E-02
90.00	1.89	3.671	0.82	.194E-02
120.00	2.75	4.865	1.16	.176E-02
178.00	4.97	7.037	1.02	.142E-02

TABLE I 65

EXPERIMENTAL RUN NO. = 147
SPHALERITE LEACHING IN AQUEOUS H2SO4

SPHAL. TYPE LEACHED		= -17+12 ZCR
TEMPERATURE	(K)	= 318.00
INITIAL MASS	(KG)	= 0.0450
STIRRER SPEED	(RPM)	= 1000.0
INITIAL H2SO4	(KG-MOL/M3)	= 1.0000
SPEC.SURFACE AREA	(M2/KG)	= 420.0

KDCALC (KPA M3/KG-MOL) = .1654E 04

TIME (MINS)	PH2S (KPA)	$[Zn^{2+}]$ $\times 10^3$ (kg-mol/m^3)	$[Fe]_{TOT}$	ZN2+/PH2S (KG-MOL/M3 KPA)
2.60	0.06	0.881	0.842	.130E-01
60.00	1.97	2.94	0.896	.149E-02
120.00	6.81	9.026	1.033	.133E-02
180.00	11.40	11.40	1.219	.100E-02
240.00	18.05	12.70	1.434	.703E-03
300.00	23.21	13.77	1.613	.593E-03
360.00	26.96	14.07	1.703	.522E 00
420.00	30.08	16.22	2.366	.539E-03

TABLE I 66

EXPERIMENTAL RUN NO. = 145
SPHALERITE LEACHING IN AQUEOUS H2SO4

SPHAL. TYPE LEACHED		= -125+106 PR
TEMPERATURE	(K)	= 318.00
INITIAL MASS	(KG)	= 0.0450
STIRRER SPEED	(RPM)	= 1000.0
INITIAL H2SO4	(KG-MOL/M3)	= 1.0000
SPEC.SURFACE AREA	(M2/KG)	= 130.0

KDCALC (KPA M3/KG-MOL) = .1654E 04

TIME (MINS)	PH2S (KPA)	$[Zn^{2+}]$ $\times 10^3$ (kg-mol/m^3)	$[Fe]_{TOT}$	ZN2+/PH2S (KG-MOL/M3 KPA)
4.00	0.44	0.291	0.717	.659E-03
20.00	1.07	0.26	0.43	.243E-03
60.00	2.01	1.101	0.556	.546E-03
90.00	4.22	1.897	0.878	.451E-03
120.00	7.36	3.014	0.95	.409E-03
240.00	14.75	4.406	1.79	.299E-03
300.00	26.84	5.92	2.10	.221E-03
360.00	27.34	6.72	2.545	.246E-03

TABLE I 67

EXPERIMENTAL RUN NO. = 146
SPHALERITE LEACHING IN AQUEOUS H2SO4

SPHAL. TYPE LEACHED		= -75+53 PR
TEMPERATURE	(K)	= 318.00
INITIAL MASS	(KG)	= 0.0450
STIRRER SPEED	(RPM)	= 1000.0
INITIAL H2SO4	(KG-MOL/M3)	= 1.0000
SPEC.SURFACE AREA	(M2/KG)	= 160.0

KDCALC (KPA M3/KG-MOL) = .1654E 04

TIME (MINS)	PH2S (KPA)	$[Zn^{2+}]$ $\times 10^3$ (kg-mol/m^3)	$[Fe]_{TOT}$	ZN2+/PH2S (KG-MOL/M3 KPA)
4.00	0.16	0.199	0.448	.127E-02
40.00	2.52	1.346	0.896	.536E-03
65.00	5.95	2.493	1.61	.419E-03
180.00	22.74	6.31	4.122	.278E-03
240.00	28.63	6.884	4.48	.240E-03
330.00	36.50	8.23	5.37	.225E-03
360.00	37.60	8.23	5.91	.219E-03
390.00	38.70	8.261	5.914	.214E-03

TABLE I 68

EXPERIMENTAL RUN NO. = 144
SPHALERITE LEACHING IN AQUEOUS H2SO4

SPHAL. TYPE LEACHED		= -17+12 PR
TEMPERATURE	(K)	= 318.00
INITIAL MASS	(KG)	= 0.0450
STIRRER SPEED	(RPM)	= 1000.0
INITIAL H2SO4	(KG-MOL/M3)	= 1.0000
SPEC.SURFACE AREA	(M2/KG)	= 420.0

KDCALC (KPA M3/KG-MOL) = .1654E 04

TIME (MINS)	PH2S (KPA)	$[Zn^{2+}]$ $\times 10^3$ (kg-mol/m^3)	$[Fe]_{TOT}$	ZN2+/PH2S (KG-MOL/M3 KPA)
2.00	0.02	0.612	N.D.	.262E-01
14.00	0.19	0.642	0.806	.338E-02
40.00	-1.73	1.209	0.896	N.D.
60.00	-2.28	2.54	1.147	N.D.
140.00	2.22	6.195	2.01	.279E-02
240.00	12.84	9.255	5.02	.720E-03
304.00	20.55	9.974	7.348	.485E-03
374.00	28.30	10.56	11.11	.373E-03
453.00	36.24	10.63	15.23	.293E-03

A P P E N D I X J

TABULATED EXPERIMENTAL RESULTS

FOR LEACHING UNDER CASE (ii) CONDITIONS

($[Fe^{3+}]_o$: $[H_2SO_4]_o \geq 1,8$)

The procedure adspted for processing case (ii) experimental leaching results is described in section G. 2.

TABLE J 1

SPHALERITE LEACHING IN ACIDIC FE2(SO4)3
EXPERIMENTAL RUN NO. = 122 (-125,0+106,0 µm)
SPHAL. TYPE LEACHED = WBM
TEMPERATURE (K) = 358,0
STIRRER SPEED (RPM) = 800.0
INITIAL FE3+ (KG-MOL/M3) = 0.9848
INITIAL H2SO4 (KG-MOL/M3) = N.D.
INITIAL AREA (M2/KG) = 65.0
INITIAL SOLIDS MASS (KG) = 0.1000

TIME (MINS)	ZN2+ (KG-MOL/M3)	FE3+ (KG-MOL/M3)	H2SO4 (KG-MOL/M3)
7,50	.152 E-01	.985E 00	N.D.
32,00	.537 E-01	.888E 00	N.D.
90,00	.985 E-01	.788E 00	N.D.
165,00	.136 E 00	.716E 00	N.D.

FINAL EXTENT X (-) = 0.2703
FINAL AREA (M2/KG) = 102.00
TOTAL DRY RESIDUE (KG) = 0.0769
SULPHUR EXTRACTED (KG) = 0.0076

MEAS. INTL RATE(KG-MOL/MIN M3) = 0.0019

TABLE J 2

SPHALERITE LEACHING IN ACIDIC FE2(SO4)3
EXPERIMENTAL RUN NO. = 130
SPHAL. TYPE LEACHED = WBM(-30,0+75,0)
TEMPERATURE (K) = 318.00
STIRRER SPEED (RPM) = 1000.0
INITIAL FE3+ (KG-MOL/M3) = 1.0386
INITIAL H2SO4 (KG-MOL/M3) = 0.8224
INITIAL AREA (M2/KG) = 80.0
INITIAL SOLIDS MASS (KG) = 0.1500

TIME (MINS)	ZN2+ (KG-MOL/M3)	FE3+ (KG-MOL/M3)	H2SO4 (KG-MOL/M3)
6,00	.612E-02	.104E 01	N.D.
30,00	.184E-01	.967E 00	N.D.
60,00	.283E-01	.950E 00	N.D.
122,00	.428E-01	.949E 00	N.D.
240,00	.629E-01	.870E 00	N.D.
560,00	.109E 00	.741E 00	N.D.
1230,00	.179E 00	.600E 00	N.D.

FINAL EXTENT X (-) = 0.1171
FINAL AREA (M2/KG) = 77.00
TOTAL DRY RESIDUE (KG) = 0.1110
SULPHUR EXTRACTED (KG) = 0.0058

MEAS. INTL RATE(KG-MOL/MIN M3) = .667E-03

TABLE J 3

SPHALERITE LEACHING IN ACIDIC FE2(SO4)3
EXPERIMENTAL RUN NO. = 46
SPHAL. TYPE LEACHED = WBM (-75,0+63,0µm)
SIZE FRACTION X10^{6} (M) = -75,0 + 63,0
TEMPERATURE (K) = 343,0
STIRRER SPEED (RPM) = 800,0
INITIAL FE3+ (KG-MOL/M3) = 0,8147
INITIAL H2SO4 (KG-MOL/M3) = 0,337
INITIAL AREA (M2/KG) = 80,0
INITIAL SOLIDS MASS (KG) = 0,1

TIME (MINS)	ZN2+ (KG-MOL/M3)	FE3+ (KG-MOL/M3)	H2SO4 (KG-MOL/M3)
1,5	0,00466	0,824	0,337
5,5	0,0116	0,815	0,316
10,0	0,0185	0,788	0,326
30,0	0,0382	0,761	0,332
65,0	0,0598	0,695	0,326
122,0	0,0918	0,632	0,337
180,0	0,12	0,60	0,326
435,0	0,199	0,442	0,339
495,0	0,214	0,405	0,342

Final extent X (-) = 0,2102
Final area (m^{2}/kg) = 90,1
Total dry residue (kg) = 0058
SULPHUR extracted (kg) = 0,034
Meas. Intl. rate (mol/min m^{3}) = 0,0033

TABLE J 4

SPHALERITE LEACHING IN ACIDIC FE2(SO4)3
EXPERIMENTAL RUN NO. = 48
SPHAL. TYPE LEACHED = WBM(-75,0 +63,0 µm)
TEMPERATURE (K) = 355.50
STIRRER SPEED (RPM) = 800.0
INITIAL FE3+ (KG-MOL/M3) = 0.7950
INITIAL H2SO4 (KG-MOL/M3) = 0.2980
INITIAL AREA (M2/KG) = 80.0
INITIAL SOLIDS MASS (KG) = 0.1000

TIME (MINS)	ZN2+ (KG-MOL/M3)	FE3+ (KG-MOL/M3)	H2SO4 (KG-MOL/M3)
2.00	.627E-02	.768E 00	.306E 00
5.00	.217E-01	.750E 00	.311E 00
15.00	.451E-01	.725E 00	.317E 00
30.00	.642E-01	.698E 00	.300E 00
45.00	.814E-01	.671E 00	.316E 00
75.00	.113E 00	.609E 00	.332E 00

FINAL EXTENT X (-) = 0.1111
FINAL AREA (M2/KG) = 90.10
TOTAL DRY RESIDUE (KG) = 0.0024
SULPHUR EXTRACTED (KG) = 0.0035

MEAS. INTL RATE(KG-MOL/MIN M3) = .429 E-02

TABLE J 5

SPHALERITE LEACHING IN ACIDIC FE2(SO4)3
EXPERIMENTAL RUN NO. = 47
SPHAL. TYPE LEACHED = WBM(-75,0+63,0µm)
TEMPERATURE (K) = 368.00
STIRRER SPEED (RPM) = 800.0
INITIAL FE3+ (KG-MOL/M3) = 1.5041
INITIAL H2SO4 (KG-MOL/M3) = 0.5612
INITIAL AREA (M2/KG) = 80.0
INITIAL SOLIDS MASS (KG) = 0.1000

TIME (MINS)	ZN2+ (KG-MOL/M3)	FE3+ (KG-MOL/M3)	H2SO4 (KG-MOL/M3)
2.00	.181E-01	.149E 01	.571E 00
5.00	.467E-01	.145E 01	.566E 00
10.00	.704E-01	.139E 01	.582E 00
30.00	.150E 00	.127E 01	.612E 00
45.00	.196E 00	.124E 01	.600E 00
77.00	.277E 00	.103E 01	.638E 00
137.00	.356E 00	.843E 00	.648E 00
197.00	.392E 00	.716E 00	.684E 00

FINAL EXTENT X (-) = 0.3844
FINAL AREA (M2/KG) = 105.70
TOTAL DRY RESIDUE (KG) = 0.0630
SULPHUR EXTRACTED (KG) = 0.0116

MEAS. INTL RATE(KG-MOL/MIN M3) = .125 E-0

TABLE J 6

SPHALERITE LEACHING IN ACIDIC FE2(SO4)3
EXPERIMENTAL RUN NO. = 128
SPHAL. TYPE LEACHED = WBM (-32,0+24,0µm)
TEMPERATURE (K) = 318.00
STIRRER SPEED (RPM) = 1000.0
INITIAL FE3+ (KG-MOL/M3) = 0.2256
INITIAL H2SO4 (KG-MOL/M3) = 0.1224
INITIAL AREA (M2/KG) = 140.0
INITIAL SOLIDS MASS (KG) = 0.0500

TIME (MINS)	ZN2+ (KG-MOL/M3)	FE3+ (KG-MOL/M3)	H2SO4 (KG-MOL/M3)
2.00	.214E-02	.217E 00	.871E 00
10.00	.490E-02	.202E 00	N.D.
30.00	.106E-01	.193E 00	.880E 00
130.00	.259E-01	.149E 00	N.D.

FINAL EXTENT X (-) = 0.0512
FINAL AREA (M2/KG) = 199.00
TOTAL DRY RESIDUE (KG) = 0.0707
SULPHUR EXTRACTED (KG) = 0.0022

MEAS. INTL RATE(KG-MOL/MIN M3) = .555 E-03

TABLE J 7

SPHALERITE LEACHING IN ACIDIC FE2(SO4)3
EXPERIMENTAL RUN NO. = 127
SPHAL. TYPE LEACHED = WBM
SIZE FRACTION $X10^6$ (M) = -24.0+17.0
TEMPERATURE (K) = 318.0
STIRRER SPEED (RPM) = 1000.0
INITIAL FE3+ (KG-MOL/M3) = 0.2131
INITIAL H2SO4 (KG-MOL/M3) = 0.1235
INITIAL AREA (M2/KG) = 320.0
INITIAL SOLIDS MASS (KG) = 0.05

TIME (MINS)	ZN2+ (KG-MOL/M3)	FE3+ (KG-MOL/M3)	H2SO4 (KG-MOL/M3)
1.8	0.179 E-02	0.220	0.112
7.0	0.314 E-02	0.213	0.110
30.0	0.788E-02	0.200	0.116

Meas. intl. rate (kg-mol/m^3) = 0.001

TABLE J 8

SPHALERITE LEACHING IN ACIDIC FE2(SO4)3
EXPERIMENTAL RUN NO. = 74
SPHAL. TYPE LEACHED = WBM (-17.0+12.0 μm)
TEMPERATURE (K) = 323.00
STIRRER SPEED (RPM) = 800.0
INITIAL FE3+ (KG-MOL/M3) = 0.1468
INITIAL H2SO4 (KG-MOL/M3) = 0.0612
INITIAL AREA (M2/KG) = 420.0
INITIAL SOLIDS MASS (KG) = 0.0300

TIME (MINS)	ZN2+ (KG-MOL/M3)	FE3+ (KG-MOL/M3)	H2SO4 (KG-MOL/M3)
5.50	.291E-02	.134E 00	.602E-01
15.00	.459E-02	.133E 00	.592E-01
30.00	.688E-02	.131E 00	.602E-01
60.00	.118E-01	.122E 00	.602E-01

FINAL EXTENT X (-) = 0.3854
FINAL AREA (M2/KG) = 359.40
TOTAL DRY RESIDUE (KG) = 0.0261
SULPHUR EXTRACTED (KG) = 0.0003

MEAS. INTL RATE(KG-MOL/MIN M3) = .580 E-03

TABLE J 9

SPHALERITE LEACHING IN ACIDIC FE2(SO4)3
EXPERIMENTAL RUN NO. = 116
SPHAL. TYPE LEACHED = VMWBM
TEMPERATURE (K) = 318.00
STIRRER SPEED (RPM) = 800.0
INITIAL FE3+ (KG-MOL/M3) = 0.1504
INITIAL H2SO4 (KG-MOL/M3) = 0.0510
INITIAL AREA (M2/KG) = 3272.0
INITIAL SOLIDS MASS (KG) = 0.0200

TIME (MINS)	ZN2+ (KG-MOL/M3)	FE3+ (KG-MOL/M3)	H2SO4 (KG-MOL/M3)
5.50	.110E-01	.118E 00	.500E-01
15.50	.161E-01	.113E 00	.469E-01
33.00	.236E-01	.949E-01	.531E-01
69.00	.333E-01	.788E-01	.490E-01

FINAL EXTENT X (-) = 0.2110
FINAL AREA (M2/KG) = 1637.00
TOTAL DRY RESIDUE (KG) = 0.0164
SULPHUR EXTRACTED (KG) = 0.0012

MEAS. INTL RATE(KG-MOL/MIN M3) = .210E-02

TABLE J 10

SPHALERITE LEACHING IN ACIDIC FE2(SO4)3
EXPERIMENTAL RUN NO. = 118
SPHAL. TYPE LEACHED = VMWBM
TEMPERATURE (K) = 338.00
STIRRER SPEED (RPM) = 800.0
INITIAL FE3+ (KG-MOL/M3) = 0.3044
INITIAL H2SO4 (KG-MOL/M3) = 0.0735
INITIAL AREA (M2/KG) = 3272.0
INITIAL SOLIDS MASS (KG) = 0.0200

TIME (MINS)	ZN2+ (KG-MOL/M3)	FE3+ (KG-MOL/M3)	H2SO4 (KG-MOL/M3)
4.50	.260E-01	.272E 00	N.D.
15.00	.382E-01	.210E 00	N.D.
45.00	.512E-01	.188E 00	N.D.
74.50	.630E-01	.183E 00	N.D.
255.00	.956E-01	.118E 00	N.D.

FINAL EXTENT X (-) = 0.5600
FINAL AREA (M2/KG) = 1309.00
TOTAL DRY RESIDUE. (KG) = 0.0121
SULPHUR EXTRACTED (KG) = 0.0023

MEAS. INTL RATE(KG-MOL/MIN M3) = .690E-02

TABLE J 11

SPHALERITE LEACHING IN ACIDIC FE2(SO4)3
EXPERIMENTAL RUN NO. = 10
SPHAL. TYPE LEACHED = ZCR
SIZE FRACTION $X10^6$ (M) = -212.0
TEMPERATURE (K) = 303.00
STIRRER SPEED (RPM) = 800.0
INITIAL FE3+ (KG-MOL/M3) = 0.3760
INITIAL H2SO4 (KG-MOL/M3) = 0.1837
INITIAL AREA (M2/KG) = 450.5
INITIAL SOLIDS MASS (KG) = 0.0200

TIME (MINS)	ZN2+ (KG-MOL/M3)	FE3+ (KG-MOL/M3)	H2SO4 (KG-MOL/M3)
1.50	.734E-02	.358E 00	.184E 00
7.00	.795E-02	.358E 00	.176E 00
60.00	.144E-01	.347E 00	.173E 00
90.00	.165E-01	.340E 00	.178E 00
120.00	.199E-01	.333E 00	N.D.

MEAS. INTL. RATE (kg-mol/m^3.min) = 0.101 E-03
MEAS INTL [Zn^{2+}] (kg-mol/m^3) = 0.0068

TABLE J 12

SPHALERITE LEACHING IN ACIDIC FE2(SO4)3
EXPERIMENTAL RUN NO. = 11
SPHAL. TYPE LEACHED = ZCR
SIZE FRACTION $X10^6$ (M) = -212.0
TEMPERATURE (K) = 323.00
STIRRER SPEED (RPM) = 800.0
INITIAL FE3+ (KG-MOL/M3) = 0.3760
INITIAL H2SO4 (KG-MOL/M3) = 0.1837
INITIAL AREA (M2/KG) = 450.5
INITIAL SOLIDS MASS (KG) = 0.0200

TIME (MINS)	ZN2+ (KG-MOL/M3)	FE3+ (KG-MOL/M3)	H2SO4 (KG-MOL/M3)
1.00	.704E-02	.376E 00	.184E 00
20.00	.159E-01	.355E 00	.184E 00
120.00	.428E-01	.304E 00	N.D.
150.00	.482E-01	.297E 00	N.D.

MEAS. INTL.RATE(kg-mol/m^3min) = 0.372 E-03
MEAS. INTL.[Zn^{2+}] (kg-mol/m^3) = 0.0064

TABLE J 13

SPHALERITE LEACHING IN ACIDIC FE2(SO4)3
EXPERIMENTAL RUN NO. = 9
SPHAL. TYPE LEACHED = ZCR
SIZE FRACTION $X10^6$ (M) = -212.0
TEMPERATURE (K) = 358.00
STIRRER SPEED (RPM) = 800.0
INITIAL FE3+ (KG-MOL/M3) = 0.3760
INITIAL H2SO4 (KG-MOL/M3) = 0.1939
INITIAL AREA (M2/KG) = 450.5
INITIAL SOLIDS MASS (KG) = 0.0200

TIME (MINS)	ZN2+ (KG-MOL/M3)	FE3+ (KG-MOL/M3)	H2SO4 (KG-MOL/M3)
1.50	.147E-01	.322E 00	.176E 00
5.00	.245E-01	.322E 00	.176E 00
15.00	.398E-01	.308E 00	N.D.
30.00	.566E-01	.265E 00	.184E 00
45.00	.704E-01	.244E 00	.204E 00
61.00	.826E-01	.215E 00	N.D.
75.00	.878E-01	.197E 00	.194E 00
90.00	.933E-01	.192E 00	.190E 00
120.90	.102E 00	.172E 00	.194E 00
150.00	.112E 00	.158E 00	.194E 00

MEAS. INTL.RATE(kg-mol/m^3min) = 0,1176 E-02
MEA S. INTL.(Zn^{2+})(kg-mol/m^3) = 0,0279

TABLE J 14

SPHALERITE LEACHING IN ACIDIC FE2(SO4)3
EXPERIMENTAL RUN NO. = 12
SPHAL. TYPE LEACHED = ZCR
SIZE FRACTION $X10^6$ (M) = -212.0
TEMPERATURE (K) = 373.00
STIRRER SPEED (RPM) = 800.0
INITIAL FE3+ (KG-MOL/M3) = 0.3671
INITIAL H2SO4 (KG-MOL/M3) = 0.1878
INITIAL AREA (M2/KG) = 450.5
INITIAL SOLIDS MASS (KG) = 0.0200

TIME (MINS)	ZN2+ (KG-MOL/M3)	FE3+ (KG-MOL/M3)	H2SO4 (KG-MOL/M3)
1.00	.272E-01	.356E 00	.184E 00
5.00	.324E-01	.322E 00	.185E 00
10.00	.474E-01	.283E 00	N.D.
15.00	.548E-01	.265E 00	N.D.
30.00	.765E-01	.222E 00	N.D.
60.00	.973E-01	.168E 00	N.D.
90.00	.115E 00	.147E 00	.206E 00
120.00	.121E 00	.125E 00	N.D.
150.00	.126E 00	.111E 00	.214E 00
205.00	.137E 00	.931E-01	.133E-01
223.00	.141E 00	.859E-01	N.D.

MEAS. INTL.RATE (kg-mol/m^3min) = 0,2357 E-02
MEAS INTL (Zn^{2+}) (kg-mol/m) = 0,0229

TABLE J 15

SPHALERITE LEACHING IN ACIDIC FE2(SO4)3
EXPERIMENTAL RUN NO. = 14
SPHAL. TYPE LEACHED = ZCR
SIZE FRACTION $X10^6$ (M) = -106.0+90.0
TEMPERATURE (K) = 343.00
STIRRER SPEED (RPM) = 800.0
INITIAL FE3+ (KG-MOL/M3) = 0.3832
INITIAL H2SO4 (KG-MOL/M3) = 0.1878
INITIAL AREA (M2/KG) = 140.0
INITIAL SOLIDS MASS (KG) = 0.0200

TIME (MINS)	ZN2+ (KG-MOL/M3)	FE3+ (KG-MOL/M3)	H2SO4 (KG-MOL/M3)
2.00	.434E-02	.383E 00	.188E 00
6.00	.120E-01	.383E 00	N.D.
15.00	.160E-01	.365E 00	N.D.
30.00	.212E-01	.351E 00	N.D.
45.00	.297E-01	.337E 00	.188E 00
60.00	.344E-01	.324E 00	N.D.
90.00	.428E-01	.304E 00	N.D.
120.00	.520E-01	.286E 00	.186E 00
150.00	.578E-01	.269E 00	N.D.
210.00	.661E-01	.251E 00	.190E 00
303.00	.747E-01	.231E 00	.191E 00
325.00	.872E-01	.215E 00	.192E 00
360.00	.884E-01	.210E 00	N.D.

MEAS. INTL.RATE (kg-mol/m^3min) = 0,421 E-03
MEAS INTL (Zn^{2+}) (kg-mol/m^3) = 0,0092

TABLE J 16

SPHALERITE LEACHING IN ACIDIC FE2(SO4)3
EXPERIMENTAL RUN NO. = 124
SPHAL. TYPE LEACHED = ZCR
SIZE FRACTION $X10^6$ (M) = -106.0+ 90.0
TEMPERATURE (K) = 358.00
STIRRER SPEED (RPM) = 800.0
INITIAL FE3+ (KG-MOL/M3) = 0.3438
INITIAL H2SO4 (KG-MOL/M3) = N.D.
INITIAL AREA (M2/KG) = 140.0
INITIAL SOLIDS MASS (KG) = 0.0500

TIME (MINS)	ZN2+ (KG-MOL/M3)	FE3+ (KG-MOL/M3)	H2SO4 (KG-MOL/M3)
6.00	.262E-01	.299E 00	N.D.
15.00	.421E-01	.258E 00	N.D.
30.00	.598E-01	.215E 00	N.D.
50.00	.750E-01	.201E 00	N.D.

FINAL EXTENT X (-) = 0.1590
FINAL AREA (M2/KG) = 295.30
TOTAL DRY RESIDUE (KG) = 0.0400
SULPHUR EXTRACTED (KG) = 0.0020

MEAS. INTL RATE(KG-MOL/MIN M3) = .187E-02
MEAS. INTL. ZN2+ (KG-MOL/M3) = 0.0150

TABLE J 17

SPHALERITE LEACHING IN ACIDIC FE2(SO4)3
EXPERIMENTAL RUN NO. = 18
SPHAL. TYPE LEACHED = ZCR
SIZE FRACTION $X10^6$ (M) = -106.0+90.0
TEMPERATURE (K) = 368.00
STIRRER SPEED (RPM) = 800.0
INITIAL FE3+ (KG-MOL/M3) = 0.3617
INITIAL H2SO4 (KG-MOL/M3) = 0.1867
INITIAL AREA (M2/KG) = 140.0
INITIAL SOLIDS MASS (KG) = 0.0200

TIME (MINS)	ZN2+ (KG-MOL/M3)	FE3+ (KG-MOL/M3)	H2SO4 (KG-MOL/M3)
2.00	.857E-02	.358E 00	.187E 00
6.00	.177E-01	.337E 00	N.D.
10.00	.268E-01	.315E 00	N.D.
15.00	.337E-01	.297E 00	N.D.
30.00	.502E-01	.254E 00	.190E 00
45.00	.636E-01	.229E 00	N.D.
60.00	.728E-01	.204E 00	N.D.
90.00	.849E-01	.174E 00	N.D.
140.00	.959E-01	.143E 00	N.D.
180.00	.109E 00	.122E 00	N.D.

MEAS. INTL.RATE (kg-mol/m^3min) = 2.32×10^{-3}
MEAS INTL (Zn^{2+}) (kg-mol/m^3) = 0.0033

TABLE J 18

SPHALERITE LEACHING IN ACIDIC FE2(SO4)3
EXPERIMENTAL RUN NO. = 23
SPHAL. TYPE LEACHED = ZCR
SIZE FRACTION $X10^6$ (M) = -106.0+ 90.0
TEMPERATURE (K) = 368.00
STIRRER SPEED (RPM) = 800.0
INITIAL FE3+ (KG-MOL/M3) = 0.9270
INITIAL H2SO4 (KG-MOL/M3) = 0.4692
INITIAL AREA (M2/KG) = 140.0
INITIAL SOLIDS MASS (KG) = 0.0500

TIME (MINS)	ZN2+ (KG-MOL/M3)	FE3+ (KG-MOL/M3)	H2SO4 (KG-MOL/M3)
2.00	.242E-01	.906E 00	.459E 00
5.00	.471E-01	.865E 00	.473E 00
10.00	.765E-01	.777E 00	.482E 00
20.00	.116E 00	.686E 00	.488E 00
30.00	.151E 00	.616E 00	.490E 00
45.00	.181E 00	.537E 00	.498E 00
60.00	.208E 00	.480E 00	.504E 00
62.00	.223E 00	.476E 00	.512E 00
70.00	.231E 00	.455E 00	N.D.
80.00	.237E 00	.444E 00	N.D.
90.00	.263E 00	.423E 00	.518E 00
105.00	.266E 00	.401E 00	.524E 00
135.00	.281E 00	.347E 00	.527E 00
165.00	.297E 00	.313E 00	.524E 00

FINAL EXTENT X (-) = 0.4420
FINAL AREA (M2/KG) = 337.40
TOTAL DRY RESIDUE (KG) = 0.0292
SULPHUR EXTRACTED (KG) = 0.0043

MEAS. INTL RATE(KG-MOL/MIN M3) = .600E-02
MEAS. INTL. ZN2+ (KG-MOL/M3) = 0.0150

TABLE J 19

SPHALERITE LEACHING IN ACIDIC FE2(SO4)3
EXPERIMENTAL RUN NO. = 120
SPHAL. TYPE LEACHED = ZCR
SIZE FRACTION $X10^6$ (M) = -90.0+ 75.0
TEMPERATURE (K) = 338.00
STIRRER SPEED (RPM) = 800.0
INITIAL FE3+ (KG-MOL/M3) = 0.3044
INITIAL H2SO4 (KG-MOL/M3) = N.D.
INITIAL AREA (M2/KG) = 150.0
INITIAL SOLIDS MASS (KG) = 0.0500

TIME (MINS)	ZN2+ (KG-MOL/M3)	FE3+ (KG-MOL/M3)	H2SO4 (KG-MOL/M3)
4.00	.903E-02	.286E 00	N.D.
20.00	.207E-01	.272E 00	N.D.
75.00	.444E-01	.224E 00	N.D.

FINAL EXTENT X (-) = 0.0940
FINAL AREA (M2/KG) = 308.50
TOTAL DRY RESIDUE (KG) = 0.0418
SULPHUR EXTRACTED (KG) = 0.0013

MEAS. INTL RATE(KG-MOL/MIN M3) = .970E-03
MEAS. INTL. ZN2+ (KG-MOL/M3) = 0.0050

TABLE J 20

SPHALERITE LEACHING IN ACIDIC FE2(SO4)3
EXPERIMENTAL RUN NO. = 24
SPHAL. TYPE LEACHED = ZCR
SIZE FRACTION $X10^6$ (M) = -90.0+ 75.0
TEMPERATURE (K) = 343.00
STIRRER SPEED (RPM) = 800.0
INITIAL FE3+ (KG-MOL/M3) = 0.9132
INITIAL H2SO4 (KG-MOL/M3) = 0.4592
INITIAL AREA (M2/KG) = 150.0
INITIAL SOLIDS MASS (KG) = 0.0500

TIME (MINS)	ZN2+ (KG-MOL/M3)	FE3+ (KG-MOL/M3)	H2SO4 (KG-MOL/M3)
1.00	.106E-01	.911E 00	.455E 00
5.00	.200E-01	.906E 00	.451E 00
10.00	.359E-01	.859E 00	.459E 00
15.00	.451E-01	.845E 00	.471E 00
30.00	.704E-01	.757E 00	.469E 00
45.00	.803E-01	.734E 00	.469E 00
60.00	.109E 00	.695E 00	.465E 00

FINAL EXTENT X (-) = 0.2309
FINAL AREA (M2/KG) = 311.20
TOTAL DRY RESIDUE (KG) = 0.0390
SULPHUR EXTRACTED (KG) = 0.0019

MEAS. INTL RATE(KG-MOL/MIN M3) = .240E-02
MEAS. INTL. ZN2+ MOL/M3) = 0.0100

TABLE J 21

SPHALERITE LEACHING IN ACIDIC FE2(SO4)3
EXPERIMENTAL RUN NO. = 26
SPHAL. TYPE LEACHED = ZCR
SIZE FRACTION $X10^6$ (M) = -90.0+ 75.0
TEMPERATURE (K) = 368.00
STIRRER SPEED (RPM) = 800.0
INITIAL FE3+ (KG-MOL/M3) = 1.4826
INITIAL H2SO4 (KG-MOL/M3) = 0.8041
INITIAL AREA (M2/KG) = 150.0
INITIAL SOLIDS MASS (KG) = 0.1000

TIME (MINS)	ZN2+ (KG-MOL/M3)	FE3+ (KG-MOL/M3)	H2SO4 (KG-MOL/M3)
5.00	.102E 00	.136E 01	.790E 00
15.00	.223E 00	.111E 01	.788E 00
30.00	.312E 00	.867E 00	.794E 00
46.00	.382E 00	.738E 00	.806E 00
60.00	.416E 00	.648E 00	.812E 00
90.00	.477E 00	.501E 00	.822E 00
150.00	.581E 00	.344E 00	.841E 00
215.00	.639E 00	.201E 00	.841E 00

FINAL EXTENT X (-) = 0.6830
FINAL AREA (M2/KG) = 234.30
TOTAL DRY RESIDUE (KG) = 0.0454
SULPHUR EXTRACTED (KG) = 0.0138

MEAS. INTL RATE(KG-MOL/MIN M3) = .118E-01
MEAS. INTL. ZN2+ (KG-MOL/M3) = 0.0300

TABLE J 22

SPHALERITE LEACHING IN ACIDIC FE2(SO4)3
EXPERIMENTAL RUN NO. = 27
SPHAL. TYPE LEACHED = ZCR
SIZE FRACTION $X10^6$ (M) = -90.0 +75.0
TEMPERATURE (K) = 368.00
STIRRER SPEED (RPM) = 800.0
INITIAL FE3+ (KG-MOL/M3) = 0.9025
INITIAL H2SO4 (KG-MOL/M3) = 0.4745
INITIAL AREA (M2/KG) = 150.0
INITIAL SOLIDS MASS (KG) = 0.1000

TIME (MINS)	ZN2+ (KG-MOL/M3)	FE3+ (KG-MOL/M3)	H2SO4 (KG-MOL/M3)
3.00	.589E-01	.818E 00	.456E 00
6.00	.987E-01	.731E 00	.445E 00
10.00	.133E 00	.630E 00	.451E 00
15.00	.170E 00	.573E 00	.459E 00
30.00	.237E 00	.415E 00	.471E 00
60.00	.323E 00	.231E 00	.482E 00
75.00	.361E 00	.159E 00	.484E 00

FINAL EXTENT X (-) = 0.3840
FINAL AREA (M2/KG) = 316.70
TOTAL DRY RESIDUE (KG) = 0.0482
SULPHUR EXTRACTED (KG) = 0.0084

MEAS. INTL RATE(KG-MOL/MIN M3) = .120E-01
MEAS. INTL. ZN2+ (KG-MOL/M3) = 0.0250

TABLE J 23

SPHALERITE LEACHING IN ACIDIC FE2(SO4)3
EXPERIMENTAL RUN NO. = 49
SPHAL. TYPE LEACHED = ZCR
SIZE FRACTION $X10^6$ (M) = -75.0+ 63.0
TEMPERATURE (K) = 323.00
STIRRER SPEED (RPM) = 800.0
INITIAL FE3+ (KG-MOL/M3) = 0.8864
INITIAL H2SO4 (KG-MOL/M3) = 0.4541
INITIAL AREA (M2/KG) = 150.0
INITIAL SOLIDS MASS (KG) = 0.1000

TIME (MINS)	ZN2+ (KG-MOL/M3)	FE3+ (KG-MOL/M3)	H2SO4 (KG-MOL/M3)
1.00	.182E-01	.877E 00	.416E 00
6.50	.269E-01	.876E 00	.417E 00
15.00	.344E-01	.836E 00	.414E 00
30.00	.485E-01	.817E 00	.417E 00
60.00	.688E-01	.748E 00	.415E 00
90.00	.904E-01	.698E 00	.415E 00

FINAL EXTENT X (-) = 0.0960
FINAL AREA (M2/KG) = 216.80
TOTAL DRY RESIDUE (KG) = 0.0771
SULPHUR EXTRACTED (KG) = 0.0028

MEAS. INTL RATE(KG-MOL/MIN M3) = .132E-02
MEAS. INTL. ZN2+ (KG-MOL/M3) = 0.0180

TABLE J 24

SPHALERITE LEACHING IN ACIDIC FE2(SO4)3
EXPERIMENTAL RUN NO. = 17
SPHAL. TYPE LEACHED = ZCR
SIZE FRACTION $X10^6$ (M) = -45.0+38.0
TEMPERATURE (K) = 343.00
STIRRER SPEED (RPM) = 800.0
INITIAL FE3+ (KG-MOL/M3) = 0.3671
INITIAL H2SO4 (KG-MOL/M3) = 0.1857
INITIAL AREA (M2/KG) = 185.0
INITIAL SOLIDS MASS (KG) = 0.0200

TIME (MINS)	ZN2+ (KG-MOL/M3)	FE3+ (KG-MOL/M3)	H2SO4 (KG-MOL/M3)
1.00	.500E-02	.365E 00	N.D.
7.00	.104E-01	.355E 00	N.D.
15.00	.182E-01	.329E 00	.202E 00
31.00	.312E-01	.304E 00	.186E 00
45.00	.393E-01	.286E 00	N.D.
60.00	.488E-01	.269E 00	N.D.
90.00	.584E-01	.247E 00	N.D.
120.00	.670E-01	.227E 00	.186E 00
155.00	.750E-01	.195E 00	N.D.
180.00	.812E-01	.168E 00	.185E 00

MEAS. INTL RATE (kg-mol/m^3min) = 0.914×10^{-3}
MEAS. INTL (Zn^{2+}) (kg-mol/m3) = 3.3×10^{-3}

TABLE J 25

SPHALERITE LEACHING IN ACIDIC FE2(SO4)3
EXPERIMENTAL RUN NO. = 15
SPHAL. TYPE LEACHED = ZCR
SIZE FRACTION $X10^6$ (M) = -45.0+38.0
TEMPERATURE (K) = 368.00
STIRRER SPEED (RPM) = 800.0
INITIAL FE3+ (KG-MOL/M3) = 0.3671
INITIAL H2SO4 (KG-MOL/M3) = 0.1878
INITIAL AREA (M2/KG) = 185.0
INITIAL SOLIDS MASS (KG) = 0.0200

TIME (MINS)	ZN2+ (KG-MOL/M3)	FE3+ (KG-MOL/M3)	H2SO4 (KG-MOL/M3)
1.00	.704E-02	.367E 00	.184E 00
5.00	.212E-01	.329E 00	.188E 00
10.00	.344E-01	.299E 00	.189E 00
15.00	.440E-01	.272E 00	.191E 00
25.00	.620E-01	.233E 00	.194E 00
40.00	.783E-01	.197E 00	.197E 00
60.00	.903E-01	.165E 00	.200E 00
90.00	.103E 00	.136E 00	.203E 00
120.00	.114E 00	.111E 00	.206E 00
180.00	.125E 00	.895E-01	.206E 00

MEAS. INTL.RATE (kg-mol/m3min) = $3,44 \times 10^{-3}$
MEAS INTL $[Zn^{2+}]$ (kg-mol/m3) = $3,0 \times 10^{-3}$

TABLE J 26

SPHALERITE LEACHING IN ACIDIC FE2(SO4)3
EXPERIMENTAL RUN NO. = 21
SPHAL. TYPE LEACHED = ZCR
SIZE FRACTION $X10^6$ (M) = -45.0+38.0
TEMPERATURE (K) = 368.00
STIRRER SPEED (RPM) = 800.0
INITIAL FE3+ (KG-MOL/M3) = 0.3617
INITIAL H2SO4 (KG-MOL/M3) = 0.1878
INITIAL AREA (M2/KG) = 185.0
INITIAL SOLIDS MASS (KG) = 0.0100

TIME (MINS)	ZN2+ (KG-MOL/M3)	FE3+ (KG-MOL/M3)	H2SO4 (KG-MOL/M3)
1.50	.490E-02	.362E 00	.187E 00
5.00	.128E-01	.344E 00	.187E 00
11.00	.228E-01	.322E 00	.189E 00
15.00	.292E-01	.308E 00	.193E 00
20.00	.347E-01	.290E 00	.194E 00
30.00	.433E-01	.276E 00	.198E 00
45.00	.509E-01	.251E 00	.199E 00
60.00	.554E-01	.240E 00	.201E 00
75.00	.612E-01	.229E 00	.202E 00
90.00	.639E-01	.229E 00	.201E 00
120.00	.655E-01	.218E 00	.204E 00
151.00	.695E-01	.206E 00	.203E 00
180.00	.698E-01	.202E 00	.204E 00
210.00	.725E-01	.201E 00	.204E 00
240.00	.750E-01	.199E 00	.204E 00

MEAS. INTL.RATE (kg-mol/m3min) = $2,5 \times 10^{-3}$
MEAS INTL $[Zn^{2+}]$ (kg-mol/m3) = $1,0 \times 10^{-3}$

TABLE J 27

SPHALERITE LEACHING IN ACIDIC FE2(SO4)3
EXPERIMENTAL RUN NO. = 75
SPHAL. TYPE LEACHED = ZCR
SIZE FRACTION $X10^6$ (M) = -17.5 + 12.7
TEMPERATURE (K) = 323.00
STIRRER SPEED (RPM) = 800.0
INITIAL FE3+ (KG-MOL/M3) = 0.1450
INITIAL H2SO4 (KG-MOL/M3) = 0.0592
INITIAL AREA (M2/KG) = 420.0
INITIAL SOLIDS MASS (KG) = 0.0200

TIME (MINS)	ZN2+ (KG-MOL/M3)	FE3+ (KG-MOL/M3)	H2SO4 (KG-MOL/M3)
5.00	.566E-02	.141E 00	.531E-01
15.00	.887E-02	.140E 00	.541E-01
30.00	.138E-01	.122E 00	.531E-01
45.00	.193E-01	.115E 00	.551E-01
120.00	.333E-01	.824E-01	N.D.

FINAL EXTENT X (-) = 0.1770
FINAL AREA (M2/KG) = 525.30
TOTAL DRY RESIDUE (KG) = 0.0146
SULPHUR EXTRACTED (KG) = 0.0010

MEAS. INTL RATE (KG-MOL/MIN M3) = .330E-03
MEAS. INTL. ZN2+ (KG-MOL/M3) = 0.0040

TABLE J 28

SPHALERITE LEACHING IN ACIDIC FE2(SO4)3
EXPERIMENTAL RUN NO. = 104
SPHAL. TYPE LEACHED = VMZCR

TEMPERATURE (K) = 318.0
STIRRER SPEED (RPM) = 800.0
INITIAL FE3+ (KG-MOL/M3) = 0.144
INITIAL H2SO4 (KG-MOL/M3) = 0.0633
INITIAL AREA (M2/KG) = 2708.0
INITIAL SOLIDS MASS (KG) = 0.02

TIME (MINS)	ZN2+ (KG-MOL/M3)	FE3+ (KG-MOL/M3)	H2SO4 (KG-MOL/M3)
7.0	0.199 E-01	0.1074	0.0694
16.0	0.289 E-01	0.0798	N.D.
25.0	0.344 E-01	0.0609	N.D.
45.0	0.408 E-01	0.0466	N.D.

FINAL EXTENT X (-) = 0.2171
FINAL AREA (m^2/kg) = 1801.0
TOTAL DRY RESIDUE (kg) = 0.0141
SULPHUR EXTRACTED (kg) = 0.0012

MEAS. INTL. RATE (kg-mol/m3min) = $3,5 \times 10^{3}$

TABLE J 29

SPHALERITE LEACHING IN ACIDIC FE2(SO4)3
EXPERIMENTAL RUN NO. = 119
SPHAL. TYPE LEACHED = VMZCR
TEMPERATURE (K) = 338.00
STIRRER SPEED (RPM) = 800.0
INITIAL FE3+ (KG-MOL/M3) = 0.2990
INITIAL H2SO4 (KG-MOL/M3) = N.D.
INITIAL AREA (M2/KG) = 2708.0
INITIAL SOLIDS MASS (KG) = 0.0200

TIME (MINS)	ZN2+ (KG-MOL/M3)	FE3+ (KG-MOL/M3)	H2SO4 (KG-MOL/M3)
10.00	.421E-01	.193E 00	N.D.
30.00	.597E-01	.175E 00	N.D.
75.00	.795E-01	.133E 00	N.D.
120.00	.883E-01	.110E 00	N.D.

FINAL EXTENT X (-) = 0.4790
FINAL AREA (M2/KG) = 2442.00
TOTAL DRY RESIDUE (KG) = 0.0136
SULPHUR EXTRACTED (KG) = 0.0029

MEAS. INTL RATE (KG-MOL/MIN M3) = .700E-02
MEAS. INTL. ZN2+ (KG-MOL/M3) = 0.0000

TABLE J 30

SPHALERITE LEACHING IN ACIDIC FE2(SO4)3

EXPERIMENTAL RUN NO. = 123
SPHAL. TYPE LEACHED = PR
SIZE FRACTION $X10^6$ (M) = -106.0+90.0
TEMPERATURE (K) = 318.00
STIRRER SPEED (RPM) = 800.0
INITIAL FE3+ (KG-MOL/M3) = 0.3438
INITIAL H2SO4 (KG-MOL/M3) = ND
INITIAL AREA (M2/KG) = 140.0
INITIAL SOLIDS MASS (KG) = 0.0200

TIME (MINS)	ZN2+ (KG-MOL/M3)	FE3+ (KG-MOL/M3)	H2SO4 (KG-MOL/M3)
5.00	.367E-02	.337E 00	N.D.
20.00	.109E-01	.322E 00	N.D.
65.00	.219E-01	.301E 00	N.D.
120.00	.291E-01	.286E 00	N.D.

FINAL EXTENT X (-) = 0.1732
FINAL AREA (M2/KG) = 176.60
TOTAL DRY RESIDUE (KG) = 0.0180
SULPHUR EXTRACTED (KG) = 0.0005

MEAS. INTL RATE(KG-MOL/MIN M3) = .400E-03
MEAS. INTL. ZN2+ (KG-MOL/M3) = 0.0020

TABLE J 31

SPHALERITE LEACHING IN ACIDIC FE2(SO4)3

EXPERIMENTAL RUN NO. = 131
SPHAL. TYPE LEACHED = PR
SIZE FRACTION $X10^6$ (M) = -106.0+ 90.0
TEMPERATURE (K) = 318.00
STIRRER SPEED (RPM) = 1000.0
INITIAL FE3+ (KG-MOL/M3) = 0.4656
INITIAL H2SO4 (KG-MOL/M3) = 0.6306
INITIAL AREA (M2/KG) = 140.0
INITIAL SOLIDS MASS (KG) = 0.0500

TIME (MINS)	ZN2+ (KG-MOL/M3)	FE3+ (KG-MOL/M3)	H2SO4 (KG-MOL/M3)
0.01	.142E 00	.466E 00	N.D.
2.00	.144E 00	.466E 00	N.D.
15.00	.144E 00	.466E 00	N.D.
61.00	.146E 00	.451E 00	N.D.
180.00	.150E 00	.412E 00	N.D.
240.00	.160E 00	.412E 00	N.D.
300.00	.165E 00	.390E 00	N.D.
420.00	.177E 00	.376E 00	N.D.
600.00	.190E 00	.347E 00	N.D.
780.00	.196E 00	.340E 00	N.D.

FINAL EXTENT X (-) = 0.1270
FINAL AREA (M2/KG) = 705.00
TOTAL DRY RESIDUE (KG) = 0.0437
SULPHUR EXTRACTED (KG) = 0.0024

MEAS. INTL RATE(KG-MOL/MIN M3) = .800E-04
MEAS. INTL. ZN2+ (KG-MOL/M3) = 0.142

Note. The leach solution used in this experiment contained 0.8% of the final filtered solution of the experiment reported on table J 2.

TABLE J 32

SPHALERITE LEACHING IN ACIDIC FE2(SO4)3

EXPERIMENTAL RUN NO. = 76
SPHAL. TYPE LEACHED = PR
SIZE FRACTION $X10^6$ (M) = -90.0+ 75.0
TEMPERATURE (K) = 343.00
STIRRER SPEED (RPM) = 800.0
INITIAL FE3+ (KG-MOL/M3) = 0.7628
INITIAL H2SO4 (KG-MOL/M3) = 0.4133
INITIAL AREA (M2/KG) = 150.0
INITIAL SOLIDS MASS (KG) = 0.1500

TIME (MINS)	ZN2+ (KG-MOL/M3)	FE3+ (KG-MOL/M3)	H2SO4 (KG-MOL/M3)
5.00	.317E-01	.670E 00	.410E 00
15.00	.803E-01	.564E 00	.408E 00
30.00	.128E 00	.455E 00	.416E 00
60.00	.194E 00	.260E 00	.414E 00
90.00	.248E 00	.143E 00	.414E 00
120.00	.298E 00	.842E-01	N.D.

FINAL EXTENT X (-) = 0.2340
FINAL AREA (M2/KG) = 764.00
TOTAL DRY RESIDUE (KG) = 0.1150
SULPHUR EXTRACTED (KG) = 0.0098

MEAS. INTL RATE(KG-MOL/MIN M3) = .688E-02
MEAS. INTL. ZN2+ (KG-MOL/M3) = 0.0000

TABLE J 33

SPHALERITE LEACHING IN ACIDIC FE2(SO4)3

EXPERIMENTAL RUN NO. = PR 79 *
SPHAL. TYPE LEACHED = PR residue from Run 76 (Table 32)
SIZE FRACTION $X10^6$ (M) = -90.0+ 75.0
TEMPERATURE (K) = 343.00
STIRRER SPEED (RPM) = 800.0
INITIAL FE3+ (KG-MOL/M3) = 0.4118
INITIAL H2SO4 (KG-MOL/M3) = 0.2224
INITIAL AREA (M2/KG) = 764.0
INITIAL SOLIDS MASS (KG) = 0.1000

TIME (MINS)	ZN2+ (KG-MOL/M3)	FE3+ (KG-MOL/M3)	H2SO4 (KG-MOL/M3)
2.50	.119E-01	.389E 00	.231E 00
10.00	.428E-01	.322E 00	.228E 00
30.00	.968E-01	.195E 00	.233E 00
45.00	.126E 00	.132E 00	.231E 00
60.00	.143E 00	.770E-01	.233E 00
70.00	.151E 00	.460E-01	N.D.

FINAL EXTENT X (-) = 0.3690
FINAL AREA (M2/KG) = 1075.00
TOTAL DRY RESIDUE (KG) = 0.0779
SULPHUR EXTRACTED (KG) = 0.0047

MEAS. INTL RATE(KG-MOL/MIN M3) = .530E-02
MEAS. INTL. ZN2+ (KG-MOL/M3) = 0.0000

* Residue from Run 76 was CCl washed to remove elemental sulphur prior to its use in this run

TABLE J 34

SPHALERITE LEACHING IN ACIDIC FE2(SO4)3

EXPERIMENTAL RUN NO. = 69
SPHAL. TYPE LEACHED = PR
SIZE FRACTION $X10^6$ (M) = -75.0+63.0
TEMPERATURE (K) = 308.00
STIRRER SPEED (RPM) = 800.0
INITIAL FE3+ (KG-MOL/M3) = 0.1397
INITIAL H2SO4 (KG-MOL/M3) = 0.0633
INITIAL AREA (M2/KG) = 150.0
INITIAL SOLIDS MASS (KG) = 0.0500

TIME (MINS)	ZN2+ (KG-MOL/M3)	FE3+ (KG-MOL/M3)	H2SO4 (KG-MOL/M3)
2.00	.199E-02	.138E 00	.629E-01
12.00	.367E-02	.133E 00	.631E-01
30.00	.688E-02	.110E 00	.633E-01
60.00	.138E-01	.115E 00	N.D.

FINAL EXTENT X (-) = 0.0321
FINAL AREA (M2/KG) = 241.10
TOTAL DRY RESIDUE (KG) = 0.0446
SULPHUR EXTRACTED (KG) = 0.0005

MEAS. INTL RATE(KG-MOL/MIN M3) = .210E-03
MEAS. INTL. ZN2+ (KG-MOL/M3) = 0.0013

TABLE J 35

SPHALERITE LEACHING IN ACIDIC FE2(SO4)3

EXPERIMENTAL RUN NO. = 70
SPHAL. TYPE LEACHED = PR
SIZE FRACTION $X10^6$ (M) = -75.0+ 63.0
TEMPERATURE (K) = 318.00
STIRRER SPEED (RPM) = 800.0
INITIAL FE3+ (KG-MOL/M3) = 0.2793
INITIAL H2SO4 (KG-MOL/M3) = 0.1112
INITIAL AREA (M2/KG) = 150.0
INITIAL SOLIDS MASS (KG) = 0.0500

TIME (MINS)	ZN2+ (KG-MOL/M3)	FE3+ (KG-MOL/M3)	H2SO4 (KG-MOL/M3)
2.00	.260E-02	.275E 00	.114E 00
11.00	.688E-02	.263E 00	.116E 00
30.00	.162E-01	.249E 00	.114E 00
60.00	.303E-01	.211E 00	.114E 00
92.00	.421E-01	.174E 00	.118E 00
120.00	.473E-01	.168E 00	.118E 00

FINAL EXTENT X (-) = 0.1100
FINAL AREA (M2/KG) = 462.00
TOTAL DRY RESIDUE (KG) = 0.0412
SULPHUR EXTRACTED (KG) = 0.0016

MEAS. INTL RATE(KG-MOL/MIN M3) = .500E-03
MEAS. INTL. ZN2+ (KG-MOL/M3) = 0.0020

TABLE J 36

SPHALERITE LEACHING IN ACIDIC FE2(SO4)3
EXPERIMENTAL RUN NO. = 52
SPHAL. TYPE LEACHED = PR
SIZE FRACTION $X10^6$ (M) = -75.0+ 63.0
TEMPERATURE (K) = 323.00
STIRRER SPEED (RPM) = 800.0
INITIAL FE3+ (KG-MOL/M3) = 0.8022
INITIAL H2SO4 (KG-MOL/M3) = 0.2959
INITIAL AREA (M2/KG) = 150.0
INITIAL SOLIDS MASS (KG) = 0.1000

TIME (MINS)	ZN2+ (KG-MOL/M3)	FE3+ (KG-MOL/M3)	H2SO4 (KG-MOL/M3)
1.50	.119E-01	.779E 00	.289E 00
5.00	.109E-01	.770E 00	.298E 00
15.00	.259E-01	.722E 00	.293E 00
30.00	.535E-01	.677E 00	.292E 00
60.00	.926E-01	.594E 00	.300E 00
70.00	.111E 00	.580E 00	.301E 00

FINAL EXTENT X (-) = 0.1480
FINAL AREA (M2/KG) = 499.00
TOTAL DRY RESIDUE (KG) = 0.0833
SULPHUR EXTRACTED (KG) = 0.0039

MEAS. INTL RATE(KG-MOL/MIN M3) = .179E-02
MEAS. INTL. ZN2+ (KG-MOL/M3) = 0.0040

TABLE J 37

SPHALERITE LEACHING IN ACIDIC FE2(SO4)3
EXPERIMENTAL RUN NO. = 50
SPHAL. TYPE LEACHED = PR
SIZE FRACTION $X10^6$ (M) = -75.0+ 63.0
TEMPERATURE (K) = 343.00
STIRRER SPEED (RPM) = 800.0
INITIAL FE3+ (KG-MOL/M3) = 0.8774
INITIAL H2SO4 (KG-MOL/M3) = 0.4439
INITIAL AREA (M2/KG) = 150.0
INITIAL SOLIDS MASS (KG) = 0.1000

TIME (MINS)	ZN2+ (KG-MOL/M3)	FE3+ (KG-MOL/M3)	H2SO4 (KG-MOL/M3)
1.50	.116E-01	.851E 00	.446E 00
5.50	.315E-01	.811E 00	.439E 00
15.00	.757E-01	.709E 00	.441E 00
30.50	.145E 00	.578E 00	.459E 00
45.00	.181E 00	.469E 00	.456E 00

FINAL EXTENT X (-) = 0.2110
FINAL AREA (M2/KG) = 674.70
TOTAL DRY RESIDUE (KG) = 0.0760
SULPHUR EXTRACTED (KG) = 0.0056

MEAS. INTL RATE(KG-MOL/MIN M3) = .571E-02
MEAS. INTL. ZN2+ (KG-MOL/M3) = 0.0000

TABLE J 38

SPHALERITE LEACHING IN ACIDIC FE2(SO4)3
EXPERIMENTAL RUN NO. = 121
SPHAL. TYPE LEACHED = PR
SIZE FRACTION $X10^6$ (M) = -75.0+ 63.0
TEMPERATURE (K) = 358.00
STIRRER SPEED (RPM) = 800.0
INITIAL FE3+ (KG-MOL/M3) = 0.7162
INITIAL H2SO4 (KG-MOL/M3) = 0.1551
INITIAL AREA (M2/KG) = 150.0
INITIAL SOLIDS MASS (KG) = 0.0800

TIME (MINS)	ZN2+ (KG-MOL/M3)	FE3+ (KG-MOL/M3)	H2SO4 (KG-MOL/M3)
6.00	.566E-01	.705E 00	N.D.
42.00	.156E 00	.408E 00	N.D.
88.00	.220E 00	.251E 00	N.D.
205.00	.288E 00	.609E-01	N.D.

FINAL EXTENT X (-) = 0.4210
FINAL AREA (M2/KG) = 884.00
TOTAL DRY RESIDUE (KG) = 0.0534
SULPHUR EXTRACTED (KG) = 0.0095

MEAS. INTL RATE(KG-MOL/MIN M3) = .940E-02
MEAS. INTL. ZN2+ (KG-MOL/M3) = 0.0000

TABLE J 39

SPHALERITE LEACHING IN ACIDIC FE2(SO4)3
EXPERIMENTAL RUN NO. = 51
SPHAL. TYPE LEACHED = PR
SIZE FRACTION $X10^6$ (M) = -75.0+ 63.0
TEMPERATURE (K) = 368.00
STIRRER SPEED (RPM) = 800.0
INITIAL FE3+ (KG-MOL/M3) = 0.8058
INITIAL H2SO4 (KG-MOL/M3) = 0.3224
INITIAL AREA (M2/KG) = 150.0
INITIAL SOLIDS MASS (KG) = 0.1000

TIME (MINS)	ZN2+ (KG-MOL/M3)	FE3+ (KG-MOL/M3)	H2SO4 (KG-MOL/M3)
1.00	.283E-01	.763E 00	.317E 00
5.00	.895E-01	.568E 00	.337E 00
10.00	.142E 00	.483E 00	.333E 00
20.00	.220E 00	.328E 00	.339E 00
30.00	.259E 00	.252E 00	.344E 00
40.00	.285E 00	.188E 00	.367E 00

FINAL EXTENT X (-) = 0.3330
FINAL AREA (M2/KG) = 181.60
TOTAL DRY RESIDUE (KG) = 0.0678
SULPHUR EXTRACTED (KG) = 0.0090

MEAS. INTL RATE(KG-MOL/MIN M3) = .305E-01
MEAS. INTL. ZN2+ (KG-MOL/M3) = 0.0000

TABLE J 40

SPHALERITE LEACHING IN ACIDIC FE2(SO4)3
EXPERIMENTAL RUN NO. = 129
SPHAL. TYPE LEACHED = PR
SIZE FRACTION $X10^6$ (M) = -24.0+ 17.0
TEMPERATURE (K) = 318.00
STIRRER SPEED (RPM) = 1000.0
INITIAL FE3+ (KG-MOL/M3) = 0.2256
INITIAL H2SO4 (KG-MOL/M3) = 0.8735
INITIAL AREA (M2/KG) = 320.0
INITIAL SOLIDS MASS (KG) = 0.0300

TIME (MINS)	ZN2+ (KG-MOL/M3)	FE3+ (KG-MOL/M3)	H2SO4 (KG-MOL/M3)
1.25	.311E-02	.218E 00	N.D.
5.00	.375E-02	.208E 00	.857E 00
15.00	.681E-02	.193E 00	N.D.
45.00	.165E-01	.172E 00	.851E 00
75.00	.245E-01	.156E 00	N.D.
136.00	.361E-01	.125E 00	N.D.
180.00	.410E-01	.115E 00	N.D.

FINAL EXTENT X (-) = 0.1600
FINAL AREA (M2/KG) = 437.00
SULPHUR EXTRACTED (KG) = 0.0015

MEAS. INTL RATE(KG-MOL/MIN M3) = .200E-03
MEAS. INTL. ZN2+ (KG-MOL/M3) = 0.0030

TABLE J 41

SPHALERITE LEACHING IN ACIDIC FE2(SO4)3
EXPERIMENTAL RUN NO. = 73
SPHAL. TYPE LEACHED = PR
SIZE FRACTION $X10^6$ (M) = -17.5+ 12.7
TEMPERATURE (K) = 323.00
STIRRER SPEED (RPM) = 800.0
INITIAL FE3+ (KG-MOL/M3) = 0.1468
INITIAL H2SO4 (KG-MOL/M3) = 0.0622
INITIAL AREA (M2/KG) = 420.0
INITIAL SOLIDS MASS (KG) = 0.0200

TIME (MINS)	ZN2+ (KG-MOL/M3)	FE3+ (KG-MOL/M3)	H2SO4 (KG-MOL/M3)
5.00	.612E-02	.139E 00	.653E-01
15.00	.122E-01	.117E 00	.643E-01
30.00	.200E-01	.104E 00	.663E-01
60.00	.320E-01	.734E-01	.673E-01

FINAL EXTENT X (-) = 0.1810
FINAL AREA (M2/KG) = 680.00
TOTAL DRY RESIDUE (KG) = 0.0161
SULPHUR EXTRACTED (KG) = 0.0011

MEAS. INTL RATE(KG-MOL/MIN M3) = 0.213 -02
MEAS. INTL. ZN2+ (KG-MOL/M3) = 0.0030

TABLE J 42

SPHALERITE LEACHING IN ACIDIC FE2(SO4)3
EXPERIMENTAL RUN NO. = 105
SPHAL TYPE LEACHED = VMPR
TEMPERATURE (K) = 318.0
STIRRER SPEED (RPM) = 800.0
INITIAL FE3+ (KG-MOL/M3) = 0.1432
INITIAL H2SO4 (KG-MOL/M3) = 0.0633
INITIAL AREA (M2/KG) = 2630.0
INITIAL SOLIDS MASS (KG) = 0.02

TIME (MINS)	ZN2+ (KG-MOL/M3)	FE3+ (KG-MOL/M3)	H2SO4 (KG-MOL/M3)
1.0	.1436E-01	.113E 00	.055
6.0	.2486E-01	.820E-01	.053
15.0	.3519E-01	.570E-01	.054
25.0	.4092E-01	.460E-01	N.D.

FINAL EXTENT X (X) = 0.2392
FINAL AREA (M2/KG) = 1365.0
TOTAL DRY RESIDUE (KG) = 0.0141
SULPHUR EXTRACTED (KG) = 0.0012

MEAS. INITIAL RATE (KG-MOL/MIN M3) = 23.75×10^{-3}

TABLE J 43

SPHALERITE LEACHING IN ACIDIC FE2(SO4)3
EXPERIMENTAL RUN NO. = 117
SPHAL. TYPE LEACHED = VMPR
TEMPERATURE (K) = 318.00
STIRRER SPEED (RPM) = 800.0
INITIAL FE3+ (KG-MOL/M3) = 0.3080
INITIAL H2SO4 (KG-MOL/M3) = N.D.
INITIAL AREA (M2/KG) = 2630.0
INITIAL SOLIDS MASS (KG) = 0.0200

TIME (MINS)	ZN2+ (KG-MOL/M3)	FE3+ (KG-MOL/M3)	H2SO4 (KG-MOL/M3)
2.30	.263E-01	.256E 00	N.D.
8.50	.303E-01	.248E 00	N.D.
19.00	.408E-01	.227E 00	N.D.

FINAL EXTENT X (-) = 0.5600
FINAL AREA (M2/KG) = 982.30
TOTAL DRY RESIDUE (KG) = 0.0105
SULPHUR EXTRACTED (KG) = 0.0034

MEAS. INTL RATE(KG-MOL/MIN M3) = 24.0×10^{-3}

TABLE J 44

SPHALERITE LEACHING IN ACIDIC FE2(SO4)3
EXPERIMENTAL RUN NO. = 71
SPHAL. TYPE LEACHED = BDH
TEMPERATURE (K) = 323.00
STIRRER SPEED (RPM) = 800.0
INITIAL FE3+ (KG-MOL/M3) = 0.2901
INITIAL H2SO4 (KG-MOL/M3) = 0.1112
INITIAL AREA (M2/KG) = 7200.0
INITIAL SOLIDS MASS (KG) = 0.0500

TIME (MINS)	ZN2+ (KG-MOL/M3)	FE3+ (KG-MOL/M3)	H2SO4 (KG-MOL/M3)
5.00	.203E-01	.252E 00	.104E 00
15.00	.338E-01	.224E 00	.105E 00
30.00	.428E-01	.208E 00	.106E 00
60.00	.627E-01	.174E 00	.104E 00
95.00	.760E-01	.145E 00	N.D.

FINAL EXTENT X (-) = 0.1480
FINAL AREA (M2/KG) = 7610.00
TOTAL DRY RESIDUE (KG) = 0.0371
SULPHUR EXTRACTED (KG) = 0.0018

MEAS. INTL RATE(KG-MOL/MIN M3) = .900E-02
MEAS. INTL. ZN2+ (KG-MOL/M3) = 0.0000

TABLE J 45

SPHALERITE LEACHING IN ACIDIC FE2(SO4)3
EXPERIMENTAL RUN NO. = 78
SPHAL. TYPE LEACHED = BDH
TEMPERATURE (K) = 343.00
STIRRER SPEED (RPM) = 800.0
INITIAL FE3+ (KG-MOL/M3) = 0.1432
INITIAL H2SO4 (KG-MOL/M3) = 0.0633
INITIAL AREA (M2/KG) = 7200.0
INITIAL SOLIDS MASS (KG) = 0.0200

TIME (MINS)	ZN2+ (KG-MOL/M3)	FE3+ (KG-MOL/M3)	H2SO4 (KG-MOL/M3)
5.00	.193E-01	.106E 00	.612E-01
15.00	.343E-01	.868E-01	.633E-01
30.00	.451E-01	.698E-01	.627E-01
45.00	.526E-01	.528E-01	.622E-01
60.00	.598E-01	.233E-01	.643E-01

FINAL EXTENT X (-) = 0.2932
FINAL AREA (M2/KG) = 8260.00
SULPHUR EXTRACTED (KG) = 0.0014

MEAS. INTL RATE(KG-MOL/MIN M3) = .600E-02
MEAS. INTL. ZN2+ (KG-MOL/M3) = 0.0000

TABLE J 46

SPHALERITE LEACHING IN ACIDIC FE2(SO4)3
EXPERIMENTAL RUN NO. = 80
SPHAL. TYPE LEACHED = BDH
TEMPERATURE (K) = 343.00
STIRRER SPEED (RPM) = 800.0
INITIAL FE3+ (KG-MOL/M3) = 0.2919
INITIAL H2SO4 (KG-MOL/M3) = 0.1071
INITIAL AREA (M2/KG) = 7200.0
INITIAL SOLIDS MASS (KG) = 0.0200

TIME (MINS)	ZN2+ (KG-MOL/M3)	FE3+ (KG-MOL/M3)	H2SO4 (KG-MOL/M3)
5.00	.321E-01	.235E 00	.106E 00
15.00	.532E-01	.192E 00	.110E 00
30.00	.685E-01	.165E 00	.110E 00
45.00	.809E-01	.127E 00	.111E 00
60.00	.867E-01	.106E 00	N.D.

FINAL EXTENT X (-) = 0.4670
FINAL AREA (M2/KG) = 8858.00
TOTAL DRY RESIDUE (KG) = 0.0122
SULPHUR EXTRACTED (KG) = 0.0024

MEAS. INTL RATE(KG-MOL/MIN M3) = .116E-01
MEAS. INTL. ZN2+ (KG-MOL/M3) = 0.0000

TABLE J 47

SPHALERITE LEACHING IN ACIDIC FE2(SO4)3
EXPERIMENTAL RUN NO. = 72
SPHAL. TYPE LEACHED = BDH
TEMPERATURE (K) = 353.00
STIRRER SPEED (RPM) = 800.0
INITIAL FE3+ (KG-MOL/M3) = 0.5802
INITIAL H2SO4 (KG-MOL/M3) = 0.2235
INITIAL AREA (M2/KG) = 7200.0
INITIAL SOLIDS MASS (KG) = 0.0500

TIME (MINS)	ZN2+ (KG-MOL/M3)	FE3+ (KG-MOL/M3)	H2SO4 (KG-MOL/M3)
5.00	.117E 00	.365E 00	.227E 00
15.00	.151E 00	.249E 00	.234E 00
25.00	.181E 00	.197E 00	.238E 00
40.00	.223E 00	.141E 00	N.D.
60.00	.242E 00	.109E 00	.237E 00

FINAL EXTENT X (-) = 0.4710
FINAL AREA (M2/KG) = 5265.00
TOTAL DRY RESIDUE (KG) = 0.0321
SULPHUR EXTRACTED (KG) = 0.0049

MEAS. INTL RATE(KG-MOL/MIN M3) = .600E-01
MEAS. INTL. ZN2+ (KG-MOL/M3) = 0.0000

A P P E N D I X K

TABULATED EXPERIMENTAL RESULTS FOR THE OXIDATION OF H_2S BY Fe^{3+} IN THE ABSENCE AND PRESENCE OF SPHALERITE OR ACTIVATED CHARCOAL

The procedure adopted for processing this type of data is described in section G. 3 .

Note that the same experimental run numbers are presented on the tables in Appendix I for the sphalerite dissolution reactions which generate H_2S , as are presented in this appendix for the results of oxidising H_2S thus generated by Fe^{3+} .

TABLE K 1

FE3+ OXIDN. OF H2S IN AQUEOUS H2SO4
EXPERIMENTAL RUN NO. = 217

SPHAL. TYPE PRESENT	=	NO SOLIDS
TEMPERATURE (K)	=	318.00
STIRRER SPEED (RPM)	=	1000.00
INITIAL FE3+ (KG-MOL/M3)	=	0.0143
INITIAL H2SO4 (KG-MOL/M3)	=	0.50
TOTAL SOLIDS AREA (M2/M3)	=	0.00
INITIAL SOLIDS (KG)	=	0.0000
KDEXP (KPA M3/KG-MOL)	=	689.6
KDCALC (KPA M3/KG-MOL)	=	1569.00
INITIAL H2S(meas)(KG-MOL/M3)	=	0.0414

TIME (MINS)	PH2S (KPA)	ZN2+ (KG-MOL/M3)
0.00	28.38	N.D.
1.00	21.62	N.D.
2.00	20.85	N.D.
3.00	20.08	N.D.
5.00	19.69	N.D.
10.00	19.11	N.D.

MEAS. INTL. RATE (KPA/MIN) = -15.4424

TABLE K 2

FE3+ OXIDN. OF H2S IN AQUEOUS H2SO4
EXPERIMENTAL RUN NO. = 217

SPHAL. TYPE PRESENT	=	NO SOLIDS
TEMPERATURE (K)	=	318.00
STIRRER SPEED (RPM)	=	1000.00
INITIAL FE3+ (KG-MOL/M3)	=	0.0286
INITIAL H2SO4 (KG-MOL/M3)	=	0.50
TOTAL SOLIDS AREA (M2/M3)	=	0.00
INITIAL SOLIDS (KG)	=	0.0000
KDEXP (KPA M3/KG-MOL)	=	559.7
KDCALC (KPA M3/KG-MOL)	=	1569.00
INITIAL H2S(calc)(KG-MOL/M3)	=	0.0343

TIME (MINS)	PH2S (KPA)	ZN2+ (KG-MOL/M3)
0.00	19.11	N.D.
0.50	7.72	N.D.
1.00	4.63	N.D.
2.00	2.51	N.D.
3.00	1.66	N.D.
5.00	0.85	N.D.
10.00	0.08	N.D.
15.00	-0.12	N.D.

MEAS. INTL. RATE (KPA/MIN) = -32.7191

TABLE K 3

FE3+ OXIDN. OF H2S IN AQUEOUS H2SO4
EXPERIMENTAL RUN NO. = 216

SPHAL. TYPE PRESENT	=	NO SOLIDS
TEMPERATURE (K)	=	318.00
STIRRER SPEED (RPM)	=	1000.00
INITIAL FE3+ (KG-MOL/M3)	=	0.0143
INITIAL H2SO4 (KG-MOL/M3)	=	1.00
TOTAL SOLIDS AREA (M2/M3)	=	0.00
INITIAL SOLIDS (KG)	=	0.0000
KDEXP (KPA M3/KG-MOL)	=	1134.0
KDCALC (KPA M3/KG-MOL)	=	1654.00
INITIAL H2S(meas)(KG-MOL/M3)	=	0.0255

TIME (MINS)	PH2S (KPA)	ZN2+ (KG-MOL/M3)
0.00	28.95	N.D.
1.00	26.72	N.D.
2.00	25.48	N.D.
5.00	23.45	N.D.
10.00	22.01	N.D.
15.00	21.54	N.D.
20.00	21.16	N.D.
25.00	20.65	N.D.
30.00	20.54	N.D.

MEAS. INTL. RATE (KPA/MIN) = -2.6171

TABLE K 4

FE3+ OXIDN. OF H2S IN AQUEOUS H2SO4
EXPERIMENTAL RUN NO. = 216

SPHAL. TYPE PRESENT	=	NO SOLIDS
TEMPERATURE (K)	=	318.00
STIRRER SPEED (RPM)	=	1000.00
INITIAL FE3+ (KG-MOL/M3)	=	0.0286
INITIAL H2SO4 (KG-MOL/M3)	=	1.00
TOTAL SOLIDS AREA (M2/M3)	=	0.00
INITIAL SOLIDS (KG)	=	0.0000
KDEXP (KPA M3/KG-MOL)	=	1118.0
KDCALC (KPA M3/KG-MOL)	=	1654.00
INITIAL H2S(calc)(KG-MOL/M3)	=	0.01838

TIME (MINS)	PH2S (KPA)	ZN2+ (KG-MOL/M3)
0.00	20.54	N.D.
1.00	16.93	N.D.
2.00	14.63	N.D.
5.00	11.29	N.D.
10.00	8.99	N.D.
15.00	7.84	N.D.
20.00	7.14	N.D.
25.00	6.64	N.D.
30.00	6.18	N.D.

MEAS. INTL. RATE (KPA/MIN) = -5.1478

TABLE K 5

FE3+ OXIDN. OF H2S IN AQUEOUS H2SO4
EXPERIMENTAL RUN NO. = 218

SPHAL. TYPE PRESENT	=	NO SOLIDS
TEMPERATURE (K)	=	318.00
STIRRER SPEED (RPM)	=	1000.00
INITIAL FE3+ (KG-MOL/M3)	=	0.0143
INITIAL H2SO4 (KG-MOL/M3)	=	2.00
TOTAL SOLIDS AREA (M2/M3)	=	0.00
INITIAL SOLIDS (KG)	=	0.0000
KDEXP (KPA M3/KG-MOL)	=	1120.0
KDCALC (KPA M3/KG-MOL)	=	1824.00
INITIAL H2S(meas)(KG-MOL/M3)	=	0.0258

TIME (MINS)	PH2S (KPA)	ZN2+ (KG-MOL/M3)
0.00	28.95	N.D.
1.00	28.18	N.D.
2.00	27.72	N.D.
5.00	26.27	N.D.
10.00	24.75	N.D.
20.00	22.86	N.D.
30.00	21.77	N.D.
40.00	21.23	N.D.

MEAS. INTL. RATE (KPA/MIN) = -0.6451

TABLE K 6

FE3+ OXIDN. OF H2S IN AQUEOUS H2SO4
EXPERIMENTAL RUN NO. = 218

SPHAL. TYPE PRESENT	=	NO SOLIDS
TEMPERATURE (K)	=	318.00
STIRRER SPEED (RPM)	=	1000.00
INITIAL FE3+ (KG-MOL/M3)	=	0.0286
INITIAL H2SO4 (KG-MOL/M3)	=	2.00
TOTAL SOLIDS AREA (M2/M3)	=	0.00
INITIAL SOLIDS (KG)	=	0.0000
KDEXP (KPA M3/KG-MOL)	=	1137.0
KDCALC (KPA M3/KG-MOL)	=	1824.00
INITIAL H2S(calc) (KG-MOL/M3)	=	0.0187

TIME (MINS)	PH2S (KPA)	ZN2+ (KG-MOL/M3)
0.00	21.23	N.D.
1.00	19.30	N.D.
2.00	17.57	N.D.
5.00	14.28	N.D.
10.00	11.20	N.D.
20.00	8.11	N.D.
30.00	6.56	N.D.

MEAS. INTL. RATE (KPA/MIN) = -1.544

TABLE K 7

FE3+ OXIDN. OF H2S IN AQUEOUS H2SO4
EXPERIMENTAL RUN NO. = 172

SPHAL. TYPE PRESENT	=	VMWBM
TEMPERATURE (K)	=	318.00
STIRRER SPEED (RPM)	=	1000.00
INITIAL FE3+ (KG-MOL/M3)	=	0.0055
INITIAL H2SO4 (KG-MOL/M3)	=	0.48
TOTAL SOLIDS AREA (M2/M3)	=	22972.59
INITIAL SOLIDS (KG)	=	0.0100
KDEXP (KPA M3/KG-MOL)	=	1698.00
KDCALC (KPA M3/KG-MOL)	=	1569.00

TIME (MINS)	PH2S (KPA)	ZN2+ (KG-MOL/M3)
0.00	11.04	.791E-02
1.00	9.93	N.D.
2.00	9.66	N.D.
3.00	9.31	N.D.
5.00	8.83	N.D.
10.00	8.35	N.D.
15.00	8.26	N.D.
20.00	8.32	N.D.

MEAS. INTL. RATE (KPA/MIN) = -0.7110

TABLE K 8

FE3+ OXIDN. OF H2S IN AQUEOUS H2SO4
EXPERIMENTAL RUN NO. = 172

SPHAL. TYPE PRESENT	=	VMWBM
TEMPERATURE (K)	=	318.00
STIRRER SPEED (RPM)	=	1000.00
INITIAL FE3+ (KG-MOL/M3)	=	0.0138
INITIAL H2SO4 (KG-MOL/M3)	=	0.48
TOTAL SOLIDS AREA (M2/M3)	=	22972.59
INITIAL SOLIDS (KG)	=	0.0100
KDEXP (KPA M3/KG-MOL)	=	1698.00
KDCALC (KPA M3/KG-MOL)	=	1569.00

TIME (MINS)	PH2S (KPA)	ZN2+ (KG-MOL/M3)
0.00	6.28	.875E-02
1.00	6.11	N.D.
2.00	4.97	N.D.
5.00	3.00	N.D.
10.00	1.64	N.D.
15.00	1.17	N.D.
20.00	1.23	.978E-02

MEAS. INTL. RATE (KPA/MIN) = -1.9924

TABLE K 9

FE3+ OXIDN. OF H2S IN AQUEOUS H2SO4
EXPERIMENTAL RUN NO. = 176

SPHAL. TYPE PRESENT	=	VMWBM
TEMPERATURE (K)	=	318.00
STIRRER SPEED (RPM)	=	1000.00
INITIAL FE3+ (KG-MOL/M3)	=	0.0055
INITIAL H2SO4 (KG-MOL/M3)	=	0.97
TOTAL SOLIDS AREA (M2/M3)	=	19154.35
INITIAL SOLIDS (KG)	=	0.0100
KDEXP (KPA M3/KG-MOL)	=	1698.00
KDCALC (KPA M3/KG-MOL)	=	1654.00

TIME (MINS)	PH2S (KPA)	ZN2+ (KG-MOL/M3)
0.00	17.52	N.D.
1.00	17.15	N.D.
2.00	16.86	N.D.
2.00	16.86	N.D.
5.00	16.17	N.D.
10.00	15.56	N.D.

MEAS. INTL. RATE (KPA/MIN) = -0.3667

TABLE K 10

FE3+ OXIDN. OF H2S IN AQUEOUS H2SO4
EXPERIMENTAL RUN NO. = 176

SPHAL. TYPE PRESENT	=	VMWBM
TEMPERATURE (K)	=	318.00
STIRRER SPEED (RPM)	=	1000.00
INITIAL FE3+ (KG-MOL/M3)	=	0.0138
INITIAL H2SO4 (KG-MOL/M3)	=	0.97
TOTAL SOLIDS AREA (M2/M3)	=	19155.35
INITIAL SOLIDS (KG)	=	0.0100
KDEXP (KPA M3/KG-MOL)	=	1698.00
KDCALC (KPA M3/KG-MOL)	=	1654.00

TIME (MINS)	PH2S (KPA)	ZN2+ (KG-MOL/M3)
0.00	15.21	.140E-01
1.00	13.83	N.D.
2.00	12.81	N.D.
5.00	10.99	N.D.
10.00	9.30	N.D.
15.00	8.39	N.D.
20.00	7.91	.153E-01

MEAS. INTL. RATE (KPA/MIN) = -1.2804

TABLE K 11

FE3+ OXIDN. OF H2S IN AQUEOUS H2SO4
EXPERIMENTAL RUN NO. = 175

SPHAL. TYPE PRESENT	=	VMWBM
TEMPERATURE (K)	=	318.00
STIRRER SPEED (RPM)	=	1000.00
INITIAL FE3+ (KG-MOL/M3)	=	0.0055
INITIAL H2SO4 (KG-MOL/M3)	=	1.95
TOTAL SOLIDS AREA (M2/M3)	=	13393.50
INITIAL SOLIDS (KG)	=	0.0100
KDEXP (KPA M3/KG-MOL)	=	1792.00
KDCALC (KPA M3/KG-MOL)	=	1824.00

TIME (MINS)	PH2S (KPA)	ZN2+ (KG-MOL/M3)
0.00	33.03	N.D.
2.00	32.30	N.D.
5.00	31.57	N.D.
10.00	30.73	N.D.
15.00	30.27	N.D.
10.00	30.27	N.D.

MEAS. INTL. RATE (KPA/MIN) = -0.2037

TABLE K 12

FE3+ OXIDN. OF H2S IN AQUEOUS H2SO4
EXPERIMENTAL RUN NO. = 175

SPHAL. TYPE PRESENT	=	VMWBM
TEMPERATURE (K)	=	318.00
STIRRER SPEED (RPM)	=	1000.00
INITIAL FE3+ (KG-MOL/M3)	=	0.0138
INITIAL H2SO4 (KG-MOL/M3)	=	1.95
TOTAL SOLIDS AREA (M2/M3)	=	13393.50
INITIAL SOLIDS (KG)	=	0.0100
KDEXP (KPA M3/KG-MOL)	=	1792.00
KDCALC (KPA M3/KG-MOL)	=	1824.00

TIME (MINS)	PH2S (KPA)	ZN2+ (KG-MOL/M3)
0.00	30.27	.235E-01
2.00	27.66	N.D.
5.00	24.97	N.D.
10.00	22.20	N.D.
15.00	21.05	N.D.
20.00	20.82	N.D.

MEAS. INTL. RATE (KPA/MIN) = -1.1504

TABLE K 13

FE3+ OXIDN. OF H2S IN AQUEOUS H2SO4
EXPERIMENTAL RUN NO. = 200

SPHAL. TYPE PRESENT	=	BDH
TEMPERATURE (K)	=	318.00
STIRRER SPEED (RPM)	=	1000.00
INITIAL FE3+ (KG-MOL/M3)	=	0.0057
INITIAL H2SO4 (KG-MOL/M3)	=	0.48
TOTAL SOLIDS AREA (M2/M3)	=	24273.42
INITIAL SOLIDS (KG)	=	0.0040
KDEXP (KPA M3/KG-MOL)	=	N.D.
KDCALC (KPA M3/KG-MOL)	=	1569.00

TIME (MINS)	PH2S (KPA)	ZN2+ (KG-MOL/M3)
0.00	10.47	.888E-02
1.00	9.68	N.D.
2.00	9.20	N.D.
5.00	8.49	N.D.
10.00	8.20	N.D.
14.20	8.07	.967E-02

MEAS. INTL. RATE (KPA/MIN) = -0.9196

TABLE K 14

FE3+ OXIDN. OF H2S IN AQUEOUS H2SO4
EXPERIMENTAL RUN NO. = 200

SPHAL. TYPE PRESENT	=	BDH
TEMPERATURE (K)	=	318.00
STIRRER SPEED (RPM)	=	1000.00
INITIAL FE3+ (KG-MOL/M3)	=	0.0143
INITIAL H2SO4 (KG-MOL/M3)	=	0.48
TOTAL SOLIDS AREA (M2/M3)	=	24273.42
INITIAL SOLIDS (KG)	=	0.0040
KDEXP (KPA M3/KG-MOL)	=	N.D.
KDCALC (KPA M3/KG-MOL)	=	1569.00

TIME (MINS)	PH2S (KPA)	ZN2+ (KG-MOL/M3)
0.00	7.97	.967E-02
1.00	6.01	N.D.
2.00	4.71	N.D.
3.00	3.82	N.D.
5.00	2.78	N.D.
10.00	1.63	N.D.
15.00	1.38	.110E-01

MEAS. INTL. RATE (KPA/MIN) = -2.1301

TABLE K 15

FE3+ OXIDN. OF H2S IN AQUEOUS H2SO4
EXPERIMENTAL RUN NO. = 199

SPHAL. TYPE PRESENT	=	BDH
TEMPERATURE (K)	=	318.00
STIRRER SPEED (RPM)	=	1000.00
INITIAL FE3+ (KG-MOL/M3)	=	0.0143
INITIAL H2SO4 (KG-MOL/M3)	=	0.96
TOTAL SOLIDS AREA (M2/M3)	=	18614.80
INITIAL SOLIDS (KG)	=	0.0040
KDEXP (KPA M3/KG-MOL)	=	N.D.
KDCALC (KPA M3/KG-MOL)	=	1654.00

TIME (MINS)	PH2S (KPA)	ZN2+ (KG-MOL/M3)
0.00	26.64	.179E-01
1.00	24.90	N.D.
2.00	23.55	N.D.
5.00	21.54	N.D.
10.00	19.96	N.D.
15.00	19.30	N.D.
25.00	18.61	N.D.
30.00	18.92	.192E-01

MEAS. INTL. RATE (KPA/MIN) = -1.7062

TABLE K 16

FE3+ OXIDN. OF H2S IN AQUEOUS H2SO4
EXPERIMENTAL RUN NO. = 199

SPHAL. TYPE PRESENT	=	BDH
TEMPERATURE (K)	=	318.00
STIRRER SPEED (RPM)	=	1000.00
INITIAL FE3+ (KG-MOL/M3)	=	0.0286
INITIAL H2SO4 (KG-MOL/M3)	=	0.96
TOTAL SOLIDS AREA (M2/M3)	=	18614.80
INITIAL SOLIDS (KG)	=	0.0040
KDEXP (KPA M3/KG-MOL)	=	N.D.
KDCALC (KPA M3/KG-MOL)	=	1654.00

TIME (MINS)	PH2S (KPA)	ZN2+ (KG-MOL/M3)
0.00	19.30	.192E-01
1.00	16.41	N.D.
2.00	14.09	N.D.
5.00	10.81	N.D.
10.00	8.49	N.D.
15.00	7.34	N.D.
20.00	6.49	N.D.
25.00	5.68	N.D.
30.00	5.02	.211E-01

MEAS. INTL. RATE (KPA/MIN) = -3.6055

TABLE K 17

FE3+ OXIDN. OF H2S IN AQUEOUS H2SO4
EXPERIMENTAL RUN NO. = 201

SPHAL. TYPE PRESENT	=	BDH
TEMPERATURE (K)	=	318.00
STIRRER SPEED (RPM)	=	1000.00
INITIAL FE3+ (KG-MOL/M3)	=	0.0143
INITIAL H2SO4 (KG-MOL/M3)	=	1.95
TOTAL SOLIDS AREA (M2/M3)	=	9809.35
INITIAL SOLIDS (KG)	=	0.0040
KDEXP (KPA M3/KG-MOL)	=	N.D.
KDCALC (KPA M3/KG-MOL)	=	1827.00

TIME (MINS)	PH2S (KPA)	ZN2+ (KG-MOL/M3)
0.00	45.67	.285E-01
1.00	43.90	N.D.
2.00	42.39	N.D.
5.00	39.57	N.D.
10.00	36.98	N.D.
20.00	34.05	N.D.
30.00	33.20	.290E-01

MEAS. INTL. RATE (KPA/MIN) = -1.7179

TABLE K 18

FE3+ OXIDN. OF H2S IN AQUEOUS H2SO4
EXPERIMENTAL RUN NO. = 201

SPHAL. TYPE PRESENT	=	BDH
TEMPERATURE (K)	=	318.00
STIRRER SPEED (RPM)	=	1000.00
INITIAL FE3+ (KG-MOL/M3)	=	0.0286
INITIAL H2SO4 (KG-MOL/M3)	=	1.95
TOTAL SOLIDS AREA (M2/M3)	=	9809.35
INITIAL SOLIDS (KG)	=	0.0040
KDEXP (KPA M3/KG-MOL)	=	N.D.
KDCALC (KPA M3/KG-MOL)	=	1827.00

TIME (MINS)	PH2S (KPA)	ZN2+ (KG-MOL/M3)
0.00	33.28	.290E-01
1.00	30.50	N.D.
2.00	28.45	N.D.
5.00	24.40	N.D.
10.00	20.85	N.D.
20.00	17.57	N.D.
30.00	15.36	N.D.

MEAS. INTL. RATE (KPA/MIN) = -3.0186

TABLE K 19

FE3+ OXIDN. OF H2S IN AQUEOUS H2SO4
EXPERIMENTAL RUN NO. = 201

SPHAL. TYPE PRESENT		= BDH
TEMPERATURE	(K)	= 318.00
STIRRER SPEED	(RPM)	= 1000.00
INITIAL FE3+	(KG-MOL/M3)	= 0.0286
INITIAL H2SO4	(KG-MOL/M3)	= 1.95
TOTAL SOLIDS AREA	(M2/M3)	= 9842.92
INITIAL SOLIDS	(KG)	= 0.0040
KDEXP	(KPA M3/KG-MOL)	= N.D.
KDCALC	(KPA M3/KG-MOL)	= 1827.00

TIME (MINS)	PH2S (KPA)	ZN2+ (KG-MOL/M3)
0.00	15.13	N.D.
1.00	14.09	N.D.
2.00	13.13	N.D.
3.00	12.35	N.D.

MEAS. INTL. RATE (KPA/MIN) = -1.1000

TABLE K 20

FE3+ OXIDN. OF H2S IN AQUEOUS H2SO4
EXPERIMENTAL RUN NO. = 170

SPHAL. TYPE PRESENT		= VMZCR
TEMPERATURE	(K)	= 318.00
STIRRER SPEED	(RPM)	= 1000.00
INITIAL FE3+	(KG-MOL/M3)	= 0.0055
INITIAL H2SO4	(KG-MOL/M3)	= 0.48
TOTAL SOLIDS AREA	(M2/M3)	= 17851.25
INITIAL SOLIDS	(KG)	= 0.0100
KDEXP	(KPA M3/KG-MOL)	= 1861.00
KDCALC	(KPA M3/KG-MOL)	= 1569.00

TIME (MINS)	PH2S (KPA)	ZN2+ (KG-MOL/M3)
0.00	13.16	N.D.
1.00	12.31	N.D.
2.00	11.64	N.D.
5.00	11.14	N.D.
8.00	10.87	N.D.
10.00	10.92	N.D.

MEAS. INTL. RATE (KPA/MIN) = -0.8255

TABLE K 21

FE3+ OXIDN. OF H2S IN AQUEOUS H2SO4
EXPERIMENTAL RUN NO. = 170

SPHAL. TYPE PRESENT		= VMZCR
TEMPERATURE	(K)	= 318.00
STIRRER SPEED	(RPM)	= 1000.00
INITIAL FE3+	(KG-MOL/M3)	= 0.0138
INITIAL H2SO4	(KG-MOL/M3)	= 0.48
TOTAL SOLIDS AREA	(M2/M3)	= 17851.25
INITIAL SOLIDS	(KG)	= 0.0100
KDEXP	(KPA M3/KG-MOL)	= 1861.00
KDCALC	(KPA M3/KG-MOL)	= 1569.00

TIME (MINS)	PH2S (KPA)	ZN2+ (KG-MOL/M3)
0.00	10.87	.964E-02
1.00	8.66	N.D.
2.00	7.45	N.D.
3.00	6.72	N.D.
5.00	5.65	N.D.
10.00	4.09	N.D.
15.00	3.57	N.D.
20.00	3.67	N.D.

MEAS. INTL. RATE (KPA/MIN) = -2.4968

TABLE K 22

FE3+ OXIDN. OF H2S IN AQUEOUS H2SO4
EXPERIMENTAL RUN NO. = 170

SPHAL. TYPE PRESENT		= VMZCR
TEMPERATURE	(K)	= 318.00
STIRRER SPEED	(RPM)	= 1000.00
INITIAL FE3+	(KG-MOL/M3)	= 0.0138
INITIAL H2SO4	(KG-MOL/M3)	= 0.48
TOTAL SOLIDS AREA	(M2/M3)	= 17851.25
INITIAL SOLIDS	(KG)	= 0.0100
KDEXP	(KPA M3/KG-MOL)	= 1861.00
KDCALC	(KPA M3/KG-MOL)	= 1569.00

TIME (MINS)	PH2S (KPA)	ZN2+ (KG-MOL/M3)
0.00	3.67	.103E-01
1.00	2.55	N.D.
2.00	1.98	N.D.
3.00	1.58	N.D.
4.00	1.36	N.D.
5.00	1.27	N.D.
6.00	1.19	N.D.

MEAS. INTL. RATE (KPA/MIN) = -0.8148

TABLE K 23

FE3+ OXIDN. OF H2S IN AQUEOUS H2SO4
EXPERIMENTAL RUN NO. = 168

SPHAL. TYPE PRESENT		= VMZCR
TEMPERATURE	(K)	= 318.00
STIRRER SPEED	(RPM)	= 1000.00
INITIAL FE3+	(KG-MOL/M3)	= 0.0055
INITIAL H2SO4	(KG-MOL/M3)	= 0.97
TOTAL SOLIDS AREA	(M2/M3)	= 4795.32
INITIAL SOLIDS	(KG)	= 0.0050
KDEXP	(KPA M3/KG-MOL)	= 1698.00
KDCALC	(KPA M3/KG-MOL)	= 1654.00

TIME (MINS)	PH2S (KPA)	ZN2+ (KG-MOL/M3)
0.00	17.42	.121E-01
1.00	17.10	N.D.
2.00	17.00	N.D.
5.00	16.63	N.D.
10.00	15.17	N.D.
15.00	14.79	N.D.

MEAS. INTL. RATE (KPA/MIN) = -0.3938

TABLE K 24

FE3+ OXIDN. OF H2S IN AQUEOUS H2SO4
EXPERIMENTAL RUN NO. = 168

SPHAL. TYPE PRESENT		= VMZCR
TEMPERATURE	(K)	= 318.00
STIRRER SPEED	(RPM)	= 1000.00
INITIAL FE3+	(KG-MOL/M3)	= 0.0138
INITIAL H2SO4	(KG-MOL/M3)	= 0.97
TOTAL SOLIDS AREA	(M2/M3)	= 4795.32
INITIAL SOLIDS	(KG)	= 0.0050
KDEXP	(KPA M3/KG-MOL)	= 1698.00
KDCALC	(KPA M3/KG-MOL)	= 1654.00

TIME (MINS)	PH2S (KPA)	ZN2+ (KG-MOL/M3)
0.00	14.79	.120E-01
1.00	13.48	N.D.
2.00	12.66	N.D.
5.00	11.10	N.D.
10.00	9.60	N.D.
15.00	8.60	N.D.
20.00	7.64	N.D.
25.00	7.20	N.D.

MEAS. INTL. RATE (KPA/MIN) = -1.0321

TABLE K 25

FE3+ OXIDN. OF H2S IN AQUEOUS H2SO4
EXPERIMENTAL RUN NO. = 168

SPHAL. TYPE PRESENT	=	VMZCR
TEMPERATURE (K)	=	318.00
STIRRER SPEED (RPM)	=	1000.00
INITIAL FE3+ (KG-MOL/M3)	=	0.0138
INITIAL H2SO4 (KG-MOL/M3)	=	0.97
TOTAL SOLIDS AREA (M2/M3)	=	4795.32
INITIAL SOLIDS (KG)	=	0.0050
KDEXP (KPA M3/KG-MOL)	=	1698.00
KDCALC (KPA M3/KG-MOL)	=	1654.00

TIME (MINS)	PH2S (KPA)	ZN2+ (KG-MOL/M3)
0.00	6.97	.123E-01
1.00	6.53	N.D.
2.00	6.20	N.D.
5.00	5.42	N.D.
10.00	4.51	N.D.

MEAS. INTL. RATE (KPA/MIN) = -0.3385

TABLE K 26

FE3+ OXIDN. OF H2S IN AQUEOUS H2SO4
EXPERIMENTAL RUN NO. = 174

SPHAL. TYPE PRESENT	=	VMZCR
TEMPERATURE (K)	=	318.00
STIRRER SPEED (RPM)	=	1000.00
INITIAL FE3+ (KG-MOL/M3)	=	0.0055
INITIAL H2SO4 (KG-MOL/M3)	=	1.94
TOTAL SOLIDS AREA (M2/M3)	=	8980.71
INITIAL SOLIDS (KG)	=	0.0100
KDEXP (KPA M3/KG-MOL)	=	1861.00
KDCALC (KPA M3/KG-MOL)	=	1824.00

TIME (MINS)	PH2S (KPA)	ZN2+ (KG-MOL/M3)
0.00	40.33	.275E-01
2.00	39.95	N.D.
4.00	39.56	N.D.
6.00	39.18	N.D.
8.00	38.80	N.D.
10.00	38.53	N.D.
16.00	36.88	N.D.

MEAS. INTL. RATE (KPA/MIN) = -0.1853

TABLE K 27

FE3+ OXIDN. OF H2S IN AQUEOUS H2SO4
EXPERIMENTAL RUN NO. = 174

SPHAL. TYPE PRESENT	=	VMZCR
TEMPERATURE (K)	=	318.00
STIRRER SPEED (RPM)	=	1000.00
INITIAL FE3+ (KG-MOL/M3)	=	0.0138
INITIAL H2SO4 (KG-MOL/M3)	=	1.94
TOTAL SOLIDS AREA (M2/M3)	=	8980.71
INITIAL SOLIDS (KG)	=	0.0100
KDEXP (KPA M3/KG-MOL)	=	1861.00
KDCALC (KPA M3/KG-MOL)	=	1824.00

TIME (MINS)	PH2S (KPA)	ZN2+ (KG-MOL/M3)
0.00	30.86	N.D.
1.00	35.03	N.D.
2.00	33.76	N.D.
5.00	31.42	N.D.
10.00	28.89	N.D.
15.00	27.54	N.D.
20.00	26.93	N.D.
25.00	26.81	N.D.
30.00	26.81	N.D.

MEAS. INTL. RATE (KPA/MIN) = -1.2047

TABLE K 28

FE3+ OXIDN. OF H2S IN AQUEOUS H2SO4
EXPERIMENTAL RUN NO. = 174

SPHAL. TYPE PRESENT	=	VMZCR
TEMPERATURE (K)	=	318.00
STIRRER SPEED (RPM)	=	1000.00
INITIAL FE3+ (KG-MOL/M3)	=	0.0138
INITIAL H2SO4 (KG-MOL/M3)	=	1.94
TOTAL SOLIDS AREA (M2/M3)	=	8980.71
INITIAL SOLIDS (KG)	=	0.0100
KDEXP (KPA M3/KG-MOL)	=	1861.00
KDCALC (KPA M3/KG-MOL)	=	1824.00

TIME (MINS)	PH2S (KPA)	ZN2+ (KG-MOL/M3)
0.00	26.81	.277E-01
2.00	25.01	N.D.
4.00	23.74	N.D.
6.00	22.78	N.D.
10.00	21.24	N.D.
15.00	19.97	N.D.
20.00	19.09	N.D.
30.00	17.90	N.D.
35.00	17.90	N.D.

MEAS. INTL. RATE (KPA/MIN) = -0.8032

TABLE K 29

FE3+ OXIDN. OF H2S IN AQUEOUS H2SO4
EXPERIMENTAL RUN NO. = 171

SPHAL. TYPE PRESENT	=	VMPR
TEMPERATURE (K)	=	318.00
STIRRER SPEED (RPM)	=	1000.00
INITIAL FE3+ (KG-MOL/M3)	=	0.0055
INITIAL H2SO4 (KG-MOL/M3)	=	0.48
TOTAL SOLIDS AREA (M2/M3)	=	17649.56
INITIAL SOLIDS (KG)	=	0.0100
KDEXP (KPA M3/KG-MOL)	=	1308.00
KDCALC (KPA M3/KG-MOL)	=	1569.00

TIME (MINS)	PH2S (KPA)	ZN2+ (KG-MOL/M3)
0.00	8.45	.754E-02
0.33	6.72	N.D.
0.66	6.05	N.D.
1.00	5.76	N.D.
2.00	5.67	N.D.
3.00	5.67	N.D.

MEAS. INTL. RATE (KPA/MIN) = -8.4506

TABLE K 30

FE3+ OXIDN. OF H2S IN AQUEOUS H2SO4
EXPERIMENTAL RUN NO. = 171

SPHAL. TYPE PRESENT	=	VMPR
TEMPERATURE (K)	=	318.00
STIRRER SPEED (RPM)	=	1000.00
INITIAL FE3+ (KG-MOL/M3)	=	0.0138
INITIAL H2SO4 (KG-MOL/M3)	=	0.48
TOTAL SOLIDS AREA (M2/M3)	=	17649.56
INITIAL SOLIDS (KG)	=	0.0100
KDEXP (KPA M3/KG-MOL)	=	1308.00
KDCALC (KPA M3/KG-MOL)	=	1569.00

TIME (MINS)	PH2S (KPA)	ZN2+ (KG-MOL/M3)
0.00	5.72	.826E-02
0.33	3.73	N.D.
0.66	2.46	N.D.
1.00	1.59	N.D.
2.00	0.31	N.D.
3.00	0.00	N.D.
5.00	0.00	N.D.

MEAS. INTL. RATE (KPA/MIN) = -5.7230

TABLE K 31

FE3+ OXIDN. OF H2S IN AQUEOUS H2SO4
EXPERIMENTAL RUN NO. = 169

SPHAL. TYPE PRESENT	=	VMPR
TEMPERATURE (K)	=	318.00
STIRRER SPEED (RPM)	=	1000.00
INITIAL FE3+ (KG-MOL/M3)	=	0.0055
INITIAL H2SO4 (KG-MOL/M3)	=	0.97
TOTAL SOLIDS AREA (M2/M3)	=	206468.23
INITIAL SOLIDS (KG)	=	0.0850
KDEXP (KPA M3/KG-MOL)	=	1698.00
KDCALC (KPA M3/KG-MOL)	=	1654.00

TIME (MINS)	PH2S (KPA)	ZN2+ (KG-MOL/M3)
0.00	16.28	.115E-01
1.00	14.40	N.D.
2.00	13.70	N.D.
3.00	13.31	N.D.
4.00	13.13	N.D.
5.00	13.07	N.D.

MEAS. INTL. RATE (KPA/MIN) = -2.7373

TABLE K 32

FE3+ OXIDN. OF H2S IN AQUEOUS H2SO4
EXPERIMENTAL RUN NO. = 169

SPHAL. TYPE PRESENT	=	VMPR
TEMPERATURE (K)	=	318.00
STIRRER SPEED (RPM)	=	1000.00
INITIAL FE3+ (KG-MOL/M3)	=	0.0138
INITIAL H2SO4 (KG-MOL/M3)	=	0.97
TOTAL SOLIDS AREA (M2/M3)	=	4514.41
INITIAL SOLIDS (KG)	=	0.0050
KDEXP (KPA M3/KG-MOL)	=	1698.00
KDCALC (KPA M3/KG-MOL)	=	1654.00

TIME (MINS)	PH2S (KPA)	ZN2+ (KG-MOL/M3)
0.00	13.16	.116E-01
1.00	11.24	N.D.
2.00	10.40	N.D.
30.00	9.87	N.D.
5.00	9.10	N.D.
10.00	7.78	N.D.
15.00	7.01	N.D.
20.00	6.29	N.D.
25.00	5.81	N.D.
30.00	5.38	N.D.

MEAS. INTL. RATE (KPA/MIN) = -2.6413

TABLE K 33

FE3+ OXIDN. OF H2S IN AQUEOUS H2SO4
EXPERIMENTAL RUN NO. = 101

SPHAL. TYPE PRESENT	=	VIBR PR
TEMPERATURE (K)	=	318.00
STIRRER SPEED (RPM)	=	800.00
INITIAL FE3+ (KG-MOL/M3)	=	0.0045
INITIAL H2SO4 (KG-MOL/M3)	=	0.95
TOTAL SOLIDS AREA (M2/M3)	=	35267.28
INITIAL SOLIDS (KG)	=	0.0200
KDEXP (KPA M3/KG-MOL)	=	1561.00
KDCALC (KPA M3/KG-MOL)	=	1654.00

TIME (MINS)	PH2S (KPA)	ZN2+ (KG-MOL/M3)
0.00	20.30	.214E 02
0.33	17.18	N.D.
0.66	16.08	N.D.
1.00	15.40	N.D.

MEAS. INTL. RATE (KPA/MIN) = -24.9872

TABLE K 34

FE3+ OXIDN. OF H2S IN AQUEOUS H2SO4
EXPERIMENTAL RUN NO. = 101

SPHAL. TYPE PRESENT	=	VIBR PR
TEMPERATURE (K)	=	318.00
STIRRER SPEED (RPM)	=	800.00
INITIAL FE3+ (KG-MOL/M3)	=	0.0045
INITIAL H2SO4 (KG-MOL/M3)	=	0.95
TOTAL SOLIDS AREA (M2/M3)	=	35267.28
INITIAL SOLIDS (KG)	=	0.0200
KDEXP (KPA M3/KG-MOL)	=	1561.00
KDCALC (KPA M3/KG-MOL)	=	1654.00

TIME (MINS)	PH2S (KPA)	ZN2+ (KG-MOL/M3)
0.00	16.24	.220E-01
0.33	13.43	N.D.
0.66	11.93	N.D.
1.00	11.37	N.D.

MEAS. INTL. RATE (KPA/MIN) = -12.8059

TABLE K 35

FE3+ OXIDN. OF H2S IN AQUEOUS H2SO4
EXPERIMENTAL RUN NO. = 173

SPHAL. TYPE PRESENT	=	VMPR
TEMPERATURE (K)	=	318.00
STIRRER SPEED (RPM)	=	1000.00
INITIAL FE3+ (KG-MOL/M3)	=	0.0055
INITIAL H2SO4 (KG-MOL/M3)	=	1.95
TOTAL SOLIDS AREA (M2/M3)	=	8547.58
INITIAL SOLIDS (KG)	=	0.0100
KDEXP (KPA M3/KG-MOL)	=	1850.00
KDCALC (KPA M3/KG-MOL)	=	1824.00

TIME (MINS)	PH2S (KPA)	ZN2+ (KG-MOL/M3)
0.00	27.48	.242E-01
0.33	34.67	N.D.
0.66	34.11	N.D.
1.00	33.82	N.D.
2.00	33.76	N.D.
4.00	33.88	N.D.
6.00	33.92	N.D.

MEAS. INTL. RATE (KPA/MIN) = -8.4506

TABLE K 36

FE3+ OXIDN. OF H2S IN AQUEOUS H2SO4
EXPERIMENTAL RUN NO. = 173

SPHAL. TYPE PRESENT	=	VMPR
TEMPERATURE (K)	=	318.00
STIRRER SPEED (RPM)	=	1000.00
INITIAL FE3+ (KG-MOL/M3)	=	0.0055
INITIAL H2SO4 (KG-MOL/M3)	=	1.95
TOTAL SOLIDS AREA (M2/M3)	=	8547.58
INITIAL SOLIDS (KG)	=	0.0100
KDEXP (KPA M3/KG-MOL)	=	1850.00
KDCALC (KPA M3/KG-MOL)	=	1824.00

TIME (MINS)	PH2S (KPA)	ZN2+ (KG-MOL/M3)
0.00	33.92	N.D.
0.33	32.25	N.D.
0.66	31.42	N.D.
1.00	30.86	N.D.
2.00	30.36	N.D.
3.00	30.36	N.D.
5.00	30.46	N.D.

MEAS. INTL. RATE (KPA/MIN) = -5.5988

TABLE K 37

FE3+ OXIDN. OF H2S IN AQUEOUS H2SO4
EXPERIMENTAL RUN NO. = 173

SPHAL. TYPE PRESENT	=	VMPR
TEMPERATURE (K)	=	318.00
STIRRER SPEED (RPM)	=	1000.00
INITIAL FE3+ (KG-MOL/M3)	=	0.0138
INITIAL H2SO4 (KG-MOL/M3)	=	1.95
TOTAL SOLIDS AREA (M2/M3)	=	8547.58
INITIAL SOLIDS (KG)	=	0.0100
KDEXP (KPA M3/KG-MOL)	=	1861.00
KDCALC (KPA M3/KG-MOL)	=	1824.00

TIME (MINS)	PH2S (KPA)	ZN2+ (KG-MOL/M3)
0.00	30.36	.245E-01
0.50	27.71	N.D.
1.00	26.31	N.D.
2.00	24.45	N.D.
3.00	23.07	N.D.
5.00	21.40	N.D.
8.00	20.53	N.D.

MEAS. INTL. RATE (KPA/MIN) = -7.6824

TABLE K 38

FE3+ OXIDN. OF H2S IN AQUEOUS H2SO4
EXPERIMENTAL RUN NO. = 173

SPHAL. TYPE PRESENT	=	VMPR
TEMPERATURE (K)	=	318.00
STIRRER SPEED (RPM)	=	1000.00
INITIAL FE3+ (KG-MOL/M3)	=	0.0121
INITIAL H2SO4 (KG-MOL/M3)	=	1.95
TOTAL SOLIDS AREA (M2/M3)	=	8547.58
INITIAL SOLIDS (KG)	=	0.0100
KDEXP (KPA M3/KG-MOL)	=	1861.00
KDCALC (KPA M3/KG-MOL)	=	1824.00

TIME (MINS)	PH2S (KPA)	ZN2+ (KG-MOL/M3)
0.00	20.59	.245E-01
0.33	18.82	N.D.
0.66	18.13	N.D.
1.00	17.73	N.D.
2.00	16.77	N.D.
5.00	15.15	N.D.
10.00	13.58	N.D.
15.00	12.46	N.D.
20.00	12.23	N.D.

MEAS. INTL. RATE (KPA/MIN) = -5.2816

TABLE K 39

FE3+ OXIDN. OF H2S IN AQUEOUS H2SO4
EXPERIMENTAL RUN NO. = 222

SPHAL. TYPE PRESENT	=	NO SOLIDS
TEMPERATURE (K)	=	298.00
STIRRER SPEED (RPM)	=	1000.00
INITIAL FE3+ (KG-MOL/M3)	=	0.0491
INITIAL H2SO4 (KG-MOL/M3)	=	1.00
TOTAL SOLIDS AREA (M2/M3)	=	0.00
INITIAL SOLIDS (KG)	=	0.0000
KDEXP (KPA M3/KG-MOL)	=	N.D.
KDCALC (KPA M3/KG-MOL)	=	1225.00

TIME (MINS)	PH2S (KPA)	ZN2+ (KG-MOL/M3)
0.00	26.21	N.D.
1.00	23.47	N.D.
3.00	20.39	N.D.
5.00	18.36	N.D.
10.00	15.28	N.D.
15.00	13.53	N.D.
20.00	12.17	N.D.
30.00	10.62	N.D.
10.00	9.74	N.D.

MEAS. INTL. RATE (KPA/MIN) = -3.4299

TABLE K 40

FE3+ OXIDN. OF H2S IN AQUEOUS H2SO4
EXPERIMENTAL RUN NO. = 220

SPHAL. TYPE PRESENT	=	ACT. CHAR.
TEMPERATURE (K)	=	298.00
STIRRER SPEED (RPM)	=	1000.00
INITIAL FE3+ (KG-MOL/M3)	=	0.0491
INITIAL H2SO4 (KG-MOL/M3)	=	1.00
TOTAL SOLIDS AREA (M2/M3)	=	0.00
INITIAL SOLIDS (KG)	=	0.0030
KDEXP (KPA M3/KG-MOL)	=	N.D.
KDCALC (KPA M3/KG-MOL)	=	1225.00

TIME (MINS)	PH2S (KPA)	ZN2+ (KG-MOL/M3)
0.00	26.77	N.D.
1.00	19.16	N.D.
2.00	16.07	N.D.
3.00	14.11	N.D.
4.00	12.63	N.D.
5.00	11.50	N.D.
7.00	9.66	N.D.
10.00	8.05	N.D.
15.00	6.41	N.D.
20.00	5.51	N.D.
25.00	4.90	N.D.
30.00	4.73	N.D.

MEAS. INTL. RATE (KPA/MIN) = -9.2102

TABLE K 41

FE3+ OXIDN. OF H2S IN AQUEOUS H2SO4
EXPERIMENTAL RUN NO. = 221

SPHAL. TYPE PRESENT	=	ACT. CHAR.
TEMPERATURE (K)	=	298.00
STIRRER SPEED (RPM)	=	1000.00
INITIAL FE3+ (KG-MOL/M3)	=	0.0491
INITIAL H2SO4 (KG-MOL/M3)	=	1.00
TOTAL SOLIDS AREA (M2/M3)	=	0.00
INITIAL SOLIDS (KG)	=	0.0100
KDEXP (KPA M3/KG-MOL)	=	N.D.
KDCALC (KPA M3/KG-MOL)	=	1225.00

TIME (MINS)	PH2S (KPA)	ZN2+ (KG-MOL/M3)
0.00	26.35	N.D.
0.50	16.42	N.D.
1.00	13.21	N.D.
2.00	9.92	N.D.
3.00	8.30	N.D.
4.00	7.44	N.D.
5.00	6.95	N.D.
7.00	6.24	N.D.
10.00	5.66	N.D.
15.00	5.15	N.D.
20.00	4.84	N.D.
25.00	4.60	N.D.

MEAS. INTL. RATE (KPA/MIN) = -22.3304

TABLE K 42

FE3+ OXIDN. OF H2S IN AQUEOUS H2SO4
EXPERIMENTAL RUN NO. = 223

SPHAL. TYPE PRESENT	=	ACT. CHAR.
TEMPERATURE (K)	=	298.00
STIRRER SPEED (RPM)	=	1000.00
INITIAL FE3+ (KG-MOL/M3)	=	0.0491
INITIAL H2SO4 (KG-MOL/M3)	=	1.00
TOTAL SOLIDS AREA (M2/M3)	=	0.00
INITIAL SOLIDS (KG)	=	0.0200
KDEXP (KPA M3/KG-MOL)	=	N.D.
KDCALC (KPA M3/KG-MOL)	=	1225.00

TIME (MINS)	PH2S (KPA)	ZN2+ (KG-MOL/M3)
0.00	26.85	N.D.
0.25	16.28	N.D.
0.50	13.34	N.D.
1.00	10.42	N.D.
2.00	8.34	N.D.
3.00	7.44	N.D.
4.00	6.92	N.D.
5.00	6.54	N.D.
7.00	5.93	N.D.
10.00	5.47	N.D.
15.00	4.76	N.D.

MEAS. INTL. RATE (KPA/MIN) = -52.9998

A P P E N D I X L

TABULATED EXPERIMENTAL RESULTS FOR LEACHING UNDER CASE (iii) CONDITIONS

($[Fe^{3+}]_o$: $[H_2SO_4]_o \leq 0,1$)

This type of data was qualitatively interpreted as discussed in section G. 4.

TABLE L 1

EXPERIMENTAL RUN NO. = 180
SPHALERITE LEACHING IN AQUEOUS H2SO4

SPHAL. TYPE LEACHED		=	VMWBM+FE3+ at t=0)
TEMPERATURE	(K)	=	318.00
INITIAL MASS	(KG)	=	0.0100
STIRRER SPEED	(RPM)	=	1000.0
INITIAL H2SO4	(KG-MOL/M3)	=	0.5000
INITIAL FE3+	(KG-MOL/M3)	=	0.0138
SPEC.SURFACE AREA	(M2/KG)	=	3272.0
KDCALC	(KPA M3/KG-MOL)	=	.1569E 04

TIME (MINS)	PH2S (KPA)	ZN2+ (KG-MOL/M3)
1.00	0.00	.294E-02
5.00	0.00	.550E-02
15.00	0.00	.592E-02
62.00	0.00	.601E-02
90.00	0.00	.604E-02

TABLE L 2

EXPERIMENTAL RUN NO. = 177
SPHALERITE LEACHING IN AQUEOUS H2SO4

SPHAL. TYPE LEACHED		=	VMWBM+FE3+ at t=0)
TEMPERATURE	(K)	=	318.00
INITIAL MASS	(KG)	=	0.0100
STIRRER SPEED	(RPM)	=	1000.0
INITIAL H2SO4	(KG-MOL/M3)	=	1.0000
INITIAL FE3+	(KG-MOL/M3)	=	0.0138
SPEC.SURFACE AREA	(M2/KG)	=	3272.0
KDCALC	(KPA M3/KG-MOL)	=	.1654E 04

TIME (MINS)	PH2S (KPA)	ZN2+ (KG-MOL/M3)
1.00	3.75	.430E-02
5.00	4.90	.765E-02
10.00	5.28	.948E-02
21.50	7.49	.115E-01
30.00	8.93	.116E-01
45.00	10.47	.131E-01
60.00	11.43	N.D.
75.00	12.29	.144E-01

TABLE L 3

EXPERIMENTAL RUN NO. = 178
SPHALERITE LEACHING IN AQUEOUS H2SO4

SPHAL. TYPE LEACHED		=	VMWBM+FE3+ at t=0)
TEMPERATURE	(K)	=	318.00
INITIAL MASS	(KG)	=	0.0100
STIRRER SPEED	(RPM)	=	1000.0
INITIAL H2SO4	(KG-MOL/M3)	=	1.0000
INITIAL FE3+	(KG-MOL/M3)	=	0.0275
SPEC.SURFACE AREA	(M2/KG)	=	3272.0
KDCALC	(KPA M3/KG-MOL)	=	.1654E 04

TIME (MINS)	PH2S (KPA)	ZN2+ (KG-MOL/M3)
1.00	1.44	N.D.
5.00	3.07	.878E-30
10.00	0.05	N.D.
15.00	0.00	N.D.
30.00	0.38	.120E-01
45.00	0.84	.329E-29
60.00	1.58	.132E-01
90.00	2.78	.145E-01

TABLE L 4

EXPERIMENTAL RUN NO. = 179
SPHALERITE LEACHING IN AQUEOUS H2SO4

SPHAL. TYPE LEACHED		=	VMWBM+FE3+ at t=0)
TEMPERATURE	(K)	=	318.00
INITIAL MASS	(KG)	=	0.0100
STIRRER SPEED	(RPM)	=	1000.0
INITIAL H2SO4	(KG-MOL/M3)	=	1.0000
INITIAL FE3+	(KG-MOL/M3)	=	0.0550
SPEC.SURFACE AREA	(M2/KG)	=	3272.0
KDCALC	(KPA M3/KG-MOL)	=	.1654E 04

TIME (MINS)	PH2S (KPA)	ZN2+ (KG-MOL/M3)
0.33	0.67	N.D.
0.66	0.72	N.D.
1.00	0.53	.535E-02
2.00	0.26	N.D.
5.00	0.10	.981E-02
17.00	0.00	.782E-29
25.00	0.00	N.D.
30.00	0.00	.217E-01
45.00	0.00	N.D.
60.00	0.00	.259E-01

TABLE L 5

EXPERIMENTAL RUN NO. = 210
SPHALERITE LEACHING IN AQUEOUS H2SO4

SPHAL. TYPE LEACHED		=	VMWBM+FE3+ at t=0)
TEMPERATURE	(K)	=	318.00
INITIAL MASS	(KG)	=	0.0100
STIRRER SPEED	(RPM)	=	1000.0
INITIAL H2SO4	(KG-MOL/M3)	=	1.0000
SPEC.SURFACE AREA	(M2/KG)	=	3272.0
KDCALC	(KPA M3/KG-MOL)	=	.1654E 04
INITAL FE3+	(KG-MOL/M3)	=	0.0570

TIME (MINS)	PH2S (KPA)	ZN2+ (KG-MOL/M3)
0.25	0.53	N.D.
0.50	0.50	N.D.
1.00	0.34	.600E-02
5.00	0.07	.110E-01
10.00	0.00	N.D.
15.00	0.05	.175E-01
30.00	0.36	.205E-01
45.00	0.82	.215E-01
60.00	1.10	.219E-01
75.00	1.49	.216E-28

TABLE L 6

EXPERIMENTAL RUN NO. = 181
SPHALERITE LEACHING IN AQUEOUS H2SO4

SPHAL. TYPE LEACHED		=	VMWBM+FE3+ at t=0)
TEMPERATURE	(K)	=	318.00
INITIAL MASS	(KG)	=	0.0100
STIRRER SPEED	(RPM)	=	1000.0
INITIAL H2SO4	(KG-MOL/M3)	=	2.0000
INITIAL FE3+	(KG-MOL/M3)	=	0.0138
SPEC.SURFACE AREA	(M2/KG)	=	3272.0
KDCALC	(KPA M3/KG-MOL)	=	.1824E 04

TIME (MINS)	PH2S (KPA)	ZN2+ (KG-MOL/M3)
0.33	3.00	N.D.
0.66	4.30	N.D.
1.00	5.22	.617E-02
2.00	6.38	N.D.
6.00	7.61	.102E-01
10.00	8.45	N.D.
15.00	10.64	.133E-01
30.00	15.44	.173E-01
15.00	18.52	.179E-01
60.00	20.36	N.D.

TABLE L 7

EXPERIMENTAL RUN NO. = 182
SPHALERITE LEACHING IN AQUEOUS H2SO4

SPHAL. TYPE LEACHED	=	VMWRM+A.C.at t=0)
TEMPERATURE (K)	=	318.00
INITIAL MASS(sphal.) (KG)	=	0.0100
STIRRER SPEED (RPM)	=	1000.0
INITIAL H2SO4 (KG-MOL/M3)	=	1.0000
SPEC.SURFACE AREA (M2/KG)	=	3272.0
INTL. ACT. CHARCOAL (KG)	=	0.0050

KDCALC (KPA M3/KG-MOL) = .1654E 04

TIME (MINS)	PH2S (KPA)	ZN2+ (KG-MOL/M3)
1.30	7.11	.770E-02
5.00	11.62	.104E-01
10.00	13.25	N.D.
15.00	14.02	.128E-01
30.00	15.17	.144E-01

MEASURED (DP/DT)0 (KPA/MIN)	=	9.22
FITTED (DP/DT)0 (KPA/MIN)	=	9.87
MEASURED (P)EQ (KPA)	=	15.46
FITTED (P)EQ (KPA)	=	15.40

TABLE L 8

EXPERIMENTAL RUN NO. = 212
SPHALERITE LEACHING IN AQUEOUS H2SO4

SPHAL. TYPE LEACHED	=	VMWRM+A.C.at t=0)
TEMPERATURE (K)	=	318.00
INITIAL MASS (KG)	=	0.0100
STIRRER SPEED (RPM)	=	1000.0
INITIAL H2SO4 (KG-MOL/M3)	=	1.0000
SPEC.SURFACE AREA (M2/KG)	=	3272.0
INTL. ACT. CHARCOAL (KG)	=	0.0100

KDCALC (KPA M3/KG-MOL) = .1654E 04

TIME (MINS)	PH2S (KPA)	ZN2+ (KG-MOL/M3)
0.50	3.94	N.D.
0.80	5.95	.737E-02
2.00	9.03	N.D.
5.00	11.62	.119E-01
10.00	12.91	.134E-01
20.00	14.21	.145E-01
30.00	14.87	N.D.
40.00	15.27	.155E-01

MEASURED (DP/DT)0 (KPA/MIN)	=	10.45
FITTED (DP/DT)0 (KPA/MIN)	=	11.30
MEASURED (P)EQ (KPA)	=	15.27
FITTED (P)EQ (KPA)	=	15.10

TABLE L 9

EXPERIMENTAL RUN NO. = 183
SPHALERITE LEACHING IN AQUEOUS H2SO4

SPHAL. TYPE LEACHED	=	VMWRM+FE+AC.at t=0)
TEMPERATURE (K)	=	318.00
INITIAL MASS (KG)	=	0.0100
STIRRER SPEED (RPM)	=	1000.0
INITIAL H2SO4 (KG-MOL/M3)	=	1.0000
SPEC.SURFACE AREA (M2/KG)	=	3272.0
KDCALC (KPA M3/KG-MOL)	=	.1654E 04

TIME (MINS)	PH2S (KPA)	ZN2+ (KG-MOL/M3)
0.33	1.08	N.D.
0.66	1.31	N.D.
1.00	1.34	.433E-02
2.00	1.15	N.D.
5.00	1.97	.765E-02
10.00	4.99	.107E-01
30.00	7.25	.128E-01
45.00	8.60	.141E-01

INTL. ACT. CHARCOAL (KG) = 0.0050

TABLE L 10

EXPERIMENTAL RUN NO. = 215
SPHALERITE LEACHING IN AQUEOUS H2SO4

SPHAL. TYPE LEACHED	=	VMWRM+FE3+ACT. CHAR)
TEMPERATURE (K)	=	318.00
INITIAL MASS(sphal.) (KG)	=	0.0100
STIRRER SPEED (RPM)	=	1000.0
INITIAL H2SO4 (KG-MOL/M3)	=	1.0000
INITIAL FE3+ (KG-MOL/M3)	=	0.0573
SPEC.SURFACE AREA (M2/KG)	=	3272.0
KDCALC (KPA M3/KG-MOL)	=	.1654E 04

TIME (MINS)	PH2S (KPA)	ZN2+ (KG-MOL/M3)
1.0	0	6.042×10^{-3}
5.0	0	11.473×10^{-3}
15.0	0	18.051×10^{-3}
30.0	0	22.793×10^{-3}
45.0	0	23.56×10^{-3}
60.0	0	23.925×10^{-3}

MASS OF ACT. CHARCOAL (kg) = 0.01

TABLE L 11

EXPERIMENTAL RUN NO. = 214
SPHALERITE LEACHING IN AQUEOUS H2SO4

SPHAL. TYPE LEACHED	=	VMWRM+FE3+ACT.CHAR.)
TEMPERATURE (K)	=	318.00
INITIAL MASS (KG)	=	0.0100
STIRRER SPEED (RPM)	=	1000.0
INITIAL H2SO4 (KG-MOL/M3)	=	1.0000
INITIAL FE3+ (KG-MOL/M3)	=	0.0573
SPEC SURFACE AREA (M2/KG)	=	3272.0

KDCALC (KPA M3/KG-MOL) = .1654 E 04

TIME (MINS)	PH2S (KPA)	ZN2+ (KG-MOL/M3)
1.0	0	5.997×10^{-3}
5.0	0	11.779×10^{-3}
15.0	0	17.286×10^{-3}
30.0	0	21.493×10^{-3}
45.0	0	21.952×10^{-3}
60.0	0	22.411×10^{-3}

MASS OF ACT CHARCOAL (kg) = 0.02

TABLE L 12

EXPERIMENTAL RUN NO. = 184
SPHALERITE LEACHING IN AQUEOUS H2SO4

SPHAL. TYPE LEACHED	=	VMWRM+SUL.at t=0)
TEMPERATURE (K)	=	318.00
INITIAL MASS (KG)	=	0.0100
STIRRER SPEED (RPM)	=	1000.0
INITIAL H2SO4 (KG-MOL/M3)	=	1.0000
SPEC.SURFACE AREA (M2/KG)	=	3272.0
CDEXP (KG-MOL/M3 KPA)	=	.7320E-03
KDEXP (KPA M3/KG-MOL)	=	.1669E 04
KDCALC (KPA M3/KG-MOL)	=	.1654E 04
INTL.S° POWDER ADDED (KG)	=	0.0100

TIME (MINS)	PH2S (KPA)	ZN2+ (KG-MOL/M3)	ZN2+/PH2S (KG-MOL/M3 KPA)
0.50	4.61	N.D.	N.D.
1.20	8.83	.696E-02	.788E-03
5.00	14.40	.110E-01	.762E-03
16.00	17.29	.114E-01	.660E-03
30.00	18.63	N.D.	N.D.
45.00	19.21	.141E-01	.733E-03

MEASURED (DP/DT)0 (KPA/MIN)	=	15.36
FITTED (DP/DT)0 (KPA/MIN)	=	12.30
MEASURED (P)EQ (KPA)	=	19.21
FITTED (P)EQ (KPA)	=	19.50

TABLE L 13

EXPERIMENTAL RUN NO. = 188
SPHALERITE LEACHING IN AQUEOUS H2SO4

SPHAL. TYPE LEACHED	=	VMWBM+ZN+FEatt=0)
TEMPERATURE (K)	=	318.00
INITIAL MASS (KG)	=	0.0100
STIRRER SPEED (RPM)	=	1000.0
INITIAL H2SO4 (KG-MOL/M3)	=	1.0000
SPEC.SURFACE AREA (M2/KG)	=	3272.0
KDCALC (KPA M3/KG-MOL)	=	.1654E 04

TIME (MINS)	PH2S (KPA)	ZN2+ (KG-MOL/M3) (
0.33	0.48	N.D.
0.66	0.57	N.D.
1.00	0.49	.299E-01
2.00	0.35	N.D.
3.00	0.14	N.D.
5.00	0.08	N.D.
10.00	0.00	N.D.
20.00	0.00	.419E-01
40.00	0.00	.434E-01
60.00	0.24	.465E-01
80.00	0.67	N.D.
90.00	0.75	.499E-01

INITIAL ZN2+ (KG-MOL/M3) = 0.0299
INITIAL FE3+ (KG-MOL/M3) = 0.0550

TABLE L 14

EXPERIMENTAL RUN NO. = 207
SPHALERITE LEACHING IN AQUEOUS H2SO4

SPHAL. TYPE LEACHED	=	VMZCR+FE3+att=0)
TEMPERATURE (K)	=	318.00
INITIAL MASS (KG)	=	0.0100
STIRRER SPEED (RPM)	=	1000.0
INITIAL H2SO4 (KG-MOL/M3)	=	1.0000
INITIAL FE3+ (KG-MOL/M3)	=	0.0287
SPEC.SURFACE AREA (M2/KG)	=	2700.0
KDCALC (KPA M3/KG-MOL)	=	.1654E 04

TIME (MINS)	PH2S (KPA)	ZN2+ (KG-MOL/M3)
0.50	1.92	N.D.
1.00	2.54	.475E-02
2.00	2.88	N.D.
3.00	2.84	N.D.
6.00	2.53	.962E-02
10.00	1.98	N.D.
15.00	1.46	.128E-01
20.00	1.46	N.D.
25.00	1.46	N.D.
30.00	1.65	.145E-01
40.00	2.69	N.D.
62.00	4.74	.159E-01
80.00	6.15	N.D.
100.00	7.68	N.D.
105.70	8.07	.180E-01

TABLE L 15

EXPERIMENTAL RUN NO. = 211
SPHALERITE LEACHING IN AQUEOUS H2SO4

SPHAL. TYPE LEACHED	=	VMZCR(+FE3+att=0)
TEMPERATURE (K)	=	318.00
INITIAL MASS (KG)	=	0.0100
STIRRER SPEED (RPM)	=	1000.0
INITIAL H2SO4 (KG-MOL/M3)	=	1.0000
INITIAL FE3+ (KG-MOL/M3)	=	0.0573
SPEC.SURFACE AREA (M2/KG)	=	2700.0
KDCALC (KPA M3/KG-MOL)	=	.1654E 04

TIME (MINS)	PH2S (KPA)	ZN2+ (KG-MOL/M3)
0.50	0.84	N.D.
1.00	1.05	.525E-02
5.00	1.13	.106E-01
10.00	1.13	N.D.
14.70	1.19	.168E-01
29.80	1.34	.208E-01
45.00	1.54	.226E-01
60.00	3.76	.236E-01

TABLE L 16

EXPERIMENTAL RUN NO. = 206
SPHALERITE LEACHING IN AQUEOUS H2SO4

SPHAL. TYPE LEACHED	=	BDH(+FE3+att=0)
TEMPERATURE (K)	=	318.00
INITIAL MASS (KG)	=	0.0040
STIRRER SPEED (RPM)	=	1000.0
INITIAL H2SO4 (KG-MOL/M3)	=	1.0000
INITIAL FE3+ (KG-MOL/M3)	=	0.0287
SPEC.SURFACE AREA (M2/KG)	=	7200.0
KDCALC (KPA M3/KG-MOL)	=	.1654E 04

TIME (MINS)	PH2S (KPA)	ZN2+ (KG-MOL/M3)
1.00	2.50	.326E-02
2.00	3.78	N.D.
3.00	4.37	N.D.
5.00	4.80	.888E-02
10.00	4.80	.128E-01
13.00	4.76	N.D.
15.00	4.86	N.D.
20.00	5.17	N.D.
25.00	5.72	N.D.
30.00	6.82	.178E-01
40.00	8.83	N.D.
60.00	11.24	.202E-01

TABLE L 17

EXPERIMENTAL RUN NO. = 208
SPHALERITE LEACHING IN AQUEOUS H2SO4

SPHAL. TYPE LEACHED	=	BDH(+FE3+att=0)
TEMPERATURE (K)	=	318.00
INITIAL MASS (KG)	=	0.0040
STIRRER SPEED (RPM)	=	1000.0
INITIAL H2SO4 (KG-MOL/M3)	=	1.0000
INITIAL FE3+ (KG-MOL/M3)	=	0.1146
SPEC.SURFACE AREA (M2/KG)	=	7200.0
KDCALC (KPA M3/KG-MOL)	=	.1654E 04

TIME (MINS)	PH2S (KPA)	ZN2+ (KG-MOL/M3)
0.50	0.79	N.D.
1.25	1.06	.409E-02
2.00	0.91	N.D.
7.00	0.58	.123E-01
15.00	0.55	N.D.
20.70	0.48	.216E-01
40.00	0.79	.259E-01
50.00	0.79	N.D.
60.00	0.79	.281E-01

TABLE L 18

EXPERIMENTAL RUN NO. = 209
SPHALERITE LEACHING IN AQUEOUS H2SO4

SPHAL. TYPE LEACHED	=	VMPR(+FE3+att=0)
TEMPERATURE (K)	=	318.00
INITIAL MASS (KG)	=	0.0100
STIRRER SPEED (RPM)	=	1000.0
INITIAL H2SO4 (KG-MOL/M3)	=	1.0000
INITIAL FE3+ (KG-MOL/M3)	=	0.0143
SPEC.SURFACE AREA (M2/KG)	=	2630.0
KDCALC (KPA M3/KG-MOL)	=	.1654E 04

TIME (MINS)	PH2S (KPA)	ZN2+ (KG-MOL/M3)
1.60	0.13	.579E-02
5.00	0.38	.785E 01
10.00	0.60	N.D.
19.50	0.77	.861E-02
30.00	0.88	N.D.
39.70	1.10	.852E-02
50.00	2.38	N.D.
60.00	3.99	.999E-02
70.00	5.60	N.D.
80.00	6.91	N.D.
90.00	7.88	.129E-01

TABLE L 19

EXPERIMENTAL RUN NO. = 205
SPHALERITE LEACHING IN AQUEOUS H2SO4

SPHAL. TYPE LEACHED		=	VMPR(+FE3+att=0)
TEMPERATURE	(K)	=	318.00
INITIAL MASS	(KG)	=	0.0100
STIRRER SPEED	(RPM)	=	1000.0
INITIAL H2SO4	(KG-MOL/M3)	=	1.0000
INITIAL FE3+	(KG-MOL/M3)	=	0.0287
SPEC.SURFACE AREA	(M2/KG)	=	2630.0
KDCALC	(KPA M3/KG-MOL)	=	.1654E 04

TIME (MINS)	PH2S (KPA)	ZN2+ (KG-MOL/M3)
1.00	0.10	.598E-02
5.00	0.19	.973E-02
20.00	0.44	.138E-01
30.00	0.56	.140E-01
60.00	1.31	.141E-01
90.00	1.60	.139E-01

A P P E N D I X M

LIST OF TABLES AND FIGURES

M 1 LIST OF TABLES

Table

activation energies E_a representing the origin and slope of the lines appearing on figure 3.13.

3.9 Summary of pre-exponential constants A_E calculated using equation 3.40.

3.10 Summary of constants appearing in the general initial rate leaching equation 3.41.

3.11 Summary of conditions and initial rate results for WBM and VMWBM sphalerites leaching under case (ii) conditions.

3.12 Summary of conditions and initial rate results for BDH sphalerite leaching under case (ii) conditions.

3.13 Summary of leaching conditions and initial rate results for ZCR and VMZCR sphalerites leaching under case (ii) conditions.

3.14 Summary of conditions and initial rate results for PR and VMPR sphalerite leaching under case (ii) conditions.

3.15 Summary of activation energies E_a and pre-exponential constants A_E for the indicated best fit lines for leaching various sphalerites under case (ii) conditions ($[Fe^{3+}]_o : [H_2SO_4]_o \geq 1,8$). Concentrations of major impurities (copper and iron) are also summarised.

3.16 Summary of concentrations of major impurities (Cu and Fe) and $\lambda(\overline{D})$ for the indicated sphalerites.

4.1a Determination of $\psi_4(X)$ for VMWBM leaching results reported in table J.9.

4.1b Determination of $\psi_4(X)$ for VMWBM leaching results reported in table J.10.

Table

M 2 LIST OF FIGURES

Figure

Figure

and fitted initial rate values for the BDH sphalerite.

3.18 Arrhenius plot demonstrating the effect of temperature on k_{18} (as defined by equation 3.44) for the WBM, VMWBM and BDH sphalerites.

3.19 Arrhenius plot demonstrating the effect of temperature on k_{18} (where k_{18} is defined by equation 3.44) for ZCR and VMZCR sphalerites.

3.20 Arrhenius plot demonstrating the effect of temperature on k_{18} (where k_{18} is defined by equation 3.44) for the PR and VMPR sphalerites.

3.21 Mean diameter $\overline{D}$ versus rate constant ratio $\lambda(\overline{D})$ (where $\lambda(\overline{D})$ is defined by equation 3.45) for the WBM, VMWBM and BDH sphalerites.

3.22 Mean diameter $\overline{D}$ versus rate constant ratio $\lambda(\overline{D})$ (where $\lambda(\overline{D})$ is defined by equation 3.45) for the ZCR and VMZCR sphalerites.

3.23 Mean diameter $\overline{D}$ versus rate constant ratio $\lambda(\overline{D})$ (where $\lambda(\overline{D})$ is defined by equation 3.45) for the PR and VMPR sphalerites.

3.24 Comparison of best fit Arrhenius plots presented on figures 3.18 (WBM and BDH); 3.19 (ZCR) and 3.20 (PR).

3.25 Comparison of best fit $\lambda(\overline{D})$ versus $\overline{D}$ curves off figures 3.21, 3.22 and 3.23.

4.1 Comparison of active site area ratio functions $\psi_1(X)$, $\psi_2(X)$, $\psi_3(X)$ and $\psi_4(X)$ with $\psi_4(X)$ values calculated for WBM and VMWBM sphalerites leaching under case (ii) conditions.

4.2 Example of graphically determining $\psi_4(X)$ and

Figure

k_{13} solutions to equation 4.5 for VMWBM sphalerite leaching under case (i) conditions at two different $[H^+]_o$ values.

4.3 Example of graphically determining $\Psi_4(X)$ and k_{13} solutions to equation 4.5 for VMWBM sphalerite leaching under case (i) conditions at two different temperatures.

4.4 Example of graphically determining $\Psi_4(X)$ and k_{13} solutions to equation 4.5 for VMWBM spalerite leaching under case (i) conditions with two different masses of sphalerite initially present.

4.5 Summary of $\Psi_4(X)$ versus X solution values shown on figures 4.2 , 4.3 and 4.4 .

4.6 Summary of k_{13} versus X solution values shown on figures 4.2 , 4.3 and 4.4 .

4.7 Comparison of all case (i) $\Psi_4(X)$ versus X data (from figure 4.5) with all case (ii) $\Psi_4(X)$ versus X data (from figure 4.1)

4.8 Reverse rate constant ratio $\Omega(X)$ versus X for VMWBM sphalerite leached under case (i) conditions. $\Omega(X)$ is defined by equation 4.10 .

4.9 Arrhenius - type plot illustrating the effect of temperature on the reverse rate constant k_{13} for VMWBM sphalerite leaching under case (i) conditions.

4.10 Comparison of calculated $\Psi_4(X)$ versus X values for the VMZCR sphalerite (leaching under case (i) and case (ii) conditions) and for the ZCR sphalerite (leaching under case (ii) conditions) with the functions $\Psi_1(X)$, $\Psi_2(X)$, $\Psi_3(X)$ and $\Psi_4(X)$.

Figure

4.11 Rate curve for ZCR sphalerite leaching under case (ii) conditions, demonstrating the effect of removing the sulphur from the particles at $X = 0,49$.

4.12 Comparison of reverse rate constant k_{13} calculated for VMZCR sphalerite (using data reported in tables I 13 and I 15) with the best fit k_{13} curve (off figure 4.6) for VMWBM sphalerite.

4.13 Comparison of calculated $\psi_4(X)$ versus X values for the PR and VMPR sphalerites leaching under case (ii) conditions with the functions $\psi_1(X)$, $\psi_2(X)$, $\psi_3(X)$ and $\psi_4(X)$.

4.14 Reverse rate constant values k_{13} calculated for BDH sphalerite leaching under various case (i) conditions (using equation 4.5 with the assumption that $\phi(X)$ varies according to the shrinking core model equation 4.2).

4.15 Comparison of $\psi_4(X)$ versus X values for BDH sphalerite leaching under case (ii) conditions with the functions $\psi_1(X)$, $\psi_2(X)$, $\psi_3(X)$ and $\psi_4(X)$.

4.16 Comparison between $\psi_4(X)$ versus X best fit and calculated curves for each of the sphalerites presented previously on figures 4.7, 4.10, 4.13 and 4.15.

5.1 H_2S oxidation rate constant $(k_{I_o})_{exp}$ versus $[H_2SO_4]_o$. $(k_{I_o})_{exp}$ was calculated using the Verhulst model as expressed by equation 5.3.

5.2 H_2S oxidation rate constant ratio ω (defined by equation 5.5) versus the total VMPR sphalerite surface area A present.

Figure

5.3a & 5.3b Comparison between case (i) and case (iii) experimental $[Zn^{2+}]$ and P_{H_2S} leaching results for VMWBM sphalerite.

5.4 Effect of initial $[Fe^{3+}]$ on the amount of Zn^{2+} produced from VMWBM sphalerite during different time intervals.

5.5a & 5.5b Comparison between case (i) and case (iii) experimental $[Zn^{2+}]$ and P_{H_2S} results for VMWBM sphalerite at different $[H_2SO_4]_o$ values.

5.6a & 5.6b Comparison between case (i) and case (iii) experimental $[Zn^{2+}]$ and P_{H_2S} leaching data for VMZCR sphalerite.

5.7a & 5.7b Comparison between case (i) and case (iii) experimental $[Zn^{2+}]$ and P_{H_2S} leaching data for BDH sphalerite.

5.8a & 5.8b Comparison between case (i) and case (iii) experimental $[Zn^{2+}]$ and P_{H_2S} leaching data for VMPR sphalerite.

5.9a & 5.9b Comparison of the experimental $[Zn^{2+}]$ and P_{H_2S} rate curves for the VMWBM, VMZCR, VMPR and BDH sphalerites leaching under case (iii) conditions.

6.1 S.E.M. photograph of unleached WBM sphalerite.

6.2 S.E.M. photograph of unleached ZCR sphalerite particles.

6.3 S.E.M. photograph of CCl_4 washed leached ZCR sphalerite particles.

6.4 S.E.M. photograph of unleached PR sphalerite particles.

6.5 S.E.M. photograph of CCl_4 washed leached PR sphalerite particles.

Figure

6.6 S.E.M. photograph of the unwashed surface of a single leached PR particle.

6.7 S.E.M. photograph of an unwashed leached PR sphalerite particle.

6.8 S.E.M. photograph of a CCl_4 washed leached PR sphalerite particle.

6.9 S.E.M. photograph of an unleached ZCR sphalerite particle.

6.10 S.E.M. photograph of the unwashed surface of a single ZCR particle.

6.11 S.E.M. photograph of the CCl_4 washed surface of a ZCR sphalerite particle.

6.12 S.E.M. photograph of an unwashed leached WBM sphalerite particle.

6.13 S.E.M. photograph of a CCl_4 washed leached WBM sphalerite particle.

6.14 O.M. photograph of a polished section of WBM sphalerite particles.

6.15 O.M. photograph of a polished section of ZCR sphalerite particles.

6.16 O.M. photograph of a polished section of PR sphalerite particles.

6.17 O.M. photograph of a polished section of PR sphalerite particles.

6.18 O.M. photograph of a polished section of a single ZCR sphalerite particle.

6.19 Plot of $[Zn^{2+}]$ versus elemental S^o recovered, demonstrating the stoichiometric production of S^o during the leaching of the various sphalerites under case (ii) conditions.

Figure

6.20 Experimental rate curves for leaching various size fractions of WBM sphalerite under case (i) conditions ($[Fe^{3+}]_o$: $[H_2SO_4]_o \geq 0,0$)

6.21 Experimental rate curves for leaching various size fractions of ZCR sphalerite in H_2SO_4 .

6.22 Experimental rate curves for leaching various size fractions of PR sphalerite in H_2SO_4 .

6.23 Comparison of the leaching rate curves for the -17,0 + 12,0 μm size fraction of WBM , ZCR and PR leaching in H_2SO_4 .

6.24 Comparison of rate curves for WBM , ZCR and PR sphalerite (-17,0 + 12,0 μm size fraction) leaching under case (i) conditions.

6.25 Experimental rate curves comparing the dissolution of iron during the leaching of PR , ZCR and WBM sphalerites (-17,0 + 12,0 μm size fraction) in H_2SO_4 .

6.26 Comparison of zinc and iron dissolution rate curves for PR and VMPR sphalerites leaching in H_2SO_4 .

6.27 Comparison between zinc and iron dissolution rate curves for VMPR sphalerite leaching in H_2SO_4 .

6.28 Comparison of the selectivities associated with the dissolution of zinc and iron from three sizes of PR sphalerite, and from VMPR sphalerite leaching in H_2SO_4 .

6.29 Demonstration of the catalytic effect of activated charcoal on the oxidation of H_2S by Fe^{3+}. The initial oxidation rate ratio ω^* is defined by equation 6.5 .

6.30a & 6.30b Comparison of experimental $[Zn^{2+}]$ and P_{H_2S} rate curves for VMWVM sphalerite leaching in H_2SO_4 without and with Fe^{3+} and/or activated charcoal initially present.

Figure

6.31 Experimental $[Zn^{2+}]$ rate curves for VMWBM sphalerite leaching in H_2SO_4 with sufficient Fe^{3+} initially present so that no P_{H_2S} is detectable, and with activated charcoal present.

6.32 Comparison between the $[Zn^{2+}]$ and P_{H_2S} rate curves for ball milled (WBM) and vibratory milled (WVM) sphalerite leaching under case (i) conditions.

6.33 Comparison between the specific surface areas of WBM and WVM sphalerites.

6.34 Plots of case (ii) leaching data for BDH, VMWBM, and VMPR sphalerites.

6.35 Plots of case (ii) leaching data for WBM, ZCR and PR sphalerites.

A.1 Schematic diagram of leaching apparatus.

A.2 Overall view of leaching apparatus.

A.3 Close-up view of the reactor bowl and head.

E.1 Effect of temperature on the distribution coefficient K_D for H_2S dissolved in water.

E.2 Plot of $(C_D)_{exp}$ (where $(C_D)_{exp} = P_{H_2S} / [Zn^{2+}]$) versus time for various sphalerites leaching under case (i) conditions.

E.3 Plot of experimental H_2S distribution coefficient $(K_D)_{exp}$ versus $[H_2SO_4]_o$.

E.4 Arrhenius - type plot demonstrating the effect of temperature on the H_2S distribution coefficient K_D.

F.1 Comparison of specific surface areas of PR and ZCR sphalerites before and after acid pre-treatment, with A_o values calculated for solid spheres.

F.2 Comparison of the specific surface area of WBM

Figure

sphalerite before and after acid pre-treatment with A_o calculated for solid spheres using equation F. 2 .

F.3 Comparison of the ratios A_o (for a sphalerite) to A_o (calculated for solid spheres) for the ZCR, PR and WBM sphalerites.

F.4 Comparison between experimental and calculated fractional area remainder η versus extent leached X results.

F.5 Fractional area remainder versus the extent of reaction X for PR sphalerite.

F.6 Fractional area change η versus extent leached X for ZCR sphalerite.

F.7 Examples of plotting A' versus X for PR and ZCR sphalerites, and of measuring $\frac{dA'}{dX}$ from the slopes of the best fit lines.

F.8 $\frac{dA'}{dX}$ versus $\overline{D}$ for PR and ZCR sphalerites.

H.1a Comparison of $^{P}H_2S$ versus time rate curves at different stirrer speeds for VMWBM sphalerite.

H.1b Comparison of $^{P}H_2S$ versus time rate curves at different stirrer speeds for VMPR sphalerite.

H.1c Comparison of $^{P}H_2S$ versus time rate curves at different stirrer speeds for BDH sphalerite.

H.2a Plot demonstrating the effect of M_o on the $^{P}H_2S$ versus time rate curves for VMWBM sphalerite.

H.2b Plot demonstrating the effect of M_o on the $^{P}H_2S$ versus time rate curves for BDH sphalerite.